

THE JOURNAL OF PHYSICAL CHEMISTRY

มหาวิทยาลัยเกษตรศาสตร์
(Registered in U. S. Patent Office)

กระทรวงอุตสาหกรรม

CONTENTS

35th NATIONAL COLLOID SYMPOSIUM, University of Rochester, Rochester, New York, June 14-16, 1961

D. S. MacIver and H. H. Tobin: The Chemisorption of Gases on Cobalt Oxide Surfaces at Low Temperatures.	1665	John A. Thoma and Dexter French: The Starch-Iodine-Iodide Interaction. II. Potentiometric Investigations.	1825
J. J. Chessick and A. C. Zettlemoyer: A Comparison of Integral Enthalpies, Free Energies and Entropies of Adsorption.	1672	Lyle R. Dawson, Richard C. Sheridan and Hartley C. Eckstrom: Solvents Having High Dielectric Constants. XI. Electromotive Force Measurements of the Cell Pt, H ₂ ; HCl(m); AgCl-Ag in N-Methylacetamide at 40°.	1829
J. W. Whalen: Thermodynamic Properties of Water Adsorbed on Quartz.	1676	Donald Barton: Deuterium Isotope Effects in the Gas Phase Oxidation of Formaldehyde by Nitrogen Dioxide.	1831
W. H. Wade and N. Hackerman: Heats of Immersion. V. The TiO ₂ -H ₂ O System—Variations with Particle Sizes and Outgassing Temperature.	1681	Richard H. Boyd: Solution Conductance of Cyanocarbon Salts.	1834
Willard D. Bascom and C. R. Singletary: The Adsorption of Oil-Soluble Sulfonates at the Metal/Oil Interface.	1683	J. Fischer, L. Trevorrow and W. Shinn: The Kinetics and Mechanism of the Thermal Decomposition of Plutonium Hexafluoride.	1843
C. F. Schadt and R. D. Cadie: Thermal Forces on Aerosol Particles.	1689	Elmer J. Huber, Jr., Earl L. Head, Charles E. Holley, E. K. Storms and N. H. Krikorian: The Heats of Combustion of Niobium Carbides.	1846
Wasył S. Hnojewy and Lloyd H. Reyerson: Further Studies on the Sorption of H ₂ O and D ₂ O Vapors by Lysozyme and the Deuterium-Hydrogen Exchange Effect.	1694	Carl E. Johnson and Jack Fischer: Kinetics of the Reaction of Sulfur Tetrafluoride with Uranium Trioxide and Uranyl Fluoride.	1849
Martin Blank: The Effect of Vapors on Monolayer Permeability to Carbon Dioxide.	1698	J. J. Jurinak and D. H. Volman: Cation Hydration Effects on the Thermodynamics of Water Adsorption by Kaolinite.	1853
Henri L. Rosano, Paul Duby and Jack H. Schulman: Mechanism of the Selective Flux of Salts and Water Migration through Non-Aqueous Liquid Membranes.	1704	J. L. Ryan: Actinide(IV) Chloride Species Absorbed by Anion Exchange Resins from Chloride Solutions.	1856
Richard C. Goodknight and Irving Fatt: The Diffusion Time-Lag in Porous Media with Dead-End Pore Volume.	1709	Herman Pines and Jean Ravoire: Alumina: Catalyst and Support. XII. The Effect of Intrinsic Acidity of Aluminas upon Hydrogen-Deuterium Exchange.	1859
M. Kerker, J. P. Kratochvil and E. Matijević: Light Scattering Functions for $m = 1.80$ (0.04) 2.08 and $\alpha = 0.1$ (0.1) 10.0. I. Mie Scattering Coefficients.	1713	Kang Yang and Preston L. Gant: Ethane Radiolysis at Very Low Conversion.	1861
N. G. Ainslie, J. D. Mackenzie and D. Turnbull: Melting Kinetics of Quartz and Cristobalite.	1718	D. G. Hill and M. Elander: Electromotive Force Measurements in the System AgNO ₃ and NaCl in Equimolar NaNO ₃ -KNO ₃ Mixtures and their Comparison with the Quasi-Lattice Theory.	1866
E. Matijević, M. B. Abramson, R. H. Ottewill, K. F. Schulz and M. Kerker: Adsorption of Thorium Ions on Silver Iodide Sols.	1724	Stanley Bruckenschein and Jiro Osugi: Spectrophotometric Determination of the Dissociation Constant of Silver Chloride in Pyridine.	1868
Alan S. Michaels and Frederick W. Tausch, Jr.: Modification of Growth Rate and Habit of Adipic Acid Crystals with Surfactants.	1730	R. E. Glick: Exact Nuclear Magnetic Resonance Shielding Constants for Hydride, Helium, Lithium(I), Oxygen(VI).	1871
Gerald W. Sears: The Origin of Spherulites.	1738	Helmuth E. Jorgensen and Ulrich P. Strauss: Exploratory Studies on the Surface Activity of Polysoaps.	1873
Wilson J. Barnes, William G. Luetzel and Fraser P. Price: Crystallization of Poly-(ethylene oxide) in Bulk.	1742	A. Narten and T. I. Taylor: Separation of Nitrogen and Oxygen Isotopes by Exchange of Nitric Oxide with Non-Aqueous Solutions of Nitric Oxide Complexes.	1877
Philip R. Wilson, S. Krimm and Richard S. Stein: An Optical Diffractometer Analysis of Light Scattering Patterns Obtained from Polyethylene Films.	1749	Charles M. Huggins: Proton Magnetic Resonance Study of the Basicity of the Silicon-Oxygen Bond.	1881
J. L. Bethune and Gerson Kegeles: Countercurrent Distribution of Chemically Reacting Systems. II. Reactions of the Type $A + B \rightleftharpoons C$.	1755	Kōzō Shinoda and Joel H. Hildebrand: Critical Composition in Liquid Mixtures of Components of Very Different Molar Volumes.	1885
J. L. Bethune and Gerson Kegeles: Countercurrent Distribution of Chemically Reacting Systems. III. Analogs of Moving Boundary Electrophoresis and Sedimentation.	1761	C. B. McGough and G. Houghton: Catalytic Activity of the Lanthanide Oxides for the Dehydrogenation of Cyclohexane.	1887
Alan S. Michaels and Richard G. Miekka: Polycation-Polyanion Complexes: Preparation and Properties of Poly-(vinylbenzyltrimethylammonium)-Poly-(styrene sulfonate).	1765	NOTES	
Irving Cohen and Tony Vassiliades: Critical Phenomena in Aqueous Solutions of Long Chain Quaternary Ammonium Salts. II. Specificity and Light Scattering Properties.	1774	Francis P. Dwyer and Alan M. Sargeson: The Rate of Electron Transfer between the Tris-(ethylenediamine)-cobalt(II) and Cobalt(III) Ions.	1892
Irving Cohen and Tony Vassiliades: Critical Phenomena in Aqueous Solutions of Long Chain Quaternary Ammonium Salts. III. Viscosity, Diffusion and Charge Properties.	1781	J. Feney and L. H. Sutcliffe: Conformation of Fluorinated Cyclohexanes.	1894
C. W. Diggins, Jr. and R. J. Bolen: Ultracentrifugal Determination of the Micellar Character of Non-Ionic Detergent Solutions. II.	1787	Clifford J. McGinn: Diastereoazotropes as a Means of Resolution.	1896
John Bugosh: Colloidal Alumina-The Chemistry and Morphology of Colloidal Boehmite.	1789	F. B. Baker and T. W. Newton: The Reaction between Uranium (IV) and Hydrogen Peroxide.	1897
David F. Waugh: Casein Interactions and Micelle Formation.	1793	Mihir Chowdhury: Tetrachlorophthalic Anhydride-Azahydrocarbon Complexes.	1899
Arthur Veis: Phase Separation in Polyelectrolyte Solutions. II. Interaction Effects.	1798	G. N. Malcolm, H. N. Parton and I. D. Watson: Enthalpies and Entropies of Formation of Mercury(II)-Halide 1:1 Complex Ions.	1900
Horst W. Hoyer, Anne Marmo and Margaret Zoellner: Some Colloidal Properties of Decyl- and Dodecyltrimethylammonium Dodecyl Sulfate.	1804	Norman C. Li, LeRoy Johnson and James Shoolery: Proton Magnetic Resonance of Glycylglycinate, Glycineamide, and their Metal Complexes.	1902
Horst W. Hoyer and Anne Marmo: The Electrophoretic Mobilities and Critical Micelle Concentrations of the Decyl-, Dodecyl- and Tetradecyltrimethylammonium Chloride Micelles and their Mixtures.	1807	A. R. Lawrence and A. J. Matuszko: The Electric Moments of Some Nitrate Esters.	1903
W. Taylor, J. E. Cluskey and F. R. Senti: Water Sorption by Dextrans and Wheat Starch at High Humidities.	1810	L. V. Gregor, J. J. Fritz and P. E. Field: Hydrated and Anhydrous Bisethylenediamine Copper(II) Sulfate.	1904
W. Taylor, H. F. Zobel, Milford White and F. R. Senti: Deuterium Exchange in Starches and Amylose.	1816	P. W. Allen: The Effect of Copper Alkanoates on Oxidizing Olefins.	1906
Richard Turse and Wm. Rieman III: Kinetics of Ion Exchange in a Chelating Resin.	1821	Carl A. Heller, Dwight A. Fine and Ronald A. Henry: Photochromism.	1908
		S. S. Parikh and Thomas R. Sweet: Determination of the Ionization Constants of Some Phenylmercury Compounds.	1909



THE JOURNAL OF PHYSICAL CHEMISTRY

(Registered in U. S. Patent Office)

W. ALBERT NOYES, JR., EDITOR

ALLEN D. BLISS

ASSISTANT EDITORS

A. B. F. DUNCAN

EDITORIAL BOARD

A. O. ALLEN
C. E. H. BAWN
J. BIGEISEN
D. D. ELEY

D. H. EVERETT
S. C. LIND
F. A. LONG
K. J. MYSELS

J. E. RICCI
R. E. RUNDLE
W. H. STOCKMAYER
A. R. UBBELOHDE

E. R. VAN ARTSDALEN
M. B. WALLENSTEIN
W. WEST
EDGAR F. WESTRUM, JR.

Published monthly by the American Chemical Society at 20th and Northampton Sts., Easton, Pa.

Second-class mail privileges authorized at Easton, Pa. This publication is authorized to be mailed at the special rates of postage prescribed by Section 131.122.

The *Journal of Physical Chemistry* is devoted to the publication of selected symposia in the broad field of physical chemistry and to other contributed papers.

Manuscripts originating in the British Isles, Europe and Africa should be sent to F. C. Tompkins, The Faraday Society, 6 Gray's Inn Square, London W. C. 1, England.

Manuscripts originating elsewhere should be sent to W. Albert Noyes, Jr., Department of Chemistry, University of Rochester, Rochester 20, N. Y.

Correspondence regarding accepted copy, proofs and reprints should be directed to Assistant Editor, Allen D. Bliss, Department of Chemistry, Simmons College, 300 The Fenway, Boston 15, Mass.

Business Office: Alden H. Emery, Executive Secretary, American Chemical Society, 1155 Sixteenth St., N. W., Washington 6, D. C.

Advertising Office: Reinhold Publishing Corporation, 430 Park Avenue, New York 22, N. Y.

Articles must be submitted in duplicate, typed and double spaced. They should have at the beginning a brief Abstract, in no case exceeding 300 words. Original drawings should accompany the manuscript. Lettering at the sides of graphs (black on white or blue) may be pencilled in and will be typeset. Figures and tables should be held to a minimum consistent with adequate presentation of information. Photographs will not be printed on glossy paper except by special arrangement. All footnotes and references to the literature should be numbered consecutively and placed in the manuscript at the proper places. Initials of authors referred to in citations should be given. Nomenclature should conform to that used in *Chemical Abstracts*, mathematical characters be marked for italics, Greek letters carefully made or annotated, and subscripts and superscripts clearly shown. Articles should be written as briefly as possible consistent with clarity and should avoid historical background unnecessary for specialists.

Notes describe fragmentary or incomplete studies but do not otherwise differ fundamentally from articles and are subjected to the same editorial appraisal as are articles. In their preparation particular attention should be paid to brevity and conciseness. Material included in Notes must be definitive and may not be republished subsequently.

Communications to the Editor are designed to afford prompt preliminary publication of observations or discoveries whose value to science is so great that immediate publication is imperative. The appearance of related work from other laboratories is in itself not considered sufficient justification for the publication of a Communication, which must in addition

meet special requirements of timeliness and significance. Their total length may in no case exceed 1000 words or their equivalent. They differ from Articles and Notes in that their subject matter may be republished.

Symposium papers should be sent in all cases to Secretaries of Divisions sponsoring the symposium, who will be responsible for their transmittal to the Editor. The Secretary of the Division by agreement with the Editor will specify a time after which symposium papers cannot be accepted. The Editor reserves the right to refuse to publish symposium articles, for valid scientific reasons. Each symposium paper may not exceed four printed pages (about sixteen double spaced typewritten pages) in length except by prior arrangement with the Editor.

Remittances and orders for subscriptions and for single copies, notices of changes of address and new professional connections, and claims for missing numbers should be sent to the American Chemical Society, 1155 Sixteenth St., N. W., Washington 6, D. C. Changes of address for the *Journal of Physical Chemistry* must be received on or before the 30th of the preceding month.

Claims for missing numbers will not be allowed (1) if received more than sixty days from date of issue (because of delivery hazards, no claims can be honored from subscribers in Central Europe, Asia, or Pacific Islands other than Hawaii), (2) if loss was due to failure of notice of change of address to be received before the date specified in the preceding paragraph, or (3) if the reason for the claim is "missing from files."

Subscription rates (1961): members of American Chemical Society, \$12.00 for 1 year; to non-members, \$24.00 for 1 year. Postage to countries in the Pan-American Union \$0.80; Canada, \$0.40; all other countries, \$1.20. Single copies, current volume, \$2.50; foreign postage, \$0.15; Canadian postage, \$0.10; Pan-American Union, \$0.10. Back volumes (Vol. 56-64) \$30.00 per volume; foreign postage, per volume \$1.20, Canadian, \$0.40; Pan-American Union, \$0.80. Single copies: back issues, \$3.00; for current year, \$2.50; postage, single copies: foreign, \$0.15; Canadian, \$0.10; Pan-American Union, \$0.10.

The American Chemical Society and the Editors of the *Journal of Physical Chemistry* assume no responsibility for the statements and opinions advanced by contributors to THIS JOURNAL.

The American Chemical Society also publishes *Journal of the American Chemical Society*, *Chemical Abstracts*, *Industrial and Engineering Chemistry*, International Edition of *Industrial and Engineering Chemistry*, *Chemical and Engineering News*, *Analytical Chemistry*, *Journal of Agricultural and Food Chemistry*, *Journal of Organic Chemistry*, *Journal of Chemical and Engineering Data*, *Chemical Reviews*, *Chemical Titles* and *Journal of Chemical Documentation*. Rates on request.

Daniel Berg and William M. Hickam: Sorption of Sulfur Hexafluoride by Artificial Zeolites.....	1911
Leo Brewer, John L. Margrave, Richard F. Porter and Karl Wieland: The Heat of Formation of C ₂ F ₂	1913
Vincent J. DeCarlo and F. O. Rice: Reaction of Atomic Hydrogen with Solids at -195°.....	1913
R. M. Izatt, J. W. Wrathall, and K. P. Anderson: Studies of the Copper(II)-Alanine and Phenylalanine Systems in Aqueous Solution. Dissociation and Formation Constants as a Function of Temperature.....	1914
George Van Dyke Tiers: Proton Nuclear Magnetic Resonance	

Spectroscopy. XII. Tetramethylsilane: Some Observations Concerning Line Width and Line Shape.....	1916
R. A. McDonald and D. R. Stull: The Heat Content and Heat Capacity of Boron Nitride from 298 to 1689°K.....	1918

COMMUNICATIONS TO THE EDITOR

James K. Fogo: Electron Spin Resonance of Aromatic Hydrocarbons on Silica-Alumina Catalysts.....	1919
Norman A. Krohn and Hilton A. Smith: The Influence of X-Rays on Catalytic Activity as Related to Incorporated Radioactivity.....	1919

THE JOURNAL OF PHYSICAL CHEMISTRY

(Registered in U. S. Patent Office) (© Copyright, 1961, by the American Chemical Society)

VOLUME 65

OCTOBER 26, 1961

NUMBER 10

THE CHEMISORPTION OF GASES ON COBALT OXIDE SURFACES AT LOW TEMPERATURES

By D. S. MACIVER AND H. H. TOBIN

Gulf Research & Development Company, Pittsburgh 30, Pa.

Received March 7, 1961

The adsorption of oxygen, hydrogen and carbon monoxide by cobalt oxides of various compositions has been studied. In addition, measurements have been made of the electrical conductances of the oxides and their activities in the hydrogen-deuterium exchange catalysis. It was found that while stoichiometric CoO would not chemisorb hydrogen to any appreciable extent at low temperatures (-195 to -78°) carbon monoxide was chemisorbed over most of the surface at -195° . Hydrogen was adsorbed at -195° on an oxidized (non-stoichiometric) CoO surface in the form of a rapid, reversible chemisorption. At -78° , on the same surface, hydrogen was chemisorbed in two forms, a fast, reversible adsorption and a slow, irreversible chemisorption which poisoned the surface with respect to the hydrogen-deuterium exchange catalysis. Carbon monoxide was chemisorbed to about the same extent at -195° on both the oxidized and unoxidized CoO surfaces. These results are discussed in terms of the d-electron configurations of the surface cations. In general, it was concluded that the low temperature hydrogen-deuterium exchange activities of cobalt oxides are more directly related to the oxidation states of their surfaces than to their bulk electrical conductivities. Further, high exchange activity seems to be associated with the $3d^6$ cation electron configuration (Co^{+3}) rather than with the $3d^7$ configuration (Co^{+2}).

Introduction

For a number of years attempts have been made to explain the catalytic properties of transition metal oxides in terms of their semiconductor characteristics.¹ It has been suggested recently,²⁻⁵ however, that considerations involving the d-electron configurations of the surface cations in these oxides may provide an alternative and, in some cases, a more comprehensive basis for understanding variations in catalytic activities. Experimentally, the latter viewpoint has been based to a large extent upon a study^{2,3} of the hydrogen-deuterium exchange reaction at low temperatures over a number of oxides within and immediately succeeding the first transition period; this work indicated that the oxides most active in the exchange catalysis were Cr_2O_3 , NiO and Co_3O_4 . For the first two oxides the surface cation d-electron configuration was taken to be $3d^3$ and $3d^8$, respectively, and

high activity was accordingly associated with these configurations. In the case of Co_3O_4 , however, there are two types of cations present, $\text{Co}^{+2}(3d^7)$ and $\text{Co}^{+3}(3d^6)$, and since this was the only oxide of cobalt studied, the question naturally arises as to whether the activity may be uniquely assigned to either one of the above configurations.

In a broader sense, these same considerations of the d-electrons relate to the general subject of chemisorption⁵ and it would appear that a need exists for information concerning the chemisorption of various gases on transition metal oxides, especially at fairly low temperatures where extensive oxidation or reduction of the bulk adsorbent is not a problem. As far as the case of the cobalt oxides is concerned, little relevant information seems to exist in the literature outside of the recent work by Stone, Rudham and Gale.⁶ These latter workers investigated the interaction of oxygen, carbon monoxide and ethylene with cobaltous oxide in the vicinity of room temperature and obtained considerable information on the variation of heats of adsorption with coverage. Their work, however, was concerned primarily with elucidating the mechanism of certain oxidation reactions and no attempt was made to relate the activity to the

(1) F. S. Stone, "Chemistry of the Solid State," ed. by W. E. Garner, Academic Press, New York, N. Y., 1955, Chapter 15.

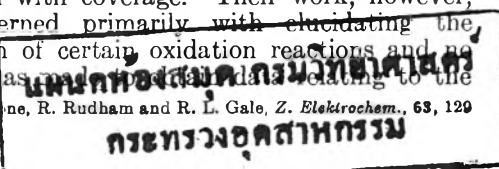
(2) D. A. Dowden, N. Mackenzie and B. M. W. Trapnell, *Proc. Roy. Soc. (London)*, **237A**, 245 (1956).

(3) D. A. Dowden, N. Mackenzie and B. M. W. Trapnell, *Advances in Catalysis*, **9**, 65 (1957).

(4) D. A. Dowden, "Chemisorption," ed. by W. E. Garner, Academic Press, New York, N. Y., 1957, Chapter 1.1.

(5) D. A. Dowden and D. Wells, "The Second International Congress on Catalysis," Paris, France, July 4-9, 1960, Paper No. 73.

(6) F. S. Stone, R. Rudham and R. L. Gale, *Z. Elektrochem.*, **63**, 129 (1959).



adsorption of hydrogen or to the hydrogen-deuterium exchange reaction.

In consideration of the foregoing discussion, a study of the low temperature adsorption of a number of gases by various cobalt oxides was undertaken with special attention being given to those factors influencing the interaction of hydrogen with these surfaces. It was intended that this study would provide a basis for comparison with a similar investigation reported earlier involving chromia.⁷

Experimental

Materials.—The gases employed in the present study were prepared and purified in the manner described earlier⁷; in all cases mass spectrometric analyses indicated purities of at least 99.9%. Cobaltous oxide (CoO) was obtained for each experiment in which it was required by thermally decomposing Reagent Grade cobaltous carbonate *in vacuo*.⁸ The carbonate was evacuated at room temperature for two hours and the temperature then increased to 300° over a one-hour period. After the bulk of the decomposition had taken place (a process requiring about two hours), the temperature was raised to 350° and the evacuation continued for another 17 hours. The weight change resulting from this procedure corresponded to complete conversion of the carbonate to the monoxide; the finished product was an olive green material whose X-ray diffraction pattern was that of CoO. Cobaltic oxide (Co₂O₃) was prepared by two techniques; either the cobaltous oxide obtained as described above was heated in a 100 mm. pressure of oxygen for several hours at 200° or the original carbonate was heated in air for 72 hours at 400°; in both cases the weight change and the X-ray diffraction pattern indicated the black product to be Co₂O₃. Before use, this Co₂O₃ was evacuated for 17 hours at 200°.

A sample of silica gel used as a reference in some of the experiments to be described was prepared by the hydrolysis of tetraethyl orthosilicate. The gel after drying at 100° was calcined for two hours at 600°.

Apparatus and Procedure.—Adsorption data were obtained either volumetrically or gravimetrically depending upon the requirements of the particular experiment being considered. The volumetric system and the procedures followed in its use have been described earlier.⁷ A special gas buret was added in which the mercury level could be continuously varied thus permitting the measurement of adsorption rates at constant pressure. The gravimetric adsorption apparatus consisted of a silica spring balance⁹ having a sensitivity of 1.78 mg./mm. mounted within a thermostated tube of 25 mm. diameter; the silica balance pan containing about 400 mg. of adsorbent was suspended via a silica fiber from the end of the spring into the lower part of the tube, around which could be placed either a furnace or a dewar. Extensions of the spring relative to an internal reference point were measured with a traveling microscope to ±0.001 mm. The tube containing the spring was connected through a liquid nitrogen trap to a vacuum system capable of producing a vacuum of 10⁻⁶ mm. The system included the usual gas storage and handling facilities; adsorbate pressures were read to ±0.1 mm. on a mercury manometer.

Hydrogen-deuterium exchange activities were determined using the volumetric adsorption system in the manner described earlier.⁷ The results were computed in terms of the usual first-order rate constant

$$k = -\frac{1}{S\tau} \ln(1 - x_\tau/x_\infty)$$

where τ is the time in minutes, S the surface area in m.² and x_τ and x_∞ the mole fraction of HD in the gas phase at time τ and at equilibrium, respectively. In cases where no reaction took place over a 20-hour period, the rate constant was assumed to be essentially zero.

Electrical conductances of the powdered oxides were obtained using a special vacuum conductivity cell. The

sample chamber consisted of a 12 mm. diameter glass tube closed at one end by a platinum disk serving as an electrode. A thin (about 2 mm.) bed of cobaltous carbonate was placed in the tube on top of this electrode and a perforated platinum disk (the second electrode) was rested on top of the powder; over this latter disk a steel weight was suspended in such a fashion that it could be caused to descend upon the sample by means of an external magnet. The entire assembly was enclosed in a glass envelope and sealed onto a high vacuum system. After the carbonate had been decomposed to cobaltous oxide, the powder was compacted by dropping the weight onto the bed of powder several times and finally allowing it to remain there. The d.c. conductances were measured with a vacuum tube ohmmeter; the measuring voltages were applied only momentarily in order to minimize polarization effects as much as possible.

The BET surface areas of the several oxide samples employed in the present work were determined with nitrogen at -195° using a cross sectional of 16.2 Å.² for an adsorbed nitrogen molecule.

Results

Preliminary experiments showed that CoO prepared as indicated above had a surface area of about 80 m.²/g. and reacted readily with oxygen at room temperature to give a material whose X-ray pattern was that of Co₃O₄. The initial chemisorption step in this oxidation process probably involved the transfer of electrons from the adsorbent to the adsorbate with the concurrent production of Co⁺³ ions.¹⁰ It seemed reasonable, therefore, to expect that if extensive oxidation of the bulk adsorbent could be prevented, then it might be possible to vary the oxidation state of the surface (*i.e.*, the number of surface Co⁺³ ions) in a systematic manner. In order to explore this possibility, a number of experiments were carried out in which the chemisorption of oxygen on CoO was studied at -195° using the gravimetric adsorption system. Preliminary studies indicated that contact of CoO with oxygen at -195° resulted in an extensive (*i.e.*, several monolayers) oxygen uptake due apparently to a non-selective adsorption process brought about by the highly exothermic character of the initial chemisorption.⁶ In order to avoid this situation, the following procedure involving the use of helium as a heat transfer agent was employed in determining the amount of oxygen chemisorbed at -195°. The CoO was cooled to -195° in 10 mm. of helium and then 50 mm. of oxygen was added; after 15 minutes the gas mixture was evacuated until the total pressure was 10 mm. and then another 50 mm. of oxygen added. Two more such withdrawals and additions were made at 15-minute intervals. The sample then was evacuated for one hour at -195° and one hour at -78°. The amount of oxygen taken up in this sequence of operations was defined as the amount chemisorbed at -195°; future reference to oxygen chemisorption will assume this definition.

The results of a number of oxygen adsorption experiments performed in this manner are indicated in Table I. Here the surface area of each sample as measured with nitrogen just prior to the oxygen adsorption is indicated in column 3 and the oxygen chemisorbed during each step in column 4. The excess oxygen, that is, the amount of oxygen associated with the sample in excess of that required for stoichiometric CoO, is given in column 5 in

(7) D. S. MacIver and H. H. Tobin, *J. Phys. Chem.*, **64**, 451 (1960).

(8) M. Le Blanc and E. Möbius, *Z. physik. Chem.*, **142**, 151 (1929).

(9) J. W. McBain and A. M. Bakr, *J. Am. Chem. Soc.*, **48**, 690 (1926).

(10) B. M. W. Trapnell, "Chemisorption," Butterworths Scientific Publications, London, 1955, p. 190.

TABLE I
OXYGEN ADSORPTION ON COBALTOUS OXIDE AT -195°

Expt. no.	Description	Surface area, $m.^2/g.$ sample	Incremental oxygen adsorption, cc. (STP)/ $m.^2$	Excess oxygen, cc. (STP)/g. CoO	θ^a
1	CoO—initial adsorption	90.7	0.096	8.70	0.54
1	Above—repeat adsorption	90.7	.016	10.15	.62
1	Above—repeat adsorption	90.7	.008	10.87	.67
1	Above—repeat adsorption	90.7	~ 0	10.87	.67
2	CoO—initial adsorption	87.0	0.095	8.29	.53
2	Above—heated 16 hr. at 200°	83.7	...	8.29	.53
2	Above—repeat adsorption	83.7	.069	14.14	.90
2	Above—heated 16 hr. at 200°	82.7	...	14.12	.90
2	Above—repeat adsorption	82.7	.071	20.08	1.33
2	Above—heated 16 hr. at 200°	78.4	...	20.05	1.31
2	Above—repeat adsorption	78.4	.070	25.75	1.65
2	Above—heated 16 hr. at 200°	76.0	...	25.73	1.64
2	Above—repeat adsorption	76.0	.068	31.11	1.99
2	Above—heated 2 hr. at 200°	30.48	1.95
3	CoO—initial adsorption	98.4	.093	9.08	0.52
3	Above—heated 16 hr. at 300°	79.7	...	8.41	0.49
3	Above—repeat adsorption	79.7	.084	15.19	0.87

^a θ = total oxygen uptake expressed in monolayers.

terms of the volume of gas per unit weight of the original CoO. Finally, in column 6 the total oxygen uptakes are expressed in monolayers, a monolayer of adsorbed gas in this case being defined as one oxygen atom per surface cobalt ion assuming a cation density of $9.5 \times 10^{18}/m.^2$ (based on an average of the (100) and (110) planes).

Experiment 1 of Table I indicated that it was indeed possible to more or less confine the oxygen uptake to the surface region since less than a monolayer was adsorbed initially and only a small additional adsorption took place upon re-exposure to oxygen. It may be noted that the adsorbent changed color from an olive green to a dark brown upon contact with oxygen at -195° . If the adsorbent with a layer of chemisorbed oxygen was evacuated at 200° then, as demonstrated by experiment 2, surface sites capable of chemisorbing oxygen were regenerated, presumably by incorporation of the adsorbed oxygen into the bulk of the adsorbent. That this oxygen was incorporated rather than merely desorbed from the surface is indicated by the fact that there was no weight loss during the evacuation process (column 5). With the aid of the foregoing information, it was possible to establish a cyclic procedure in which the surface could be alternately covered with chemisorbed oxygen (*i.e.*, the surface oxidized to Co^{+3}) and then partially regenerated (*i.e.*, reduced to Co^{+2}) by "annealing" the adsorbed oxygen into the adsorbent lattice by heating at 200° *in vacuo* for 16 hours. In experiment 2 of Table I, where five such cycles were carried out, it will be noted that the amount adsorbed per unit area after each annealing step was remarkably constant and that the decrease in total area as a result of heating was relatively small. When the annealing temperature was increased to 300° , as in experiment 3, both the number of sites regenerated and the degree of sintering were increased.

It was to be expected that, since CoO containing an excess of oxygen is a p-type semiconductor, the incorporation of successive layers of chemisorbed

oxygen into the bulk of the oxide should result in an increase in electrical conductivity of the oxide. This effect was demonstrated in a series of experiments in which the conductivity of CoO was measured before and after the introduction of excess oxygen. In these experiments the conductivity of CoO, prepared *in situ* as described in the previous section, was first measured as a function of temperature. The adsorbent then was cooled to -195° , oxygen adsorbed in the usual fashion, and the adsorbent evacuated for 17 hours at 200° ; the conductivity then was remeasured. The effect of a second adsorption and annealing cycle was next determined and the sample then oxidized to Co_3O_4 by heating in 100 mm. of oxygen for several hours followed by evacuation for 16 hours at 200° ; once again the conductivity was determined. In all these cases, the conductivity was measured as a function of temperature over several rising and falling temperature cycles in order to establish the reproducibility of the conduction measurements; in each instance satisfactory reproducibility was obtained. It was found that, for the sample in each oxidation state, the conductivity λ could be expressed in the form

$$\lambda = \lambda_0 e^{-E/RT}$$

where λ_0 and E are constants. The results obtained are presented in Table II in terms of these two constants.

TABLE II
ELECTRICAL CONDUCTANCE OF COBALT OXIDES
 $\lambda = \lambda_0 e^{-E/RT}$

Sample	λ_0 , mhos	E , kcal./mole	Temp. range, $^{\circ}C.$
CoO	6.3×10^{-10}	20	150–340
Above-first O_2 adsorption and annealing	6.4×10^{-8}	13	100–200
Above-second O_2 adsorption and annealing	3.6×10^{-8}	12	100–200
Above-oxidized to Co_3O_4	4.9×10^{-6}	10	100–200

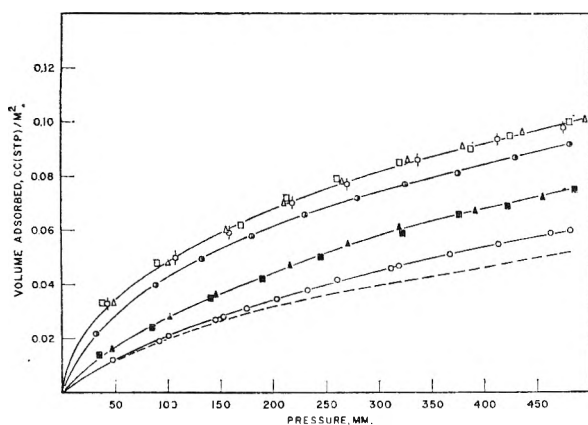


Fig. 1.—Adsorption of hydrogen on cobalt oxide surfaces at -195° : (O) adsorption on CoO; (\square , Δ , \diamond) adsorption on CoO after 1st, 2nd and 3rd oxygen chemisorptions, respectively; (\blacksquare , \blacktriangle) adsorption on CoO after "annealing" 1st and 2nd oxygen chemisorption, respectively; (\odot) adsorption on Co_3O_4 ; dotted line represents adsorption on silica.

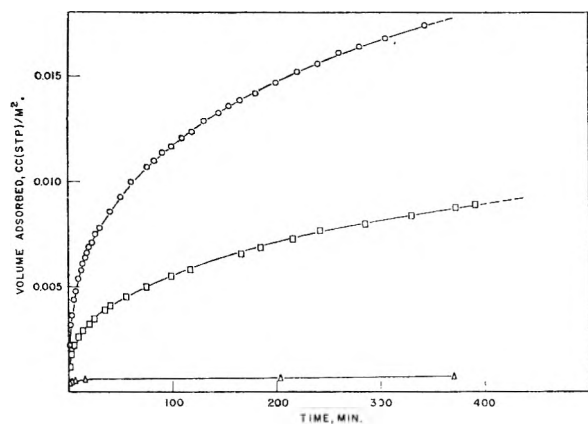


Fig. 2.—Hydrogen adsorption on cobalt oxide surfaces at -78° and 100 mm. (\square) adsorption on Co_3O_4 ; (O) adsorption on CoO after chemisorbing oxygen; (Δ) adsorption on CoO after "annealing" chemisorbed oxygen.

From the foregoing experimental work it appeared that both the oxidation state of the surface and the conductivity (*i.e.*, the defect state or stoichiometry) of the oxide could be varied by chemisorbing and annealing successive layers of oxygen; attention was therefore directed toward studying the accompanying changes in the adsorptive properties of the oxide.

The adsorption of hydrogen at -195° was investigated, using the volumetric adsorption system, by determining isotherms first on a fresh CoO surface and then on the same surface after chemisorbing oxygen at -195° and again after annealing the adsorbent with its chemisorbed oxygen at 200° for 16 hours; this adsorption and annealing cycle was repeated twice more and the sample finally oxidized to Co_3O_4 . The hydrogen isotherms at each step in the oxidation procedure are shown in Fig. 1. In all cases the hydrogen adsorption was rapid and also reversible in that it could be removed by evacuation for one hour at -78° . As is evident from Fig. 1 the amount of hydrogen adsorption was directly related to the oxidation state of the surface, the adsorption on CoO increasing upon chemisorption of oxygen (*i.e.*, oxidation of the surface) and de-

creasing when this chemisorbed oxygen was annealed into the bulk oxide (*i.e.*, reduction of the surface).

In order to obtain some indication of the amount of hydrogen that could be physically adsorbed at -195° , an adsorption isotherm, shown in Fig. 1, was measured on a silica surface where one would not expect any low temperature chemisorption. As is apparent, the amount of hydrogen physically adsorbed by the silica was, on a unit area basis, quite close to the total amount adsorbed by the CoO.

At -78° the hydrogen adsorption phenomena were quite different from those observed at -195° . There was no appreciable adsorption of hydrogen on CoO at -78° even at pressures as high as 500 mm. When oxygen was first chemisorbed at -195° , however, a slow hydrogen chemisorption process was observed at -78° ; a typical example of this chemisorption as a function of time is shown in Fig. 2. If, before contact with hydrogen, the chemisorbed oxygen layer was annealed in the usual fashion at 200° the subsequent hydrogen chemisorption was greatly reduced; this is again illustrated in Fig. 2. In the case of Co_3O_4 , a similar slow hydrogen adsorption process was observed at -78° , although as indicated in Fig. 2 this was less extensive than on the oxygen-covered CoO surface. The hydrogen adsorption at -78° , in addition to being slow, also differed from the adsorption observed at -195° in that it was principally irreversible. In other words it could not be desorbed. For example, if the adsorption of hydrogen on an oxygen-covered CoO surface at -78° was interrupted by evacuation at 25 mm, the adsorption was found to recommence at the point on the rate curve at which the interruption took place. In another experiment a sample of oxygen-covered CoO was allowed to chemisorb hydrogen at -78° , evacuated for several hours at this same temperature and then isolated from the diffusion pump. The sample was opened to a McLeod gauge and then slowly heated to 200° . During this process no evolution of gas as evidenced by a build-up of pressure was observed until around 200° ; at this point a small amount of water was desorbed. As a further check on the irreversible nature of the adsorption process, an attempt was made to exchange the adsorbed hydrogen with deuterium. A sample of CoO upon which oxygen had been previously chemisorbed at -195° was allowed to adsorb 1.5 cc. (STP)/g. of hydrogen at -78° . Pure deuterium then was circulated over the sample, first at -195° and then at -78° for 18-hour periods, and the gas phase analyzed. There was no exchange with the adsorbed hydrogen at -195° and only a slight exchange at -78° involving about 2% of the adsorbed hydrogen.

Another feature of the -78° hydrogen chemisorption which was of interest was that it decreased the amount of subsequent hydrogen chemisorption at -195° . Oxygen was chemisorbed at -195° on a sample of CoO and a hydrogen isotherm determined at -195° . The sample then was warmed to -78° and 0.019 cc.(STP)/m.² of hydrogen chemisorbed after which the sample was recooled to

−195° and a hydrogen isotherm again determined. The results, shown in Fig. 3, indicated that the high temperature adsorption caused a definite decrease in the amount of low temperature adsorption.

It was found that the rates of hydrogen chemisorption both on Co_3O_4 and on oxygen-covered CoO at −78° obeyed the familiar Elovich equation.¹¹ The integrated form of this equation is

$$q = \frac{1}{\alpha} \ln(\tau + k) - \frac{1}{\alpha} \ln k$$

where q is the amount adsorbed in time τ and α and k are pressure and temperature dependent constants. Using properly chosen k values, plots of q versus $\ln(\tau + k)$ were linear for both surfaces and extrapolation to $\tau = 0$ indicated that there was, in addition to the adsorption described by the Elovich equation, a rapid initial adsorption process which amounted, in both cases, to the order of 0.001 cc.(STP)/m.² at 100 mm.

Having explored in some detail the adsorption of hydrogen by cobalt oxides, attention next was directed toward the adsorption of another reducing gas, carbon monoxide. A number of adsorption isotherms of carbon monoxide on various cobalt oxide surfaces were measured at −195°. The general procedure was to obtain isotherms before and after evacuation for one hour at −78°. The results of the work with carbon monoxide are shown in Fig. 4 along with several nitrogen isotherms determined at the same temperature.¹² It will be noticed that the nitrogen isotherms on Co_3O_4 and CoO and the carbon monoxide isotherm on Co_3O_4 after evacuation at −78° are all in quite close agreement; this would be expected for purely physical adsorption of carbon monoxide in the latter case since the cross-sectional areas of adsorbed carbon monoxide and nitrogen are about the same.¹³ It seems reasonable, therefore, to assert that the lowest isotherm in Fig. 4 represents a close approximation to the amount of carbon monoxide physically adsorbed by a cobalt oxide surface. On this basis then it is obvious that chemisorption of carbon monoxide takes place at −195° on all the surfaces considered in Fig. 4. On the CoO surface the chemisorption was largely reversible in the sense that it could be removed at −78° (see Fig. 4); when the CoO surface was oxidized, the total carbon monoxide adsorption was not greatly enhanced, as in the case of hydrogen chemisorption, but instead became less reversible. With Co_3O_4 the adsorption seemed to be almost entirely irreversible. The effect of carbon monoxide chemisorption upon subsequent hydrogen adsorption at −195° is illustrated in Fig. 3. Here the various surfaces were exposed to carbon monoxide at −195° and then evacuated for one hour at −78°. Obviously, the chemisorbed carbon monoxide blocked some of the hydrogen adsorption sites.

As a final phase of this work the hydrogen-deu-

(11) H. A. Taylor and N. Thon, *J. Am. Chem. Soc.*, **74**, 4169 (1952).

(12) It should be remarked that, in contrast to chromia,⁷ the oxides of cobalt showed no tendency to chemisorb nitrogen at −195°. The adsorbed nitrogen was readily removed by evacuation at −78° and nitrogen surface areas agreed with those obtained using argon to within the uncertainty involved in estimating adsorbate cross-sectional areas.

(13) H. L. Pickering and H. C. Eckstrom, *J. Am. Chem. Soc.*, **74**, 4775 (1952).

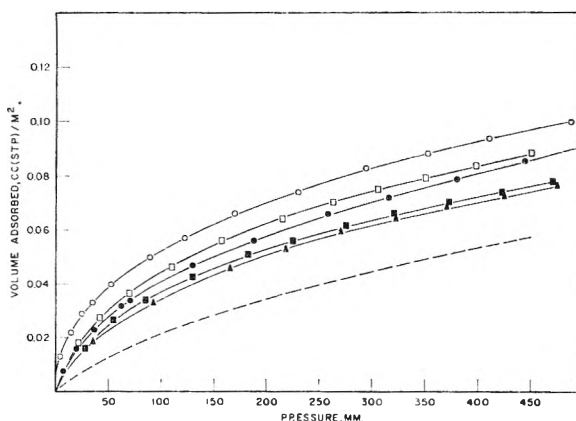


Fig. 3.—Adsorption of hydrogen on cobalt oxide surfaces at −195°: (○, ●) adsorption on oxygen-covered CoO before (○) and after (●) chemisorbing hydrogen at −78°; (□, ■) adsorption on Co_3O_4 before (□) and after (■) chemisorbing carbon monoxide at −195°; (▲) adsorption on oxygen-covered CoO after chemisorbing carbon monoxide at −195°; dotted line represents adsorption on CoO.

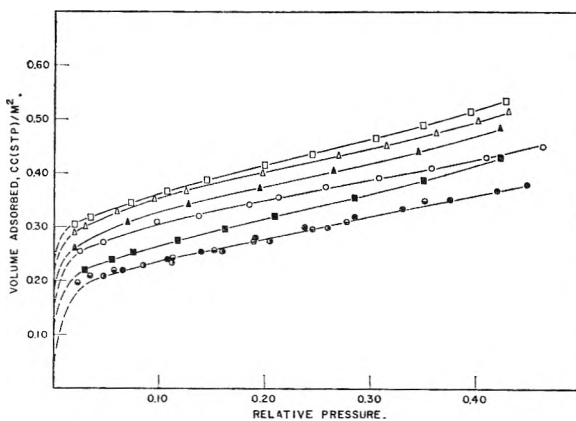


Fig. 4.—Carbon monoxide and nitrogen adsorption on cobalt oxide surfaces at −195°. Open and solid symbols represent adsorption before and after evacuation for one hour at −78°: (○, ●) CO on Co_3O_4 ; (△, ▲) CO on CoO; (□, ■) CO on CoO after chemisorbing oxygen; (●) N_2 on Co_3O_4 ; (●) N_2 on CoO.

terium exchange activities of cobalt oxides were determined as a function of various pretreatments. The results obtained at −78 and −195° are summarized in Table III. Since cobalt oxide surfaces other than that of CoO tend to irreversibly chemisorb hydrogen at −78°, exchange measurements were not made in certain of the experiments at this temperature. Generally speaking, the results given in Table III are self-explanatory and require little elaboration. As indicated in experiments 1 and 6, a CoO surface was a relatively inert catalyst for the exchange until oxidized. Experiment 2 would suggest that it was the oxidation state of the surface rather than factors related to the stoichiometry of the bulk phase which was directly associated with activity. Further, according to experiments 4, 5 and 7, both chemisorbed carbon monoxide and hydrogen, chemisorbed at −78°, poisoned the various oxide surfaces for the exchange catalysis.

It should perhaps be remarked at this point that the activity of Co_3O_4 or oxygen-covered CoO cannot be the result of trace amounts of a metallic phase formed *via* reduction of the oxide by stop-

TABLE III
HYDROGEN-DEUTERIUM EXCHANGE ACTIVITIES OF COBALT
OXIDE SURFACES

Expt. no.	Surface	k (-195°), min. ⁻¹ m. ⁻²	k (-78°), min. ⁻¹ m. ⁻²
1	CoO	~ 0	7.5×10^{-8}
1	Above—adsorbed O ₂ at -195°	2.0×10^{-4}	7.8×10^{-8}
2	CoO	~ 0
2	Above—adsorbed O ₂ at -195°	2.6×10^{-4}
2	Above—heated 16 hr. at 200°	0.4×10^{-4}
2	Above—adsorbed O ₂ at -195°	1.7×10^{-4}
2	Above—heated 16 hr. at 200°	0.8×10^{-4}
2	Above—adsorbed O ₂ at -195°	1.9×10^{-4}
3	CoO	~ 0
3	Above—adsorbed O ₂ at -195°	2.5×10^{-4}
3	Above—adsorbed H ₂ at -78°	0.2×10^{-4}
4	CoO	~ 0	6.9×10^{-8}
4	Above—adsorbed CO at -195°	~ 0	2.6×10^{-8}
5	CoO	~ 0
5	Above—adsorbed O ₂ at -195°	2.2×10^{-4}
5	Above—adsorbed CO at -195°	4.2×10^{-8}	1.9×10^{-7}
6	Co ₃ O ₄	1.6×10^{-6}	2.2×10^{-7}
7	Co ₃ O ₄	1.2×10^{-6}
7	Above—adsorbed CO at -195°	1.8×10^{-7}	2.1×10^{-6}

cock grease as was formed in the case of nickelous oxide by Dry and Stone.¹⁴ In the first place, the cobalt oxide samples were protected with cold traps from such contamination and, in the second place, a CoO surface became active at -195° only after treatment with oxygen in a fashion such as would certainly oxidize any metallic surface.

Discussion

Oxygen chemisorption on an ionic solid such as CoO is generally considered to involve an electron transfer process in which the cations of the adsorbent are oxidized and an ionic adsorbed species formed, the latter consisting, in all probability, of either O²⁻ or O⁻ ions.¹⁰ At low temperatures where ionic mobility is small, this adsorbed oxygen will not be incorporated into the bulk lattice and the oxidation will be confined more or less to the surface region. Under these conditions, the amount of oxygen taken up by the solid would not be expected to exceed that required to oxidize those cations associated with the surface. In the present case of CoO the number of surface cations was estimated, as indicated earlier, to be about $9.5 \times 10^{18}/\text{m}^2$. If the oxygen adsorption process at -195° results in the formation of O²⁻ ions, the amount of oxygen required to oxidize these cobaltous ions to cobaltic ions is 0.09 cc. (STP)/m.², a value which agrees rather well with the observed oxygen chemisorption of 0.095 cc. (STP)/m.². It must be recognized, of course, that this agreement may be fortuitous and other possibilities exist. For example, if O⁻ ions are formed, only one-half of the surface cobalt ions would be oxidized. In addition, it is conceivable that, due to the exothermicity of the adsorption process,⁶ local heat effects resulted in some incorporation of oxide ions into the bulk lattice; in other words, it is possible that the oxidation involved some of the bulk cations. The facts remain, however, that the amount of oxygen chemisorbed by cobaltous oxide at -195° did not exceed that required for complete oxidation of the surface and that after evacuation of the adsorbent at -78° the surface did not

chemisorb additional oxygen at -195° to any great extent. On this basis it seems reasonable to conclude that the low temperature chemisorption of oxygen on CoO resulted in the oxidation of the majority of surface cobaltous ions to cobaltic ions and that little incorporation of oxygen into the bulk oxide took place.

As noted earlier, the adsorption of hydrogen by cobalt oxide was strongly dependent upon the oxidation state of the surface. The fact that CoO itself was inactive in the exchange catalysts at -195° suggests that the hydrogen adsorption at this temperature was either physical or a weak molecular chemisorption. This latter possibility seems rather unlikely since the results obtained using silica as the sorbent indicate that the major portion of the hydrogen taken up by CoO at -195° may be accounted for in terms of a physical adsorption. At -78° , although some isotopic exchange was observed, the relatively low level of this activity coupled with the lack of any measurable adsorption indicates that, even at this temperature, the surface of CoO does not chemically interact with hydrogen to any great extent. In terms of the discussions of Dowden and others,²⁻⁵ this would imply that the 3d⁷ electron configuration of the metal ion is relatively unfavorable for the activation of hydrogen.

The oxidation of a CoO surface caused a substantial increase in the hydrogen adsorption at -195° and since this oxidized surface also had a high exchange activity, it may be assumed that at least part of the increased adsorption was in the form of a dissociative chemisorption. The fact that this adsorption was related to the oxidation state of the surface and that it was completely reversible, further suggests a direct interaction between the adsorbate and the surface cations.¹⁰ Assuming that this interaction was one in which each hydrogen molecule was dissociated into atoms which were in turn bonded to separate cations, it may be calculated from the data of Fig. 1 that only about 25% of the possible adsorption sites (*i.e.*, Co⁺³ ions) were occupied at the highest pressures studied.¹⁵ This value appears to be somewhat pressure dependent and presumably at sufficient pressures most of the surface cations would be occupied by chemisorbed hydrogen.

At -78° , hydrogen appeared to be chemisorbed on an oxidized CoO surface in at least two forms, a weak dissociative adsorption and a slow irreversible adsorption. The former was evidenced by the high exchange activity of the surface and, less directly, by the finite values for q_0 , the initial adsorption, obtained from the Elovich equation. It is obvious from these latter data that, at the pressures employed, only a small portion (*i.e.*, less than 1%) of the surface was engaged in this weak adsorption. Presumably this chemisorption involves the surface cations¹⁰ and may perhaps be identified with the adsorption occurring in larger amounts at -195° . The slow adsorption at -78° appeared completely different in that it was irre-

(14) M. E. Dry and F. S. Stone, *Disc. Faraday Soc.*, **28**, 192 (1959).

(15) This figure may be compared with earlier results⁷ for the adsorption of hydrogen on a reduced chromia surface at -195° . In this latter case almost the entire surface was covered with hydrogen at pressures in excess of about 100 mm.

versible and was not directly associated with the exchange reaction, although, as noted earlier, it did poison the surface for the exchange catalysis at -195° . It seems possible that this adsorption involved the reaction of hydrogen with surface oxide ions, perhaps to form surface hydroxyl groups.¹⁰ In this sense the slow adsorption may be considered as a reduction of the surface and the poisoning action to result from a decrease in the number of cobaltic ions, the latter apparently being necessary for the low temperature exchange activity. It is interesting to note that other surfaces, notably those of chromia¹⁶ and certain iron catalysts,¹⁷ adsorb hydrogen in two or more forms and that in these cases also, poisoning phenomena are found when hydrogen is chemisorbed at "high" temperatures.

It should be pointed out again that activity for the low temperature catalysis did not appear to be directly related to electrical conductivity of the cobalt oxide, but rather to the oxidation state of the surface (*i.e.*, the electron configuration of the surface cations). It is interesting in this respect to compare the behavior of CoO with that of Cr₂O₃. In the former case, increasing the p-typeness of the oxide increased the activity, while in the latter case a decrease in activity was observed.¹⁸ This further emphasizes the difficulty, pointed out by other workers,² of relating the hydrogen-deuterium exchange activity of the transition metal oxides to their bulk semiconductivities.

The chemisorption of carbon monoxide on an oxide surface is, like hydrogen, often considered¹⁰ to occur in two general forms: a weak reversible adsorption taking place at low temperatures which is usually regarded as some sort of covalent bonding with surface cations, and an irreversible high temperature adsorption in which, in the case of carbon monoxide, surface carbonate ions may be formed. The more or less reversible nature of the low temperature carbon monoxide chemisorption on the CoO surface, both before and after oxidation, would seem to suggest that the former type adsorption predominated under the given experimental conditions. The fact that the total adsorption was not greatly changed when the surface was oxidized seems to indicate that no additional adsorption sites were created during the oxidation process, although the greater difficulty with which the chemisorbed gas was desorbed from the oxidized adsorbent suggests, in this case, a higher heat of adsorption. In other words, if the adsorption sites are indeed cobalt ions then the bonding energy of carbon monoxide with cobaltic ions is greater than with cobaltous ions.

The data represented in Fig. 4 indicate a total carbon monoxide chemisorption on the CoO surface of about 3.5×10^{18} molecules/m.². This is quite close to the value observed earlier for carbon monoxide chemisorption on a reduced chromia surface.⁷ In the latter case the possibility was discussed

that each carbon monoxide molecule was effectively bonded to two surface cations. If such a situation prevailed in the case of CoO then about 7×10^{18} ions/m.² would be occupied, a figure which agrees quite well with the total number of surface cobalt ions (*i.e.*, 9.5×10^{18} /m.²). It would appear, therefore, that carbon monoxide is chemisorbed over most of the available surface of CoO at liquid nitrogen temperatures.

The facts that carbon monoxide, chemisorbed on the oxidized CoO surface at -195° , poisoned this surface both with respect to subsequent hydrogen adsorption and to the hydrogen-deuterium exchange activity may be taken as evidence that carbon monoxide occupies sites involved in the hydrogen adsorption process. It is further apparent that not all the hydrogen chemisorbed on an oxidized CoO surface at -195° is equally active in the exchange reaction. This may be seen by referring to Fig. 3 where it will be noticed that the strongly chemisorbed carbon monoxide (*i.e.*, that carbon monoxide not desorbed at -78°) does not completely destroy the subsequent hydrogen chemisorption although, as indicated in Table III, it does deactivate the surface in the exchange reaction.

It is interesting to observe that although a CoO surface will not chemisorb hydrogen at -195° it will chemisorb carbon monoxide. Presumably the necessity of dissociating the hydrogen molecule makes the chemisorption of this adsorbate less energetically favorable than for the case of carbon monoxide where no dissociation is involved.

Acknowledgments.—The authors take this opportunity to thank Mr. E. L. Brozek for making the mass spectrometric analyses. Thanks are also due to Drs. C. W. Montgomery and Frank Morgan for their interest and encouragement and to Gulf Research & Development Company for permission to publish.

DISCUSSION

G. L. ROBERTS (American Cyanamid Company).—Did you measure particle size by either X-ray diffraction line broadening or electron microscopy during the cycles?

D. S. MACIVER.—Such particle size measurements were not made. The surface area values given in Table I indicate that the area, and hence the particle size, of the oxide did not change greatly during the cycles.

A. C. ZETTEMAYER (Lehigh University).—In principle, the conductivity measurements should be made on single crystals rather than on compacted powders. Would it be likely that correlation with conductivity measurements would be achieved if the single crystal measurements could be made?

D. S. MACIVER.—It is doubtful whether measurements on single crystals would result in a correlation. The fact is, that as excess oxygen is added to CoO, the conductivity increases regardless of whether the oxide is a powder or a single crystal; the H₂-D₂ activity, on the other hand, is not directly related to the total amount of excess oxygen, but rather to the oxidation state of the surface.

A. C. ZETTEMAYER.—I am concerned about the complications involved in measuring the electrical conductivity of powdered materials.

D. S. MACIVER.—Such complications are, of course, serious in any attempt to quantitatively relate conductivity and, say, catalyst activity. In the present case, however, it is a qualitative relation which is of interest and here I believe these complications do not influence the general observation that as excess oxygen is introduced into the CoO lattice the conductivity increases.

(16) S. W. Weller and S. E. Voltz, *J. Am. Chem. Soc.*, **76**, 4695 (1954).

(17) J. T. Kummer and P. H. Emmett, *J. Phys. Chem.*, **56**, 258 (1952).

(18) S. E. Voltz and S. W. Weller, *J. Am. Chem. Soc.*, **75**, 5227 (1953).

A COMPARISON OF INTEGRAL ENTHALPIES, FREE ENERGIES AND ENTROPIES OF ADSORPTION

By J. J. CHESSICK AND A. C. ZETTMEOYER

Surface Chemistry Laboratory, Lehigh University, Bethlehem, Pa.

Received March 9, 1961

Integral heats of formation of monolayers of water and organic vapors on various polar solids, silicas, and a graphitic surface were compared with the free energies of adsorption and the entropy terms. In most of the cases studied, the $-\Delta H$ values increased linearly with the $-T\Delta S$ values. The correlation with $-\Delta F$ values was not as good. Dangers of employing heats of immersion to represent the wetting process when complexities arise due to the perturbation of the surface, the formation of non-duplex films, or the possible formation of double layers, are described. A remarkable correlation between the heats of formation of the monolayer and the $T\Delta S$ terms occurs for several diverse materials interacting with water; the correlation persists for several silicas of widely different surface areas. Much less agreement occurs between trends in $-\Delta H$'s and $-\Delta F$'s. The integral thermodynamic quantities for organic vapors adsorbed on a graphitic surface require much more detailed study in order to elucidate their behavior.

Heats of immersion, as described in detail in a recent review,¹ have been employed to: (1) rate the polarity of solid surfaces^{2,3} by employing different simple organic liquids as the setting liquids; (2) establish the energy of adhesion⁴ which is the energy required to separate a solid from a liquid; (3) give the integral and differential heats of adsorption which then may be compared with usually less accurate vapor adsorption measurements; (4) determine the distribution of adsorption site energies so that surface heterogeneities of the solid can be mapped¹; and (5) establish the areas of non-porous solids⁵ when the particles are not too small so that interparticle condensation measurements are insensitive. Calorimeters are available which produce any of several orders of sensitivity, and the techniques are well established.

The adsorption free energy may be calculated from isotherm data. To perform the required integration according to the Gibbs equation, quite low pressure adsorption data are required,⁶⁻⁸ and to carry the summation successfully for non-porous powders to the condensation pressure, a compaction procedure has been developed⁹ to produce a conclusive limiting value to the amount adsorbed. Another approach is to combine measured temperature coefficients of heats of immersion with the heat quantities according to the Gibbs-Helmholtz equation. The few available values^{9,10} are mostly negative, but zero and positive coefficients have also been reported. Much work remains to be done on this subject; compared to enthalpy

changes, relatively few estimations of free energies of adsorption have been made.

Even though it would be more significant to compare systems on the basis of the free energy changes, most analyses of the interaction of solids with liquids or vapors have been based on enthalpy changes. Seldom have both the enthalpy changes and the free energy changes been determined on the same system. It is the purpose of this paper to bring together such reliable related data as exists and to report calculations made on the same basis so that comparisons of the free energy and enthalpy changes could be made. Concomitantly, it was of interest to compare the entropy changes with these values.

Attention was restricted to the integral quantities for the formation of the first adsorbed layer. Almost all interpretations of solid/liquid or vapor interactions are related to molecular behavior in this first layer. Furthermore, for polar solids the heat of adsorption often falls close to the heat of liquefaction as the first layer is completed. The specific influence of the surface would be masked if the comparisons were made at the saturation pressures and here also complications due to capillary condensations may occur.^{8,9}

Calculations and Results

Heats of immersionsal wetting were used to establish the integral heats of adsorption of the monolayer for the systems tabulated in Tables I and II. All of the systems in Tables I and II have water as the adsorbate. Those in Table III are for organic vapors onto graphite. The surface enthalpy of water, 118.5 ergs/cm.², had to be subtracted to obtain the integral heat quantities for the silica-water systems since heat of immersion data for monolayer covered silica samples were not measured here. This monolayer heat value was assumed to be equal to h_I , the surface enthalpy of the wetting liquid, water. In all other cases, the heats of wetting with coverage were available so that more reliable estimations of the contributions of the first layer could be made from the $h_{I(SL)}$'s. The free energies of adsorption were determined by applying the Gibbs equation to the isotherm data. These quantities have been put on a kcal./mole basis so that the comparisons could be made on the basis of the adsorbate molecules. On an ergs/cm.² basis, as often reported, this comparison

(1) J. J. Chessick and A. C. Zettlemoyer, "Advances in Catalysis XI," Academic Press, 1959, New York, N. Y., p. 263.

(2) J. J. Chessick, A. C. Zettlemoyer, F. H. Healey and G. J. Young, *Canadian J. Chem.*, **23**, 251 (1955); A. C. Zettlemoyer, J. J. Chessick and C. M. Hollabaugh, *J. Phys. Chem.*, **62**, 489 (1958); A. C. Zettlemoyer, *Official Digest*, **28**, 1238 (1957).

(3) B. V. Il'in, V. F. Kiselev and G. I. Alexandrova, *Doklady Akad. Nauk S.S.S.R.*, **102**, 1155 (1955).

(4) W. D. Harkins, F. E. Brown and E. C. H. Davies, *J. Am. Chem. Soc.*, **39**, 354 (1917).

(5) W. D. Harkins, *J. Chem. Phys.*, **9**, 552 (1951); W. D. Harkins and G. Jura, *J. Am. Chem. Soc.*, **66**, 919 (1944).

(6) L. E. Drain and J. A. Morrison, *Trans. Faraday Soc.*, **48**, 316 (1952).

(7) D. H. Bangham, *ibid.*, **33**, 805 (1937); D. H. Bangham and R. I. Razouk, *ibid.*, **33**, 1463 (1937).

(8) R. L. Every, W. H. Wade and N. Hackerman, *J. Phys. Chem.*, **65**, 25 (1961).

(9) R. G. Craig, J. J. Van Voorhis and F. E. Bartell, *ibid.*, **60**, 1225 (1956); J. J. Van Voorhis, R. G. Craig and F. E. Bartell, *ibid.*, **61**, 1513 (1957).

(10) G. Jura, Ph.D. Thesis, University of Chicago.

TABLE I

INTEGRAL THERMODYNAMICS QUANTITIES FOR THE ADSORPTION OF WATER VAPOR ON SOLIDS AT MONOLAYER COVERAGE									
Adsorbent	Ref.	Evac. T., °C.	Ads. T., °C.	$-(H_A - H_L),^i$ kcal./mole	$-(F_A - F_L),^i$ kcal./mole	$-T(\Delta S),^i$ kcal./mole	$-(S_A - S_L),$ e.u.	$S_A',$ e.u.	
A Kaolin	a	25	25	8.5	2.9	5.6	18.7	-2.0	
Anatase	b	500	25	5.2	1.8	3.4	11.4	5.3	
Ferric oxide	c	25	25	4.8	3.4	1.4	4.7	12.0	
Cellulose	d	25	25	3.9	1.9	2.0	6.9	9.9	
Wool keratin	e	80	24.6	3.6	1.6	2.0	6.8	10.0	
Asbestos	f	25	20	2.2	0.81	1.4	4.7	12.0	
Graphon	g	27	25	-1.3	1.7	-3.0	-13.3	30.0	
B Silica A	h	160	25	18.4	2.0	16.4	55.0	-38.3	
B	h	160	25	11.3	1.9	9.4	32.4	-15.7	
C	h	160	25	9.3	2.2	7.1	24.5	-7.8	
D	h	160	25	6.0	2.3	3.7	12.9	3.8	
E	h	160	25	4.85	2.2	2.6	8.7	8.0	

^a From unpublished data, Lehigh Surface Chemistry Laboratory, Bethlehem, Pa. ^b W. D. Harkins, "The Physical Chemistry of Surface Films," Reinhold Publ. Corp., New York, N. Y., 1952, p. 256. ^c F. H. Healey, J. J. Chessick and A. V. Fraioli, *J. Phys. Chem.*, **60**, 1001 (1956). ^d J. L. Morrison and J. F. Hanlan, *Nature*, **179**, 528 (1957). ^e A. C. Zettlemoyer, G. J. Young, J. J. Chessick and F. H. Healey, *J. Phys. Chem.*, **57**, 649 (1953). ^f G. J. Young, J. J. Chessick, F. H. Healey and A. C. Zettlemoyer, *ibid.*, **58**, 313 (1954). ^g Ref. 8; Professor N. Hackerman kindly provided the integrated π values in ergs/cm.² at 0.2 relative pressure from which the above calculations were made. These values differ little from those at the actual v_m 's. ^h $H_A - H_L = (H_{I(SL)} - h_{I(SL)})/\Gamma$. $F_A - F_L = \phi/\Gamma - kT \ln p/p_0$.

TABLE II

INTEGRAL THERMODYNAMIC QUANTITIES FOR THE ADSORPTION OF WATER VAPOR ON SILICAS AT 0.9 p/p_0^a

Adsorbent	Ref.	Evac. T., °C.	Ads. T., °C.	$-(H_A - H_L),$ kcal./mole	$-(F_A - F_L),$ kcal./mole	$-T(\Delta S),$ kcal./mole	$-(S_A - S_L),$ e.u.	$S_A',$ e.u.
Silica	A	160	25	4.2	0.81	3.4	11.3	5.4
	B	160	25	2.6	0.82	1.8	6.3	10.4
	C	160	25	2.7	1.00	1.7	5.7	11.0
	D	160	25	1.4	0.93	0.47	1.6	15.1
	E	160	25	1.25	0.91	0.34	1.1	15.6

^a Calculated from ref. 8.

is lost. The equation of Jura and Hill¹¹

$$T(S_A - S_L) = [h_{I(SL)} - h_{I(SL)}]/\Gamma + \frac{\phi}{\Gamma} - kT \ln p/p_0$$

was employed to calculate the entropy changes. S_A and S_L are the entropies per mole of the adsorbate and the bulk liquid, respectively; $h_{I(SL)}$ and $h_{I(SL)}$ are the heats of immersion of the bare and monolayer coated sample, respectively; and $\Gamma = N_A/\Sigma$, or the surface concentration of N_A moles on Σ surface area when the relative pressure at equilibrium is p/p_0 at temperature T . The S_A' values were calculated from the $-(S_A - S_L)$ values using the entropy of the liquid adsorbate and assuming the adsorbent was unperturbed by the adsorption process; the S_A' values also can be considered to contain the perturbation effects.

Discussion

In Fig. 1, the integral enthalpy changes for the monolayer formation of water on the various substrates of Table IA are plotted against the corresponding $T\Delta S$ and ΔF values. It may be seen that both $-T\Delta S$ and $-\Delta F$ generally increase linearly with $-\Delta H$. Only the points for ferric oxide and Graphon do not coincide fairly closely with the straight lines. The $-\Delta H$ vs. $-T\Delta S$ plot, however, if extended below zero, would also fall close to the point for the Graphon. The parallelism of the thermodynamic quantities for these quite diverse systems is quite evident. It is borne out also by the fairly regular increase of the S_A' values with the regular decreases in the ex-

(11) G. Jura and T. L. Hill, *J. Am. Chem. Soc.*, **74**, 1958 (1952).

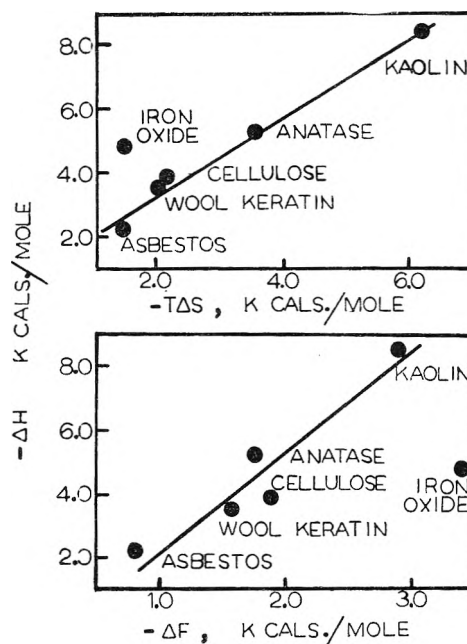


Fig. 1.—Integral heats vs. free energies and temperature-entropy products for the adsorption of monolayers of water at 25° on various polar solids.

thermic heats of formation of the monolayer as tabulated in Table IA. The systems respond sensitively in so far as enthalpy changes are concerned, whereas the variations in the changes in free energy are much less severe.

The heat of formation of the monolayer of

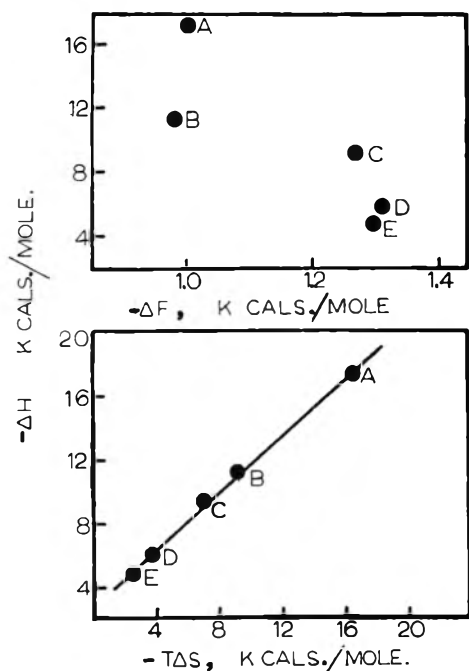


Fig. 2.—Integral heats vs. free energies and temperature-entropy products for the adsorption of water at 25° at a relative pressure of 0.2 on silica samples which increase in area from sample A to E.⁸

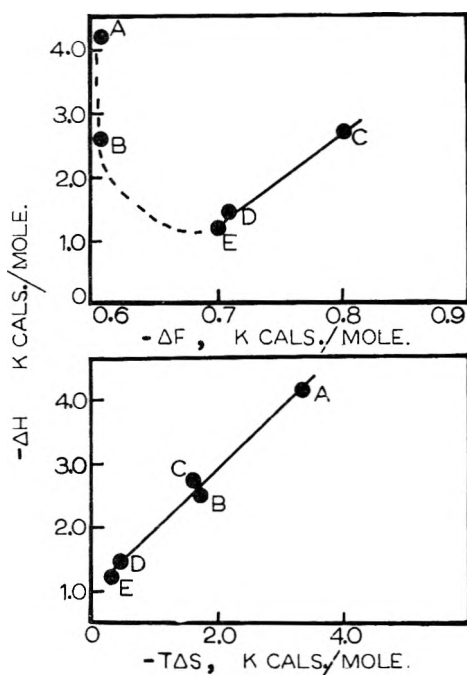


Fig. 3.—Integral heats vs. free energies and temperature-entropy products for the adsorption of water at 25° at a relative pressure of 0.9 on silica samples which increase in area from sample A to E.⁸

water on the hydrogen kaolin reflects strong interaction and the calculated negative S_A' implies that the surface is strongly perturbed by the adsorption process. Presumably, hydration of surface ion is responsible for this abnormal result. The next highest heat of formation of the monolayer is for anatase. The evidence of Chessick and Hollabaugh¹² obtained on a rutile TiO_2 sug-

gests that in this case some of the water is chemisorbed. Adsorption of water on the ferric oxide is peculiar¹³ in that, after the mild degassing at 25°, the co-area of the adsorbed water molecule in the BET range is large; the co-area only approaches 10.5 Å.² as the activation temperature approaches 450°. Although the S_A' 's for the ferric oxide and chrysotile asbestos are the same, the heat of immersion or isosteric heat vs. coverage curves are distinctly different. Asbestos presents a homogeneous surface toward water, iron oxide a quite heterogeneous surface. Configurational entropy effects account in part for the low value of S_A' for water on asbestos, compared to 16.7 e.u. for liquid water, even though the surface is homogeneous (see pertinent ref., Table I, for more detail).

The cellulose and wool keratin after 25° outgassing are materials which interact with water only mildly. Entropy contributions due to swelling¹⁴ appear to be small for the monolayer formation as indicated by the concurrence of the thermodynamic quantities with those for the other system.

That the Graphon-water system has a heat of adsorption below the heat of liquefaction is now firmly established.¹⁵ The BET v_m for water vapor is 1/1500 of that for nitrogen. Therefore, the "monolayer" film of water is not duplex and $h_{I(SFL)}$ of the "monolayer" covered sample is definitely required to determine $-(H_A - H_I)$. Sometimes the enthalpies of the surface of the bulk liquid have been incorrectly used in such situations.^{8,16}

The enthalpies of formation of monolayers of water for the silicas are listed in decreasing order in Table IB and this is the increasing order of surface areas.⁸ On the mole basis there is a fourfold variation in the integral enthalpies, whereas on a square centimeter basis as presented by Every, Wade and Hackerman,⁸ there is only a twofold difference. Even more striking are the small differences in the $-\Delta F$'s. When the $-\Delta H$'s are plotted against the $-T\Delta S$ terms, as in Fig. 2, a remarkably linear increase is seen. The first three S_A' values are so absurdly low as to reflect doubt on the reported heats of immersion which are unexpectedly high for 160° outgassed samples. The measurements should be reliable since a precision microcalorimeter was employed.¹⁷

Any lack of parallel variation in $-\Delta H$ with $-\Delta F$ in Fig. 2 doubtless is the result of lack of sensitivity for the scale as plotted. On the other hand, and quite contrary to the presentation of Every, Wade and Hackerman⁸ on a unit area basis, the integral free energies on a mole basis show no maximum in their variation with surface area. Certainly in these systems enthalpy changes or free energy changes on a unit area basis are a doubtful criterion for considering the driving tendency for the process.

(12) C. M. Hollabaugh and J. J. Chessick, *J. Phys. Chem.*, **65**, 109 (1961).

(13) F. H. Healey, J. J. Chessick and A. V. Fraioli, *ibid.*, **60**, 1001 (1956).

(14) J. L. Morrison and J. F. Hanlan, *Nature*, **179**, 528 (1957).

(15) G. J. Young, J. J. Chessick, F. H. Healey and A. C. Zettle-moyer, *J. Phys. Chem.*, **58**, 313 (1954).

(16) F. E. Bartell and R. M. Suggitt, *ibid.*, **58**, 36 (1954).

(17) W. H. Wade, R. L. Every and N. Hackerman, *ibid.*, **64**, 355 (1960).

TABLE III

INTEGRAL THERMODYNAMIC QUANTITIES FOR THE ADSORPTION OF ORGANIC VAPORS ON GRAPHITE AT MONOLAYER COVERAGE

Adsorbate	Ref.	Evac. T , °C.	Ads. T , °C.	$-(H_A - H_L)$, kcal./mole	$-(F_A - F_L)$, kcal./mole	$-T(\Delta S)$, kcal./mole	$-(S_A - S_L)$, e.u.	SA' , e.u.
Toluene	<i>a</i>	25	25	6.4	3.9	2.5	8.3	8.4
CCl ₄	<i>a</i>	25	25	5.1	3.2	1.9	6.4	10.3
Cyclohexane	<i>a</i>	25	25	5.2	3.3	1.9	6.4	10.3
<i>n</i> -Heptane	<i>a</i>	25	25	3.9	4.0	-0.1	-0.2	16.9
1-Propanol	<i>a</i>	25	25	-0.78	3.5	-4.3	-14.5	ca. 31.2

* Ref. 18. Professor Bartell kindly provided the $-\Delta F'$ values and the corresponding v_m 's.

E., W. and H. applied the Gibbs equation up to $0.9p^\circ$ because of the unreliability of the isotherms beyond this point. Differences from the p° values are small. In Table II, the calculated results for the integral quantities are presented. The most significant point about these results is that the sharp differences encountered in the monolayer values are masked at or near saturation pressures. The $-\Delta H$ vs. $-T\Delta S$ plot in Fig. 3 remains remarkably linear and although there is a sharp minimum in the $-\Delta H$ vs. $-\Delta F'$ plot, the lack of reliability of the $-\Delta F'$ results for the scale plotted sheds doubt on this finding. Certainly if the one plot is truly linear, then the other also must be linear.

The integral thermodynamic quantities for five organic vapors adsorbed on a graphite are presented in Table III. There is again a parallelism between the $-\Delta H$'s and the $-\Delta F'$'s; also the variations in the $-\Delta F'$'s are less than in the $-\Delta H$'s. The results for toluene, carbon tetrachloride and

cyclohexane are not surprising. The integral heats and free energies fall in the order expected. It is noteworthy, however, that the entropy of the adsorbed heptane is approximately equal to the entropy of the liquid, and that of the adsorbed propanol is much higher than that of the liquid. Some tentative explanations have been offered,¹⁸ but much more work with these systems is needed. This work is in progress.

Acknowledgment.—The writers acknowledge the encouragement and support of the Materials Laboratory, Wright Air Development Division, Wright-Patterson Air Force Base, Ohio, in this work. Special thanks are extended to Messrs. Schwenker, Christian and Adamczak. Some of this work also was performed under NSF Research Grant No. G16265.

(18) J. J. Chessick, A. C. Zettlemyer and Y. Yu, *J. Phys. Chem.* **64**, 530 (1960).

THERMODYNAMIC PROPERTIES OF WATER ADSORBED ON QUARTZ

BY J. W. WHALEN

*Socony Mobil Oil Company, Inc., Field Research Laboratory, Dallas, Texas**Received March 7, 1961*

Thermodynamic functions for the adsorbed aqueous phase on a quartz surface have been obtained from adsorption isotherm and immersion heat measurements. The equilibrium heats of adsorption obtained from the two sets of data are compared. Integral adsorption entropies were calculated from the immersion heat data. There is evidence that the adsorbed phase is predominantly immobile at low surface coverages.

Introduction

The water molecule-hydroxyl group interaction in the silica-water system has been the subject of considerable recent attention.¹⁻³ It is of interest to obtain energy and entropy changes for the interaction on crystalline particles in the absence of internal porosity. Entropy data are usually obtained by appropriate treatment of adsorption isotherms relating the quantity adsorbed on a fixed area of solid surface to the pressure of vapor in equilibrium with the sorbed phase at two temperatures. Integral as well as differential entropies of adsorption may be obtained.^{4,5} To obtain integral entropies of adsorption the spreading pressure, φ , defined by the relationship^{6,7}

$$\varphi = RT \int_0^{\Gamma} \Gamma d \ln p$$

where Γ is the quantity, in moles, adsorbed on unit area of solid surface, must be obtained over the entire pressure range from zero to condensation pressure for the adsorbate vapor at two adsorption temperatures. Adsorption data down to very low pressures are required for accurate extrapolation to zero pressure.⁸ The accuracy of adsorption data at low surface coverage is often quite poor, particularly for crystalline solids having surface areas below 10 square meters per gram. Entropy data based on such calculations can be meaningless in view of experimental inadequacies in the adsorption measurement.

Jura and Hill⁹ have shown that more precise measurements of the integral entropy of the adsorbed phase can be derived from heats of immersion in the condensed adsorbate when spreading pressures are available for the adsorbed phase at a single temperature. Immersion heat data are obtained for the clean solid sample and for the solid containing a known quantity of adsorbed vapor. The integral entropy of adsorption, referred to the bulk liquid adsorbate phase is

$$T(S_S - S_L') = \frac{U - U_0}{N_S} + \varphi/\Gamma - kT \ln x$$

S_S is the average entropy per molecule for the

- (1) A. V. Kiselev and G. G. Muttik, *Kolloid Zhur.*, **19**, 562 (1957).
- (2) V. A. Nikitin, A. N. Sidorov and A. V. Karyakin, *Zhur. Fiz. Khim.*, **30**, 117 (1956).
- (3) J. R. Zimmerman and J. A. Lasater, *J. Phys. Chem.*, **62**, 1157 (1958).
- (4) D. H. Everett, *Trans. Faraday Soc.*, **46**, 453 (1950).
- (5) T. L. Hill, *J. Chem. Phys.*, **17**, 520 (1949).
- (6) D. H. Bangham, *Trans. Faraday Soc.*, **33**, 605 (1937).
- (7) G. E. Boyd and H. K. Livingston, *J. Am. Chem. Soc.*, **64**, 2363 (1942).
- (8) T. L. Hill, P. H. Emmett and L. G. Joyner, *ibid.*, **73**, 5102 (1951).
- (9) G. Jura and T. L. Hill, *ibid.*, **74**, 1598 (1952).

sorbed vapor, S_L' the average entropy per molecule in the condensed liquid phase in equilibrium with vapor at temperature T , U_0 , and \bar{U} the heats of immersion of the clean solid and the solid with N_S sorbed moles, respectively, and x the relative pressure of vapor in equilibrium with the sorbed film.

This paper presents adsorption and immersion heat data obtained for the aqueous film on a crushed and sized quartz sample. Differential and equilibrium heats of adsorption were calculated from the adsorption isotherms. Equilibrium heats of adsorption and integral entropies, relative to the bulk liquid phase, were calculated from the immersion heat data.

Experimental

Adsorption.—The gravimetric adsorption system consisted of a sensitive capacitance gauge isolating the adsorption manifold from a balance manifold, an oil manometer measuring pressure in the balance manifold, a quartz spring from which the adsorbent was suspended, and appropriate means of introducing water vapor into the system. The entire adsorption system was housed in an air thermostat in which the temperature was maintained constant to within $\pm 0.05^\circ$. Adsorbate quantities were obtained by measuring the total length of the quartz spring with a cathetometer which could be read to ± 0.02 mm. A number of spring length observations were averaged for each point. The quartz spring had a capacity of 2.5 g. and a sensitivity of 20.08 mg./mm. elongation.

Pressure in the adsorption manifold was measured indirectly with an Apiezon "B" oil manometer. To prevent contamination of the adsorbate vapor and the manometer oil, the adsorption manifold was separated from a balance manifold by a differential pressure device operating on the capacitance principle. The elastic element of this device was a brass bellows having 8 active convolutions (Sylphon Bellows #2070) supplied by the Robertshaw Fulton Company. The bellows was attached to a rigid brass lid and sealed in a glass housing. A fixed reference plate, also supported from the lid, provided an air capacitance with reference to the closed end of the brass bellows. With adsorption manifold pressure inside the bellows and balance manifold pressure outside, deviation of the capacitance from a null value provided a sensitive measure of pressure difference between the adsorption and balance manifolds. The null position was established under equalized pressure conditions during assembly and checked under high vacuum prior to operation. A maximum usable sensitivity was obtained with about 325 mmf. capacitance between the reference and bellows plates.

Capacitance change was detected by making the gauge one arm in a capacitance bridge consisting of two capacitance and two resistive arms. Bridge power was provided by a Southwestern Industrial Electronics Model M oscillator of high frequency and amplitude stability. The bridge was operated at 1500 cycles. Bridge unbalance was indicated by a logarithmic scale vacuum tube voltmeter. A calibration curve related bridge unbalance to differential pressure across the gauge and provided small correction to the measured balance manifold pressure for off-null readings. Approximately 2 mm. of oil pressure difference between adsorption and balance manifolds corresponded to full scale (40 mv.) deflection.

Pressure in the balance manifold was measured, with reference to high vacuum, by reading both arms of the oil

manometer with a cathetometer. Reproducible readings to ± 0.02 mm. oil were obtained. Absolute accuracy for the pressure measurement, including corrections indicated by the differential pressure device, was ± 0.05 mm. of oil.

Greaseless conditions were maintained in the adsorption system by using Teflon seated Hoke bellows valves throughout with Glyptal sealed, standard taper joints for the spring housing assembly. A two-stage oil diffusion pump and manifold bakeout procedures reduced the pressure to less than 10^{-6} mm. prior to adsorption runs.

Immersion Heats.—The adiabatic twin calorimeter used in these studies was based on a system described by Gucker.¹⁰ Major modifications made desirable by the availability of improved instrumentation were in the adiabatic control device and in the differential thermopile output measurement. Modifications required to accommodate the particular requirements of immersion heat studies included the use of spun silver calorimeter vessels to provide rapid thermal equilibrium, more rigid tops and supports to accommodate the shock of breaking sample bulbs and more elaborate sealing and stirring precautions to permit the evaluation of thermal contributions of long duration.

The calorimeter assembly consisted of two silver calorimeter vessels having 500-cc. fluid capacity. Each calorimeter was attached to a rigid, silver plated brass lid spaced three inches from a surrounding, highly polished silver plated copper jacket. Supporting spacers for each lid were three half-inch diameter Nylon rods. Evacuation of the jacket proved unnecessary in light of the sufficiently low heat transfer rate across the dead air space. Additional thermal isolation was provided by Nylon inserts in the stirring shafts and sample breaker rod. The calorimeter assembly and surrounding air jacket was immersed in an oil-bath. Adiabatic control between one of the calorimeters, used as a reference vessel, and the jacket wall was accomplished by utilizing the error signal from a ten junction copper-constantan thermopile to proportion heat input into the oil-bath. A Minneapolis-Honeywell 100 X Brown recorder and balancing motor provided amplification and servo action for the error signal. Maximum deviation from adiabatic conditions was $\pm 10^{-4}$ °.

Each calorimeter vessel contained two heaters, one for calibration and one for balancing, a stirrer, sample support and breaker mechanism, and appropriate wells to accommodate the thermopiles for control and measurement. Stirrers were matched in construction to provide similar heat inputs during operation and were, in addition, driven at constant speed. A hysteresis-synchronous motor operating on closely controlled 100 cycle power was used with a Gilmer timing belt drive to provide power for the two stirrers.

Matching wells projected 1.5 inches into the calorimeter vessels to accommodate a 42 junction copper-constantan thermopile used to determine the temperature difference between reaction and reference vessels. The thermopile consisted of number 36 B & S gauge copper wires and number 28 B & S gauge constantan wires spaced on opposite sides of a mica card. The junctions were timed using low thermal e.m.f. solder, careful temperature control and no flux. Insulation and rigidity were provided by a thin mica sheet folded over each end of the completed junctions, followed by a copper foil sheath. Dimensions were closely controlled to provide a tight fit of the completed thermopile in the calorimeter side wells. Adiabatic control thermopiles, constructed in the same manner, fitted into smaller side wells and made spring contact with the jacket enclosure. Either calorimeter could be used as the reference control or the reaction calorimeter.

Differential temperature was obtained by measuring the output of the 42 junction thermopile potentiometrically. A Rubicon Microvolt potentiometer, a Liston-Becker DC amplifier and box-type galvanometer were used, together with thermally isolated reversing switches, to obtain precise measurement to $\pm 10^{-8}$ volt, corresponding to a temperature difference of 5×10^{-6} °.

In order to obtain significant measurements at thermal levels corresponding to 10^{-4} ° temperature rise on immersion, quite elaborate sealing precautions are required to minimize and equalize evaporation losses from the calorimeter pair. Calorimeter-lid seals consisted of "O" rings compressed between the highly polished calorimeter lip and inside lid

surface. Compression was obtained by a locking device consisting of pins in the calorimeters and tapered slots in the lids. Two Teflon bearing surfaces were provided for each stirring shaft. The shafts were ground and highly polished at the bearing points. The Teflon bearings were machined to close tolerance and replaced frequently. Breaker rod seals were similarly ground and polished and operated through a single Teflon bearing surface.

Calibration and balance heat input were accomplished using two number 38 B & S gauge manganin wire heaters threaded through holes in the outer edge of mica cards. The calibration heater was wound (non-inductively) near the bottom of the card, the balance heater was located above the calibration heater. The manganin wires were terminated well down the body of the heater. Number 30 B & S gauge copper wires served as current leads, down the mica card, to the heating elements. The completed heaters, sheathed with mica and copper foil, were inserted in silver wells welded into the calorimeter lids and projecting into the immersion fluid. Number 36 B & S gauge copper current and potential leads were connected to the heater assembly above the calorimeter lid.

For calibration heat input an external 19.80 ohm manganin resistor was placed in series with the calibration heater. Five two-volt lead storage cells in parallel, drained across an identical load prior to calibration heat input, provided a constant power input with variation of -1×10^{-6} volt during the 200-300 second heating period. Current and potential measurements were made using standard techniques and precautions.¹¹ Heating time was measured by electronic counting of a crystal controlled 100 cycle signal. Residual unbalance in stirring heat input and evaporation loss were eliminated by heat input into the lagging calorimeter. Three two-volt lead storage cells, discharged to a stable power level, provided power for these heaters. With proper experience the unbalance between the two calorimeters could be maintained readily at 5×10^{-6} or less under constant operating conditions prior to immersion. Drift rate under operating conditions could be reduced to 10^{-7} ° per minute.

Following assembly, the calorimeter system was allowed to stand overnight to attain thermal equilibrium. Immersion samples were contained in thin wall glass bulbs, sealed off under vacuum or controlled atmosphere. Sample bulbs were broken manually by depression of a rod to which the sample bulb was attached.

A series of calibration runs demonstrated the validity of Newton's law of cooling to the reaction calorimeter

$$K_1 = \frac{d \ln \Theta}{dt}$$

where Θ is the temperature difference between the two calorimeters. For the usual case, where $d\Theta/dt \cong 0$ prior to a heat input, the correction to the measured value of Θ for heat transferred to the surroundings and to the reference calorimeter is

$$\Delta\Theta = -(K_1 + k) \int_0^t \Theta dt$$

where t is the time in seconds measured from the beginning of the heat input period, K_1 is the experimentally determined heat transfer coefficient for the reaction calorimeter ($5.50 \pm 0.03 \times 10^{-6}$ sec.⁻¹) and k the calculated value for the heat transfer coefficient (1.30×10^{-6} sec.⁻¹) to the reference vessel along the 80 thermopile wires. Corrections, obtained by graphical integration of measured values of Θ vs. t during the cooling period following a heat input, permit a straight line extrapolation to the time of origination of the heat input. The thermal response to the reaction calorimeter was determined to be 1.352 ± 0.001 joules/microvolt using water as the immersion fluid. Slow heat inputs following a preliminary rapid heat input have been measured to duplicate the conditions during an immersion process in which a portion of the heat is liberated slowly. In a typical experiment of this nature 17.24 joules of heat was introduced at 0.096 joule/sec. followed by 3.24 joules introduced at 0.0054 joule/sec. for a total heat input of 20.48 joules. Using the correction technique described, the heat input obtained graphically from measured values of Θ vs. t yielded a value of 20.47 joules. From these and other experimental results an

(10) F. T. Gucker, H. B. Pickard and R. W. Planck, *J. Am. Chem. Soc.*, **61**, 459 (1939).

(11) W. Swietoslowski, "Microcalorimetry," Reinhold Publ. Corp., New York, N. Y., 1946.

accuracy of ± 0.04 joule in the determination of a heat input is indicated.

Materials and Techniques.—Finely ground quartz (99.82% SiO_2) obtained from the Standard Silica Company, Ottawa, Illinois, was sized by sedimentation in water and air dried at 110° . The material selected for this study was that corresponding in settling time to spherical particles less than 5μ in diameter. The BET surface area using nitrogen adsorption was found to be $7.5 \text{ m}^2/\text{g}$.

Thin walled glass sample bulbs used in the immersion study were blown from carefully cleaned Pyrex glass and reworked several times in the flame. Bulb diameters were approximately 20 mm. A number of trial runs indicated no measurable heat input on breakage. Although some investigators report correction quantities ranging from 0.3 to 1.6 joules,^{12,13} others find no breakage heat.^{14,15} With small, thin walled bulbs the bulb breakage heat is apparently almost exactly cancelled by the evaporation effect.

Adsorption on samples prepared for immersion studies followed outgassing under vacuum at 110° or at 250° until the residual pressure in the system was less than 5×10^{-6} mm. Outgassing times were never less than 3 days. These conditions were found to result in reproducible immersion heat values for clean quartz samples for all outgassing temperatures from 110 to 450° . The samples were equilibrated for approximately two hours with a water (or ice) reservoir maintained at an appropriate fixed temperature. The relative pressure of water vapor at these temperatures was calculated from vapor pressure data¹⁵ and referred to the adsorption isotherm to obtain the adsorbed quantity Γ . The sample bulb was maintained at 25° throughout the adsorption. Sample bulbs were carefully sealed off under equilibrium conditions by slowly increasing the wall thickness of the tubulation in several steps to avoid heating the sample. The final seal-off could be made very quickly in this manner.

Results and Discussion

Gravimetric adsorption isotherms were obtained at 25 and 35° for water vapor on the quartz surface. In view of the relatively low surface area of the quartz material each isotherm was repeated several times. The 25° isotherm represents smoothed data for four complete isotherm studies on two separate samples. Two isotherms on separate samples were smoothed to obtain the 35° isotherm. Isothermic heats of adsorption, given by

$$\left(\frac{\partial \ln p}{\partial T}\right)_\Gamma = -\frac{\Delta \bar{H}}{RT^2}$$

were calculated using the integrated form of the above equation. The smoothed isotherm data together with calculated isosteric heats of adsorption are given in Table I. The surface coverage Θ was obtained using the BET measured quartz surface area and assigning a coverage of 10.6 \AA^2 to the water molecule.

Spreading pressures for the aqueous film on quartz were obtained by graphical integration of the smoothed isotherm data in the conventional manner.⁸ Suggestions made by Hill⁵ were followed in relating the adsorbed quantity to the spreading pressure. The data were extrapolated from relative pressures of approximately 0.9 to 1.0 to obtain φ_{25} . Spreading pressure values were used to obtain enthalpy changes (Table II) associated with the transfer of a mole of water from the bulk liquid to the adsorbed phase⁵

(12) F. E. Bartell and R. M. Suggitt, *J. Phys. Chem.*, **57**, 36 (1953).

(13) A. C. Zettlemoyer, G. J. Young, J. J. Chessick and F. H. Healey, *ibid.*, **57**, 649 (1953).

(14) F. LaPorte, *Ann. Phys.*, **5**, 5 (1950).

(15) E. J. Westrum, Jr., and L. Eyring, *J. Am. Chem. Soc.*, **74**, 2045 (1952).

(16) "International Critical Tables," McGraw-Hill Book Co., New York, N. Y.

TABLE I

ISOSTERIC HEAT OF ADSORPTION WATER VAPOR ON QUARTZ

Quantity adsorbed (mg. HOH/g. SiO_2)	Equilibrium relative pressure		Isosteric heat of adsorption $-\Delta H$, kcal./mole HOH	Θ
	(P/P_0) 25°	(P/P_0) 35°		
0.50	0.012	0.024	23.11	0.24
.67	.029	.064	24.86	.32
.83	.068	.116	20.11	.39
1.00	.122	.174	16.89	.47
1.17	.183	.241	14.60	.56
1.33	.258	.319	14.34	.63
1.50	.342	.406	13.59	.71
1.67	.437	.502	13.59	.79
2.00	.622	.672	11.87	.95
2.17	.660	.709	11.77	1.03
2.33	.698	.739	11.48	1.11
2.50	.727	.766	11.39	1.19
2.84	.788	.808	10.90	1.35
3.17	.822	.838	10.79	1.51
3.67	.857	.869	10.70	1.74
4.17	.876	.887	10.70	1.98

$$\left(\frac{\partial \ln x}{\partial T}\right)_\varphi = -\left(\frac{\mathcal{H}_S - H_L'}{RT^2}\right)$$

Equilibrium heats of adsorption were calculated from the above data utilizing the expression

$$\Delta \mathcal{H}_{ad} = \mathcal{H}_S - H_L' - \Lambda$$

where Λ is the molar heat of vaporization of the adsorbate vapor. Spreading pressure values reported in this work are in considerable disagreement with those previously reported for the quartz-water system.^{7,17}

TABLE II

SPREADING PRESSURES FOR WATER VAPOR ON QUARTZ AT 25 AND 35°

Equilibrium relative pressure, P/P_0	φ_{25} , ergs/cm. ²	φ_{35} , ergs/cm. ²
0.02	15.88	15.44
.04	23.81	20.03
.06	29.12	24.61
.08	33.41	28.23
.10	37.10	31.48
.25	51.32	44.65
.30	60.91	54.39
.40	69.04	62.20
.50	75.87	68.89
.60	82.15	75.17
.70	88.23	80.89
.80	94.33	87.19
.90	102.8	96.16
(1.00)	$\varphi_{25} = 120$	

Recent investigations have shown that the immersion heats of small quartz particles are dependent on the particle size. The semi-amorphous character of small crystalline particles produced by crushing and grinding processes has been well established.^{18,19} The carefully sized quartz particles used in this work give a clean surface immersion heat of 310 ergs/cm^2 of solid surface area. A broad

(17) N. Hackerman and A. C. Hall, *J. Phys. Chem.*, **62**, 1212 (1958).

(18) G. S. Khodakov and E. R. Plutais, *Doklady Akad. Nauk S.S.S.R.*, **123**, 725 (1958).

(19) P. B. Dempster and P. D. Ritchie, *J. Appl. Chem.*, **3**, 182 (1953).

variety of particle sizes exhibits much higher immersion heats²⁰ due to the higher crystal order existing in the large particle content of the sample. The low immersion heat exhibited by small particles has been discussed^{20,21} in terms of decreased crystal order in the surface. In view of the lower total surface energy, quartz particles in the size range of materials used in this work would be expected to exhibit a low free energy change on adsorption.

Boyd and Livingston⁷ report a value of 240 ergs/cm.² for the free energy change of water vapor adsorption on quartz. These authors did not describe their quartz material. Later work from that laboratory²² reports immersion heats of quartz in water as 600 ergs/cm.². If it is assumed that unsized quartz particles having approximately the same surface characteristics were used in both of these studies, the discrepancy between spreading pressure values for the completed aqueous film on quartz may be attributed to the low surface energy of particles used in this work. Hackerman and Hall¹⁷ list an extrapolated value of 209 ergs/cm.² on a quartz sample reported as having a surface area 5.5 m.²/g. The particle size and degree of amorphicity in their sample cannot be greatly different from that used in this work. Isotherms in their study were obtained volumetrically as opposed to the gravimetric determinations used in this work and that of Boyd and Livingston.

Measured heats of immersion for samples containing adsorbed water are shown in Fig. 1. The solid curve refers to the adsorbed film on samples outgassed at 110°, the dotted curve to the adsorbed film on samples outgassed at 250°. The immersion heat curve for the 110° pretreatment sample is characterized by a very sharp minimum at $P/P_0 = 0.05$ and a slight maximum at $P/P_0 = 0.6$, corresponding to the point on the requirement. The data obtained following 250° sample pretreatment do not show the minimum at low relative pressures but a sharp and heightened maximum at $P/P_0 = 0.75$. The data point occurring at the maximum in this latter case was verified by a repeat measurement. Data smoothing to eliminate the sharp minimum at $P/P_0 = 0.05$ would require assignment of entirely unreasonable experimental error to three data points. Within our experience in this study, such action would not be permissible.

Heat functions associated with the transfer of molecules from the aqueous liquid phase to the adsorbed phase on quartz were calculated from the immersion heat data. Where h_i^0 is the heat of immersion in ergs/cm.² for the clean solid and h_i^p that for the solid containing Γ moles of adsorbate per square centimeter of solid surface

$$H_S - H_L' = \frac{h_i^p - h_i^0}{\Gamma}$$

These values were combined with spreading pressure data to obtain the equilibrium heat function as defined by Hill⁵

(20) J. W. Whalen, Southwestern Regional American Chemical Society Meeting, San Antonio, Texas, Dec. 1958.

(21) N. Hackerman and A. C. Makrides, *J. Phys. Chem.*, **63**, 594 (1959).

(22) G. E. Boyd and W. D. Harkins, *J. Am. Chem. Soc.*, **64**, 1195 (1942).

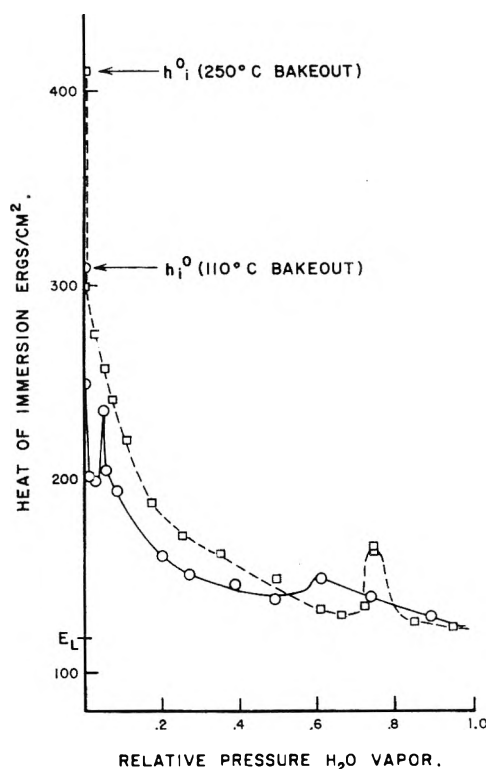


Fig. 1.—Heats of immersion in water of the aqueous film on quartz.

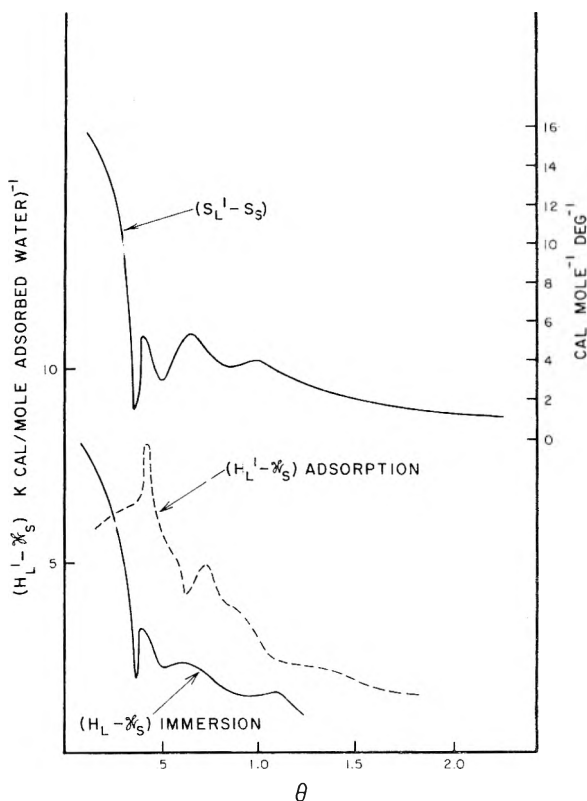


Fig. 2.—Thermodynamic functions for the aqueous film on quartz as calculated from immersion heat and adsorption isotherm data.

$$\bar{\mathcal{C}}_S - H_L' = (H_S - H_L' + \varphi/\Gamma)$$

Equilibrium heat functions, referred to the liquid phase, as obtained from adsorption (dotted curve)

and immersion (solid curve) studies are compared in Figure 2. Little significance can be attached to values obtained from adsorption data below $\theta = 0.4$ in view of the inability to discriminate experimentally between amounts adsorbed at 25° and at 35° in this region. Otherwise the experimental data are remarkably consistent in form although the heat function derived from isotherm data is significantly higher throughout. The major characteristic of the heat function derived from immersion data is the very sharp minimum occurring at a surface coverage of 0.38. At this point each water molecule may be associated with 29 Å.² of solid surface. Localized interaction is quite probable in systems of this nature where the adsorbate species is also a constituent of the surface structure.

Adsorption entropies, referred to the bulk liquid phase, are obtained from the equilibrium heat function and the free energy change associated with transfer of vapor from the bulk liquid phase to the presorbed phase⁹

$$S_S = S_L' = \frac{1}{T} (\mathcal{H}_S - H_L') - R \ln P/P_0$$

Entropy data derived from the immersion heat study are shown in Fig. 2. The same characteristics are shown in the entropy data as are indicated by the equilibrium heat function. There is a minimum in the entropy curve near the monolayer as required by adsorption theory.

Comparison of immersion heat values (Fig. 1) for samples outgassed at 110 and at 250° show that the initial adsorption process is different for the two sample sets. The sites responsible for localized interaction in the first instance are either not available in the case of the 250° outgassed sample or the interactions involving these sites are obscured by other processes involving the altered surface structure and the bulk liquid phase.

Previous investigators, using more direct techniques have shown that water exists in two states on the Vycor² and silica gel³ surfaces. It has been suggested that the more strongly adsorbed water is adsorbed on surface silicon atoms while the less strongly adsorbed water is associated with surface hydroxyl groups. The thermodynamic functions calculated from immersion heat data on the 110° outgassed sample in the very low surface coverage region tend to verify these suggestions. A decrease in the number of surface hydroxyl groups with increasing pretreatment temperature has been well established for silica gels.²³ Although similar behavior would not be anticipated for the quartz surface, the semiamorphous, small quartz particles have been shown^{20,21} to possess some of the dehydration characteristics of gel surfaces. Vapor adsorption studies^{20,24} have demonstrated that water adsorption on a quartz surface outgassed at temperatures in excess of 150° is irreversible and that rehydration of the quartz surface is not complete from the vapor phase at low relative pressures. Immersion heat data for the aqueous film on such surfaces is obscured by extraneous slow heat evolution associated with further rehydration on immer-

sion in the bulk liquid phase. These immersion heat data indicate that rehydration from the sorbed phase is associated with the completion of a monolayer. In view of the irreversibility of water vapor adsorption data on quartz outgassed at 250°, complete thermodynamic calculations were not attempted for these samples.

Conclusions

Immersion heat data for water adsorbed on a quartz surface have been shown to be more informative than adsorption data with regard to thermodynamic functions for the adsorbed phase. Spreading pressure values considerably lower than those previously reported for the aqueous film on quartz are believed to be characteristic of the disordered surface of small quartz particles. Variation of the equilibrium heat function ($\mathcal{H}_S - H_L'$) with coverage indicates that the adsorption of water vapor on quartz is immobile in the region of low surface coverage. A mobile film structure apparently exists at higher coverages. Conclusions reached in this study relative to the characteristics of the aqueous phase sorbed on quartz must be qualified as pertaining to a quartz sample of less than 5 μ particles outgassed in the manner described.

Acknowledgment.—The author wishes to express appreciation to the Socony Mobil Oil Company, Inc., for permission to publish the results of this study.

DISCUSSION

A. C. ZETTMAYER (Lehigh University).—It would be helpful if you would give the uncertainty in your determinations of enthalpy changes or entropy changes by the two methods. The uncertainties might be indicated by vertical lines at several points on your Fig. 2. Such lines should overlap (see, e.g., *J. Phys. Chem.*, 58, 313 (1954)) unless one or both of the methods are suspect.

J. W. WHEALEN.—Let me emphasize two points. First, the presentation of the data in Fig. 2 in terms of ($\mathcal{H}_S - H_L'$) tends to magnify the discrepancy between the values obtained from immersion data and those obtained from adsorption isotherms. The more conventional presentation ($\mathcal{H}_S - H_C$) would indicate a maximum difference of approximately 20% between the sets of values. Second, a major objective of this work was to demonstrate that reasonably precise enthalpy values can be obtained using the immersion heat technique in cases where the sample area is very small, in this case 7.5 m.²/g., and where adsorption data are not adequate to provide values of high confidence.

With respect to the values obtained from adsorption data alone, the error limits usually applied (see ref. 8) consider only the uncertain extrapolation to zero pressure. For low surface area material the uncertainty in the adsorption isotherm can introduce uncertainty in the values of φ throughout the entire relative pressure range. The comparison of φ values for two temperatures thus yields a large uncertainty in the equilibrium heat of adsorption. For example, an uncertainty of 1 erg/cm.² in φ leads to an uncertainty of ± 4 kcal./mole H₂O in ($\mathcal{H}_S - H_L'$) at $P/P_0 = 0.1$ and an uncertainty of ± 1 kcal./mole H₂O at $P/P_0 = 0.6$. These uncertainties are sufficiently large to invalidate conclusions based on the character of the ($\mathcal{H}_S - H_L'$)_{ad.} curve. The situation with regard to ($\mathcal{H}_S - H_L'$) derived from immersion data is entirely different. Here the major uncertainty is in Γ , the absorbed water in the film prior to immersion. The uncertainties are not appreciably influenced by uncertainty in φ/Γ which is not large in comparison to ($\mathcal{H}_S - H_L'$). Total heats of immersion ranged from 8.33 joules at $\theta = 0.26$ to 2.73 joules at $\theta = 3.9$. In all cases the heat evolution was instantaneous. In such cases the calorimetric error is less than ± 0.04 joule. All immersion heat errors in the range of major interest ($\theta < 1$) have a measurement error of less than 1%. Uncertainties $\delta(\Delta\mathcal{H})$, kcal./mole H₂O in ($\mathcal{H}_S -$

(23) R. K. Iler, "The Colloid Chemistry of Silica and Silicates," Cornell University Press, Ithaca, N. Y., 1955.

(24) S. P. Zhdanov, *Doklady Akad. Nauk, SSSR*, 123, 716 (1958).

H_L')_{imm.} are: at $\theta = 0.11$, $\delta(\Delta\mathcal{C}) = \pm 2$; $\theta = 0.24$, $\delta(\Delta H) = \pm 1$; $\theta = 0.30$, $\delta(\Delta\mathcal{C}) = \pm 0.5$; $\theta = 0.37$, $\delta(\Delta\mathcal{C}) = \pm 0.30$; $\theta = 0.42$, $\delta(\Delta\mathcal{C}) = \pm 0.25$, $\theta = 1.07$, $\delta(\Delta\mathcal{C}) = \pm 0.1$. These uncertainties are not large enough to influence the character of the $(\mathcal{C}_s - H_L')$ _{imm.} data and do not influence the character of the derived entropy curve.

D. R. ROSSINGTON (Alfred University).—Is the concept of spreading pressure invalidated by some chemisorption?

J. W. WHALEN.—I believe the consensus is that: the concept of "spreading pressure" is confined to non-localized adsorption, *i.e.*, free mobility is required in the film; in cases involving localized adsorption the concept of "spreading pressure" is not valid; however, we have lost only the physical concept; the function defined by the equation utilized in this work is not influenced by localization or non-localization of the film.

HEATS OF IMMERSION. V. THE TiO₂-H₂O SYSTEM—VARIATIONS WITH PARTICLE SIZES AND OUTGASSING TEMPERATURE

BY W. H. WADE AND N. HACKERMAN

Department of Chemistry, University of Texas, Austin, Texas

Received March 20, 1961

The heats of immersion of both anatase and rutile in water have been obtained as a function of particle size and outgassing temperature. The heats of immersion of both crystalline modifications were found to decrease with decreasing particle size for samples whose specific surface area varied from approximately 7 to 250 m.²/g. All samples showed a similar variation of immersional heat with outgassing temperature, namely, maxima were observed at 300–350°.

Introduction

Previous measurements from this Laboratory^{1–3} demonstrated two trends in the immersional heats per cm.² (ΔH_i) of SiO₂ and Al₂O₃ in H₂O: (i) a marked dependence of ΔH_i on particle size, and (ii) rather characteristic behaviors with outgassing temperature. For SiO₂ in H₂O, in general, ΔH_i increases, passes through a maximum, and then decreases with increasing outgassing temperature. On the other hand, Al₂O₃ in H₂O exhibits a monotonic increase of ΔH_i with outgassing temperature. This interpretation has been in terms of gradual endothermic loss of physically adsorbed water at lower outgassing temperatures and surface hydroxyl groups at higher temperatures. The difference between SiO₂ and Al₂O₃ is that the dehydroxylated SiO₂ surface does not rehydrate rapidly, whereas the Al₂O₃ surface does. The variation of ΔH_i with particle size has been explained as a fundamental variation of surface amorphous character with particle size.^{1–3}

Several studies pertinent to the present work have been reported for TiO₂. Harkins and co-workers⁴ selected a barrel of anatase with a specific surface area of 13.8 m.²/g. as a standard of comparison for surface studies. They reported a ΔH_i of 512 ergs/cm.² for this material outgassed at 500°. Zettlemoyer, *et al.*,⁵ made this measurement for a 7.3 m.²/g. rutile sample outgassed at 400°, and obtained 550 ergs/cm.². Recently, Yates⁶ obtained the infrared spectra of several anatase and rutile samples. They demonstrated the loss of physically adsorbed water below 350° outgassing temperature. This was shown by the absence of any H–C–H bending modes although there were prominent OH

stretching modes at 350°, indicating surface hydroxyl groups. This conflicts with Zettlemoyer,⁷ who assumes there are no surface OH groups on TiO₂ since the bulk hydroxide is unstable.

The present study was undertaken to assess the ΔH_i of anatase and rutile as a function of both particle size and of outgassing temperature.

Experimental

Samples.—The source of all samples was the National Lead Company, South Amboy, N.J. They are listed in Table I. Samples F and I are those Yates used in his infrared studies.⁶ The samples A₁, A₂, and A₃ were prepared in this Laboratory by grinding large single crystals in an agate mortar, with subsequent sedimentation and fractionation in water. Only three of the many fractions obtained are reported on here.

The B.E.T. surface areas were measured by Kr adsorption as previously described.⁸ The samples prior to immersion were outgassed at 10⁻⁶ mm. for three days in Pyrex bulbs and were sealed off on the outgassing apparatus. The outgassing temperatures in Table II are accurate to $\pm 5^\circ$.

Calorimeter.—The calorimeter already has been described¹ and likewise the sample bulbs.³ Heat output from sample immersion continued over a 5 to 10 minute period. Sample weights varied from 0.1 to 5 g., depending on the specific surface area. All measurements were run in duplicate with a usual agreement of 2 to 3%.

Results

The variations of ΔH_i with outgassing temperature for samples A–I are listed in Table II and illustrated in Fig. 1.

Particle Size Effect.—A variation with particle size is once again prominent, and both crystalline modifications of TiO₂ were obtained in a reasonable spectrum of particle sizes. If at any given outgassing temperature the ΔH_i 's for the two modifications are considered separately, there is a general decrease of ΔH_i with decreasing particle size. Moreover, at a given outgassing temperature, the ΔH_i for anatase is approximately 80 to 180 ergs/cm.² greater than for rutile samples with approximately the same particle size. This might be inferred from Yates' infrared data⁶ in which his ana-

(1) A. C. Makrides and N. Hackerman, *J. Phys. Chem.*, **63**, 594 (1959).

(2) W. H. Wade, R. L. Every and N. Hackerman, *ibid.*, **64**, 355 (1960).

(3) W. H. Wade and N. Hackerman, *ibid.*, **64**, 1196 (1960).

(4) W. D. Harkins, "The Physical Chemistry of Surface Films," Reinhold Publ. Corp., New York, N. Y., 1952.

(5) A. C. Zettlemoyer, G. J. Young, J. J. Chessick and F. H. Healey, *J. Phys. Chem.*, **57**, 649 (1953).

(6) D. J. C. Yates, *ibid.*, **65**, 746 (1961).

(7) A. C. Zettlemoyer, *Chem. Revs.*, **59**, 937 (1959).

(8) M. J. Joncich and N. Hackerman, *J. Phys. Chem.*, **57**, 674 (1953).

TABLE I

Sample	Manufacturers Code	Crystalline modification	Purity %	Impurities				Surface area (m. ² /g.)
				SiO ₂	ZnO	Nb	Other	
A's	MP 1643-1	rutile	99.9	0.04	0.01	0.01	0.001	1.11, 9.4, 24.5
B	MP 1634	rutile	99.9	0.04	0.01	0.01	0.001	6.45
C	MP 1663-4	anatase	99.5	0.05			0.5	7.65
D	MP 1663-2	anatase	99.8	0.2				10.50
E	MP 1643-2	rutile	99.7	0.2			0.1	114
F	MP 1208	rutile	99.8				0.2	158
G	MP 1643-4	anatase	99.5	0.1		0.1	0.25	174
H	MP 1663-1	rutile	99.8	0.2				188
I	MP 1579	anatase	99.4				0.65	251

TABLE II
 ΔH_i (ERGS/CM.²)

μ , (°C.)	Sample, m. ² /g.										
	A ₁ 1.11	A ₂ 9.40	A ₃ 24.5	B 6.45	C 7.65	D 10.50	E 114	F 158	G 174	H 188	I 251
100				407	592	504	328	204	415	293	352
150				484	701	575	419	286	493	345	441
200				542	779	628	496	308	557	376	506
250	619	580	529	593	852	672	563	326	585	401	552
300				640	891	695	573	330	586	409	570
350				657	908	693	544	317	570	408	557
400				645	909	677	449	281	540	398	515
450				612	902	650	413	226	507	384	456

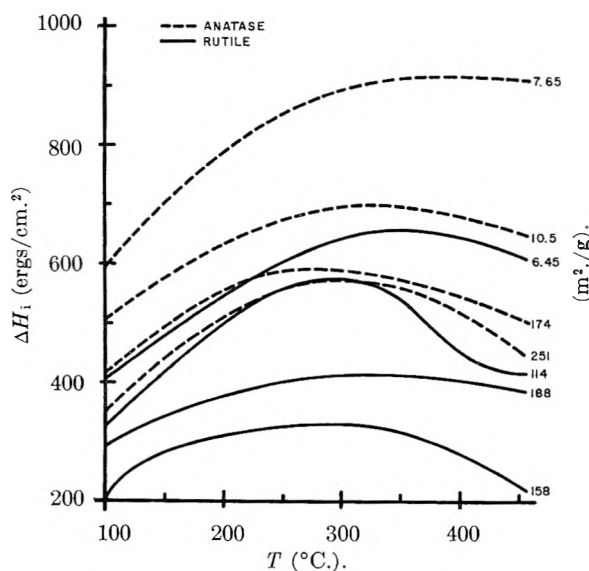


Fig. 1.

tase samples showed two OH bands, and rutile only one. However, the somewhat risky assumption must be made that the extent of OH coverage correlates with the energetics of physical adsorption. It should be noted that the present authors consider TiO₂ a poor choice for a "standard" adsorbent in adsorption studies. This material apparently cannot be obtained in greater than 99.9% purity (this is best found as seen from Table I), its surface is quite reactive,⁶ and there appears to be some chemical reduction (as evidenced by color changes when heated *in vacuo*).^{6,9} This last property has been attributed to adsorbed organic dyes used as pH indicators in the precipitation of TiO₂. It was to eliminate this last difficulty, as well as to obtain large particle size samples, that the rutile single crystals were ground and fractionated. These samples A₁, A₂, and A₃ which had never been

(9) A. C. Zettlemoyer, private communication.

in contact with organic substances displayed the same color change behavior as did samples F and G. Color changes were not observed for samples other than A, F and G.

The three samples A₁, A₂ and A₃ could be prepared in only small amounts due to a limited supply of starting material, and it was not feasible to subdivide them to the extent that ΔH_i could be obtained as a function of outgassing temperature. Instead, the three samples were outgassed at 250° only. For these samples there is a regular decrease of ΔH_i with decreasing particle size. The values are reasonably consistent with the other rutile samples outgassed at 250°.

Effect of Outgassing Temperature.—The effect of outgassing temperature is similar to that for the SiO₂-H₂O system in that the immersional heats for both anatase and rutile increase, pass through a maximum, and then decrease. The prominence of the maximum varies from sample to sample and is barely discernible for the coarsest anatase sample. The maximum occurs at 300 and 350°, whereas for SiO₂ the usual position of the maximum was at 250°, indicative of a higher bond energy for titanol groups than for silanol groups.

By analogy to SiO₂ the removal of titanol groups might be irreversible on the time scale of the calorimetric measurements, hence the decrease of ΔH_i with outgassing temperature above 300° because of the reduced opportunity for hydrogen bonding. An infrared study for the kinetics of rehydration with outgassing temperatures higher than those used by Yates⁶ is necessary to shed more light on this problem.¹⁰

(10) After preparation of this manuscript, recent work by Holabough and Chesick¹¹ introduces an added complication to the behavior with outgassing temperature. They find that samples vacuum outgassed at 450° have ΔH_i 's considerably higher than for the same samples subsequently treated with O₂ at 450°, the indication being that there is a direct connection between ΔH_i and the extent of reduction of the Ti⁴⁺ to a lower oxidation state on outgassing. Applied to the present work, this would indicate more pronounced maxima since the reduction is undoubtedly more extensive the higher the

Conclusions

The data continue to affirm that there is an inherent characteristic of adsorptive behavior, namely that the heats of adsorption are directly dependent on particle size. There is a uniform trend for both crystalline modifications of TiO_2 . The behavior with outgassing temperature is similar to that for SiO_2 ; it is interpretable in terms of the progressive loss of physically adsorbed water and chemically bonded surface hydroxyl groups. It is fruitless to say that any one of the TiO_2 samples could be picked as the "representative one" without more insight into its surface structure.

Acknowledgment.—The authors express appreciation to the American Petroleum Institute for their continued interest and support. Some surface areas were measured by Mr. H. D. Cole and his assistance was greatly appreciated. Dr. D. J. C. Yates was very helpful in supplying both TiO_2 samples and a preprint of his paper⁶ which had been submitted to *Journal of Physical Chemistry*.

DISCUSSION

D. S. MACIVER (Gulf Research and Development Company).—Concerning Professor Wade's observations relative to the heats of immersion of Al_2O_3 and TiO_2 in water, I might make two comments. In the first place, the heat of immersion of Al_2O_3 is dependent not only on such factors as particle size, outgassing temperature, etc., but also on the crystalline structure of the Al_2O_3 . In the case of the high area aluminas such as $\gamma\text{-Al}_2\text{O}_3$, several crystalline modifications

outgassing temperature and only becomes important at temperatures above 200 to 300°. Presumably, the ΔH_i measurements at higher outgassing temperatures for samples not treated with oxygen also include a heat source in that oxygen in the calorimeter oxidizes the reduced TiO_2 during the immersionsal measurements.

(11) C. M. Hollabaugh and J. J. Chessick, *J. Phys. Chem.*, **65**, 109 (1961).

exist and attempts to compare immersionsal heats of a series of aluminas must take this factor into consideration. Secondly, I would think that, in the case of TiO_2 , plots of ΔH_i vs. weight loss during outgassing might be more informative than plots of ΔH_i vs. outgassing temperature (Fig. 1). Have the former plots been made?

W. H. WADE.—I would hasten to concur that gamma, chi, etc. aluminas have not been characterized; however, the α -aluminas which are well characterized show a uniform decrease in ΔH_i with decreasing particle size. Your point regarding TiO_2 is well taken and no plots of the type you mention have been made. Many TiO_2 samples lose weight in excess of that attributable to surface losses. Presumably, decomposition occurs at higher outgassing temperatures.

L. H. REYERSON (University of Minnesota).—How were your samples outgassed? Outgassing can remove oxygen atoms from the surface so that the surface is Ti_2O_3 , not TiO_2 . This was proved in our laboratories by sorption of NO_2 and magnetic susceptibility studies on TiO_2 . NO_2 gave up an oxygen atom to fill each hole which had lost oxygen during outgassing.

W. H. WADE.—All TiO_2 samples were outgassed at the temperatures noted and at 10^{-6} mm. for approximately 100 hours.

W. D. ROSS (E. I. du Pont Company).—The comment has been made that TiO_2 can lose oxygen upon heating, even if not contaminated by organic material. A distinction should be made between anatase and rutile. Rutile is the more stable and can be heated strongly with no appreciable loss of oxygen. Anatase loses oxygen more readily; I am not sure how strongly it can be outgassed. It has been remarked that some metallic impurities affect oxygen loss; with this I agree.

W. H. WADE.—One of the rutile samples reported in the present study showed some evidence of decomposition although it is of the highest purity attainable. I am not sure whether the correct explanation has yet been offered for the loss of oxygen by some TiO_2 samples.

A. C. ZETTMAYER (Lehigh University).—Our laboratory has shown that the loss of oxygen from rutile may be identified with the presence of traces of organic substances.

THE ADSORPTION OF OIL-SOLUBLE SULFONATES AT THE METAL/OIL INTERFACE

BY WILLARD D. BASCOM AND C. R. SINGLETERRY

U. S. Naval Research Laboratory, Washington 25, D. C.

Received March 20, 1961

It has been found possible to isolate adsorbed films of the salts of dinonylnaphthalenesulfonic acid on stainless steel surfaces by retraction from aromatic hydrocarbon solution. The wetting behavior of various series of liquids on the resulting film-coated surfaces suggests that the molecules adsorb to give monomolecular films by attachment of the polar sulfonate heads to the metal oxide surface with the hydrocarbon tails outward. The molecules are sufficiently close packed to yield a surface having properties similar to those of polyethylene. A study of the wettability of the soap monolayers by a series of alkylnaphthalene liquids indicates that adsorption from water-saturated solution is independent of the soap cation and is the result of dipole interactions between the hydrated sulfonate ion-pair with the metal oxide surface. Adsorption from anhydrous solution does depend upon the choice of cation. Here dipole interactions between the unhydrated ion-pair and the metal-oxide surface appear to be supplemented by coordination of the cation with the oxygen of the oxide film.

Introduction

Many studies have been made of the adsorption of polar-non-polar solutes from non-aqueous solution onto oxide-coated metal surfaces. Most of these investigations, however, have been concerned with the carboxylic acid and amine derivatives of straight-chain hydrocarbons and fluorocarbons. The adsorptive behavior of the soaps of high molecular weight acids has received relatively minor attention despite their wide use as corrosion inhibitors and sludge dispersants in lubricating oils. A

more complete knowledge of soap adsorption at the solid-oil interface would permit a better understanding of the role of such soaps in these technological areas. It has been found at this Laboratory, for instance, that the effectiveness of oil-soluble soaps in diminishing ice adhesion in lubricated systems is in part related to their adsorption at the oil-metal interface.

The work reported here concerns the adsorption of various salts of dinonylnaphthalenesulfonic acid on stainless steel. These compounds, well char-

acterized in studies concerning their micelle-forming properties in non-polar solvents,¹ were adsorbed from isopropylbiphenyl solution. This solvent has a sufficiently high surface tension to be non-spreading on the adsorbed monolayers, thus permitting isolation of the film-covered surfaces by retraction² from the soap solutions. No previous use has been made of the retraction technique for the isolation and study of soap films. The few investigations that have been made of soap adsorption have either employed the Langmuir-Blodgett technique to form soap films on solid surfaces³ or have simply washed the adsorbate solution from metal specimens with a volatile solvent to isolate film-covered surfaces.⁴

Zisman and co-workers have investigated the spreading behavior of liquids on organic polymer surfaces and on oleophobic monolayers obtained by retraction from non-polar solution. They have been able to establish⁵ a relationship between wettability and the chemical constitution of the solid surface. These concepts have been utilized in this study to infer the molecular configuration of soap monolayers.

Experimental

Materials.—The dinonylnaphthalenesulfonic acid was especially synthesized for research use. The hydrocarbon radical of the compound was prepared by alkylation of naphthalene with a propylene trimer and this then was sulfonated. Analysis⁶ has indicated no detectable mono- or tri-alkyl hydrocarbon. It is reasonable to assume from the method of preparation that the nonyl groups are highly branched and that the more abundant homologs have both alkyl groups in the same ring. Also, it is reasoned that sulfonation occurs on the ring opposite the alkyl substituents.

The purification of the acid and the preparation and purification of the metal sulfonates has been described previously.⁶ The acid was exactly neutralized with the appropriate base to form the sodium and cesium soaps and the divalent soaps were prepared by metathesis of the sodium soap with appropriate inorganic salts. Each preparation was lyophilized and stored in sealed ampoules under nitrogen. The octadecylamine was used as received. Solvents used were isopropylbiphenyl, obtained as a mixture of *meta* and *para* isomers, and practical grade hexadecane. Each liquid was repeatedly perchlorated through a column of Florisil adsorbent to remove polar contaminants. Their purity in this respect was demonstrated by the fact that they showed no tendency to spread on a freshly swept surface of distilled water or on the surface of water that was made slightly acid or alkaline.

The wetting liquids studied are listed in Table I along with their surface tensions as determined using the ring method and employing the corrections given by Harkins.⁷ It was found for many of these liquids that only after repeated percolation through Florisil adsorbent did the ring method give the maximum and reproducible surface tensions listed in Table I. The lower, less precise, values were undoubtedly due to the adsorption of polar contaminants on the platinum ring.

Molecular distillation of a few of the liquids was necessary to remove minor amounts of isomers and homologs. This was never fully achieved for nonyl- and dinonylnaphthalene, although molecular weight determinations showed that they

differed sufficiently in constitution to be considered separate members of the series of alkylnaphthalenes.

Surface Preparation and Film Isolation.—Stainless steel cylinders, three-quarters inch in diameter and in height, had one face ground flat and then polished to a mirror finish with fine alumina powder on a metallographic wheel. Alumina powder loosely retained on the surface was flooded off in a stream of hot tap water followed by a distilled water rinse. Microscopic examination revealed a small number of particles on the polished surface that were probably alumina. They appeared to constitute less than 1% of the total surface area. The polishing procedure yields a metal oxide surface that is completely wet by water (0° contact angle). Any tendency for water to wet the surface incompletely sug-

TABLE I

SURFACE TENSIONS OF THE WETTING LIQUIDS

Liquids	Surface tension, γ _{LV} , dyne/cm.
Alkylnaphthalenes	
1-methylnaphthalene	38.5
1,6-dimethylnaphthalene	37.7
1-ethylnaphthalene	37.6
<i>t</i> -amylnaphthalene	34.3
<i>t</i> -butylnaphthalene	Mixed isomers
nonylnaphthalene	
dinonylnaphthalene	32.6
Alkylbiphenyls	
1,1-diphenylethane	37.7
2-methylbibenzyl	36.4
isopropylbiphenyl (<i>ortho, meta</i>)	34.8
amylbiphenyl	34.2
diphenyldodecane	32.5
Miscellaneous Liquids	
water	72.8
methyl iodide	50.8
1-bromonaphthalene	44.6
isopropylbiphenyl (<i>ortho, meta</i>)	34.8
bis-(2-ethylhexyl) sebacate	31.1
octane	21.8

gested the presence of adsorbed organic contamination and required the alumina polishing procedure to be repeated. The specimens were dried in an evacuated chamber at 70–80°. The platinum surface was prepared by polishing one face of a disc one inch in diameter and one-sixteenth inch thick. This surface was cleaned of organic contamination before each experiment by heating the disc to redness in a gas flame. A specularly reflective polytetrafluoro-ethylene surface was prepared by cutting one face of a small block with a microtome and then pressing the fresh surface against a smooth glass plate at 180° and 1000 p.s.i.⁸ The polyethylene was obtained as a powder and molded under heat and pressure to obtain a specularly reflective surface.

The adsorbed sulfonate films were obtained by exposing stainless steel specimens for 16 to 20 hours at 20° to solutions containing 0.5% of adsorbate in isopropylbiphenyl. The specimens then were withdrawn and the solution allowed to retract from their surfaces.

Octadecylamine monolayers were deposited on the platinum surfaces by adsorption from a 0.1% solution in hexadecane and isolated by retraction.

Contact Angle Measurement.—Using a telescope-goniometer, the sessile drop method was employed to determine advancing contact angles when they were above 10°. A drop 1 mm. in diameter was placed on a surface and then advanced by two successive additions of liquid. Three such drops were observed on both sides for each liquid, giving a total of twelve measurements. The average deviation was less than two degrees.

It was necessary that contact angles considerably less than 10° be measured with some precision. It is difficult to make measurements with a telescope-goniometer in this low

(1) S. Kaufman and C. R. Singleterry, *J. Colloid Sci.*, **12**, 465 (1957).

(2) W. C. Bigelow, D. L. Pickett and W. A. Zisman, *ibid.*, **1**, 513 (1946).

(3) J. E. Young, *Australian J. Chem.*, **8**, 173 (1955).

(4) V. Hong, S. L. Eisler, D. Bootzin and H. Harrison, *Corrosion*, **10**, 343 (1954).

(5) E. G. Shafrin and W. A. Zisman, *J. Phys. Chem.*, **64**, 519 (1960).

(6) S. Kaufman and C. R. Singleterry, *J. Colloid Sci.*, **10**, 139 (1955).

(7) W. D. Harkins and H. F. Jordan, *J. Am. Chem. Soc.*, **52**, 1751 (1930).

(8) R. C. Bowers, W. C. Clinton and W. A. Zisman, *J. Appl. Phys.*, **24**, 1066 (1953).

range but a micro-interference technique proved to be useful. A metallographic microscope fitted with a 540 $m\mu$ light source for vertical incident light was focused at the drop edge. When the contact angle was less than ten degrees it was possible to resolve the interference bands resulting from normal reflection from the upper and lower surfaces of the thin liquid wedge. The interference patterns were photographed and the band spacing measured to obtain the contact angle. It was found that contact angles measured in this way on two separate drops on the same surface rarely differed by more than one-half degree. All contact angle measurements and surface tension measurements were carried out at 20°. Robbins and LaMer also have reported an interference method for contact angle measurement.⁹

Numerous attempts were made to detect any tendency for the adsorbed sulfonate molecules to dissolve into the wetting liquids. These efforts were unsuccessful. The deliberate addition of sulfonate to the wetting liquids did not result in contact angles different from those obtained using the pure liquids. There was no observable change with time in the contact-angles for drops allowed to remain on the retracted films for as long as 20 hours. The resistance of the adsorbed films to solvent desorption was further tested by placing a drop of wetting liquid on a surface and noting the contact angle. This initial drop then was retracted after a few moments and the contact angle determined for a second drop on the same area. No significant difference was apparent in these instances.

Results

The purpose of this work was to study the properties of the films adsorbed on stainless steel from solutions containing dinonylnaphthalenesulfonic acid or its metal salts. The most important property of such films is the surface energy, but this cannot be measured directly; inferences concerning the surface energy of solids are most conveniently derived from contact angle or wetting phenomena. Although some information can be gained by comparing the contact angles of a single liquid, such as methylene iodide, on various surfaces, a more reliable and convenient index of surface energy is furnished by the determination of the critical surface tension of wetting, γ_c , the surface tension of a liquid which will just spread on the solid surface. Zisman and co-workers⁵ have determined γ_c by measuring the contact angles, θ , of a suitably chosen series of liquids on the surface and plotting the cosine of the contact angle as a function of the surface tension, γ_{LV} , of the liquids. They found $\cos \theta$ to be a linear function of γ_{LV} and extrapolated the data to $\cos \theta = 1$ to obtain γ_c . For the study of polytetrafluoroethylene surfaces and adsorbed monolayers of straight chain polar-non-polar compounds, they measured the contact angles of a series of n -alkanes from C_{16} to C_8 .^{10,11} These liquids, however, all spread on the films formed by the dinonylnaphthalene sulfonates. Zisman, *et al.*, when studying surfaces of higher energy than the paraffin chain monolayers, used a series of miscellaneous liquids ranging in surface tension from 30 to 70 dynes/cm.,^{12,13} but in the present work this series was found to give poorly reproducible results on several of the films. However, two series of alkyl-substituted aromatic compounds were found which had sufficiently high surface tensions, and which gave linear plots of $\cos \theta$ vs. γ_{LV} for the organic surfaces

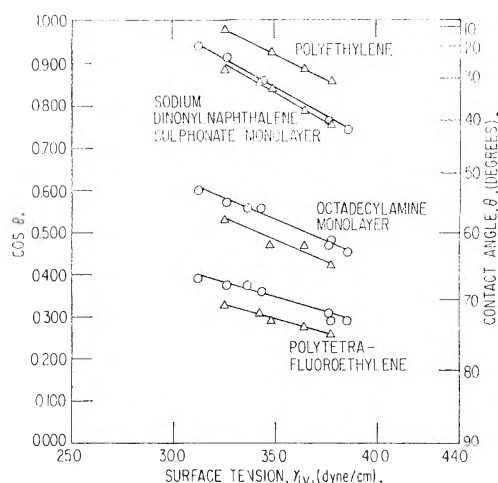


Fig. 1.—The spreading behavior of a series of alkylnaphthalenes, O, and a series of alkylbiphenyls, Δ , on various oleophobic surfaces.

previously investigated by Zisman and co-workers and also for the soap films of this study (Fig. 1). One series consisted of alkylnaphthalenes and the other of hydrocarbons containing two non-fused benzene rings. The alkylnaphthalenes were selected for most of the work because they have structures closer to that of the dinonylnaphthalene sulfonate radical of which the outer surface of the monolayer was presumed to be composed.

The surfaces studied and the conditions of film formation were selected to provide information on (1) the variation of γ_c for a given surface with the choice of liquid series, (2) the effect of water present during adsorption or the properties of the film formed by a given sulfonate and (3) the effect of different cations on the nature of the films.

Figure 1 summarizes data for the two series of alkyaromatic hydrocarbons on polytetrafluoroethylene, octadecylamine monolayer, sodium dinonylnaphthalene sulfonate monolayer and polyethylene. These data show that the liquid series rank the critical surface tensions of solid polytetrafluoroethylene, octadecylamine monolayer, and solid polyethylene surfaces in the order previously assigned by measurements with miscellaneous liquids (Table II) and by friction studies.¹⁴

The alkylbiphenyl series indicates a lower value of γ_c than does the alkylnaphthalene series, the difference being greater for surfaces of lower critical surface tension. For the surface coated by sodium dinonylnaphthalene sulfonate, the difference is comparable with the uncertainty of the extrapolation. The value of γ_c for the sodium sulfonate monolayer indicated by the two alkyl aromatic series is approximately 29 dynes/cm., which is distinctly lower than γ_c for polyethylene but higher than for octadecylamine monolayer.

Figure 2 compares the data for the alkylnaphthalenes and for the miscellaneous series of liquids on copper dinonylnaphthalene sulfonate monolayer. The alkylnaphthalene data have a steeper slope and extrapolate to a γ_c higher by three dynes than that indicated by the miscellaneous series. Data

(9) M. L. Robbins and V. K. LaMer, *J. Colloid Sci.*, **15**, 151 (1960).

(10) H. W. Fox and W. A. Zisman, *ibid.*, **5**, 514 (1950).

(11) E. G. Shafrin and W. A. Zisman, *ibid.*, **7**, 166 (1952).

(12) H. W. Fox and W. A. Zisman, *ibid.*, **7**, 438 (1952).

(13) A. H. Ellison and W. A. Zisman, *J. Phys. Chem.*, **58**, 503 (1954).

(14) W. A. Zisman in "Friction and Wear," edited by R. Davies, Elsevier Publishing Co., Amsterdam, 1959, p. 110.

TABLE II
THE CRITICAL SURFACE TENSIONS, γ_c , OF VARIOUS OLEOPHOBIC SURFACES

Surface	Surface constitution	γ_c , dynes/cm.					
		<i>n</i> -Alkanes	Ref.	Misc. liquids	Ref.	Alkyl-naphthalenes ^b	Alkyl-biphenyls ^b
Polytetrafluoroethylene	—CF ₂ —	18	10	18-20	10	0	0
Octadecylamine monolayer	—CH ₃ —	22	11	18-24	11	12	10
Dinonylnaphthalene sulfonate monolayer ^a	—CH ₃ —, —CH ₂ —			26 (Cu)	^b	29 (Na)	29 (Na)
Polyethylene	—CH ₂ —			31	12		32
Polystyrene	—CH ₂ —, C ₆ H ₅ —			35	13		

^a Isolated by retraction from water-saturated isopropylbiphenyl solution. ^b This investigation.

for the miscellaneous liquids on the other soap films were not reproducible and are not reported.

In Fig. 3 the wetting data for the alkyl-naphthalenes on surfaces obtained from a solution of dinonylnaphthalenesulfonic acid and from a solution of the copper soap of this acid indicate a slightly smaller value of γ_c for the acid film.

The water content of the solutions from which the sulfonate films were deposited had a distinct effect on the properties of the monolayer, the magnitude of the effect being specific to the cation present. The pertinent data are shown in Fig. 4, which has been divided into two sections to avoid confusion in the plots. The solid line in the upper section refers to the composite data for all the sulfonate films retracted from water-saturated oil solution. For such films the wetting data, within experimental uncertainty, gave the same linear relationship for all of the metal sulfonates. Adsorption from anhydrous solutions, on the other hand, gave surfaces for which the data fell on distinctly different lines which are presented as dotted lines in Fig. 4a. The difference from the corresponding water-saturated solution was greatest for the barium compound and, as indicated in Fig. 4b, was negligible for copper dinonylnaphthalene sulfonate. Separate experiments demonstrated that the results were not influenced by variations of the relative humidity with which the metal surface was equilibrated before deposition of the film.

The time required for film adsorption to be completed for any given soap solution was found to be greater than five hours for the sodium soap in water-saturated solution but less than ten minutes for the dry sodium soap solution and also less than ten minutes for the copper soap in either water-saturated or anhydrous oil solution. This was determined by observing when α -methylnaphthalene gave a maximum contact angle against surfaces retracted from the solution at various time intervals.

It also was found that reduction of the sodium soap concentration from 0.5 to 0.0005 weight % in water-saturated oil solution did not diminish the maximum contact angle obtainable with α -methylnaphthalene.

Discussion

The Significance of γ_c Values.—The use of the experimental quantity γ_c as an indication of surface properties or surface configuration of adsorbed molecules needs to be examined critically when γ_c must be obtained by the extrapolation of contact angle data from a series of hydrocarbons

not previously employed for this purpose. As Zisman and Fox pointed out¹⁰ in their first paper on the subject, γ_c is not the surface tension, γ_{SV} , of the solid, but is smaller by the magnitude of the interfacial tension, γ_{SL} , between the solid and that liquid which just spreads on the solid surface. This can be seen from the Young-Dupre equation which relates the interfacial tensions and $\cos \theta$ for a liquid on a solid surface in equilibrium with the saturated vapor of the wetting liquid

$$\cos \theta = \frac{\gamma_{SV} - \gamma_{SL}}{\gamma_{LV}} \quad (1)$$

Extrapolation of the wetting data for a series of liquids on a given solid to $\cos \theta = 1$ gives γ_c which may be thought of as the surface tension of a hypothetical member of the series that just spreads. Equation 1 then becomes

$$\gamma_c = \gamma_{SV} - \gamma_{SL}, \text{ at } \cos \theta = 1 \quad (2)$$

In this instance, γ_{SL} is the interfacial tension against the solid surface for the liquid that just spreads and will be small provided γ_{SL} for the actual members of the series of wetting liquids is small or becomes small as the contact angle decreases.

This interfacial tension is believed to be small when the molecular structure of the wetting liquids approaches that of the outer layer of the solid surface as the contact angle approaches zero. This belief is supported by several lines of evidence. Two liquids having similar molecular structures are usually miscible, *i.e.*, the interfacial tension between them is zero. The critical surface tensions of a number of organic solids are not far removed from the surface tension of liquids that closely resemble them in molecular structure. As an example, the wetting data for the alkylbiphenyls on polyethylene (Fig. 1) extrapolate to a γ_c value slightly higher than 31 dynes/cm. Fox, *et al.*,¹⁵ determined the surface tension of a high molecular weight liquid polyethylene to be 30.7. This close agreement between γ_{LV} and γ_c for polyethylene implies that for the alkylbiphenyl liquids γ_{SL} becomes very small in the extrapolation to $\cos \theta = 1$.

It is possible to arrive at the same conclusions if one interprets the interfacial tensions between non-polar phases as resulting from the difference between the magnitudes of unsatisfied molecular interaction or dispersion forces at the surfaces of two phases. London¹⁶ has related these forces of

(15) H. W. Fox, E. F. Hare and W. A. Zisman, *J. Phys. Chem.*, **59**, 1097 (1955).

(16) F. London, *Trans. Faraday Soc.*, **33**, 8 (1937).

interaction for non-polar liquids with their molecular polarizability, so the difference in polarizability of the atomic groups at an interface may be taken to reflect the imbalance of dispersion forces. This difference will be least when the atomic groups in the two substances forming the interface are most nearly the same. There may, of course, be residual differences because of different packing densities in the two phases or because of the entropy effect associated with confining the molecules in the solid surface to fixed positions. When the solid surface is made up of oriented polar-non-polar molecules, as it is in this study of sulfonate adsorption, comparisons of molecular structure must be made between the average surface of the liquid and the atomic groups composing the outermost part of the monolayer. Zisman has demonstrated that the surface properties of close-packed films are determined by the nature of the outermost atomic groups and not by the dipole forces associated with the polar heads held on the substrate surface.⁵

The criteria that must be met for a series of liquids to be useful in the determination of the γ_c for non-polar solids are (1) that their wetting behavior on the solid surface give a linear relation between $\cos \theta$ and γ_{LV} and (2) that the molecular structures of the liquids approach that of the atomic groups prevailing at the solid surface with decreasing surface tension of the liquids. There is one further limitation. It was demonstrated by Zisman and co-workers¹² and also in the present investigation that it was not possible to obtain an unambiguous extrapolation to $\cos \theta = 1$ of the wetting data for a group of alkylbenzenes on octadecylamine monolayer. This difficulty may well be a result of the very narrow range of surface tensions of the alkylbenzenes. Even though the solid-liquid interfacial tensions for a group of liquids against a non-polar solid may be small, this quantity does not necessarily change in the same way as the surface tension changes with decreasing contact angle. This irregularity may be neglected if the surface tensions of the liquids cover a relatively wide range, *i.e.* if the increments in surface tension are large compared with the probable change in γ_{SL} between the same members. However, the alkylbenzenes have surface tensions between 28.5 and 30.5 dynes/cm., a much smaller range than that covered by the alkylnaphthalenes, alkylbiphenyls or the *n*-alkanes.

Therefore, it is concluded that a third condition for a series of liquids to be useful for the determination of γ_c is that their surface tensions vary systematically over a substantial range. The three conditions necessary for a series of wetting liquids are seen to be satisfied when the *n*-alkanes are used as contact angle liquids on a paraffin surface or on a paraffin-chain monolayer. They also are satisfied when alkylnaphthalene liquids are observed on monolayers of the dinonylnaphthalene sulfonates, but not when these alkyl-aromatics are applied to a paraffin or close packed methyl surface. In the latter instance the solid-liquid interfacial energy is appreciable because it arises as a result of an imbalance of dispersion forces between solid surfaces comprised of weakly polarizable methyl or perfluoro

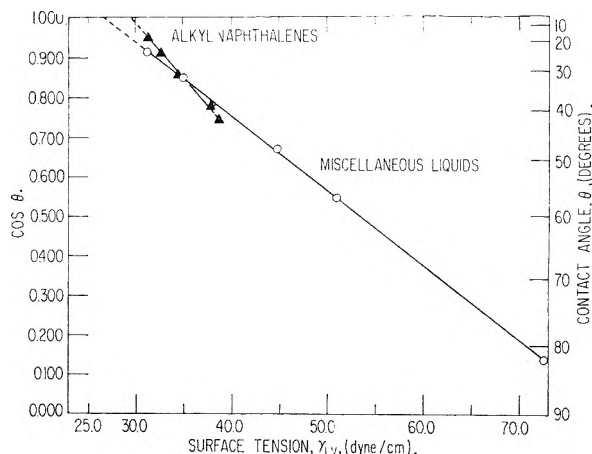


Fig. 2.—The spreading behavior of a series of alkylnaphthalenes and a series of miscellaneous liquids on copper dinonylnaphthalene sulfonate monolayer retracted from a water-saturated solution of the sulfonate in isopropylbiphenyl.

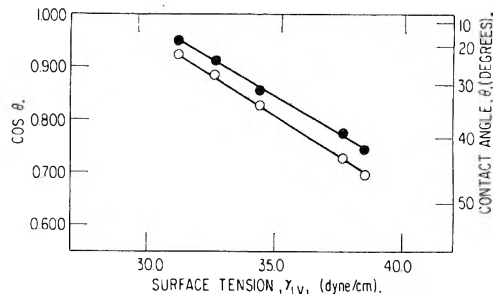


Fig. 3.—The spreading behavior of a series of alkylnaphthalenes on dinonylnaphthalenesulfonic acid monolayers, O, and on copper dinonylnaphthalene sulfonate monolayer, ●, retracted from water-saturated isopropylbiphenyl solution.

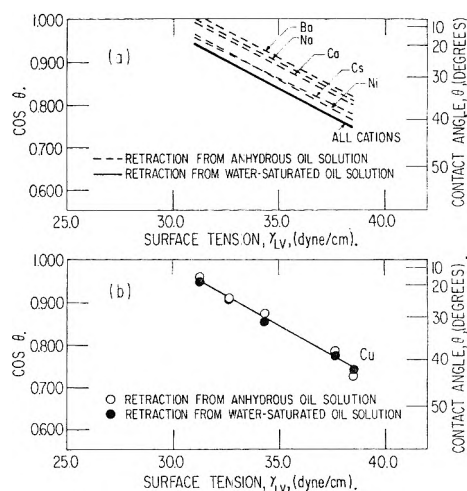


Fig. 4.—The effect of water in the adsorbate solution and the choice of soap cation on the spreading behavior of alkylnaphthalenes on dinonylnaphthalene sulfonate monolayers.

functions and liquids which contain the more polarizable methylene groups and aromatic rings. It is, therefore, not surprising that extrapolation of the contact angle data for the alkylnaphthalenes or the alkylbiphenyls on an octadecylamine monolayer gives much smaller numbers for the critical surface tension than were obtained with the *n*-alkanes. This confirms the generalization made by Zisman¹²

that from among the various series of wetting liquids that can be employed on a given non-polar surface, the surface tension of the solid will be best approximated by the series giving the highest value of γ_c .

In spite of the limitation imposed by the uncertain magnitude of γ_{SL} , the critical surface tensions obtained on the non-polar surfaces listed in Table II using the *n*-alkanes, alkylnaphthalenes, alkylbiphenyls and the miscellaneous liquids all agree in ranking the surfaces in the same order of increasing surface tension. Therefore, the differences between various monolayers prepared from the dinonylnaphthalene sulfonates which are revealed by γ_c values estimated with the alkylnaphthalenes may be accepted with considerable confidence to represent real differences in the surface energies of these monolayers resulting from differences in the closeness of packing of the adsorbed molecules.

Soap Monolayers.—There is little doubt that the sulfonate films isolated and studied in this investigation are monolayers. This belief is based on the fact that the γ_c values for those adsorbed films are all less than that for the surface of polyethylene which is comprised primarily of methylene groups. Also, the γ_c values for the soap films are all greater than the value obtained on the methyl-rich surface of a close-packed octadecylamine monolayer. Thus, the surface properties of the sulfonate monolayers correspond to those of an admixture of methyl and methylene groups. This requires that the molecules be adsorbed on the stainless steel surfaces by attachment of their polar sulfonate heads with their hydrocarbon tails oriented more-or-less normal to the surface. The molecules must be sufficiently close-packed so that the nonyl groups shield the naphthalene rings and the polar sulfonate groups from interaction with the spreading liquids. This is similar to the orientation and packing that has been observed for the monolayers adsorbed from oil solutions of many other polar-non-polar materials. Multilayer adsorption of the soap would involve only van der Waals or dispersion force interaction between the soap molecules in solution and the hydrocarbon end-groups of the initially adsorbed soap. The energy available from such an attachment would be considerably less than the energy necessary to release the ionic interaction that holds a soap molecule in the core of a soap micelle¹⁷ so that such a second layer could not be in equilibrium with a solution containing micelles.

It has been experimentally determined here that, for the soap monolayers isolated from anhydrous oil solution, the critical surface tensions determined using the alkylnaphthalenes are specific to the soap cation. On the other hand, surfaces isolated from water-saturated oil solution have the same critical surface tension regardless of the soap cation, and this common value of γ_c is lower than the γ_c values obtained for the various monolayers from anhydrous systems. If we interpret differences in γ_c as indicating differences in packing of the molecules in the adsorbed films we must conclude that the cation

determines the closeness of packing in monolayers from anhydrous sulfonate solution and that the monolayers obtained from water-saturated oil solutions of all the sulfonates have essentially the same packing and are generally more closely packed than the monolayers obtained from anhydrous oil solution.

The effect of water in these experiments is not believed to result from hydrolysis of the sulfonate to give the free acid. Baker and Singleterry¹⁸ have shown that the salts of dinonylnaphthalenesulfonic acid are not significantly hydrolyzed in oil solution in the presence of excess water and carbon dioxide.

The effect of water on sulfonate adsorption is controlled by the water content of the solutions and not by the previous history of the metal surface with respect to adsorbed water. This is evidenced by the fact that the experimental result could not be altered by equilibrating the metal specimens with various relative humidities prior to their contact with either water-saturated or anhydrous sulfonate solution. That is, a surface carrying adsorbed water, upon exposure to anhydrous sulfonate solution, develops a monolayer which is indistinguishable from that deposited on an intensively dried surface. It must be concluded either that adsorbed water does not alter the binding of the monolayer or that the anhydrous sulfonate system removes the water from the surface during the establishment of adsorption equilibrium. The latter alternative is more probable. The first water solubilized by sulfonates¹⁹ has a high apparent density and low vapor pressure which suggests it is firmly held in the soap micelles. The amount of water required for a monolayer on all surfaces of the metal button is only 0.01% of that corresponding to one molecule per mole of sulfonate present in the adsorbate solution. In the face of competition with sulfonate molecules for adsorption sites on the metal it may be expected that the partition of water between the surface and the micelles will leave much less than a monolayer of water molecules directly adsorbed on the metal. Thus in the presence of anhydrous solutions, trace amounts of water introduced during experimental manipulations will have negligible effects on the adsorbed monolayer.

Sulfonate soap adsorption from anhydrous systems then must involve adsorbate molecules in which the cation is not hydrated but is more-or-less strongly associated with the anion. Attachment of the adsorbate on the metal-oxide surface could involve specific coordination of the cation with oxygen of the oxide surface or a general dipole interaction between the polar sulfonate group of the soap molecule and the polar metal surface. Consequently, it is not surprising that the closeness of packing of the various sulfonate monolayers from anhydrous oil solution is determined by the soap cation. The tendency to coordinate with surface oxygen would vary with the cation, and the cation size would determine the charge separation and

(18) H. R. Baker and C. R. Singleterry, *Ind. Eng. Chem.*, **48**, 1190 (1956).

(19) J. B. Mathew and E. Hirshhorn, *J. Colloid Sci.*, **12**, 465 (1957).

(17) W. D. Bascom, S. Kaufman and C. R. Singleterry, Fifth World Petroleum Congress, Section VI, Paper 18, 1959.

thus the dipole strength of the various sulfonate groups. There is no simple correlation between the γ_0 values for the various monolayers and the probable coordinating tendency of the cations or the probable dipole strengths of the various sulfonates. It is possible that the two mechanisms are both operative but to different relative degrees for different soaps. In water-saturated solution the cation will be hydrated; this will increase the charge separation in the sulfonate ion pair as well as saturate the coordination tendency of the cation. The ion-pair may dissociate sufficiently to permit the sulfonate anion to be adsorbed independently. The data are not adequate, however, to distinguish this possibility from a simple dipole interaction between the hydrated sulfonate ion pair and the oxide surface. It is also possible that water adsorbed on the metal oxide is involved in linking the sulfonate molecules to the surface. The water present on the metal oxide will be in equilibrium with water in the micelles and the exact amount held on the surface will depend upon the ability of water to compete with sulfonate for adsorption sites and the ability of the surface to compete with the micelles for water.

Acknowledgments.—Grateful acknowledgment is made of the considerable assistance and encouragement given us by Dr. W. A. Zisman and the members of his research group, Mrs. E. G. Shafrin, Mrs. M. K. Bennett and Dr. N. L. Jarvis.

DISCUSSION

E. D. GODDARD (Lever Brothers Company).—The authors express the view that the adsorbed surfactant is in monolayer form and advance an explanation of this view which is based on energetic considerations involving the presence of micelles in the solution. Has adsorption been carried out from solutions where there are no micelles present, if need be from water-free solutions or from very dilute surfactant solutions? Although it might be that a monolayer is the equilibrium adsorbed species when the solution is in contact with metal, this might well change when the liquid retracts and a situation obtains which is somewhat similar to that in multilayer deposition by the Langmuir-Blodgett technique.

W. D. BASCOM.—The suggestion is, of course, that above the critical micelle concentration (CMC) the sulfonate soaps are adsorbed at the air/organic liquid interface and that as

the adsorbate solution retracts from the metal oxide surface a second monolayer is deposited. We have not studied the adsorption of these sulfonates at concentrations below their CMC since this would involve the use of inordinately dilute adsorbate solutions (1×10^{-7} m./l.). However, the presence of any appreciable surface excess of solute at the air/organic liquid interface should be detectable from the difference in surface tension between the solutions and the pure solvents. Measurement of the surface tension of a 1% copper dinonylnaphthalenesulfonate solution in isopropylbiphenyl using the pendant drop method did not differ from the value obtained for the solvent.

A. S. MICHAELS (Massachusetts Institute of Technology).—Is the difference between the "critical surface tension" of an aromatic surface sufficiently different from that of an aliphatic surface to justify your conclusions about molecular orientations in these monolayers?

W. D. BASCOM.—The critical surface tension of polyethylene is 4 dynes/cm. less than the value obtained using comparable liquids on polystyrene (Table II). This difference is many times greater than the limiting difference in γ_0 that could be called experimentally significant.

A. S. MICHAELS.—How do you reconcile your conclusions about molecular packing in these monolayers with L. S. Bartell's observations on the wettability of incomplete monolayers—*i.e.*, small differences in contact angle often were observed over rather large changes in fractional surface coverage.

W. A. ZISMAN (U. S. Naval Research Laboratory).—In L. S. Bartell's work no change in contact angle was observed over an apparent large change in fractional coverage because he used a liquid which was able to fill the pores in the adsorbed film with adlined hydrocarbon molecules. Hence, he formed a mixed film and didn't know that because both solute and solvent molecules in the monolayer were exposing $-\text{CH}_2$ groups to the contacting liquid sessile drop. His work does not contradict that reported by me or in the present paper.

W. D. BASCOM.—L. S. Bartell has reported a more or less proportional and consistent decrease in contact angle with monolayer depletion for wetting liquids that would not be expected to "fit" into the spaces left by the removed adsorbate molecules. The wetting liquids employed in our study of the sulfonate soaps could not participate in such quasi-crystalline penetration into the monolayer.

HOWARD SHEFFER (Union College).—Which isomeric dinonylnaphthalenesulfonic acids were used in the studies? Do you plan to do further work varying the studies of the dialkyl-naphthalenesulfonic acids?

W. D. BASCOM.—The alkyl groups were on the same ring and the sulfonic acid groups were on the other ring. These products are difficult to prepare and are a mixture of isomers, so no further work along these lines is planned.

THERMAL FORCES ON AEROSOL PARTICLES¹

BY C. F. SCHADT AND R. D. CADLE

Stanford Research Institute, Menlo Park, California

Received March 7, 1961

A modified Millikan oil drop apparatus has been used to investigate thermal forces on individual aerosol particles of varying size and widely varying thermal conductivity. The results confirm previous indications that thermal forces on particles of high thermal conductivity are very much larger than predicted by Epstein's equation. Thermal forces on particles whose size is about that of the mean free path are in fair agreement with predictions from Cawood's equation, regardless of thermal conductivity.

Introduction

One of the more useful tools for collecting aerosol particles in the 0.1 to 1.0 μ size region is the thermal precipitator. According to the generally accepted

radiometer theory of Epstein,² particles having high thermal conductivities should be very difficult to collect by this method. However, no such difficulties have been reported in the literature. In a previous study of the efficiency of a thermal pre-

(1) This work was supported by Grant S-30 of the U. S. Public Health Service.

(2) P. S. Epstein, *Z. Physik*, **54**, 537 (1929).

cipitator for collection of aerosol particles, the authors³ found good agreement with the Epstein theory for stearic acid, a material with low thermal conductivity. Similar agreement had been found for such particles by earlier workers.^{4,5} However, for materials with relatively high thermal conductivities, namely, sodium chloride and iron, thermal forces measured with the thermal precipitator were 20 to 50 times the theoretical values. This is a startling disagreement with generally accepted physical theory.

The thermal precipitator was designed to collect particles, not to measure thermal forces, and the results mentioned above are difficult to interpret. This paper describes measurements of thermal forces on individual particles in apparatus of the Millikan oil drop type, in which a thermal gradient as well as an electrical field can be produced. The results obtained for particles of tricresyl phosphate, sodium chloride and mercury confirm the results obtained with the thermal precipitator. The Epstein theory was derived for particles that are large relative to the mean free path of the gas molecules. The studies were also extended to include the cases for particles smaller than the mean free path and the intermediate region, and the results were compared with the equations of Cawood⁶ and Waldmann.⁷

Theory.—The theories that explain the force that acts on a particle suspended in a gas in which a thermal gradient exists are quite different for the case in which the mean free path of the gas molecules is smaller than the particle diameter and for the case in which it is larger. The intermediate region has not been covered by any generally accepted theory.

The case in which the mean free path is smaller than the particle diameter has been treated in detail by Epstein.² He considered a spherical particle in a gas in which a uniform thermal gradient exists at appreciable distance from the particle. On the basis of the thermal conductivities of the particle and of the gas and assuming the applicability of the Fourier equation for heat conduction without convection, he calculated the temperature distribution on the surface of the particle. Then, using the concept of thermal creep (first developed by Maxwell) for flow of gas molecules along an unevenly heated surface and integrating over a sphere, he obtained an expression for gas flow along the surface of the particle. This he used as a boundary condition for solving the Navier-Stokes equations to obtain an expression for thermal force on the particle. It is interesting to note that this boundary condition conflicts with the condition of zero velocity at the surface used in obtaining the usual Stokes law equation, which in turn has been used in measuring thermal force. Interestingly enough this does not seem to cause any great discrepancy between measurements made by observing

an electrically charged particle in motion or by balancing the thermal force with an electrical field⁴ as will be discussed in a later section. This raises some question as to the validity of the theory.

The Epstein equation is

$$F = -9\pi r \left(\frac{k_a}{2k_a + k_i} \right) \frac{\eta^2}{\rho T} \times G$$

where

- F = thermal force
- r = radius of the particle
- k_a = thermal conductivity of the gas
- k_i = thermal conductivity of the particle
- η = viscosity of the gas
- ρ = density of the gas
- T = absolute temperature (average)
- G = thermal gradient

Waldmann⁷ treats the case for mean free path larger than the particle diameter. In this case the thermal conductivity of the particles is of no significance and the thermal force is a result of the net impulse in the direction of the gradient imparted to the particle by the impinging gas molecules

$$F = -\frac{8}{15} r^2 \sqrt{\frac{2\pi m}{kT}} \times \lambda_{tr} \times G$$

where

- λ_{tr} = translational thermal conductivity of gas
- m = mass of a gas molecule
- k = Boltzmann's constant
- T = absolute temperature of the gas (av.)

Using the equations of classical gas kinetics, this can be put in the form

$$F = -\frac{4.0PL}{T} \times r^2G$$

where L is the mean free path and P is the pressure of the gas. The Cawood equation,⁶ the validity of which has been questioned,⁴ was derived for the case of mean free path approximately equal to the particle diameter

$$F = -\frac{\pi}{2} \frac{PL}{T} r^2G$$

It is of interest to note its similarity to the Waldmann equation, derived for $L \gg r$.

Experimental

The apparatus used to measure thermal force on single particles was similar to those of Saxton and Ranz,⁴ and Rosenblatt and La Mer.⁵ The observation cell consisted essentially of two machined and polished brass rods, 3/4 inch in diameter, separated by 0.30 cm., and enclosed in a Kel-F housing. The upper rod was electrically heated by an internal heating element. Copper-constantan thermocouples were embedded near the end surfaces of each rod to provide measurements of the temperature of each surface. Uniform or converging electrical fields could be produced between the two surfaces in a manner described by Rosenblatt and La Mer.⁵ A beam of light filtered with copper sulfate solution passed through two glass windows in the cell to illuminate the particles. A low-power microscope was used to observe the particles through a third window. A reticule in the eyepiece provided two reference lines (upper and lower) to measure the distance of fall of a particle. This corresponded to a distance in the middle of the cell of 0.085 cm. A small port was provided to evacuate the cell and introduce aerosol particles. The cell could be very slowly evacuated while a particle was being studied, so that the behavior of the same particle could be observed at different pressures.

The general procedure was to evacuate the cell partially and then let it suck in some prepared aerosol, bringing the pressure up to one atmosphere. A particle with suitable electrical charge and of desired settling velocity (approx-

(3) C. F. Schadt and R. D. Cadle, *J. Colloid Sci.*, **12**, 356 (1957).

(4) R. L. Saxton and W. E. Ranz, *J. Appl. Phys.*, **23**, 917 (1952).

(5) P. Rosenblatt and V. K. La Mer, *Phys. Rev.*, **70**, 385 (1946).

(6) W. Cawood, "Disperse Systems in Gases; Dust, Smoke and Fog," p. 1068, Faraday Society General Discussion, Gurney and Jackson, London, 1936.

(7) L. Waldmann, *Z. Naturforsch.*, **14a**, 589 (1959).

mate) was selected. By repeated reversal of the electrical field, the cell could be cleared of other particles. Then, with zero temperature difference and zero electrical field (*i.e.*, with the rods electrically shorted), the settling velocity (v_0) was measured several times by timing the fall of the particle past the two lines in the eyepiece reticule with a stopwatch. The particle was raised each time by momentarily applying an electrical field. From the known density of the material, and by applying the Stokes-Cunningham equation, the particle size and weight (w) were computed. The electrical field (E_0) required to balance its weight could then be measured with a vacuum tube voltmeter. The temperature of the upper rod then was increased, and, after stabilization of the thermal field, migration velocities (v) were measured as before. Thermal force was in the same direction as gravitational force. Thermal force could be obtained from the expression

$$F = \frac{v - v_0}{v} W$$

and by measuring the new electrical field (E) required to balance gravity plus thermal force one could obtain

$$F = \frac{E - E_0}{E} W$$

Tricresyl phosphate (TCP) was obtained from Monsanto Chemical Company. It was clear, had a specific gravity of 1.165 ± 0.008 at $25^\circ/25^\circ$, acidity 0.01% maximum. The sodium chloride was of reagent grade and was dissolved in distilled water. The mercury was triple-distilled. TCP aerosol was produced in a De Vilbiss nebulizer with dry air.

Sodium chloride aerosol was first produced from saturated aqueous solution in a De Vilbiss nebulizer and allowed to dry in a 1/2-liter flask before use, particle numbers 1, 2, 3. For the rest of the particles studied, numbers 4, 5, 6, 7, the aerosol was passed through a tube 2.5 cm. in diameter and 20 cm. long, filled with molecular sieve material⁸ to absorb the water vapor.

Mercury aerosol was produced with a condensation-type aerosol generator,⁹ using dry nitrogen and a very small amount of NO_2 to produce condensation nuclei. Electron microscope samples were obtained with a thermal precipitator. Examination of many samples indicated that the particles were spherical drops which must have been coated by a very thin layer of some material, perhaps an oxide of mercury, which prevented their evaporation. However, the layer must have been very thin relative to the drop size, because the drops evaporated, leaving no trace of material, whenever the electron beam intensity was raised above a very low level.

Results and Conclusions

The results were compared with the Epstein equation by plotting measured F/r versus thermal gradient for a given average absolute temperature.

Measurements of thermal force on tricresyl phosphate (TCP) droplets, which have a low thermal conductivity, 4.8×10^{-4} cal./cm. sec. $^\circ\text{C}$., indicate fairly close agreement with the Epstein equation (Fig. 1), in general agreement with previous results mentioned above.

Thermal force measurements on particles of sodium chloride, which has a much higher thermal conductivity, 1.55×10^{-2} cal./cm. sec. $^\circ\text{C}$., agree with the predicted dependence on thermal gradient, particle radius and density of gas (or on mean free path) (Fig. 2). However, the magnitude of the thermal force is about 30 times that predicted by the Epstein theory. This could be explained if the thermal conductivity of the particles could be shown to be comparable to that of tricresyl phosphate. This would be approximately 0.03 times the bulk value for sodium chloride. This great a difference is difficult to account for. Two conceivable explanations have been considered. First,

(8) Obtained from the Linde Company.

(9) D. Sinclair and V. K. La Mer, *Chem. Revs.*, **44**, 245 (1949).

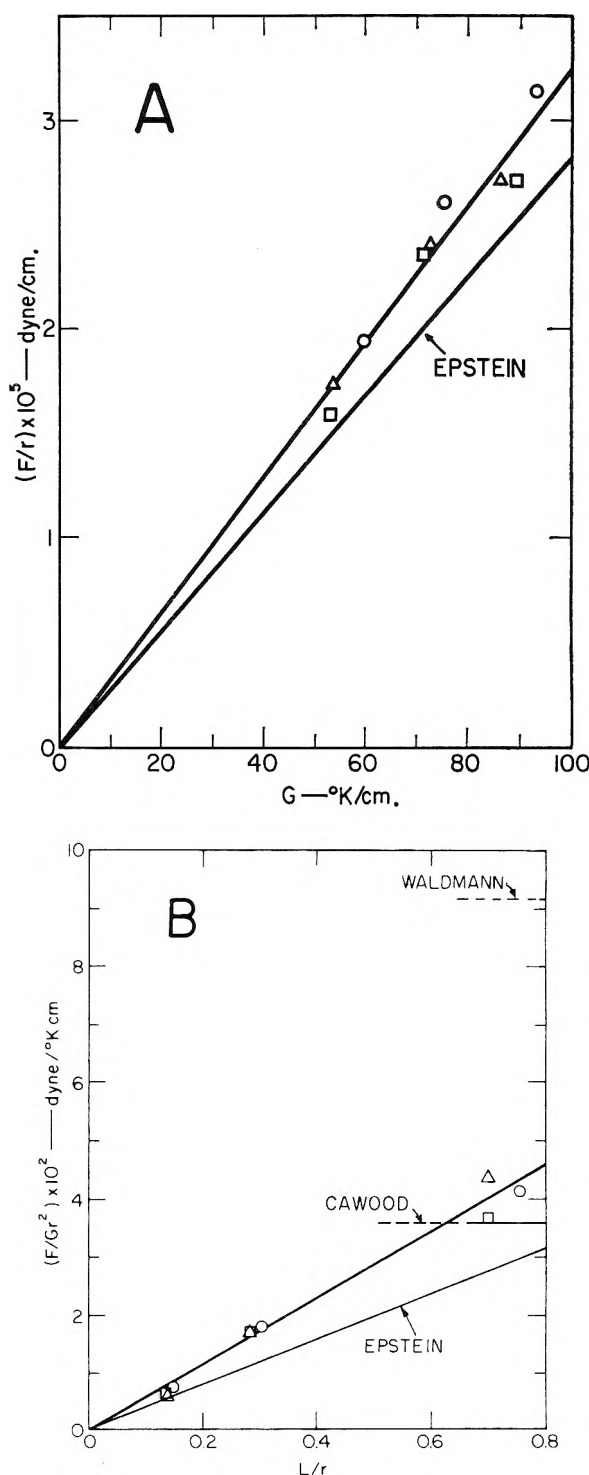


Fig. 1.—Tricresyl phosphate droplets. Radius of each droplet in μ : \odot , 0.46; \square , 0.49; \triangle , 0.49. A. Dependence of thermal force on thermal gradient and particle radius. B. The effect of the ratio of mean free path to particle radius. Average temperature was 307°K .

the particles might have a microcrystalline structure. This was ruled out by electron microscope pictures of samples of the particles which indicated that they were single crystals, mostly cubic, though not all perfect cubes, occasional particles being somewhat enlarged along one dimension, with some variations from perfect cube or rectangular solid

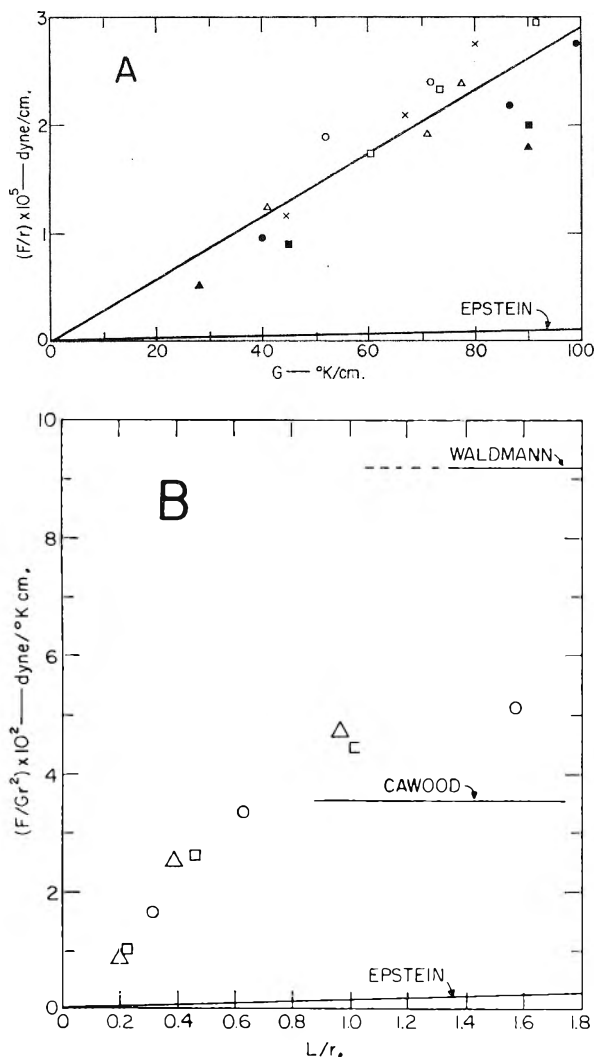


Fig. 2.—Sodium chloride particles, radius of each particle in μ :

No. 1	○	0.22 μ	No. 5	●	0.41 μ
No. 2	□	0.30 μ	No. 6	■	1.02 μ
No. 3	△	0.35 μ	No. 7	▲	1.15 μ
No. 4	×	0.40 μ			

A. Dependence of thermal force on thermal gradient and particle radius at atmospheric pressure. B. The effect of the ratio of mean free path to particle radius. Average temperature was 307°K .

shapes. This would certainly be expected to produce some scatter in results from a number of particles, and may explain some of the scatter observed. The second possibility is that the particles were actually drops of supersaturated salt solution while suspended in air. However, in an attempt to preclude this possibility, the majority of the particles were obtained by passing the aerosol through a bed of molecular sieve pellets to reduce the relative humidity of the air to a very low value. It seems very unlikely that supersaturated salt solution droplets could remain stable for the period of two or more hours required for measurements on each particle.

The fact that the sodium chloride particles are not spherical, although the particle size determinations, based on Stokes-Cunningham calculations from velocity of fall assumed they were, would in-

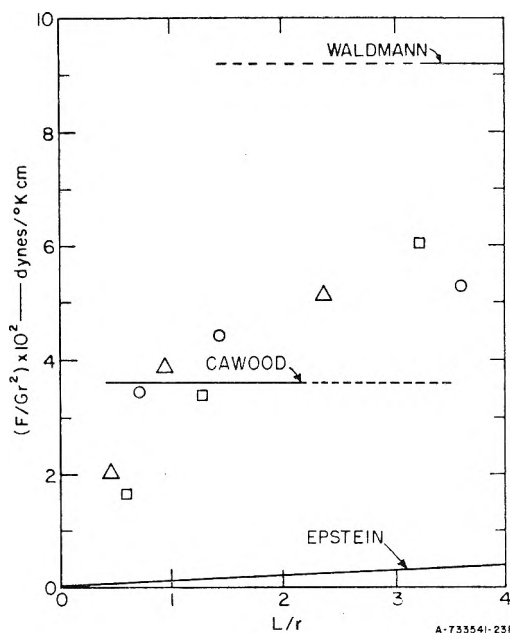


Fig. 3.—Mercury droplets: the effect of the ratio of mean free path to particle radius. Average temperature was 307°K . Radius of each droplet in μ : ○, 0.096; □, 0.115; △, 0.145.

produce error and some uncertainty as to the exact significance of the size measurements. This would not account for a discrepancy of a factor of 30.

To derive the Epstein theory for the case of a cube, for example, would be a very difficult problem and might be complicated by the need to consider tumbling of the particle. However, one would expect greater thermal stress along the surface near an edge or corner than could exist on a spherical particle. Thus one might qualitatively expect a higher thermal force on particles with sharp edges.

The droplets of mercury, which has a thermal conductivity of 2.8×10^{-2} cal./cm. sec. $^\circ\text{C}$., also behaved in agreement with the Epstein theory in the same sense as sodium chloride particles did, that is with regard to particle size, thermal gradient and density of gas. However, the thermal force was approximately 50 times the theoretical value. In fact the droplets behaved as if their thermal conductivity were about the same as that of TCP. This represents a difference by a factor of 50, which would be difficult to conceive of unless the droplets were composed largely of some material other than mercury, for example a very thick oxide coating. This seems unlikely as explained earlier in the section on experimental method.

For each of the materials some measurements of thermal force were made both by observing the velocity of a particle in a combined thermal and gravitational field, and by balancing the fields with a measured electrical field. The latter method generally yielded somewhat higher values of thermal force. This might be related to the contradictory boundary conditions assumed for thermal velocity. Or it might be explained by the moving particle disturbing the thermal field in the gas. An intermediate method also was used to measure thermal force on the largest sodium chloride parti-

cles because their weights were large relative to the thermal force. For several particles, velocity measurements were made both with and without the weight balanced out by an electrical field. The differences in velocities were fairly large. For the balanced (and thus lower velocity) cases, the thermal force values were somewhat greater. The same interpretations apply as for the completely balanced case.

For each of the three materials thermal force measurements were made at different pressures for the same particle. These results are plotted in Figs. 1B, 2B and 3 as F/r^2 versus L/r . The corresponding theoretical lines for Cawood's, Waldmann's, and Epstein's theories are included. The F/r^2 values increase with increasing L/r values, exceeding the Cawood theoretical value, and appear to approach the Waldmann theoretical values. The Cawood equation, though of different theoretical basis, happens to give values similar to those from the Waldmann equation. The largest L/r value, 3.6, was not large enough to determine where the curves level off, if at all.

In conclusion, the results confirm the earlier indication that the Epstein equation, although fairly satisfactory for particles of low thermal conductivity, is highly unsatisfactory for particles of high thermal conductivity. The results show that the thermal forces are relatively insensitive to thermal conductivity. The reason is not known. The Cawood equation is fairly satisfactory for particles about the same size as the mean free path of the gas, regardless of the thermal conductivity.

DISCUSSION

T. W. WILSON (Georgia Institute of Technology).—The validity of the experimental observations as a test of Epstein's equation seems questionable on the grounds that the characteristic Knudsen numbers are near unity. Particularly in the case of experiments with mercury, it is not certain that the requirements are fulfilled for a continuous fluid medium with respect to particle dimensions. It seems possible that the observations might be representative of the transition region where neither the Epstein nor Waldmann equation is expected to describe the force accurately. There is some experimental indication of this, e.g., as the particle size increases, the experimental force more nearly approaches that defined by Epstein's equation.

C. F. SCHADT.—It is true that the Epstein equation was developed for particles large relative to the mean free path. Therefore, one should consider the variation of F/Gr^2 with decreasing values of L/r . In Fig. 2B, within the limits of accuracy of the experimental data, the approach to the origin is linear as are the values predicted by the Epstein equation. This is true even if we include data from 2A, which to avoid confusion were not plotted in 2B and correspond to values of L/r as small as 0.057. Similar rough linearity to the origin seems to exist in Fig. 3 although the smallest value of L/r is only about 0.5. Certainly there is no suggestion of an approach to the Epstein equation for smaller values of L/r .

The results appear to validate previous work with a thermal precipitator (Ref. 3) in which values of L/r as small as about 0.066 were employed using carbonyl iron and no significant approach to the values predicted by the Epstein equation was observed. Thus it seems unlikely that the discrepancies between our data and the Epstein predictions are due to a transition region.

In Fig. 2A there does indeed appear to be a small tendency for the larger particles to be subjected to smaller thermal forces than the smaller particles for corresponding values of thermal gradient. However, even if this trend is significant, it is too small to suggest an approach of the thermal forces to those predicted by the Epstein equation.

M. KERKER (Clarkson College of Technology).—When we first made mercury aerosols, nucleated with oxides of mercury, our observation that these droplets were stable under a low intensity electron microscope beam led us to carry out the following experiment. Small mercury droplets were formed by shearing mercury between two glass microscope slides. These were collected upon electron microscope grids and examined without any further treatment. Rather than evaporate, they would increase in size, slightly, over a period of about 20 minutes exposure to the electron beam, presumably owing to accretion of contaminating material. An electron micrograph of such a droplet has been published (*J. Coll. Sci.*, 10, 413 (1955)).

W. D. ROSS (E. I. du Pont Co.)—Epstein used the temperature distribution parallel to the surface of the particle to calculate the thermal creep. The gradient results in more molecules, at lower velocity, striking a surface element from the quadrant at the lower temperature side than from the quadrant at the higher temperature side. The rebounding molecules are distributed in equal numbers and equal velocities into both quadrants. Maxwell's equation assumes that the temperature gradient does not change with distance perpendicularly to the surface.

In the present experiments, when $k_i \gg k_a$, and L is comparable with r , the gradient at a distance L from the surface is much greater than that at the surface. The temperature gradient which determines the creep is that which exists at a distance L_0 from the surface; this is the average distance of the start of all trajectories, weighted in proportion to the distance parallel to the surface, along the gradient, from the element. Measuring the trajectories in terms of polar angle θ from the normal to the surface

$$L_0 = \frac{L \int \sin^2 \theta \cos^2 \theta d\theta}{\int \sin^2 \theta \cos \theta d\theta} = 0.58L$$

Following Epstein's procedure to find the gradient at this distance from the surface, we find that his equation should be modified by replacing his term

$$(k_a/(2k_a + k_i))$$

with

$$\left[1 - \left(\frac{k_i - k_c}{k_i + 2k_a} \right) \left(\frac{r}{r + L_c} \right)^2 \right]$$

This greatly decreases the effect of k_i on F , in agreement with the findings of Schadt and Cadle.

C. F. SCHADT.—This represents basically a modification of the Maxwell theory of thermal creep, in which the creep velocity is calculated as before, except that $\partial T/\partial S$ is taken at a distance of L_0 from the surface of the particle. The comments apparently imply that this modification is intended to apply only to the case $L \approx r$. I am not sure of the exact meaning of L_c and whether it should depend on r . In order to make comparisons with our data, we have tacitly assumed $L_c = 0.58L$ for all values of L/r . The consequent modification of the Epstein equation results in rough agreement with the experimental data presented in our paper. The additional dependence on particle radius, $(r/r + L_c)^2$, not present in the Epstein equation, predicts a change in F/r (Fig. 2A, NaCl particles) of about fourfold between particles of radii 0.22 and 1.15 micron, which is considerably greater than the experimental difference of only about 50%. For TCP particles of 0.5 micron radius, it predicts roughly twice the experimental and Epstein values. These may not be unreasonable disagreements in view of the complexity of the phenomenon and the numerous approximations and assumptions involved in the theories. The term results in a very large change for large values of L/r and approximates the Epstein form if L/r is very small. It would be interesting to apply Ross' form to experimental data for considerably smaller L/r values than the minimum used in our work (namely, 0.057). However, I think it is questionable to expect the modified equation to apply to the transition region ($L \approx r$), as seems to be implied in Ross' comments. Further theoretical and experimental investigation of Ross' proposed modification seem worthwhile.

W. A. ZISMAN (U. S. Naval Research Laboratory).—Since the electrostatic field of force used in your experiments serves to balance the gravitational field acting on an oil drop, you should know the total field accurately. Have you

allowed for the contribution to that field from the volta potential difference between your two metal electrodes? This field is rarely zero; even between two pieces of like metals it can be significant. Magnitudes of 0.2 to 0.8 volt are common.

C. F. SCHATZ.—A copper-constantan thermocouple was imbedded in each brass block so that the temperature of each block could be measured independently, or by connection in series a difference temperature measured. At

zero temperature difference, switching between the "shorting" connection and the series thermocouple connection did not produce any obvious change in the motion of charged particles. The potentials required to balance different particles varied from about 5 to 200 volts, being about 20 to 70 volts for most particles. Thus, we conclude that possible volta potential differences (even as great as 1 volt) could not account for the lack of agreement with the Epstein theory, although they might account for some scatter of data.

FURTHER STUDIES ON THE SORPTION OF H₂O AND D₂O VAPORS BY LYSOZYME AND THE DEUTERIUM-HYDROGEN EXCHANGE EFFECT¹

WASYL S. HNOJEWYJ² AND LLOYD H. REYERSON

The School of Chemistry, University of Minnesota, Minneapolis 14, Minnesota

Received March 7, 1961

Isotherm data are reported for the sorption of H₂O and D₂O vapors by dry (lyophilized) lysozyme at 17, 27, 37 and 47° as well as for D₂O at 57°. A definite exchange effect was found at each of these temperatures but it was evident that a fraction of the hydrogens exchanged very slowly. The first isotherms, for both H₂O and D₂O, were determined at 17° and these were followed successively by measurement at 27, 37, 47 and 57° (for D₂O). At the conclusion of the experiments at the highest temperatures, new measurements were carried out by lowering the temperature 10°. The first isotherm then obtained at 37° gave results lower than those found previously at this temperature. Following desorption a repeat isotherm at 37° checked the values obtained before heating the protein to 47°. Similar results were found upon lowering the temperature to 27° and 17°. Thus carrying out a complete isotherm at higher temperatures followed by cooling of the protein results in a reduced capacity to adsorb H₂O and D₂O until the protein had adsorbed rather large amounts of vapors. Following such adsorption, successive isotherms check those originally found at a given temperature prior to an increase in temperature. This suggests that the protein undergoes structural changes as the temperature of sorption is increased. These changes are not reversible until the protein has adsorbed relatively large amounts of H₂O and D₂O.

Previous work in this Laboratory³ presented evidence that, upon completion of an adsorption-desorption isotherm of D₂O on lyophilized lysozyme, the protein had permanently gained weight. Upon completion of three such isotherms the protein had gained 1.37% by weight. The study, here reported, extended the previous work over a wider range of temperatures and much longer time periods. Additional sorption of D₂O by the protein, that had readily exchanged deuterium for labile hydrogen to give the 1.37% gain in weight, showed a very slow additional exchange at more than one temperature. The maximum gain in weight, following additional long-time adsorption-desorptions of D₂O, turned out to be about 1.6%. This suggests that about 15% of the labile hydrogens that finally exchange are present in the protein structure at sites that are only occasionally adsorbing D₂O in such a way that exchange takes place.

The present study began by a careful determination of an isotherm for H₂O vapor on lysozyme at 17°. Following a complete desorption, the weight of the protein was found to be unchanged. An adsorption-desorption at 27° showed, once again, that there had been no change in weight. However, similar determinations at 37 and 47° showed a small loss of weight. Repeated adsorption-desorptions at 37° showed a maximum loss of weight of 0.37%. At 47° a further small loss occurred and here, after many runs up to high relative vapor pressures, the total loss reached 0.609%. No

further loss occurred when the temperature was lowered. This protein then was used in all of the experiments reported here.

This loss of weight suggests that, in the case of enzymatic proteins, the method of preparation may leave traces of strongly adsorbed material which are only removed by adsorption-desorption of H₂O at the higher temperatures. The other possibility involves the loss of bound water but this does not seem likely, because once the protein had lost this weight, the final weight after desorption always remained the same at the end of each run no matter at what temperature the measurements were made.

Experimental

The experimental procedures essentially followed those previously reported.^{3,4} The sample of lysozyme used in this study came from the same larger batch that provided the material for the earlier work.³ The sample was weighed into the light glass bucket and suspended from a hook at the lower end of the quartz helical spring. After pumping at 10⁻⁶ mm. pressure for five days at 47°, the sample weighed 337.5 mg. Triply distilled H₂O and D₂O (99.5%) were subjected to a series of freezings and thawings while pumping down to a pressure of 10⁻⁶ mm. The quartz helix spring had a sensitivity of 25.215 mg./cm. and the cathetometer, having an accuracy of ± 0.015 mm., permitted precise measurements of the spring extension during sorption.

After the protein had sustained its maximum loss in weight during sorptions up to 47° it was cooled at 17°. Several adsorption-desorptions were carried out on it at this temperature with no further change in weight. Carefully determined isotherms, for H₂O on this protein, then were successively obtained at 17, 27, 37 and 47°. These were followed by several isotherms at 37°, then 27° and finally at 17°. In each case the protein weighed the same at the end of the desorption runs as it did at the beginning of the first of the whole series. Following these experiments with

(1) This study was supported by Research Grant No. H2972 from the National Institutes of Health.

(2) Research Associate, University of Minnesota.

(3) W. S. Hnojewyj and L. H. Reyerson, *J. Phys. Chem.*, **63**, 1653 (1959).

(4) L. H. Reyerson and W. Hnojewyj, *ibid.*, **64**, 811 (1960).

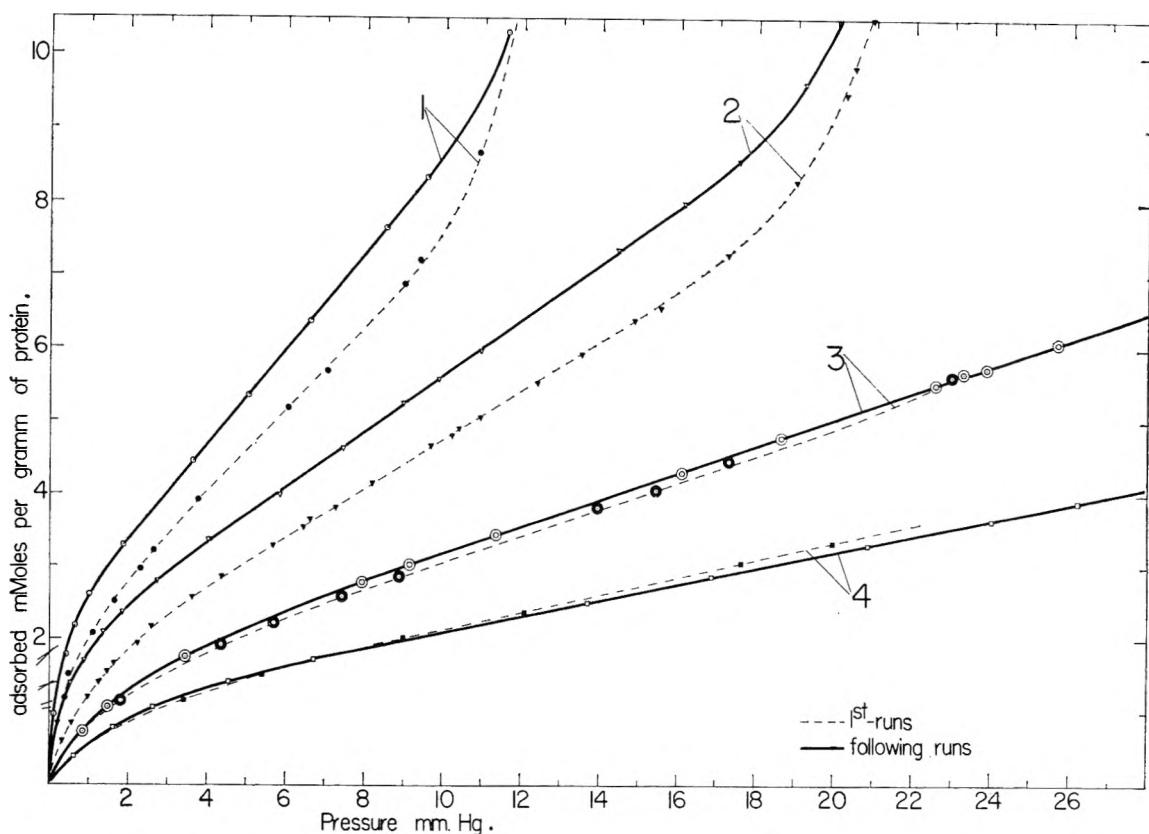


Fig. 1.—Adsorption isotherms of H₂O vapor upon the lysozyme at various temperatures: 1, at 17°; 2, at 27°; 3, at 37°; 4, at 47°.

H₂O vapor, D₂O vapor was adsorbed up to high relative pressures and then desorbed a sufficient number of times to complete the maximum exchange which amounts to a gain of 1.6% of the original weight of the protein. The final exchanges were carried out at 47°. This deuterated protein then was used as the adsorbent and isotherms for D₂O vapor, sorbed by the protein, were obtained at 17, 27, 37, 47, and 57°. After a repeat determination at 57° the temperature was lowered to 47° and at least three isotherms determined at this temperature. Similar determinations followed at 37°, then 27° and finally at 17°.

Results

As was stated, the lysozyme sample, used in this study and prior to the precise isotherm determination, lost a maximum of 0.609% of its original weight at 27° as a result of absorbing and then desorbing H₂O several times up to relatively high vapor pressures and at temperatures up to 47°. These weight losses appeared to have no effect on the amounts of water sorbed, since successive isotherms at a given temperature were essentially identical when referred to the initial weight at the beginning of each run. Figure 1 gives the adsorption isotherm values determined, at the four temperatures indicated, on the sample that had reached constant weight. The solid lines show the results obtained first at 17°, then at 27°, then 37° and finally at 47°. The protein was then slowly warmed to 57° and then cooled to 47°. The dashed line numbered 4, gives the results of the first adsorption isotherm run at 47°, following cooling to this temperature. A second complete isotherm, at 47°, coincided with the solid line isotherm obtained at this temperature before heating. Upon

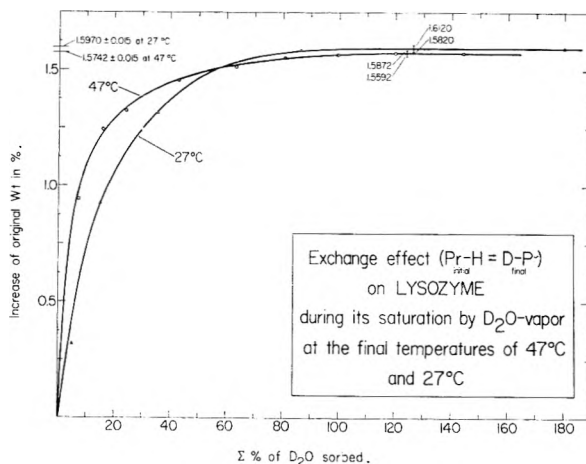


Fig. 2.

cooling the sample to 37°, the first isotherm values gave the results shown by the dashed curve labeled 3. The second isotherm run at 37° matched the isotherms obtained at this temperature before heating to 47° and coincides with the solid line labeled 3.

Similar results were found each time the temperature was lowered but differences between the first and succeeding runs at 27 and 17° exceeded those at 37 and 47°. It seems evident that this enzymatic protein loses some capacity to adsorb water vapor as it is heated. It only regains this capacity, upon cooling, after first adsorbing H₂O up to relatively high vapor pressures and then desorbing it.

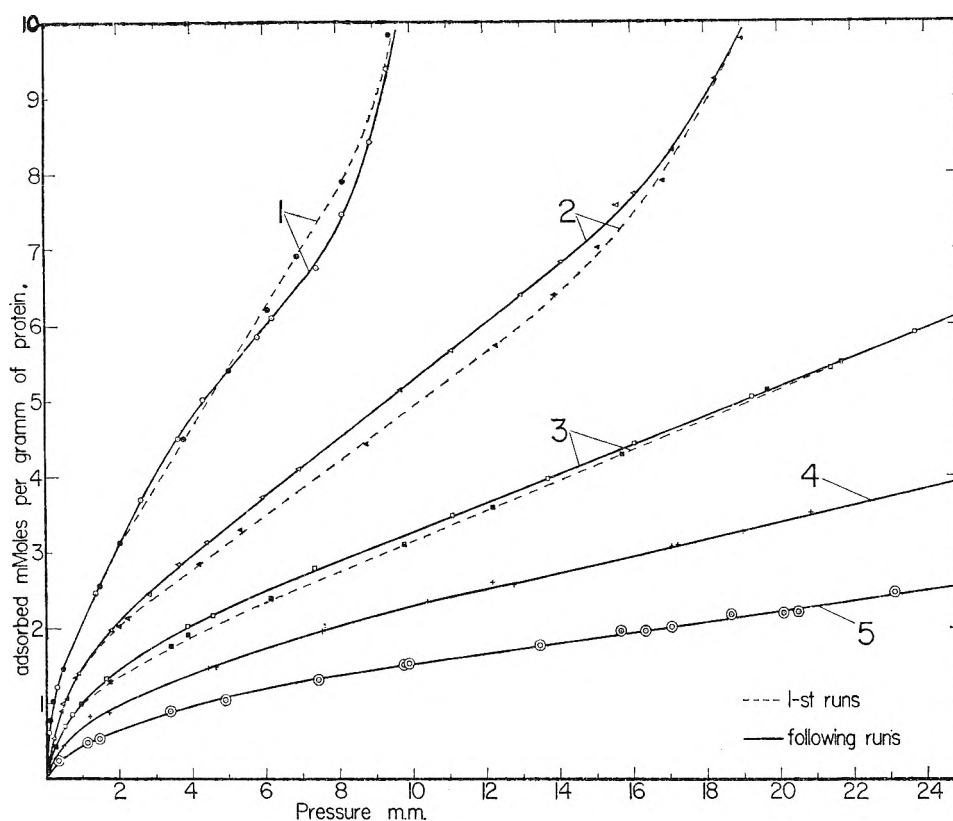


Fig. 3.—Adsorption isotherms of D_2O vapor upon the deuterized lysozyme at various temperatures: 1, at 17° ; 2, at 27° ; 3, at 37° ; 4, at 47° ; 5, at 57° .

The greater differences found between first and succeeding runs, after cooling to 27° and then to 17° , suggest that somewhat greater structural changes followed the warming from 17 to 27° and from 27 to 37° than occurred upon further heating. This may be due to greater adsorptive capacity at the lower temperatures but the isotherms do not indicate it.

Upon completing the isotherms for H_2O , the same sample was used to adsorb D_2O in order to exchange D for H on all exchangeable sites at 47° . In this work equilibrium between the protein and D_2O vapor was established at a given vapor pressure and the weight of adsorbed D_2O recorded. The sorbed D_2O then was desorbed completely and the increase in weight, due to deuterium exchange, determined. This partially deuterated protein was again exposed to pure (99.5%) D_2O vapor until it had adsorbed roughly the same amount of D_2O as before. The protein again showed a gain in weight due to exchange. Similar adsorption-desorptions followed until no further gain in weight was observed on long standing at rather high relative pressures. Figure 2 shows these results, the ordinate giving the percentage gain in weight of the protein as the result of successive adsorptions followed by desorptions. The abscissa gives the cumulative amounts of D_2O that were adsorbed successively and then desorbed to reach the maximum exchange. As shown in Fig. 2 the maximum gain in weight due to exchange turned out to be 1.59 to 1.61% of the original weight of the protein. This weight gain accounts for an actual exchange of slightly more than 90% of the hydrogens that are theoret-

ically exchangeable. Actually, if one takes a molecular weight value of $14,500 \pm 500$ for lysozyme together with the most recently accepted values⁵ for the number of each kind of amino acid residues present in the protein, it turns out that the maximum exchange found in this work is 91% of the theoretical. Thus 9% of the hydrogens that are present in the protein do not come in contact with adsorbed D_2O , even at high relative pressures, in a way that permits exchange.

The deuterated sample of the protein from the exchanges carried out at 47° was used to determine an isotherm for D_2O at the same temperatures and under the same conditions as had been carried out for H_2O on the undeuterated sample except that a complete isotherm was obtained at 57° . Figure 3 gives the results obtained for this complete set of experiments. Again the dashed lines show the first isotherm obtained after cooling the deuterated protein from 47 to 37° , then 37 to 27° and finally from 27 to 17° . Values from second runs at each of these three temperatures coincided with the original isotherm values found prior to each ten degree increase in temperature. It should be noted that the first runs that followed the lowering of the temperature differed less from the final equilibrium values than was the case for H_2O being adsorbed on the undeuterated sample. This suggests that the deuterated protein underwent smaller structural changes on heating than did the original protein.

In order to determine a possible effect of temperature on the exchange between the dry protein

(5) G. R. Tristram, *Advances in Protein Chem.*, **5**, 83 (1959).

and adsorbed D₂O, a second sample of lysozyme from the original batch was subjected to adsorption-desorption of H₂O until a constant weight was reached at 27°. Successive amounts of D₂O were adsorbed and then desorbed until maximum exchange had been reached at 27°. The results appear in Fig. 2 as the curve marked 27°. It is evident from these two exchange studies that the protein exchanges more D for H during the first three or four adsorption-desorptions of D₂O at 47° than at 27°. However, when the maximum exchange has been reached at the two temperatures, slightly more D remains a part of the protein at 27°. This difference is so slight that the highest of several experimental values at 47° overlaps the lowest value at 27°. Thus it may be said that deuterium, from D₂O, exchanges more easily at 47° during the early stages of the process but that at maximum exchange, the very slight difference, if any, favors the lower temperature. It should also be noted that if one extrapolates the straight line portions of the solid isotherms out to the vapor pressure of H₂O at the respective temperatures, then the intersections at all of these temperatures give approximately the same value for the amount of H₂O adsorbed. Furthermore this value again equals the amount of D₂O that must have been adsorbed for the total exchange.

From the data of the isotherms of Fig. 1 and 3, differential heats of adsorption were calculated by the Clausius-Clapeyron expression. These results are shown in Fig. 4 for H₂O and Fig. 5 for D₂O. The solid lines of Fig. 4 are determined from the well established, reproducible isotherms while the dashed curves are from the first runs following a lowering of the temperature by 10°. The calculated heats rise following initial adsorption and then fall as increasing amounts of H₂O are taken up by the protein. The ΔH values for the temperature interval 27-37° are far higher than for the other two ten-degree intervals. This suggests that there has been a larger structural change in the protein in this range and that the isotherm at 37° represents considerably lower amounts adsorbed than would have been the case if there had been no structural change. The next lower ΔH values (at least for amounts of H₂O adsorbed up to 2-3 moles per gram of protein) come from the isotherms at 17 and 27° but there is the same type of rise and then fall of the heat values. Structural changes probably start in this temperature range. Since the isotherms following each temperature lowering (dashed curves) indicate that the protein does not reverse its structural change until it has adsorbed relatively large amounts of water vapor, it is not surprising that the ΔH values determined from such isotherms tend to be different from those of the reproducible values. In the 17 to 27° interval, the heat values calculated from first runs (dashed curves) do not differ too much from those obtained from reproducible isotherms and this seems reasonable since the first run isotherms at each of these temperatures lie below the solid curves by about the same amount. Figure 5 gives the results of similar ΔH value calculations for the adsorption of D₂O by the deuterated protein.

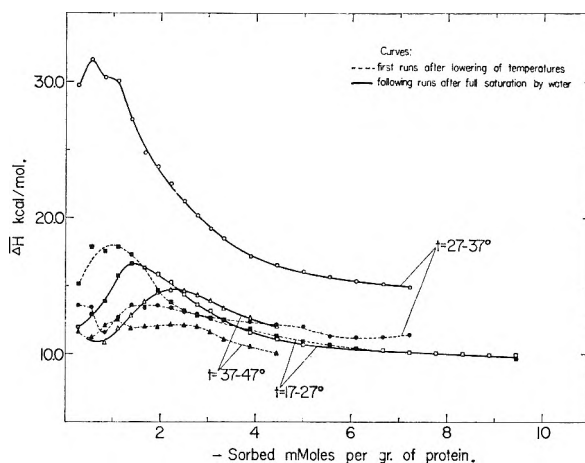


Fig. 4.—Heats of H₂O adsorption by dry lysozyme as functions of coverages and temperatures.

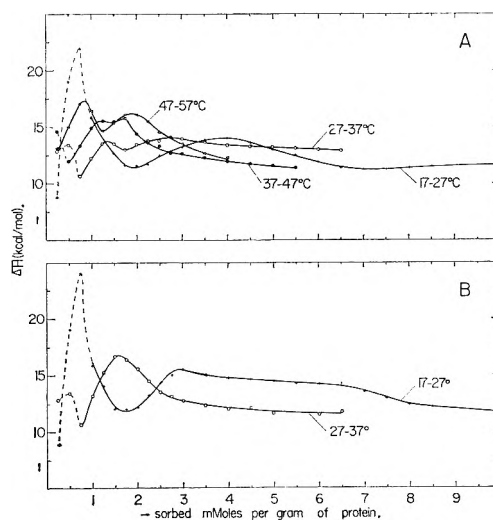


Fig. 5.—Heats of D₂O adsorption by dry deuterated lysozyme as a function of coverages and temperatures: A, determined from well established, reproducible isotherms; B, —, —, the first run isotherms, following a 10° lowering of temperature.

Since there is little difference between the reproducible adsorption values and the first runs, following a temperature lowering, the ΔH values from the two sets of isotherms ought to be similar. Examination of Sections A and B of this figure show considerable similarity. There is no single curve well above the others. The dashed parts of these curves represent values that are uncertain due to the difficulties involved in precisely determining the early adsorption values. As yet there is no explanation of the variation in the positions of the maxima in the heat values as calculated and shown in the graphs.

Conclusions

The results, here presented, strongly suggest that lysozyme before deuteration has quite an open structure when compared to β -lactoglobulin.⁴ This protein undergoes structural changes, perhaps a form of denaturation, in the temperature range studied. This form of denaturation holds, upon lowering the temperature, until the protein has adsorbed H₂O up to high relative pressures. It

then appears to relax and return to the structure that it had previously at this temperature. Upon deuteration the protein seems to be structurally more stable because it shows much smaller changes in adsorptive capacity than did the hydrogen protein when the temperature was raised and then

lowered. Lysozyme also shows that mono site coverage by water molecules as proved by deuterium exchange may be determined by extrapolating straight line portions of the isotherms out to the abscissa for the saturated vapor pressure at a given temperature.

THE EFFECT OF VAPORS ON MONOLAYER PERMEABILITY TO CARBON DIOXIDE*

BY MARTIN BLANK

Department of Physiology, College of Physicians and Surgeons, Columbia University, New York, N. Y.

Received March 7, 1961

Changes in the vapor pressure of water or methanol, which are present in the subphase, greatly affect the permeability of an octadecanol monolayer to carbon dioxide. Water vapor decreases the permeability while methanol vapor increases the permeability at low concentrations and decreases it at high concentrations. Both vapors are present in the monolayer as additional resistances to the passage of carbon dioxide but it is not known if the vapor is trapped or if the carbon dioxide-vapor collisions are more effective in a monolayer. The permeability of octadecanol to carbon dioxide appears to vary linearly with water vapor pressure so it is possible to extrapolate the values to a zero vapor pressure state. This result is compared with octadecanol permeability to water and the ratio of the permeabilities agrees approximately with a Boltzmann expression where the energy is the work that must be done by the gas to pass through the monolayer. Since this energy depends on the diameter of the penetrating molecule, the effect of molecular size appears to be an important factor in the energy barrier to penetration.

I. Introduction

Recent studies^{1,2} on monolayer permeability to several gases have indicated that water vapor is operationally present in the monolayer as an additional resistance. In brief, the supporting evidence is the following.

(a) The permeabilities of several monolayers to carbon dioxide, oxygen and nitrous oxide are approximately two orders of magnitude lower than the previously observed permeability to water vapor.³⁻⁵ These two measurements, however, do not relate to monolayers under the same conditions. When one measures the permeability of a monolayer to water, the system includes a monolayer on an aqueous subphase. In the experiments with other gases, the gases are always additional components since an aqueous subphase is always necessary for the existence of a monolayer. As a result, the water that must be in the monolayer, due to the equilibrium between the aqueous subphase and the gas phase, can act as an extra resistance to the passage of other gases.

(b) On raising the temperature, the large increase in monolayer permeability observed in the case of water is not observed for the other gases. The activation energies for the processes are about 15 kcal./mole for water, 1 kcal./mole for carbon dioxide and 2 kcal./mole for nitrous oxide. The explanation offered in line with the above hypothesis is that a rise in temperature has two opposing effects on the total process. First, it causes an increase in the kinetic energy of the penetrating mole-

cules and a decrease in the cohesion of the monolayer, both resulting in a sharp increase in permeability. (This is observed in the case of water vapor permeability.) However, the temperature rise also causes a rise in the vapor pressure of the water, increasing the amount of water operationally present in the monolayer during the penetration of carbon dioxide and nitrous oxide. The net result, a smaller change in permeability, has a magnitude that can be predicted² semi-quantitatively on the basis of the above assumptions.

(c) The permeability of monolayers on very concentrated solutions such as glycine buffers, hemoglobin solutions, etc., are much greater than on the more dilute solutions. This may be partly due to other factors but the more concentrated solutions also have lower vapor pressures which would give less of a resistance due to water vapor and, therefore, a greater permeability.

(d) Langmuir and Langmuir⁶ estimated the amount of water vapor present in a monolayer during a steady state evaporation process. Recalculation using newer data shows approximately the same concentration of water in the monolayer as in saturated air. This supports the idea that the amount of water operationally present in the monolayer can be given by the vapor pressure.

(e) The presence of water vapor in monolayers has been suggested as the cause of a peculiarity in another physical property, namely, the limiting area of molecules. On a surface it is about 10% greater than the cross sectional area of long straight hydrocarbon chain compounds in crystals. N. K. Adam⁷ stated that the water in the subphase causes a "... disruptive force antagonistic to the lateral adhesions between the long chains." He also suggested that "... it is probable that a

* This investigation was supported by a Senior Research Fellowship (SF-482) from the U. S. Public Health Service.

(1) M. Blank and F. J. W. Roughton, *Trans. Faraday Soc.*, **56**, 1832 (1960).

(2) M. Blank, A.C.S. Symposium "Transport Processes Through Monolayers," in press.

(3) R. J. Archer and V. K. La Mer, *J. Phys. Chem.*, **59**, 200 (1955).

(4) H. L. Rosano and V. K. La Mer, *ibid.*, **60**, 348 (1956).

(5) G. T. Barnes and V. K. La Mer, A.C.S. Symposium as in ref. 2.

(6) I. Langmuir and D. Langmuir, *J. Phys. Chem.*, **31**, 1719 (1927).

(7) N. K. Adam, "The Physics and Chemistry of Surfaces," Oxford, 1941, p. 52.

certain number of water molecules are entrapped among the film molecules . . .” Although the expansion of monolayers in a surface has been ascribed generally to the effect of bonding with the subphase, the above possibilities remain.

The hypothesis of water in a monolayer affecting permeability raises an important problem since foreign substances in monolayers have been shown to increase rather than decrease the permeability. Archer and La Mer³ found that benzene impurities greatly increased the permeability of a monolayer to water. Rosano and La Mer⁴ found that mixed monolayers always had lower resistances than the more impermeable monolayer. Extensive work by Robbins and La Mer⁵ showed that occluded solvent molecules disrupted the monolayer and their results correlated with water evaporation resistance measurements. Cook and Ries⁶ also showed the deleterious effects of several solvents on the low surface pressure region of stearic acid isotherms. These studies demonstrate that foreign substances in a monolayer have a disrupting effect that is accompanied by a greater permeability. However, there is a considerable difference between water vapor and the hydrocarbon molecules, such as benzene, that were studied and that are known to affect cohesion in monolayers.

In this paper the effect of water and methanol vapors on monolayer permeability will be determined. The results will be discussed in terms of the process of monolayer permeability and, specifically, the effect of molecular size on the energy barrier.

II. Experimental Results

To test the hypothesis outlined in the Introduction, octadecanol was used as the monolayer since it is relatively impermeable and, therefore, has a fairly large effect on the gas transport rate. Many physical properties of octadecanol monolayers have been investigated and the permeabilities to water vapor and several other gases are known. They have a further advantage in that the OH group is relatively insensitive to changes in the subphase, *e.g.*, octadecanol permeability is unaffected by subphase pH over a very wide range.

In the experiments, an excess of octadecanol was deposited from a spreading solution in 40–60° petroleum ether onto the surface of a carbon dioxide absorbing solution. The solvent was pumped away leaving an octadecanol monolayer at its maximum surface pressure and a small solid phase which was shown not to affect the gas absorption. This method ensured the deposition of a monolayer at a reproducible surface pressure in a cell which did not permit quantitative deposition.

The measurements involved the use of a temperature compensated differential manometer (described in detail in a previous publication¹) to detect the absorption of carbon dioxide at a monolayer free gas-solution interface and at an interface with an octadecanol monolayer. From the two rates, it was possible to calculate a permeability for the monolayer, assuming an initial steady state. This permeability is equivalent to that calculated in experiments on water evaporation.

Carbon dioxide was chosen as the gas since it has been studied fairly extensively in this system. The absorption, which is free from convection effects within rather wide limits of the rate, is easy to control by varying the pH of the absorbing solution since this does not affect the monolayer.

To see if one could vary the amount of water operationally present in the monolayer by varying the vapor pressure of the subphase, LiCl solutions at various concentrations were

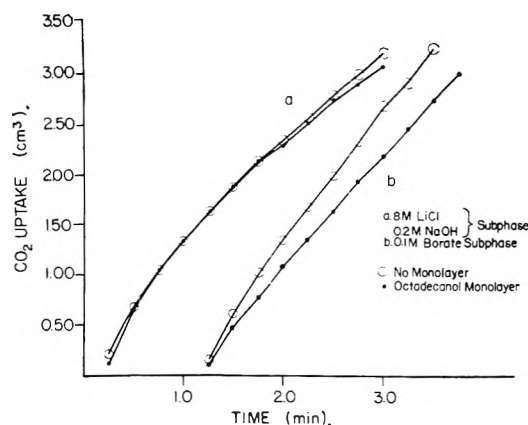


Fig. 1.—Absorption rate of carbon dioxide on two different subphases with and without octadecanol monolayers (25.0°).

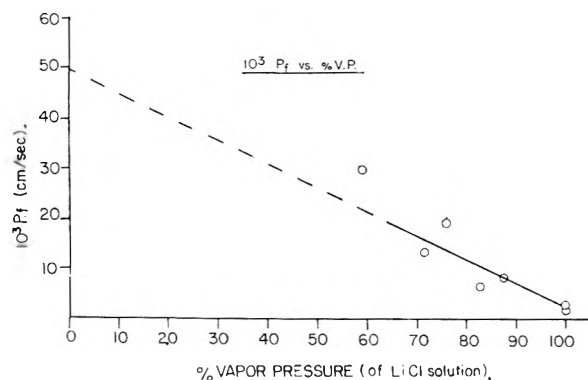


Fig. 2.—The measured monolayer permeability to carbon dioxide as a function of the subphase water vapor pressure (25.0°).

used. LiCl is among the most soluble salts and therefore gives a wide range of vapor pressure decrease. The water vapor pressure as a function of LiCl concentration is taken from the "Handbook of Chemistry and Physics." (The data are given for 100° but the fractional decreases in vapor pressure are independent of temperature.)

Figure 1 gives the uptake of carbon dioxide as a function of time for two subphases of differing vapor pressure. (Curves b are displaced by one minute from curves a to make the diagram clear.) The curves represent averages of at least three determinations and the individual points are good to about ± 2 to 3%. In the absence of LiCl, the vapor pressure is about the same as for 0.1 M solutions previously used to absorb the carbon dioxide, and it is possible to observe a large difference between a clean and an octadecanol covered interface. (See curves b for a borate subphase.) On the 8 M LiCl subphase shown in curves a, the data for the octadecanol monolayer and for the clean surface fit approximately on the same curve. This solution has a much lower vapor pressure and the data show a much greater permeability of the monolayer to carbon dioxide.

Experiments were done on a number of different subphases and Fig. 2 is a plot of the monolayer permeability (P_1) to carbon dioxide as a function of the % vapor pressure of the subphase (with pure water taken as equal to 100%). The graph shows that the permeability increases as the vapor pressure decreases and that the variation is approximately linear. The data have been extrapolated to zero vapor pressure to give a value of about 50×10^{-3} cm²/sec.

To examine the possibility that gases other than water vapor might have similar effects on the permeability of a monolayer to carbon dioxide, experiments were done with subphases of water-methanol mixtures. The method of varying the concentration of methanol in a monolayer by adding it to the spreading solvent leads to variations in concentration as a result of different degrees of evaporation, solution in subphase, diffusion rate in subphase, etc. With subphases of varying methanol concentrations, it is possible

(8) M. L. Robbins and V. K. La Mer, *J. Colloid Sci.*, **15**, 123 (1960).

(9) H. D. Cook and H. E. Ries, *J. Phys. Chem.*, **60**, 1533 (1956).

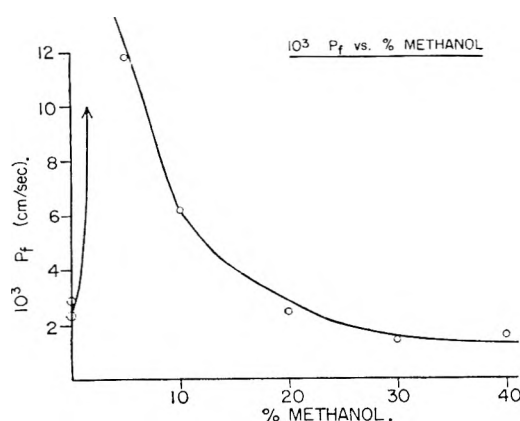


Fig. 3.—The measured monolayer permeability to carbon dioxide as a function of the concentration of methanol in the subphase (25.0°).

to know the equilibrium vapor pressure of the methanol and, therefore, the amount of methanol "in" the monolayer at all times. Methanol, which is somewhat similar to the hydrocarbons used as solvents in monolayer studies, is a simple molecule that is miscible with water in all proportions. The solutions exhibit a wide range of vapor pressures which are known over the complete range of mixtures.

The experiments on these subphases yielded the same type of raw data as are given in Fig. 1. The results for 5% methanol are similar to those for 8 *M* LiCl (curves a), and the data for 20% methanol are similar to those given for no LiCl in the subphase (curves b). From experiments with subphases of varying water methanol ratio, the permeability of octadecanol to carbon dioxide was calculated and these values are given in Fig. 3 as a function of methanol concentration in the subphase. The graph shows that the presence of small amounts of methanol in the monolayer increases the permeability very markedly. This parallels the results, mentioned earlier, of studies on water permeability where small amounts of molecules such as benzene greatly increase monolayer permeability. However, when one increases the vapor pressure of methanol, the monolayer becomes less permeable to carbon dioxide. Apparently, after one subtracts the initial disrupting effect of methanol on monolayer cohesion, increasing methanol concentration has the same effect as increasing water vapor concentration. When the vapor pressure of methanol is approximately equal to that of the water vapor, the monolayer permeability drops below its initial value, demonstrating that the blocking effect is not just a return to the initial value after the monolayer disruption but, rather, a definite decrease in permeability.

III. Discussion

A. The Effect of Vapors.—The observed decrease in monolayer permeability to carbon dioxide in the presence of water and methanol vapors is not a matter of simple collisions between the vapor and carbon dioxide because a comparison of the results obtained with octadecanol monolayers and those obtained in the absence of monolayers should keep the number of collisions constant. However, the monolayer may affect the number of collisions between the carbon dioxide and the vapor molecules in a non-specific manner. It also may trap some of the vapor molecules and, therefore, cause a change in the permeability.

Let us consider some changes in the pattern of molecular collisions that may occur as a result of the presence of a monolayer. For example, the point at which a vapor molecule enters the monolayer can become a preferred site for the entrance of another molecule, since the vapor has already done part of the work of pushing the monolayer chains apart. A carbon dioxide molecule may be

channeled into this "hole," thereby increasing the chances for collisions. Collisions also can be more effective if the monolayer chains act as intermediaries in collision processes. In other words, in cases where carbon dioxide and vapor molecules just avoid each other *in vacuo*, in a monolayer the carbon dioxide may collide with a CH₂ group which in turn collides with the vapor molecule. These effects may be considerable despite the small number of vapor molecules simultaneously present in the monolayer, since the turnover rate is very high.

Let us now consider the possibility that molecules of the vapor are trapped in the monolayer. One can ask why should the monolayer trap the vapor and not the carbon dioxide. If the carbon dioxide were trapped there would be a difference in the P_f depending on the partial pressure and this is not found over a tenfold range of pressure. Therefore, one also would have to explain specificity if the above explanation is used. Furthermore, a calculation of the number of water molecules present simultaneously in a monolayer, assuming the same concentration as in saturated air [see I(d) above], gives about one molecule to every 10⁴ monolayer molecules. The amount is negligible in terms of the ability to compress the monolayer and also in terms of the ability to act as a physical barrier. However, the idea of occlusion of vapor in the monolayer is supported to some extent by the data of Fig. 3. At low values of methanol vapor pressure the permeability of octadecanol is greatly enhanced, while at higher values the permeability decreases and one observes the blocking effects shown by water vapor. Considerable evidence favors the idea that an increase in permeability is associated with the occlusion of a foreign molecule in the monolayer. If there is occlusion at low vapor pressures, it seems equally possible at higher vapor pressures.

We, therefore, have two possibilities for explaining the extra resistance due to water or methanol vapors which involve either short (collision effects) or long (occlusion effects) lifetimes in the monolayer. In either case, there must be collisions between the carbon dioxide and the vapor (that is either transient or trapped), so collision effects is the simpler hypothesis and, therefore, the more desirable one.

The variation of P_f with water vapor pressure (Fig. 2) appears to be linear and the data have been treated as such. The independent variable, the % vapor pressure, can be replaced by the actual vapor pressure or the number of molecules per unit volume in the gas phase to give equivalent graphs. This shows that the value of P_f is proportional to the number of molecules of vapor in a unit volume of the gas phase and, presumably, in a unit volume of monolayer. Therefore, a reasonable explanation for the observed linear variation is that the decrease in permeability is due to collisions of carbon dioxide with the vapor and that the number of collisions varies linearly with the concentration of vapor, as in the case of binary collisions.

[Although this serves as a rationalization for the extrapolation to zero vapor pressure, the as-

sumed linearity of P_f has not been proven. In fact, the linear behavior has no meaning above 100% vapor pressure since P_f will approach but will not equal zero nor will it become negative as implied by the straight line. However, points above 100% vapor pressure cannot be obtained on water since one must raise the temperature which in and of itself increases P_f . If one adds a volatile substance such as methanol, the data (Fig. 3) do show a leveling off of P_f when the vapor pressure becomes very high. This may demonstrate a non-linear mechanism, but it may be relevant only at higher concentrations of vapor. In addition, these data are complicated by having both water and methanol vapors as well as a disrupting effect on the monolayer so they may not be relevant at all. However, if one considers the possibility that the originally proposed linear variation is not the case, then the extrapolated value may be higher.]

The value of P_f extrapolated to zero vapor pressure represents the P_f that would be obtained using a pure carbon dioxide gas phase. Since the most reliable points of Fig. 2 are those of lowest P_f , the extrapolation is made subject to error over and above that due to the scatter of the points and to the fact that they extend over only half of the range. Nevertheless, the trend of the points is clear and an error in the extrapolated value should not affect the qualitative conclusions to be drawn.

B. The Effect of Molecular Size.—The movement of gases through monolayers cannot be described as a classical diffusion process because the calculated diffusion coefficients vary with the monolayer thickness. However, the monolayer does impede the movement of the gas, and it is necessary to formulate the effect in some way. Langmuir and co-workers^{6,10} originally described the effect of a monolayer in terms of an extra energy barrier to the passage of gas. This has proved to be a fruitful approach and there have been many attempts to characterize the energy barrier by studying the effects of surface pressure, the chain length and nature of the polar group of monolayers, as well as the effect of temperature. Recently, Blank and La Mer¹¹ attempted to characterize the molecular processes involved during penetration by calculating the energy for the penetration, by water, of a single layer of CH_2 groups in fatty alcohol monolayers as a function of the separation of the CH_2 groups. They found a dependence on separation distance which indicates that the water molecule must compress the CH_2 groups against the repulsion forces. This is reasonable in close packed monolayers and it is also in line with Langmuir's original hypothesis of the energy barrier where a gas must do work against the surface pressure (the repulsive forces) of a monolayer.

Langmuir's formulation of the energy barrier was at near equilibrium conditions, where a Boltzmann factor gives the variation in the fraction (f) of molecules that can penetrate a monolayer in terms of extra energy (E) needed by the molecules. E can be evaluated in terms of monolayer proper-

ties by setting it equal to the work done by the gas (of cross-sectional area a_0) against the surface pressure (π) of the monolayer. Therefore

$$f = e^{-E/kT} = e^{-\pi a_0/kT} \quad (1)$$

where k = Boltzmann constant and T = absolute temperature. The rate of penetrating the monolayer is proportional to f , so equation 1 can be looked upon as (proportional to) a permeability and the inverse as a resistance.

Since the early studies were confined almost exclusively to water penetration, a_0 was constant and in succeeding papers it was neglected. Recent studies with several penetrating gases have made it possible to examine the applicability of equation 1 to the penetration process. The first results¹ on carbon dioxide permeability could not be compared directly to the water vapor permeability measurements since they were affected by the water vapor. However, the permeability extrapolated to zero water vapor pressure (50×10^{-3} cm./sec.) represents the permeability of a "water free" octadecanol monolayer to carbon dioxide and is comparable to the measurements of water permeability. Two values are in the literature for octadecanol permeability (at maximum surface pressure) to water. They are approximately^{4,5} 300×10^{-3} and 250×10^{-3} cm./sec. when converted to the same units. The ratio of P_f 's therefore is about 5-6 to 1, the monolayer being more permeable to water. The values of a_0 for water and carbon dioxide are not known accurately since they depend on the techniques used in their evaluation. One can get an approximate idea from data summarized by Moelwyn-Hughes,¹² which include effective radii and incompressible radii based on gas viscosity measurements and so constitute a fair range of values. Substituting values for the cross-sectional area as measured by the square of the radius, (into equation 1) one obtains a permeability ratio of about 3-6 to 1, the monolayer being more permeable to water.

This is a reasonable demonstration that the effect of molecular size can be predicted approximately from the equation originally proposed by Langmuir. The carbon dioxide values are the most reliable at the present time for this kind of test but data for nitrous oxide also indicate reasonable agreement. Nitrous oxide has approximately the same radius as carbon dioxide and octadecanol has approximately the same permeability to both gases. The available data for oxygen, which has the same permeability as carbon dioxide but a smaller radius, do not agree with equation 1. However, the statements about nitrous oxide and oxygen assume that the interference due to water vapor has the same effect as in the case of carbon dioxide. This assumption is not valid in the case of oxygen if the interference effects are due to collisions with transient or occluded water vapor. Carbon dioxide and nitrous oxide have the same molecular weight but oxygen is considerably lighter and, therefore, makes many more collisions at the same pressure. The greater number of collisions

(10) I. Langmuir and V. J. Schaefer, *J. Franklin Inst.*, **235**, 119 (1943).

(11) M. Blank and V. K. La Mer, A.C.S. Symposium as in ref. 2.

(12) E. A. Moelwyn-Hughes, "Physical Chemistry," Pergamon 1957, p. 597.

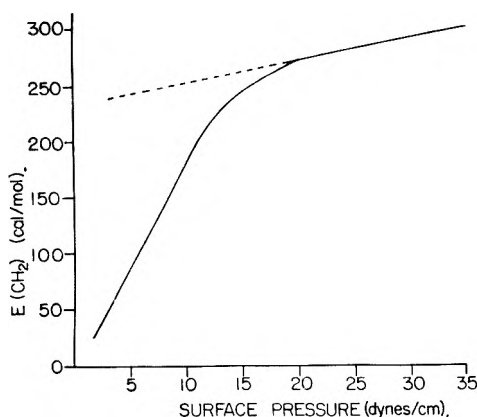


Fig. 4.—The calculated energy for water penetrating a layer of CH_2 groups (in fatty alcohol monolayers) as a function of the surface pressure (25.0°).

would cause greater interference, hence a higher permeability on extrapolation to zero pressure and the possibility of agreement with equation 1. Therefore, the generality of equation 1 with regard to the dependence of the permeability on molecular size of penetrating molecule is still to be demonstrated but it does seem to apply to the available data. It might be added in passing that dependence of the rate on the size of the penetrating molecule makes the monolayer permselective (*i.e.*, it endows the monolayer with functional "pores").

In addition to predicting an effect due to molecular size, equation 1 predicts that the logarithm of the permeability or the resistance (τ) should vary linearly with the surface pressure. This has been observed in some cases. Archer and La Mer³ showed this for the S phase of fatty acids. Rosano and La Mer⁴ and Barnes and La Mer⁵ have given data for the high pressure phases of fatty alcohols which agree approximately with the prediction. Blank and La Mer¹¹ showed that the value of E for penetrating a CH_2 group, $E(\text{CH}_2)$, in the high pressure region of fatty alcohols is approximately linear with π (see Fig. 4). (This condition is equivalent to $\ln \tau$ being proportional π .) In these cases of agreement as to functional dependence, the proportionality constant leads to variable values of a_0 that are about an order of magnitude too small and that, therefore, indicate a lack of quantitative agreement. There are many cases where even the qualitative dependence of the permeability on π is not as predicted, so that equation 1 cannot be a general statement of the energy barrier. Equation 1 appears to be but one of the factors in the energy barrier and one can expect agreement only under conditions that will become evident upon examination of the energy barrier as a whole.

C. The Energy Barrier to Monolayer Penetration.—Aside from the molecular size factor given in equation 1, Langmuir¹⁰ found the need for a monolayer chain length term. Archer and La Mer³ found that each CH_2 group in an LC phase fatty acid monolayer contributes about 300 cal./mole to the energy barrier for water penetration. The magnitude of the contribution is π independent, but in the S phase, where it is also π independent, the magnitude is about 200 cal./mole. Blank²

found that for the penetration of carbon dioxide, oxygen and nitrous oxide, about 350 cal./mole were added per CH_2 group. It was not possible to check the π dependence here but Blank and La Mer¹¹ showed that the contribution per CH_2 group can be π dependent. Figure 4 shows that $E(\text{CH}_2)$ varies with π in fatty alcohol monolayers and that the variation can explain the three different values quoted as being due to different states of monolayer packing. The π dependence of the monolayer chain length factor can account for the inability to determine the correct value of a_0 from the $\ln \tau$ vs. π data and it also points up the complexity of π as a variable in penetration experiments.

There are other factors that enter into the energy barrier since monolayers of the same length (number of CH_2 groups) and at the same π do not have equal permeabilities to the same penetrating species. Rosano and La Mer⁴ found that incompressible monolayers are far less permeable than compressible ones, but compressibility *per se* does not determine permeability. Cholesterol monolayers are relatively incompressible and the surface pressure can exceed 40 dynes/cm., yet these films have little or no effect on the passage of gases. Since the saturated straight chain compounds are the least permeable, the important factor that appears to be significant is the effect of the structure of the polar and hydrocarbon parts of the molecule on the ability to pack in an interface. (The polar group is also important in causing an orientation of water molecules in the liquid, which should affect the permeability of a monolayer as well as its stability.) This factor, which can be called intrinsic to the monolayer type, may also be π dependent, especially if the molecule can be easily deformed upon compression.

It is possible to summarize our knowledge of the energy barrier by combining the various factors that have been discussed.

$$E = f[K(\pi), l(\pi), \pi a_0] \quad (2)$$

where $K(\pi)$ is the intrinsic factor, $l(\pi)$ is the chain length factor and πa_0 has been given in equation 1. By using the same gas so that πa_0 is constant and by using a homologous series so that $K(\pi)$ is constant, it has been possible to determine $l(\pi)$. In this paper, $K(\pi)$ and $l(\pi)$ were kept constant so that the πa_0 dependence could be investigated. For these and other reasons E has been broken up into a number of factors even though the surface pressure, monolayer chain length and packing are all inter-related. As a matter of fact, $l(\pi)$ definitely varies with the monolayer state³ so it probably would be more meaningful to lump $K(\pi)$ and $l(\pi)$ together as a monolayer factor [that is distinct from πa_0 which depends on the gas that is penetrating]. If E , as in equation 2 or as modified by combining $K(\pi)$ and $l(\pi)$ in a single term, is substituted into equation 1, the effects of the above variables on the penetration rate become apparent and one also sees the framework for considering the temperature dependence.

Aside from the interfering effects of water vapor, there is a further complication in the analysis of the permeability that is due to the possibility of hydration of the gas in the aqueous phase. Hawke and

Alexander¹³ determined monolayer permeability to carbon dioxide and hydrogen sulfide where the gas moved from the aqueous phase to the gas phase. In the cases where the systems were the same as those studied by the author's technique, the results agreed as to order of magnitude but the permeabilities were always lower. Furthermore, the values for hydrogen sulfide were lower still. Carbon dioxide and hydrogen sulfide have approximately equal diameters¹² so that all the factors in equation 2 are approximately equal. However, if one considers that there can be some penetration as a hydrated species thus increasing a_0 , or what seems more likely, that there is an additional restraining step due to the need for dehydration before the gas can penetrate, then one can account for the differences observed. The Bunsen coefficient would be a measure of the affinity for water and, since the value is about three times higher for hydrogen sulfide (than for carbon dioxide), it would have less of a tendency to dehydrate. Therefore, hydrogen sulfide would pass through more slowly and carbon dioxide would pass more slowly from the aqueous phase than from the gas phase. There are many data available for the penetration of plasma membranes (which are

(13) J. G. Hawke and A. E. Alexander, A.C.S. Symposium as in ref. 2.

bimolecular layers about 75 Å. thick) that can be explained on the basis of a process measured by the partition coefficient. This would support the above explanation and account for the differences observed.

DISCUSSION

A. S. MICHAELS (Massachusetts Institute of Technology).—Is there any possibility that convective processes (created by temperature, density, or surface tension gradients) in the liquid film in the absence of a deposited monolayer are eliminated in the presence of a monolayer, thereby increasing the persistence to mass transfer independent of any specific barrier action of the monolayer itself?

M. BLANK.—This question has been considered (ref. 1) and it seems unlikely that convective processes play a role in the systems studied. In brief, the reasons are:

1. Calculations of the absorption rate when no monolayer is present (assuming a liquid diffusion limited process) coincide with the observed rate data. This indicates that there are no convective processes during absorption in the absence of monolayers. The reason for this may be that the increase in temperature due to heats of solution and reaction cancels the effect of an increase in density due to mass absorption. The absence of convection may also be due to the relatively short times of the experiments.

2. Certain monolayers offer no measurable diffusion barrier but nevertheless affect the transfer across interfaces in stirred systems by interfering with convective processes near the interface. Bovine serum albumin and cholesterol are examples of these substances and they were found to have no effect on the transport of gases.

MECHANISM OF THE SELECTIVE FLUX OF SALTS AND WATER MIGRATION THROUGH NON-AQUEOUS LIQUID MEMBRANES

BY HENRI L. ROSANO, PAUL DUBY AND JACK H. SCHULMAN

Stanley-Thompson Laboratory, Henry Krumb School of Mines, Columbia University, New York 27, New York

Received March 9, 1961

The mechanism of migration of different salts through different non-aqueous liquid membranes has been studied under varying conditions. It has been demonstrated that a rate-controlling step is not diffusion in either the aqueous or organic phase but is governed by the migration through the interface. The energies of activation for NaCl and KCl migrating through 1-butanol have been found to be 6 and 5.2 kcal., respectively. Electrical potential measurements across the non-aqueous liquid membrane show that K^+ ions migrate more easily than Na^+ ions through the oil-water interface which agrees with the activation energy values. Finally the water migration across non-aqueous liquid membranes has been investigated

In previously published papers^{1,2} it has been shown that valuable information about the diffusion mechanism through living cell membranes can be derived by studying the selective flux of various salts through non-aqueous liquid membranes. The diffusion of different salts through different oil layers has been studied under varying conditions. This phenomenon was called diffusion transport. In the presence of an amphoterie phospholipid (carrier) in the oil-membrane interface, the transport is markedly increased when salts are opposed; this phenomena was called carrier transport. This carrier transport functions also when the diffusion process has been blocked.

In the present paper, the study of the laws of these phenomena with more emphasis on the diffusion transport is made. This effect is present in any membrane and it is worthwhile to determine the parameters on which it depends before the study of the carrier transport.

Baniel³ has investigated the transfer of water between aqueous systems by a partially miscible solvent, in view of its industrial application as a dehydration process. The transport of water and the kinetics of this transfer can be described, and consequently predicted, in the same way as the transport of the salts.

From the order of magnitude of the observed diffusion rates, it will be shown that the rate-controlling step is not diffusion in either the aqueous or organic phase, as it is usually assumed, but is governed by the migration through the interface. It is shown that the kinetics of the transport can be described by considering only the differential flux in terms of chemistry of the salts with the different phases.

Experimental

Diffusion and Carrier Transport.—The apparatus consisted essentially of polystyrene boxes with covers placed in a constant temperature bath, 30° for most of the experiments. Each box was divided into two, with a thick (0.5 cm.) partition. Into each compartment an aqueous solution of 350 cc. was placed, leaving approximately 0.8 cm. free barrier between the two aqueous solutions. Over the two compartments 300 cc. of a non-aqueous liquid membrane was placed, permitting transfer of ions and salts from one aqueous system to the other *only* through the "oil" phase. The "oil"

phase membrane was approximately 2.0 cm. thick and was stirred at constant speed by a motor stirrer. The oil-water interfacial area in each compartment was 83.7 cm.². Influence of the above described variables on the migration was tried out, and except for the temperature, no radical effects were observed in the rates of salt or ion transports.

Water Migration.—A 600-cc. glass container with a glass divider 5.5 cm. high was used for studying the water diffusion through permeable oil membranes. Two side tubes allowed the change in height of the two oil-water interfaces to be measured. Each cell compartment contained 100 cc. of an aqueous solution and 250 cc. of an "oil" membrane floating over the two compartments. The glass container was thermostated at 30°. A Gaertner precision cathetometer was used for measuring the difference between the two oil-water interface levels as a function of time.

Electrical Potential Measurements.—Electric potentials across the oil membrane were measured by using two KCl bridges in the two aqueous compartments of the diffusion cell and by using two reversible calomel electrodes connected to a Keithley 610A electrometer allowing 0.2 mv. precision.

Partition Coefficient Measurements.—One hundred and forty ml. of the salt solution presaturated with the alcohol to be studied was vigorously agitated with 150 ml. of the alcohol presaturated with distilled water. The system was maintained several hours in a thermostated water-bath. After complete separation of the phases 100 ml. of the alcohol phase was removed and evaporated to dryness and the residue was re-dissolved in 10 cc. of distilled water. An analysis of this solution was performed on a Process and Instrument flame photometer by using an internal standard method. Next, the partition coefficient was calculated.

Theoretical

The experiment is equivalent to a system consisting of two aqueous phases separated by an oil layer.

The transport of salt from compartment A to compartment B consists of the following steps: (a) diffusion through a variable concentration layer at the interphase I; (b) transport across the interface I; (c) diffusion through a variable concentration layer at the interphase of the oil phase; (d) same as c; (e) transport across the interface II; (f) same as a. Since good mechanical stirring was given in all the three phases, bulk diffusion can be considered as a fast step.

Fick's law gives for the flux density $F = D \times \text{grad } C$ where D is the diffusion coefficient and C the concentration of the diffusing species. D is of the order of 10^{-5} cm.²/sec. in most liquid systems.⁴ In these experiments, because of stirring, the diffusion layers are very thin, and have been experimentally estimated to be approximately 30μ .⁵

Experimentally, it has been shown that the salt

(1) J. H. Schulman and H. L. Rosano, in a Monograph on "Transport Processes through Monolayers," in publication Academic Press, New York, N. Y., 1961; 3rd Int. Congr. Surface Activity, Cologne, 1960. Vol. II, p. 112.

(2) H. L. Rosano, J. H. Schulman and J. B. Weisbuch, *Ann. N. Y. Acad. Sci.*, **92**, art. 2 (1961).

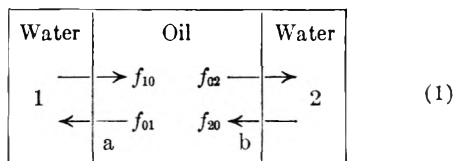
(3) A. Baniel, *J. Appl. Chem.*, **9**, 521 (1959).

(4) S. Glasstone, K. J. Laidler and H. Eyring, "The Theory of Rate Processes," McGraw-Hill Book Co., New York, N. Y., 1941, pp. 526-527.

(5) J. H. Schulman and T. Teorell, *Trans. Faraday Soc.*, **34**, 1338 (1938).

concentration, in 1-BuOH for example, is smaller than 1 mM/l. for a starting 50 mM/l. concentration in the aqueous compartment. The difference in salt concentration on each side of the interfacial zone (49 mM/l.) can be considered as: (a) slow drop in salt concentration in the quiet aqueous interfacial zone; (b) a sharp drop at the very interface; (c) another slow drop in the quiet "oil" phase. Since the partition coefficient for NaCl and KCl at 30° for 1-BuOH is 1.8×10^{-2} , this indicates that the drop of the salt concentration at the very interface for a 50 mM/l. salt concentration is at least 49.1 mM/l. Then a reasonable estimate of the maximum drop in concentration in each quiet layer is of the order of 0.9 mM/l. Consequently, the concentration gradient which is the driving force in Fick's law mechanism is 0.9 mM/l. per 30 μ . The resulting flux is $10^{-5} \times 0.9 \times 10^{-3} \times 3600/30 \times 10^{-4} = 10.3 \times 10^{-3}$ mM/cm.²/hr. The actual rate observed for KCl is 1.1×10^{-3} mM/cm.²/hr. which is much smaller than the above estimation. Consequently, the diffusion in these concentration interphase layers is not the rate determining factor. The determining step is the flux across the interface and not a diffusion along a concentration gradient according to Fick's law.

The system consists of two aqueous phases separated by an oil layer.



Let us now define: a and b, the two interphases separating, respectively, the oil from aqueous phases (1) and (2). The following notations are

- V_1, V_2, V_0 , volumes of the three phases (in l.)
- C_1, C_2, C_0 , concn. of the salt in the three phases (mM/l.)
- $f_{10}, f_{01}, f_{20}, f_{02}$, flux densities of salt through the interface
- Φ , resulting flux
- A , area of the interphase (equal for a and b)
- P_{ow} , partition coefficient of the salt between oil and water
- k_{ow}, k_{wo} , rate constants of the salt exchange reaction between oil-water and water-oil
- R , gas constant
- T , absolute temperature
- T_m , average mean temperature
- t , time

Mathematical Description of Salt Diffusion through a Non-aqueous Liquid Membrane.— It can be stated:

$$\begin{aligned} f_{10} &= k_{wo}C_1 & f_{01} &= k_{ow}C_0 \\ f_{20} &= k_{wo}C_2 & f_{02} &= k_{ow}C_0 \end{aligned} \quad (2)$$

at equilibrium: $f_{10} = f_{01}$ or

$$\frac{(C_0)_{eq}}{(C_1)_{eq}} = \frac{k_{wo}}{k_{ow}} = P_{ow} \quad (3)$$

When transport proceeds, a steady state is rapidly reached, and the salt concentration in the oil remains approximately constant. The follow-

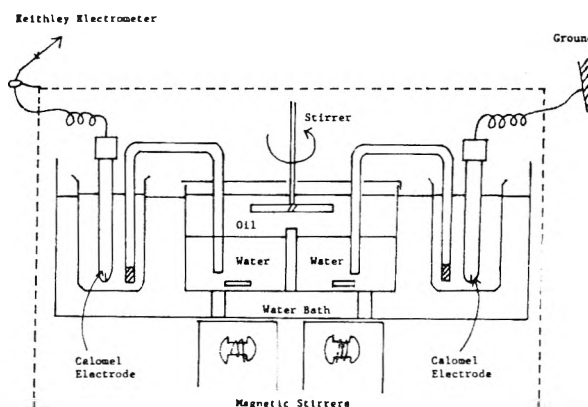


Fig. 1.—Transport cell.

ing equation expresses the equality of the resulting fluxes through the two membranes a and b

$$f_{10} - f_{01} = f_{02} - f_{20} = \frac{\Phi}{A} \quad (4)$$

or

$$k_{wo}C_1 - k_{ow}C_0 = k_{ow}C_0 - k_{wo}C_2 = \frac{\Phi}{A}$$

from which

$$C_0 = \frac{1}{2} \frac{k_{wo}}{k_{ow}} (C_1 + C_2) = \frac{P_{ow}}{2} (C_1 + C_2) \quad (5)$$

and the flux is

$$\Phi = A \frac{k_{ow} P_{ow}}{2} (C_1 - C_2) = A \frac{k_{wo}}{2} (C_1 - C_2) \quad (6)$$

Equation 6 is slightly different from the equation quoted by Teorell⁶; $\Phi = Ak(PC_1 - C_2)$, where k is rate constant and P , the partition coefficient. The disagreement between equation 6 and the one proposed by Teorell derive from the fact that the two interfaces have been considered here.

For the small temperature range of the experiments, it can be assumed that enthalpy and entropy corresponding to the free energy of activation are constant and the rate constant k_{ow} can be expressed by the Arrhenius equation

$$k_{ow} = ke^{-Q/RT} \quad (7)$$

The change of concentration as a function of time is

$$\Phi = \frac{d(V_2C_2)}{dt} = - \frac{d(V_1C_1)}{dt} \quad (8)$$

From equations 8 and 6, for $V_1 = V_2$

$$\frac{dC_2}{dt} = \frac{A}{V_1} \frac{k_{ow} P_{ow}}{2} (C_1 - C_2) \quad (9)$$

experimentally, the salt concentration in the alcohol is constant and small. The total amount of salt is constant and equal to the initial quantity.

$$V_1(C_1 + C_2) + V_0C_0 = \text{constant} = V_1C_1 \text{ initial} \quad (10)$$

from (5)

$$V_1(C_1 + C_2) + \frac{P_{ow} V_0}{2} (C_1 + C_2) = V_1C_1 \text{ initial}$$

and

$$C_1 + C_2 = \frac{V_1}{V_1 + \frac{P_{ow} V_0}{2}} C_1 \text{ initial} = C_1^* \quad (11)$$

(6) T. Teorell, *Discussions Faraday Soc.*, **21**, 9 (1956).

TABLE I

Salt	Initial concn., mM/l.	Alcohol	Slope, hr. ⁻¹	k_{ow} , cm. hr. ⁻¹	P_{ow}	k_{ow} , cm. hr. ⁻¹
KCl opposed to NaCl	50	1-BuOH	6.5×10^{-3}	0.027	1.8×10^{-2}	1.5
KCl opposed to LiCl	50	1-BuOH	6.3×10^{-3}	.026	1.8×10^{-2}	1.45
KCl opposed to Ca(NO ₃) ₂	50	1-BuOH	6.7×10^{-3}	.028	1.8×10^{-2}	1.55
KCl opposed to Ca(NO ₃) ₂	1000	1-BuOH	6.5×10^{-3}	.027	1.6×10^{-2}	1.7
KCl opposed to HCl	50	1-BuOH	4.5×10^{-3}	.019	1.0×10^{-2}	1.9
NaCl opposed to KCl	50	1-BuOH	5.5×10^{-3}	.023	1.8×10^{-2}	1.28
NaCl opposed to KCl	50	2-BuOH	2.4×10^{-3}	.10	6.4×10^{-2}	1.55

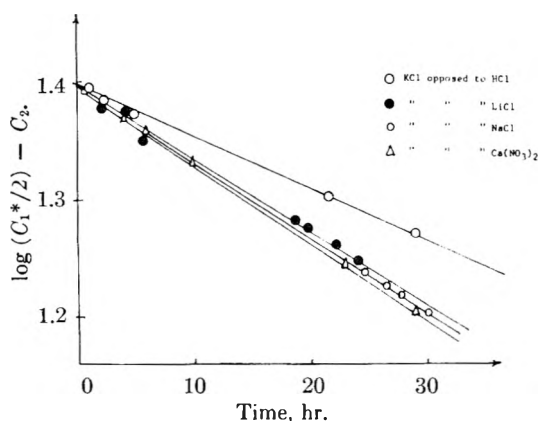


Fig. 2.—Logarithmic representation of the diffusion of 50 mM/l. of KCl opposed to 50 mM/l. of various salts through 1-butanol at 30°.

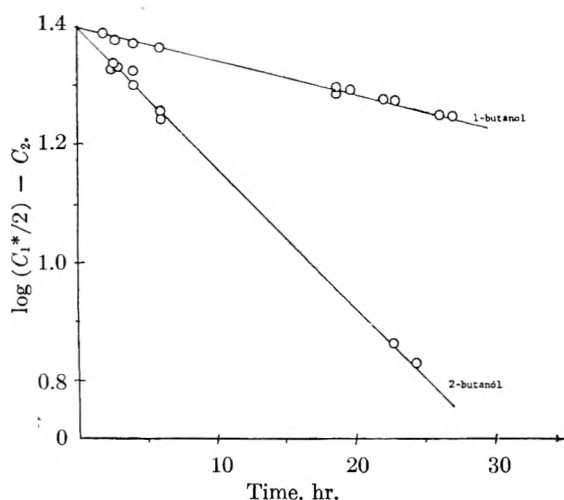


Fig. 3.—Logarithmic representation of the diffusion of 50 mM/l. of NaCl opposed to M/20 HCl through 1-butanol and 2-butanol.

When P_{ow} is small, C^* is close to the initial concentration in compartment 1. From equations 9 and 11

$$\frac{dC_2}{dt} = \frac{A}{V_1} \frac{k_{ow} P_{ow}}{2} [C_1^* - 2C_2] \quad (12)$$

For the initial condition $t = 0$, $C_2 = 0$, then

$$C_2 = \frac{C_1^*}{2} (1 - e^{-(A/V_1)k_{ow} P_{ow} t}) \quad (13)$$

By plotting the experimental results on a semi-logarithmic graph experimental values of $k_{ow}P_{ow}$ are obtained.

Results

Diffusion Transport.—The diffusion transport

results can be plotted according to equation 13. Figure 2 represents the diffusion of KCl opposed to NaCl and HCl and Ca(NO₃)₂ and Fig. 3 represents the Na ion diffusing through various alkyl alcohols. Table I summarizes the partition coefficient, the slope, and the resulting rate constant for the various diffusion experiments.

Activation Energy.—The diffusion transport of NaCl and KCl through 1-butanol at different temperatures has been carried out. The partition coefficients of NaCl and KCl as a function of temperature were determined. It was found that they are constant in the range 17 to 45°. It was also observed for both KCl and NaCl that the partition coefficient decreases slightly while the salt concentration increases. From the results of the diffusion transport at various temperatures and the partition coefficients, the rate constants were determined. According to equation 7 by plotting $\ln k$ vs. $1/T$ we calculate the following activation energies values

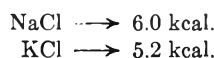


Figure 4 gives the results.

Electrical Potentials.—The electrical potential measured across the non-aqueous membrane varies linearly with the logarithm of the salt concentration ratio. No electrical potential was measured when the two bridges were placed in the same aqueous compartment. Ten mM/l. of NaCl were opposed to 100, 250, 500, 1000 mM/l. of NaCl and identical experiments were performed with KCl. As expected no potentials were measured if the non-aqueous membrane was replaced by a salt bridge. The results are plotted on Fig. 5. The slopes of the curves were appreciably smaller than those expected from the classical Nernst equation which predicts a change of 58 mv. for a tenfold change in salt concentration. This model can be compared to a diffusion potential due to a salt concentration difference on each side of the membrane. The Henderson equation

$$E = \frac{u-v}{u+v} RT \ln \frac{C_1}{C_2}$$

(where E is the electrical potential, u , v are, respectively, the cationic and anionic mobilities) cannot be applied directly. Because of the stirring, the phenomenon does not depend upon the ionic mobilities differences in the oil. Instead, the chemical differential flux of the cations and anions crossing the interfaces should be considered: k_+ and k_-

$$E = \frac{k_+ - k_-}{k_+ + k_-} RT \ln \frac{C_1}{C_2} = \frac{k_+/k_- - 1}{k_+/k_- + 1} RT \ln \frac{C_1}{C_2} \quad (14)$$

From Fig. 5 and by using equation 14, the ratio of rates can be calculated: $(k_+/k_-)_{KCl} = 0.66$ and $(k_+/k_-)_{NaCl} = 0.57$. Similar experiments were carried out with K_2SO_4 which also gave a linear log plot. But, in this case the potentials were found negative in contrast to the positive potentials found with KCl and NaCl. This indicated the following order of ionic mobilities $Cl > K > Na > SO_4$.

Water Migration Across Non-aqueous Liquid Membranes.—In all the other experiments, isotonic systems were used. The study of the water migration, when two solutions of different salt concentration are opposed, was attempted. The first experiments were designed to study the influence of the chemistry of the oil membrane. Figure 6 represents the water transport (increase in volume in the saline solution plus the decrease in volume in the water compartment *vs.* time) across 2-butanol; 2-methyl-1-propanol; 1-butanol for a NaCl saturated solution at room temperature (24°). It can be seen that water migrates rapidly through 2-butanol which has volumetric water content (at 30°) of 27.5%. 2-Methyl-1-propanol and 1-butanol have, respectively, a water content of 7.1 and 6.9%, but the partition coefficients for NaCl (see Table I) are smaller for 2-methyl-1-propanol (1.5×10^{-2}) as compared to 1-butanol (1.8×10^{-2}). There are, therefore, two transport phenomena working in opposite directions, *e.g.*, the water migrating towards the concentrated salt compartment and the salt towards the dilute salt compartment. With time, the salt concentration in both compartments equalizes (the volumes being different). The rate of the water migration appears to be proportional to the water content and to a rate factor. As in the case of the salt it is proportional to the partition coefficient and to a rate constant; consequently, in the case of a salt completely insoluble in oil, the system would act as an osmometer. Figure 6 represents the migration of water for KCl and K_2SO_4 at various concentrations. K_2SO_4 is much less soluble than KCl in 1-BuOH. The slopes at the origin of these water migration curves *vs.* time appear to depend on the molar salt concentration, but the curvature is certainly dependent on the salt partition coefficient. On Fig. 7 it can be seen that 20 mM/l. of K_2SO_4 and 100 mM/l. of KCl produce the same water migration after 120 hours although the slopes at the origin are different. Quantitative investigations dealing with the water transport are now in progress.

Discussion

It can be seen from the flux equation 6 that two parameters control the rate of migration. P_{ow} is the partition coefficient which shows that several salts migrating through the same alcohol have a flux controlled by their partition coefficients. This can be altered by the counterflow of other salts which can increase or decrease the partition coefficient of the original migrating salt. See Table I and ref. 2. It also can be seen in Table I that the same salts diffusing through different alcohols have rates about equivalent to their partition coefficients P_{ow} . The second parameter,

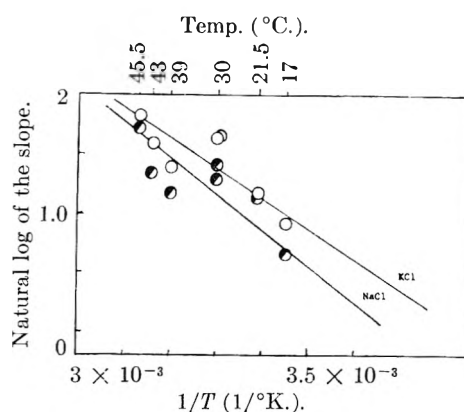


Fig. 4.—Logarithm of the rate of diffusion *vs.* $1/T$.

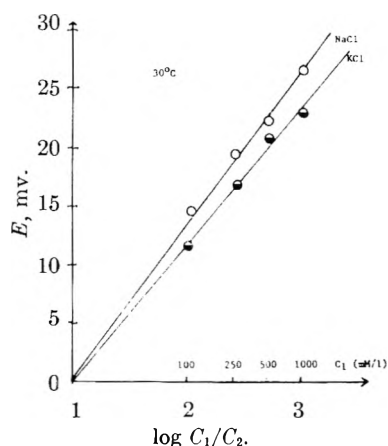


Fig. 5.—Electrical potential variation across 1-butanol (at 30°) for identical salt at various concentrations.

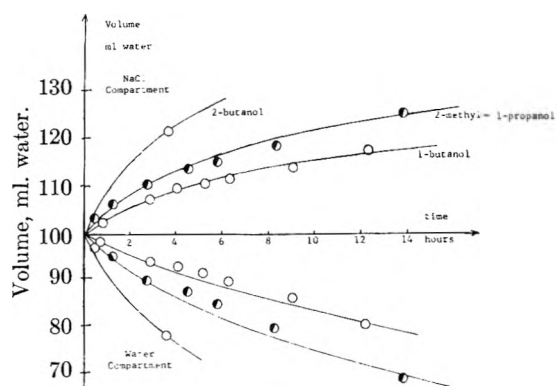


Fig. 6.—Increase and decrease of opposing volumes of 100 ml. of NaCl saturated solution to 100 ml. of water separated by various alcohols as a function of time.

which controls the rate of diffusion, k_{ow} is a rate constant which may indicate a hydration change of the ions as they cross the boundary from the aqueous to the non-aqueous phase.

This is equivalent to an analogy of the retardation of water evaporation due to the presence of a monolayer of a condensed alkyl alcohol, or fatty acid film on the surface of the water. An activation energy is necessary to bring the water molecule off the surface in the presence of an array of orientated hydroxyl groups attached the film forming molecules. This has been calculated for penta-decylic acid to be of the order of 11 kcal. for the

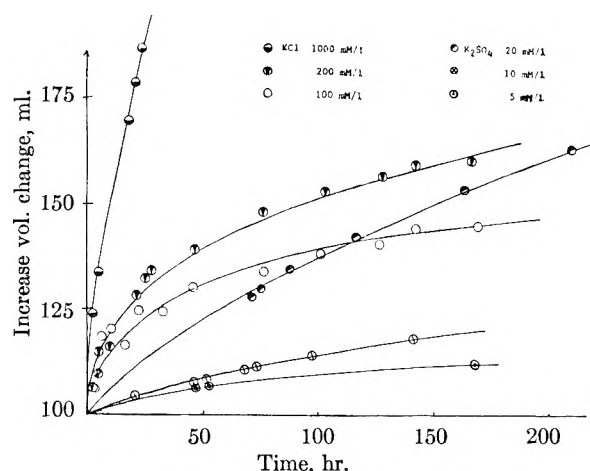


Fig. 7.—Increase of volume of 100 ml. of various salts at various concentrations opposed to 100 ml. of water separated by 1-butanol (at 30°).

polar end of the molecule.⁷ In the case described in this work, it would be considered that the hydrated ions would lose a water molecule as they crossed the boundary into the non-aqueous liquid membrane phase. The activation energies calculated from measuring the rates of migration at different temperatures for KCl and NaCl for 1-butanol system (equation 8) gave a value of 5.2 kcal. for KCl and 6.0 kcal. for NaCl migration.

This difference in the activation energies could explain why K^+ ions always migrate quicker than Na^+ ions, although the partition coefficients for the two salts in the various alcohols under the concentrations used were approximately the same. This probably substantiates the effect of the rate constant k_{ow} in the flux equation 6.

The activation energy is related to that for breaking one hydroxyl bond which could be obtained by the removal of one water molecule from each Na^+ or K^+ ion on crossing the interface.

The difference in the migration rate of the Na and K chlorides would now be interpreted by the differences in their hydration.³

It would be interesting to measure the activa-

(7) R. D. Archer, Ph.D. dissertation, Columbia University, p. 30, April, 1954.

tion energy for other chloride salts in relation to the hydration of the cations on migration across an aqueous-non-aqueous liquid membrane interface.

The stirring of the non-aqueous liquid membrane is important in the mechanism of migration discussed in this work. This makes the system equivalent to a very thin membrane in which the activation energy found for the salt migration corresponds to the energy barrier on taking a hydrated ion from the aqueous into the non-aqueous liquid membrane.

Acknowledgments.—This investigation was supported by P.H.S. Research Grant No. B-2067 (C) from the National Institute of Neurological Diseases and Blindness.

DISCUSSION

I. R. MILLER (Columbia University).—Your interpretation assumes that the rate determining step is the crossing of the interface boundary, based on the assumption that the thickness of the diffusion layer is of the order of 30 μ . The second assumption does not seem to be justified for the experimental set-up since no convection currents resulting from instable density distributions occur. As vigorous stirring was avoided the flow near the interface was laminar. Under these conditions the thickness of the diffusion layer might be higher by several orders of magnitude than the values assumed.

I would like to point out that the activation energies measured are practically the same as one would obtain by writing the diffusion constant in the form $D = D_0 e^{-A/KT}$ and assuming a constant diffusion gradient under the steady state and independent of temperature. In this case $d(\ln D/dT)_{x=0} = d(\ln D_0/dT) = -A/R$. Diffusion as the rate controlling step would help to explain the difference in rates of transport of NaCl and of KCl although their distribution coefficients are the same.

H. L. ROSANO.—As to the thickness of the quiet diffusion layer at the liquid/oil interface, the results of diffusion or carrier transport were found reproducible from a relatively slow rate of stirring up to rotation corresponding to breaking of the interfaces (30 to 80 rotations per minute). Our experiments were performed around 60 r.p.m. and slight oscillation of the interface was always visible. Talcum powder at the interface was found moving in all the cases of diffusion transport. So, we question that the layer might be thicker by several orders. Mention can be made of the work of Peterson and Gregor (*J. Electrochem. Soc.*, 106, 1051–1061 (1959)) in which they calculated the thickness of the unstirred film at the surface of a solid ion exchange membrane to be 1 to 30 microns upon decreasing the stirring. In the case of a liquid/liquid interface the thickness reasonably should be even lower.

THE DIFFUSION TIME-LAG IN POROUS MEDIA WITH DEAD-END PORE VOLUME

BY RICHARD C. GOODKNIGHT AND

California Research Corporation, La Habra, California

IRVING FATT

Department of Mineral Technology, University of California, Berkeley, California

Received March 7, 1961

The time-lag phenomenon, observed during non-steady state diffusion or fluid flow in porous media, is often used to determine the diffusivity coefficient. The effect of dead-end pore volume on diffusivity determined in this way has not been previously described. It is shown here that the diffusivity calculated from the time-lag is a function of the sum of the flow channel volume and the dead-end pore volume. The non-steady state diffusion equation is solved for a system with dead-end pore volume and with initial and boundary conditions encountered in the time-lag measurement. The dead-end pore volume is shown to influence only the early portion of the time-lag curve.

Introduction

When material begins to diffuse across a barrier there is a time delay in achieving steady state transport. As a result of this delay an extrapolation of the steady state portion of the mass transport *versus* time curve intercepts the time axis at a finite, positive time. This intercept has been called the time-lag by Barrer.¹ The interpretation of the time-lag in terms of the diffusivity coefficient has been described by Barrer for a constant diffusivity and by Frisch²⁻⁵ for systems in which diffusivity may be a function of concentration or time.

Most time-lag measurements have been applied to molecular diffusion. Fatt⁶ has shown however that the diffusivity coefficient, $k/\phi\mu c$, which appears in the equation describing non-steady state fluid flow through porous media can be obtained from a time-lag measurement. In this case the delay in establishment of steady state fluid flow is the time-lag.

The simplicity of the time-lag measurement in both diffusion and fluid flow systems makes it a convenient method for obtaining the diffusion coefficient, tortuosity (when diffusion takes place in the fluid contained in a porous medium), and the term $k/\phi\mu c$ when fluid flows through a porous medium. Previous treatments of the time-lag method have not included the situation where there is dead-end volume in the medium through which diffusion or fluid flow takes place. Goodknight, Klikoff and Fatt (GKF)⁷ solved the general equation for non-steady state diffusion or fluid flow in such systems but did not include the time-lag initial and boundary conditions. It is the purpose of this paper to present the solutions for the time-lag initial and boundary conditions and to compare these solutions with experimental data on a laboratory flow system.

Nomenclature

A cross-sectional area of porous flow channel
 A_o cross-sectional area of orifice

c compressibility
 C variable concentration
 C_2 concentration in sink (variable)
 D diffusion coefficient
 D_o effective diffusion coefficient
 H a constant coefficient
 I pressure gradient multiplied by time
 k permeability of porous flow channel
 k_o permeability of orifice
 l_o length of orifice
 L length of porous medium
 P' dimensionless pressure in flow channels, $P' = (P_2 - P_o)/(P_b - P_o)$
 P_2' dimensionless pressure in dead-end pores, $P_2' = (P_2 - P_o)/(P_b - P_o)$
 P pressure (variable)
 P_o initial pressure (constant)
 P_b boundary pressure (constant)
 P_2 pressure in dead-end pore (variable)
 q volumetric flow rate
 S parameter of La Place transform
 t time
 T_L time-lag
 T_{L2} time-lag
 V_1 pore volume of flow channel (not including dead-end volume)
 V_2 total volume of all dead-end pores
 V_o volume of individual dead-end pores
 X distance coordinate
 Z cumulative volume
 Z_L cumulative volume past
 $Z_{L\alpha}$ cumulative volume past $X = L$ when Z_L is linear function of time
 α diffusivity coefficient for liquid, $\alpha = k/\phi_1\mu c$
 β a constant
 θ tortuosity = diffusion path length/ L
 ϕ_1 V_1/AL
 ϕ_2 V_2/AL
 μ viscosity

Theory

GKF have shown that equations 1 and 2 below describe non-steady state diffusion in the fluid contained in a porous medium in which there are dead-end pores.

$$\frac{\partial C}{\partial t} = \frac{D}{\theta^2} \frac{\partial^2 C}{\partial X^2} - \frac{V_2}{V_1} \frac{\partial C_2}{\partial t} \quad (1)$$

$$\frac{\partial C_2}{\partial t} = \frac{DA_o}{l_o V_o} (C - C_2) \quad (2)$$

The analogous equations for non-steady state flow of a slightly compressible liquid through a porous medium containing dead-end pores are

$$\frac{\partial P}{\partial t} = \frac{k}{\phi_1\mu c} \frac{\partial^2 P}{\partial X^2} - \frac{V_2}{V_1} \frac{\partial P_2}{\partial t} \quad (3)$$

and

- (1) R. M. Barrer, *J. Phys. Chem.*, **57**, 35 (1953).
- (2) H. L. Frisch, *ibid.*, **61**, 93 (1957).
- (3) H. L. Frisch, *ibid.*, **62**, 401 (1958).
- (4) H. O. Pollack and H. L. Frisch, *ibid.*, **63**, 1022 (1959).
- (5) H. L. Frisch, *ibid.*, **63**, 1249 (1959).
- (6) I. Fatt, *Trans. Am. Inst. Mining Met. Engrs.*, **216**, 449 (1959).
- (7) R. C. Goodknight, W. A. Klikoff, Jr., and I. Fatt, *J. Phys. Chem.*, **64**, 1162 (1960).

$$\frac{\partial P_2}{\partial t} = \frac{k_0 A_0}{\mu l_0 c V_0} (P - P_2) \tag{4}$$

For convenience the coefficients are defined as

$$\frac{k}{\phi_1 \mu c} = \alpha \tag{5}$$

and

$$\frac{k_0 A_0}{\mu l_0 c V_0} = H \tag{6}$$

Equations 3 and 4 are solved here but it is to be understood that the same solutions apply to equations 1 and 2 since

$$C \equiv P, C_2 \equiv P_2, (D/\theta^2) \equiv \alpha \\ (DA_0/l_0 \nu_0) \equiv H$$

The initial and boundary conditions for the time lag measurement are

$$P'(X, 0) = P_2'(X, 0) = 0 \tag{7}$$

$$P'(L, t) = 0 \tag{8}$$

$$P'(0, t) = 1, t > 0 \tag{9}$$

The solution of equations 3 and 4 with the above conditions is carried out in the manner already described by GKF. The result is

$$P'(X, t) = 1 - \frac{X}{L} - \sum_{n=1}^{\infty} \frac{\sin \beta_n X}{S_n L \left(\frac{\partial \beta}{\partial S}\right)_n} \exp(S_n t) \tag{10}$$

where

$$\beta_n = \frac{n\pi}{L}, n = 1, 2, \dots \tag{11}$$

$$2S_n = - \left\{ H \left(1 + \frac{V_2}{V_1} \right) + \alpha \beta_n^2 \right\} \pm \sqrt{\left\{ H \left(1 + \frac{V_2}{V_1} \right) + \alpha \beta_n^2 \right\}^2 - 4\alpha \beta_n^2 H} \tag{12}$$

$$\left(\frac{\partial \beta}{\partial S}\right)_n = - \frac{1}{2\alpha \beta_n} \left\{ 1 + \frac{V_2}{V_1} \left(\frac{H}{S_n + H} \right)^2 \right\} \tag{13}$$

Equation 10 can be differentiated to obtain the pressure gradient at any point and time

$$\frac{\partial P'}{\partial x} = \frac{-1}{L} - \sum_{n=1}^{\infty} \frac{\beta_n \cos \beta_n X}{S_n L \left(\frac{\partial \beta}{\partial S}\right)_n} \exp(S_n t) \tag{14}$$

Let the volume that has flowed past any point X be Z , then

$$Z = - \frac{kA}{\mu} I \tag{15}$$

where

$$I = \int_0^t \left(\frac{\partial P'}{\partial X}\right) dt \tag{16}$$

Inserting equation 14 into 16 gives

$$I = - \frac{t}{L} + \sum_{n=1}^{\infty} \frac{\beta_n \cos \beta_n X}{S_n^2 L \left(\frac{\partial \beta}{\partial S}\right)_n} - \sum_{n=1}^{\infty} \frac{\beta_n \cos \beta_n X}{S_n^2 L \left(\frac{\partial \beta}{\partial S}\right)_n} \exp(S_n t) \tag{17}$$

The first summation on the right-hand side in equation 17 can be simplified by substituting into it S_n^2 from equation 12. This summation then becomes

$$\sum_{n=1}^{\infty} \frac{\beta_n \cos \beta_n X}{S_n^2 L \left(\frac{\partial \beta}{\partial S}\right)_n} = \frac{\left(1 + \frac{V_2}{V_1}\right) L}{\alpha} \left[\frac{X}{L} - \frac{1}{3} - \frac{X^2}{2L^2} \right] \tag{18}$$

Note that equation 18 is independent of H . Equation 17 then can be written

$$I = - \frac{t}{L} + \frac{\left(1 + \frac{V_2}{V_1}\right) L}{\alpha} \left[\frac{X}{L} - \frac{1}{3} - \frac{X^2}{2L^2} \right] - \sum_{n=1}^{\infty} \frac{\beta_n \cos \beta_n X}{S_n^2 L \left(\frac{\partial \beta}{\partial S}\right)_n} \exp(S_n t) \tag{19}$$

Equations 15 and 19 can now be used to obtain an expression for the volume that has flowed past $X = L$ from $t = 0$ to t . This is

$$Z_L = - \frac{kA}{\mu} \left[- \frac{t}{L} + \frac{L}{\alpha} \left(1 + \frac{V_2}{V_1} \right) - \sum_{n=1}^{\infty} (-1)^n \frac{n\pi}{L} \frac{\exp(S_n t)}{S_n L \left(\frac{\partial \beta}{\partial S}\right)_n} \right] \tag{20}$$

As t increases Z_L approaches the asymptote

$$Z_{L\infty} = - \frac{kA}{\mu} \left[- \frac{t}{L} + \frac{L}{\alpha} \left(1 + \frac{V_2}{V_1} \right) \right] \tag{21}$$

This asymptotic straight line in a plot of Z_L versus t intercepts the time axis, $Z_L = 0$, at the time-lag T_L .

$$T_L = \frac{L^2}{\alpha} \left(1 + \frac{V_2}{V_1} \right) \tag{22}$$

If α is replaced by its equivalent, equation 5, we obtain

$$T_L = \frac{(V_1 + V_2)\phi_1 \mu c L^2}{6kV_1} \tag{23}$$

or

$$T_L = \frac{(V_1 + V_2)\mu c L}{6kA} \tag{24}$$

Equation 20, together with equations 11, 12 and 13, give the complete curve of volume throughput versus time, in the time-lag experiment. Equation 23 or 24 gives the time-lag.

If only the time-lag is desired then equation 3 can be solved by a simple procedure due to Frisch.⁸ Equation 3 is rearranged to

$$\frac{\partial P}{\partial t} + \frac{V_2}{V_1} \frac{\partial P}{\partial t} = \alpha \frac{\partial^2 P}{\partial X^2} \tag{25}$$

Integrating both sides

$$\int_0^t \int_0^L \int_x^L \left(\frac{\partial P}{\partial t} + \frac{V_2}{V_1} \frac{\partial P}{\partial t} \right) dy dx dt = \alpha \int_0^t \int_0^L \int_x^L \left(\frac{\partial^2 P}{\partial X^2} \right) dy dx dt \tag{26}$$

Then

$$\int_0^L \int_x^L \left(P + \frac{V_2}{V_1} P_2 \right) dy dx = \alpha \int_0^t \int_0^L \left(\frac{\partial P}{\partial X}(L) - \frac{\partial P}{\partial X} \right) dx dt \tag{27}$$

$$\int_0^L \int_x^L \left(P + \frac{V_2}{V_1} P_2 \right) dy dx = - \alpha \int_0^t \int_0^L \frac{\partial P}{\partial X}(L, t) dx dt - \alpha \int_0^t \int_0^L \frac{\partial P}{\partial X} dx dt \tag{28}$$

(18)

(8) H. L. Frisch, private communication.

q^* is defined by

$$q^* = - \frac{q(L, \alpha)}{(kA/\mu)} = \frac{\Delta P}{L} = \frac{1}{L} \quad (29)$$

for unit pressure difference. Equation 28 now can be rewritten as

$$\int_0^L \int_x^L \left(P + \frac{V_2}{V_1} P_2 \right) dy dx = \alpha L I_L + \alpha \Delta P t \quad (30)$$

But from equation 29 $\Delta P = q^* L$, then

$$I_L = -q^* t + \frac{\int_0^L \int_x^L \left(P + \frac{V_2}{V_1} P_2 \right) dy dx}{\alpha L} \quad (31)$$

For the asymptote I_{La} we get from equation 31

$$I_{La} = q^*(t - T_L) \quad (32)$$

From equation 32 we find

$$T_L = \frac{q^* t + I_{La}}{q^*} \quad (33)$$

If we use equation 31 for I_{La} we obtain

$$T_L = - \frac{\int_0^L \int_x^L \left(P + \frac{V_2}{V_1} P_2 \right) dy dx}{\alpha L q^*} \quad (34)$$

In the limit $t = \infty$ we have steady state, then

$$\lim_{t \rightarrow \infty} P = \lim_{t \rightarrow \infty} P_2 = 1 - \frac{X}{L} \quad (35)$$

Equation 34 now becomes

$$T_L = \frac{\left(1 + \frac{V_2}{V_1} \right)}{\alpha L q^*} \int_0^L \int_x^L \left(1 - \frac{X}{L} \right) dy dx \quad (36)$$

or

$$T_L = \frac{\left(1 + \frac{V_2}{V_1} \right) L^2}{6 \alpha L q^*} \quad (37)$$

But from equation 29 $q^* = 1/L$ then

$$T_L = \frac{\left(1 + \frac{V_2}{V_1} \right) L^2}{6 \alpha} \quad (38)$$

This is the same result given in equation 22 from the general solution.

Equation 20 was evaluated by means of a FORTRAN program on an IBM 704 digital computer. The results for various combinations of α , V_1 , V_2 and H are shown in Fig. 1 and 2. The time-lags for the theoretical curves were calculated by fitting a straight line to the calculated volume *versus* time data. The line was fitted to points where the incremental volume was constant to within one part in 10,000 for a five second time increment. For the four systems shown in Fig. 1 and 2 the time when this condition was met was as follows: curve 1, 65 sec.; curve 2, 230 sec.; curve 3, 155 sec.; and curve 4, 110 sec. The time-lags and system parameters are tabulated in Fig. 1.

Experimental

The laboratory model has been adequately described in previous publications.^{6,7} In brief, the model was a 2'' x 2'' x 60'' piece of sandstone coated with epoxy resin and equipped with an inlet port, an outlet port, and nine equally-spaced connectors along one side. At these nine points could be connected a chamber, or a chamber and orifice in series, or the point could be sealed over. The sandstone had a permeability of 1.46 Darcys, and a porosity of 23.6%. The

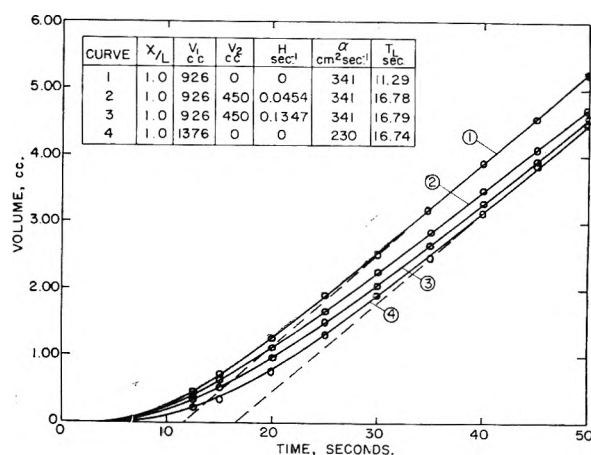


Fig. 1.—Volume of gas produced at downstream end of linear system as a function of time after applying 0.01 atm. pressure at upstream end. System parameters are shown in insert table. Solid and dashed lines are calculated from theory. Open circles are experimental points.

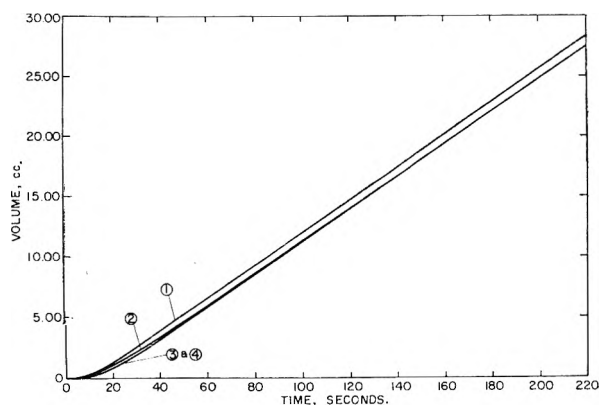


Fig. 2.—Volume of gas produced at downstream end of linear system as a function of time after applying 0.01 atm. pressure at upstream end. Legend same as in Fig. 1. Note that curves 2, 3 and 4 coincide at larger times indicating no influence of flow restriction between flow channels and dead-end volume.

nine side chambers could be either 50, 125 or 174 cm.³ each. The orifices could be 0.122, 0.0615 or 0.0411 Darcy-cm. each.

Air pressure at 0.01 atm. was applied to one end of the model by opening a quick-acting toggle valve. At the same time a stopwatch was started. The air emerging from the downstream end moved a slug of water along a calibrated, horizontal glass tube. The volume produced as a function of time was obtained by noting the time the slug passed previously calibrated volume markers. For larger volumes of air than could be handled in the horizontal tube the air was fed into the bottom of a vertical, water-filled buret set in a large pan of water. The volume so collected was recorded as a function of time after opening the upstream end to air pressure.

The experimental data are shown as open circles in Fig. 1. The curves in these figures are calculated from equation 20. The experimental time-lags equivalent to those for curves 1, 2, 3 and 4 in Fig. 1 and 2 are 11.1, 16.9, 16.8 and 16.9 sec., respectively. These are in excellent agreement with the theoretically predicted time-lags for the laboratory model. In addition, there is good agreement of experiment and theory at the lower, curved portion of the volume *versus* time curve, as shown in Fig. 1.

Discussion

Equation 24 or 38, developed from the theory shows clearly that the time-lag in a system containing dead-end pores is influenced only by the total pore volume (flow channels plus dead-end pores),

and not at all by the resistance to flow between the flow channels and the dead-end pores. This is borne out by the experimental results.

Note in Fig. 1 that in a system with dead-end pores connected to the main flow channels through resistance the volume output rises faster than in a system of the same total pore volume but with no resistance between dead-end pores and the main flow channels. Both systems have the same linear asymptote, however, and the time-lag is identical.

These results are not in agreement with some experimental data obtained by Fatt,⁶ and by Barrer and Gabor.^{9,10} They found the time-lag at constant total pore volume to be dependent upon H . A possible reason for this discrepancy now can be advanced. Although the asymptote is independent of H , the time required to reach this asymptote is dependent on H . Experiments in which H is finite must be carried out for much longer times to assure that the asymptote is reached. Extrapolation of data that had not reached the steady-state asymptote would lead to low time-lags as observed by Fatt.

There are two procedures whereby the values of V_1 , V_2 , α and H can be estimated from application of the theoretically derived equations to experimental data. The sum $V_1 + V_2$ usually can be obtained by a static volumetric measurement. From $V_1 + V_2$ and the time-lag, α can be calculated. The ratio V_2/V_1 can be calculated only if V_1 or V_2 can be estimated. This may be done by observing

the time required for the pressure transient to reach the closed end of a linear system after a sudden increase of pressure is applied to the open end.^{6,11} This is usually a function of only V_1 and is given by

$$T_{L2} = \frac{0.0471LV_1\mu c}{kA} \quad (39)$$

for small values of H . V_2 does not appear in equation 39 because the first part of the transient to arrive at $X = L$ does not "see" the dead end volume if this volume is connected to the main flow channels through a resistance for which H is small. Having obtained V_1 , V_2 and α , various values of H can be substituted into equation 20 and Z_L evaluated until a match is obtained with experimental data.

An alternative method for estimating V_1 , V_2 , α and H is available through use of the "alternating flow" technique developed by Stewart, *et al.*¹² In their procedure a sinusoidally alternating gas pressure is applied upstream. The amplitude and phase shift of the sinusoidally varying output volume, relative to the input pressure, can be interpreted in terms of V_1 , V_2 , α and H .

Acknowledgment.—The authors wish to thank the donors of the Petroleum Research Fund, administered by the American Chemical Society, for their support of the research which led to this paper. G. H. Thomas and T. H. Blanco, Jr., assisted in the experimental work.

(11) J. A. Putnam, Ph.D. Dissertation, University of California, Berkeley, 1943.

(12) C. R. Stewart, A. Lubinski and K. A. Blenkarn, *J. Pet. Tech.*, **13**, 383 (1961).

(9) R. M. Barrer and T. Gabor, *Proc. Roy. Soc. (London)*, **A251**, 353 (1959).

(10) R. M. Barrer and T. Gabor, *ibid.*, **A256**, 267 (1960).

LIGHT SCATTERING FUNCTIONS FOR $m = 1.60$ (0.04) 2.08 AND $\alpha = 0.1$ (0.1) 10.0. I. MIE SCATTERING COEFFICIENTS¹

BY M. KERKER, J. P. KRATOHVIL AND E. MATIJEVIĆ

Department of Chemistry, Clarkson College of Technology, Potsdam, New York

Received March 20, 1961

Mie scattering coefficients, K , have been calculated for refractive indices $m = 1.60$ (0.04) 2.08 and particle size parameters $\alpha = 0.1$ (0.1) 10, as well as for $m = 1.4821$ and 2.105 in the range of $\alpha = 0.1$ (0.1) 22.9 and 23 (2) 53. A graphical survey of the available scattering coefficients in the m - α domain is given. The applicability of various approximate methods for calculating K , the change of K with m , and the influence of small differences in m on K are discussed.

Despite great interest in the application of the Mie theory of scattering to fields as diverse as colloid chemistry, chemical engineering, meteorology, astrophysics and space science, the number of available scattering functions is still quite limited and many workers, especially in colloid chemistry, continue to be impeded in their work because of this. The scattering functions depend upon two parameters: the refractive index of the particle relative to the medium, m , and the size parameter, $\alpha = 2\pi r/\lambda$, where r is the particle radius and λ is the wave length of the radiation in the medium. Van de Hulst² has discussed the range of validity of the various approximations to the Mie theory for non-absorbing spheres in terms of location in the m - α domain and Penndorf³ has used this graphical device in order to survey the regions for which computations of the Mie scattering coefficients are available. Although the m - α domain is well filled for $m < 1.60$ and small values of α , there is an almost complete void for those higher refractive indices which are of interest in many areas of colloid chemistry. We have, accordingly, calculated scattering functions for $m = 1.60$ (0.04) 2.08 and $\alpha = 0.1$ (0.1) 10.0. These include not only the scattering coefficients, K , but the intensity functions for each of the components of the scattered radiation at angles of observation 0° (10°) 180° . These latter quantities will be discussed in a later paper.

The availability of these new functions permit an evaluation of various approximation and interpolation schemes which have been proposed to fill the lacunae in the m - α domain. Also, the general behavior of K with both increasing α and increasing m now can be delineated in this region of higher refractive index. Furthermore, the experience of carrying out the *complete* computation of scattering coefficient and intensity functions on a high speed digital computer now permits one to estimate the effort and cost of machine computation relative to either the effort of hand computing or that needed to obtain results using the approximation methods.

The scattering coefficient, K , is defined by

$$I/I_0 = e^{-K\pi r^2 nl} \quad (1)$$

where I_0 is intensity of an incident parallel beam of light and I is the intensity of the beam after traversing a distance, l , through the dispersion containing n spherical particles of radius r per unit volume of the dispersion. The reader is referred to the standard literature for the basic equations from which K may be calculated.^{2,4-11}

The computations were carried out with the aid of the IBM 704 computer, using a program developed for the theory of scattering of electromagnetic radiation by a sphere encased in a concentric spherical shell.¹² This theory reduces to the single sphere case when the inner radius either goes to zero or equals the outer radius. In addition to K , the output of the computer program consists of the angular functions $\text{Re}(i_1^*)$, $\text{Im}(i_1^*)$, $\text{Re}(i_2^*)$, $\text{Im}(i_2^*)$, i_1 and i_2 for angles of observation 0° (10°) 180° . The first four functions are the real and imaginary parts of the complex quantities from which the intensity functions i_1 and i_2 are obtained. These latter are proportional to the intensities of the plane-polarized components of the light scattered by a single particle. For definitions the reader is again referred to the literature.^{2,9-11} A more detailed description of the computing program will be given in a future publication where results for a sphere encased in the concentric spherical shell will be considered.

In addition to the values of m cited above, computations also have been carried out for $m = 1.4821$ and 2.1050 for $\alpha = 0.1$ (0.1) 22.9 and for $\alpha = 23.0$ (2) 53.0. These were computed in connection with an experimental study of scattering by coated aerosols.¹³ In a previous publication¹⁴ 61 of the 253 results for $m = 2.1050$ were reported. The value of $m = 1.4821$ is very close to Penndorf's^{3,7} value of $m = 1.486$, and provides an example of the influence of a very small increment in refractive index on the scattering coefficient. For

(4) R. Penndorf, *J. Meteorol.*, **13**, 219 (1956).

(5) R. Penndorf, *J. Opt. Soc. Am.*, **46**, 1001 (1956).

(6) R. B. Penndorf, *ibid.*, **47**, 603 (1957).

(7) R. B. Penndorf, *ibid.*, **47**, 1010 (1957).

(8) R. B. Penndorf, *J. Phys. Chem.*, **62**, 1537 (1958).

(9) A. N. Lowan, "Tables of Scattering Functions for Spherical Particles," Natl. Bur. Standards, Appl. Math. Series 4, Washington, D. C., 1948.

(10) R. O. Gumprecht and C. M. Sliepcevich, "Light Scattering Functions for Spherical Particles," University of Michigan Press, Ann Arbor, Michigan, 1951.

(11) W. J. Pangonis, W. Heller and A. W. Jacobson, "Tables of Light Scattering Functions for Spherical Particles," Wayne State University Press, Detroit, Michigan, 1957.

(12) A. L. Aden and M. Kerker, *J. Appl. Phys.*, **22**, 1242 (1951).

(13) E. Matijević, M. Kerker and K. F. Schulz, *Discussions Faraday Soc.*, **30**, 178 (1960).

(14) M. Kerker and E. Matijević, *J. Opt. Soc. Am.*, **51**, 87 (1961).

(1) Supported by U. S. Atomic Energy Commission Contract No. AT(30-1)-1801.

(2) H. C. van de Hulst, "Light Scattering by Small Particles," John Wiley and Sons, New York, N. Y., 1957.

(3) R. B. Penndorf, "New Tables of Mie Scattering Functions for Spherical Particles. Part 6: Total Mie Scattering Coefficients for Real Refractive Indices." Geophysical Research Papers No. 45, Air Force Cambridge Research Center, Bedford, Mass., March 1956. Parts of this report appear in references 4-8.

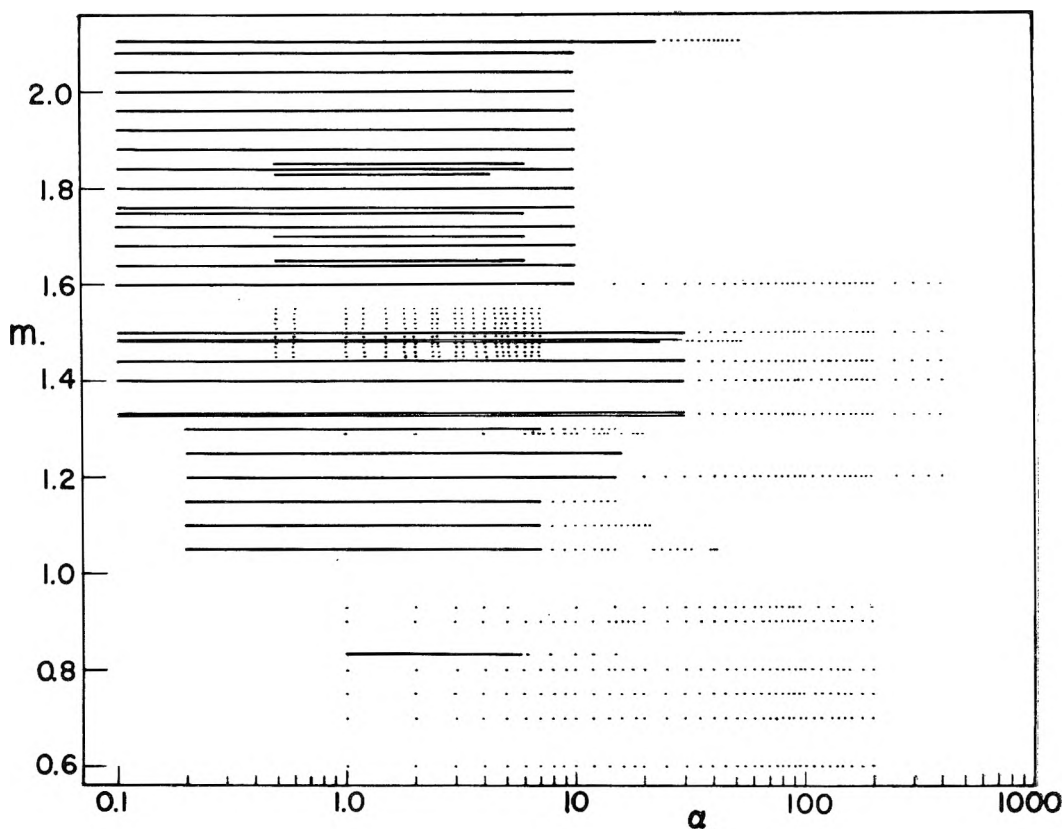


Fig. 1.—Values of available Mie scattering coefficients, K , plotted in the m - α domain. The solid lines were drawn where K values are computed for intervals of $\Delta\alpha \leq 0.2$. This compilation was made using the following references (in parenthesis): Refractive index m 0.60, 0.70, 0.75, 0.80, 0.90, 0.93 (18, 19); 0.8333 (20); 1.05, 1.10, 1.15 (11); 1.20 (10, 11); 1.25 (11, 29) 1.29 (21); 1.30 (11); 1.33 (3, 7, 9, 10, 17, 22); $4/3$ (i.e., 1.333 or 1.3333) (23–25); 1.40 (3, 7, 9, 10); 1.44 (3, 7, 9, 10); 1.45, 1.46, 1.47, 1.48 (9); 1.4821 (16); 1.486 (3, 7, 26); 1.49 (9); 1.50 (3, 7, 9, 10); 1.51, 1.52, 1.53, 1.54, 1.55 (9); 1.60 (10, 16); 1.64 (16); 1.65 (27); 1.68 (16); 1.70 (27); 1.72 (16); 1.75 (27, 28); 1.76 (16); 1.80 (16, 27); 1.831 (27, 29); 1.84 (16); 1.85 (27); 1.88, 1.92, 1.96 (16); 2.00 (3, 7, 9, 16); 2.105 (14, 16).

$\alpha > 15$, the IBM 7090 computer was used rather than the IBM 704.

The accuracy of the computer program has been checked three ways. A number of cases for $\alpha = 1$ were hand computed. A number of cases up to $\alpha = 30$ were computed using a program developed by the National Bureau of Standards for the IBM 704. This independently obtained program was utilized only for checking since it ran considerably slower than the one utilized for this work. Finally, the results were checked where they overlapped with those of Gumprecht and Sliepcevic¹⁰ at $m = 1.60$ for values of K and against those of Lowan⁹ at $m = 2.00$ for K as well as the angular functions. Complete agreement was obtained in all cases.

A comparison with K values calculated by Penndorf³ for $m = 2.00$ using the amplitude functions hand-computed by Kerker, *et al.*,¹⁵ for 23 sizes in the range of $\alpha = 1.3$ to 12.5 showed a satisfactory agreement, except for $\alpha = 4.4, 5.5, 6.5$ and 8.0.

The running time for the 1300 cases [$\alpha = 0.1$ (0.1) 10.0, $m = 1.60$ (0.04) 2.08] was 1.89 hours or 5.23 seconds per case. Each case includes the 42 intensity functions as well as the scattering coefficient. At current rates, this amounts to a cost of less than one dollar per case.

(15) M. Kerker and H. E. Perlee, *J. Opt. Soc. Am.*, **43**, 49 (1953); M. Kerker and A. L. Cox, *ibid.*, **45**, 1080 (1955).

The computed scattering coefficients, K , are presented elsewhere.¹⁶

In Fig. 1 Penndorf's survey of the available scattering coefficients in the m - α domain is extended to comprise the complete range of particle sizes (up to $\alpha = 400$) and to include the new values¹⁶ as well as additional functions that appeared after the Penndorf report³ was published. Values for $m < 1$ as well as $m > 1$ are included. As the diagram clearly shows, the domain for $m > 1$ is now very well filled up to $\alpha = 10.0$ and $m = 2.105$. Perhaps the most significant gaps are between $m = 1.33$ and 1.40.

A critical review of K values published to 1956 was made by Penndorf.³ It appears that all functions published after that date can be accepted as reliable except a few of the K values for $m = 1.75$ hand-computed by Meehan and Beattie.²⁸ How-

(16) Deposited with the American Documentation Institute, Library of Congress, Washington 25, D. C., Serial Number 6663; photographs \$3.75; microfilm \$2.00, payable in advance.

(17) R. O. Gumprecht and C. M. Sliepcevic, *J. Phys. Chem.*, **57**, 90 (1953).

(18) R. H. Boll, R. O. Gumprecht and C. M. Sliepcevic, *J. Opt. Soc. Am.*, **44**, 18 (1954).

(19) R. H. Boll, J. A. Leacock, G. C. Clark and S. W. Churchill, "Tables of Light Scattering Functions: Relative Indices of Less than Unity, and Infinity," University of Michigan Press, Ann Arbor, 1958.

(20) V. C. Anderson, *J. Acoust. Soc. Am.*, **22**, 426 (1950).

(21) J. C. Johnson and J. R. Terrell, *J. Opt. Soc. Am.*, **45**, 451 (1955).

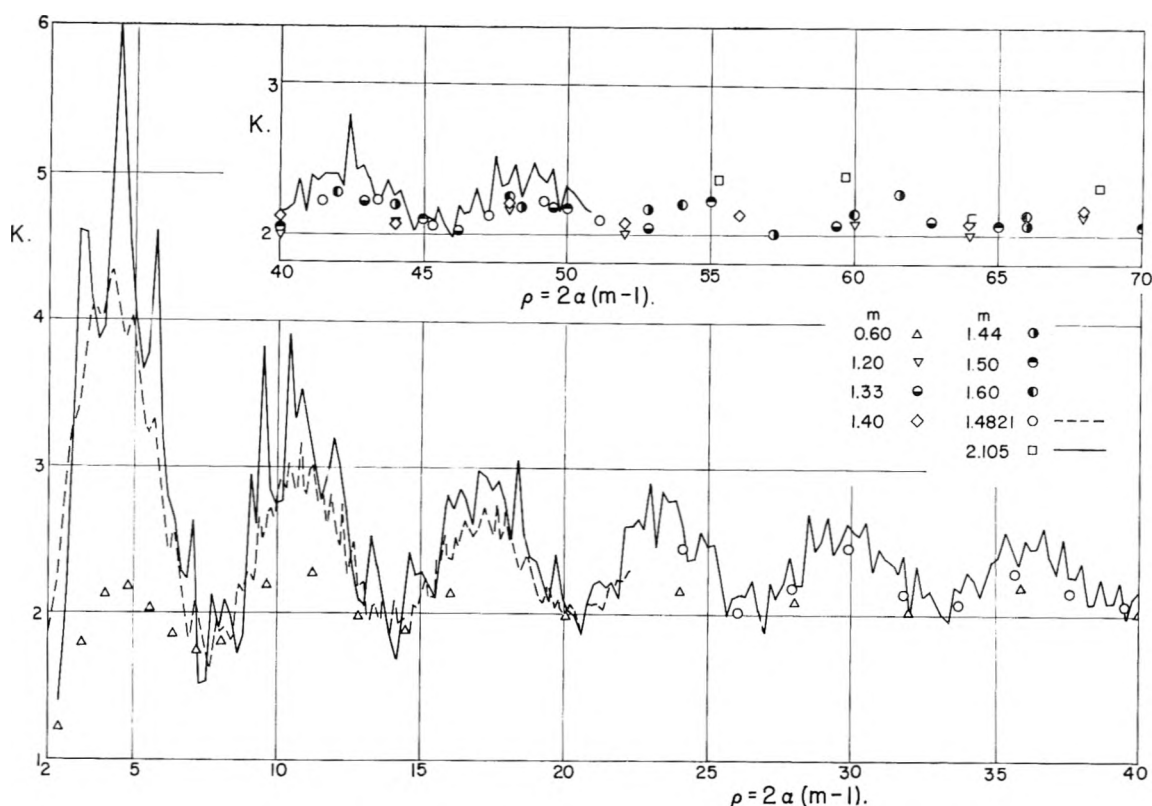


Fig. 2.—Mie scattering coefficient K as function of normalized size parameter ρ for $m = 1.4821$ (dashed line and \circ), 2.105 (full line and \square), and 0.60 (Δ), and, in the inset, for several other refractive indices.

ever, the latter data have recently been machine recomputed and corrected.²⁷

Except for a few selected values of m , given by Penndorf^{3,7} and in this paper, scattering coefficients for $\alpha > 10$ are available only in large steps of α (Gumprecht and Sliepcevich^{10,17} and Boll, *et al.*^{18,19}).

In Fig. 2, K is plotted versus the parameter $\rho = 2\alpha(m - 1)$ for $m = 1.4821$ and 2.105 . To extend the range of refractive indices, the values of Boll, *et al.*¹⁹ for $m = 0.60$ are also plotted (using the absolute values of $2\alpha(m - 1)$). The main part of the diagram covers the values for $\alpha < 50$ for $m = 0.60$, $\alpha < 40$ for $m = 1.4821$ and $\alpha < 18$ for $m = 2.105$. The plot continues in the inset, where other available functions for higher α -values for m between 1.33 and 1.60 are represented as separate points. This plot clearly extends, at least up to $m = 2.105$, the validity of van de Hulst's suggestion^{2,30} that the major oscillations of all curves of K versus ρ are similar. This point had been analyzed and confirmed first by Hawksley³¹ and

later in more detail by Penndorf.^{3,8} The results for intermediate values of m also have been plotted and they follow the same pattern indicated in Fig. 2. It is difficult to discern any regularity in the pattern in the range $\rho > 70$ since a very limited number of K values is available beyond this point. Also, the amplitude of the oscillations at high α -values becomes small, all values of K being close to 2.

The ripples superimposed upon the major oscillations do not follow any simple pattern and, in fact, the ratio of the ripple amplitude to that of the major oscillations increases with increasing m . For $m = 2.105$, this ratio ranges from about 0.25 to 0.50.

Penndorf^{3,8,32} has put much effort in working out an empirical method of computing K for arbitrary values of m and α . The method is based upon the location of the phase (or position) of the extreme values of the available curves of K vs. ρ and estimating the absolute value of K at the extrema. His final result is a smooth function which behaves somewhat like a damped sine function. According to Penndorf, if a smoothed out function is considered sufficient, this permits an estimation of K for $m \leq 2$ with an accuracy of better than $\pm 3\%$ as compared with values computed from the exact Mie theory. Higher accuracy is not possible be-

(22) F. T. Gucker, Jr., cited in ref. 2.
 (23) J. A. Stratton and H. G. Houghton, *Phys. Rev.*, **38**, 159 (1931).
 (24) H. Holl, *Optik*, **1**, 213 (1946); **4**, 173 (1948).
 (25) H. G. Houghton and W. R. Chalker, *J. Opt. Soc. Am.*, **39**, 955 (1949).
 (26) J. D. Riley, "Calculations of Light Intensity Functions," U. S. Nav. Res. Lab., Radio Div. III, ORB Info. Bull. No. 9, 1949.
 (27) E. J. Meehan, personal communication, November 1960; E. J. Meehan and Z. Z. Hugus, published in *J. Opt. Soc. Am.*, **51**, 260 (1961).
 (28) E. J. Meehan and W. H. Beattie, *ibid.*, **49**, 735, (1959).
 (29) R. D. Murley, *J. Phys. Chem.*, **64**, 161 (1960).
 (30) H. C. van de Hulst, "Optics of Spherical Particles," *Recherches Astron. Obser. Utrecht*, **11**, part 1, 56 (1946).

(31) P. G. W. Hawksley, *British Coal Utilisation Research Assn. Monthly Bull.*, **16**, 117, 181 (1952).
 (32) R. Penndorf, "Research on Aerosol Scattering in the Infrared. Sci. Report No. 1: Results of an Approximation Method to the Mie Theory for Colloidal Spheres." Technical Report RAD-TR-59-36, Air Force Cambridge Research Center, Bedford, Mass., September 1959.

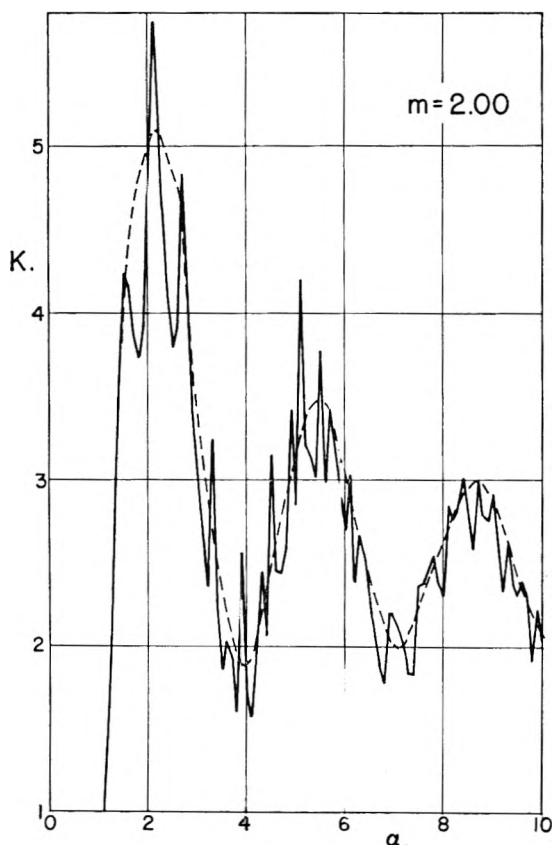


Fig. 3.—Mie scattering coefficient K as function of size parameter α for $m = 2.00$. Full line, exact computations (in $\Delta\alpha$ steps of 0.1); dashed line, Penndorf's approximate curve³² ($\Delta\alpha = 0.2$).

cause for $m \leq 1.50$ this is about the magnitude of the ripples. Furthermore, as Penndorf points out, since the error of 3% represents a considerable fraction of the absolute amplitude of the major oscillations of K , results for which errors are in excess of this amount are useless.

For $m > 1.50$ the magnitude of ripple amplitude becomes more and more pronounced not only around the first maximum, as Penndorf³² (p. 14), was aware but also around other maxima. This point is effectively illustrated in Fig. 3, where K values for $m = 2.00$ computed by the exact Mie theory¹⁶ are compared with those calculated by Penndorf's approximate method (Table AIII in ref. 32). Even for values around the third maximum, differences of up to 16% can be noticed. It should be mentioned also that a random check of Penndorf's approximate values in the range of $m \leq 1.50$ revealed in some cases differences greater than $\pm 3\%$. Thus, Penndorf's statement (ref. 32, p. 6) that "the K function is completely determined if the phase (in terms of ρ) and the amplitude (in terms of K) of the scattering function at the extreme values are known as a function of m " does not seem to be acceptable.

It is obvious, then, that an approximate method of this type is quite impractical for $m > 1.50$ where the ratio of ripple amplitude to that of major oscillation becomes so large. We had suggested this limitation,¹⁴ as had Murley,²⁹ and

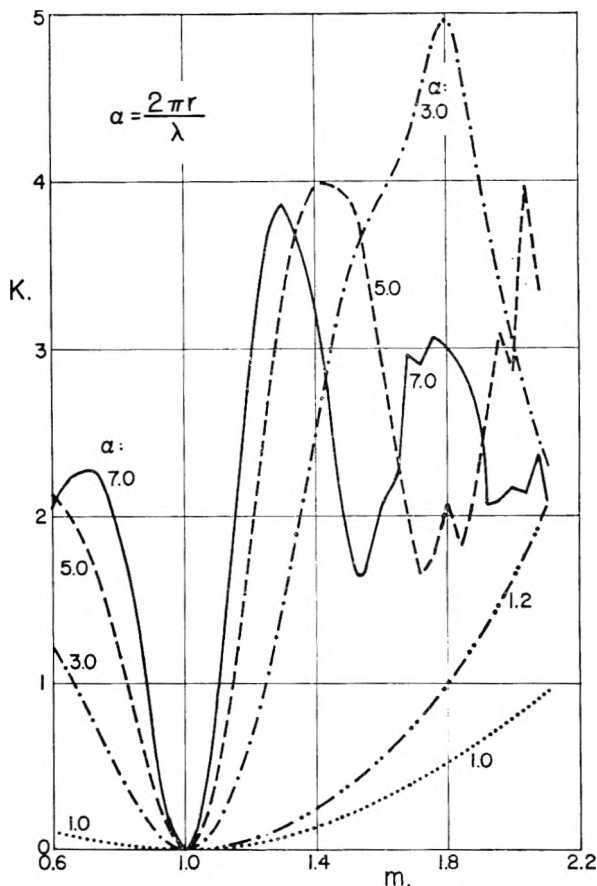


Fig. 4.—Mie scattering coefficient K as function of refractive index m for $\alpha = 1.0, 1.2, 3.0, 5.0$ and 7.0 .

our new computations make this point conclusive.

Van de Hulst² has explored the feasibility of interpolating between available values by plotting in the complex domain the complex quantities from which the functions are obtained. He has shown that for a refractive index as low as $m = 1.33$ it is necessary to have α intervals at least as close as 1. For the higher range of m presented here, the increase in the ripple structure of these functions makes this interpolative method even more precarious.

It would appear that approximate procedures for estimating Mie theory functions are no longer feasible. The methods proposed are cumbersome and time consuming, are seriously limited in accuracy and usually require some exact computations as a starting point. The ease and cost of performing such calculations by machine is such that it is more expedient to fill the m - α domain with a sufficiently high density of points as has been done for the range of m and α presented in this paper in order to permit simple graphical interpolation. Recently, Deirmedjian, *et al.*,³³ arrived at the same conclusion in an analysis of Mie scattering by absorbing spheres.

A second approach to simplifying the calculation of K is by expanding the Mie coefficients into a power series in α and utilizing only the terms in-

(33) D. Deirmedjian, R. Clasen and W. Viezee, "Mie Scattering with Complex Index of Refraction," P-2079, August 1960, RAND Corp., Santa Monica, Calif.

volving powers of α^n where $n \leq 10$.³⁴ Penndorf has shown that in no case is the method applicable to $\alpha > 1.0$ and for $m = 2$ it is restricted to values of $\alpha < 0.65$. For these values of α , computation of the exact value of K with a desk calculator is not significantly more time consuming than use of the approximate formulas themselves.

The abundance of functions in the m - α domain now permits a more detailed insight into the change of K with m . We have plotted K versus m for almost all α -values (up to $\alpha = 10$) and a few selected curves are reproduced in Fig. 4. For the range $m = 1.0$ to 2.105, K increases monotonically with m for values of $\alpha \leq 2$, allowing, thus, safe interpolation for intermediate values of m . There is an exception for $\alpha = 1.6$ where K reaches a maximum at $m = 2.04$. This is due to the occurrence of the first ripple in the K versus α curve in the region of this combination of m and α . For $\alpha > 2$ there is one maximum and at larger values of α the relationship becomes more and more oscillatory. This means that there will be regions where particles of a more refractive material will scatter the same as or even less than the particles of the same size of a less refractive material. This kind of multivaluedness might create major problems in interpreting light scattering data for systems (a) containing homogeneous particles of various refractive indices or (b) containing particles of a central core of one material coated with a shell of a second material. Obviously light scattering may be impractical for determining particle size and particle size distribution in such cases because of this refractive index effect and it should be considered in planning work with such systems.

For $m < 1$ the pattern is very similar over the range of values covered by the computations. The first maximum appears at α about 6.

From Fig. 4 and other similar plots, not reproduced here, it seems most likely that for closer intervals of m , the K versus m curve would be even more oscillatory than we have drawn it. This calls for extreme caution in attempting to obtain, by simple graphical or analytical interpolation, the K functions for those m values for which there are no exact computations available. This point once again makes the use of high-speed computers the only realistic approach to the problem of obtaining accurate Mie theory functions.

The values of α_M and m_M at which the first maximum of K versus m appears are plotted in Fig. 5. Although there may be some uncertainty in location of the first maximum in the K versus m plot, depending on the number of computed functions around first maximum, the graph clearly shows where the multivaluedness in K versus m can be expected. Corresponding to each pair of values in this curve, K increases monotonically with m up to m_M provided $\alpha < \alpha_M$.

The need for exact computations and the insufficiency of approximate values are once more made obvious if K values for two slightly different refractive indices, e.g., for $m = 1.4821$ presented in this paper and for $m = 1.4860$ given by Penndorf,³⁷

(34) R. Penndorf, "Research on Aerosol Scattering in the Infrared. Sci. Report No. 3. Scattering Coefficients for Absorbing and Nonabsorbing Aerosols." Technical Report RAD-TR-60-27, Air Force Cambridge Research Laboratories, Bedford, Mass., October 1960.

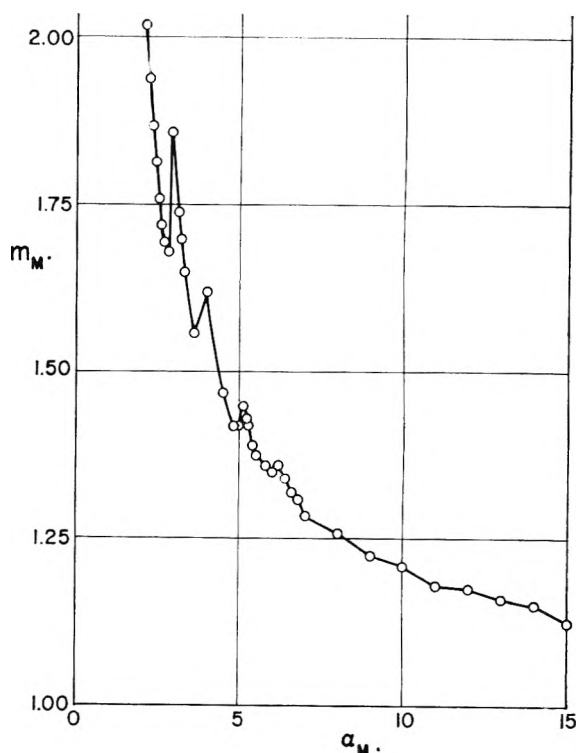


Fig. 5.—Location of the first maximum in the K versus m plot for various α -values.

are compared. Both sets of data overlap in the range of $\alpha = 0.1$ –23.0 in equal steps of $\Delta\alpha (= 0.1)$. It was found that this small difference in m of only 0.26% results in an average difference of 1.8% between the two sets of scattering coefficients (230 values) with a standard deviation of 2.4% in the limits 0–12.4%. The differences generally increase with increasing particle size (e.g., in the region of first and third maximum of the K versus α curve the average differences are 1.2 and 2.2%, respectively). Since at higher α values the scattering coefficient itself oscillates no more than 20% from the mean, such differences between two sets of values are significant. This fact indicates that it is necessary to know the refractive index of the particles to a high degree of precision and to control it properly during experiments.

DISCUSSION

J. R. CANN (University of Colorado Medical School).—I wonder whether the ripples superimposed upon the major oscillations in the K - α plots would be eliminated by using $\Delta\alpha$ steps smaller by, say, a factor of 100 in the computer computations.

M. KERKER.—Yes. A group at the National Bureau of Standards has explored this point and found that in the range $\alpha = 2$ –10, for $m = 2.1050$, for $\Delta\alpha$ as small as 0.001, the functions are quite smooth. The interval for which the functions become smooth decreases with increasing values of α and m . The ripple arises from the superposition of the terms for the various partial electric and magnetic oscillations, each of which varies smoothly.

W. D. ROSS (E. I. du Pont Company).—When and how will you publish your angular intensity tables.

M. KERKER.—These tables will be submitted for publication shortly, but we would be willing to supply any results.

G. A. CAVE (S. C. Johnson Company).—What is the effect of oscillations in the range 1.40–1.60?

M. KERKER.—We have found that in this range the oscillations are quite high. It would be expected that here the effect on angular intensity functions would be even greater. It would be dangerous to extrapolate or to interpolate over more than short intervals.

MELTING KINETICS OF QUARTZ AND CRISTOBALITE

BY N. G. AINSLIE, J. D. MACKENZIE AND D. TURNBULL

*General Electric Research Laboratory, Schenectady, New York**Received March 1, 1961*

The melting of quartz single crystals and polycrystalline cristobalite has been investigated by the use of a microscopic technique. Melting was heterogeneous even at the highest superheating attained, which was 300° for quartz and 40° for cristobalite. It began at the free surfaces and grain boundaries, but never within a crystal, and propagated inward. The rate of propagation of the quartz-fused silica interface was measured as a function of superheating. It was independent of time at constant temperature and the form of its variation with temperature was about the same as that of the relation calculated from the viscosity of fused silica. However, the observed relation was higher, in growth rate, than the calculated relation by an approximately constant factor of 40.

I. Introduction

In some models of melting (see review of Temperley¹) it is assumed that the crystalline phase, when heated, becomes intrinsically unstable at some characteristic temperature, T_c , and then transforms continuously or homogeneously to the liquid phase. In the earliest of such models, due to Lindemann,² this characteristic temperature was identified with the thermodynamic melting temperature, T_m . In later developments the model was modified in such a way as to place T_c above but still near T_m .

In contrast with this view there are the models according to which melting, like crystallization, is a discontinuous transition which occurs by nucleation and growth.³ Then the frequency, I , of nucleation of liquid domains and their rate of growth, u , ought to be governed by the same thermodynamic and kinetic parameters which constitute the corresponding quantities for crystallization.

The experience that most crystals melt at slight superheating has sometimes been cited as support for the view that melting is nearly a continuous process. Actually all observations reported so far indicate that melting is a heterogeneous process in which a liquid film forms on the external surface of the crystal and then grows inward, all at slight superheating. The essential difference then between melting and crystallization is that nucleation of liquid on a crystal surface is very easy whereas the converse process is very difficult. If the melt is quite fluid, growth and the concurrent heat absorption is so rapid that the interior of the crystal cannot become appreciably superheated; for such liquids u/K , where K is the thermal conductivity, is relatively large.

On the other hand if the melt is very viscous, growth is slow (for review see Turnbull and Cohen⁴) and u/K is relatively small so that it should be possible to superheat the crystal by relatively large amounts unless melting becomes continuous. In fact it has been demonstrated already that crystals of albite⁵ and quartz,⁶ which form very

viscous melts, can sustain large superheating (>100° for albite and >300° for quartz) for considerable periods of time. With these systems, there is the opportunity to investigate quantitatively the propagation of the crystal-liquid interface as a function of superheating. We decided to do this for the melting of quartz and cristobalite.

II. Experimental

A. Control of Impurity Effects.—Turnbull and Cohen⁷ pointed out that for covalently bound systems it may be expected that small amounts of certain impurities will strongly catalyze the movement of the crystal-liquid interface. Recently Ainslie, Morelock and Turnbull⁸ have shown that small amounts of water and/or oxygen, which enter the silica from the gas phase, indeed increase the velocity of propagation of the cristobalite-fused silica interface by one or two orders of magnitude at least. This effect, though observed in crystallization, should, of course, also occur in melting. Therefore in quantitative measurements of the rate of melting it is essential to minimize the effects of gas phase impurities. One way to do this is to introduce "getters" into the system. It has been shown⁸ that pure graphite, silicon, chromium or germanium do suppress markedly the rate of propagation of the cristobalite-fused silica interface in closed systems.

When quartz is heated in air above its melting point but below 1710° it usually is transformed rapidly to cristobalite. Actually this transformation may occur *via* fused silica which may not be observed because of the rapidity of the impurity catalyzed propagation of the cristobalite-fused silica interface. Indeed Mackenzie⁹ found that the cristobalite-quartz transformation in the range 1500–1700° is promoted by atmospheric impurities. To observe directly the fusion of quartz these impurities must be eliminated.

B. Quartz.—The majority of the quartz specimens used in this work were obtained from selected single crystals of Brazilian quartz. Spectrographic analysis indicated that the upper limits for Li, Na, Ca, Pt, Pb, Sn, Fe and B were 0.001% for K, Rb, Sr, Ba and Al, 0.01% and for Cs, 0.1%. Limited experiments also were carried out with Herkimer natural quartz crystals and with synthetic quartz crystals from the Western Electric Company and Sawyer Engineering Associates. The concentrations of the metallic impurities present in these samples are approximately equal to those in the Brazilian quartz. Infrared analysis indicated that the OH concentrations of all four samples were similar in magnitude.

Single crystal specimens were cut in the form of parallelepipeds, 1 cm. × 0.5 cm. × 0.1 cm. in dimensions, polished, degreased, acid-washed and dried. The samples were placed on a thin Pt-40% Rh sheet inside a Pt-40% Rh boat and loosely covered with a sheet of the same material. The boat was in turn placed inside a 1-inch diameter Morganite "impervious" alumina tubing situated inside a horizontal Pt-40% Rh resistance furnace of length 12 inches and internal diameter 1 1/4 inches. The two ends of the alumina tube were sealed onto glass tubings which carried side-arms for gas flow and a special adaptor for a thin platinum rod used in the horizontal movement of the boat within the tube. After the boat had been placed at the cold end of the tube, the latter

(1) H. N. V. Temperley, "Changes of State," Cleaver-Hume Press, Ltd., London, 1956, Chapter 5.

(2) F. A. Lindemann, *Physik. Z.*, **11**, 609 (1910).

(3) G. Tammann, "The States of Aggregation," D. Van Nostrand Co., New York, N. Y., 1925, Chapter 9.

(4) D. Turnbull and M. H. Cohen, "Modern Aspects of the Vitreous State," Vol. 1, Edited by J. D. Mackenzie, Butterworth, London, 1960, pp. 38–62.

(5) A. L. Day and E. T. Allen, *Carnegie Inst. Wash. Publ.*, **31** (1905).

(6) J. D. Mackenzie, *J. Am. Ceram. Soc.*, **43**, 615 (1960).

(7) D. Turnbull and M. H. Cohen, *J. Chem. Phys.*, **29**, 1049 (1958).

(8) N. G. Ainslie, C. R. Morelock and D. Turnbull, submitted to *J. Am. Ceram. Soc.*

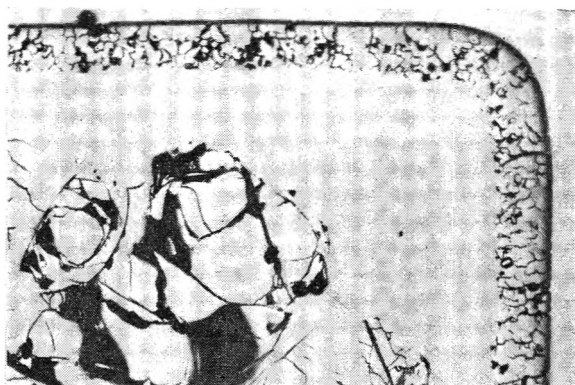


Fig. 1.—Section of quartz single crystal heated at 1710° for 40 min. in argon, showing direct fusion to give glass phase which then transformed to give external cristobalite layer. (200×).



Fig. 2.—Section of quartz single crystal heated at 1730° for 15 min. in air, showing formation of glass phase G over quartz substrate Q. (200×).

was sealed and then purged overnight with dry argon. When the furnace had reached the desired temperature, the boat was first moved slowly into a hot region and kept at about 600° for 30 minutes to allow for the completion of the α - β transition of quartz. It then was transferred rapidly into the central hot zone of the furnace and maintained at various intervals up to 4 hours. Temperature equilibrium in the tube, as indicated by a thermocouple, was usually restored in about a minute after the sample was admitted. A further 2 minutes was allowed for the sample to reach the temperature of the experiment.

To suppress the quartz-cristobalite transformation so that quartz fusion can be observed, a small piece of graphite (National Carbon Co. "Spectroscopic pure" grade) was placed inside the boat so as to maintain a reducing atmosphere. At the end of the fusion experiment, the boat was quickly withdrawn and the specimens subsequently mounted, metallographically polished and the thickness of the glassy layer measured. The presence of a glassy layer rather than a cristobalite layer on the surface of the quartz was easily discernible under the microscope (see Fig. 1) and was confirmed by X-ray analysis. Fusion experiments at temperatures in excess of 1720° were carried out in an air atmosphere. Temperature measurements were made with a calibrated Pt-20% Rh thermocouple.

C. Cristobalite.—As single crystals of cristobalite were not available, polycrystalline samples were prepared by the devitrification of General Electric No. 204 fused silica for various periods in air at about 1600°. Both 1/2 inch diameter tubing and 1/8 inch diameter rod were used. The concentrations of metallic impurities are similar to those in the quartz samples. The glass tubing and rod were first partially or completely devitrified in an internally-wound Pt-40% Rh resistance furnace. Some specimens were "up-quenched" from the devitrification temperature through the melting point of cristobalite (1710°) to about 1750° by rapidly transferring to another furnace. Other specimens were allowed to cool through the α - β inversion of cristobalite

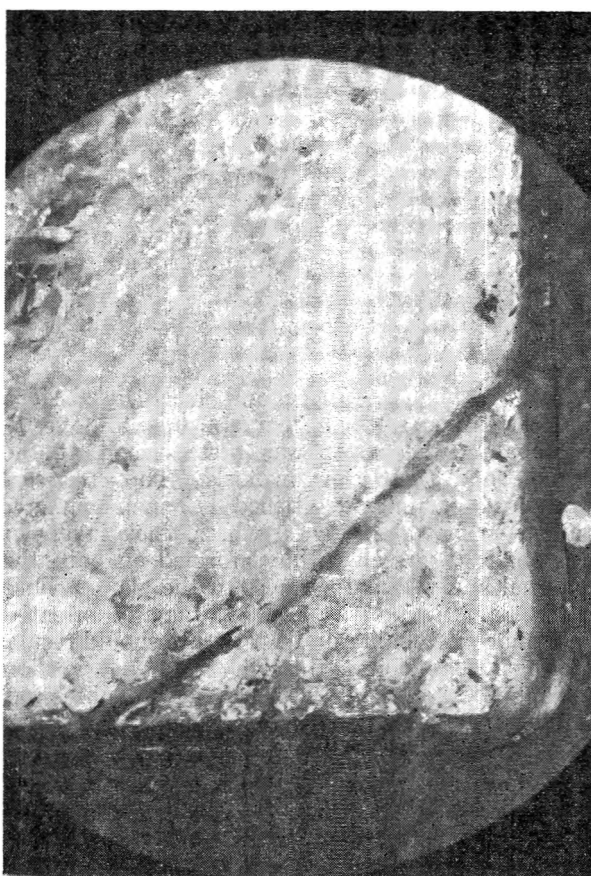


Fig. 3.—Section of quartz single crystal heated at 1740° for 20 min. in air, showing fusion at external surfaces and along crack. (50×).

(\sim 250°) to room temperature and then reheated first to 1600° for 10 minutes for the attainment of thermal equilibrium and then to 1750° for the melting experiment. During firing, all the specimens were wrapped in platinum foil. The ambient atmosphere was air in all cases. After heat treatment, the samples were mounted, sectioned and metallographically polished for examination.

III. Results

A. Quartz.—Fusion experiments were carried out between 1550 and 1750°. The lower limit was imposed by the extremely slow fusion rate although this is still approximately 150° above the melting point of quartz (\sim 1400°).⁷ At 1550°, for instance, the linear melting rate was only 3×10^{-6} cm. per minute. In general, prolonged heatings at these lower temperatures were subject to uncertainty due to the increasing tendency of the formation of cristobalite from the melted quartz (Fig. 1). At temperatures above 1750° melting had become too rapid for accurate rate determinations. The results obtained for samples from the four different sources mentioned were approximately equal. This is probably due to the similarity of their impurity contents.

In all the experiments carried out, melting invariably proceeded from the surface inwards. The result of a typical experiment is shown in Fig. 2. In no case was fusion observed to have taken place in the interior of a crystal except at along cracks which had formed when the quartz was rapidly heated (Fig. 3). The viscosity of liquid silica at these temperatures was so high,

about 10^8 poise at 1600° , that the geometry of the heated specimen was still preserved for the duration of the experiments. This is clearly illustrated in Fig. 1 and 3. The accurate measurement of the thickness of the melted layer was therefore possible. As the coefficient of thermal expansion of vitreous silica is negligibly small, the thickness of the solid glass at room temperature was considered to be that of the liquid layer at the experimental temperature. Within the limits of uncertainty, fusion-time relationships were linear as illustrated in Fig. 4. The observed melting rates at different temperatures between 1550 and 1750° are presented in Table I.

B. Cristobalite.—In general, when fused silica was devitrified at high temperatures to give β -cristobalite, the latter was first formed at the surface and then grew inwards. The cross-section of a partially devitrified $1/2$ inch diameter tubing is shown in Fig. 5 where thick layers of cristobalite are seen to have formed on both the external and internal surfaces of the glass. Since a circular tubing was used, a radially oriented columnar cristobalite grain structure should result. However, on cooling through the α - β inversion at about 250° , finer grained α -cristobalite was formed together with internal cracking due to the density difference between the two phases. Despite this, the room temperature microstructure still retains vestiges of the high temperature columnar structure as shown in Fig. 5.

A $1/2$ inch diameter tubing specimen which had been partially devitrified at 1600° , "up-quenched" to 1750° by quickly transferring to another furnace, and then maintained at this temperature for 4 minutes is shown in Fig. 6. A portion of the same specimen at higher magnification is shown in Fig. 7. It can be seen that melting had occurred on both the external and internal surfaces and proceeded inwards *via* the columnar grain boundaries. No fusion is observed to have occurred along the α -cristobalite grain boundaries which cross the columnar grains laterally. This is because the α -cristobalite was formed only after the fusion treatment. This experiment thus represents the superheating of β -cristobalite to approximately 40° above its melting point for 4 minutes. A significant feature revealed by Figs. 6 and 7 is that while extensive melting had taken place at both the internal and external surfaces, that occurring at the two *internal* vitreous silica-cristobalite interfaces was negligible. A rod specimen which had been completely devitrified, brought through the α - β inversion to room temperature, reheated to 1600° for 10 minutes and then kept at 1750° for 6 minutes is shown in Fig. 8. This heat treatment had resulted in the formation of many additional grain boundaries before fusion. It is seen that unlike Figs. 6 and 7, melting had now occurred along both the columnar and the new lateral grain boundaries.

IV. Discussion

A. Evidence of Superheating.—Experimental evidence of the superheating of crystalline solids, even to the extent of a few degrees above the melting temperature for a matter of only seconds, is

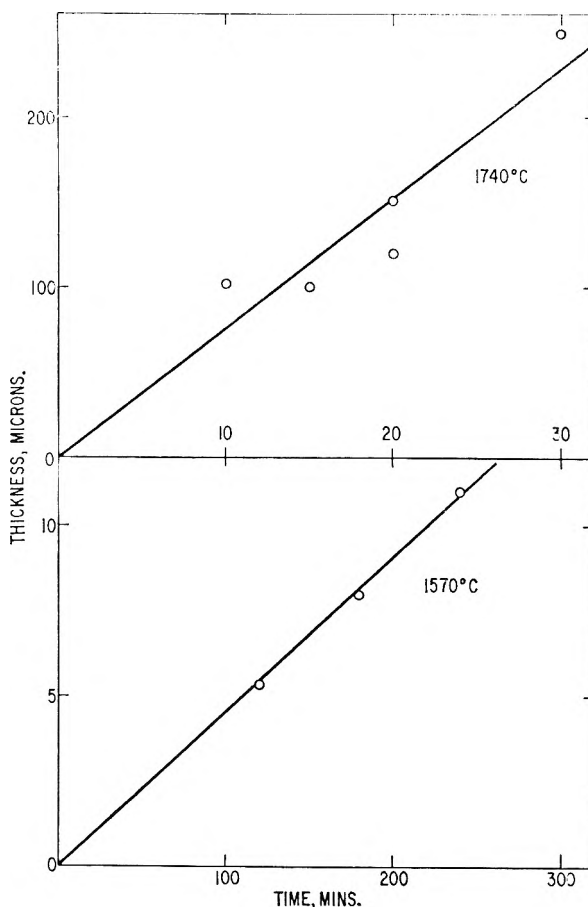


Fig. 4.—Growth of liquid phase with time for the fusion of crystalline quartz at 1740 and 1570° , respectively.

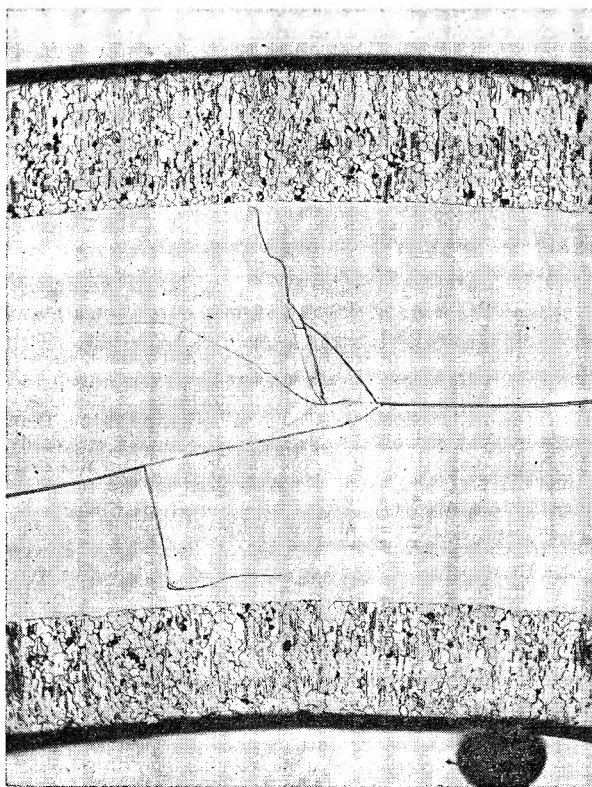


Fig. 5.—Formation of cristobalite by the incomplete devitrification of a $1/2$ inch diameter vitreous silica tubing. ($100\times$).

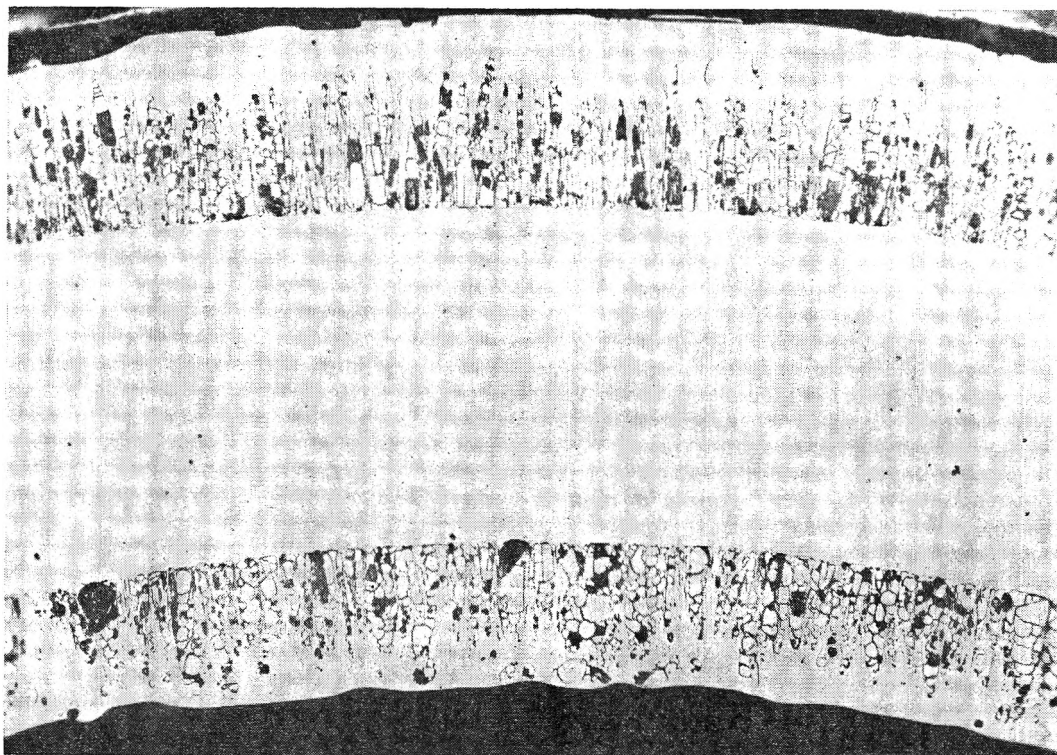


Fig. 6.—Section of two layers of cristobalite obtained from a partially devitrified vitreous silica tubing (as Fig. 5) heated to 1750° for 4 min. in air, showing melting at both external and internal surfaces. (100×).

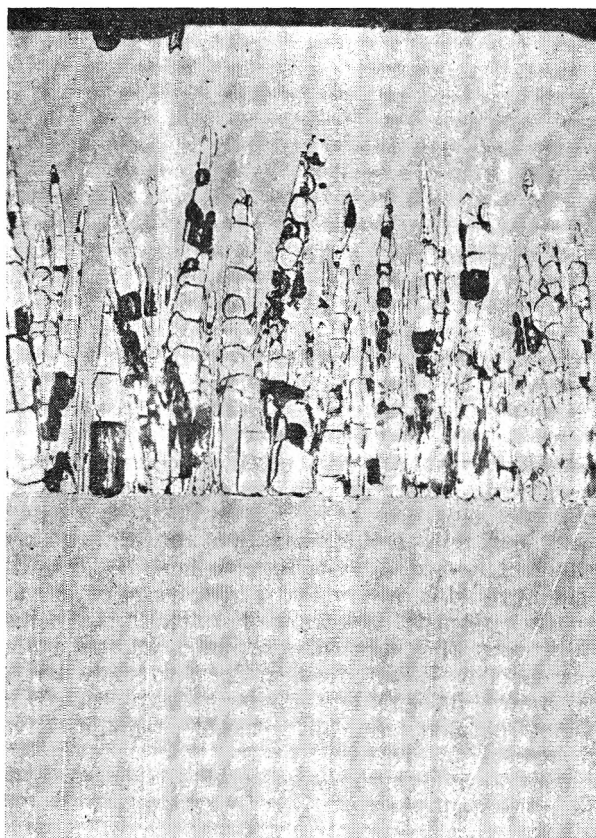


Fig. 7.—Magnified view of a part of Fig. 6. (300×).

extremely rare. The present work indicates that quartz has been superheated some 300° and cristobalite some 40° above their respective melting temperatures for periods in excess of 10 minutes.

That this was actually achieved under the present experimental conditions can be easily demonstrated. We will adopt the fusion of quartz as an example.

The dimensions of the samples used were 0.1 cm. × 0.5 cm. × 1.0 cm. and their average weight only about 0.15 g. The heat source of the furnace thus may be considered large relative to the sample. From the known thermal conductivity and heat capacity of quartz, and ignoring radiation effects, it is estimated that only seconds are necessary for the sample to reach about 1400°, the assumed melting point of quartz. More than two minutes were allowed for the sample to reach this temperature. Once this temperature is exceeded, heat flow will be primarily controlled by the latent heat of fusion of quartz. Since the thermal conductivity of quartz and vitreous silica is similar in magnitude¹⁰ ($\sim 10^{-2}$ cal. sec.⁻¹ cm.⁻¹ degree C.⁻¹), the time for the center of the specimen to reach the temperature of superheat is simply given by

$$t = \frac{Hd}{KA(T_1 - T_2)} \quad (1)$$

where T_1 is the temperature of the surface of the specimen (1700°, say), T_2 is the temperature at its center (1400°), K is the mean thermal conductivity of quartz and vitreous silica over this temperature range, A is the surface area (0.5 cm.²), d is half the thickness of the specimen (0.05 cm.) and H is the sum of the latent heat of fusion (~ 50 cal. g.⁻¹) and the integrated heat capacity (~ 0.3 cal. degree⁻¹ g.⁻¹) over the range 1400–1700° for half the mass of the sample. H is approximately 5 cal. and therefore t is only about 2 seconds. Since some experiments were conducted at 1740° for as

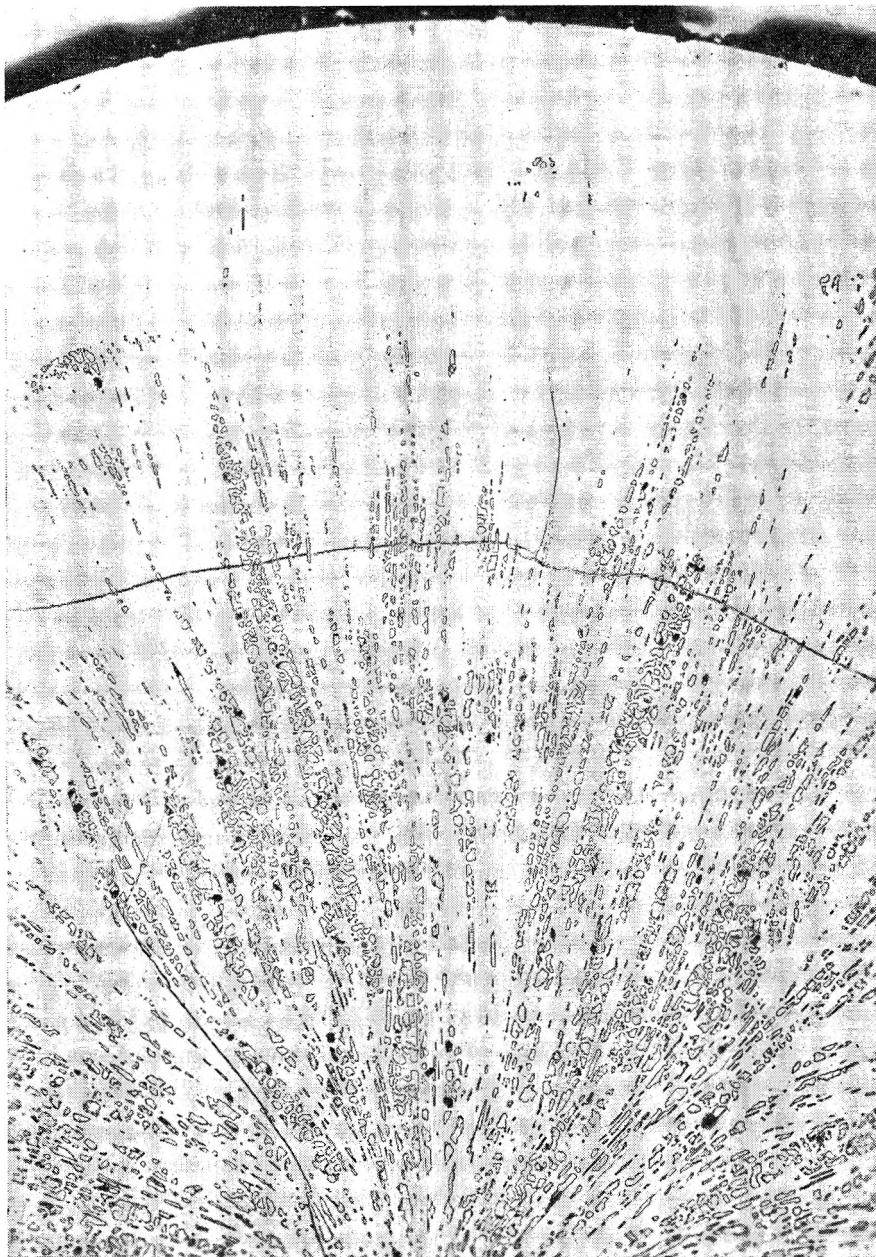


Fig. 8.—Section of cristobalite specimen obtained from a completely devitrified vitreous silica rod heated to 1750° for 6 min., showing melting at both columnar and lateral grain boundaries due to heat treatment described in text. (100×).

long as 30 minutes, there is little doubt that superheating was achieved.

B. Inapplicability of Homogeneous Mechanism of Fusion.—This investigation has clearly demonstrated that, contrary to the suggestions of Weyl and Marboe,⁹ the melting of quartz (see Figs. 1–3) and cristobalite (see Figs. 6–8) is not homogeneous but heterogeneous. Further the melting of quartz is heterogeneous even at 300° superheating.

Neglecting strain energy, the time required for homogeneous melting, if it is not limited by heat flow, should be of the order of the time, τ , for molecular relaxation within the crystal. For the homogeneous melting mechanism to be consistent

(9) W. A. Weyl and E. C. Marboe, *J. Soc. Glass Technol.*, **43**, 417 (1959).

with our results the relaxation time for quartz would have to exceed 10^4 seconds at 2000°K. which would correspond to a free energy of activation of at least 160 kcal./mole. This time, being 10^7 times the approximate relaxation time for viscous flow in fused silica, is improbably large. Therefore, it seems that homogeneous melting, if it were thermodynamically possible, should have occurred.

It is possible that homogeneous melting of quartz is prevented by the large strain energy which could develop from the accompanying volume change (15%). This energy, if unrelieved, would be sufficient to raise the melting temperature of quartz far above the temperatures used in this investigation. However, it might be largely relieved, for example, by the formation and move-

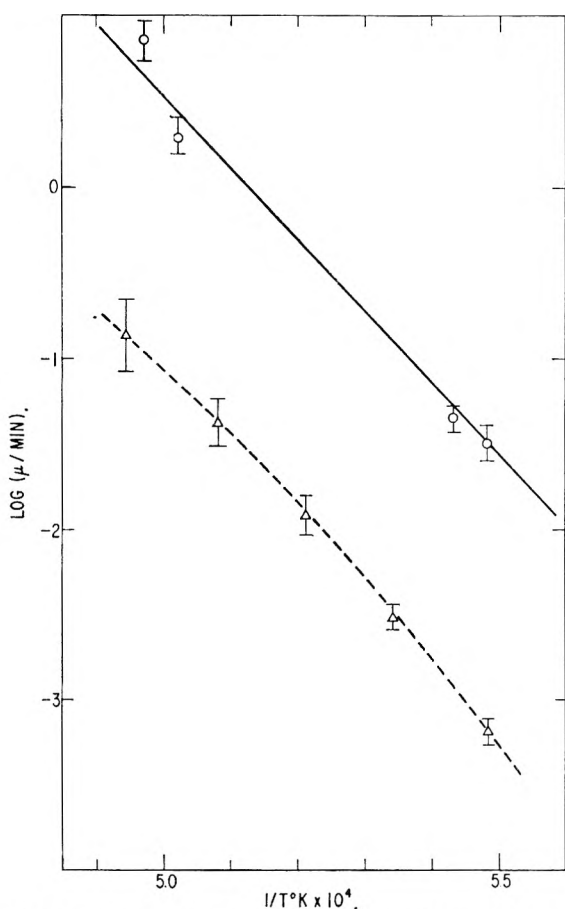


Fig. 9.—Relationship between the logarithm of melting rate and $1/T$ for quartz at 1550–1750°: O, observed data; Δ , calculated from equation 4.

ment of point defects in the quartz. To what extent this occurs cannot be decided because we lack information on the behavior of point defects in quartz. In cristobalite, however, the strain energy would hardly be sufficient to prevent homogeneous fusion since the volume change on melting is negligible.¹⁰

C. Application of Heterogeneous Melting Mechanism.—In our experiments liquid films quickly formed at the free surfaces and grain boundaries and grew inwards. The formal theory for the rate of propagation of liquid–crystal interfaces has been discussed fully elsewhere.^{11,4} It leads to the following relation

$$u = \frac{fD}{\lambda} [1 - \exp(\Delta g/kT)] \quad (2)$$

where D is the kinetic constant for interface motion in $\text{cm.}^2 \text{sec.}^{-1}$, f is the fraction of interface sites at which reaction can occur, λ is the “jump” distance and Δg is the motivating free energy. Provided D is identified with the coefficient of self-diffusion in the liquid and then related to the viscosity through the Stokes-Einstein relation, equation 2 becomes

$$u = \frac{fkT}{8\pi\lambda^2\eta} [1 - \exp(\Delta g/kT)] \quad (3)$$

This equation satisfactorily describes the rate of

(10) R. B. Sosman, “Properties of Silica,” Chemical Catalog Co., Inc., New York, N. Y., 1927, Chapter 21.

(11) W. B. Hillig and D. Turnbull, *J. Chem. Phys.*, **24**, 914 (1956).

crystal growth in undercooled glycerin and selenium with reasonable values of f .¹¹ However, even with catalyst impurities removed from the gas phase, it underestimates the rate of propagation of the cristobalite–fused silica interface by about an order of magnitude.⁸ This disparity may have been due to catalytic impurities originally present in the fused silica.

For testing equation 3 with our results we have set $f = 1$ and $\Delta g = (\Delta H_f/N)((T_m - T)/T_m)$ where ΔH_f is the molar heat of fusion, N is Avogadro’s number and T_m is the thermodynamic melting temperature. Also making use of the condition fulfilled in our experiments that $kT \gg \Delta g$ we obtain

$$u = \frac{\Delta H_f(T - T_m)}{T_m 3\pi\lambda^2\eta N} \quad (4)$$

To calculate u for quartz, we have put $\Delta H_f = 3$ kcal./mole,¹⁰ $\lambda = 3 \times 10^{-8}$ cm. (*i.e.*, approximately twice the Si–O bond distance) and η equal to the average values of the interpolated viscosity^{12–14} over the temperature range 1550 to 1750°. Values of u so calculated are compared with the measured values for quartz in Table I and the calculated and measured variations of the logarithmic rates with reciprocal temperature are compared in Fig. 9. Perhaps the most significant feature of the comparison is the good agreement between the variation of the two relations with reciprocal temperature. The *average* slopes of the curves are not significantly different, that of the calculated relation being the greater by only 1–2%. The actual magnitudes of the observed rates (see Table I) are at all temperatures about a factor of

TABLE I

COMPARISON OF OBSERVED FUSION RATES OF QUARTZ AND VALUES CALCULATED FROM EQUATION 4

T , °C.	Approximate superheat	Fusion rate, μ /minute Obsd.	Calcd.	Obsd./calcd.
1550	150	3.0×10^{-2}	6.6×10^{-4}	45
1600	200	1.3×10^{-1}	3.0×10^{-3}	43
1650	250	4.5×10^{-1}	1.2×10^{-2}	38
1700	300	1.5	4.3×10^{-2}	35
1750	350	6.0	1.5×10^{-1}	40

40 greater than the calculated rates. This disparity is of the same magnitude as found for the movement of the cristobalite–fused silica interface in devitrification with the catalytic impurities removed from the gas phase.⁸ A considerable part of the difference may arise from the uncertainties in the values of the variables in equation 4. Thus values of ΔH_f for quartz have been reported¹⁰ which are more than double the value used in our calculations. We have indicated by the spreads in the calculated values of u in Fig. 9 our estimate of the uncertainties in the viscosity. Also just what value should be assigned to λ is far from clear. Apart from these uncertainties the difference between the observed and calculated rates also may

(12) N. V. Solomin, *J. Phys. Chem., U.S.S.R.*, **14**, 235 (1940).

(13) J. O’M. Bockris, J. D. Mackenzie and J. A. Kitchener, *Trans. Faraday Soc.*, **51**, 1734 (1955).

(14) M. P. Vclarovich and A. A. Leontieva, *J. Soc. Glass Technol.*, **20**, 139 (1936).

reflect some inadequacy of the model or the catalytic effect of certain impurities (*e.g.*, H₂O) originally present in the quartz.

Acknowledgment.—One sample of synthetic quartz was kindly supplied by Dr. R. A. Laudise of the Bell Telephone Laboratories. We are grateful to Mrs. M. Houle for metallographic preparation of the samples, Mr. W. K. Murphy for experimental assistance and Dr. W. B. Hillig for valuable discussions.

DISCUSSION

A. VAN HOOK (Holy Cross College).—What is the temperature coefficient of thermal conductivity in this system? Have you tried any seeding experiments?

J. D. MACKENZIE.—The temperature coefficient of thermal conductivity at high temperatures is not available. However, the coefficients for both crystalline and vitreous silica are negligibly small at the lower temperatures as compared to that for viscous flow, for instance.

No seeding experiments were attempted nor necessary

since nucleation occurred readily at free surfaces and grain boundaries.

R. A. ORIANI (U. S. Steel Corporation).—Can you account for the much greater difficulty of superheating in other materials?

J. D. MACKENZIE.—The primary reason is probably the high fluidity of the melt of most materials. Thus the viscosity at the melting temperature is about 10⁻² poise for most materials whereas that for quartz is about 10¹⁰ poise. If we assume that the presently suggested mechanism is applicable and ignoring heat flow, then for $\eta = 10^{-2}$ and $(T - T_m) = 1^\circ$, equation (4) reduces to $u \approx 10\Delta H_f/T_m$, where the units of ΔH_f are calories per mole. The approximate fusion rates thus calculated for a variety of substances at a superheating of only one degree are given in the table.

Substance	Fusion rate, cm./sec.
Al	20
Pb	20
LiNO ₃	100
NaCl	70
Naphthalene	130
Benzene	100

ADSORPTION OF THORIUM IONS ON SILVER IODIDE SOLS¹

By E. MATIJEVIĆ, M. B. ABRAMSON,² R. H. OTTEWILL,³ K. F. SCHULZ AND M. KERKER

Clarkson College of Technology, Potsdam, N. Y.

Received March 9, 1961

The adsorption of thorium ions on dialyzed silver iodide sols over a pH range from 2.5–7.0 was determined using Th²³⁴ as a tracer. It was found that the amount of thorium adsorbed depends on pH, increasing sharply at pH > 4. It is above this pH that thorium ions show strong hydrolysis effects. Thus, it is believed that hydrolyzed thorium species adsorb more strongly than unhydrolyzed thorium ions. Electrophoresis and coagulation experiments indicate a strong reversal of charge of silver iodide particles in accordance with the adsorption effects.

Introduction

The role of adsorption of counterions on sol particles in the process of coagulation has been a subject of extensive investigation; yet, the results are still indecisive. The fact that adsorption takes place was demonstrated early in this century^{4,5} and attempts were made to connect the adsorbability of the counterions with the Schulze–Hardy rule.^{6–11} Freundlich proposed a theory of equivalent adsorption of counterions on the sol particles at and above the coagulation concentration.^{12,13} This theory was strongly criticized by Weiser^{14,15} who showed that although adsorption of counterions does take place, the quantities of different ions adsorbed are by no means equivalent. After

further experiments and study of the results, Freundlich himself recognized that his theory did not hold.¹⁶

There are several reasons for the discrepancy in conclusions reached by the early investigators. Firstly, the determination of the extremely small quantities of adsorbed materials was experimentally precarious because they were determined by difference. Secondly, the colloidal precipitates used as adsorbents were frequently very poorly defined systems (such as metal hydroxides, sulfides, etc.) which did not justify a direct comparison of data or a generalization of results. Finally, the results with various types of coagulating ions (such as dyes, colloidal electrolytes, organic ions, complex inorganic ions, simple inorganic ions, etc.) were indiscriminately compared and treated as if the coagulation mechanism in all cases was identical.

In connection with the last statement one must distinguish among three different groups of coagulating ions. Firstly, there are ions and molecules which are preferentially adsorbed on colloidal particles due to strong adsorption forces (*e.g.*, by chemisorption forces). In this group are large organic ions and polar molecules such as dyes, detergents, polymeric substances, and alkaloids such as strychnine, morphine, etc. For this case we have suggested the term “adsorption coagulation.”¹⁷ Secondly, there are ions which

(1) Supported by the Office of Ordnance Research Contract No. DA-ORD-10.

(2) Participant in the NSF Summer Research Project, 1960.

(3) On leave from Department of Colloid Science, University of Cambridge, England.

(4) H. Schulze, *J. prakt. Chem.*, [2] **25**, 431 (1882); **27**, 32 (1883).

(5) W. B. Hardy, *Proc. Roy. Soc. (London)*, **A66**, 110 (1900).

(6) D. B. Ganguly and N. R. Dhar, *J. Phys. Chem.*, **26**, 836 (1922).

(7) N. G. Chatterjee and N. R. Dhar, *Kolloid-Z.*, **33**, 18 (1923).

(8) N. R. Dhar, K. C. Sen and H. Ghosh, *J. Phys. Chem.*, **28**, 457 (1924).

(9) H. B. Weiser, *ibid.*, **29**, 955 (1925).

(10) W. R. Whitney and J. E. Ober, *Z. physik. Chem.*, **39**, 630 (1902); *J. Am. Chem. Soc.*, **23**, 842 (1903).

(11) S. Linder and H. Picton, *Z. physik. Chem.*, **73**, 385 (1910).

(12) H. Freundlich, *Kolloid-Z.*, **1**, 321 (1907); *Z. physik. Chem.*, **73**, 385 (1910).

(13) H. Freundlich and H. Schucht, *ibid.*, **85**, 641 (1913).

(14) H. B. Weiser and J. L. Sherrick, *J. Phys. Chem.*, **23**, 205 (1919).

(15) H. B. Weiser and E. B. Middleton, *ibid.*, **24**, 30, 630 (1920).

(16) H. Freundlich, K. Joachimson and G. Ettisch, *Z. physik. Chem.*, **A141**, 249 (1929).

(17) E. Matijević and R. H. Ottewill, *J. Colloid Sci.*, **13**, 242 (1958).

form a sparingly soluble salt or a strong complex with the crystal lattice ions of the adsorbent and particularly with the potential-determining ions on the surface. For this case the adsorption rules expressed by Paneth, Fajans, and Hahn are applicable.¹⁸⁻²⁴ Finally, there are ions which do not show either effect mentioned above. These are usually simple inorganic and organic ions whose compounds with the crystal lattice or potential-determining ions are quite soluble. When referring to their coagulation effects, they are usually called "neutral electrolytes."

After the obvious failure of the Freundlich theory of coagulation by equivalent adsorption, there was a general feeling that the adsorption data with these "neutral electrolytes" were doubtful, and it was tacitly accepted that such adsorption is negligible. However, with refinements in experimental techniques (especially the use of radio-isotopes) and new advances in coagulation theories, the interest in accurate determination of adsorption of "neutral" ions and the role of this adsorption in coagulation has been revived. Recently, Herak^{25,26} measured the adsorption of simple di- and trivalent counterions on a silver iodide sol and found a pronounced adsorption. Moreover, the adsorbed quantities seemed to be equivalent.

In this work, we have attempted to determine the adsorption of thorium ions on silver iodide sols over various pH ranges, using Th²³⁴ as a tracer. There is little doubt that the ionic thorium species are adsorbed onto the sol particles since thorium shows the "reversal of charge" phenomenon which is understood to be caused by adsorption of counterions. Differences in adsorption at various pH's should reveal the influence of the hydrolysis of counterions upon adsorption since it is well known that the thorium ion is subject to very pronounced hydrolysis.²⁷⁻²⁹ Since the coagulation concentrations of thorium salt solutions are very low (in the range of $<10^{-5}$ moles/l.), the system lends itself both to direct adsorption measurements and measurements by difference. It was hoped that adsorption measurements of this type would shed further light on the mechanism of coagulation.

Experimental

Materials.—All materials used were of highest purity grade, and the water was doubly distilled, the second distillation being carried out from an all-Pyrex still.

Preparation of the Silver Iodide Sol.—Concentrated silver iodide sols were prepared in essentially the same manner as that described by Harmsen, van Schooten and Overbeek.³⁰ Five hundred ml. of a 50 mM solution of silver nitrate was added with vigorous stirring to 500 ml.

- (18) F. Paneth, *Physik-Z.*, **15**, 924 (1914).
- (19) K. Horovitz and F. Paneth, *Z. physik. Chem.*, **89**, 513 (1915).
- (20) K. Fajans and K. Beckerath, *ibid.*, **97**, 478 (1921).
- (21) K. Fajans and T. Erdey-Grúz, *ibid.*, **A168**, 117 (1931).
- (22) O. Hahn, O. Erbacher and N. Fechtinger, *Naturwissenschaften*, **14**, 1196 (1926).
- (23) O. Hahn, *Ber.*, **59B**, 2014 (1926).
- (24) O. Hahn and L. Imre, *Z. physik. Chem.*, **A144**, 161 (1929).
- (25) M. J. Herak, Dissertation, Univ. of Zagreb, 1960.
- (26) M. J. Herak and M. Mirnik, *Kolloid-Z.*, **168**, 139 (1960).
- (27) E. Matijević, M. B. Abramson, K. F. Schulz and M. Kerker, *J. Phys. Chem.*, **64**, 1157 (1960).
- (28) S. Hietanen and L. G. Sillén, *Acta Chem. Scand.*, **13**, 533 (1959).
- (29) K. A. Kraus and R. W. Holmberg, *J. Phys. Chem.*, **58**, 325 (1954).

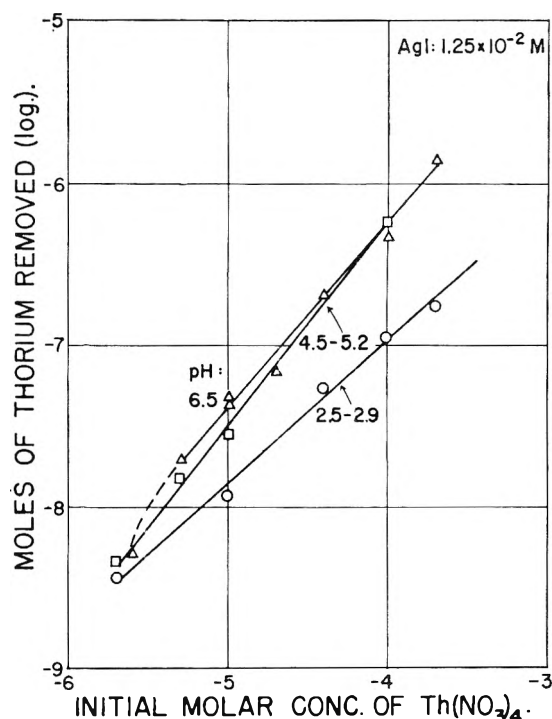


Fig. 1.—Moles of thorium ions adsorbed on AgI sol (1.25×10^{-2} mole/l.), plotted against the initial concentration of thorium nitrate in solution for three pH ranges: 2.5-2.9, 4.5-5.2 and 6.5.

of a 55 mM potassium iodide solution. The resultant sol was immediately electrodialed, aged at 80° for 24 hours, re-electrodialyzed, and then electrodeccanted. The concentrated sol was then diluted with distilled water to give a stock solution of appropriate concentration. This concentration was determined by withdrawing an aliquot and drying to constant weight at 110°. In the present work a stock solution of 2.56×10^{-2} M silver iodide was employed.

Preparation of Th²³⁴(UX₁).—This was prepared following a method described by Dyrssen,³¹ using ion-exchange separation of Th²³⁴ from uranium on a bed of Amberlite IR-112. The thorium was extracted from the resin using oxalic acid solution, and the eluate was evaporated to dryness under an infrared lamp to decompose the oxalate. The ThO₂ remaining was dissolved in concentrated nitric acid, evaporated to dryness to remove excess nitric acid and then taken up in dilute nitric acid (10^{-3} M). The Th²³⁴ solution was kept as a stock solution in 10^{-3} M nitric acid, and its activity was checked daily. The half-life time was checked and found to be 24.6 days; this is in good agreement with the literature value of 24.5 days.³²

Adsorption Measurements.—Adsorption determinations were performed either at constant initial Th²³⁴ concentration or at constant Th²³⁴/Th ratio. The solutions for measurements at constant Th²³⁴ concentrations were prepared by taking 1 ml. of Th²³⁴ stock solution, 0.5 ml. of 2×10^{-3} M potassium iodide solution and a volume of a thorium nitrate stock solution (either 2×10^{-4} or 2×10^{-3} M) chosen to give the desired final concentration of thorium nitrate. The pH of this solution was then adjusted by addition of either sodium hydroxide or nitric acid and the volume made up to 10 ml. Four ml. of this solution was then added to 4 ml. of the silver iodide sol. The blank was prepared by adding 4 ml. of the thorium nitrate solution to 4 ml. of distilled water. The solutions were mixed in test-tubes and allowed to stand for 30 minutes. During this time, particularly at low pH and thorium nitrate concentrations in the region of 10^{-4} M, the sol coagulated and settled out. The

(30) G. J. Harmsen, J. Van Schooten and J. Th. G. Overbeek, *J. Colloid Sci.*, **8**, 72 (1953).

(31) D. Dyrssen, *Svensk Kemisk Tidskr.*, **62**, 153 (1950).

(32) G. Friedlander and J. W. Kennedy, "Introduction to Radiochemistry," John Wiley and Sons, Inc., New York, N. Y., 1949.

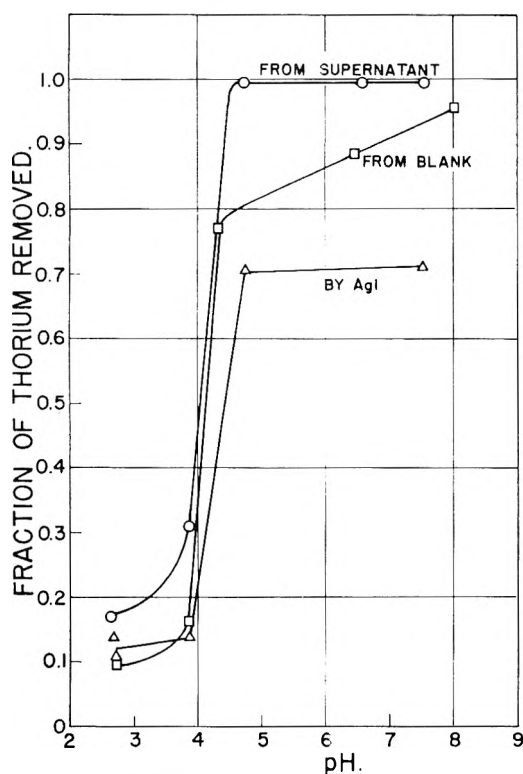


Fig. 2.—Fraction of thorium removed from a 1×10^{-4} molar solution of thorium nitrate as determined from adsorption on AgI (Δ), from loss in the blank (no AgI present) (\square) and from loss from supernatant (sol containing AgI) for different pH values.

tubes were then re-agitated and both blank and sol centrifuged for 5 minutes at approximately 8,000 r.p.m. Four ml. of the centrifuged supernatant was withdrawn, the pH measured, and the count taken. A further 1 ml. was then added and the count repeated. The solution then was evaporated under an infrared lamp and counts taken on the dry sample. A similar procedure was employed for the blank.

When a constant $\text{Th}^{234}/\text{Th}$ ratio was used, the procedure remained the same, except that the ratio of active to inactive thorium was kept constant.

The solid material left after removal of the supernatant was washed with 5 ml. of distilled water, centrifuged and rewashed (ca. 5 ml.). Periodically the washings were checked for activity. Finally, the silver iodide was quantitatively transferred, as an aqueous sludge to a specimen cup, the water removed by evaporation under an infrared lamp, and then the activity determined.

Counting Technique.—Counts were taken by means of a Nuclear Chicago Model 186 Decade scaler in conjunction with a GM tube operated at 1300 volts. Glass cups of 2-cm. diameter, inserted directly on the platform of the lead tower were used, and counts were taken for at least 5 minutes. Usually duplicate determinations were made, but if erratic readings were obtained several more measurements were taken.

Microelectrophoresis Measurements.—Mobility determinations were made in an equipment described in detail previously.³³

Sols for electrophoresis were prepared in the following manner. Aliquots of potassium iodide and thorium nitrate were mixed to give the desired concentrations and then adjusted to the required pH by addition of nitric acid or sodium hydroxide; the volume was then brought to 5 ml. and the pH confirmed. This mixture was added to 5 ml. of silver iodide sol of concentration $2 \times 10^{-4} M$. Thus the resultant systems were of silver iodide concentration $10^{-4} M$ and $pI = 4$.

Mobilities were measured within ten minutes of mixing the two solutions. After determination of mobility the pH of the sol was again measured.

Coagulation Measurements.—Coagulation of the sols was brought about by mixing solutions containing constant concentration of the sol and variable concentrations of thorium nitrate. The process was followed by measuring changes of optical density with time using a Model DU Beckman spectrophotometer. The same procedure of preparing solutions was employed as in the case of microelectrophoresis measurements.

Results

The adsorption of thorium ions on the AgI sol particles was measured over the pH range 2.5–7.0; most of determinations being made over the pH ranges 2.5–2.9, 4.5–5.2, and 6.5–7. In Fig. 1, the removal of thorium by a silver iodide sol (concn. = 1.25×10^{-2} moles/l., $pI = 4.3$) is plotted against the initial concentration of thorium nitrate in solution. The curves include data obtained using a constant Th^{234} concentration as well as a constant $\text{Th}^{234}/\text{Th}$ ratio. The agreement using both techniques is good, but the method of constant Th^{234} was preferred in view of the higher counts per unit volume. These results show that the amount of thorium ions adsorbed is greater at higher pH's.

These data, however, do not take into consideration the loss of thorium from solution due to the adsorption on glass. Adsorption of cationic species on glass has been detected and measured by a number of investigators.^{34–40} These experiments have invariably shown that cations are adsorbed on glass and that this adsorption depends strongly on pH, being always smaller (often negligible) at low pH. In particular, the adsorption of thorium ions on glass was measured by J. and B. Rydberg,⁴¹ who found that adsorption of Th^{234} by glass underwent a sharp increase at pH 4.2 reaching a maximum of 80% adsorption at this pH compared with less than 5% at pH 2 or above pH 7.

For this reason we have measured the adsorption of thorium ions on glass under conditions comparable to the experiments with the AgI sols. Figure 2 shows the amount of Th removed at various pH's from the supernatant and from the blank and also the amount adsorbed by the solid AgI for an initial concentration of $1 \times 10^{-4} M \text{Th}(\text{NO}_3)_4$.

In Fig. 3 the lower curve gives the moles of thorium ions removed by silver iodide at pH 2.6 as a function of the equilibrium concentration of thorium nitrate. At such a low pH, there is no significant adsorption on glass relative to that on AgI. This is especially true at higher concentrations of thorium, and the adsorption data can be used unambiguously. Excellent agreement is obtained here between adsorption as measured by loss from the supernatant and that from the activity on the solid.

(34) I. Beloni, M. Haissinsky and H. N. Salama, *ibid.*, **63**, 881 (1959).

(35) M. Haissinsky and Y. Laflamme, *J. chim. phys.*, **55**, 510 (1958).

(36) I. E. Starik and M. C. Lambert, *Zhur. Neorg. Khim.*, **3**, 136 (1958).

(37) I. E. Starik and A. B. Kossitsyn, *ibid.*, **2**, 444 (1957).

(38) S. Otani, M. Miura and H. Monda, *J. Sci. Hiroshima Univ.*, **A22**, 61 (1958).

(39) T. Schonfeld and E. Broda, *Mikrochem. ver. Mikrochim. Acta*, **36/37**, 537 (1951).

(40) J. F. King and A. Romer, *J. Phys. Chem.*, **37**, 663 (1933).

(41) J. Rydberg and B. Rydberg, *Svensk Kemisk Tidsskr.*, **64**, 200 (1952).

(33) E. Matijević, K. G. Mathai, R. H. Ottewill and M. Kerker, *J. Phys. Chem.*, **65**, 826 (1961).

The upper curve on Fig. 3 gives the adsorption for the pH range 6.6-6.8 as a function of initial concentration of thorium. As is already clear from the above, there is considerable adsorption of thorium ions on both glass and AgI at $pH > 4$. Since most of our data on AgI were obtained by direct measurement of the activity of the solid, we were unable to relate quantitatively the adsorption on AgI to the *equilibrium* concentration of thorium in solution. However, it is quite obvious that there is much greater adsorption of thorium on the AgI at higher pH and a correction for the loss of thorium on glass would give even higher values for the amount adsorbed on AgI as a function of the equilibrium concentration of Th.

Coagulation and Electrophoresis.—The coagulation effects of thorium upon silver iodide sol have been investigated previously with sols *in statu nascendi*^{27,42} and dialyzed sols.⁴³ However, it was desirable to obtain coagulation concentrations of thorium ions under the same conditions as used in adsorption measurements presented here. Figure 4 (lower) gives the coagulation curves for silver iodide sols ($1 \times 10^{-4} M$ AgI, $pI = 4$) at pH values of 2.6, 4.5 and 6.5, respectively. The coagulation concentrations, which were obtained by extrapolating the steep part of the coagulation limit (A) to zero turbidity, agree very well with the values for silver iodide sols *in statu nascendi*.²⁷ It is of interest that in both cases the magnitude of the turbidity is in the order $\tau_{2.6} > \tau_{4.5} > \tau_{6.5}$. The stability limits (B) of both dialyzed sols and sols *in statu nascendi* are in perfect agreement at pH 4.5. At pH 6.5 there are no data for sols *in statu nascendi* for comparison. At pH 2.6 there is a disagreement between the two results. The sols *in statu nascendi* exhibit a stability limit at much higher concentrations of thorium than the dialyzed sols, and at still lower pH, no stability limit was observed.

The mobility of the AgI particles was measured as a function of thorium nitrate concentration over the range $5 \times 10^{-7} M$ to $10^{-4} M$ at pH values of 2.6, 4.5 and 6.5. The mobility against log concentration curves are illustrated in Fig. 4 (upper). In all three cases, as would be expected from the coagulation effects, reversal of charge takes place. There is considerable difference between the gradients of the curves at the reversal of charge concentration, the steepness increasing with increasing pH.

Addition of distilled water to sols with a positive charge resulted in a *very* slow decrease in positive mobility, the decrease during the first ten minutes after dilution being negligible. Thus it would appear that the desorption of the thorium ion from the surface is a slow process and confirms that the errors introduced into the adsorption measurements by washing the solid with distilled water are negligible.

Discussion

Our present results on the adsorption of ionic

(42) K. F. Schulz and E. Matijević, *Kolloid-Z.*, **168**, 143 (1960).

(43) G. N. Goroehowski and J. R. Protass, *Z. physik. Chem.*, **A174**, 122 (1935); H. R. Kruyt and S. A. Troelstra, *Kolloid-Beihfte*, **54**, 262 (1943).

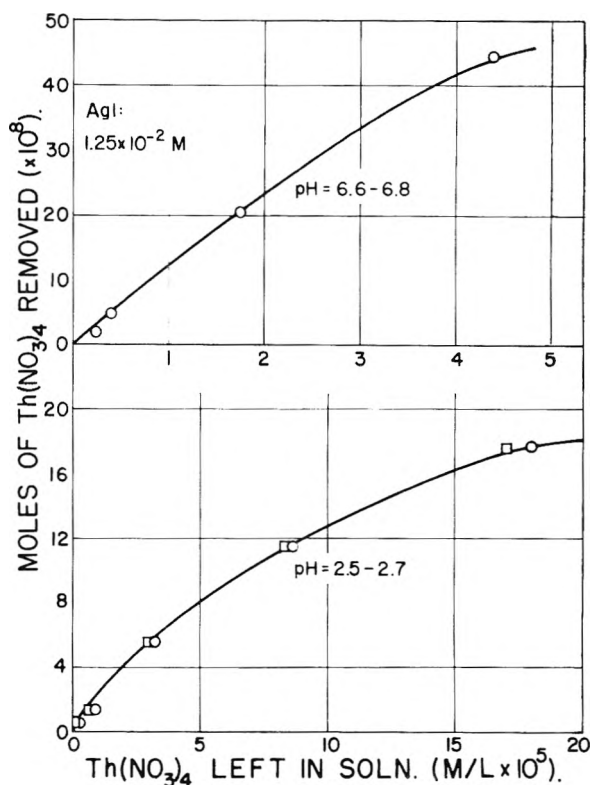


Fig. 3.—Moles of thorium ions adsorbed on AgI sols (1.25×10^{-2} mole/l.) in two pH ranges: 2.5-2.7 and 6.6-6.8 plotted against thorium nitrate left in solution (calculated from the difference). \circ , adsorption determined directly on the solid; \square , adsorption determined from the loss from supernatant.

thorium species on silver halides using dialyzed sols are in qualitative agreement as far as pH effects with earlier work on sols *in statu nascendi*.⁴⁴ However, in the earlier work the measurements were not sensitive enough to detect adsorption at low pH's.

From Fig. 3, it is apparent that at pH 2.6 adsorption increases with increasing concentration of $\text{Th}(\text{NO}_3)_4$ in solution to a limiting value which corresponds to 6×10^{-3} g. equiv. of thorium/mole of AgI. Herak²⁵ found for several trivalent ions and one divalent ion a corresponding adsorption of $\sim 3 \times 10^{-3}$ g. equiv./mole of AgI. These values are remarkably close, especially if one considers that the sols were prepared differently and that different sol concentrations were used. From the surface area of this uncoagulated sol, as determined from a particle size distribution obtained by electron microscopy, these results correspond to one thorium ion adsorbed per 400 \AA^2 of the surface. This is about the average density of potential determining ions (I^-) adsorbed on a negative silver iodide sol.⁴⁵⁻⁴⁷ Thus, it appears that at low pH the limiting adsorption with thorium is reached when one thorium ion is adsorbed per approximately one potential determining ion. The thorium con-

(44) K. F. Schulz and M. J. Herak, *Croat. Chem. Acta*, **30**, 127 (1958).

(45) E. J. W. Verwey and H. R. Kruyt, *Z. physik. Chem.*, **A167**, 137 (1933).

(46) M. Mirnik and B. Težak, *Trans. Faraday Soc.*, **50**, 65 (1954).

(47) G. L. Mackor, *Rec. trav. chim.*, **70**, 763 (1951).

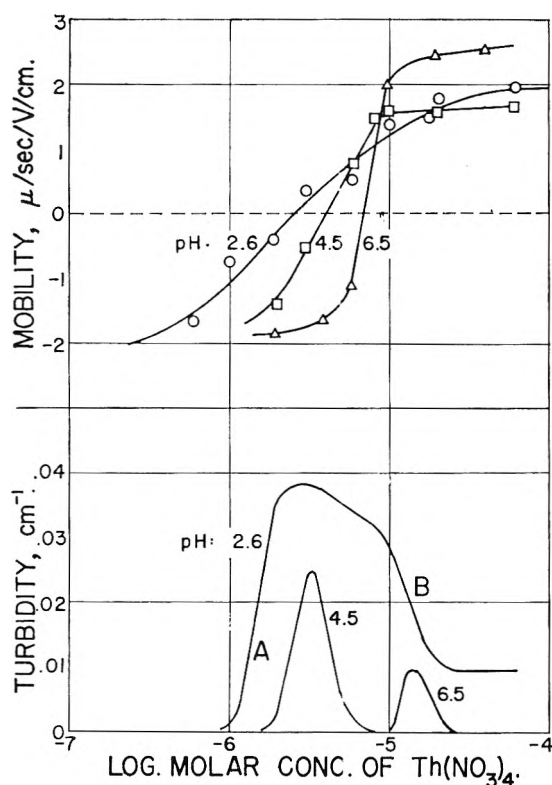
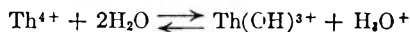


Fig. 4.—Turbidity and mobility curves of a dialyzed silver iodide sol (AgI : 1×10^{-4} mole/l., $pI = 4$) coagulated by thorium nitrate at the different pH values of the sol, *viz.*, 2.6, 4.5 and 6.5.

centration at which this "saturation" effect occurs corresponded to the reversal of charge region in the coagulation curve (Fig. 4) as one would expect. In the concentration range for critical coagulation (Fig. 4, limit A), the amount of thorium adsorbed is considerably lower.

The most striking effect is that of the pH influence. At higher pH values the adsorption of thorium on AgI appears to be higher, a sharp increase taking place at a $pH \sim 4$ (Fig. 2). It is precisely at this pH , however, that a sharp upturn in coagulation concentration occurs (Fig. 2, ref. 27). This change was explained in terms of the following hydrolysis reaction²⁷



which becomes predominant at very low concentrations of thorium.^{27,29} It appears, then, that this hydrolyzed species is more readily adsorbed. Using the equilibrium constant of 5×10^{-6} , given by Kraus and Holmberg²⁹ for this reaction, we find that the increased adsorption of thorium on both glass and silver iodide (Fig. 3), occurs at a pH where the hydrolyzed species becomes predominant. This is a further indication that hydrolyzed species of Th ion are more strongly adsorbed than the simple hydrated ion.

Similar effects on the influence of pH on the adsorption of metal ions have been detected before.^{21,43,49} One common explanation was that "radiocolloids" were formed at higher pH 's and

are more strongly adsorbed than simple ions,²⁴ but this *ad hoc* explanation is questionable.³⁴ Such "radiocolloids" are presumed to be finely dispersed metal hydroxides. Although the solubility product for thorium hydroxide^{50,51} has been reported to be as low as $\sim 10^{-45}$, it seems unlikely that thorium hydroxide does form at the concentrations and pH 's employed in these experiments. We have never observed the formation of a precipitate of thorium hydroxide under our experimental conditions. Data reported on solubilities of metal hydroxides are often quite unreliable. Furthermore, the simple application of solubility product constant principle cannot be employed when equilibria with hydrolyzed species, rather than simple ions are involved. Also, other kinds of complexes—such as thorium-halide complex ions—will retard the formation of thorium hydroxide. For these reasons we believe that it is the formation of hydrolyzed ionic species at higher pH that accounts for increased adsorption on both the glass and AgI surfaces.

In support of this position we might point out that at low pH aluminum ions do not reverse the charge, whereas at higher pH 's where hydrolyzed aluminum complexes are formed a very strong reversal of charge is observed.³³

It appears then that the hydrolyzed ionic species adsorb more strongly on the surface of silver halides than the simple hydrated ion, even though the latter may carry a higher charge. We believe this enhanced adsorption is due to the presence of the hydroxyl group. This may not be obvious in the case of thorium where the hydrolyzed ion is presumed to be a monomer, ThOH^{3+} . However, in the case of aluminum, where the ionized species is a polynuclear complex,^{33,52} and no direct attachment of the metal atom to the solid surface can occur, contact of counterion through the hydroxyl group becomes the only possibility. (It is tacitly assumed that upon adsorption, the simple metal ion loses at least part of its hydration shell.)

The difference in adsorption between the hydrolyzed and the non-hydrolyzed species might be due to the effect of exchange adsorption of H^+ ions on the heteropolar surface. Since simple Th^{4+} (hydrated) are present only in media of high concentrations of hydrogen ions they may actually be replaced by them. It is known that highly valent ions can be desorbed by lower valent ions.^{41,53} Recently, Herak has demonstrated^{25,26} by direct adsorption measurement that this exchange appears to be equivalent.

Another factor that should be considered in discussing the adsorption of non-hydrolyzed thorium ions is the strong complexing tendency of thorium ions with various anions.^{54,55} Although there are no data available for iodide, thorium is known to complex with chloride.⁵⁴ Such complexes between the stabilizing ions and counterions (in our case

(50) Y. Oka, *J. Chem. Soc. Japan*, **61**, 311 (1940).

(51) I. M. Korenman, *Zhur. Obshchei Khim.*, **25**, 1801 (1955).

(52) C. Brosset, G. Biedermann and L. G. Silén, *Acta Chem. Scand.*, **9**, 1917 (1954).

(53) J. F. King and U. T. Greene, *J. Phys. Chem.*, **37**, 1047 (1933).

(54) E. L. Zebroski, H. W. Alter and F. K. Heumann, *J. Am. Chem. Soc.*, **73**, 5646 (1951).

(55) R. A. Day and R. W. Stoughton, *ibid.*, **72**, 5662 (1950).

(48) J. F. King and P. R. Pine, *J. Phys. Chem.*, **37**, 851 (1933).

(49) H. Leng, *Sitzber. Akad. Wiss. Wien. [IIA]*, **136**, 19 (1927).

thorium) may play a significant role. Coagulation and electrophoresis experiments on AgI with another quadrivalent ion, *viz.*, zirconium, show quite different effects than observed with thorium under identical conditions.⁵⁶ It is quite possible that specific complexing effects may play a role here and experiments which may give us a better insight into these problems are at present underway.

In our earlier coagulation experiments with sols *in statu nascendi*, we did not detect a stability limit at the lower pH values even at high Th ion concentrations, and we concluded from this that non-hydrolyzed Th ions, which constitute the prevalent species at such pH's, do not reverse the charge. The adsorption, coagulation and mobility measurements described in this work show that at sufficiently high concentrations, Th⁺⁴ ions do actually reverse the charge.

This apparent contradiction arises because the absence of a stability limit in the case of our earlier experiments is not sufficient proof that there has not been reversal of charge. We have now determined the mobility of the particles of a AgI sol *in statu nascendi* (AgNO₃ 1×10^{-4} M, KI 2×10^{-3} M) at pH 2 in the presence of 1×10^{-3} M Th(NO₃)₄. The particles were positively charged showing reversal of charge but had a mobility of only 0.34 μ /sec./v./cm. This is considerably lower than the mobility observed with a dialyzed sol under comparable conditions.

The explanation of the absence of a stability limit for the recharged sols *in statu nascendi* is

(56) E. Matijević, K. G. Mathai and M. Kerker, to be published.

as follows. It is known that the concentration of anions necessary to produce coagulation decreases very sharply with decreasing surface charge density of the sol particles.⁵⁷ Apparently, then, the very weakly charged sols *in statu nascendi* were coagulated by the rather low concentration of anions (nitrate) present in solution. Thus, even though the particles had undergone reversal of charge, they were not stabilized. On the other hand, with the dialyzed sols, the surface charge density is sufficiently high so that coagulation by the existing anions does not occur. The coagulation curves for these sols do show a stability limit at the lowest pH.

We are planning experiments to explore these differences more fully.

DISCUSSION

R. K. ILER (E. I. du Pont Company).—In regard to the basic aluminum ions that are strongly adsorbed, does increasing the temperature of an aluminum salt solution have any effect, especially when at pH 6?

E. MATIJEVIĆ.—We have studied the influence of temperature upon aluminum salt solutions by means of coagulation effects and reported these results in a previous paper (E. Matijević and B. Težak, *J. Phys. Chem.*, **57**, 951 (1953)). However, we did not study directly the adsorption changes of aluminum ionic species at different temperatures.

E. D. GODDARD (Lever Brothers Company).—The explanation advanced for the pH effect on coagulation which involves the formation of basic salts brings to mind the work of Wolstenholme and Schulman, who advanced a similar explanation to account for the effect of a number of different salts on fatty acid monolayers at various pH levels.

(57) J. Herak and B. Težak, *Archiv. kem.*, **25**, 87 (1953).

MODIFICATION OF GROWTH RATE AND HABIT OF ADIPIC ACID CRYSTALS WITH SURFACTANTS

BY ALAN S. MICHAELS AND FREDERICK W. TAUSCH, JR.

Department of Chemical Engineering, Massachusetts Institute of Technology, Cambridge, Massachusetts

Received March 1, 1961

The isothermal (32.7°) growth of crystals of adipic acid from aqueous solution under carefully controlled conditions has been studied as a function of (a) supersaturation level (1 to 13%) and (b) concentration of various anionic and cationic surfactants (0 to 360 mg./l.), using a specially designed crystallizing apparatus. Growth rates of the characteristic faces ((001), (010) and (110)) of the crystals were determined microscopically. Sorption of surfactants on the crystals was independently determined. While results are in general qualitative agreement with earlier work on this system, a number of very significant and unusual effects have been detected which could not have been observed without control of temperature and supersaturation. The growth-retardation on certain faces is far greater than previously reported, and the effect of additive is strongly dependent on supersaturation level; at low supersaturation, increasing additive concentration results in drastic reduction or cessation of growth on certain faces, while at high supersaturation levels the additives have relatively little effect on growth, regardless of concentration. A particularly interesting result is that anionic additives actually significantly accelerate growth on the (001) face. It is also found that additives increase the supersaturation level at which extensive three-dimensional nucleation occurs, and also result in better-formed crystals. The results are interpreted in terms of two-dimensional nucleation and dislocation theories of crystal growth, and mechanisms for growth and habit modification are developed.

I. Introduction

It has long been known that trace concentrations of certain additives can have profound effects on crystal growth rate and habit. These effects are of great importance in many fields of science and technology, but the mechanisms by which additives affect crystal growth are not clear. It is generally agreed that additives must adsorb to some extent on a crystal surface in order to affect growth on that face. There has also been some evidence that the effectiveness of additives decreases with increasing "tempo" of crystallization.^{1,2} Previous studies of the effect of additive on crystal growth from solution, however, have generally involved neither measurements of additive adsorption nor careful control of the factors which determine growth rate.

Recent work^{3,4} has shown that certain surface active agents modify the habit of adipic acid crystals grown from aqueous solution. Adipic acid crystallizes from distilled water as thin hexagonal plates (see Fig. 1) with prominent hexagonal (001) faces (referred to as C faces), (010) side faces (B faces), and (110) end faces (A faces). X-Ray studies⁵ have shown that the linear, six-carbon, dicarboxylic adipic acid molecules are lined up in this crystal end-to-end so that the C faces represent an end view of the molecule and are entirely carboxyl in nature, while the A and B faces represent side views of the adipic acid molecule and are therefore partially carboxyl and partially hydrocarbon in nature. As little as one mg./liter of a cationic surfactant modifies the habit from thin hexagonal plates to even thinner hexagonal plates (see Fig. 1), while as little as 25 mg./liter of an anionic surfactant results in thicker

hexagonal plates or prisms. It has been postulated that the partially-ionized negatively-charged surface carboxyls on all faces result in coulombic adsorption of the cationic surfactant on all faces, but more extensively on the C faces (due to higher carboxyl density) than on the A and B faces, resulting in relatively greater retardation of growth on the C faces and hence thinner plates. The anionic surfactant, on the other hand, is coulombically repelled from all faces by the surface carboxyls, but can adsorb amphipathically (non-ionically) on the partially-hydrocarbon A and B faces, thus retarding growth on these faces more than on the C faces and resulting in thicker plates and prisms.

In the light of previous work, the present investigation has involved direct measurement of isothermal (32.7°) growth rates normal to each of the three faces of adipic acid crystals grown from seeds in aqueous solution, under carefully controlled constant conditions, as a function of supersaturation level and additive concentration, and correlation of the effects of additives on growth with measurements of additive adsorption.

II. Experimental

A. Materials.—Distilled water free of surface active impurities was used throughout.

Commercial adipic acid was further purified by crystallizing three times from distilled water, and was found to contain no significant amount of surface active contaminant.

Three pure, well-characterized surface active additives were used: (1) sodium dodecyl-(tetrapropyl)-benzene sulfonate, an anionic surfactant referred to as SDBS; (2) sodium nonyl-(tripropyl)-benzene sulfonate, another anionic referred to as SNBS; and (3) trimethyloctadecylammonium chloride, a cationic surfactant referred to as TMOAC. The two anionic surfactants were specially prepared and were reported to be free of sodium sulfate and to contain less than 0.1% unsulfonated hydrocarbon; the SDBS was the same as that used in previous work.⁴ Although these surfactants were not further purified before use, foam-fractionation of a sample of the SDBS revealed no significant amount of highly surface active contaminant.

B. Adsorption Measurements.—Calibration plots of surface tension versus surfactant concentration, in both distilled water and saturated adipic acid solution, were prepared from measurements on solutions of known concentration, using a Cenco-Du Nouy Interfacial Tensiometer. All surface tension measurements were carried out in a constant temperature room maintained at $25 \pm 1^\circ$, on solutions

(1) H. E. Buckley, "Crystal Growth," John Wiley and Sons, Inc., New York, N. Y., 1951, p. 378.

(2) F. C. Frank, "Growth and Perfection of Crystals," Doremus, Roberts and Turnbull, editors, John Wiley and Sons, Inc., New York, N. Y., 1958, p. 8.

(3) D. Fysh, reported in "Surface Activity," J. L. Moilliet and B. Collie, editors, Third Ed., D. Van Nostrand and Co., New York, N. Y., 1951, p. 133-145.

(4) A. S. Michaels and A. R. Colville, Jr., *J. Phys. Chem.*, **64**, 13 (1960).

(5) R. H. Morrison and A. R. Robertson, *J. Chem. Soc.*, 987 (1949).

which were equilibrated for at least 24 hours in that room. Crystals for the adsorption measurements were grown from solution by cooling, and were always kept in saturated adipic acid solution to avoid contamination. Crystals of various shapes were obtained by controlling cooling rate and by using SDBS to modify crystal habit; when SDBS was used to obtain needles, crystals were washed several times to remove adsorbed surfactant. Specific surface area of each batch of crystals was estimated by microscopic examination of a sample of ten crystals chosen at random.

The procedure for determining isotherms for adsorption of surfactant on adipic acid crystals consisted of: (1) equilibrating at 25° about 25 g. of the specially prepared crystals with a measured volume of saturated adipic acid solution containing a known concentration of surfactant; (2) after 24 hours, removing the supernatant solution for determination of surfactant concentration by surface tension measurement; (3) washing the crystals with two 10-ml. portions of warm distilled water to dissolve the crystals partially and remove the adsorbed surfactant. The concentration of adipic acid in the wash solution generally corresponded almost exactly to saturation at 25°, at which surface tension was measured. Material balances on the surfactant indicated that all of the original surfactant could usually be accounted for in the supernatant and the wash solution, although with very high concentrations of surfactant there was an apparent loss of surfactant due to incomplete washing of the crystals. For this reason, calculated values for adsorption, assuming that all surfactant not remaining in solution or mechanically entrained in the crystal cake is adsorbed, are more reliable and hence are reported.

C. Crystal Growth Rate Measurements.—A schematic drawing of the apparatus developed for growing crystals is presented in Fig. 2. The crystallizer consisted of a 500-ml. three-neck flask fitted with a thermometer readable to 0.01°. Vigorous agitation was provided in the crystallizer by a specially-designed magnetically-driven stirrer, and the crystallizer was immersed in a water-bath maintained at 32.7 ± 0.01°. Supersaturation was maintained in the crystallizer by circulating the solution (by means of a peristaltic-type pump operating on a short length of silicone rubber tubing) through a crystal separating column (to prevent carryover of crystals in the crystallizer), thence through a bed of adipic acid crystals in the dissolver maintained at a slightly higher temperature than the crystallizer, and finally through a filter (to prevent carryover of crystals from the dissolver) and back to the crystallizer. The circulating solution dissolved some of the crystals in the dissolver and became virtually saturated at the temperature of the dissolver; upon returning to the crystallizer, and cooling to the temperature of the crystallizer, the solution became supersaturated. Preliminary work showed that at steady-state the supersaturation level in the crystallizer remained constant and the temperature of the solution in the crystallizer was constant within 0.01°. The absolute temperature level in the crystallizer varied from zero to several tenths of a degree higher than the 32.7° water bath, due to heat from the warmer entering solution. The entire apparatus in contact with the solution was constructed of glass, except for the Teflon and stainless steel stirrer and the short length of silicone rubber tubing in the pump. Great care was exercised to avoid contamination of the solution, and periodic surface tension measurements on the solution indicated absence of surface-active impurities.

All the seeds used in the SDBS and SNBS runs were thin plates from a single batch, grown from pure adipic acid solution, dried, sieved, and the 30–40 mesh fraction collected for use; these seeds were well formed and, because of the sieving, of quite uniform size (average dimensions, referring to Fig. 1, $L = 0.767$ mm., $W = 0.50$ mm., $T = 0.14$ mm.). Thick prisms were used for seeds in the TMODAC runs, since thin seeds would have resulted in extremely thin plates which would have been hard to handle and measure. The prisms for all TMODAC runs were prepared in a single batch by growing the thin plate seeds mentioned above in solution containing SDBS, then drying; these prisms were also well formed and, because of the uniformity of the seeds, quite uniform ($L = 0.934$ mm., $W = 0.473$ mm., $T = 1.58$ mm.).

The procedure for growing crystals involved: (1) establishing steady-state in the apparatus with the desired supersaturation level and additive concentration in the crystallizer; (2) adding about 100 seeds which were briefly washed in distilled water just prior to addition to the crystallizer in

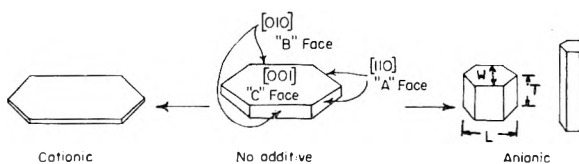


Fig. 1.—Effect of additives on adipic acid crystal habit.

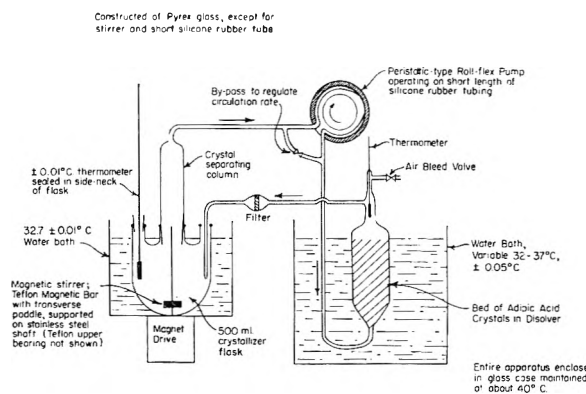


Fig. 2.—Schematic cross-section of crystallizer (approximately to scale).

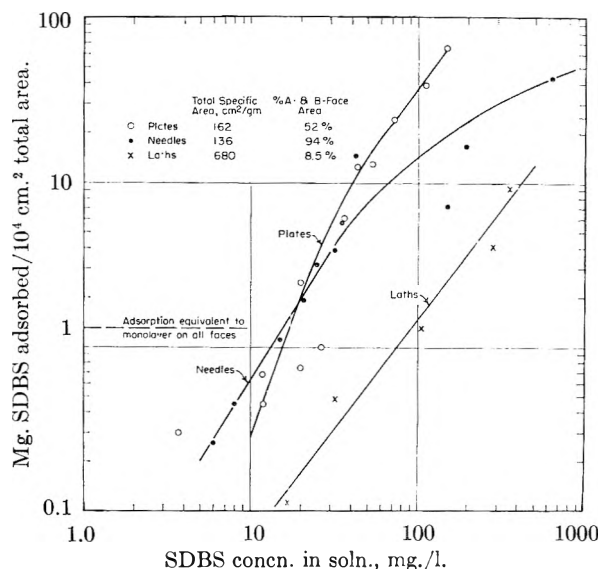


Fig. 3.—Adsorption of SDBS on adipic acid crystals of various shapes.

order to remove surface impurities; (3) permitting growth to occur on the freely-suspended seeds for periods of one-half hour to several days until about one to five millimeters growth had occurred on the fastest growing faces; (4) after growth had occurred for the desired period of time, pipetting a 10-ml. sample of solution from the crystallizer for determination of adipic acid concentration by titration and surfactant concentration by surface tension measurement; and (5) simultaneously sucking the crystals out of the crystallizer, drying them, and microscopically measuring the crystal dimensions of ten crystals chosen at random. Since the seeds were very uniform and no nucleation occurred, the entire sample was of uniform size within about 10%. From the difference in average dimensions of the seeds and the grown crystals, along with the duration of growth and the crystal geometry, growth rates normal to the A, B and C faces were calculated. The supersaturation level was calculated from the solubility of adipic acid at the temperature of the crystallizer (C_0 , about 33 g. per liter at 32.7°) and the actual concentration of adipic acid in the crystallizer (C), i.e., $S = (C/C_0)$ = supersaturation ratio, and $(C - C_0/C_0) = (S - 1)$ = supersaturation.

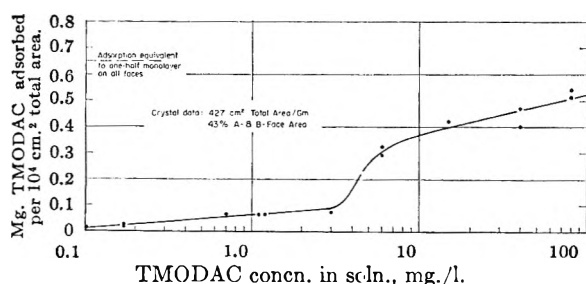


Fig. 4.—Adsorption of TMODAC on adipic acid crystals (plates).

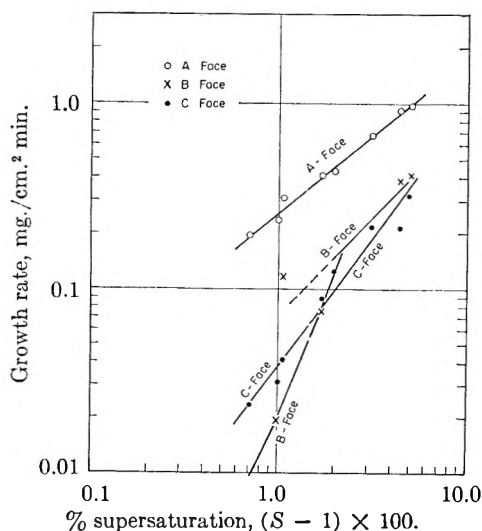


Fig. 5.—No additive, \ln (growth rate) versus \ln (supersaturation) for all three faces.

III. Results

A. Adsorption Isotherms.—Figure 3 shows that SDBS adsorbed about ten times more extensively, per unit total surface area, on plate- and needle-shaped crystals than on laths. Referring to the specific surface areas for the various crystal shapes (see Fig. 3), however, the surface of the lath-shaped crystals consisted almost entirely of C faces, with only 8.5% A and B faces, while 52% of the area of the plates and 94% of the area of the needles consisted of A and B faces. In fact, adsorption values based on mg. SDBS adsorbed per unit A- and B-face area correlate reasonably well on a single curve for all three crystal shapes, indicating that adsorption of SDBS is far stronger on the A and B faces than on the C faces.

The amount of SDBS adsorbed increased rapidly with SDBS concentration in solution. An adsorbed monolayer of SDBS, based on 50 \AA^2 per molecule, corresponds to about 1.3 mg. SDBS per 10^4 cm^2 ; according to Fig. 3, this level of adsorption is reached with as little as 15–25 mg./l. SDBS in solution, and perhaps fifty monolayers form at higher concentrations. While adsorption of this magnitude is not common, it is also not improbable; the critical micelle concentration of SDBS was lowered from over 1000 mg./l. in distilled water to about 300 mg./l. in saturated adipic acid solution, and adipic acid crystals may induce a sort of micellar or pseudo-crystalline adsorption of SDBS. It is, however, possible that the crystal faces are highly stepped, resulting in higher specific

surface area than indicated by microscopic measurements of crystal size and shape, although a "rugosity factor" of 50 for a solution-grown crystal face seems improbably high.

An isotherm for adsorption of TMODAC on adipic acid crystal plates is presented in Fig. 4. A monolayer of TMODAC also corresponds to about 1.3 mg. per 10^4 cm^2 , and Fig. 4 shows that no more than a monolayer adsorbed at even very high concentrations, thus supporting the validity of the procedure and, in turn, supporting the hypothesis of multilayer adsorption of SDBS.

B. Crystal Growth Rate Studies.—Using the apparatus developed in this investigation, growth rates normal to each of the three faces of adipic acid crystals grown at 32.7° were directly measured as a function of supersaturation level (from less than 1% up to the point where extensive three-dimensional nucleation occurred) and additive concentration and character. The latter included: no additive; SDBS at concentrations of 10, 25, 45, 80 and 360 mg./l., SNBS at a concentration of 100 mg./l.; and TMODAC at concentrations of 30 and 100 mg./l. The growth rate results, for each crystal face and additive concentration, are presented in Fig. 5 to 10.

The maximum supersaturation level at which crystals could be grown from seeds without extensive secondary nucleation increased with additive concentration from about 5% in the absence of additive to over 20% at very high additive concentration. Although high supersaturation levels could not be maintained after extensive nucleation occurred, measurements on the nucleated crystals showed that the relative growth rates on the various faces were the same as, and the absolute growth rates approximately the same as, crystals grown simultaneously from seeds.

In the absence of additive, and at low supersaturation levels, growth on the A faces was more rapid than on the B and C faces, resulting in thin elongated-hexagonal plates (laths). At higher supersaturation levels growth rate on the B faces approached growth rate on the A faces, resulting in more regular, hexagonal, thin plates. Figure 5 shows that growth rate on the A faces increased with the first power of supersaturation, growth rate on the C faces increased with approximately the $3/2$ power of supersaturation, and growth rate on the B faces increased with the second power of supersaturation at low levels and the first power of supersaturation at high supersaturation levels.

Low concentrations of SDBS (25 mg./l. and less) had little effect on growth rate on any face, as shown in Fig. 6 to 8, but higher concentrations caused drastic retardation of growth on the A and B faces. The retardation was strongly dependent on SDBS concentration and supersaturation level (or growth rate), resulting in complete stoppage of growth at high additive concentration and low supersaturation levels, but having very little effect at high supersaturation levels regardless of additive concentration. Because of this, growth rate on the A and B faces increased with as much as the fifth power of supersaturation.

At the same time that growth on the A and B

faces was retarded by SDBS, growth rate on the C faces increased with increasing additive concentration (see Fig. 8 and 10). With 80 mg./l. SDBS and low supersaturation, growth rate on the C faces was about five times higher than in the absence of additive; still higher concentrations of SDBS resulted in slightly decreased growth rate, although still significantly higher than in the absence of additive.

The only concentration of SNBS studied was 100 mg./l., and the growth results were virtually the same, for all three faces, as with 80 mg./l. SDBS, indicating that the effects of these two anionic additives are almost identical.

Concentrations of both 30 and 100 mg./l. TMODAC resulted in complete stoppage of growth on the C faces at all supersaturation levels, and significantly retarded growth on the A and B faces, with the retardation most marked at lower supersaturation levels, as shown in Fig. 9. As a result, growth rate on both the A and B faces, in the presence of both 30 and 100 mg./l. TMODAC, increased with the second power of supersaturation level.

IV. Discussion

A. Effect of Additives on Three-dimensional Nucleation.—The observed effect of additives on three-dimensional nucleation is consistent with numerous reports that additives inhibit nucleation.⁶ Since there appears to be no mechanism by which additives that reduce the crystal-solution interfacial free energy can thermodynamically inhibit homogeneous nucleation, it is believed that the inhibition of nucleation is due to poisoning of either heterogeneous nuclei or homogeneously-formed embryos. The chain lengths of the surfactants used in this investigation are of the order of 50–100 Å., which is of the same order as the estimated edge length of a critical-sized three-dimensional nucleus. It might therefore be expected that the surfactants would preferentially adsorb on (and poison) the larger (and more active) embryos, thereby resulting in progressively increased critical supersaturation levels as additive concentration is increased and smaller potential nuclei are poisoned.

B. Effect of Additives on Crystal Quality—Needle-like Formations.—It was found that, for a given supersaturation level, crystals grown in the presence of additives were better formed and had smoother faces than crystals grown in the absence of additives. Needle-like projections did not generally occur on either the A or the B faces at growth rates below about 0.2 mg./cm.² min., corresponding to about 30 molecular layers per second, and additives which reduced growth rate below this level were found to improve crystal quality by preventing needle-like formations. The C faces were generally quite smooth except at the very high C-face growth rates occurring at the very high supersaturation levels (*e.g.*, 10%) which could be maintained in the presence of high concentrations of SDBS; needle-like projections then occurred profusely on the C faces at growth rates above

(6) P. M. Egli and S. Zarfass, *Discussiones Faraday Soc.*, 5, 61 (1949).

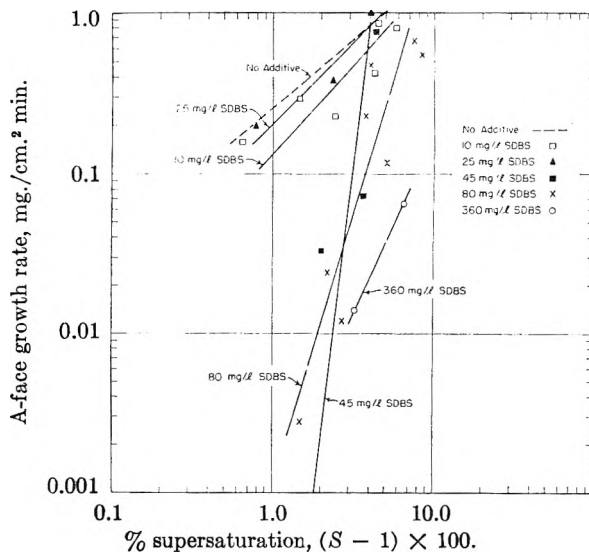


Fig. 6.—Effect of SDBS on A-face growth rate.

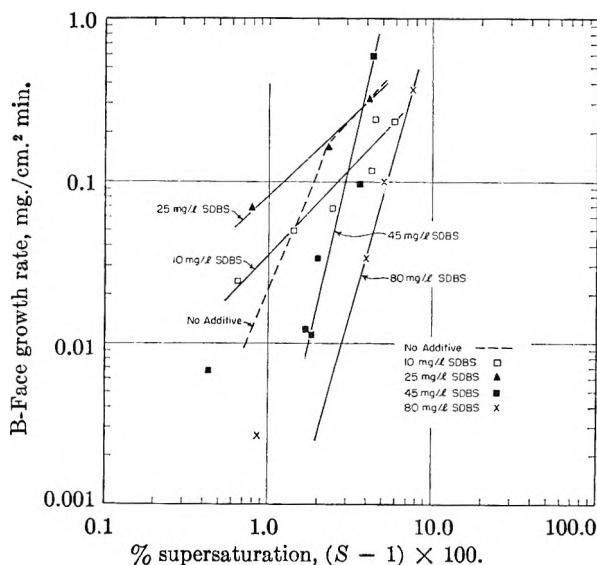


Fig. 7.—Effect of SDBS on B-face growth rate.

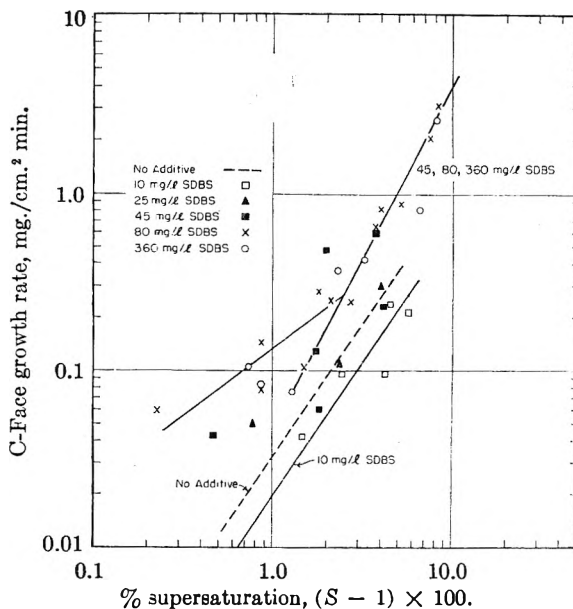


Fig. 8.—Effect of SDBS on C-face growth rate.

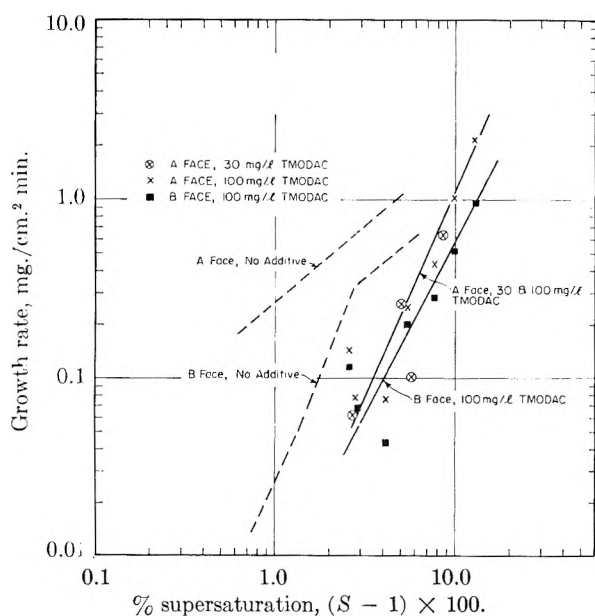


Fig. 9.—Effect of TMODAC on A- and B-face growth rate.

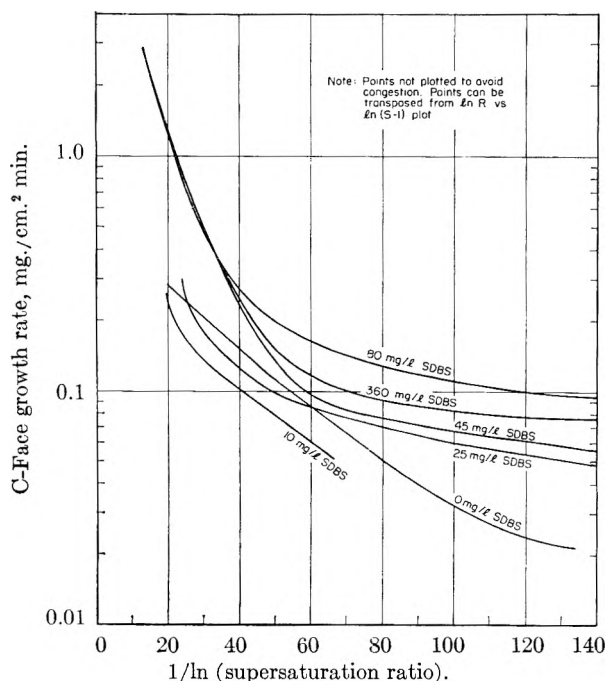


Fig. 10.—Effect of SDBS on C-face growth rate.

about 1.0 mg./cm.² min., which also corresponds to about 30 layers per second.

These results indicate that there is a critical rate of initiation of new layers, at about 30 layers per second, above which needle-like projections form. In the light of the mechanism of dendritic and whisker growth (e.g., ref. 7, 8), the following interpretation is proposed. The rate of initiation of new layers increases, in most cases, with supersaturation to a power greater than unity, while the rate of advance of a layer across the crystal surface increases more or less directly with supersaturation.^{9,10} With increasing supersaturation

level, therefore, a point will eventually be reached at which the rate of initiation of new layers is much faster than the rate of advance of these layers away from the point of initiation, so that a small surface protrusion forms (i.e., the layers pile up); because of the more favorable diffusion environment of this protrusion, it will become unstable and grow into the solution faster than, and at the expense of, the adjacent surface. Since additives were found to improve crystal quality, it appears that additives retard initiation of new layers more than advance of layers across the crystal surface.

C. Relation between Additive Adsorption and Effect on Growth.—The observation that SDBS adsorbs far more extensively on the A and B faces than on the C faces is consistent with the postulated pattern of adsorption (i.e., amphipathic adsorption on the A and B faces despite coulombic repulsion from all faces) and with the observed effects of SDBS on growth (i.e., retardation on A and B faces, but accelerated growth on C faces). The fact that concentrations of SDBS below about 25 mg./l. had little effect on growth, despite the indicated monolayer adsorption, indicates that very extensive adsorption (involving a complete monolayer and perhaps multilayers) is necessary for SDBS to retard A- and B-face growth. Since both additive adsorption and growth retardation increased with increasing SDBS concentration, it appears that the degree of retardation is related to the amount of adsorption, although increased rate of adsorption from more concentrated additive solution may also be a factor.

Although adsorption of TMODAC on the various crystal faces could not be resolved because only one crystal shape was used, the distinct step in the adsorption isotherm (Fig. 4) presumably corresponds to completion of a monolayer on the C faces, since the cationic TMODAC would be expected (from the postulated pattern of adsorption) to adsorb most strongly on the high-carboxyl-density C faces; the fact that TMODAC retarded growth on the C faces more than on the A and B faces supports this. Furthermore, the fact that both 30 and 100 mg./l. TMODAC retarded growth on the A faces to the same extent indicates that the maximum retardation had been reached; the adsorption isotherm indicates that little additional adsorption occurs above 30 mg./l. TMODAC in solution, and presumably even very high concentrations of TMODAC would not further retard growth. This suggests that additive diffusion is not the limiting step for growth retardation, at least for TMODAC at 30 and 100 mg./l., and that with increasing additive concentration additional adsorption either does not occur or does not further retard growth.

Comparison of the anionic and cationic additives with regard to adsorption and effect on growth indicates that less-than-monolayer adsorption of TMODAC (e.g., at 30 mg./l. in solution) retards growth on the A and B faces more than multilayer adsorption of SDBS (e.g., at 360 mg./l.). Since

(7) F. R. N. Nabarro and P. J. Jackson, in ref. 2.

(8) D. D. Saratovkin, "Dendritic Crystallization," translated from Russian, Consultant Bureau, Inc., New York, N. Y., 1959.

(9) W. K. Burton, N. Cabrera and F. C. Frank, *Phil. Trans. Roy. Soc. (London)*, **A249**, 299 (1951).

(10) A. R. Verma, "Crystal Growth and Dislocations," Academic Press, Inc., New York, N. Y., 1953.

TMODAC is attracted to the A and B faces both coulombically and amphipathically, while SDBS is adsorbed amphipathically despite coulombic repulsion, it appears that adsorptive-bond-strength (which probably influences sorbate mobility) is a more important factor than sorbate surface concentration.

D. Mechanism of Growth. 1. Comparison with Theory.—The experimentally observed dependence of growth rate on supersaturation level to powers greater than unity, and the fact that crystals generally grew as well-formed polyhedra, indicate that the diffusional resistance is not the rate-controlling mechanism.

Correlation in terms of two-dimensional nucleation^{9,11-13} was found to be unsatisfactory because of the non-linearity of plots of $\ln R$ versus $1/\ln S$; in most cases the curves exhibited two rather linear regions, with a low slope at low supersaturation levels and a high slope at high supersaturation levels, and with a distinct break between them (e.g., see Fig. 10). Furthermore, even the highest values of crystal-solution interfacial free energy deduced from this correlation were only one to three ergs/cm.², which seems unreasonably low even for the crystal-solution interface. With this correlation, however, slopes were found to increase with additive concentration, which is consistent with a mechanism involving increased activation energy for nucleus formation due to contamination of the crystal surface on which nucleation occurs.

The dislocation mechanism of growth^{9,10,12,14-16} was found to be an attractive possibility for growth in the absence of additive, because of the observed dependence of growth rate on the second power of supersaturation level at low growth rates and on the first power at high growth rates. In the presence of SDBS, however, the observed dependence of growth rate on powers of supersaturation as high as five is difficult to explain in terms of growth from dislocations alone.

2. Proposed Mechanisms of Growth Retardation.—The two-dimensional nucleation mechanism would be attractive if the very low activation energies for nucleus formation could be justified. The dislocation mechanism would also be attractive if the strong dependence of growth rate on supersaturation level (in the presence of SDBS) could be accounted for. It was found that the effects of both supersaturation level and additive concentration on growth retardation could be accounted for in terms of the following analysis.

Although the solubility of a particle (either three- or two-dimensional) increases with decreasing size, and in general the critical radius of curvature of a particle in equilibrium with supersaturated solution is given by the well-known relation $r \sim 1/\ln S$, it is nevertheless possible for a stable two-dimensional sub-critical embryo to exist on a crystal surface, e.g., the step created by the intersection

of two closely spaced screw dislocations of opposite sign.⁹ The supersaturation level necessary to activate such an embryo to initiate a growth layer is far less than the supersaturation level necessary for initiation of a layer on a perfect crystal surface, i.e., two-dimensional nucleation. Furthermore, the probability of activation of such an embryo at a given supersaturation level increases exponentially with increasing embryo size. It is proposed that the effect of these stable two-dimensional sub-critical embryos on crystal growth (initiation of new layers) is analogous to the well-known effect of heterogeneous nuclei on three-dimensional nucleation (initiation of a new phase).

According to this proposed mechanism of growth, the rate of growth can be expressed as

$$R = \sum_{i=0}^{i=n} C_i \exp(-\beta_i/\ln S) \quad (1)$$

where

- i represents a class of embryos characterized by a specific value of β_i
- C_i is the surface concn. of embryos of size i
- β_i corresponds to an energy of activation to permit growth of an embryo of size i
- $\exp(-\beta_i/\ln S)$ can be considered as the probability of activation of an embryo of size i

Actually, it was found that all of the growth rate results could be fitted by only two terms of such an expression, i.e.

$$R = C_1 \exp(-\beta_1/\ln S) + C_2 \exp(-\beta_2/\ln S) \quad (2)$$

with the constants C_1 , C_2 , β_1 and β_2 functions of additive concentration. The use of only two terms of the expansion can be justified by assuming a distribution of embryo sizes which favors small embryos, which is rather likely; this leads to the conclusion that only the very large embryos (which are present in low concentration but have a very high probability of activation) and the small embryos (which are present in very high concentration but have a low probability of activation) may contribute significantly to the summation. Values of the constants determined from the experimental growth rate results are consistent with this model: the first term is characterized by very low values of the constants C_1 and β_1 and this term predominates at low supersaturation levels and therefore apparently represents the contribution of the group of large embryos, while the second term is characterized by high values of the constants C_2 and β_2 and therefore predominates at high supersaturation levels and apparently represents the contribution of the small embryos.

The effect of additive on the values of the constants was also found to be consistent with the proposed mechanism. Values of β_1 and β_2 were found to increase with increasing additive concentration (reflecting increasing slopes on plots of $\ln R$ versus $1/\ln S$), indicating that additives inhibit activation of embryos of all sizes. Additive also decreased values of C_1 , indicating poisoning of larger embryos (as might be expected and in agreement with the postulated effect of additives on three-dimensional nucleation), but additive actually increased values of C_2 ; the latter observation is interpreted to indicate that, as larger embryos are preferentially

(11) W. Becker and R. Doring, *Ann. Physik*, **24**, 719 (1935).

(12) W. K. Burton and N. Cabrera *Disc. Faraday Soc.*, **5**, 33 (1949).

(13) M. Volmer and H. Flood, *Z. physik. Chem.*, **A170**, 273 (1934).

(14) N. Cabrera and D. A. Vermilyea, in ref. 2.

(15) F. C. Frank, *Discussions Faraday Soc.*, **5**, 49 (1949).

(16) W. T. Read, Jr., "Dislocations in Crystals," McGraw-Hill Book Co., New York, N. Y., Chapter 10, 1953.

poisoned, the contribution of smaller embryos becomes more important and is reflected in higher values of C_2 .

The foregoing analysis does not, however, take into consideration the inescapable reality that the surface-concentration of an adsorbed additive on a growing crystal face must be different from (and probably less than) the equilibrium concentration on a non-growing face. In the case of TMODAC, at least at the concentrations studied, the kinetics of additive adsorption are apparently not important since the same degree of retardation was obtained with 30 and 100 mg./l. With SDBS, however, the degree of retardation increased with additive concentration and the kinetics of additive adsorption may be important. If it is postulated that a propagating lattice layer on a growing face sweeps the surface clean of adsorbed additive, then clearly, the steady-state average surface-concentration of additive during growth will be directly related to (a) the rate of diffusion of additive to the surface, and (b) the rate of advance of a lattice layer and the time-interval between successive layer-depositions. These postulates lead to the prediction that the growth-inhibitory action of a surfactant must increase with the surfactant concentration in solution, and decrease with increasing growth rate (or level of supersaturation), in complete agreement with the experimental observations. The authors have had fair success in developing kinetic expressions, incorporating these concepts, which are qualitatively consistent with the observed growth-rate data; proper test and refinement of these relations will, however, require more extensive experimental information than is presently available.

3. Mechanism of Growth Acceleration.—While additives have generally been found to retard growth, it has often been suggested that incorporation of additives into a growing crystal could increase growth rate by creating dislocations (*e.g.*, ref. 14), and there is evidence that additives can increase the rate of two-dimensional nucleation by reducing edge free energy (*e.g.*, ref. 17). The increasing C-face growth rate with SDBS concentration (see Fig. 10) may well be due to additive incorporation; with 360 mg./l. SDBS, perhaps the retarding effect of SDBS adsorption begins to overshadow the accelerating effect. Increased rate of two-dimensional nucleation does not seem likely, however, since the results of this investigation indicate that growth does not involve two-dimensional nucleus formation as such, and it also seems unlikely that sufficient additive could adsorb on a nucleus edge during its formation to significantly influence its free energy of formation.

It might be mentioned that the results suggest that the accelerated C-face growth may be directly related to retarded A- and B-face growth; C-face growth increased with SDBS concentration at the same time that A- and B-face growth decreased, but with 360 mg./l. SDBS (when A- and B-face growth had been virtually stopped) C-face growth rate did not further increase. While there is evidence that surface diffusion is an important factor

in growth from the vapor phase (*e.g.*, ref. 8, 18), however, rapid surface flow of solute on crystals growing from concentrated solutions seems more difficult to justify.

V. Conclusions

The major conclusions drawn from this investigation are the following. (1) Surfactants increase the supersaturation level at which adipic acid crystals can be grown from seeds without occurrence of secondary nucleation, apparently by poisoning sub-critical embryos or heterogeneous nuclei.

(2) All of the additives studied greatly modify adipic acid crystal habit and relative growth rates on different crystal faces by adsorbing in a specific manner. The anionic surfactants adsorb far more extensively on the A and B faces than on the C faces. The cationic surfactant adsorbs only to the extent of one monolayer, and apparently adsorbs more strongly on the C faces than on the A and B faces.

(3) The effects of additives on growth rate are strongly dependent on additive concentration and on supersaturation level (or growth rate itself), resulting in drastic effects at low supersaturation levels and high additive concentration, but having very little effect at high supersaturation levels, regardless of additive concentration.

(4) Both anionic surfactants studied produce similar effects. Concentrations less than 25 mg./l. (corresponding to monolayer adsorption) have little effect on growth rate, but higher concentrations (at which very extensive multilayer adsorption on the A and B faces occurs) result in greatly reduced growth rate on the A and B faces, while at the same time growth rate on the C faces increases by as much as fivefold over the rate without additive. Two possible explanations for the accelerated growth on the C faces due to anionic surfactants are: (1) creation of dislocations by additive incorporation; and (2) surface flow of solute from faces retarded by additive.

(5) The cationic surfactant, with less than monolayer adsorption on all faces, virtually stops growth on the C faces at all supersaturation levels and significantly decreases growth rate on the A and B faces.

(6) Combination of the concepts of two-dimensional nucleation and growth from dislocations permits satisfactory correlation of the growth rate results. This proposed mechanism explains both the effect of supersaturation level and the effect of additive concentration on growth rate. The kinetics of additive adsorption also appear to be of importance, however, at least with anionic additives.

Acknowledgment.—The authors gratefully acknowledge the financial support of the Solar Energy Research Fund (in the form of Fellowship aid to the junior author), and of the Esso Education Foundation (in the form of a Research Award to the

(17) G. W. Sears, in ref. 2.

(18) M. Volmer and I. Estermann, *Z. Physik*, **7**, 13 (1921).

senior author), which made this study possible. The assistance of Mr. R. W. Swisher of the Monsanto Chemical Company in providing surfactant samples is appreciated.

DISCUSSION

A. C. ZETTMAYER (Lehigh University).—We have reported that SDBS on graphite surfaces does not form more than one adsorbed layer. Hence, on a hydrocarbon surface, such as your A- and B-faces, similar adsorption characteristics would be expected. Fifty adsorbed layers seem very unlikely especially since the hydrocarbon portions of the SDBS would adsorb next to the A- and B-faces of the adipic acid crystals with the polar anion group outward surrounded diffusely by counterions. It seems unlikely that micelles (hydrocarbon tails turned in) could be adsorbed.

A. S. MICHAELS.—The apparent (and anomalous) high level of sorption of SDBS on the A- and B-faces would, we think, hardly be expected if these faces closely resembled the apolar surfaces of graphite or other hydrocarbons. We are prompted to wonder whether specific interactions between SDBS and the carboxyl groups of the adipic acid molecules located on the crystal surface, or in the adsorbed, hydrated layer adjacent to the crystal surface, may be contributory to sorption of the surfactant. The observation that the CMC of SDBS in saturated adipic acid solution is about one-third of the value in distilled water suggests that adipic acid-SDBS complexes, or "mixed micelles," may form in the solution; perhaps a rather thick, hydrous, poorly ordered "mixed micellar" layer is deposited on the A- and B-faces whose SDBS content is sufficient to account for such high level of surfactant sorption.

LEO SHEDLOVSKY (Colgate-Palmolive Company).—To what extent is the surface tension method of estimating adsorption suitable? Unless foam fractionation was estimated over the concentration range shown in the adsorption isotherms, the possibility of selective adsorption on adipic acid crystals may not be ruled out. Would this influence the surface tension especially in the steep portion of the curve at low concentrations and lead to uncertainty for such a method of calibration?

A. S. MICHAELS.—The use of surface tension measurements to estimate surfactant sorption on solid surfaces is

unquestionably open to serious criticism when applied to commercial surfactants, which usually are mixtures of compounds of differing interfacial activity. Since the surfactants used in this study were specially prepared, highly purified compounds, the surface tension technique appeared to be much less objectionable, although not completely defensible for this reason alone. The experimental facts that (a) foam-fractionation of quite dilute solutions (100 p.p.m.) of SDBS caused no significant change in solution surface tension, and (b) surface-tension analysis of adipic acid crystals containing sorbed SDBS yielded essentially the same surfactant content as estimated from the surface tension change of the contacting solution, lend confidence to our belief that the surface-tension technique for estimating sorption is of reasonable accuracy for the system studied.

W. A. ZISMAN (Naval Research Laboratory).—At what pH were these experiments run? Also, might there have been inorganic impurities in the distilled water used. In dealing with carboxylic acids there is always the possibility that any multivalent metallic ion present will form a film of insoluble soap. The formation of insoluble carboxylates would be promoted above a pH of 2 or 3. In these experiments such soaps could form on the single crystals of adipic acid and inhibit or restrict crystal growth. However, any water soluble surface active agents present, such as an alkyl sulfate or sulfonate, might serve as a dispersing or solubilizing agent to remove the insoluble carboxylate from the crystal face and so let it resume growing.

A. S. MICHAELS.—In all cases, crystals were grown from pure, aqueous adipic acid solutions in the absence of added strong acid or alkali. Since the ionization constant of adipic acid is approximately 4×10^{-5} , and since saturated solutions are roughly 0.2 molar, the pH of the solutions was approximately 5.3. Because of the large ratio of un-ionized to ionized acid in these solutions, they are quite highly buffered, and the pH is virtually invariant over the range of conditions studied.

No specific attempts were made to avoid multivalent cation contamination beyond use of low-conductivity distilled water. However, the process of multistep recrystallization of the adipic acid used for crystal growth measurements should have allowed removal of any insoluble carboxylate salts formed by the presence of traces of such cations.

THE ORIGIN OF SPHERULITES

BY GERALD W. SEARS

*Research Division, General Dynamics/Electronics, Rochester, New York**Received March 1, 1961*

The initiation of spherulites is considered on the basis of Cahn-Hilliard theory of non-classical nucleation. It is shown that polycrystalline nuclei can originate at high supersaturations by a single nucleation event. Empirical examples are cited to indicate the methods by which non-classical nucleation can be experimentally identified.

Spherulitic crystallization has been recognized for many years¹ by mineralogists. The term has been used to describe polycrystalline aggregates, spherical in form, and radial or concentric in structure. Closely related aggregates are called reniform, botryoidal, pisolytic, mammillary and globular. When spherulites are formed from a doubly refracting mineral or from a crystalline substance having a birefringent character caused by internal strain, they commonly exhibit a dark cross in the microscope under crossed Nicols.

In the past decade it has been established that spherulitic crystallization is the usual way in which a bulk sample of high polymer crystallizes. In 1945 Bunn and Alcock² first observed spherulites in a polymer system. They studied polyethylene. Similar structures were subsequently observed in polyurethan³ and polyamides.⁴ The first detailed study of the kinetics of spherulite formation was made by Price.⁵ It is now recognized as the usual mode of crystallization in high polymers.^{6,7}

The optical behavior of spherulites is dependent upon optical properties of bulk material, the state of elastic strain of individual crystallites and the relative crystallite orientations. The spherulitic structure can also be described by what is called a texture. Texture describes the relationship of common crystallographic directions of individual crystallites to particular directions in the polycrystalline aggregate. If each crystallite of a spherulite had a (100) direction nearly radial to the spherulite center, this could be called a radial (100) texture. If spherulitic growth is constrained to two dimensions, or if it is restricted to less than 2π planar angle or 4π solid angle, it is still properly described as spherulitic.

It is the purpose of the present paper to relate the initiation of spherulites to the theory of non-classical nucleation, which has been developed by Cahn and Hilliard.⁸ Although they have treated nucleation energetics only in a two component incompressible fluid, it is assumed that the main conclusions of their treatment are applicable to the nucleation of a real crystalline phase from a fluid parent phase. It will be shown that when a spherulite originates from a single nucleation

event, the nucleus is non-classical and may be properly described by the Cahn-Hilliard theory. The final spherulitic structure that develops from a spherulitic nucleus is determined by the conditions under which growth, as distinct from nucleation, occurs.

It is expected that non-classical nucleation may occur heterogeneously on foreign particles at smaller undercoolings than would be necessary for homogeneous nucleation.

Resume of Non-classical Nucleation.—It has long been recognized that the classical analysis of the nucleation event in phase transformations must be invalid at sufficiently large supersaturations. The radius, r_c , of a critical sized nucleus is given by

$$r_c = - \frac{\gamma}{\Delta F_v} \quad (1)$$

where ΔF_v is the volume free energy of the transformation and γ is the interfacial free energy between the parent phase and the embryo or nucleus. In the limit it can be formally written

$$\lim_{\Delta F_v \rightarrow \infty} r_c = 0 \quad (2)$$

When a new phase is nucleated from a parent phase the critical radius of a classical nucleus can be made arbitrarily small by increasing the free energy of transformation.

Consider the nucleation of a crystalline phase from a fluid medium. The classical analysis of nucleation must become invalid when the critical radius becomes smaller than the radius of the unit cell. With a complex unit cell it is conceivable that a nucleus might be smaller than a unit cell, still crystalline, but certainly possessing a different volume free energy (in hypothetical bulk) from the bulk phase having the complex cell. Even at larger critical radii, *e.g.*, smaller free energies of transformation, the classical treatment becomes invalid because of the impossibility of distinguishing the volume of a nucleus from its interface.

Classical nucleation theory derives from Gibbs' theory⁹ of phase stability. He recognized that the relative stability of a phase with respect to its environment was a function of the particle size of the phase. He realized that a small nucleus of a bulk phase might be completely inhomogeneous in composition. However, he developed a self-consistent method of describing a nucleus by treating it as though it were homogeneous up to

(9) J. W. Gibbs, "Collected Works," Yale University Press, New Haven, Conn., 1948, Vol. 1, pp. 105-115, pp. 252-258.

(1) E. S. Dana, "Textbook of Mineralogy," 4th Ed., by W. E. Ford, John Wiley and Sons, New York, N. Y., 1932, p. 329.

(2) C. W. Bunn and T. C. Alcock, *Trans. Faraday Soc.*, **41**, 317 (1945).

(3) E. Von Jenckel and H. Wilsing, *Z. Elektrochem.*, **53**, 4 (1949).

(4) R. Gabler, *Naturwissenschaften*, **35**, 284 (1948).

(5) F. P. Price, *J. Am. Chem. Soc.*, **74**, 311 (1952).

(6) W. M. D. Bryant, *J. Polymer Sci.*, **2**, 547 (1947).

(7) A. Keller, *ibid.*, **17**, 291 (1955).

(8) J. W. Cahn and J. E. Hilliard, *J. Chem. Phys.*, **31**, 688 (1959).

a sharp interface with its environmental phase. The total work of forming such a nucleus involved a negative free energy for the transformed volume and a positive free energy for the new interface.

In the classical theory of nucleation¹⁰ which has been developed from Gibbs' theory of phase stability, the specific interfacial free energy is equated to the free energy of a flat interface and the volume free energy is equated to the value characteristic of the bulk phase. From the preceding discussion it is apparent that Gibbs would have been well aware of the limitations of this procedure.

In order to make a more accurate analysis of the free energy barrier to nucleation for large driving forces it is necessary to treat the thermodynamics of systems having a gradient in composition. Recently Cahn and Hilliard¹¹ have developed a thermodynamic treatment of non-uniform systems. They have found that the free energy of a small volume is the sum of two terms—one equal to the free energy of a uniform system at the local composition and a second that is very closely proportional to the square of the local composition gradient. Hart¹² has confirmed that Cahn and Hilliard analysis by a classical thermodynamic formulation using undetermined multipliers and redundant variables. Cahn¹³ later established the equivalence of the two treatments.

A knowledge of the free energy of non-uniform systems allows the energetics of a nucleation event to be treated without the use of an artificially defined nucleus. Cahn and Hilliard⁸ have recently treated nucleation energetics in a two component incompressible fluid. In the present paper the assumption is made that the general conclusions of the two fluid treatment are directly applicable to the nucleation of a crystalline phase from a fluid parent phase. This latter system has a common feature with the two fluid system—the lack of elastic strain energy terms. The Cahn-Hilliard theory predicts that the critical free energy of nucleation at large supersaturations should be less than the value calculated by classical nucleation theory.

The composition and/or structure at the center of the nucleus should deviate from that of a classical nucleus. The radius should become larger than that of a classical nucleus at sufficiently large supersaturations.

Formally we write

$$\lim_{\Delta F_v \rightarrow \infty} r_c = \infty \quad (3)$$

$$\lim_{\Delta F_v \rightarrow \infty} \Delta f^* = 0 \quad (4)$$

where Δf^* is the free energy of formation of a critical sized nucleus. At sufficiently large supersaturations no part of the nucleus should be homogeneous.

It is possible to qualitatively understand the behavior of a non-classical nucleus at high supersaturations by a simple argument. A phase boundary has an optimum thickness, which is de-

termined by a volume free energy term and a gradient free energy term. If the boundary was very thick the gradient term would be small, but a large volume would be involved. If the boundary was very sharp the volume involved would be small, but the gradient free energy term would be very large. The optimum thickness is associated with the smallest excess phase boundary free energy.

For low supersaturations and large nuclei it is possible to define what is interior and what is volume quite clearly. At very high supersaturations it becomes impossible to decide what part of a nucleus is boundary and what part interior. As previously mentioned, the composition becomes inhomogeneous throughout.

The configuration of a critical nucleus may be stated as follows: At sufficiently high supersaturations it is cheapest energetically to form a nucleus with a volume free energy algebraically larger than that of the bulk phase in order to maintain a smaller interfacial free energy term. It should be emphasized that the Cahn-Hilliard treatment is not invalid at low supersaturations. Just as quantum mechanics includes classical mechanics, the Cahn-Hilliard analysis includes the classical analysis of nucleation.

Approximate Limitations of Classical Nucleation.—It has already been mentioned that the classical analysis of nucleation cannot be valid when the critical radius is less than the radius of a unit cell of the crystalline phase involved. Another limitation is placed upon the classical analysis in that the critical radius must be greater than the thickness of the phase boundary between the nucleating phase and the parent phase. Qualitatively it may be written that

$$\bar{r}_c = r_0 + \tau_0 \quad (5)$$

where r_c is that critical radius at which classical nucleation theory certainly fails, r_0 is the radius of the unit cell, and τ_0 is the half thickness of the phase boundary. Admittedly this criterion is approximate, but it serves as a fiducial point for experimental observations. Combining equations 1 and 5 yields the maximum free energy, $\bar{\Delta F}$, at which classical nucleation can provide a valid description of the nucleation process

$$\bar{\Delta F} = - \frac{\gamma M}{\rho(r_0 + \tau_0)} \quad (6)$$

where M is the molecular weight and ρ is the density of the nucleating phase. To a first approximation the free energy of transformation is related to the supercooling, ΔT , by the relation

$$\Delta F = - \frac{\Delta H}{T} \Delta T \quad (7)$$

where ΔH is the heat of transformation and F_0 is the equilibrium temperature. The upper limit for supercooling, $\bar{\Delta T}$, at which classical nucleation can occur is written

$$\bar{\Delta T} = \frac{\gamma M T_0}{\rho \cdot \Delta H \cdot (r_0 + \tau_0)} \quad (8)$$

If nucleation occurs at a supercooling greater than $\bar{\Delta T}$ for a given system, the nuclei will be non-classical. It is the purpose of the present paper to

(10) M. Volmer, "Kinetik der Phasenbildung," Steinkopf, Dresden and Leipzig, 1939.

(11) J. W. Cahn and J. E. Hilliard, *J. Chem. Phys.*, **28**, 258 (1958).

(12) E. W. Hart, *Phys. Rev.*, **113**, 412 (1959).

(13) J. W. Cahn, *J. Chem. Phys.*, **30**, 112 (1959).

propose that spherulitic nuclei are one type of non-classical nuclei. An immediate correlation is the occurrence of spherulites at larger supercooling in a given system than single crystal nuclei.

Occurrence of Non-classical Nucleation.—Since non-classical nucleation requires a larger absolute free energy of transformation than classical nucleation, it can occur by two possible paths. Either an appreciable nucleation rate does not occur in the classical regime or the system must be quenched through the classical region.

Since

$$\Delta f^* = \Delta f^*(\Delta F) \quad (9)$$

the conditions for no classical nucleation on slow cooling are

$$\Delta f^*(\Delta F) > skT \text{ for } |\Delta F| < |\overline{\Delta F}| \quad (10)$$

where s is a number approximately 60.

The functional dependence of Δf^* upon ΔF differs according to whether nucleation occurs homogeneously or heterogeneously and in the latter case upon the nature of the nucleation catalyst.

Since the presence of a nucleation catalyst reduces the free energy of transformation at which an appreciable nucleation rate occurs, it is possible that a given system might be slow-cooled into the region for non-classical nucleation in the absence of a catalyst, while classical nucleation would occur in the presence of a nucleation catalyst.

If a system must be quenched to obtain the conditions for non-classical nucleation, the necessary quenching rate will depend on the molecular mobilities across the interface between parent phase and nuclei as well as the functional dependence of Δf^* upon ΔF . A viscous system should be quite easily cooled into the region of non-classical nucleation.

Nature of Non-classical Nuclei.—Non-classical rigid nuclei may exist in three possible structures: (a) a polycrystalline or spherulitic structure, (b) an extremely defective single crystal nucleus and (c) a glassy nucleus. The first possibility is proposed to account for spherulitic nucleation. The last two possibilities are probably empirically indistinguishable. Thus two possible structures exist for non-classical nuclei, spherulitic or glass.

The nucleation of a particular solid from a fluid phase will occur at an appreciable rate in the absence of nucleation catalysts for a certain critical free energy of transformation. Consider the case in which an appreciable nucleation rate does not occur until the region of non-classical nucleation is reached. The structure of the non-classical nuclei would be that which corresponded to the lowest free energy of nucleation. If a polycrystalline nucleus were to form it would be a necessary requirement that the intercrystalline boundary or boundaries could be fitted inside of the critical nucleus.

Fullman¹⁴ has considered the equilibrium form of macroscopic crystalline bodies. He concludes that polycrystalline configurations may have lower free energy than single crystals for sufficiently large anisotropy of specific surface free energy and suf-

ficiently large anisotropy of specific surface free energy and sufficiently small grain boundary energies. From available values of the pertinent interfacial free energies it was impossible to determine whether a polycrystalline configuration was more stable than a single crystal of an actual crystal.

Although a macroscopic isotropic crystal would never have a stable spherulitic configuration by the preceding considerations, it is quite possible that the surface energy of a cubic crystal, for example, might be anisotropic in the presence of surface active materials. Under these conditions a spherulitic form might become stable.

It is finally remarked that the relative stabilities of single crystal *versus* spherulitic configuration would be dependent upon the size of crystalline body under consideration. In practice single crystal nuclei seem to be always attainable.

Observation of Non-classical Nucleation. A.—A recent experiment by Sears and DeVries¹⁵ indicates a simple method of investigating the structure of a nucleus. A near-perfect sheet of alumina was grown by a vapor phase reaction at 1600–1700°. Such crystals presented perfect {0001} faces.

When the parent vapor phase was quenched more rapidly than reactants could diffuse to growing crystal faces, the growing crystal face could be placed temporarily in contact with a limited volume of highly supersaturated vapor phase. The crystal was then exposed to a low supersaturation of parent vapor so that any nuclei formed during the period of high supersaturation could be grown to a visible size without further nucleation.

Immediately after a perfect face was exposed to the highly supersaturated vapor phase no change could be seen in the surface at 80 \times . After about two minutes growth at low supersaturations a few white dots appeared on the perfect surface and grew to a diameter of a few microns. In a further two minutes they recrystallized to form tiny hexagonal patches each having its own uniform interference color. The hexagonal patches spread over the crystal surface.

The original structure of the nuclei could be qualitatively deduced from their developed form. To appear white the dots must have been polycrystalline. Since they were grown at a low supersaturation, the original nucleus must have been fairly large. Small nuclei could not have contained sufficient structural inhomogeneities to develop polycrystalline masses a few microns in diameter by growth at low supersaturations. Classically the nuclei should have been very small. Empirically they were relatively large and contained many structural inhomogeneities in agreement with the Cahn-Hilliard theory. Repeated nucleation at the same site on a perfect surface must occur at a negligible rate since a given nucleation event reduces the supersaturation so that a second event cannot immediately occur.

B. Organic Polymers.—The first microscopic evidence for the growth of a crystalline phase in high polymers was reported by Bunn and Alcock.² They observed spherulites in polyethylene. Only

(14) R. L. Fullman, *Acta. Met.*, **5**, 638 (1957).

(15) G. W. Sears and R. C. DeVries, *J. Chem. Phys.*, **32**, 93 (1960).

recently have single crystals of high polymers¹⁶⁻¹⁸ been grown. Non-classical nucleation theory predicts that spherulitic crystallization should be difficult to avoid empirically and single crystal nucleation and growth should occur only at very low supersaturations. The unit cell is known to be large and the crystal-melt interface is inferred to be large merely on a basis of molecular sizes. Thus the size of nucleus at which non-classical nucleation occurs must be large. On the other hand the pertinent surface energy is expected to be of the same magnitude as for a low molecular weight organic crystal. Nucleation should become non-classical for relatively small free energies of transformation and for relatively small supercoolings. This prediction is in agreement with the observation that care must be taken to avoid spherulite formation.

C. Carboxypeptidase A.—Recently Coleman and co-workers¹⁹ have grown a spherulitic morphology of carboxypeptidase A, an enzyme of molecular weight, 34,300. They nucleated and grew large polyhedral crystals at concentrations of 10 to 30 g./l. in the parent solution. At 5 g./l. they found whiskers radiating from common centers and a few polyhedra. At 2 g./l. they observed only spherulites, *i.e.*, configurations that appeared to be whiskers nucleating in all directions from common centers. The spherulitic and polyhedral crystals, when redissolved, could be interconverted by either diluting or concentrating the solution. These spherulites showed birefringent patterns common to high polymer spherulites.

These observations illustrate that the spherulitic morphology can be formed by classical nucleation events. Since the spherulites form at lower supersaturations than required for the formation of polyhedra or single crystals, it is apparent that non-classical nuclei are not involved. At supersaturations insufficient to cause an appreciable rate of two-dimensional nucleation the whisker habit^{20,21} is characteristic. The observations of Coleman, *et al.*,¹⁹ are consistent with the growth of whiskers from a multiple nucleation site at a heterogeneity in solution. The helical structure of the radiating fibers deduced from the birefringent patterns is consistent with the helical twist of a whisker bearing a screw dislocation and the internal strain associated with the dislocation.

D. Modular Cast Iron.—Within the last few years a process has been developed for producing ductile cast iron. Gray cast iron is a brittle material. It consists of an iron matrix containing precipitated flakes of graphite. In ductile cast

iron the graphite precipitate is in the form of spheroids, or spherulitic balls. The mechanical behavior is determined primarily by the shape of precipitate particles. The flakes of graphite in gray cast iron serve as stress concentrators and yield a brittle material.

Empirically an active metal, such as magnesium, is added to the molten cast iron. The resultant casting contains spheroids of graphite as opposed to flakes and is ductile.

It has been shown by studies of Keverian²² that dissolved sulfur in iron inhibits the dissolution of graphite in molten iron. From his micrographs it also appears that sulfur acts as a growth poison for graphite out of molten iron. From studies of the growth of lithium fluoride²³ and potassium chloride²⁴ from aqueous solution it has been shown that a poison for both dissolution and growth is a step poison. Finally, it has been observed that such poisons reduce the critical free energy of nucleation of the phase whose growth or dissolution is inhibited.

In the presence of sulfur, and possibly oxygen, nucleation occurs at a low supersaturation and in the classical regime. When the poison is gettered with magnesium, for example, critical supersaturation occurs at a very large supersaturation. Non-classical nucleation occurs and polycrystalline spheroids of graphite nucleate and grow.

E. Vapor Deposition of Silica Glass.—DeVries and Sears²⁵ have observed the deposition of silica in progress at 80X in the same apparatus used for the vapor deposition of aluminum oxide. Hydrogen is passed slowly over a vitreous silica rod at about 1550° and evaporates the rod by chemical reaction. The rod is heated locally by a hot tungsten coil and a silica deposit forms by the reverse reaction at the cooler region about a millimeter beyond the ends of the coil. Unlike alumina the deposit does not have a crystalline morphology. Small chunks of deposit have almost exactly the index of refraction of vitreous silica formed from the melt.

This behavior is consistent with the expectations of non-classical nucleation theory. Nucleation occurs in the non-classical regime. The grain boundaries between silicon dioxide crystals are too large to be contained in the nucleus. Thus, only a glassy nucleus could form.

Summary.—It is shown that a great amount of unity over the entire field of crystal nucleation can be made by applying the theory of non-classical nucleation to a variety of observations. The supporting evidence has been by no means exhausted. The interpretations are not to be considered as proven as final. They are for the most part illustrative of the power of the theory.

(16) P. H. Till *J. Polymer Sci.*, **17**, 447 (1957).

(17) A. Keller, *Phil. Mag.*, **2**, 21 (1957).

(18) E. W. Fischer, *Z. Naturforsch.*, **12a**, 753 (1957).

(19) J. E. Coleman, B. J. Allan and B. L. Vallee, *Science*, **131**, 350 (1960).

(20) G. W. Sears, *Acta Met.*, **1**, 457 (1953).

(21) G. W. Sears, *ibid.*, **3**, 361 (1955).

(22) J. Keverian and H. F. Taylor, *Am. Foundrymans Soc. Trans.*, **65**, 212 (1957).

(23) G. W. Sears, *J. Chem. Phys.*, **33**, 1068 (1960).

(24) G. W. Sears, *ibid.*, **29**, 979 (1953).

(25) R. C. DeVries and G. W. Sears, unpubl. results.

CRYSTALLIZATION OF POLY-(ETHYLENE OXIDE) IN BULK

BY WILSON J. BARNES, WILLIAM G. LUETZEL AND FRASER P. PRICE

*General Electric Research Laboratory, Schenectady, New York**Received March 1, 1961*

Measurements of spherulite growth rates and bulk crystallization rates have been made at a variety of temperatures on several poly-(ethylene oxide) polymers in the molecular weight range of 5000 to 30,000. Spherulite nucleation rates have been calculated. It is found that both the spherulite growth rates and the bulk crystallization rates have essentially the same temperature coefficient. This makes the spherulite nucleation rates essentially temperature independent. It is concluded that spherulite nucleation is a heterogeneous process. A theory of spherulite growth as a nucleation controlled process is presented. It is concluded that, if a constant nucleation rate per unit spherulite boundary is assumed, the growth of the crystallites comprising the spherulite is very rapid compared to their nucleation. This theory is applied to the data obtained and conclusions about the magnitude of some of the interfacial tensions are drawn.

Much of the current work on crystallization of synthetic high polymers is concerned with the investigation of tiny single crystals produced by precipitation from dilute solution.¹⁻³ Notwithstanding the intrinsic interest of these crystals, and notwithstanding the possibility that their study may ultimately lead us to a comprehension of the situation in bulk polymers, it is nevertheless fruitful to continue investigations of the crystallization of synthetic high polymers in bulk.

The development of crystallinity in bulk polymers is intimately connected with the nucleation and growth of spherulitic structures. The majority of investigations of the crystallization process have been carried out using dilatometric techniques.⁴⁻⁶ In these cases the nucleation process and the growth process are inextricably intertwined. Only in relatively few instances^{7,8} have microscopic observations of spherulite growth rate been combined with measurements of bulk crystallization rates to yield information on the rate of spherulite nucleation. In these instances it has been found that the temperature dependence of the bulk crystallization rate almost exactly equals the temperature dependence of the spherulite growth rate. Further these investigators show that, contrary to the conclusions of Mandelkern, *et al.*,⁶ the growth and crystallization rates have a dependence on the inverse first order and not on the inverse second order of the supercooling.

This paper is concerned with the rate of spherulite nucleation and growth in poly-(ethylene oxide). This material was chosen for investigation because it melts in an easily accessible region, and it is readily available in a range of molecular weights. However the principal reason was that it appeared that it might be possible by following Hibbert's procedure⁹ to prepare by stepwise synthesis, a series of monodisperse polyglycols of various molecular weights. The crystallization behavior of these materials both in bulk and from dilute solution was to be investigated. This preparative attempt has been notable only in its complete lack of success. The investigation described here

was made using well characterized polydisperse materials and is presented in the hope that, when information regarding the crystallization behavior of monodisperse polyglycols does become available, there will be a satisfactory set of data for comparison.

Experimental

Several poly-(ethylene oxide) polymers of various molecular weights were obtained from the Carbide and Carbon Chemicals Co. under the trade name Carbowax. Carbowaxes 4000, 6000 and 20M were used in the study. They were used as purchased unless otherwise noted.

Measurements of spherulite growth were made by photographing the spherulites developing in a thin film between microscope cover slips on the hot stage of the petrographic microscope. The specimens were prepared by melting a small portion of the polymer on a cover slip and placing another slip on top of the melt. In the case of the Carbowax 4000 the melt was so fluid that a specimen prepared in this manner was thin enough that it showed insufficient birefringence when crystallized. In this instance a 0.5 mil platinum shim was used to separate the cover slips. The specimen was placed on a small hot plate regulated to $\pm 1^\circ$ to melt it. It was then slid off the melting block onto the hot stage whose temperature was regulated to $\pm 0.1^\circ$ with a thermocouple controlled electric heater. A small brass cup fitted with appropriate glass ports was placed over the sample to minimize the effect of cooling by stray air currents. The development of the spherulites was followed by photographing them at appropriate intervals with a Leica camera attached to the Bausch and Lomb petrographic microscope (between crossed nicols) by means of a Mikas photomicrographic adapter. The magnification of each run was calibrated by photographing, on the same film, a stage micrometer whose smallest division was 10 μ . It was found that changing the melting temperature from 80 to 150° had no effect on the growth rate of spherulites. Therefore in all the experiments described below, the melt temperature was 100°. The Carbowax 4000 and the Carbowax 6000 developed so few spherulites in the temperature range investigated that at the higher temperatures they grew to very large size (ca. 0.5 inches diameter). Because there were so few, no attempt was made to obtain a nucleation rate by direct observation. The Carbowax 20M on the other hand developed so many spherulites that an attempt was made to remove heterogeneities by filtration and centrifugation (at 15,000 $\times g$) of a methanol solution from which the polymer was subsequently separated by evaporation of the solvent. This attempt failed.

The hot stage was also used to measure the melting points of these polymers. With a heating rate of about 0.1° per minute, the melting points are 58.2, 63.2 and 63.4° for Carbowaxes 4000, 6000 and 20M, respectively.

The investigation of the bulk rates of crystallization was carried out in conventional sealed off dilatometers modified so that the capillary came out of the bottom of the bulb and was then bent upward in the form of a U. This shape was necessary so that the mercury filling liquid could act as a seal to prevent escape of these very fluid molten polymers. The dilatometers were filled, sealed off and evacuated for at least four hours at 100° before introduction of the mercury under vacuum. The rate of crystallization was followed by first immersing the dilatometer for 15 minutes in

(1) A. Keller, *Makromol. Chem.*, **34**, 1 (1959).(2) A. Keller, *Phil. Mag.*, **2**, 21 (1957).(3) H. A. Stuart, *Kolloid-Z.*, **165**, 3 (1959).(4) L. A. Wood and N. Bekkedahl, *J. Appl. Phys.*, **17**, 362 (1946).(5) P. W. Allen, *Trans. Faraday Soc.*, **48**, 1178 (1952).(6) L. Mandelkern, F. A. Quinn, Jr., and P. J. Flory, *J. Appl. Phys.*, **25**, 830 (1954).(7) Von B. Kahle, *Z. Elektrochem.*, **61**, 1318 (1957).(8) Von B. v. Falkai and H. A. Stuart, *Kolloid-Z.*, **162**, 138 (1959).(9) E. L. Lovell and H. Hibbert, *J. Am. Chem. Soc.*, **61**, 1916 (1939).

a thermostat well above the melting temperature and then plunging it into a thermostat regulated to $\pm .01^\circ$ in the range of $40\text{--}55^\circ$ and noting the time dependence of the height of the mercury meniscus. Melting temperatures of $80, 100$ and 150° were used.

It was found with Carbowax 6000 that while changing the melting temperature from 80 to 100° decreased the rate of crystallization at 54° by a factor of about thirty, a change of melting temperature from 100 to 150° produced no significant alteration in rate. With Carbowax 4000 a change of melting temperature from 80 to 100° produced a decrease in rate of only 50% when crystallizing at 49° , and with Carbowax 20M there was essentially no change in rate when the melting temperature was varied over this range. In all the dilatometric experiments described herein, except as noted, the melting temperature was 100° and the time of residence at that temperature was 15 minutes. Since dilatometric measurements alone yield only differences in specific volume, it is necessary to determine the specific volume of the polymer at one particular temperature. This was done at 80.0° using a pycnometer with silicone oil as the filling liquid. The specific volume of Carbowaxes 4000, 6000 and 20M were found to be 0.9251, 0.9256 and 0.9233 cc./g., respectively, at that temperature.

For the interpretation of the data, it is desirable to know the specific volume of the liquid polymer at the temperature of crystallization. These figures were obtained from extrapolation of the liquid specific volume above the freezing temperatures down to the temperature of interest. In order to obtain the information on the liquid specific volumes as functions of temperature, measurements were made at a number of temperatures in the range $55\text{--}85^\circ$. It was found that plots of specific volume versus temperature were excellent straight lines. The slopes of these plots were 5.50×10^{-3} , 6.20×10^{-3} and 5.67×10^{-3} (cc.)(g.) $^{-1}$ ($^\circ\text{C.}$) $^{-1}$ for Carbowaxes 4000, 6000 and 20M, respectively. It is interesting to note that it is possible to obtain data 10° below the melting point due to the sluggishness of the crystallization process. The specific volumes of the polymer specimens at the various times were calculated using previously developed formulas which take into account the coefficients of expansion of the glass and the mercury.

Intrinsic viscosities of these polymers in water at 30° were measured using conventional suspended level Ubbelohde viscometers. These viscosities were converted to molecular weights using the equations of Bailey, *et al.*¹⁰ The results are displayed in Table I.

TABLE I
INTRINSIC VISCOSITIES OF SEVERAL POLY-(ETHYLENE OXIDE)
POLYMERS AT 30.0° IN WATER

Carbowax	$[\eta]$, cc./g.	Mol. wt. $\times 10^2$
4000	10.3	5.47
6000	19.5	12.4
20M	42.0	33.1

Bulk viscosities of the molten Carbowaxes 4000 and 6000 were measured at a series of temperatures using thermostated 1-cc. pipets which were calibrated with glycerine. In the temperature range of $60\text{--}100^\circ$ semilogarithmic plots of viscosity versus $1/T$ were good straight lines. The slopes of these lines yielded activation energies for viscous flow of 6.3 and 6.9 kcal./mole for the Carbowaxes 4000 and 6000, respectively.

Theory

It is now well established that polymer spherulites are in no sense single crystals. They are organized arrays of single crystals. Thus in order to explain the space filling properties of spherulites it is necessary to postulate dendritic growth of the crystals. This mode of growth is amply demonstrated by recent experiments.^{11,12} This type of growth im-

plies that new crystals are constantly being nucleated on the surfaces of old ones and the growth of new crystals adds to the volume of the spherulite. Now, in measurements of growth rates of spherulites, observations are taken of the boundary between the spherulite and the melt. Thus in what follows we will be concerned only with the nucleation and growth of new crystals on or near the spherulite boundary. Further we will consider only those crystals which, after nucleation, grow to some extent in a radial direction.

Consider a spherulite at time, Z , after its birth. Then the radius of the spherulite is

$$r = GZ \quad (1)$$

where G is the linear growth rate. In the time interval, dZ , the number of new crystallites that are nucleated is

$$dN = 4\pi G^2 Z^2 P dZ \quad (2)$$

where P is the nucleation rate per unit area of the spherulite-liquid interface for the crystallites with the orientation postulated above. At some time, t , later than Z the volume of each of these crystallites is

$$v = c\gamma^m(t - Z)^m \quad (3)$$

where c and m are constants characteristic of the mode of crystallite growth, and γ is the linear growth rate of the crystallites. Then the increase in volume of the spherulite due to these crystals is

$$dV = 4\pi G^2 \gamma^m c P Z^2 (t - Z)^m dZ \quad (4)$$

and the volume of the spherulite at time, t , is

$$V_t = 4\pi G^2 \gamma^m c P \int_t^0 Z^2 (t - Z)^m dZ \quad (5)$$

which leads to

$$V_t = (4\pi G^2 \gamma^m c P) \left(\frac{2}{(m+1)(m+2)(m+3)} \right) t^{3+m} \quad (6)$$

However, we know from eq. 1 that

$$V_t = 4/3\pi G^3 t^3 \quad (7)$$

which makes $m = 0$ and $v = c$. Thus if the assumption of constant nucleation rate, P , is valid, the volume of the crystallites must be constant. This can only mean that once nucleated the crystallites attain some constant size in a time very short in comparison to the nucleation time. Further, comparison of eq. 6 and 7 shows that with $m = 0$

$$G = cP \quad (8)$$

Thus the radial growth rate of the spherulite is proportional to a nucleation frequency per unit area. This is consistent with the observations and speculations of McIntyre and Flory¹³ on the sensitivity of the growth rate to temperature. Equation 8 is also consistent with the observations of Claver and Buchdahl¹⁴ on the oscillating nature of the growth of spherulites. This may be likened to periodic precipitation or Liesegang ring formation where the growth is controlled by a nucleation process that is extremely temperature sensitive. It should be noted that P is the nucleation rate referred to the gross area of the spherulite-liquid interface. On a microscopic level this interface is

(10) F. E. Bailey, J. L. Kucera and L. G. Imhof, *J. Polymer Sci.*, **32**, 517 (1958).

(11) F. P. Price, *Ann. N. Y. Acad. Sci.*, **83**, 20 (1959).

(12) H. D. Keith and F. J. Padden, Jr., *J. Polymer Sci.*, **39**, 123 (1959).

(13) A. D. McIntyre and P. J. Flory, *ibid.*, **18**, 592 (1955).

(14) G. C. Claver and R. Buchdahl, paper before Polymer Division Am. Chem. Soc., 135th Meeting, Boston, Mass., 1959.

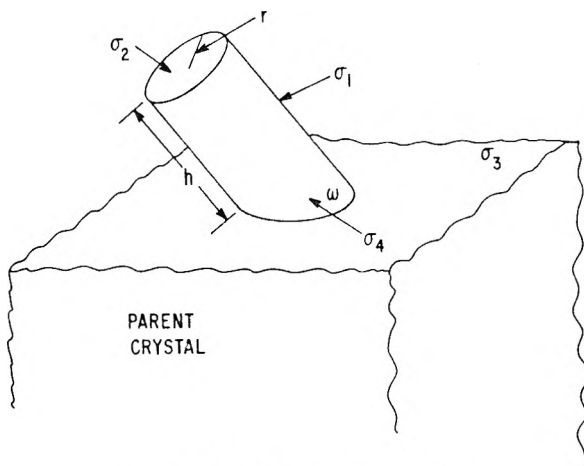


Fig. 1.—Model for dendrite nucleus.

not smooth. It must be composed of the ends of many tiny crystallites. Thus P represents only the average nucleation rate of new crystallites with some radial growth component on the appropriate side surfaces of the crystallites which comprise the rough spherulite surface at any given instant.

We now turn to a more detailed consideration of the nucleation of dendrites. In this we will not be concerned with dendritic growth in which the structure is merely a single crystal with holes in it, where all the completed regions of the structure are related as in a single crystal. Instead we will consider that each branch is a new crystal with an orientation in space differing from that of its parent. A schematic diagram of the model is shown in Fig. 1. In this diagram the nucleus is a right cylinder intersecting a plane (the parent crystal surface) with σ_1 and σ_2 the interfacial energies at the cylindrical surface-melt interface and the end surface-melt interface, respectively. The interfacial energy of the parent crystal and the melt is σ_3 and the interfacial energy between parent and daughter crystals is σ_4 .

It can be shown that the contact area and the volume of such a nucleus are $\pi r^2/\sin \omega$ and $\pi r^2(h + r \cot \omega)$, respectively. Then the energy required to construct such a nucleus from the melt is

$$\Delta F = (2\pi r\sigma_1 - \pi r^2\Delta G_V)(h + r \cot \omega) + \pi r^2 \left(\sigma_2 + \frac{\sigma_4 - \sigma_3}{\sin \omega} \right) \quad (9)$$

where ΔG_V is the bulk free energy of fusion at the temperature under consideration. Following common practice we will approximate

$$\Delta G_V = \frac{\Delta H_V}{T_m} (\Delta T) \quad (10)$$

where ΔH_V is the bulk enthalpy of fusion, T_m is the melting temperature and ΔT is the supercooling below the melting point ($\Delta T = T_m - T$, T = temperature of crystallization). If we then make $\partial \Delta F / \partial h$ and $\partial \Delta F / \partial r$ vanish, we find that r^* , h^* and ΔF^* , the critical values of r , h and ΔF , respectively, are

$$r^* = \frac{2\sigma_1}{\Delta G_V} \quad (11a)$$

$$h^* = \frac{2}{\Delta G_V} \left[\sigma_2 - 2\sigma_1 \cot \omega + \frac{\sigma_4 - \sigma_3}{\sin \omega} \right] \quad (11b)$$

and

$$\Delta F^* = \frac{4\pi\sigma_1^2}{\Delta G_V^2} \left[\sigma_2 + \frac{\sigma_4 - \sigma_3}{\sin \omega} \right] \quad (11c)$$

The important thing to note here is that when we let the nucleus vary in all three dimensions (h in one direction and r in two directions), ΔF^* varies as the inverse second power of ΔG_V or ΔT .

On the other hand, if we fix one dimension, say $h = h_1$, then the critical nucleus radius is given by solutions of the equation

$$(3/2 \Delta G_V \cot \omega) r^{*2} - \left[\sigma_2 + \frac{\sigma_4 - \sigma_3}{\sin \omega} + 2\sigma_1 \cot \omega - h_1 \Delta G_V \right] r^* - h_1 \sigma_1 = 0 \quad (12)$$

In general solution of this equation is inconvenient, first as the discriminant is not a perfect square and second as the coefficient of r^{*2} can vanish if ω is sufficiently close to $\pi/2$. However to illustrate the effect of fixing one dimension of the nucleus we will make ω so close to $\pi/2$ that the coefficient of r^{*2} vanishes. This is equivalent to making $r \cot \omega$ negligible in comparison to h (cf. eq. 9). In this particular instance

$$r^* = \frac{h_1 \sigma_1}{h_1 \Delta G_V - (\sigma_2 + \sigma_4 - \sigma_3)}$$

and

$$\Delta F^* = \frac{\pi h_1^2 \sigma_1^2}{h_1 \Delta G_V - (\sigma_2 + \sigma_4 - \sigma_3)}$$

In this case in the event that the sum, $\sigma_2 + \sigma_4 - \sigma_3$, is negligible compared to $h_1 \Delta G_V$, ΔF^* will depend inversely on the first power of the supercooling. If, as seems more probable, $\sigma_2 + \sigma_4 - \sigma_3$ is not negligible and is positive, then at small supercoolings the dependence of ΔF^* will be greater than the inverse first power of the supercooling.

It is possible to derive similar expressions for the critical nucleus dimensions and the critical free energy change for nuclei of other shapes. However the conclusions are qualitatively the same; the inverse order of the dependence of critical free energy change on supercooling is one less than the number of nucleus dimensions that are variable.

Now, it has been shown^{15,16} that the nucleation rate

$$\dot{N} = N_0 e^{-\Delta H^\ddagger/kT} e^{-\Delta F^*/kT} \quad (15)$$

where N_0 is a constant essentially independent of temperature, ΔH^\ddagger is an activation energy characteristic of the transport of material across the liquid-crystal interface (usually taken as the activation energy for viscous flow) and ΔF^* is defined as above. Since ΔH^\ddagger is essentially temperature independent and ΔF^* depends on the supercooling (ΔT) at low supercoolings the entire temperature dependence of \dot{N} is contained in the last exponential. Further we noted above in eq. 8 that for nucleation controlled growth the spherulite growth rate was proportional to the nucleation rate. If we assume that at the spherulite-liquid boundary, on the average there is a constant fraction of that

(15) R. Becker and W. Döring, *Ann. Phys.*, [5] **24**, 719 (1935).

(16) D. Turnbull and J. C. Fisher, *J. Chem. Phys.*, **17**, 71 (1949).

area made up of crystal surfaces which serve as nucleation sites for new crystals, we can write

$$P = \alpha \dot{N} \quad (16)$$

where α is that fraction. Combining eq. 8, 15 and 16 yields

$$G = \alpha c N_0 e^{-\Delta H^*/kT} e^{-\Delta F^*/kT} \quad (17)$$

Letting

$$G_0 = \alpha c N_0 e^{-\Delta H^*/kT}$$

we now note that

$$\ln G = \ln G_0 - \frac{\Delta F^*}{kT} \quad (18)$$

Then plots of $\ln G$ versus $T^{-1}[\Delta T]^{-q}$ will be linear for nuclei developing in three dimensions for $q = 2$ and will be linear for nuclei developing in only two dimensions for $q = 1$. Thus it may be possible experimentally to distinguish between these types of nuclei.

Results

Microscopic Observation.—The results of the direct observation of spherulites are shown in Table II. The figures in this table again emphasize the extreme sensitivity of the growth rate to temperature. Over a 10° temperature range the growth rate changes by three orders of magnitude. An interesting consequence of this is shown in the radical growth along the connecting center lines in two nearly touching spherulites. This is illustrated by Fig. 2 where are plotted as functions of time the changes in length of two radii of a

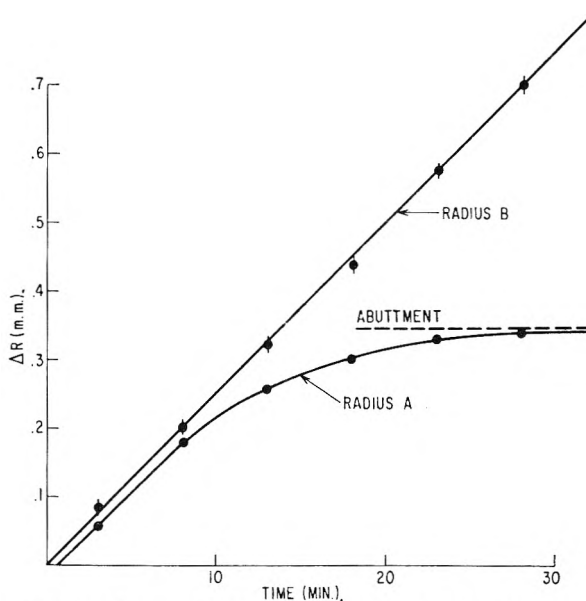


Fig. 2.—Change in radius length, ΔR , for two radii of a spherulite nearing abutment. Radius A, along center line of abutting spherulites; radius B, normal to radius A.

T_m	Melting temp., 100°		Melting time, 10 min.		
	Carbowax 4000 58.2°	Carbowax 6000 63.2°	Carbowax 6000 63.4°	Carbowax 20M 63.4°	
T ($^\circ\text{C}$)	G ($\frac{\text{mm.}}{\text{min.}}$)	T ($^\circ\text{C}$)	G ($\frac{\text{mm.}}{\text{min.}}$)	T ($^\circ\text{C}$)	G ($\frac{\text{mm.}}{\text{min.}}$)
42.0	0.826	47.2	0.705	47.6	0.107
44.2	.284	48.8	.362	48.2	.0910
45.2	.133	51.2	.0908	50.5	.0212
47.2	.0237	55.2	.00333	51.0	.0246
				51.0	.0266
				51.0	.0253
				53.8	.00565
				56.4	.000096

spherulite which is in the process of touching another spherulite. One radius is taken along the line of centers of the two abutting spherulites and the other radius is taken nearly at right angles to the first. This plot shows that initially the rate of growth is the same along both radii. However, when the radius of initial abutment gets to within about 0.15 mm. of the other spherulite, the growth rate is decreased and asymptotically approaches zero as abutment becomes increasingly imminent. Thus the spherulites seem to sense the presence of each other over considerable distances. It is possible that this effect is due to molecular orientation in the interstitial liquid resulting from contraction during crystallization. However it is more probably the result of an increase in temperature in the interstitial region resulting from the low thermal conductivity and the heat of crystallization of the polymer.

The data in Table II were manipulated to produce the plots shown in Fig. 3. While there is considerable scatter in the points, it seems clear that the $T^{-1}(\Delta T)^{-1}$ plot gives a much better straight line than would a $T^{-1}\Delta T^{-2}$ plot. Since the growth rate does seem to depend on the inverse first power of the supercooling, the dependence is expressed by eq. 18 with ΔF^* having the form shown in eq. 14. This means that the nucleus has one fixed dimension. Further since there is no detectable downward curvature, we can assume that the $\sigma_2 + \sigma_4 - \sigma_3$ term in eq. 14 is negligible compared to $h_1\Delta G_V$. Hence we can write eq. 18 in the form

$$\ln G = \ln G_0 - \frac{\pi h_1 \sigma_1^2 T_m}{k \Delta H_V} \times \frac{1}{T(\Delta T)} \quad (19)$$

The values of G_0 and the slopes of the plots in Fig. 3 are given in Table III. The slopes of these plots are all essentially the same. This is reasonable as we are dealing with polymers of the same chemical constitution varying only in molecular weight.

Carbowax	$G_0 \times 10^{-2}$	Slope $\left[\frac{\Delta(\ln G)}{\Delta(1/T\Delta T)} \right] \times 10^{-4}$
4000	3.02	-3.04
6000	2.89	-2.86
20M	0.348	-2.90
		Av. 2.93

In this situation it is to be expected that the parameters which govern the slopes of the plots would be the same for all three polymers. On the other hand, whereas the 4000 and the 6000 polymers have essentially the same G_0 , that of the 20M polymer is considerably lower. Although it is conceivable that the difference may result from a more positive value of ΔH^* for the latter polymer, this does not seem reasonable, and the real cause of the difference is not clear.

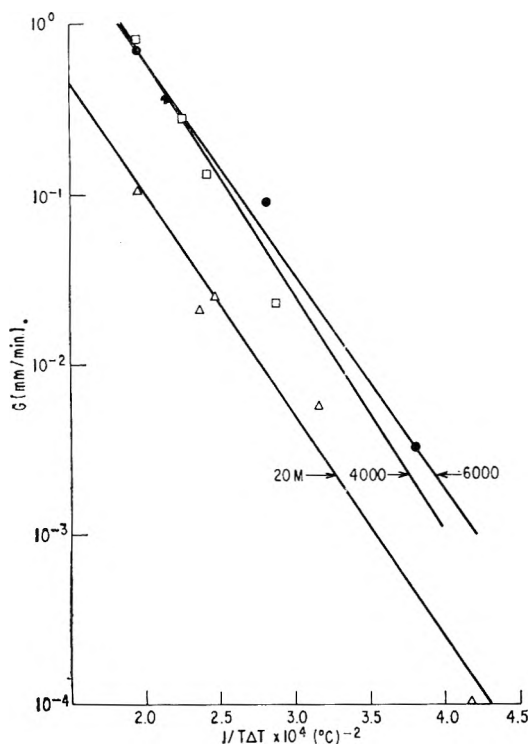


Fig. 3.—Plot of growth rate versus $1/T\Delta T$ for spherulites of several poly(ethylene oxide) polymers: ●, Carbowax 4000; □, Carbowax 6000; △, Carbowax 20M.

It is worth noting for the Carbowaxes 4000 and 6000 that, if ΔH^* in eq. 15 is equated to the activation energy for viscous flow (approx. 6.5 kcal./mole), that over the temperature range studied the effect of this term on the nucleation rate is entirely negligible. A change of 10° in temperature in this term produces only a 40% change in nucleation rate, and that in a direction opposite to that observed. This indicates the validity of the assumption of a G_0 (cf. eq. 18) that is temperature independent.

By taking $T_m = 330^\circ$ and $\Delta H_v = 45$ cal./cc., it can be calculated that the slopes in Table III are equal to $4.19 \times 10^3 h_1 \sigma_1^2$. Then by using the average value of the slopes in Table III and assuming $h_1 = 10 \text{ \AA.}$, one calculates that $\sigma_1 = 8.4$ ergs/cm.², a reasonable figure. Further, by using eq. 13, it is possible to calculate that for $\Delta T = 10^\circ$, $r^* = 14.8 \text{ \AA.}$, also a reasonable figure.

Dilatometric Experiments.—We now turn to the measurement of the bulk rate of crystallization where the nucleation of spherulites as well as their growth is involved. It has been shown by previous investigators⁶ that it is possible to characterize the course of an isothermal crystallization process by

$$\ln \left[\frac{1 - \delta}{v/v_0 - \delta} \right] = (K_n t)^n \quad (20)$$

where

- δ = density of liquid/density of crystals
- v = specific volume of liquid-crystal mixture
- v_0 = specific volume of liquid
- t = time

and K_n and n are constants characterized by the nucleation rate and the shape of the developing crystalline bodies. In general n is the sum of

the number of dimensions enlarging in the crystals plus the order of the time dependence of their nucleation rate. Thus for crystals enlarging in three dimensions and appearing at a constant rate $n = 4$. Specifically it has been shown that for radially enlarging spheres nucleating at a constant rate, $n = 4$ and

$$K_4^4 = k_s = \frac{\pi}{3\delta} AG^3 \quad (21)$$

where A = nucleation rate of the spheres per unit volume.

The form of eq. 20 implies that plots of some function of v/v_0 , say $1 - v/v_0$, versus $\log t$ should, for a given crystallizing substance, have the same shape regardless of the temperature of crystallization. Of course this happens only if the crystal growth and nucleation mechanisms do not alter. The specific shape of the plots is determined solely by the value of n and their relative positions on the $\log t$ axis are determined by K_n . Thus K_n can be measured for each experimental plot of $1 - v/v_0$ versus $\log t$ by sliding along the $\log t$ axis until a match is obtained with a curve calculated from eq. 20. This technique for analyzing rate data from dilatometric studies has been successfully applied to a wide range of polymeric systems⁶⁻⁸ and it was applied successfully here. Master plots for $n = 2, 3, 4$ with $\delta = .917$ were made and the experimental plots of $1 - v/v_0$ versus $\log t$ were fitted to them. It was found that the initial portions of the plots of all the Carbowaxes fitted the $n = 4$ curves quite well. After some crystallization (2-5%) had taken place, the Carbowax 20M seemed to go over to an $n = 3$ curve, while the Carbowaxes 4000 and 6000 fitted the $n = 2$ curves best. This led to the concept that the crystallization process in the Carbowax 20M started off with a constant spherulite nucleation rate and then after a while the spherulites stopped appearing and only those that had started continued to enlarge radially. This concept is consistent with the notion that spherulites nucleate only on heterogeneities^{17,18} and when all the heterogeneities that are active at a particular temperature have nucleated spherulites, then birth of new spherulites ceases. The change in the value of n from 4 to 2 in the case of the Carbowaxes 4000 and 6000 can be explained by assuming that the spherulites nucleate on or near the walls of the dilatometer. After the walls are completely covered, the spherulites can develop only radially inward producing the row structures frequently observed. When the surface is completely covered, if the ends of the cylindrical dilatometer bulb are neglected, it can be shown that $n = 2$ and

$$K_2 = G/(R\delta^{1/2}) \quad (22)$$

where R is the radius of the dilatometer bulb. Further it can be shown that a plot of $1 - v/v_0$ versus $\log t$ for this situation is essentially identical to that calculated from eq. 20 with $n = 2$. It is clear that the above expression for K_2 does not depend on the spherulite nucleation rate because

(17) F. P. Price, *J. Am. Chem. Soc.*, **74**, 311 (1952).

(18) F. P. Price, paper presented at the IUPAC Symposium on Macromolecules, Wiesbaden, Germany, 1959.

TABLE IV
BULK CRYSTALLIZATION RATES, SPHERULITE GROWTH RATES, AND SPHERULITE NUCLEATION RATES FOR SEVERAL POLY-(ETHYLENE OXIDE) POLYMERS

Melt temp. (°C.)	Crystln. temp.	k_s	G_{obs} ($\frac{mm.}{sec.}$) $\times 10^3$	A , $cm.^{-3} sec.^{-1}$	A' , $cm.^{-2} sec.^{-1a}$	$K_2 \times 10^4$	$G_{calc} \times 10^3$	$\frac{G_{obs}}{G_{calc}}$
Carbowax 4000								
100	46.2	1.81×10^{-12}	1.92	0.224	0.118	7.30	0.632	3.04
100	46.9	1.12×10^{-12}	1.08	.772	.400	5.15	.445	2.43
100	47.9	5.30×10^{-14}	0.483	.412	.216	2.80	.242	2.00
79	49.1	1.87×10^{-15}	.152	.467	.246	1.21	.104	1.46
100	49.1	1.22×10^{-15}	.152	.304	.159	1.12	.097	1.57
150	49.1	5.80×10^{-16}	.152	.145	.076	0.74	.064	2.38
100	50.0	1.43×10^{-17}	.0483	.110	.058	0.55	.026	1.83
Carbowax 6000								
100	50.0	2.44×10^{-12}	3.73	0.0411	0.0214	7.60	0.710	5.25
100	50.6	7.48×10^{-13}	2.78	.0305	.0160	6.00	.560	4.97
100	52.0	6.77×10^{-14}	1.19	.0351	.0184	2.90	.270	4.41
100	53.0	5.55×10^{-15}	0.566	.0268	.0141	1.53	.131	4.31
80	54.0	6.60×10^{-16}	.241	.0413	.0216	1.57	.135	1.79
100	54.0	2.36×10^{-16}	.241	.0147	.0077	0.62	.078	3.10
150	54.0	1.87×10^{-16}	.241	.0117	.0062	.58	.050	4.84
Carbowax 20M								
100	50.0	4.57×10^{-11}	.724	100				
100	52.0	2.07×10^{-12}	.233	143				
100	53.8	6.15×10^{-16}	.0558	31				
100	55.5	1.19×10^{-18}	.00049	1.9				

^a A' calculated from A using eq. 23 with $\rho = 0.262$ (a right cylinder of polymer of density 1.1, 0.9 cm. in radius weighing 3.5 g.).

in this situation no new spherulites are being born. Thus eq. 22 permits an independent calculation of G which may be compared to the microscopically observed one. If this situation is correct, then eq. 21 is no longer correct even for the initial stages of crystallization because with the spherulites starting on or near the walls they can only develop as hemispheres. Thus, for a given volume of material in the crystalline states, there would have to be twice as many hemispheres as spheres. Further since they are nucleating only on the walls and not throughout the entire volume to obtain the nucleation rate per unit wall area, we must multiply by the ratio of volume to surface of the dilatometer. Thus the nucleation rate per unit area is

$$A' = 2\rho A \quad (23)$$

where ρ is the ratio of volume to surface and A is the nucleation rate per unit volume calculated from eq. 21.

The results of the dilatometric investigations together with the calculated spherulite nucleation rates are presented in Table IV. Here the crystallization temperatures are those at which the dilatometric experiments were performed, while the values of G for these temperatures were obtained by interpolation from Fig. 3.

The values of k_s in the third column of the table again reflect the extreme temperature sensitivity of the crystallization process, varying four to five orders of magnitude over a temperature range of 4–5°.

Previous investigators⁶ have made a similar study of poly-(ethylene oxide). Their results show a temperature sensitivity of k_s similar to that evidenced by the figures in Table IV. However

the absolute magnitude of their figures is many times greater than similar ones in the table. The reason for the discrepancy is not apparent. In any event the conclusions drawn below concerning the nature of the spherulite nucleation process are not materially altered by these differences.

In the cases of the Carbowaxes 4000 and 6000 the large variation in k_s is completely the result of the temperature dependence of the spherulite growth rates, with the result that the nucleation rates given in columns five and six are essentially independent of crystallization temperature. For these two polymers there seems to be essentially no effect of growth temperature upon spherulite nucleation provided that the melting temperature is fixed. Both these polymers, however, show a consistent trend toward lower nucleation rates as the melting temperature is raised. The spherulite nucleation rate for Carbowax 4000 crystallizing at 49.1° dropped by a factor of about three when the melt temperature was raised from 79 to 150°, while the nucleation rate for the Carbowax 6000 crystallizing at 54° decreased by a factor of nearly thirty for the same change in melt temperature. The extremely small values for the nucleation rates of these two polymers are noteworthy. In this crystallization temperature range the Carbowax 4000 produces a new spherulite in each cubic centimeter about every two to five seconds, while the Carbowax 6000 takes about ten times as long. This situation produces only a very few spherulites and consequently they frequently become large enough to be visible to the unaided eye.

While the nucleation rates of the Carbowaxes 4000 and 6000 spherulites are very small and relatively independent of crystallization temperature, those of the Carbowax 20M are much larger and show a significant temperature dependence. With this latter polymer the decrease in the spherulite growth rate, large as it is, is not sufficient to account for the decrease in k_n with the result that the nucleation rate drops by a factor of about fifty when the crystallization temp. is raised from 50 to 55.5°. The relatively large magnitude of the spherulite nucleation rate in the Carbowax 20M generally resulted in so many spherulites that none ever grew to the great size of those found in the other two polymers.

The last three columns of Table IV are devoted to a summation of those portions of the bulk crystallization curves for the two lower molecular weight Carbowaxes where $n = 2$. Here G_{calc} in the penultimate column was obtained from eq. 22 with $R = 0.9$ cm. The last column gives the ratio of the observed to calculated growth rates. It is seen that sometimes this ratio is as great as five. This is a considerable variation. However in view of (a) the approximately thirty-fold variation in both the calculated and observed growth rates and (b) the simple assumptions that went into the calculation, perhaps this agreement is as good as can be expected. Certainly it is much better than an order of magnitude agreement.

In the cases of the Carbowaxes 4000 and 6000 it seems quite clear that the nucleation of the spherulites results from a heterogeneous process, either on foreign particles suspended in the melt or more probably on the glass walls of the container. The insensitivity of the spherulite nucleation rate to temperature, the small magnitude of the nucleation rate and the influence of melt temperature all indicate that this is the case. This assertion is further substantiated by an experiment wherein a thin film of Carbowax was crystallized, melted and recrystallized. Out of twenty-eight spherulites in the field of view of the first crystallization, twenty-four reappeared in identical positions in the second crystallization.

Also, experiments on the crystallization of small droplets (2–10 μ) of both Carbowax 4000 and Carbowax 6000 suspended in silicone oil,¹⁸ show that significant nucleation rates are not attained until temperatures of 0° or lower are attained. Since this temperature range is an upper limit for a homogeneous nucleation, all nucleation processes taking place 50° higher must be heterogeneous in origin.

The case of the Carbowax 20M is not as clear cut. The major difficulty is that there seemed to be no dependence of the nucleation rate on the melt temperature. Usually heterogeneous nucleation processes are accompanied by a dependence on melt temperature. The dependence is explained by the superheating necessary to melt crystalline material out of crevices in the heterogeneities.¹⁹ It is possible, although it seems improbable, that the heterogeneities could be cracked free. The dependence of the spherulite nucleation rate on crystallization temperature could be explained on the basis of a homogeneous nucleation process. However, since the temperature dependence shown is much smaller than that usually shown by homogeneous processes, we prefer to attribute nucleation to a heterogeneous process wherein the heterogeneities have a range of abilities to nucleate spherulites. Thus, the ability of a given heterogeneity depends on the crystallization temperature. Since any heterogeneity which is capable of initiating crystallization at a high temperature can also serve as a nucleation site at lower temperature, decreasing temperature will bring more heterogeneities into play and the nucleation rate will increase with decreasing temperature. One further fact that adds weight to the notion of heterogeneous nucleation for this polymer is the fact that n changes from 4 to 3 as the crystallization proceeds. It seems reasonable that, since the total volume fraction transformed was so small (less than 10%), if continuing homogeneous nucleation of spherulites were occurring, then n should have remained at 4.

(19) D. Turnbull, *J. Chem. Phys.*, **18**, 198 (1950).

AN OPTICAL DIFFRACTOMETER ANALYSIS OF LIGHT SCATTERING PATTERNS OBTAINED FROM POLYETHYLENE FILMS¹

BY PHILIP R. WILSON, S. KRIMM AND RICHARD S. STEIN

Department of Chemistry, University of Massachusetts, Amherst, Mass., and Department of Physics, University of Michigan, Ann Arbor, Mich.

Received March 1, 1961

The optical-diffraction technique is used to analyze the interpretations of light scattering patterns from polyethylene films. Three cases are considered: (1) the effect of periodicity in spherulite structure, (2) the effect of spherulite anisotropy, and (3) the effect of internal structure.

Introduction

It has been shown² that the scattering of light at low angles is a consequence of the optical anisotropy of volume filling spherulites. The anisotropic scattering patterns obtained with polarized light have been interpreted in terms of the anisotropic distribution of induced dipoles within the spherulite. The variation of the scattering patterns during the growth and melting of the spherulites has been interpreted successfully in terms of this mechanism. The theory permits one to calculate rigorously the scattering from an isolated three-dimensional spherulite. The effect of environment in a close-packed spherulitic medium is approximated by surrounding the isolated spherulite with a medium of constant refractive index equal to the average refractive index of the spherulite. A more exact treatment of the effect of surrounding spherulites is prohibitively difficult. In this paper, the optical-diffraction analog technique³ is employed to assess this effect.

Ringed Spherulite Structure.—It is now well established that the concentric rings observed in polyethylene spherulites when examined in polarized light arise from radial periodicity of crystal orientation within the spherulite.^{4,5} A theory of light scattering from such an isolated spherulite has been presented.² This theory predicts that a scattering maximum should occur at a scattering angle, θ , given by the Bragg-type equation

$$\lambda = d \sin (\theta/2) \quad (1)$$

where λ is the wave length of the light in the medium, and d is the radial repeat distance of crystal orientation. This maximum has been observed^{6,7} (Fig. 1). The effect of having the spherulite surrounded by others was examined by the optical diffraction analog technique. A full discussion of this method and of the essential

features of the diffractometer is given by Hughes and Taylor.³

Two drawings were prepared. One represents an isolated spherulite possessing a radial variation of scattering power (arising from either density or orientation variations) and the other (Fig. 2) a close-packed assembly of such spherulites. Diffraction patterns are presented in Fig. 3a and b. Three features bear noting: (1) for the single spherulite, a central ring quite close to the incident beam is seen which is absent in the pattern from the array. This results from diffraction by the entire spherulite and arises because of the boundary between the spherulite and its surroundings. (2) A new ring of greater diameter is observed in the pattern from the spherulitic array. This is a consequence of interspherulitic interference and is a result of the incompletely random distribution of spherulite centers. (3) The larger diameter ring is observable in both patterns. This is the predicted Bragg-type diffraction maximum arising from the inter-ring spacing. Its average position is the same in both patterns. This is more intense and more diffuse in the pattern from the array of spherulites. The increased intensity results from the greater number of contributing spacings while the diffuseness is probably a result of the incomplete rings at the spherulitic boundaries.

The analog patterns differ from the observed scattering maximum in that the maximum occurs as a complete circle rather than an equatorial arc. This has been explained on the basis that it is only the tangential refractive index of the spherulite which is periodic, not the radial. Consequently, periodicity in scattering power occurs only in the equatorial regions of the spherulite. The effect upon the scattering patterns of the angular variation of scattering power within the spherulite is discussed in the next section.

The Effect of Differing Radial and Tangential Polarizability.—The theory of and calculated scattering patterns for homogeneous isolated spherulites having different radial and tangential polarizabilities have been presented. The predicted scattering patterns bear a resemblance to the actual ones, and the observed angular dependency of scattered intensity is consistent with the microscopically measured spherulite size.² Again, however, the effect of interspherulitic interference is considered only in an approximate way. A more detailed analysis of this effect may be obtained from optical diffraction studies.

Polyethylene scattering patterns obtained with parallel and crossed polarization have been pub-

(1) Two of the authors (P. R. Wilson and R. S. Stein) acknowledge support, in part, by a contract with the Office of Naval Research and by grants from the Petroleum Research Fund and the Plax Corporation. The third author (S. Krimm) acknowledges support by the United States Public Health Service. The authors are indebted to Dr. Robert L. Miller, Monsanto Chemical Co., Plastics Div., Springfield, Mass., for the microdensitometer traces.

(2) R. S. Stein and M. B. Rhodes, *J. Appl. Phys.*, **31**, 1873 (1960).

(3) For a description and list of references, see W. Hughes and C. A. Taylor, *J. Sci. Instr.*, **30**, 105 (1953).

(4) (a) A. Keller, *J. Polymer Sci.*, **17**, 291 (1955); **39**, 151 (1959);

(b) F. Price, *ibid.*, **37**, 71 (1959); **39**, 139 (1959).

(5) H. D. Keith and F. J. Padden, *ibid.*, **39**, 101, 123 (1959).

(6) R. J. Clark, R. L. Miller, R. S. Stein and P. R. Wilson, *ibid.*, **42**, 275 (1960).

(7) R. S. Stein and A. Plaza, *ibid.*, **45**, 519 (1960).

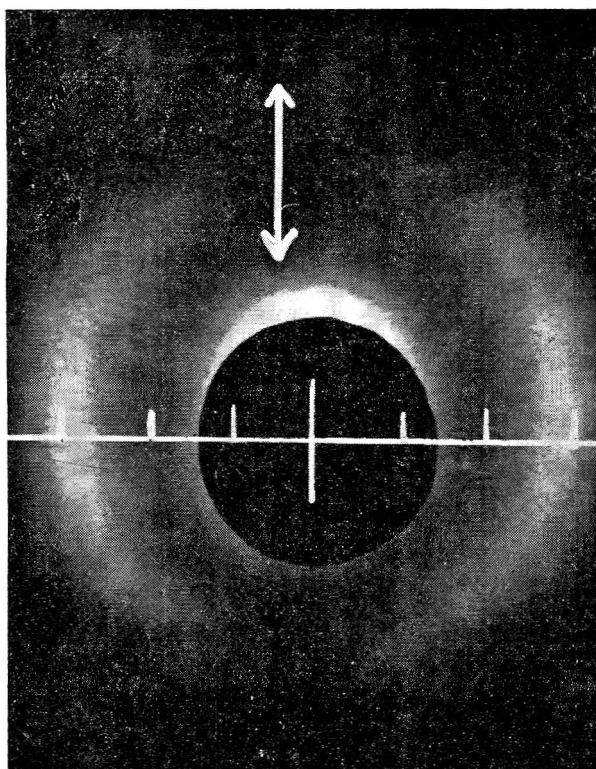


Fig. 1.—The V_V scattering pattern for a polyethylene sample having "ringed" spherulites. Five-degree angular divisions are marked. The polarization direction is vertical. The central beam and the scattering at angles less than about 7° is blocked out by a mask to avoid fogging of the film.

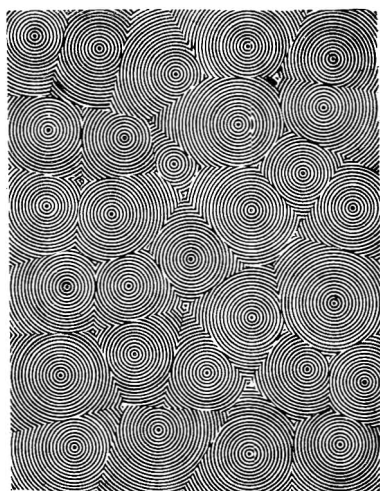


Fig. 2.—A close-packed array of two-dimensional spherulites with radial variation in scattering power.

lished² (with one polarizer in the incident beam and one in the scattered beam). In both patterns, most of the scattering occurs at angles less than 3° from the incident beam. The radial dependency of scattered intensity is a function of the size and packing of the spherulites, but the angular dependency of intensity is a function of the angular dependency of the induced dipole moment within the spherulite and the component of the scattered light from this which passes through an analyzer. This depends, of course, on the relative orientation

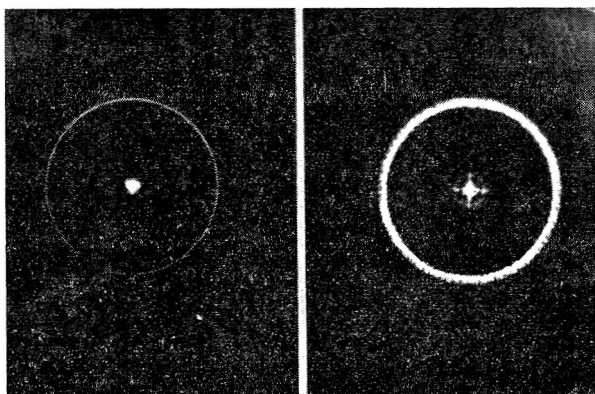


Fig. 3.—The diffraction patterns from the ringed spherulites (a) isolated spherulite, (b) close-packed array.

of the polarizer and analyzer. In the V_V pattern, the intensity concentrates along the common direction of polarization of the polarizer and analyzer; while in the H_V patterns, the intensity maxima occur in four lobes (like a four leaf clover) at 45° to both the polarizer and analyzer.

The polarization nomenclature employed here is the same as that in reference 2. The observed V_V scattering patterns, which have a more intense scattering in the angular direction corresponding to the polarization direction, have been shown to result from spherulites having a greater radial than tangential polarizability.

For simplicity of analysis by the optical diffraction technique, it will be assumed that the radial polarizability is zero and the tangential polarizability is α_t . The induced tangential dipole moment, M_t , resulting from placing such a spherulite in a plane polarized field, E , is then given by

$$M_t = \alpha_t E \cos \alpha \quad (2)$$

The components of this dipole moment transmitted by an ideal vertically and horizontally oriented analyzer are

$$M_V = \alpha_t E \cos^2 \alpha \quad (3)$$

and

$$M_H = \alpha_t E \sin \alpha \cos \alpha \quad (4)$$

The amplitude of the component of the dipole moment is greatest at $\alpha = 0$ for V_V scattering (in the polarization direction) and at $\alpha = 45^\circ$ for H_V scattering. In both cases, the scattering amplitudes vary continuously with α . The transmission of the diffraction masks should be proportional to this amplitude.

Although diffraction masks with a continuous variation in transmission are more realistic, discontinuous masks were used here because of their ease of preparation. These consist of white and black zones representing scattering and non-scattering regions, respectively. Masks for single spherulites and an array of spherulites for V_V and H_V polarization were prepared. A typical mask for an array of spherulites with V_V polarization is shown in Fig. 4. The diffraction patterns arising from three of these cases are presented in Figs. 5 and 6.

The pattern from the isolated spherulite shows the fourfold symmetry found in the observed patterns. Because of the discontinuous nature of

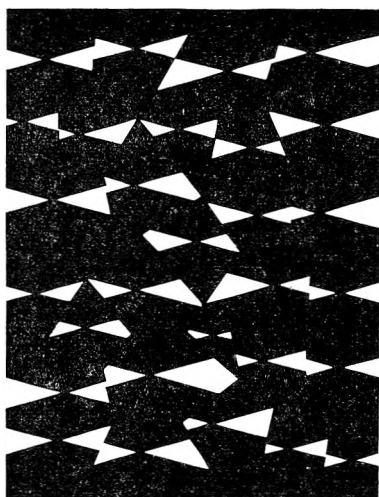


Fig. 4.—A close-packed array of tangentially polarizable spherulites with V_V polarization.

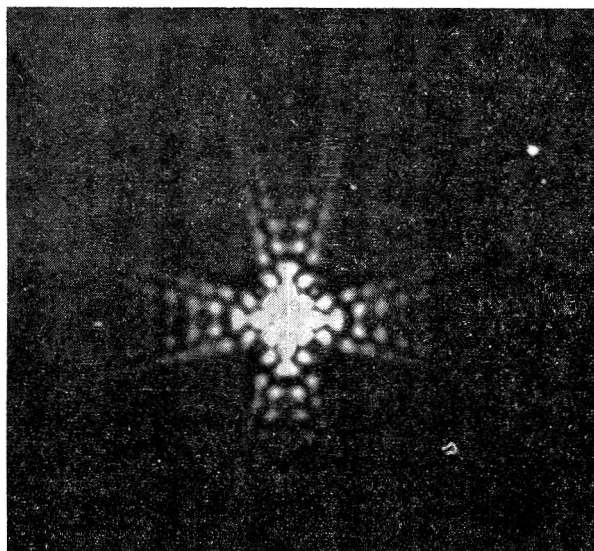


Fig. 5.—The optical diffraction pattern for an isolated idealized tangentially polarizable spherulite with H_V polarization. The polarizer and analyzer are crossed and at 45° to the vertical direction.

the two-zone model, the pattern is found to be composed of discrete spots rather than a continuous one. In the spherulite array, the fourfold symmetry is preserved, but the pattern is more continuous as a result of the randomness introduced through the distribution in size and irregular interspherulitic boundaries. Also, it should be noted that there is a reduction in scattering at low angles when compared with the isolated spherulite pattern. This reduction is a consequence of the smaller difference between the spherulite and its surroundings (other spherulites). As a result of the loss of scattering, a radial maximum occurs which is analogous to the radial maximum in intensity found in the experimental H_V pattern.²

The V_V diffraction pattern of Fig. 6a for the spherulitic array exhibits the twofold symmetry actually found with an intensification of scattering along the polarization direction.

Presumably, the diffraction patterns differ in detail from the observed scattering patterns because

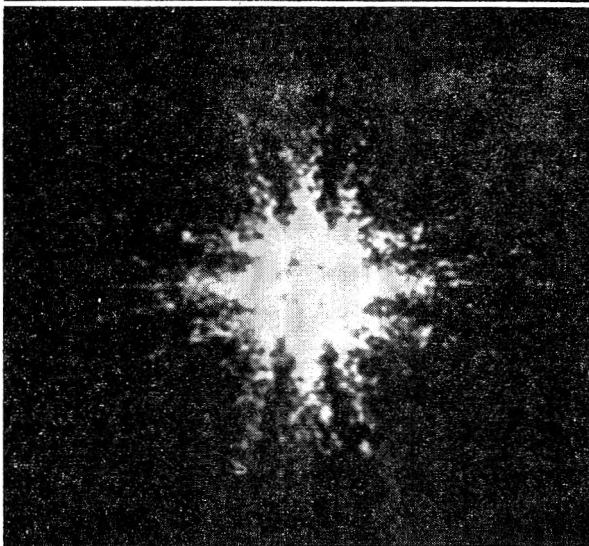
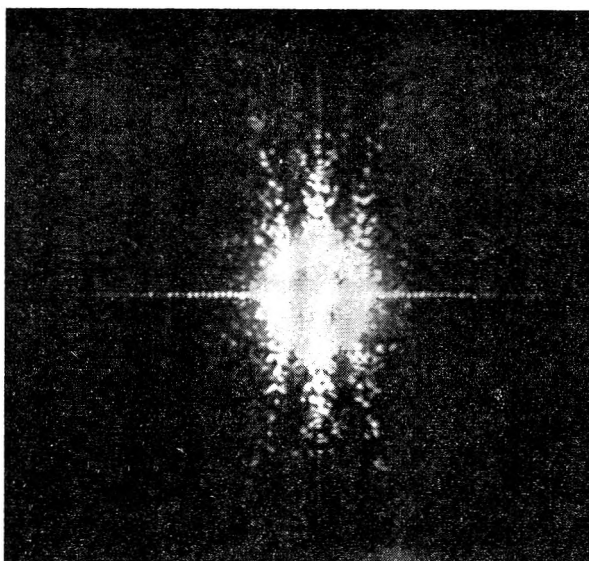


Fig. 6.—The optical diffraction patterns for a close-packed array of idealized tangentially polarizable spherulites with (a) V_V polarization, and (b) H_V polarization. The polarizer and analyzer are crossed and at 45° to the vertical direction.

of (a) the two-zone assumption, and (b) the three-dimensional nature of the actual scattering spherulites. The general features of the diffraction patterns, however, are in agreement with the observed scattering patterns and lend credence to the interpretation which has been advanced.

Contributions from the Internal Structure.—It has been pointed out that scattering at higher angles (greater than $15-20^\circ$) corresponds to fluctuations occurring over distances of a few thousand Angstrom units.⁸ These distances are considerably smaller than the dimensions of the spherulites or even of the period of radial orientation variation. It has been postulated that the scattering results from orientation fluctuations arising from a correlation in orientation of neighboring crystals.

The relationship among the various types of scattering contributions is summarized in Figure

(8) R. S. Stein, J. J. Keane, F. H. Norris, F. A. Bettelheim and P. R. Wilson, *Ann. N. Y. Acad. Sci.*, **83**, Art. 1, 37 (1959).

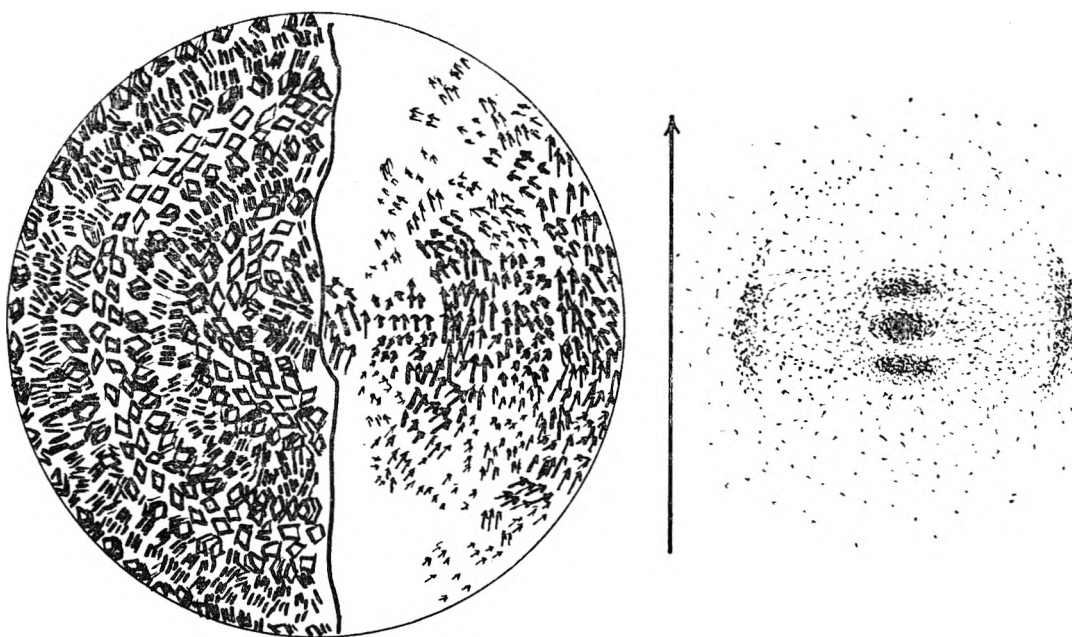


Fig. 7.—A proposed model indicating the crystallite orientation, the induced dipole distribution and the resulting scattering pattern giving rise to scattering in the low, intermediate and high angle region.

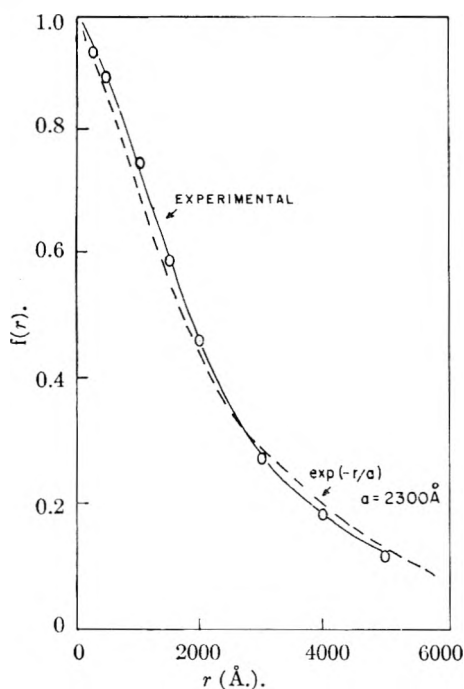


Fig. 8.—A typical variation of the correlation function $f(r)$ with r for a low density polyethylene sample compared with the empirical equation $f(r) = \exp(-r/a)$.

7. The low angle scattering (less than 5°) corresponds to distances comparable with the size of the spherulite itself. Such scattering is related to the orientational differences between spherulites and arises from the difference in radial and tangential polarizabilities. The scattering maximum, usually occurring between 10 – 20° , arises from the periodicity in orientation while the continuous tail extending out to higher angles results from this internal structure.

The higher angle scattering has been analyzed

using a generalization of the Debye–Bueche⁹ theory from which may be obtained a correlation function, $f(r)$, by a Fourier inversion. This function is believed to describe correlation in crystal orientation and is defined by

$$f(r) = \langle 3\cos^2 \theta_{ij} - 1 \rangle_r / 2 \quad (5)$$

where θ_{ij} is the angle between the optic axes of the i th and j th crystals. The average is taken over all pairs of crystals separated by the distance r . A typical such function determined for a polyethylene sample is shown in Fig. 8. It has been found that the empirical function

$$f(r) = \exp(-r/a) \quad (6)$$

proposed by Debye and Bueche for amorphous polymer scattering fits the measured $f(r)$ very well. The function indicates that two crystals very close together tend to be oriented parallel to each other, while two widely separated crystals are randomly oriented with respect to each other. a is thus an effective average radius of a volume within the medium over which orientations are correlated and is referred to as a “correlation distance.”

It has been pointed out⁸ that this correlation in orientation of neighboring crystals is probably related to the mechanism of crystal growth. The crystals are believed to grow by an autonucleation type scheme in which the presence of a crystal within a crystallizing matrix increases the probability of crystallization in its immediate vicinity. The orientation of the new crystal is controlled by that of the first and gives rise to domains of correlated orientation with the correlation decreasing with increasing separation of the crystals.

A one-dimensional theory of such correlated crystal growth employing random-walk statistics has been described¹⁰ and has been shown to give rise to the observed type of correlation function. An

(9) P. Debye and A. M. Bueche, *J. Appl. Phys.*, **20**, 518 (1949).

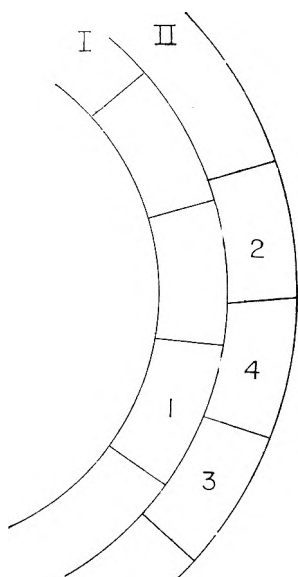


Fig. 9.—A section of the two-dimensional circular lattice considered in the assignment of probabilities.

analytical solution in two or three dimensions is difficult, but a graphical two-dimensional treatment is described here which has been tested by the optical diffraction technique.

Two-dimensional Correlated Crystal Growth.—

A two-dimensional lattice model was adopted. The dimensions of the lattice cells were adjusted so that all cells had approximately the same area. For simplicity, it was assumed that only two possible states of orientation existed and were indicated by filling in the lattice cell or not. The central cell was arbitrarily filled in; the surrounding cells were then filled in, one concentric circle at a time, proceeding outward from the center according to a set of probability rules designed to fulfill the following objectives: (1) Orientational states cluster in domains. A given state of orientation is more probable if the nearest neighbor cells are in that state. The more nearest neighbors in a given state, the greater the probability of the cell being in the same state. (2) Radial correlation in orientation is stronger than tangential orientation correlation. This postulate is adopted to take into account the observation of radial fiber structure in spherulites. (3) Correlation between cells of one orientational state (the filled-in cells), is stronger than that for the other.

A set of probabilities for the orientation in lattice cell 4 of Fig. 9 is listed in Table I. It is assumed that the two orientational states are designated by the letters A and B. Row I has been completely filled and row II is being filled. The symbol O indicates that the cell is empty. The probability of a given state in cell 4 is assumed to depend only on the state of cells 1, 2 and 3. Three situations are possible: either 2 or 3 is empty when row II is incomplete, both 2 and 3 are filled if 4 is the last cell in a row, or both 2 and 3 are empty when a new row is starting. Cells 2 and 3 are symmetrical in their effect on 4 so that an interchange in orientations between them does not result in a

(10) R. S. Stein and D. G. LeGrand, Technical Report No. 25, Office of Naval Research Project, University of Massachusetts, 1960.

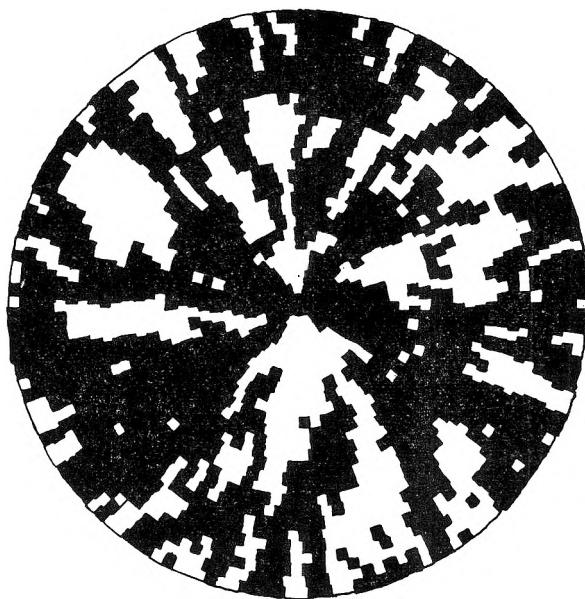


Fig. 10.—A typical orientation distribution for the two-orientation two-dimensional lattice which is generated by the probability rules of Table I.

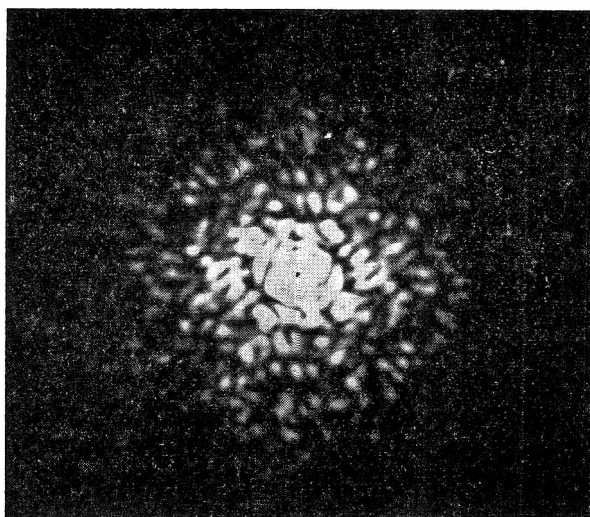


Fig. 11.—The optical diffraction pattern obtained from the orientation distribution of Fig. 10.

TABLE I

PROBABILITY RULES FOR ASSIGNING ORIENTATIONS TO LATTICE CELLS

1	Orientation in cell no. 2	3	Probability of orientation of A in cell 4
A	B	O	0.82
B	A	O	.22
B	O	O	.13
A	A	O	.89
A	O	O	.84
B	O	O	.20
A	B	B	.68
B	A	A	.40
A	A	B	.95
A	A	A	.97
B	B	B	.03
B	A	B	.07

different probability and is not considered separately. The probabilities were arbitrarily adopted in order to produce a subjectively reasonable dis-

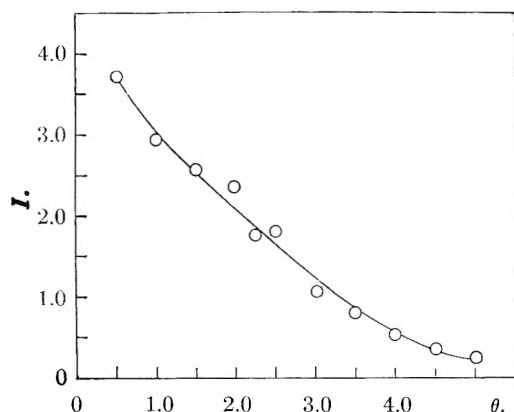


Fig. 12.—The variation in relative diffracted intensity with diffraction angle (in arbitrary units).

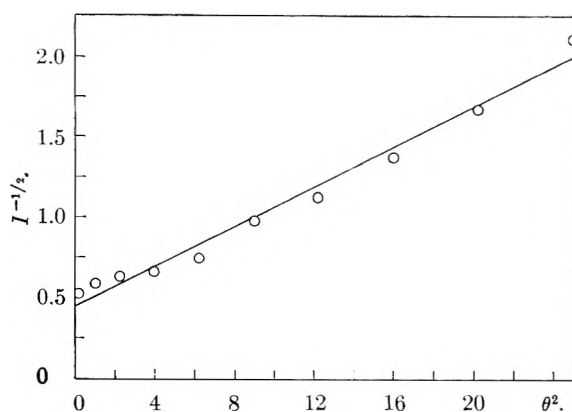


Fig. 13.—A plot of $1/I^{1/2}$ against θ^2 for the optical diffraction data.

tribution of orientations which fulfilled the preceding objectives.

Orientations were assigned serially to the cells in accordance with the probability rules with the aid of a table of random numbers. A typical orientation distribution which is generated in this way is shown in Fig. 10. The resulting fiber-like domain structure of the filled-in cells is apparent.

A diffraction mask was prepared from Fig. 10 and the optical diffraction pattern of Fig. 11 was obtained. The diffracted intensity decreases uniformly from the center in agreement with observed scattering patterns. The graininess of the pattern results from the large ratio of cell size to spherulite size and would presumably be reduced if a larger number of smaller cells was used. Radial microdensitometer traces were then made along several radii, and the average diffracted intensity at a constant radial distance from the center of the diffraction pattern was calculated. This is plotted as a function of the diffraction angle θ (measured in arbitrary units) in Fig. 12.

The above result is compared with theory in the following way: if the exponential correlation function (eq. 6) is inserted into the Debye-Bueche scattering equation

$$I = K \int_{r=0}^{\infty} f(r) \frac{\sin(hr)}{hr} r^2 dr \quad (7)$$

where $h = (4\pi/\lambda) \sin(\theta/2)$, one obtains

$$I = K' \frac{a^3}{[1 + h^2 a^2]^2} \quad (8)$$

where K and K' are constants that are independent of the scattering angle and the correlation distance a .

This may be rearranged to give

$$\frac{1}{I^{1/2}} = \frac{1}{(a^3 K')^{1/2}} (1 + h^2 a^2) \quad (9)$$

where A and B depend upon a but are independent of θ . Consequently, a plot of $(1/I^{1/2})$ against θ^2 should be a straight line.

A plot of this type made from the optical diffraction data is given in Fig. 13. The data appear to be fitted fairly well by a straight line. This indicates that the distribution of orientations giving rise to the diffraction pattern is also generated by the exponential correlation function which leads to eq. 9.

While the assumed orientation distribution is not a unique one which gives rise to an angular variation of diffracted intensity of the observed type, it appears to be a reasonable one. Thus, it is felt that the assumed type of correlated crystal orientation is consistent with the experimental observations.

A more critical test is the prediction of wide-angle scattering with polarized light. This is more sensitive to the assumed probability assignments. Analyses of these types are in progress.

DISCUSSION

B. WUNDERLICH (Cornell University).—Have you measured the refractive index difference to be 0.005? This is approximately the difference in refractive index of light vibrating parallel to the a and b axes, but not c which would have a difference 10 times as much. Were your films so thin that they allowed only two dimensional spherulites (dendrites) to grow? These are known to have the a and b axes in the plane of the film.

R. S. STEIN.—The refractive index difference of 0.005 is based on measurements of absolute intensity of scattering. We realize that this is 10 times as great as the difference between the refractive index along the c -axis of the polyethylene crystal and the average refractive index along the a and b axes. This is rationalized on the basis that the scattering entities are not the crystals but regions 5 to 10 times larger containing imperfectly oriented crystals as well as amorphous material.

In answer to the last question, the thicknesses of the films (with the exception of our studies on the very large spherulites of polyethylene oxide) were many times the spherulite diameter so that there was not preferential orientation of the c axis perpendicular to the film. This was confirmed by determinations of biaxial orientation by birefringence measurements on tilted films and by X-ray diffraction studies.

R. A. ORIANI (U. S. Steel Corporation).—How do you know *a priori* that the crystals are smaller than the correlation distance?

R. S. STEIN.—The estimates of crystal size are not from our work, but are from measurements on low angle scattering of X-rays and from the width of X-ray diffraction peaks at wider angles.

B. G. RANBY (New York State University).—It seems reasonable that a linear polyethylene, only about 10% amorphous, scatters light mainly due to fluctuations in orientation of crystallites, but is it not surprising that the same should be true for a branched polyethylene (40-50 mole % amorphous polymer) where you would expect considerable scattering due to density fluctuations?

R. S. STEIN.—If anything, there is less density fluctuation in the case of low density polyethylene than with high, and its contribution is probably responsible for less than 10% of total scattering. Even though there is more amorphous material in the low density polyethylene, the scale of mixing of this with crystalline material is finer so that its contribution to scattering is lower. From the amount of density fluctuation that we would observe, we could put an upper limit of 3000 Å. on the size of the amorphous region in low density polyethylene. This is reasonable in terms of X-ray measurements of crystal size.

COUNTERCURRENT DISTRIBUTION OF CHEMICALLY REACTING SYSTEMS. II. REACTIONS OF THE TYPE $A + B \rightleftharpoons C$

BY J. L. BETHUNE¹ AND GERSON KEGELES

Contribution from the Department of Chemistry of Clark University, Worcester, Mass.

Received March 9, 1961

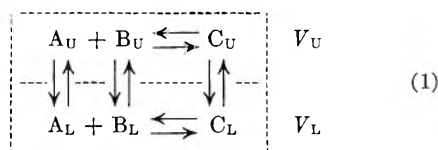
In paper I of this series,² results of computations were reported for systems undergoing reversible polymerization. In this paper a simple reaction $A + B \rightleftharpoons C$ is considered. The material balance equations are again solved by a computer for selected values of the relevant parameters. The results show that, no matter what value is assigned to the partition coefficient of the complex C, the tube containing the maximum concentration of complex must lie between the tubes containing the maximum concentrations of the reactants A and B. That is, the peak due to the complex can neither run before nor lag behind those of the reactants. The results also show that, if the partition coefficients for the three substances fall in the order $K_B < K_C < K_A$, it is possible, during the course of the distribution of such a system, to obtain a countercurrent distribution pattern exhibiting initially a single maximum, then during intermediate periods three maxima and, finally, two maxima as the system is distributed for successively larger numbers of transfers. The results finally show that, if $K_B < K_A < K_C$, one or both of the reactants may exhibit more than one concentration maximum. The application of these results to other zone separation processes is considered.

Introduction

The relevant literature has been reviewed in part I of this series.² Particular attention should be drawn to two papers by Gilbert and Jenkins^{3,4} in which the effect of a chemical reaction $A + B \rightleftharpoons C$ in moving boundary methods is considered. Since the study of countercurrent distribution of hypothetical polymerizing systems showed the possibility of obtaining disconcerting patterns even when only a single thermodynamic solute component is present in the apparatus, it was felt advisable to investigate another system in which a reaction of the type $A + B \rightleftharpoons C$ may occur.

In considering the relationships involved in the equilibration of the chemically reacting system between two phases, the following assumptions have been made: (1) the solvents are immiscible; (2) no volume changes occur as a result of either extraction or chemical re-equilibration of the solutes; (3) all solutes are considered thermodynamically ideal when described in terms of the proper reacting species; and (4) before a transfer, there is chemical as well as transport equilibrium.

The following equilibria must then hold



where A_U , B_U and C_U refer to A, B and C in upper phase of volume V_U , and A_L , B_L and C_L refer to A, B and C in lower phase of volume V_L .

Equations 2 and 3 below serve to describe the corresponding homogeneous equilibria and equation 4 describes the phase distribution equilibria in terms of the equilibrium constants on the mass per unit volume scale

$$K_U' = \frac{[C]_U^0 - \delta[C]_U}{\{[A]_U^0 - \delta[A]_U\} \{[B]_U^0 - \delta[B]_U\}} \quad (2)$$

(1) Submitted by J. L. Bethune to the Faculty of Clark University in partial fulfillment of the requirements for the Doctor of Philosophy degree, June, 1961.

(2) J. L. Bethune and G. Kegeles, *J. Phys. Chem.*, **65**, 433 (1961).

(3) G. A. Gilbert and R. C. L. Jenkins, *Nature*, **177**, 853 (1956).

(4) G. A. Gilbert and R. C. L. Jenkins, *Proc. Roy. Soc. (London)*, **A263**, 426 (1960).

$$K_L' = \frac{[C]_L^0 - \delta[C]_L}{\{[A]_L^0 - \delta[A]_L\} \{[B]_L^0 - \delta[B]_L\}} \quad (3)$$

$$K_X = \frac{[X]_U^0 - \delta[X]_U}{[X]_L^0 - \delta[X]_L}, \quad X = A, B \text{ or } C \quad (4)$$

In these equations the brackets denote concentrations on the mass per unit volume scale; the superscript 0 refers to the concentration, before equilibration, of the indicated component and δ denotes the amount by which the concentration must change, in the indicated phase, due to both transport and chemical reaction, to come to the equilibrium value of the concentration of that component.

One of these constants is redundant, for $K_L' = K_U' K_A K_B / K_C$. In this paper K_L' is chosen as the redundant parameter.

Equations 2 and 4 may be re-written in the form (5) and (6) below, if $V_U = V_L = V_S$, where V_S is the standard volume.

$$K_U = \frac{C_U^0 - \delta C_U}{(A_U^0 - \delta A_U)(B_U^0 - \delta B_U)} \quad (5)$$

$$K_X = \frac{X_U^0 - \delta X_U}{X_L^0 - \delta X_L}, \quad X = A, B \text{ or } C \quad (6)$$

Here $K_U = K_U' / V_S$, and the absence of brackets signifies that only masses are considered.

Equations 6 may be re-written in the form (7)

$$\frac{K_X(X_L^0 - \delta X_L) - (X_U^0 - \delta X_U)}{1 + K_X} = 0, \quad X = A, B \text{ or } C \quad (7)$$

If, then, the left-hand side of (7), with $X = C$, is added to the numerator of equation 5, and with $X = A$ and then $X = B$, is added to the appropriate term of the denominator of equation 5, equation 5 may be re-written as

$$K_T = \frac{C^0 - \delta C}{(A^0 - \delta A)(B^0 - \delta B)} \quad (8)$$

in which

$$K_T = \frac{K_U(1 + K_C)K_A K_B}{(1 + K_A)(1 + K_B)K_C}$$

$$X^0 = X_U^0 + X_L^0$$

$$\delta X = \delta X_U + \delta X_L, \quad X = A, B, C$$

Since, in any equilibration stage, the sole means by which a mole of C can appear is for a mole of A and

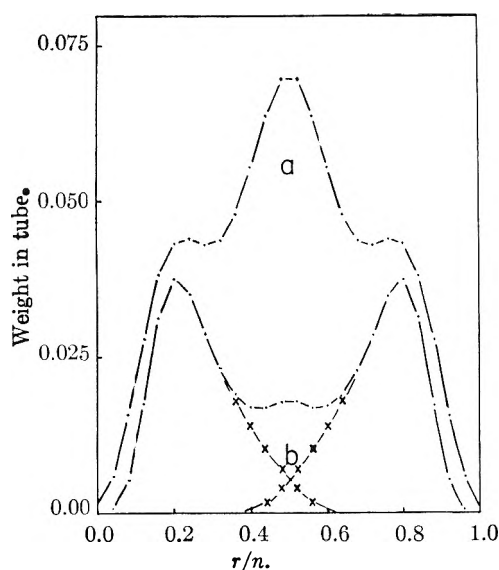


Fig. 1.—Effects of dissociation of an intermediate complex: (a) $n = 25$, (b) $n = 50$; ·—·, total; ×—× uncombined A or B.

a mole of B to disappear, the further condition, given by equation 9, may be imposed.

$$\frac{\delta C}{M_C} = -\frac{\delta A}{M_A} = -\frac{\delta B}{M_B} \quad (9)$$

in which M_A , M_B and M_C are the gram molecular weights of A, B and C, respectively. Since conservation of mass during the chemical reaction $A + B \rightarrow C$ requires that

$$M_C = M_A + M_B \quad (10)$$

when equation 10 is imposed, equations 9 may be re-written as

$$\delta C = -(R + 1)\delta A \quad (11)$$

$$\delta B = R\delta A \quad (12)$$

in which $R = M_B/M_A$.

Equations 11 and 12, when substituted in equation 8, result in

$$K_T = \frac{C^0 + (R + 1)\delta A}{(A^0 - \delta A)(B^0 - R\delta A)} \quad (13)$$

Given the initial values A^0 , B^0 and C^0 , with K_T and R assigned, this is a quadratic equation with δA as the unknown. Once δA is obtained, then δC and δB are obtained from equations 11 and 12 and the equilibrium values of the masses of A, B and C are obtained from equations 14

$$X^* = X^0 - \delta X, X = A, B, C \quad (14)$$

in which superscript e denotes the equilibrium mass of the indicated species. Then from relations (15) below, the equilibrium masses of A, B and C in the upper and lower phases are obtained.

$$X_U^* = \frac{K_X X^*}{1 + K_X}, X_L^* = \frac{X^*}{1 + K_X}, X = A, B, C \quad (15)$$

If $X_{n,r}^*$ ($X = A, B, C$) represents the initial masses of A, B and C in the r th tube after n transfers, then a distribution starts with arbitrary values of $X_{0,0}^*$ ($X = A, B, C$). Equations 11 to 15 are then solved and equilibrium values of A, B and C for both phases are obtained. This constitutes the equilibration before the first transfer. $A_{U,0,0}^*$, $B_{U,0,0}^*$ and $C_{U,0,0}^*$ are then moved to tube number

one and $A_{L,0,0}^*$, $B_{L,0,0}^*$ and $C_{L,0,0}^*$ remain in tube number zero. This constitutes the first transfer, immediately after which

$$X_{1,0}^* = X_{L,0,0}^*, X = A, B, C$$

and

$$X_{1,1}^* = X_{U,0,0}^*, X = A, B, C$$

Equations 11 to 15, containing the new initial values of A, B and C, are solved for the new equilibrium values of $X_{U,1,0}^*$, $X_{L,1,0}^*$, $X_{U,1,1}^*$ and $X_{L,1,1}^*$ ($X = A, B, C$). This constitutes the equilibration before the second transfer. The transfer is then carried out, and after it is completed

$$\left. \begin{aligned} X_{2,0}^* &= X_{L,1,0}^* \\ X_{2,1}^* &= X_{U,1,0}^* + X_{L,1,1}^* \\ X_{2,2}^* &= X_{U,1,1}^* \end{aligned} \right\} X = A, B, C$$

This constitutes the second transfer. By repetition of this process the entire countercurrent distribution patterns are obtained for every transfer up to $n = n$, where n is the assigned number of transfers.

Since the process involves the solution of large numbers of equations for even a few transfers, to investigate a range of values for K_U , K_A , K_B , K_C , R , $A_{0,0}^*$, $B_{0,0}^*$ and $C_{0,0}^*$, the parameters whose values may be arbitrarily assigned, it was necessary to use a high speed digital computer. The flow chart for the program, written in Fortran for the IBM 704, and re-written for the IBM 709, is very similar to that shown in Fig. 1 of part I.

The results of the calculations were checked in three ways:

(1) The total mass of solute in the apparatus after every transfer should equal the total mass placed initially in the machine.

(2) When K_A , K_B and K_C are chosen so that $K_C = K_A K_B = 1.0$, $R = 1.0$, $A_{0,0}^* = B_{0,0}^* = 0.0$ and $C_{0,0}^* = 1.0$, C should occupy the center of the apparatus and affect A and B equally, so that the diagram should be symmetrical about an axis passing through the tube number in which the concentration of C is a maximum.

(3) If $K_A = K_B = K_C = 1.0$, for any values of R , K_U and initial concentrations, the pattern resulting should be indistinguishable from the calculated binomial curve for a single substance with $K = 1.0$.

In any case reported here the total amount of material in all the tubes never differed from that initially placed in the apparatus by more than 7 parts in 10^6 . The second check was satisfied to 1 part in 10^6 and the third was satisfied to 1 part in 10^5 , where the binomial distribution was only calculated to 5 decimal places, but the distributions of the reacting systems were calculated to 6 decimal places.

Results

In all plots of distribution patterns the ordinate is the total mass per tube and the abscissas are tube numbers in terms of the reduced coordinate, r/n , where r is the tube number and n is the number of transfers. Plots in terms of this coordinate are useful in detection of abnormalities in distribution behavior. One effect of this type of plot should be noted. The area under the curve, as

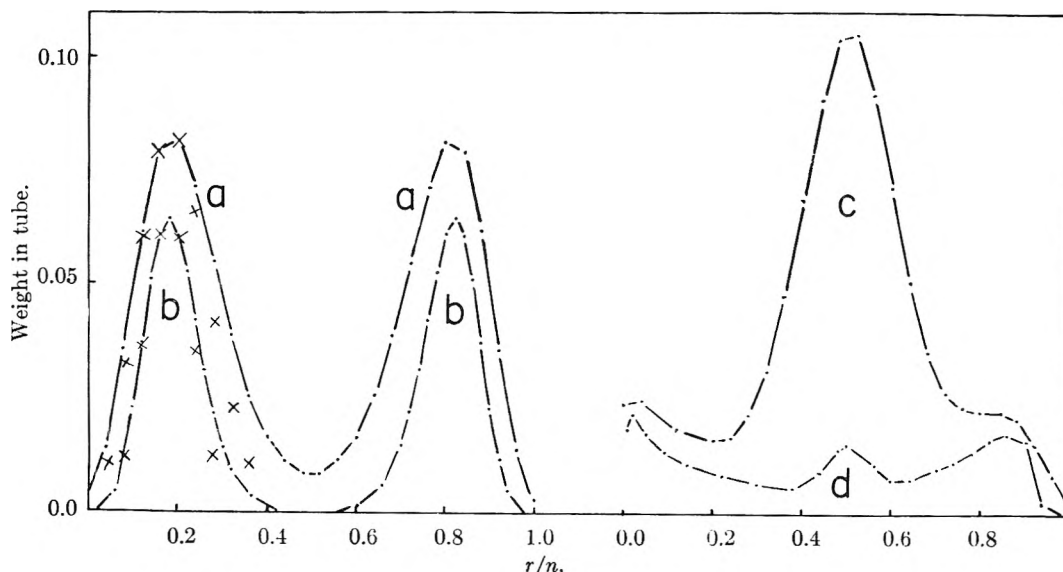


Fig. 2.—Gradual dissociation of intermediate complexes of different stabilities: (a) $n = 25$, (b) $n = 50$, in (a) and (b), $K_A K_B = K_C = 1.0$; (c) $n = 25$, (d) $n = 100$; —·—, total; ×, ×, binomial curve.

plotted, decreases as the total number of transfers increases. If the area under the curve is 1 when $n = 25$, it is 0.5 when $n = 50$. Since the abscissal units are reduced coordinates, however, involving $1/n$, both areas represent the same total mass in the apparatus.

The results divide naturally into three sets. The first set is characterized by the complex, C, moving with a partition coefficient whose value is between those of the reactants, A and B. The second set comprises cases in which the complex moves either with a partition coefficient greater or less than that of both reactants, or with a partition coefficient equal to that of either reactant. In the third set both reactants have the same partition coefficient, which differs from that of the complex. Systems in the third set, however, will exhibit the same behavior as do the dimerizing systems of part I, no matter what value is assigned to R or K_U . This is a necessary physical consequence of any separation procedure in which the degree of separation achieved depends only upon one physical constant.

Set 1. $K_B < K_C < K_A$.—In these cases,⁵ once B is left behind, without A or C, and A moves out ahead, without B or C, A and B distribute as independent solutes.

In all reported cases of this set, except one distinguished below, $K_A = 5.0$, $K_B = 0.2$, $K_C = 1.0$, $A_{0,0}^0 = B_{0,0}^0 = 0.0$ and $C_{0,0}^0 = 1.0$.

The system shown in Fig. 1, a and b, has $K_U = 1.0 \times 10^3$ and $R = 1.0$. Pattern a is for $n = 25$, pattern b for $n = 50$. The possibility of misinterpretation is obvious, for if the apparatus is stopped and the analysis carried out on a mass per tube basis after 25 transfers the interpretation of the relative amounts of the species present in the original sample would be quite different from the interpretation if the analysis were carried out after 50 transfers.

It is probable that if a large number of transfers

(5) Since A and B are only labels, this includes $K_B > K_C > K_A$.

were carried out, all of C would be removed by dissociation resulting from dilution, and A and B would be completely separated⁶ and fit binomial curves. This conjecture is lent force by the situation illustrated in Fig. 2. In this system $K_U = 1.0 \times 10^2$ and $R = 1.0$. Pattern a is for $n = 25$, b for $n = 50$. Here, after 25 transfers C has almost disappeared, and after 50 transfers C is not detectable on the graph. The crosses show the best fitting binomial curves. Since the curves are mirror images it is only necessary to calculate binomial curves for one side. The fit is better for the higher number of transfers.

In Fig. 2, c and d, the system has $K_A = 8.0$, $K_B = 0.0125$, $K_C = 1.0$, $K_U = 1.0 \times 10^5$, $R = 1.0$, $A_{0,0}^0 = B_{0,0}^0 = 0.0$ and $C_{0,0}^0 = 1.0$. Pattern c is for $n = 25$, d for $n = 100$. This is introduced to show that symmetry is artificially imposed upon the other patterns of this set by the choice $K_C = K_A K_B = 1.0$, and that the range of possible patterns is far wider than the cases reported here might imply.

The system shown in Fig. 3 may be taken as a standard for subsequent discussion in which the effect of variation in the parameter R is developed. In this system, $K_U = 1.0 \times 10^4$. Pattern a is for $n = 25$, b for $n = 50$ and c for $n = 100$ transfers. The same dilution effect is present as in the other cases, but here K_U is sufficiently high to render the complex C more stable. Here, $R = 1.0$, that is, A and B have the same molecular weight, so that when C dissociates, equal weights of A and B are produced. A range of R from 1.0 to 0.001 has been investigated.⁷ As R decreases the peak due to B decreases, at any given n , and the peak due to A increases. If $R \sim 0.001$, the portion of the weight curve due to B is indistinguishable from zero on the ordinate scale of Fig. 3. As C disappears by dissociation, if $R =$

(6) E. H. Ahrens and L. C. Craig, *J. Biol. Chem.*, **195**, 763 (1952).

(7) This is the same as a range of R from 1.0 to 1000.0, since $K_A K_B = 1.0$, that is, the distributions for A and B are mirror images of one another.

0.001, 99.9% of the mass appears as A. As a result, the pattern shows a peak, as in Fig. 3c at $r/n = 0.5$, with the same value for the weight in the tube, but the peak at $r/n = 0.16$ has vanished and the peak at $r/n = 0.83$ now has a maximum ordinate value of 0.0270. Consequently, the pattern has the appearance given by a system containing two independent solute components. By suitable selection of the value of R , it is therefore possible to get a wide variety of patterns, ranging from a single peak, if C is stable (*i.e.*, K_U very high), unstable (K_U very low, $R \ll 1.0$ and $K_C \sim K_A$), to two peaks (K_U intermediate and $R \ll 1.0$), to three peaks, as illustrated in the figures.

Of course, as has already been pointed out,⁶ in all of the cases, if a sufficient number of transfers is applied, all of C vanishes and, if $K_A \neq K_B$, A and B may be separated, probably to fit curves calculated for a binomial distribution. However, if the system should be observed *only* at this stage, a misleading impression would be obtained of the chemical constitution of the initial sample. Hence if there is reason to suspect the existence of chemical reaction to form or dissociate a complex, it is of advantage to analyze the counter-current distribution train at small, as well as large numbers of transfers.

Set 2. $K_B < K_A \leq K_C$.—Each diagram in this set shows total mass in the tubes, as well as the individual masses of the various species.

The first system, shown in Fig. 4a has $K_A = 2.5$, $K_B = 0.4$, $K_C = 10.0$, $K_U = 1.0 \times 10^3$, $R = 1.0$, $A_{0,0} = B_{0,0} = 0.0$, $C_{0,0} = 1.0$ and $n = 25$. This diagram immediately illustrates two points. First, even though C has been given a partition coefficient of 10.0, it does not pass beyond A, which has been given a partition coefficient of 2.5. Second, in contrast to the systems shown in set 1, B exhibits two maxima, one at $r/n \sim 0.34$, the other at $r/n \sim 0.86$. This may be contrasted with Fig. 1b in which neither A nor B shows more than one maximum. If a system of set 1, with $K_B < K_C < K_A$, is selected, and a series of similar systems with K_C approaching K_A are observed, it is seen that species B gradually smears across the whole zone until, as K_C becomes very near K_A , B, considered alone, forms a very broad, asymmetric peak. When $K_C = K_A$, an extra inflection point appears in the B part of the mixed peak. This inflection point may be the only evidence of the tendency to exhibit two maxima even if $K_C > K_A$, if the amount of complex present in the apparatus is small.

The maximum, in Fig. 4a, due to the reactant with the lowest partition coefficient, is not greatly affected by the presence of an excess of this reactant, as is shown in Fig. 4b. Here the system is the same as that of Fig. 4a but with initial conditions $A_{0,0} = 0.0$, $B_{0,0} = C_{0,0} = 1.0$. Here the great increase in the concentration of B has brought the total concentration of free A down from 0.2323 to 0.2251, and free C up from 0.5355 to 0.5498, while free B has increased from 0.2323 to 1.2251. If, however, the system is one in which $K_A = 1.2$, $K_B = 0.3$, $K_C = 5.0$, $K_U = 1.0 \times 10^3$, $R = 1.0$ and $n = 25$, then if the initial conditions are

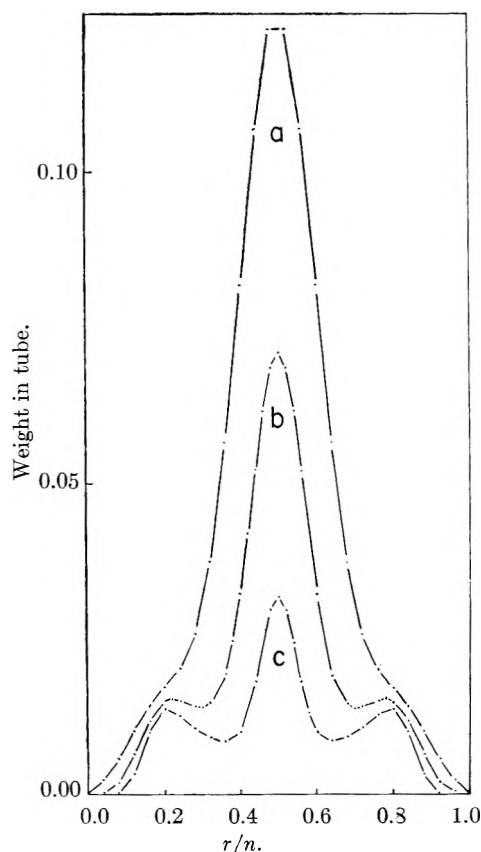


Fig. 3.—Gradual generation of skewed side peaks from dissociation of a persistent intermediate complex: (a) $n = 25$, (b) $n = 50$, (c) $n = 100$; weight in tube only plotted.

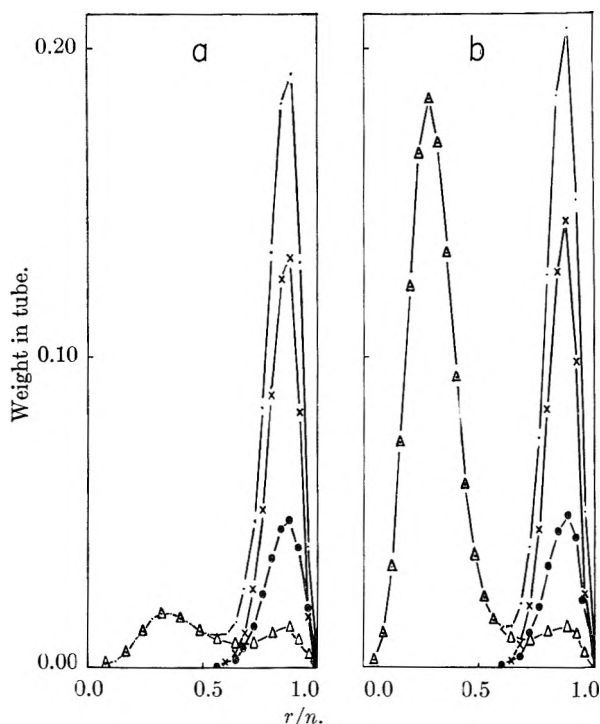


Fig. 4.—The effect of adding the slower moving reactant B when the complex is no longer intermediate but tends to move faster than either reactant. The total weight in the tube as well as the weights of the individual species are plotted: ·—·, total; ●—●, uncombined A; Δ—Δ, uncombined B; ×—×, C, $n = 25$.

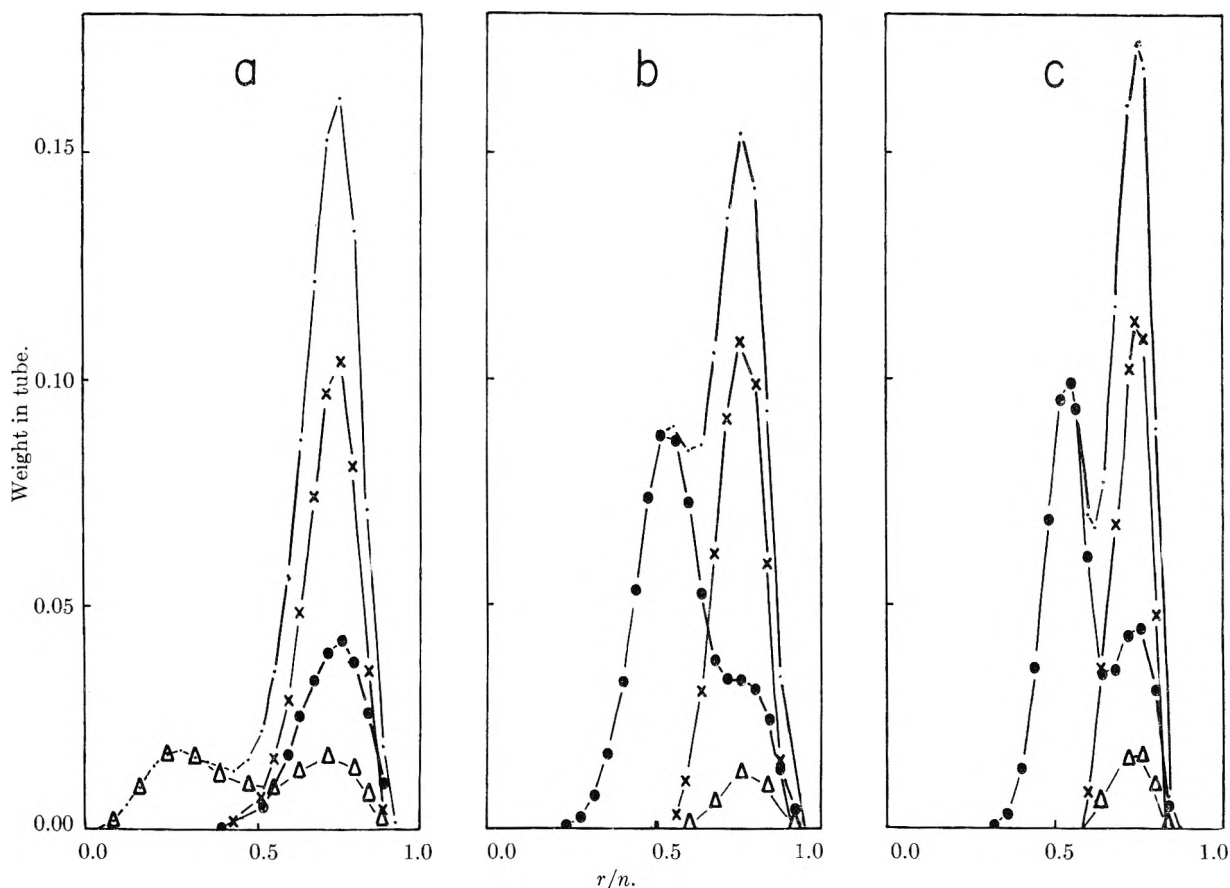


Fig. 5.—The effect of varying the amount of the faster moving reactant A when the complex tends to move faster than either reactant. The total weight per tube and the weights of the individual species are plotted: ---, total; ●—●, uncombined A; Δ—Δ, uncombined B; ×—×, C, (a) $n = 25$, (b) $n = 25$, (c) $n = 50$.

$A_{0,0}^0 = B_{0,0}^0 = 0.0$, $C_{0,0}^0 = 1.0$, the situation illustrated in Fig. 5a results. Here the double peak due to B is more clearly emphasized than in Fig. 4. If the initial conditions for this system are changed to $B_{0,0}^0 = 0.0$ and $A_{0,0}^0 = C_{0,0}^0 = 1.0$, the result is shown in Fig. 5b. Now all B, free or combined, has, on the scale of this graph, vanished from its expected place at $r/n \sim 0.23$, and appears at $r/n \sim 0.76$. There is actually a second peak due to B at $r/n \sim 0.23$, but on the scale selected for this graph it is indistinguishable from zero. The concentration of free B has decreased from 0.2506, in Fig. 5a, to 0.1010 here, C has increased from 0.4987 to 0.7980 while A has increased from 0.2506 to 1.1010. Therefore a change in the concentration of the reactant which travels with the complex affects a major change in the situation existing in the apparatus.

Figure 5c shows the system of Fig. 5b after 50 transfers. Both A and B now exhibit double peaks, although the peak for B at $r/n \sim 0.23$ is not apparent on this graph.

Figure 6, a and b, shows the effect of varying K_U . In a the system is $K_A = 0.6$, $K_B = 0.4$, $K_C = 20.0$, $R = 1.0$, $K_U = 1.0 \times 10^3$, with initial conditions $A_{0,0}^0 = B_{0,0}^0 = 0.0$, $C_{0,0}^0 = 1.0$. In b the system is altered only in that K_U now equals 1.0×10^2 . Both of these systems, when carried to $n = 50$, show a double peak for B, but the concentration of free C is dropping more rapidly in b

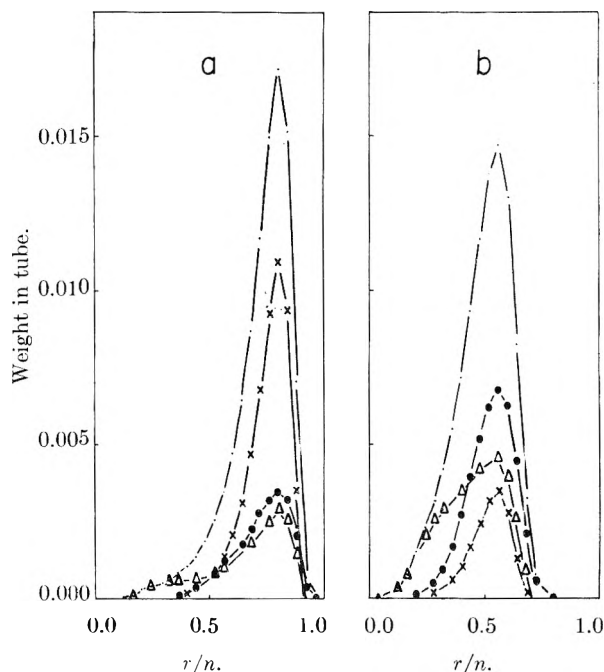


Fig. 6.—The effect of decreasing the association constant K_U : $n = 25$ for (a) and (b); (a) $K_U = 10^3$; (b) $K_U = 10^2$. The total weight per tube and the weight of the individual species are plotted: ---, total; ●—●, uncombined A; Δ—Δ, uncombined B; ×—×, C.

than in a; in b from 0.17 at $n = 25$ to 0.12 at $n = 50$, in a from 0.53 at $n = 25$ to 0.44 at $n = 50$.

One system, similar to that of Fig. 5b, has been calculated up to $n = 150$, to see if the minimum would approach the base line and yet have A in both separated peaks. This did not occur. The peak at higher values of r/n became very asymmetric but there would, on the scale of Fig. 5b, be a detectable amount of material in the tubes in which the concentration minimum occurs.

Discussion

These results are exact, under the given model and assumptions, for countercurrent distribution. They may also be applied, at least qualitatively, to any other separation technique in which a zone undergoes transport while diffusion occurs. One such technique is partition chromatography, at least while the zones remain on the column, and another is zone electrophoresis. In both of these it is possible, under certain conditions, for a substance to exhibit two concentration maxima.

This effect may be compared to the Johnston-Ogston⁸ effect in moving boundary systems, in which a substance exhibits a change in its velocity due to passage through a concentration gradient of

(8) J. P. Johnston and A. G. Ogston, *Trans. Faraday Soc.*, **42**, 789 (1946).

another substance. In Fig. 5b the velocity with which B moves is greatly affected by the presence of A, with which it reacts to give the rapidly moving C.

Figures 4 and 5 show that it is possible to obtain information about the system by changing the relative amounts of the reactants. If, on increasing the amount of one reactant, only the slower moving peak is greatly increased in size, the complex moves at least at the same rate as the faster moving reactant. If, on increasing the amount of the other reactant, the slow peak disappears and a faster moving peak appears, then the complex (considered as an entity) is characterized by a higher velocity than either reactant. If, however, the slow peak disappears and no new peak appears, the complex moves at, or very nearly at, the same velocity as the faster reactant. If, on the other hand, there is no reaction occurring, addition of either substance only increases the area of one peak and the other is undisturbed.

Acknowledgments.—This work was supported by U. S. Public Health Service Research Grant number A3508. All computations were carried out at the Massachusetts Institute of Technology Computation Center as problem number N806 under the Coöperating Colleges of New England scheme.

COUNTERCURRENT DISTRIBUTION OF CHEMICALLY REACTING SYSTEMS. III. ANALOGS OF MOVING BOUNDARY ELECTROPHORESIS AND SEDIMENTATION

BY J. L. BETHUNE AND GERSON KEGELES

Contribution from the Department of Chemistry of Clark University, Worcester, Mass.

Received March 9, 1961

Countercurrent distribution as usually carried out experimentally is a discontinuous zone separation process. If, however, the same amount of solute is first placed in every tube, each of which contains both phases, and the distribution is carried out as usual, introducing fresh upper phase into tube zero at each transfer, a discontinuous moving boundary method of analysis results. An analogous relation between calculated results from this process and results obtained from moving boundary electrophoresis or sedimentation is established. Then, using the approach described in Part I of this series, computer calculations are carried out for polymerizing systems in the ultracentrifuge. The resulting patterns show the effects of diffusion as well as transport and chemical reaction.

Introduction

Gilbert¹⁻³ and Gilbert and Jenkins^{4,5} have published a series of papers showing, theoretically, the effects of chemical reactions upon the schlieren patterns obtained from experiments using moving boundary methods of analysis. In all of their papers the effects of diffusion upon the schlieren patterns at times not infinitely long have been neglected.

Countercurrent distribution, as practiced in the laboratory, is a zone separation method. The equation⁶ relating concentration $C_{n,r}$ to position r in the apparatus after n transfers is

$$C_{n,r} = C_0 \frac{n!}{r!(n-r)!} \frac{K^r}{(K+1)^n} \quad (1)$$

where C_0 is the initial concentration of an independently partitioning solute of partition coefficient K .

For sufficiently large numbers of transfers, when the solute has a partition ratio of approximately 1.0, equation 1 may be transformed^{6,7} into equation 2

$$C_{n,r} = \frac{C_0}{\sqrt{2\pi nK}} e^{-[r-nK/(K+1)]^2/[2nK/(K+1)^2]} \quad (2)$$

If, then, the following analogies are drawn

$$n \longleftrightarrow \text{time, } t$$

$$\frac{K}{K+1} \longleftrightarrow \text{velocity, } v$$

$$r \longleftrightarrow \text{position, } x$$

$$\frac{K}{2(K+1)^2} \longleftrightarrow \text{Diffusion coefficient, } D$$

equation 2 may be re-written as equation 3

$$C_{x,t} = \frac{C_0}{\sqrt{4\pi Dt}} e^{-(x-vt)^2/4Dt} \quad (3)$$

In continuous processes, the equation describing the concentration of the zone as a function of x and t is identical with that describing the concentration gradient of the moving boundary as a func-

tion of x and t . Therefore if $C_{x,t}$ in equation 3 is replaced by $(\partial c/\partial x)$, the resulting equation should be that describing the schlieren pattern in electrophoresis or sedimentation, as indeed it is.⁸ Therefore, if a front is established in the countercurrent distribution apparatus, the derivative of this front should exhibit a pattern which is completely analogous to that experimentally obtained from electrophoresis or sedimentation in a rectangular cell, if the correct values are chosen for the parameters between which analogies are drawn. Since countercurrent distribution is a discontinuous process, this derivative curve must be approximated by taking first differences between the amounts of solute in adjacent tubes of the apparatus.

This may be verified by a step by step calculation similar to that carried out for a zone distribution.⁶ If this is done, for example, for four transfers, assuming one unit weight of solute in each of the tubes at the beginning, the weights of solute in each of the tubes are

Tube number	Total	Δ_1
(Solvent reservoir)	0	$\frac{1}{(K+1)^4}$
0	$\frac{1}{(K+1)^4}$	$\frac{4K}{(K+1)^4}$
1	$\frac{1+4K}{(K+1)^4}$	$\frac{6K^2}{(K+1)^4}$
2	$\frac{1+4K+6K^2}{(K+1)^4}$	$\frac{4K^3}{(K+1)^4}$
3	$\frac{1+4K+6K^2+4K^3}{(K+1)^4}$	$\frac{K^4}{(K+1)^4}$
4	$\frac{1+4K+6K^2+4K^3+K^4}{(K+1)^4}$	

and the first differences are indeed the usual $T_{n,r}$ as calculated from equation 1; ($T_{n,r} = C_{n,r}/C_0$). There are the first differences between tubes are

(8) L. J. Gosting, *ibid.*, **74**, 1548 (1952).

- (1) G. A. Gilbert, *Discussions Faraday Soc.*, **13**, 239 (1953).
- (2) G. A. Gilbert, *ibid.*, **20**, 68 (1955).
- (3) G. A. Gilbert, *Proc. Roy. Soc. (London)*, **A250**, 377 (1959).
- (4) G. A. Gilbert and R. C. L. Jenkins, *Nature*, **177**, 853 (1956).
- (5) G. A. Gilbert and R. C. L. Jenkins, *Proc. Roy. Soc. (London)*, **A263**, 420 (1959).
- (6) L. C. Craig and D. Craig in A. Weissberger, "Technique of Organic Chemistry," Vol. III, Interscience Publ., New York, N. Y., 1950.
- (7) R. M. Bock, *J. Am. Chem. Soc.*, **72**, 4269 (1950).

กรมวิทยาศาสตร์
กระทรวงมหาดไทย

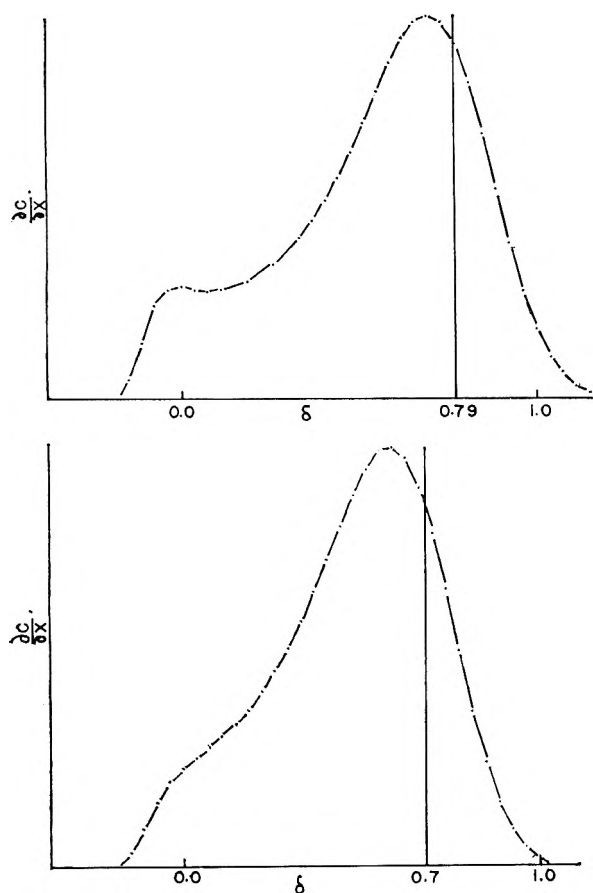


Fig. 1.—Theoretical sedimentation velocity patterns calculated from analog: upper, theoretical pattern for the case of equilibrium mixture of chymotrypsin monomers and trimers; lower, theoretical pattern for the case of equilibrium mixture of chymotrypsin monomers, dimers and trimers.

indeed those values of the function which delineates the zone.

When more than one solute is distributed, and a reaction may occur among them, the actual calculation procedure is much more difficult. In Parts I⁹ and II¹⁰ of this series, it has been shown that patterns may be calculated for countercurrent distribution of zones when a chemical reaction may occur, using material balance equations which are solved repeatedly by a computer. From the preceding discussion, it is apparent that the only changes necessary in this method of calculation, for it to be applicable to the present case, are first, that solute must initially be placed in each tube of the apparatus and second, that first differences between the contents of adjacent tubes must be calculated. This involves only obvious minor modifications of the computer program shown in Part I.

Theory

It is now desired to establish in somewhat more general terms the identity between the *first differences* in tube contents of adjacent tubes for the case of a moving front, and the corresponding *tube contents* for a moving zone.

For the purpose of this computation it is con-

venient to consider the analog of an ascending front in moving boundary electrophoresis. A countercurrent distribution train of tubes, each filled originally with unit volume of only pure lower phase solvent, may be imagined to be fed at each transfer with a unit volume of upper phase containing the amount $K/(K+1)$ of a solute having a partition coefficient K . After n transfers, the total amount of solute in the apparatus is $nK/(K+1)$, distributed over tubes numbered $r = 0$ to $r = n - 1$. This may be expressed by

$$\sum_{r=0}^{n-1} S_{n,r} = \frac{nK}{K+1} = \frac{K}{(K+1)^n} \{ (K+1)^0 (1+K)^{n-1} + (K+1)^1 (1+K)^{n-2} + \dots + (K+1)^{n-1} (1+K)^0 \} \quad (4)$$

Here each term in the expression on the right-hand side of equation 4 is individually equal to $K/(K+1)$, and there are n terms in all. The symbol $S_{n,r}$ represents the total contents of the r th tube after n transfers, as a result of the n successive additions of solute to the apparatus. To find the value of the general term $S_{n,r}$, it is necessary to combine all terms from the right-hand side of equation 4 which contain K^r multiplied by the successively increasing powers of $(1+K)$, i.e., $(1+K)^0$, $(1+K)^1$, $(1+K)^2$, etc. Enumeration of the amounts per tube for each tube after each transfer in a small number of transfers serves to verify that only such terms contribute to the contents of the r th tube. The extraction of all such terms leads to the general expression

$$S_{n,r} = \frac{K}{(K+1)^n} \left\{ (K+1)^0 \frac{(n-1)!}{r!(n-r-1)!} K^r + (K+1)^1 \frac{(n-2)!}{r!(n-r-2)!} K^r + \dots + (K+1)^{n-r} \frac{r!}{r!(r-r)!} K^r \right\} \quad (5)$$

Rearrangement of this equation leads directly to

$$S_{n,r} = \frac{K}{K+1} \left\{ \frac{(n-1)!}{r!(n-1-r)!} \frac{K^r}{(K+1)^{n-1}} + \frac{(n-2)!}{r!(n-2-r)!} \frac{K^r}{(K+1)^{n-2}} + \dots \right\} \quad (6)$$

$$\text{or } S_{n,r} = \frac{K}{K+1} \{ T_{n-1,r} + T_{n-2,r} + T_{n-3,r} + \dots + T_{r,r} \} \quad (7)$$

where each $T_{n-1,r}$ represents the binomial coefficient expression for the contents of the r th tube after $n-1$ transfers in the corresponding fundamental zone process. The first difference in tube contents for adjacent tubes is now given by

$$S_{n,r-1} - S_{n,r} = \frac{K}{K+1} \{ (T_{n-1,r-1} - T_{n-1,r}) + (T_{n-2,r-1} - T_{n-2,r}) + \dots + (T_{r,r-1} - T_{r,r}) + T_{r-1,r-1} \} \quad (8)$$

The conservation of matter now requires that in the corresponding fundamental process, the accumulation in the r th tube during the $(n+1)$ st transfer, is equal to the amount transferred into the r th tube from the $(r-1)$ st tube during the n th transfer less the amount transferred out of the r th tube to the $(r+1)$ st tube during the same transfer, i.e.

(9) J. L. Bethune and G. Kegeles, *J. Phys. Chem.*, **65**, 433 (1961).

(10) J. L. Bethune and G. Kegeles, *ibid.*, **65**, 1755 (1961).

$$\frac{K}{K+1} (T_{n,r-1} - T_{n,r}) = T_{n+1,r} - T_{n,r} \quad (9)$$

Here the right-hand side of the equation is simply the amount present in the r th tube after $n+1$ transfers less the corresponding amount after n transfers, or the accumulation during the $(n+1)$ st transfer. Application of the left side of equation 9 to each pair of T -values enclosed in parentheses in the right-hand side of equation 8 then leads to

$$S_{n,r-1} - S_{n,r} = (T_{n,r} - T_{n-1,r}) + (T_{n-1,r} - T_{n-2,r}) \\ + (T_{n-2,r} - T_{n-3,r}) + \dots + (T_{r+2,r} - T_{r+1,r}) + \\ (T_{r+1,r} - T_{r,r}) + \frac{K}{K+1} T_{r-1,r-1} \quad (10)$$

and all values except $T_{n,r}$ add out, the final term $[K/(K+1)]T_{r-1,r-1}$ being equal to $T_{r,r}$ because only the former amount can contribute to the contents of the r th tube after r transfers. Hence, the general result described above follows

$$S_{n,r-1} - S_{n,r} = T_{n,r} \quad (11)$$

To illustrate the method by which the parameters v (the velocity), D (the diffusion coefficient) and t (the time) are transformed into the analogous parameters n and K , assume that a substance M , characterized by the parameters v_M and D_M undergoes sedimentation for a time t . At the end of this time, the spread of the schlieren curve is proportional to $\sqrt{2D_M t}$ (i.e., the square root of the second moment), and the displacement undergone by the maximum of the curve is $v_M t$.

In the countercurrent distribution apparatus, after n transfers the maximum of the curve has been displaced by $nK/(K+1)$ tubes and the pattern spread is proportional to $\sqrt{nK/(K+1)^2}$. The ratio of spread to movement in the ultracentrifuge is $\sqrt{2D_M t}/v_M t$ and in the countercurrent apparatus is $1/\sqrt{nK}$. If these two ratios are equated for given values of D_M , t and v_M , and the number of transfers, n , which will give adequate detail to the curve is assigned, the value of K which will give the required ratio of spread to displacement is automatically fixed. For a fixed n , this calculation procedure corresponds to division of the ultracentrifuge cell into n compartments, determination of the amount of solute in each compartment and extraction of differences between these to obtain the analog of the schlieren pattern.

Results

The approach described above has been used to refine previous calculations done for the polymerization of α -chymotrypsin,¹¹ using Gilbert's methods.^{1,2} The same values for the sedimentation constants, equilibrium constants and time are chosen as in Fig. 5 of reference 11. A value of 10.2×10^{-7} was used for the diffusion coefficient of the monomer,¹² and from this diffusion coefficients of dimer and trimer were calculated, assuming the polymers to be spherical in shape. The calculated values are 8.1×10^{-7} and 7.1×10^{-7} for dimer and trimer, respectively. The equilibrium constant for the reaction

(11) M. S. N. Rao and G. Kegeles, *J. Am. Chem. Soc.*, **80**, 5724 (1958).

(12) G. W. Schwert and S. Kaufman, *J. Biol. Chem.*, **190**, 807 (1951).

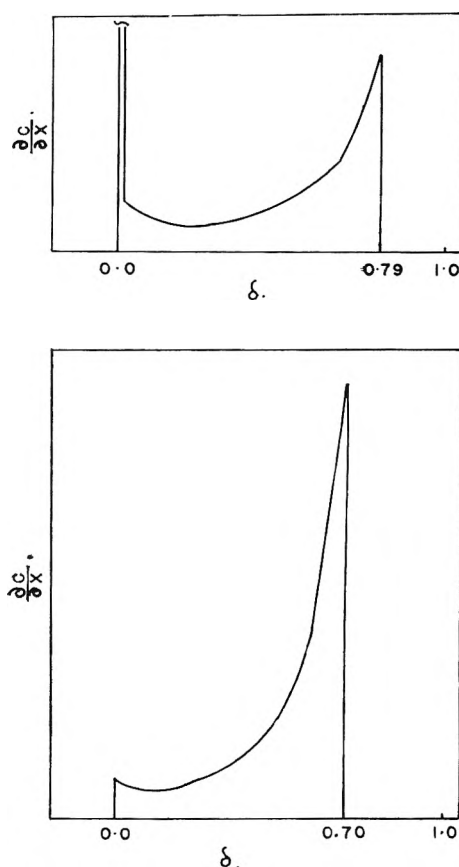


Fig. 2.—Theoretical sedimentation velocity patterns calculated from Gilbert's equations: upper, theoretical pattern for the case of equilibrium mixture of chymotrypsin monomers and trimers; lower, theoretical pattern for the case of equilibrium mixture of chymotrypsin monomers, dimers and trimers.

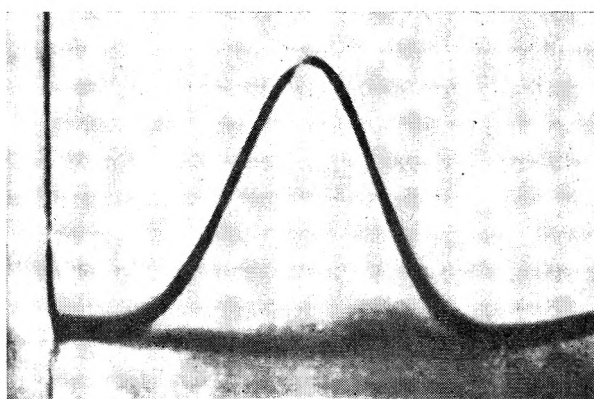
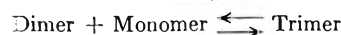
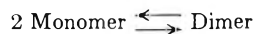


Fig. 3.—Experimental sedimentation velocity pattern of chymotrypsin.



was taken to be 50 (K_3' of reference 11) and those of the reactions



were taken to be 11.4 and 4.5, respectively (K_2 and K_3 of ref. 11).

From these, at $n = 340$, $K_M = 0.04$, $K_D = 0.13$ and $K_T = 0.24$, where K_M , K_D and K_T are the

partition coefficients of monomer, dimer and trimer, respectively. The results of this calculation are shown in Fig. 1, where the upper curve represents the pattern obtained when only monomer and trimer are present, and the lower curve that when monomers, dimers and trimers are present. These are to be compared with the Gilbert plots, for the same situation, shown in Fig. 2, and the experimental pattern of Fig. 3. None of the theoretical patterns is symmetrical, but the lower curve of Fig. 1 shows the closest approach to symmetry. The inclusion of kinetic terms in the chemical reaction could only broaden the curve, and enhance resolution, judging from the one published study including kinetic effects,¹³ and it is difficult to see how the inclusion of higher polymers in the system could remove the asymmetry which exists in the region of lowest concentrations. The most reasonable explanation of the lack of agreement is that in none of the calculations are the sedimentation and diffusion coefficients concentration dependent. If this concentration dependence could be included in the calculations it would speed up the monomer in the dilute region and retard the polymers in the regions of higher concentration, to give a more symmetrical curve.¹⁴

(13) J. R. Cann, J. G. Kirkwood and R. A. Brown, *Arch. Biochem. Biophys.*, **72**, 37 (1957).

(14) The model used for the present calculation is also in error because the slowest moving constituent (monomer) is assigned the smallest diffusion coefficient, whereas in the actual case the reverse is true, blurring the tendency for resolution of a trailing peak.

Acknowledgments.—This work was supported by U. S. Public Health Service Research Grant number A3508. All computations were carried out at the M.I.T. Computation Center as problem number N1064, under the Coöperating Colleges of New England scheme.

DISCUSSION

J. R. CANN (University of Colorado Medical School).—The important computations of Drs. Bethune and Kegeles afford a forceful demonstration of the hazards of classical interpretation of zone and moving boundary patterns of interacting systems while, at the same time, pointing up the power of these methods for studying such systems. Recently we have solved the system of differential equations describing the electrophoretic transport of two-component isomerizing systems, $A \xrightleftharpoons[k_1]{k_2} B$, by numerical solution of the corresponding difference equations (in press, *Arch. Biochem. Biophys.*). A novel feature of the results is that under certain conditions of rates of reaction and time of electrophoresis the schlieren patterns of two-component isomerizing systems may show three peaks. This is another example of how our intuition often fails us in thinking about the transport of interacting systems of macromolecules.

G. KEGELES.—Dr. Cann has kindly provided information from unpublished material mentioned in his discussion above which permitted Dr. Bethune to compute the counter-current distribution analog. It is gratifying that with this rather different approach to the computation, three peaks also were found under certain conditions. It has just been called to my attention by Dr. A. Klinkenberg that he has treated the chromatography problem for slow isomerization reactions [“(Gas Chromatography,” Edinburgh, June, 1960, R.P.W. Scott, ed. and *Chem. Eng. Sci.*, in press (1961))].

POLYCATION-POLYANION COMPLEXES: PREPARATION AND PROPERTIES OF POLY-(VINYLBENZYLTRIMETHYLAMMONIUM) POLY-(STYRENESULFONATE)

BY ALAN S. MICHAELS AND RICHARD G. MIEKKA

Department of Chemical Engineering, Massachusetts Institute of Technology, Cambridge 39, Massachusetts

Received June 30, 1961

High molecular weight poly-(vinylbenzyltrimethylammonium chloride) co-reacts in dilute (<0.2 g./dl.) aqueous solution with sodium poly-(styrenesulfonate) to form a water insoluble but hydrous polysalt which contains equi-equivalent quantities of each polyelectrolyte. The reaction product is of stoichiometric composition irrespective of whether either polymer is present in excess; the excess polymer remains dissolved in the aqueous phase. Surprisingly, the polysalt complex is found to be essentially free of micro ions (Na^+ and Cl^-), indicating virtually complete macro ion binding, and strongly suggesting that the molecules associate predominantly as randomly twisted pairs. When more concentrated solutions (>0.6 g./dl.) of the polymers are mixed, an extremely thin (ca. 200 Å.) complex film forms at the two-solution interface, which completely blocks further polymer interaction. These films can be isolated; they show very high diffusivity toward simple electrolytes (NaCl), but lower diffusivity toward larger ionic species (methylene blue chloride). Fairly fluid solutions, containing rather high concentrations (10 g./dl.) of both polymers, can be prepared in a ternary solvent system comprising ca. 20% acetone, 20% NaBr, and 60% water. Dilution of these mixtures with water, or evaporation of the acetone, results in gelation. By suitable washing techniques, amber, glassy solids, free of extraneous electrolyte, are obtained. By this route, stable complexes containing excess polycation or polyanion, as well as the neutral polysalt, can be prepared. The non-stoichiometric complexes appear to undergo structural rearrangement by a mechanism of internal ionic bond transfer when swelled in aqueous acetone solutions, or when dried. The latter also behave as cation or anion exchange resins; the neutral polysalt selectively sorbs salt from aqueous electrolyte solutions. Mechanisms of polyion interaction, and the probable structures of the complexes, are discussed in light of the experimental findings.

Introduction

The precipitation reactions occurring between oppositely-charged linear synthetic polyelectrolytes in solution, and the properties of the precipitates are of interest because of their similarities to biological systems,^{1,2,3} ion exclusion resins,⁴ and ion exchange resins and membranes. Precipitation is due to strong electrostatic attraction between oppositely-charged macromolecules which causes them to be drawn together and react ionically, giving off their associated counter-ions as free salt.^{2,5,6,7} The precipitates frequently can be dissolved, or their formation prevented, by the addition of sufficient amounts of microionic salts (e.g., NaCl) to suppress the electrostatic fields of the macromolecules. When sufficiently concentrated solutions of oppositely-charged, strongly ionized polyelectrolytes are mixed, the precipitates sometimes take the form of thin continuous films which form at the interface between the two solutions and completely block further interpolymer reaction.

Dilute solution interactions between oppositely-charged polyelectrolytes have been studied by a number of investigators.^{1,2,5,8,9,10} A study of the precipitation of pectic acid by polyethylene imine, together with an excellent review of much of the previous literature, has been given by Deuel, *et al.*⁶ They found that precipitation occurred only in a narrow range of relative concentrations of these

two weakly ionic polyelectrolytes. At the maximum precipitation point, the polyacid and polybase were quantitatively reacted, and no unreacted polyelectrolyte could be found in the supernatant liquid. Electron microscope studies indicated that the precipitates formed at this optimum reacting ratio had a cross-linked structure. Fuoss and Sadek⁵ investigated the stoichiometry of reactions occurring between 0.018 *N* polyvinyl-*N*-butylpyridinium bromide and approximately 0.005 *N* sodium polystyrenesulfonate in mixtures containing excess cationic polymer. They found a considerable variation in the weight of precipitate obtained (1.30-2.40 mg. of precipitate per cc. of sulfonate polymer solution), and the percentage of the total bromide ion trapped in the precipitate (5-10%), depending on the relative amounts and order of addition of the polyelectrolyte solutions. Although the results reported here indicate more nearly equivalent proportion between a pair of polyelectrolytes with similar structures (at higher dilutions), we too have found considerable deviations from complete equivalence at polyelectrolyte concentrations above about 0.005 *N*, which we have attributed to the beginnings of interfacial film forming tendencies.

The present study was undertaken to determine the interaction characteristics of strongly ionized, oppositely-charged polyelectrolytes of high charge density, and some of the properties of the reaction products (polysalts). The two polymers used throughout the study were poly-(sodium styrenesulfonate), NaSS, an anionic polyelectrolyte with a molecular weight of 760,000, and poly-(vinylbenzyltrimethylammonium chloride), VBTAC, a cationic polyelectrolyte with a molecular weight of about 300,000. Both polymers were furnished by the Dow Chemical Company of Midland, Michigan.

Preliminary investigations of the viscometric behavior of the individual polyelectrolytes in dilute

- (1) D. G. Dervichian, *Discussions Faraday Soc.*, **18**, 231 (1954).
- (2) H. Deuel, J. Solms and A. Dengler, *Helv. Chim. Acta*, **36**, 1671 (1953).
- (3) A. Katchalsky, *Endeavour*, **12**, 90 (1953).
- (4) M. J. Hata, J. A. Dillon and H. B. Smith, *Ind. Eng. Chem.*, **49**, 1812 (1957).
- (5) R. M. Fuoss and H. Sadek, *Science*, **110**, 552 (1949).
- (6) H. R. Kruyt, Ed., "Colloid Science," Elsevier Publishing Co., Inc., New York, N. Y., 1949, Vol. II, Ch. 10.
- (7) H. Terayama, *J. Polymer Sci.*, **8**, 243 (1952).
- (8) A. Kossel, *Z. physiol. Chem.*, **22**, 176 (1896).
- (9) R. G. Miekka, "Properties of Mixed Synthetic Polyelectrolytes," S. M. Thesis, Chem. Eng., M. I. T., 1958.
- (10) H. Morawetz and W. L. Hughes, *J. Phys. Chem.*, **56**, 64 (1952).

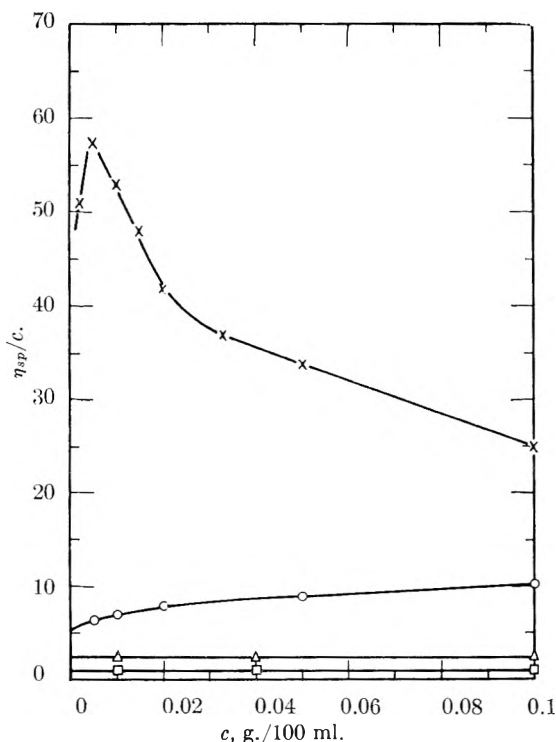


Fig. 1.—Reduced specific viscosity versus polyelectrolyte concentration for VBTAC in: \times , pure water; \circ , 0.001 M NaBr; Δ , 0.01 M NaBr; and \square , 0.10 M NaBr.

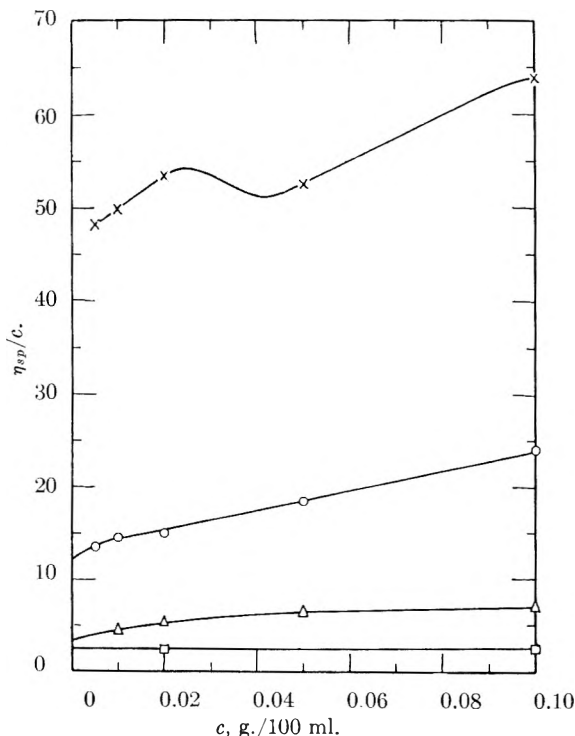


Fig. 2.—Reduced specific viscosity versus polyelectrolyte concentration for NaSS in: \times , pure water; \circ , 0.001 M NaBr; Δ , 0.01 M NaBr; and \square , 0.1 M NaBr.

aqueous solutions were made by Smith.¹¹ He obtained the plots of reduced specific viscosity vs. polyelectrolyte concentration shown in Figs. 1 and

(11) N. H. Smith, "Viscometric Study of Polyelectrolytes in Solution," S. M. Thesis, Chem. Eng. M. I. T., 1959.

2, using a modified Ostwald capillary viscometer at 25°.

The polymers reacted under three different sets of conditions, each resulting in polysalts with distinctly different properties: (1) interaction between dilute (<0.2 g./dl.) aqueous solutions of the polymers resulted in white, hydrous, particulate polysalts similar in appearance to the silver halide precipitates formed by reaction between dilute solutions of silver nitrate and the alkali halides; (2) when more concentrated solutions (>0.6 g./dl.) of the polymers were mixed, an extremely thin (ca. 200 Å.) film formed at the two solution interfaces which completely blocked further polymer interaction; and (3) polysalts containing widely varying relative amounts of the two polymers were prepared by precipitation from a ternary solvent system (NaBr-acetone-water) in which both polymers could be dissolved without interacting.

Experimental

Purification of Polyelectrolytes. Extraneous microions were removed from the polymers by adding a demineralizing resin (a mixture of cation exchange resin in the hydrogen form and anion exchange resin in the hydroxide form) to aqueous solutions containing 3–5% by weight of the polymers. After the polymer solutions had been contacted with the resin for about 12 hours, they were filtered through a fritted glass funnel to remove the resin and any contaminant particles which might be present. The solutions were dried after being passed over appropriate ion exchange resins to assure that the desired counter-ions were present on the polyelectrolytes.

Equivalent Weight Determinations. The ionic equivalent weights of the polymers were determined by standard base titrations of NaSS after it had been ion exchanged into the hydrogen form, and argentometric titrations of the chloride counterions of VBTAC. The chloride titration endpoints were determined potentiometrically using a Beckman pH meter with hydrogen and silver wire electrodes. The solutions were buffered to pH 4 to assure constant hydrogen electrode potential during the titrations. The equivalent weight of NaSS was found to be 234 ± 8 ,¹² while the value for VBTAC varied from 234 ± 10 to 264 ± 10 , depending on the batch used. The variance in equivalent weight was believed to result from degradation of some of the quaternary groups, probably by bacterial attack in solution.

Dilute Solution Interactions.—A series of mixtures containing varying relative amounts of VBTAC and NaSS were made up from dilute (<0.2 g./dl.), salt-free solutions of the polyelectrolytes. In each mixture, the total amount of the more concentrated polymer was 0.342–0.427 meq. (ca. 0.08–0.1 g.) and the final volume was 100.0 ml. An aliquot of each mixture was centrifuged to remove the precipitate, and the viscosity of the supernatant liquid was measured at $25.00 \pm 0.02^\circ$ in a Cannon-Fenske capillary type viscometer (ASTM size 100, with a flow time of 70.1 seconds for 10 ml. H₂O). For each mixture, a control sample was made up to contain the ionic excess of the more concentrated polyelectrolyte plus the amount of NaCl which would be released from the precipitate upon complete ionic interaction between the polyelectrolytes. The viscosities of these solutions were measured for comparison with the mixture supernatant viscosities. The chloride (NaCl) concentrations of the supernatant liquids of NaSS-rich mixtures were measured by potentiometrically titrating portions of the supernatants against silver nitrate.

A second, similar series of mixtures was made up from VBTAC and NaSS solutions containing 0.1 M NaBr. For this set of mixtures, no control samples were necessary since the reduced specific viscosities (η_{sp}/c) of both polyelectrolytes were independent of polyelectrolyte concentra-

(12) Reexamination of the data have indicated that a value of 230 would be a more appropriate value for the equivalent weight of NaSS, but since the small correction involved is well within the estimated experimental error, the originally assumed value of 234 has been used throughout the report.

tion and virtually unaffected by the small salt concentration increases due to release of NaCl from the precipitates.

Polyelectrolyte Interfacial Films.—The thin, complex polyelectrolyte films which formed spontaneously at the interfaces between more concentrated (>0.6 g./dl.) solutions of VBTAC and NaSS were isolated from their polymer solution environments as (1) unsupported films formed across the holes of 2-cm. i.d. plastic rings, or (2) fairly intimately supported films imbedded in filter paper on which diffusivity measurements were made:

(1) One side of a clean Plexiglas ring, 2.5 cm. o.d., 2 cm. i.d., and approximately 1.6 mm. thick was dipped into a 3% aqueous solution of NaSS in such a way that a film of the solution was formed across the hole in the ring. The ring then was turned over and dipped into a 3% aqueous VBTAC solution so that a film of the latter was formed in contact with the NaSS solution film. A coprecipitated polyelectrolyte membrane formed rapidly at the interface between the two liquid films. The ring then was suspended edgewise in a beaker of quiescent water for one hour to wash the excess unreacted VBTAC and NaSS solutions from the surfaces of the precipitated film. The plastic ring then was removed from the wash water, and the film was laminated wet onto a solid supporting surface, or placed in a desiccator at ambient temperature and 50% relative humidity to dry.

(2) A piece of filter paper (S. & S. No. 576) was clamped vertically in a diffusion cell in such a way as to form a barrier between the two compartments of the cell. A known volume of 0.1 *M* NaCl was placed in one compartment of the cell, and 0.001 *M* NaCl in the other. The compartments were fitted with stirrers and the diffusion rate of the salt through the membrane was determined by measuring the rates of change of conductivity of the solutions in the two compartments. After being washed, the filter paper was contacted on one side by a 3% NaSS solution and on the other side by a 3% VBTAC solution by pouring the solutions simultaneously into the two cell compartments. The heights of the two solutions were adjusted so that no hydraulic gradient existed across the filter paper. After sufficient time had been allowed for the polymer solutions to diffuse into the filter paper and react to form an interfacial film, the solutions were poured out, and the paper was thoroughly washed with distilled water to remove the excess polyelectrolyte solutions. The diffusion rate of NaCl (0.1 *M* diffusing to 0.001 *M*) through the treated filter paper then was measured in the same manner as described above for the untreated paper. In a test of the continuity of the imbedded interfacial film, it was found that less than 0.01 ml. of water flowed through the treated filter paper when a 8-cm. hydraulic gradient was applied across it for 24 hours. The flow rate through the untreated paper under these same conditions was several cc./hr.

Polysalt Solubilities in NaBr-Acetone-Water Mixtures.—The limiting compositions of NaBr-acetone-water solutions, in which equal amounts (0.1–0.5 g./100 ml.) of VBTAC and NaSS could be dissolved without interacting, were determined by measuring the solvent compositions at which polyelectrolyte precipitation began to occur when the concentrations of the solvent components were varied in known fashion. Some of the measurements were repeated for mixtures containing VBTAC/NaSS in the ionic ratios 2/1 and 1/2 to see whether there was any effect of polyelectrolyte ratio on the solubility limits. A third, similar set of measurements was made with mixtures containing NaSS as the only polymer to determine which of the solubility limits were due to salt-out of NaSS rather than interaction between the polymers.

Formation of Polysalts by Precipitation from NaBr-Acetone-Water Mixtures.—Solutions containing 5–10% by weight of each polyelectrolyte dissolved in a solvent comprised of 60% water, 20% NaBr, and 20% acetone were made up with polymer equivalence ratios of 2VBTAC/1NaSS, 1VBTAC/1NaSS, and 1VBTAC/2NaSS. The solutions were poured into glass petri dishes and allowed to gel by evaporation of the acetone. The samples then were placed in an oven at 50° to evaporate water until, or shortly before, a slight opacity developed at the periphery of the gels due to salt out of NaSS. The gels then were washed briefly with water to extract some of the NaBr, and replaced in the oven to again allow water evaporation to the point of incipient NaSS precipitation. This alternate washing and drying procedure was continued until the polymer content was 40–50% of the total weight of the samples.¹³

after which the polysalts were washed with demineralized water until no more salt could be extracted from them, cut into samples of the desired size, and dried at 50% humidity over a sulfuric acid-water mixture to yield amber, transparent solids.

After final washing of the polysalts, the interpolymer reactions were surprisingly complete. No sodium could be detected by flame tests made on samples cut from the quaternary-rich polysalts, and no visible silver halide precipitate was formed when silver nitrate solution was added to a tenth molar sodium nitrate solution which had been equilibrated with a sample of NaSS-rich polysalt. The neutral polysalts gave negative tests for both sodium and bromide ions, with the exception that small opaque regions (if present) at the periphery of the samples gave weak positive flame tests for sodium.

Swelling of Polysalts in NaBr-Acetone-Water Mixtures.—For swelling measurements, 0.3–0.8 g. samples of the dried polysalts were equilibrated with approximately 50 ml. volumes of various acetone-water, NaBr-water, and acetone-NaBr-water mixtures at room temperature until no further weight increase occurred in a 24-hour period. The weighings were made in a closed bottle after the samples had been blotted with tissue paper to remove excess surface liquid. One to two weeks usually were required before final equilibrium was reached. In some cases, the samples were dried without washing and reweighed to determine the amounts of NaBr absorbed with the solutions.

Results and Discussion

(1) **NaBr-Free Mixtures.** It was found that in the absence of added salts, the dilute polymers reacted in equiionic proportions regardless of the relative amounts of the two polymers being mixed. If the polymer mixtures were passed through their ionic equivalence points, the precipitates were completely flocculated, and centrifugation yielded clear supernatant liquids. The viscosities of these supernatants were almost exactly equal to those of the control samples made up to contain the ionic excess of the more concentrated polymer plus NaCl equivalent to the maximum possible counterion release from the precipitated polymers. Table I compares the measured supernatant liquid and control sample specific viscosities for the NaBr-free dilute solution VBTAC-NaSS mixtures passed through their ionic equivalence points. The maximum deviations of mixture specific viscosities from theoretical (control sample) specific viscosities were 3% (mixture 6) and 3.5% (mixture 5), corresponding to precipitate compositions of 1.03 and 1.02 meq. VBTAC/meq. NaSS, respectively. These are within the estimated error of $\pm 5\%$ in the measured (by counterion titrations) equivalent weight ratio of the polyelectrolytes.

If the mixtures deliberately were kept from being passed through their equivalence points, the precipitates could not be completely centrifuged out of the mixtures, and the specific viscosities of the resultant turbid supernatant liquids were 5–7% higher than the supernatant viscosities of similar mixtures passed through their equivalence points. It is presumed that the elevation in viscosity was due to the presence of suspended precipitate rather than a lack of complete interaction between the polymers.

(13) The purpose of this rather elaborate wash-dry procedure was to remove as much salt, water, and acetone as possible from the polysalts while keeping the over-all solvent composition near the region of polysalt solubility. If too much salt was extracted from the dilute gels by prolonged contact with water, internal porosity developed due to contraction of the polymer volume, and the final polysalts were microporous sponges rather than continuous solids.

TABLE I

SUPERNATANT LIQUID AND CONTROL SAMPLE SPECIFIC VISCOSITIES FOR NaBr-FREE DILUTE SOLUTION VBTAC-NaSS MIXTURES PASSED THROUGH THEIR IONIC EQUIVALENCE POINTS

Mixture	Mixture compositions, meq./dl.		Ionic excess VBTAC	Ionic excess NaSS	Supernatant liquid NaCl concn.	η_{sp} of mixture supernatant	$\eta_{sp,theo}$ (control sample viscosity)	$\eta_{sp}/\eta_{sp,theo}$
	VBTAC ^a	NaSS Meq./dl.						
1	0.0855	0.427	..	0.342	0.0855	5.94	5.95	0.993
2	.171	.427	..	.256	.177	2.68	2.67	.996
3	.256	.427	..	.171	.256	1.20	1.22	.984
4	.342	.342	0.00	.00	.342	0.0014	0.00	..
5	.384	.249	.135	..	.249	.198	.206	.965
6	.384	.166	.218	..	.166	.442	.456	.97
7	.384	.0829	.301	..	.0289	.943	.949	.994

^a VBTAC Batch A (equiv. wt. = 234 ± 10) used in Mixtures 1-4, Batch B (equiv. wt. 264 ± 10) used in Mixtures 5-7.

The surprising stoichiometric relations indicated by the viscosity data were corroborated by argentometric titrations made on the supernatants of the mixtures containing excess NaSS, which showed that within experimental error ($\pm 3\%$), all of the chloride counterions of the (precipitated) VBTAC were released into solution.

The results indicate that the polymers combine in some fashion other than by random interaction between the polyions, for if this were the case, a tangled, highly matted network would be formed, and one would expect that a considerable fraction of the ions of each polymer would be sterically prevented from reaction. The conclusion is that molecular pairing occurs between relatively long segments of the interacting molecules. Since the polymers used here have equal ionic spacings, pairing allows virtually complete reaction of the ions. The probable mechanism of pair formation is as follows: Initial contact between two molecules occurs randomly at some point along the polymer chains. Once an initial ionic reaction has occurred, however, the most probable points for further interaction are between ions adjacent to the reacted site, since they are of necessity very close to each other. If reactions continue to occur at sites immediately adjacent to those already reacted, the result will be a "zippering" action which will continue until the end of a molecule is reached, or until terminated by a reaction propagation from some other point on one of the molecules. Most likely the paired molecules are randomly twisted about each other rather than taking the form of regular spirals, since both polymers are atactic. The side groups need not rotate about the chains to allow the ions to approach indefinitely close to each other, since the oppositely charged ions need only be in sufficient mutual proximity to allow the escape of their counterions into the bulk solution.

It should be pointed out that, although the demineralizing resin purifications undoubtedly removed practically all monomer and very low molecular weight polymer fragments from the polyelectrolyte solutions, it is possible that some polymer of degree of polymerization as low as 5-10 remained in the solutions. Such small molecules, being quite mobile, may have enabled a degree of approach to complete and stoichiometric interaction which would not have been achieved if only very large molecules were present. Future

work with fractionated polymer samples is planned.

(2) **Mixtures Containing 0.1 M Added NaBr.** Table II gives the mixture compositions, flocculation points, and supernatant liquid specific viscosities of polyelectrolyte mixtures made in the presence of 0.1 M NaBr. The flocculation points, which were fairly reproducible, occurred before the equivalence points were reached, regardless of the order of addition of the two polymers. At the flocculation points (mixtures 11 and 12), the clear supernatant liquids were essentially free from excess polymer, having almost the same viscosity as the solvent. If polymer solution addition was continued beyond the flocculation points, some of the additional polymer entered the precipitates. When VBTAC was added in excess, more than an equivalent amount entered the precipitate within three hours from the time of mixing, and continued to enter the precipitate over longer periods of time (10 days), apparently approaching the precipitate composition at the flocculation point obtained when VBTAC was titrated by NaSS. Conversely, when NaSS was added to VBTAC, initial flocculation occurred at a ratio of about 0.65 equivalent of NaSS per equivalent of VBTAC, but when additional NaSS was added some of it entered the precipitate, increasing the ratio to 0.86 to 0.99 equivalent of NaSS per equivalent of VBTAC within three hours from the time of mixing. After 10 days the NaSS/VBTAC combining ratios had increased to 1.01-1.14, apparently approaching the ratio at the flocculation point obtained when VBTAC was added to NaSS.

Complete coprecipitation of both polyelectrolytes throughout a rather broad range of equivalent ratios is, qualitatively at least, consistent with the formation of a randomly cross-linked, polyion network. In the presence of 0.1 M NaBr, viscometric measurements on the individual polymers also indicate that both exist in solution in more or less highly coiled conformations. It is thus suggested that, in the presence of extraneous electrolytes, the coiled polymer molecules may bond together as semi-rigid, oppositely charged particles forming initially a coagulum in which only a small fraction of the available polyion pairs have reacted. Slow structural rearrangements within the precipitate may allow gradual increase in polyion bridging, with concurrent microion release. The capacity of these non-stoichiometric, incompletely

TABLE II

MEASURED AND THEORETICAL (STOICHIOMETRIC) SUPERNATANT LIQUID SPECIFIC VISCOSITIES, FLOCCULATION POINTS, AND SUPERNATANT LIQUID AND PRECIPITATE COMPOSITIONS OF DILUTE VBTAC-NASS MIXTURES CONTAINING 0.1 M NaBr

Mixture	Meq./dl.		Ionic excess VBTAC or NaSS meq./dl.	η_{sp}/c of mixture supernatant		η_{sp} for stoichio- metric reactions ^a		Meq. VBTAC/ Meq. NaSS in precipitate ^a		Flocculation point Meq. VBTAC/ Meq. NaSS
	VBTAC	NaSS		Initial	10 Days	Initial	10 Days	Initial	10 Days	
1	0.379	0.085	0.294	0.0746	0.0728	0.0788	0.0788	1.19	1.26	0.807 ^b
2	.379	.171	.208	.0456	.0423	.0557	.0557	1.22	1.29	0.817 ^b
3	.379	.171	.208	.0415	.0384	.0557	.0557	1.31	1.38	1.53 ^c
4	.379	.256	.123	.0255	.0146	.033	.033	1.11	1.27	0.817 ^b
5	.379	.427	.048	.0025	.0026	.0301	.0294	0.89	0.89	0.824 ^b
6	.379	.427	.048	.0462	.0264	.0301	.0294	1.07	.99	1.48 ^d
7	.227	.427	.200	.127	.119	.125	.122	1.01	.97	1.49 ^d
8	.152	.427	.275	.153	.146	.172	.168	0.83	.80	0.816 ^e
9	.152	.427	.275	.177	.163	.172	.168	1.05	.94	1.53 ^d
10	.0755	.427	.351	.227	.218	.220	.215	1.16	.88	1.37 ^d
11	.141	.171	.030	.00	.00	0.83	.83	0.826 ^b
12	.304	.197	.107	.00	.00	1.54	1.54	1.54 ^d

^a Values calculated assuming η_{sp}/c independent of polymer concentration for both polymers, and equal to the average of values measured for 0.04, 0.06 and 0.1 g./dl. solutions of each polymer in 0.1 M NaBr. ^b VBTAC added to NaSS. ^c NaSS added to an equivalent amount of VBTAC, then excess VBTAC added. ^d NaSS added to VBTAC. ^e VBTAC added to an equivalent amount of NaSS, then excess NaSS added.

ion-bridged structures to absorb and retain excess polycation or polyanion is readily explained by their necessarily high concentration of "unbound" segments of both positive and negative polyion charge.

The observation that the limiting sorptive capacities of these precipitates for polyanion and polycation appear to be related to the flocculation ratios for the reverse orders of addition is provocative, in that it suggests the existence of some special kind of polymer ordering in the precipitate. Further study of this phenomenon is in progress.

Polyelectrolyte Interfacial Films. When dry, the unsupported interfacial films were transparent, but in reflected light they resembled "black" soap films. The dry films adhered tenaciously to any solid surface with which they came in contact, a characteristic also observed for other polymer films below 0.22 microns in thickness.¹⁴ The unsupported films were extremely fragile and invariably broke from shrinkage stresses shortly after drying. Films plasticized by the addition of 0.2-0.5% of glycerol or dextrose to the wash water sometimes lasted for several weeks if undisturbed. Higher plasticizer concentrations resulted in thicker films as evidenced by the presence of interference patterns by reflected light.

Since the films were formed in an ionically unsymmetrical environment, some attempts were made to determine whether appreciable amounts of excess polymer were present on the film surfaces after washing. A flame test made on a sample washed half an hour gave a very faint visible flame test for sodium. Other samples were washed and then laminated to glass supporting surfaces, dried and rinsed with either methylene blue chloride solution (cationic), or an anionic kaolin suspension to see whether there was any appreciable difference in adhesion to the originally cationic and originally anionic sides of the films. There was some tendency for deeper dye

(14) J. Bryne, "Bonding Properties of Micro-dimensioned Films," Sc.D. Thesis, Chem. Eng., M.I.T., 1950.

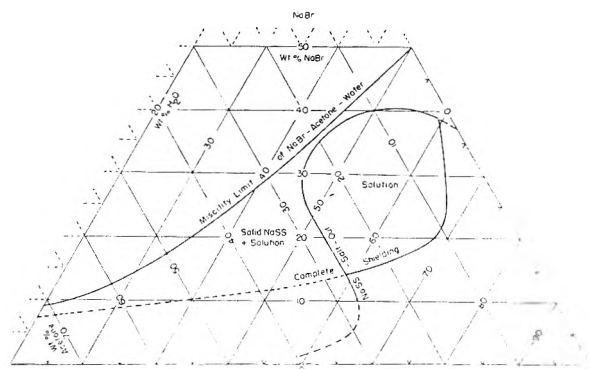
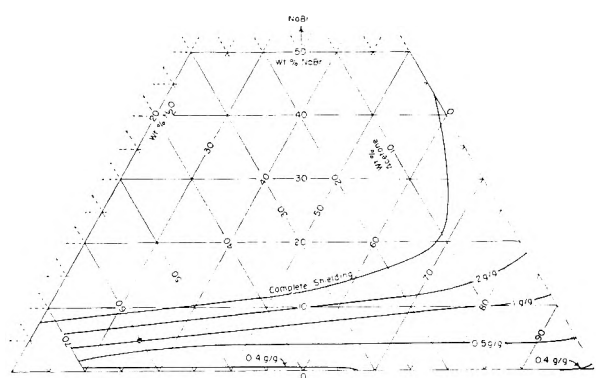


Fig. 3.—Shedding and dissolving of polysalts, and salt-out of NaSS in NaBr-acetone-H₂O mixtures at room temperature (25-30°); total polymer concentration was <1.0 g./100 ml.

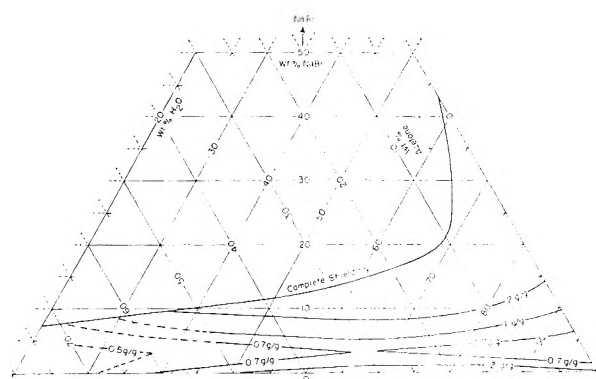
coloration of the NaSS sides, and stronger kaolin adhesion to the VBTAC sides of the films, but the differences were not great. If there were appreciable excess polymer on the film surfaces, it must have been oriented with the ions directed inward, since the surfaces were quite hydrophobic after being dried.

Reflectance spectrophotometer measurements made on an 11-film laminate showed a distinct first order reflectance minimum at an incident light wave length of 480 millimicrons, corresponding to a thickness of about 160 m μ for the 11 films or 145 Å. per dry film. Electron photomicrographs showed the films to have a uniform "pebble-grain" surface typical of amorphous polymers.

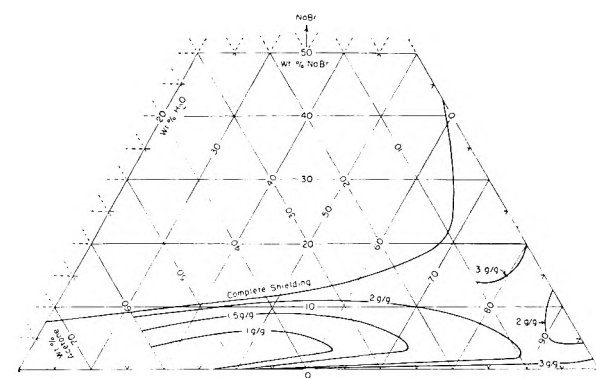
The diffusion rate of 0.1 M NaCl through a piece of filter paper treated to contain an imbedded interfacial film was 0.33 meq./hr./sq. in., which was also the value obtained for the untreated filter paper, indicating that the diffusional resistance of the interfacial membrane was very small, and negligible compared to that of the filter paper. On the other hand, the diffusional resistance of the interfacial membrane toward methylene blue chloride dye was



Acetone H₂O
 Fig. 4.—Swelling (g. solution absorbed per g. dry polysalt) of neutral polysalt in NaBr-acetone-H₂O solutions at room temperature.



Acetone H₂O
 Fig. 5.—Swelling (g. solution absorbed per dry polysalt) of polysalt composed of 2VBTAC/1NaSS in NaBr-acetone-H₂O solutions at room temperature.



Acetone H₂O
 Fig. 6.—Swelling (g. solution absorbed per g. dry polysalt) of polysalt composed of 2NaSS/1VBTAC in NaBr-acetone-H₂O solutions at room temperature.

fairly high, about 1.5 hours being required before any blue coloration could be noted in pure water placed opposite a 0.5% solution of the intensely colored dye, while only 30 minutes were required for visible dye permeation through the untreated filter paper.

Polysalt Solubilities in NaBr-Acetone-Water Solutions. Figure 3 shows the range of concentrations of NaBr, acetone, and water at which non-reacting mixed polymer solutions could be obtained at room temperature. The limiting concentrations were those at which mutual precipitation of the

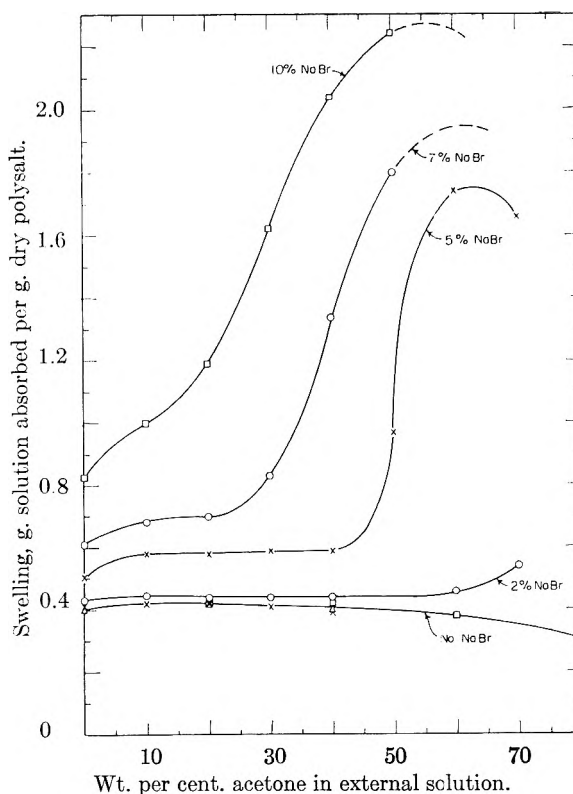


Fig. 7.—Swelling of neutral polysalt in NaBr-Acetone-H₂O solutions. Parameter: wt. per cent. NaBr in external solution.

polyelectrolytes occurred (high water concentrations), and those at which NaSS was salted out of solution (high salt and high acetone concentrations). The diagram applies to polymer concentrations totalling 1% or less, and is independent of the polyelectrolyte ratio from 2NaSS/1VBTAC to 2VBTAC/1NaSS. At polymer concentrations above 1%, gelation rather than precipitation occurred at the boundaries of the solution region, making it difficult to determine the exact position of the boundary. Within minor limits, however, the boundaries do not change until the polyelectrolytes become sufficiently concentrated so that their counter-ions add significantly to the total salt concentration, thus shifting the solubility region toward lower salt concentrations. The dotted portion of the NaSS salt-out curve (which does not border on the solution region) was made from mixed solvent solutions containing NaSS as the only polyelectrolyte.

Ionic reactions between NaSS and VBTAC also could be prevented in the region where NaSS was salted out of solution. In this region, VBTAC was leached out of (previously formed) polysalts and dissolved, leaving behind a "skeleton" of solid NaSS. The minimum salt concentrations for this total ion shielding are shown in Fig. 3 by the dotted portion of the line labeled "total shielding." The upper line on the diagram is the limit of mutual solubility of the three solvent components.

Swelling of Polysalts in NaBr-Acetone-Water Solutions. Figures 4, 5 and 6 are triangular diagrams which show the amounts of NaBr-acetone-water solutions absorbed by the solid polysalts in

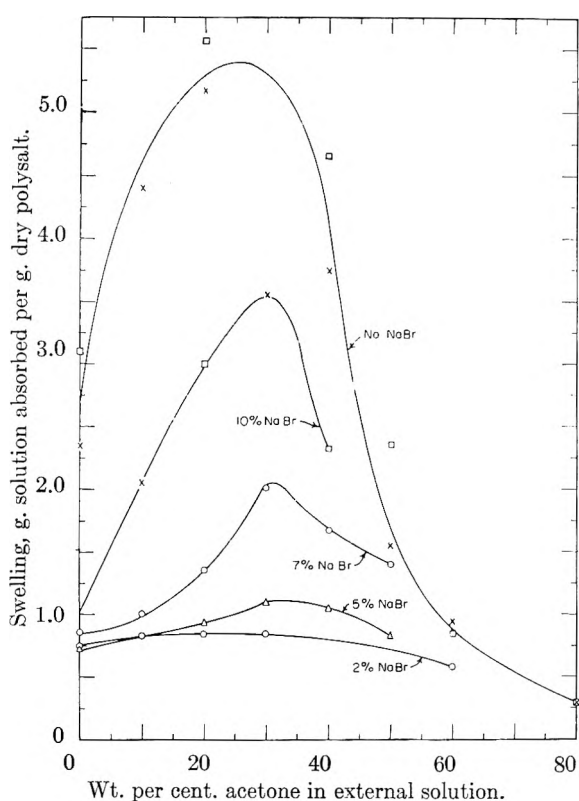


Fig. 8.—Swelling of polysalt composed of 2VBTA/1NaSS in NaBr-acetone-H₂O solutions. Parameter: wt. per cent. NaBr in external solution.

grams of solution absorbed per gram of dry polysalt. The dotted lines represent the limiting solution compositions above which complete shielding (suppression of polyelectrolyte interactions) occurred. The data are replotted in Figs. 7, 8 and 9 to show the amounts of polysalt swelling at constant salt concentrations. The values given apply to samples dried at 50% humidity before swelling (although swelling values are relative to bone-dry weights), and are reproducible to about $\pm 5\%$ below about 0.7 g. solvent absorbed per gram of polysalt, and to about $\pm 20\%$ above 1.0 g. solution absorbed per gram of polysalt. The amounts of the solutions absorbed by the non-stoichiometric polysalts were as much as 50% lower after the samples were dried over P₂O₅, but very few of these measurements were made because the samples usually shattered from unequal swelling stresses when exposed to room air after being dried to this extent.

It is interesting to note that although pure acetone is incapable of swelling the polysalts at all, mixtures containing up to 40% acetone in water induce greater swelling of the polysalts than water alone. In a separate experiment, a quaternary-rich sample which had been immersed in a solution containing 20% acetone in water was placed in pure water without intermediate drying. The sample swelled slightly¹⁵ rather than decreasing to the normal value obtained when dry polymer was equilibrated with water. After being dried, how-

(15) These slight increases in swollen weights could be accounted for by replacement of internally absorbed acetone by water so the swollen volumes probably did not increase.

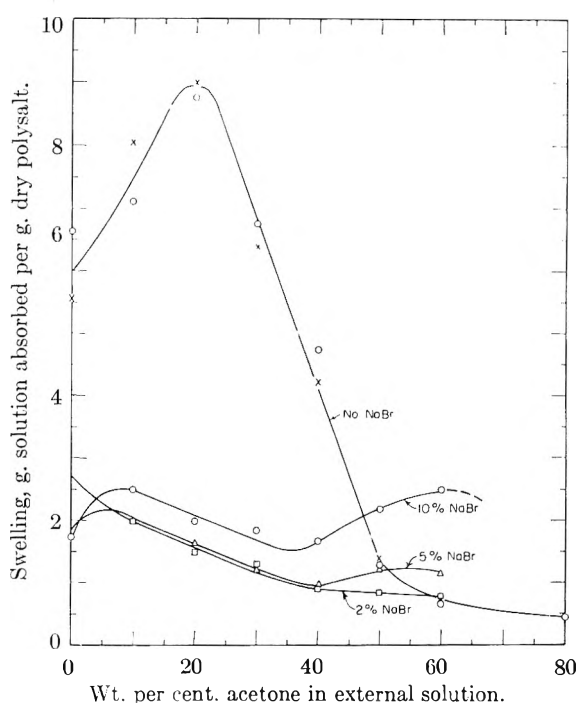


Fig. 9.—Swelling of polysalt composed of 2NaSS/1VBTA in NaBr-acetone-H₂O solutions. Parameter: wt. per cent. NaBr in external solution.

ever, the sample returned to its original water swellability. These experiments showed that the acetone in conjunction with water was able to cause some degree of rearrangement of the polysalt structure into a more expandable form. The mechanism to be described may be responsible.

When the polysalts are precipitated from the ternary solvent, the initial gelation is presumably due to random interactions between marginally unshielded molecules. As the hardening process proceeds, the molecules rearrange by ion transfer and molecular uncoiling into a structure thermodynamically more compatible with the less saline environment. By the time final drying has taken place, the polymers have achieved maximum ionic interaction. The non-stoichiometric polysalts apparently are segregated into regions of essentially neutral polysalt plus regions of unreacted excess polyelectrolyte. This heterogeneity of structure is produced by the same thermodynamic forces which induce micelle formation in surfactants: The interacted portions of the molecules, being relatively hydrophobic, are drawn together and tend to exclude water, whereas the molecular segments containing unreacted polyions are drawn into the more hydrous regions of the mixture. This tendency becomes strongest as the total water content becomes low, since at this time the repulsive forces between polyions of like charge are diminished due to the high counter-ion concentration, and the counter-ions compete strongly for the available water of hydration. Rearrangement ceases when the water content becomes sufficiently low so that the molecules are immobilized sterically.

When the dried polysalts are equilibrated with water they swell, and at least some reverse structural rearrangement into a more homogeneous,

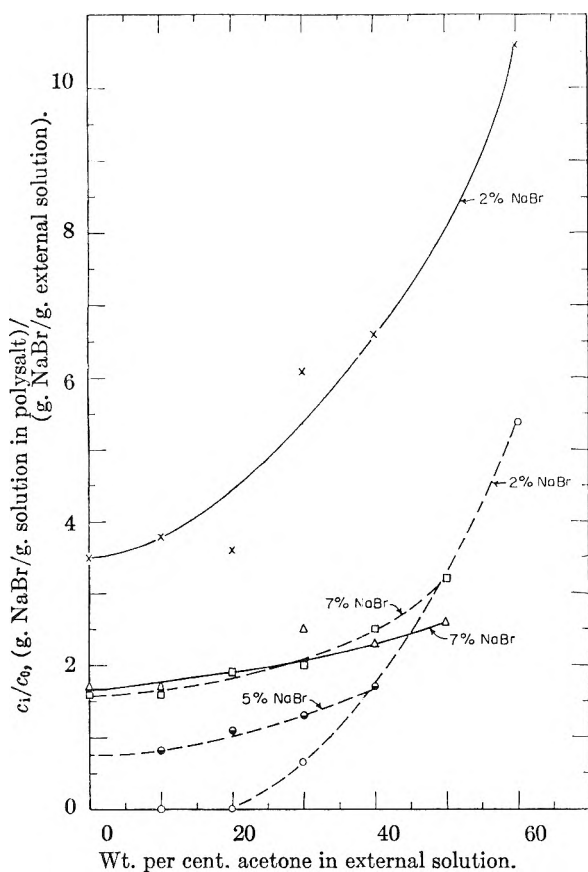


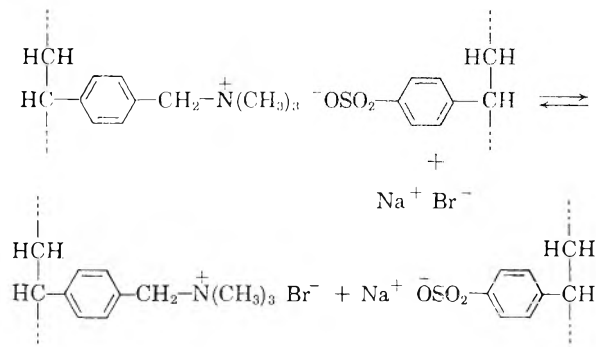
Fig. 10.—NaBr absorption by polysalts equilibrated with NaBr-acetone- H_2O solutions. Parameter: wt. per cent. NaBr in external solution: ——— neutral polysalt; - - - polysalt composed of 2VBTAC/1NaSS.

expanded configuration takes place by ionic bond transfer between the unreacted and (previously) reacted polyions. At sufficiently high degrees of swelling, the osmotic expansion forces become low enough relative to the homopolar associations between the organic portions of the molecules in the neutral regions so that the latter are able to prevent further bond rearrangements. In the presence of acetone, however, the non-ionic association forces are reduced because of increased solvent compatibility of the organic portions of the molecules. This increases the lability of the neutral regions and allows further bond transfer and structural rearrangement to occur. If the acetone is replaced by water, the homopolar association forces will again increase, making further swelling virtually impossible.

Figures 8 and 9 show that the swelling of polysalts containing excess amounts of NaSS or VBTAC is greatly suppressed by the addition of small amounts of NaBr to the acetone-water solutions, the swelling reaching a minimum at about 2% by weight of NaBr in the external solutions. This is due to the ion exclusion or Donnan equilibrium effect, which requires that the activity of an ionic species be the same within the polymer phase as in the equilibrium external liquid. Since the non-neutral polysalts already contain high internal concentrations of sodium or bromide ions present as counterions to the excess polymer molecules,

the salt in the external solution is prevented from entering the polysalts, but competes with them for water, thus reducing their swelling.

The neutral polysalt contains no excess polymer so it does not exhibit an ion exclusion effect. On the contrary, it absorbs electrolyte to such a degree that the internal salt concentration is greater than the external salt concentration (see Fig. 10). This absorption takes place primarily at the points of mutual ionic interaction of the polyelectrolytes by reversal of the precipitation process:



As the reaction takes place, the degree of ionic cross-linking is automatically reduced, allowing polysalt swelling to increase. This reaction must also take place at the quaternary sulfonate sites in the non-neutral polysalts and, at NaBr concentrations above 2% in the external solutions, the resultant decreases in ionic crosslinking allow increased polysalt swelling to occur in spite of the ion exclusion effects of the excess polyions.

At most of the added salt concentrations, the data show that polysalt swelling drops off at sufficiently high acetone concentrations. This is probably due to exclusion of acetone from the polysalts¹⁶ which produces a dehydration effect, analogous to the dehydrating effects arising from ion exclusion by the non-stoichiometric polysalts.

In addition to the swelling measurements, the amounts of salt absorbed by the polysalt samples in some of the NaBr-acetone-water solutions were determined. The results are plotted in Fig. 10 as the ratio of internal liquid to external liquid salt concentrations *vs.* per cent acetone in the external solution, with external NaBr concentration as the parameter.

At low external salt concentrations (2% NaBr \approx 0.2 M NaBr) the neutral polysalt absorbs sufficient NaBr at the double polyion sites so that the internal salt concentrations are much higher than the external salt concentrations. This absorption is undoubtedly promoted most strongly at the double polyion bonds which are strained because of steric hindrances in the structure.

The ion exclusion effect of the excess polyelectrolyte in the VBTAC-rich polysalt greatly reduces its salt absorption capacities at low salt concentra-

(16) By analogy to ion exchange resins, which quite strongly exclude acetone when contacted with aqueous acetone solutions.^{17, 18}

(17) G. Jansen, Jr., "The Anion Exchange of Complexing Cations in Mixed Solvents," Sc.D. Thesis, Chem. Eng., M.I.T., 1959.

(18) C. W. Davies and B. D. R. Owen. *J. Chem. Soc. (London)*, 1670 (1956).

tions. The markedly increased salt absorption at higher salt concentrations is due partly to decreased ion exclusion upon dilution of the excess quaternary polymer with increased polysalt swelling, and no doubt also to increasing ability of the neutral regions in the polysalt to absorb NaBr independently of the adjacent ion-excluding regions.

The greatly enhanced salt absorptions by both polysalts in the presence of added acetone can be explained as follows: The activity coefficient of NaBr in aqueous acetone solutions is higher than its activity coefficient in pure water. If the polyelectrolytes behave at all similarly to the corresponding ion exchange resins, acetone will be excluded from the resin phase. If this is the case, then as acetone is added to the external phase, the equilibrium internal salt concentrations will increase relative to the external salt concentrations until the activity of the salt is the same in both phases.

Conclusions

It is concluded that: (1) The precipitation reactions occurring between poly-(vinylbenzyltrimethylammonium chloride) and poly-(sodium styrenesulfonate) in dilute (<0.2 g./dl.), *salt-free* aqueous solution are stoichiometric and ionically complete within $\pm 5\%$, regardless of the ratio in which the two polymers are mixed. This suggests that the molecules are able to associate predominantly as randomly twisted pairs. In the presence of 0.1 *M* NaBr, the polymer molecules become rather tightly coiled, and the reactions are no longer stoichiometric, complete precipitation of both polymers occurring over a considerable range of relative concentrations of the two polymers.

(2) The interfacial films formed between more concentrated (>0.6 g./dl.) solutions of the two polymers can be isolated, are approximately 150

Å. in thickness when dry, exhibit the microadhesive properties of other polymer films below 0.22 micron in thickness, and show high diffusivity toward simple electrolytes (NaCl), but lower diffusivity toward larger ionic species (methylene blue chloride).

(3) Stable, transparent complexes containing excess polycation or polyanion, as well as neutral salts, can be obtained by precipitation from a ternary solvent (comprised of *ca.* 20% acetone, 20% NaBr, and 60% water) in which both polymers can be dissolved without coreacting. Polysalts containing excess VBTAC or NaSS undergo structural rearrangement by a mechanism of internal ionic bond transfer when swelled in aqueous acetone solutions, or when dried. The neutral polysalt selectively sorbs salt (NaBr) from aqueous electrolyte solutions, whereas the polyanion- and polycation-rich complexes exclude salt. Salt absorption by all of the polysalts is markedly increased when acetone (which is apparently quite strongly excluded from the polymer phase) is added to the external solutions.¹⁹

Acknowledgment. This research was supported in part by the Atomic Energy Commission (Contract No. AT(30-1)2574); this financial assistance is gratefully acknowledged. The authors also wish to thank Drs. G. L. Jones and R. Friederich of the Dow Chemical Company, Midland, Michigan, for providing samples of the polyelectrolytes studied, and Mr. N. H. Smith for measuring the individual polyelectrolyte viscosities. The technical assistance and advice of Professors A. C. Hardy, C. E. Hall and A. Rich, and of Mr. W. Westphal (all of M.I.T.), in carrying out microscopic, X-ray diffraction, and electrical measurements, are warmly appreciated.

(19) H. Thiele and L. Langmaack, *Z. physik. Chem. (Leipzig)*, **206**, 394 (1957).

CRITICAL PHENOMENA IN AQUEOUS SOLUTIONS OF LONG CHAIN QUATERNARY AMMONIUM SALTS. II. SPECIFICITY AND LIGHT SCATTERING PROPERTIES

By IRVING COHEN AND TONY VASSILIADES

Department of Chemistry, Polytechnic Institute of Brooklyn, Brooklyn, N. Y.

Received March 2, 1961

Aqueous solutions of a number of long chain quaternary ammonium salts at concentrations above the critical micelle concentrations have been studied as a function of added simple monovalent electrolyte and temperature. At a given temperature, there is a critical electrolyte concentration above which the system separates into two layers: the top layer is practically free of the quaternary ammonium salt and the bottom layer shows the characteristics of an oil. The volume of the bottom layer decreases with increasing electrolyte concentration. Before the onset of two phase formation, the turbidity and dissymmetry of light scattering rise sharply with increasing electrolyte concentration. An electrolyte transition range may be described, intermediate between zero electrolyte and the critical electrolyte concentration in which there is an apparent reorganization of the micellar aggregate. The phenomenon of two phase formation in these cationic soap systems shows a pronounced specificity to the anions and a lesser sensitivity to the cations of the added electrolyte. Small temperature changes produce marked changes in both the homogeneous systems and the soap-rich layer of a two phase system. A method has been devised for predicting the critical electrolyte concentration of monovalent added anions from a graphical analysis of light scattering from homogeneous systems.

Introduction

Aqueous solutions of some long chain quaternary ammonium salts at concentrations above the critical micelle concentration, in common with many "association" colloids,^{1,2} polyelectrolyte³ and polymer⁴ systems separate into two solution layers. In the case of these quaternary ammonium salts layering may be induced by the addition of small quantities of monovalent or polyvalent simple electrolytes such as NaCl, NaNO₃, NaSCN or Na₂SO₄. The layering phenomenon, classified as a form of simple coacervation by Bungenberg de Jong,² may be regarded as an arrested precipitation of the colloidal species. Two solution phase formation begins with micelles aggregating to form submicroscopic clusters; these clusters coalesce to form microscopic droplets. Further coalescence produces macroscopic droplets which tend to separate into a continuous phase. This phase appears as a top or bottom layer depending upon the density of the colloid-rich layer.

At a fixed temperature, there is a critical electrolyte concentration above which the system separates into two layers. These layers are well defined; one layer is practically free of the quaternary ammonium salt and the other layer shows the characteristics of an oil. For a fixed soap concentration, the volume of the soap-rich layer decreases with increasing electrolyte concentration and is proportional to

$$A + B/C^{1/2} + D/C^{3/2} \quad (1)$$

where A , B and D are constants and C is the concentration of the added electrolyte. At high electrolyte concentrations, the colloidal species precipitates as a solid phase. In a two phase system, the electrolyte concentration in the coacervate layer is slightly less than in the soap-free equilibrium layer.¹ This difference in electrolyte con-

centrations in the two layers may be accounted for in terms of displacement of solvent by soap with no apparent Donnan equilibrium effects.

A precondition for layering is the tremendous growth of the micellar aggregate under the influence of added electrolyte. For the systems investigated, the onset of two-phase formation is characterized by a greater than one hundred-fold increase in micellar molecular weight as compared to the salt-free micellar systems. In addition, for each of these layering systems studied, there is a narrow range of electrolyte concentration intermediate between zero electrolyte and the critical electrolyte concentration, in which the micellar aggregate grows very rapidly. The rate of micellar growth for electrolyte concentrations above and below this transition range is less than the rate of micellar growth in the characteristic electrolyte transition range.

Small temperature changes profoundly effect both the homogeneous systems and two-phase systems. Lowering the temperature of a system at constant electrolyte concentration produces effects comparable to increasing the electrolyte concentration at a fixed temperature. This may be illustrated in terms of the following: For a fixed electrolyte concentration and a fixed soap concentration, a reduction of the temperature of the system results in a growth of the micellar aggregate. Above a minimum electrolyte concentration, a transition temperature may be defined, above which relatively small changes in micellar molecular weights occur with small temperature variations and below which large changes in micellar molecular weights occur with small temperature variations. In addition, the electrolyte transition range for a fixed temperature, which is characterized by a large micellar growth, shifts to lower values as the temperature of the system is lowered.

Over a wide range of electrolyte concentration, there is a unique critical temperature for each electrolyte concentration below which the system separates into two solution phases and above which the system is homogeneous. Below the lower limit of the electrolyte concentration range, gelation

(1) I. Cohen, C. F. Hiskey and G. Oster, *J. Colloid Sci.*, **9**, 243 (1954).

(2) A. C. Bungenberg de Jong, "H. R. Kruyt Colloid Sci. II," Elsevier, Amsterdam, 1949, Chap. X.

(3) H. Eisenberg and G. R. Kohan, *J. Phys. Chem.*, **63**, 671 (1959).

(4) E. Turska and M. Laezkowki, *Roczniki Chem.*, **29**, 941 (1955); *J. Polymer Sci.*, **23**, 285 (1957).

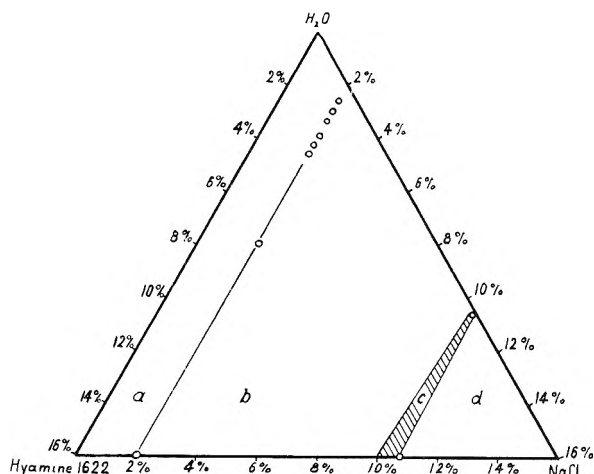


Fig. 1a.—Partial ternary phase diagram—Hyamine 1622—NaCl—H₂O. $T = 30^\circ$. a = homogeneous region; b = 2-phases, both liquid; c = indeterminant region (3-phase, 2 liquid, 1 solid); d = 2-phase, liquid—solid.

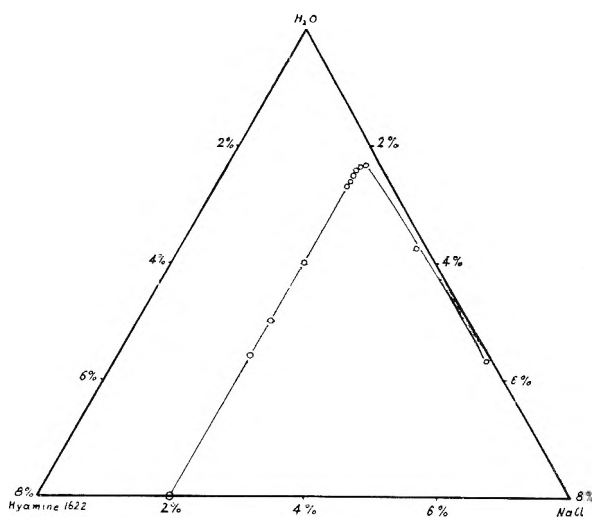
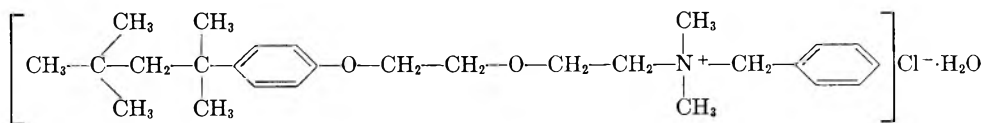


Fig. 1b.—Expanded partial ternary phase diagram Hyamine 1622—NaCl—H₂O., $T = 30^\circ$.

occurs at temperatures below -4° without two phase formation. At the upper limit of the electrolyte concentration range, the colloidal solute flocculates at the lower temperatures and is precipitated as an oil at higher temperatures.

The observed coacervation phenomenon shows a characteristic specificity with regard to the added electrolyte. Cationic soap systems are relatively insensitive to the cation of the added electrolyte. For monovalent anions of the added electrolyte, the relative effectiveness in inducing two phase formation follows a lyotropic series. Two phase systems composed of aggregates of anionic soaps, *i.e.*, alkali oleates, stearates and palmitates have been investigated by Bungenberg de Jong and associates.² We have chosen to study quaternary ammonium cationic systems because coacervation occurs at relatively low electrolyte concentrations. Large measurable changes in these systems are produced with relatively small electrolyte and temperature increments. The quaternary ammonium salt Hyamine 1622 was studied in detail because



this salt forms coacervates with a number of monovalent electrolytes at relatively low concentrations; 0.027 *M* for NaSCN to 0.336 *M* for NaCl at 26° .

This study is confined essentially to added electrolyte and temperature effects upon homogeneous systems well out of the critical region. The concern here is an attempt to characterize the onset of two solution phase formation in dilute aqueous cationic soap systems.

The experimental results obtained can be explained in terms of current concepts of critical solution phenomena related to two sets of considerations.

(a) The attraction of the micelles to each other by London-van der Waals forces, balanced by the intermicellar repulsion due to their ionic double

layers. Theories for such interaction forces have been described for idealized models⁶⁻⁷ and have been developed further by Verwey and Overbeek⁸ and Derjaguin, *et al.*⁹

(b) Where the micelles possess an anisotropic dimension,¹⁰ entropy considerations for anisotropic colloidal species in solution developed by Flory¹¹ and Onsager¹² play a decisive role in the coacervation of the aqueous cationic soap solutions studied. Michelli, *et al.*, have applied these concepts to coacervate systems.¹³

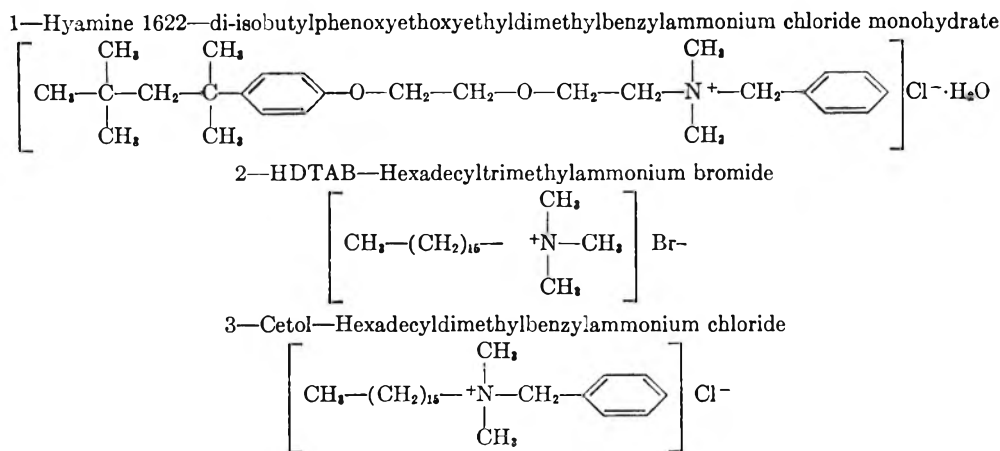
The theory predicts that in a two phase system of rod-like solute particles, one phase is a highly ordered phase. In a well-defined system of this type, aqueous Tobacco Mosaic virus solutions, this is borne out by X-ray¹⁴ and light scattering¹⁵ studies. The data developed in the study of coacervation in quaternary ammonium salt solutions show dimensional anisotropy of the colloidal aggregate in homogeneous solution prior to two phase formation. In addition, the coacervate layer of a

two phase system shows a high degree of order of the micellar aggregates.

- (5) H. Kalman and M. Willstätter, *Naturwiss.*, **20**, 952 (1932).
- (6) I. Langmuir, *J. Chem. Phys.*, **6**, 873 (1938).
- (7) B. Derjaguin, *Acta Physicochim. U.R.S.S.*, **10**, 333 (1959).
- (8) E. J. Verwey and J. Th. G. Overbeek, "Theory of Stability of Lyophobic Colloids," Elsevier, Amsterdam, 1948, p. 159 ff.
- (9) B. U. Derjaguin, A. S. Tilyevskaia, I. Abucossova and A. D. Malking, *Trans. Faraday Soc.*, **18**, 24 (1954).
- (10) P. Debye and E. W. Anacker, *J. Phys. Colloid Chem.*, **55**, 644 (1951).
- (11) P. J. Flory, *J. Chem. Phys.*, **12**, 425 (1944).
- (12) L. Onsager, *Ann. N. Y. Acad. Sci.*, **51**, 627 (1949).
- (13) I. Michelli, M. J. Voorn and J. Th. G. Overbeek, *J. Polymer Sci.*, **23**, 449 (1957).
- (14) I. Fankuchen and J. D. Bernal, *J. Gen. Physiology*, **25**, 147 (1941).
- (15) G. Oster, *ibid.*, **33**, 445 (1952).

Experimenta

Materials.—The following cationic soaps were used in this investigation



Hyamine 1622 is a pure crystalline quaternary ammonium salt monohydrate. It was obtained from Rohm and Haas and contained 1.5% H₂O as the only appreciable impurity. The hexadecyltrimethylammonium bromide (HDTAB), obtained from Eastman Organic Chemicals and the Cetol, obtained from Fine Organics, Inc. were both of technical grade. All inorganic electrolytes used in this work were of C.P. grade.

Apparatus. Light Scattering.—Light scattering measurements were performed in a Brice-Phoenix photometer, using incident unpolarized monochromatic light of wave length 4360 Å. The measurements were carried out in a cylindrical cell, with solutions which had been filtered through millipore filters of 0.45 μ pore size. Since the 3-component (soap-electrolyte-H₂O) systems are sensitive to temperature changes, a brass housing such as described by Boedtker and Doty¹⁶ was constructed to maintain constant temperature in the optical cell. The temperature control was within ±0.1°. The cell correction was determined at various angles by measuring the scattering from a fluorescein solution. Refractive index increments (dn/dc) were measured with a Zeiss dipping refractometer. For soap concentrations in excess of the critical micelle concentration, dn/dc is independent of electrolyte concentration, micellar size and micellar shape. The refractive index increments for the quaternary ammonium salts investigated are: Hyamine 1622, 0.1875; Cetol, 0.15; and HDTAB, 0.162.

Experiments of the following nature were performed.

(a) A partial ternary phase diagram was constructed for the system, Hyamine 1622–NaCl–H₂O.

(b) The critical electrolyte concentration for a number of Hyamine 1622–electrolyte–H₂O systems was determined by the interpolation method of Dervichian.¹⁷ The electrolytes used in this experiment were a number of monovalent salts, monovalent anion–divalent cation salts, and monovalent anion–trivalent cation salts.

(c) Micellar aggregate molecular weights were determined for the Hyamine 1622–NaCl–H₂O systems as a function of NaCl concentration and temperature from light scattering measurements.

(d) Charge properties of Hyamine 1622–NaCl–H₂O systems for low NaCl concentrations (below 0.05 M NaCl) were estimated from light scattering data.^{18–20}

(e) A method has been devised for predicting the critical electrolyte concentration necessary for two phase formation in systems composed of cationic soap–electrolyte–water. This method is based upon a graphical analysis of the light scattering data of the homogeneous single phase system.

(16) H. Boedtker and P. Doty, *J. Phys. Chem.*, **58**, 968 (1954).

(17) D. G. Dervichian, *Trans. Faraday Soc.*, **18**, 231 (1954).

(18) J. J. Hermans and W. Prins, *Koninkl. Ned. Akad. Wetenschap. Proc.*, **B59**, 162 (1956).

(19) J. J. Hermans and K. J. Mysels, *J. Coll. Sci.*, **12**, 594 (1957).

(20) E. W. Anacker, *J. Phys. Chem.*, **62**, 41 (1958).

Results and Discussion

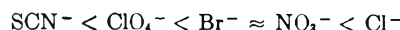
Phase Diagram.—The partial, constant temperature, ternary phase diagram of Hyamine

1622–NaCl–H₂O (Fig. 1a) was constructed by the interpolation method of Dervichian.¹⁷ The H₂O apex of the phase diagram shows four regions: (a) homogeneous region; (b) two liquid solution phases; (c) three phases—2 solution and one crystalline phase (this region is not well defined); (d) two phases—solution and a crystalline phase.

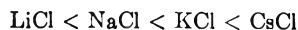
An essential feature of this partial phase diagram is the constancy of the critical electrolyte concentration (c.e.c.) necessary for two phase formation over a wide range of Hyamine 1622 concentration, i.e., 0.27% (6 × 10⁻¹³ M) to 16.20% (3.50 × 10⁻¹ M). The NaCl c.e.c. for a 0.27% Hyamine 1622 solution at 26° is 0.336 ± 0.002 M and the NaCl c.e.c. for a 16.20% Hyamine solution is 0.314 ± 0.002 M. A similar situation is indicated for the flocculation concentration of NaCl for the Hyamine 1622 system. The NaCl flocculation concentration for a 0.27% Hyamine 1622 solution is 1.8 ± 0.02 M and for 16.20% Hyamine solution is 1.71 ± 0.02 M.

Figure 1b represents an expansion of the H₂O apex of the partial ternary phase diagram for dilute Hyamine 1622 soap solutions to 0.1% (0.0031 M) slightly in excess of the critical micelle concentration. In this region of the phase diagram for soap concentrations less than 0.27%, the NaCl c.e.c. is dependent upon soap concentration and rises sharply as the solution is made more dilute in the quaternary ammonium soap.

Specificity.—Two phase formation of aqueous Hyamine 1622 solutions shows a pronounced specificity of the anions of the added electrolyte. This is indicated in Table I. This specificity follows a typical Hofmeister series for monovalent anions



The c.e.c. is much less sensitive to the cationic species of the added electrolyte. For the alkali chlorides, the c.e.c. at 26° falls within the range of 0.325 M for LiCl to 0.425 M for CsCl in the following order



With divalent and trivalent cations, there is a

small but significant increase in the critical anion concentration at a fixed temperature. For a 3% soap solution at 26°, the c.e.c. for the following salts are

NaCl—0.325 <i>M</i> in Cl ⁻	NaNO ₂ —0.067 <i>M</i> in NO ₂ ⁻
BaCl ₂ —0.420 <i>M</i> in Cl ⁻	Ba(NO ₃) ₂ —0.077 <i>M</i> in NO ₃ ⁻
FeCl ₃ —0.470 <i>M</i> in Cl ⁻	Al(NO ₃) ₃ —0.087 <i>M</i> in NO ₃ ⁻

TABLE I

CRITICAL CONCENTRATION NECESSARY FOR TWO PHASE FORMATION IN A 3% HYAMINE 1622 SOLUTION AT 26.0° OF MONOVALENT ANIONS AND MONOVALENT, DIVALENT AND TRIVALENT CATIONS

Mono-valent cations	Critical concn., <i>N</i>	TRIVALENT CATIONS		Critical concn., <i>N</i>	
		Divalent cations	Trivalent cations		
KSCN	0.027	Cu(NO ₃) ₂	0.079	Al(NO ₃) ₃	0.087
NaBr	.064	Ba(NO ₃) ₂	.078		
KClO ₃	.059	Ni(NO ₃) ₂	.078		
NaNO ₂	.067	Cd(NO ₃) ₂	.073		
NaNO ₃	.250				
LiCl	.305				
NaCl	.320	CuCl ₂	.430	FeCl ₃	.470
KCl	.325	BaCl ₂	.420		
CsCl	.425	CaCl ₂	.370		
		NiCl ₂	.400		

TABLE II

CHARGES AND AGGREGATION NUMBERS OF HYAMINE 1622 MICELLES AT LOW NaCl CONCENTRATIONS^a

NaCl (<i>M</i>)	<i>p</i>	<i>m</i>	(<i>p/m</i>) × 100	<i>M</i> ₁ × 10 ⁻⁴	1/ <i>A</i> × 10 ⁻⁴
0	1.09	13.34	8.15	0.625	0.573
0.01	12.31	75.4	16.35	3.50	3.45
.02	16.30	78.0	20.0	3.63	3.64
.03	16.25	83.0	19.6	3.87	3.94
.04	11.75	88.0	13.35	4.10	4.06
.05	10.00	100.0	10.00	4.65	4.62

^a *p* = micellar charge as computed from eq. 4, *m* = aggregation number as computed from eq. 3, *M*₁ = formula weight of Hyamine 1622, i.e., 465.5, *A* = intercept of $H(C - C_0)/(\tau - \tau_0)$ vs. $C - C_0$ plot.

A qualitative experiment that tends to indicate that specificity is related to the binding of counterions to micellar species is the following: If coacervation is produced by the addition of two electrolyte species, the effects are not additive. The greater the quantity of the more effective electrolyte in the system, the smaller the proportionate amount of the less effective electrolyte needed to produce a two phase system. For a mixed NaCl-NaBr system at 26° when the solution is 0.034 *M* in NaBr which is 1/2 the NaBr c.e.c. (0.067 *M*) coacervation may be produced with the addition of 0.10 *M* NaCl. This NaCl concentration is very much less than 1/2 the NaCl c.e.c. (0.336 *M*).

Light Scattering. Effects of Added Electrolyte.—Approximate micellar molecular weights of Hyamine 1622 in aqueous NaCl solutions were calculated from the general relationship

$$\frac{H(C - C_0)}{\tau - \tau_0} (P_{90}) = \frac{1}{M} + 2Bc \quad (2)$$

where the terms of this expression have the usual meaning. For those solutions where the medium behaved as a theta solvent (for NaCl concentration in excess of 0.05 *M*) the second term of this expression becomes negligible.

For low electrolyte concentrations where the

micellar aggregate is optically isotropic, the particle scattering factor (P_{90}) was taken as unity. For higher electrolyte concentrations for which the solutions show considerable dissymmetry of light scattering, a particle scattering factor (P_{90}) estimated for rod-shaped aggregates,²¹ was used to calculate micellar molecular weights.

For the system investigated in detail, Hyamine 1622, the micellar charge *p*, the aggregation number *m*, and the ratio of charge to aggregation number (*p/m*) were estimated from the following expressions developed by Anacker.²⁰

$$B = \frac{A(p^2 + p - AmM_1p)}{2mM_1(n_1 + n_3)} \quad (3)$$

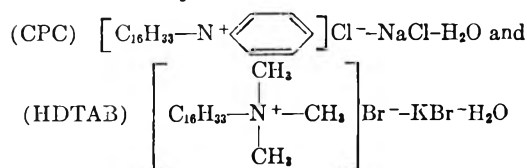
$$p = \frac{BM_1(n_1 + fn_3) + \sqrt{2B(n_1 + n_3)}}{A(1 - AM_1E/2)} \quad (4)$$

$$E = \frac{(n_1 + fn_3)}{(n_1 + n_3)} \quad (5)$$

Where *p* and *m* are the micellar charge and aggregation number, respectively, *M*₁ is the formula weight of the detergent, *A* is the intercept of a plot of $[H(C - C_0)/(\tau - \tau_0)]$ vs. $C - C_0$ and *B* its slope, *n*₁ and *n*₃ the critical micelle concentration and electrolyte concentration both expressed in moles/ml. and *f* is the ratio of molar refractive index increment of the added salt to that of the detergent (*f* = 0.17 for NaCl concn. to 0.05 *M*). This information is summarized in Table II for solutions of low NaCl concentrations. For systems of higher electrolyte concentrations where the solutions showed theta solvent properties, no attempt was made to estimate micellar charge.

The distinctive feature of the charge properties of the micellar species derived from light scattering data is the relatively low ratio of charge to aggregation number; derived *p/m* values decrease to 0.10. The *p/m* values for a non-coacervating cetylpyridinium chloride-NaCl system²⁰ range up to 0.27 for NaCl concentration up to 0.4 *M*. Philippoff²² has summarized the charge properties of a number of anionic and cationic micellar systems determined by a variety of techniques. For typical systems reported, the micellar ionization ranges from 16 to 50%.

The micellar molecular weights determined for Hyamine 1622 as a function of the NaCl concentration (Table III) show the following pattern: (a) at low NaCl concentrations, a relatively slow increase in MMW occurs; (b) between 0.17–0.19 *M* NaCl there is a sharp rise in MMW and (c) for NaCl concentrations above 0.19 *M*, the MMW increase at a rate greater than the initial rate (low NaCl concn.) but lower than the rate of increase in the interval 0.17–0.19 *M* NaCl. This pattern would indicate that in the electrolyte transition range of 0.17–0.19 *M* NaCl, a profound reorganization of the micellar structure occurs. A pertinent comparison may be made with two related systems. These systems are



Light scattering studies by Anacker and Debye^{10,20} show pronounced differences between these systems. CPC micellar molecular weight as a function of NaCl concentration shows a growth to a limiting value of 46,000 for NaCl concentrations in excess of 0.4 *M*. No further micellar growth occurs for higher NaCl concentrations. The data are consistent with a spherical model of the micelle. HDTAB at KBr concentrations of 0.178 and 0.233 *M* shows micellar molecular weights of 795,000 and 1,860,000, respectively. The data for the HDTAB system are consistent with a rod-shaped model of the micelle. A screening treatment of aqueous CPC solutions with a wide variety of monovalent and polyvalent anion salts failed to produce a coacervating effect. For a similar screening treatment of HDTAB, moderate amounts of KSCN (0.165 *M*) induced two solution phase formation. Two observations may be made here: (a) for all of the coacervating systems investigated, the micellar species were dimensionally anisotropic prior to two phase formation and (b) not all anisotropic micellar systems formed coacervates. The HDTAB-KBr solutions were homogeneous in saturated KBr systems.

TABLE III

MICELLAR MOLECULAR WEIGHTS AND DISSYMMETRIES OF HYAMINE 1622 AS A FUNCTION OF NaCl CONCENTRATION^a
AT $T = 30.0^\circ$

NaCl (<i>M</i>)	MMW $\times 10^{-6}$	$I_{45^\circ} / I_{135^\circ}$
0.11	1.23	1.03
.13	1.43	1.04
.15	1.84	1.04
.17	2.08	1.10
.18	3.06	1.11
.20	3.57	1.12
.25	5.0	1.18
.30	7.25	1.35

^a I_{45° and I_{135° are the intensities of the scattered radiation at 45 and 135°, respectively.

Dissymmetry of Light Scattering.—The dissymmetry as a function of electrolyte concentration shows the following characteristics.

At low electrolyte concentrations, external interference effects due to electrostatic interparticle interactions are evidenced by a small decrease in dissymmetry to values of less than unity. At concentrations above the electrolyte transition region, the dissymmetries begin to rise and the increase becomes more pronounced as the c.e.c. is approached. The dissymmetries of the soap-rich layer of a two-phase system show an initial sharp drop (from 1.5 to 1.18) for a 0.04 *M* increment of NaCl from 0.40 to 0.44 *M* NaCl. This sharp drop in dissymmetry would indicate destructive interference of the scattered radiation from this phase.

Temperature Effects.—Figure 2a is a plot of micellar molecular weights at fixed electrolyte concentrations (0.005 to 0.18 *M* NaCl) as a function of $1/T$ where T is the absolute temperature of the system. In the temperature range investigated (5–30°) all of the solutions studied with the exception of the 0.18 *M* NaCl solutions were homogeneous over the entire temperature range. The

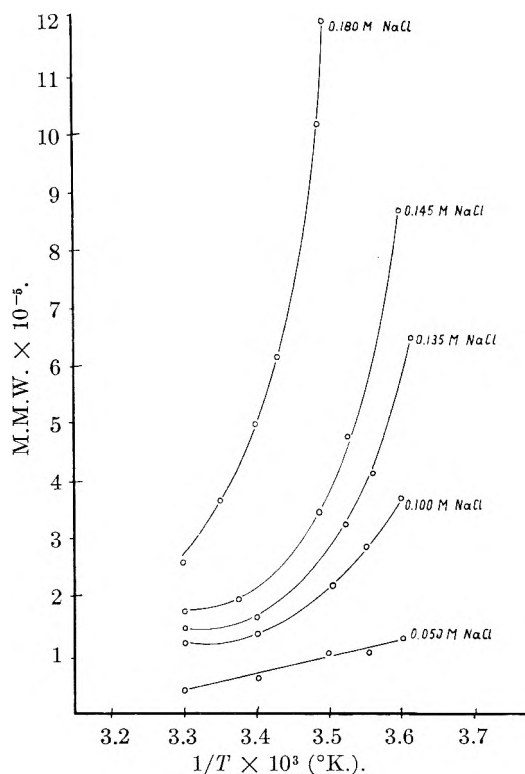


Fig. 2a.—Molecular weight of Hyamine 1622 as a function of temperature at fixed NaCl concentrations.

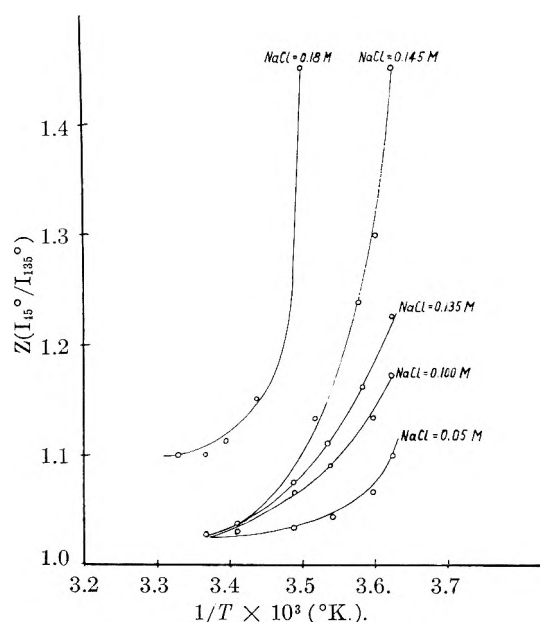


Fig. 2b.—Variation of dissymmetry with temperature for Hyamine 1622-NaCl systems; $\lambda = 4360 \text{ \AA}$.

0.18 *M* solutions separated into two phases at 11°. For all of these solutions, a reduction of the temperature of the solution results in an increase of the micellar molecular weight. For a fixed NaCl concentration of 0.05 *M*, relatively small increases in micellar molecular weight were observed. As the temperature of the system was reduced from 30 to 5°, the micellar molecular weight increment was approximately 6×10^4 MW units. For fixed NaCl concentration ($>0.1 \text{ M}$) near the electrolyte transi-

(21) P. Doty and R. Steiner, *J. Chem. Phys.*, **18**, 1211 (1950).

(22) W. Philippoff, *Discussions Faraday Soc.*, **11**, 96 (1951).

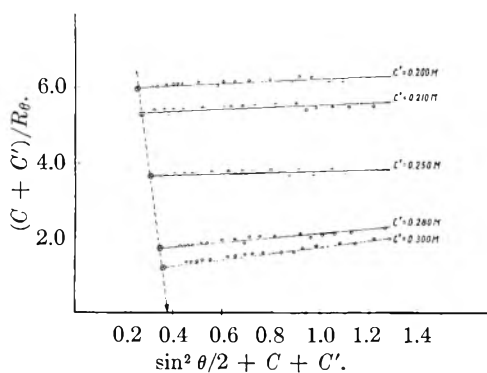


Fig. 3a.—Critical electrolyte concentration derived from the angular dependence of the modified reciprocal reduced intensity. Hyamine 1622-NaCl-H₂O system. C = Hyamine concn. = 0.0644 M ; C' = NaCl concn.; $T = 30^\circ$; $\lambda = 4360 \text{ \AA}$.

tion range, large variations in micellar molecular weights were observed as the temperature was lowered. For a one degree temperature change, for the 0.18 M NaCl system, the micellar molecular weight increment between 30 and 29° was approximately 5×10^3 MW units.

Figure 2b is a plot of dissymmetry of light scattering for several fixed electrolyte concentrations as a function of absolute temperature. For systems with NaCl concentrations below the electrolyte transition range at 30°, the dissymmetries converge to a value close to unity at the higher temperatures. For higher electrolyte concentrations (0.18 M NaCl) the dissymmetry rises very sharply as the temperature is lowered. For NaCl concentrations greater than 0.05 M the systems are more sensitive to temperature changes in the low temperature range (5–10°) than in the higher temperature range (25–30°).

C.E.C. Derived from Light Scattering Data.—A graphical analysis of light scattering data of the homogeneous Hyamine 1622-NaCl-H₂O solutions provides a means of predicting the c.e.c. required for two phase formation. For a system of fixed soap concentration, a plot of turbidity versus NaCl concentration¹ shows the following characteristics: (a) the onset of two phase formation is characterized by a sharp linear rise in turbidity; and (b) in a two phase system there is a decrease of turbidity in the soap-rich layer with increasing electrolyte concentration. The sharp rise of turbidity for homogeneous systems which is characteristic of the onset of two phase formation may be utilized to predict the c.e.c. in the following manner: For fixed NaCl concentrations (above the electrolyte transition range) and at fixed soap concentrations, the intensity of the scattered light of the homogeneous system was measured at several angles. Similar data were obtained for several electrolyte concentrations in this range, and plotted as follows.

$(c + c')/R_\theta$ vs. $(\sin^2 \theta/2 + c + c')$ is plotted where c is the molar concentration of the detergent, c' is the molar concentration of the electrolyte, R_θ is the Rayleigh ratio of scattered radiation at angle θ .

The $(c + c')/R_\theta$ for a fixed electrolyte concentration is graphically extrapolated to zero angle.

The zero angle points fall on a straight line. A linear extrapolation of the zero angle points to $(c + c')/R_\theta = 0$ yields an electrolyte concentration corresponding to the c.e.c. of the system. Essentially, the zero angle scattering is extrapolated to infinite turbidity. For very pure monodisperse systems, a very small fraction of the incident radiation is transmitted at the critical point. For the quaternary ammonium salt-electrolyte solutions investigated, the character of these systems in terms of small amounts of impurities and polydispersity is such that the assumption that all of the incident radiation is scattered at zero angle is a fair approximation of the situation.

Figure 3a represents this treatment for a 0.0644 M (3%) Hyamine 1622 solution of NaCl concentrations ranging from 0.2 to 0.31 M . The linearity of $(c + c')/R_\theta$ plot is obtained for NaCl concentrations above the electrolyte transition range (0.17–0.19 M NaCl) previously described. This method correctly predicts the relative constancy of c.e.c. over a wide range of soap concentration and was tested for several concentrations between 0.5 to 5% soap. Figure 3b represents a divalent cation system, Hyamine 1622-BaCl₂-H₂O. The divalent cation effect of increasing the critical anion concentration necessary for two phase formation is predicted quantitatively by this method. Figures 3c and 3d represent the systems Cetol-NaCl-H₂O and HDTAB-KSCN-H₂O, which form coacervates at high and low electrolyte concentrations, respectively. The values of the c.e.c. check within 2% of the c.e.c. values obtained by the standard interpolation method.

Conclusions

A tentative model of the micellar aggregate in the quaternary ammonium salt solutions studied which will account for observed phenomena is the following: In a salt-free solution of Hyamine 1622 and at low NaCl concentrations, the micelles are experimentally isotropic and are of a lower charge density than is common in the many soap and polyelectrolyte systems previously investigated. This relatively lower state of ionization is indicated from the light scattering data, and the small quantity of added NaCl ($\sim 0.05 M$) necessary to achieve theta solvent properties in Hyamine 1622 solutions. Strauss²³ has observed theta solvent effects in sodium polyphosphate solutions at NaBr concentrations of 0.415 M . The polyphosphate systems were estimated to be 30–40% ionized. For cetylpyridinium chloride solutions²⁰ in which the coacervation is not observed, theta solvent effects are observed for NaCl concentrations in excess of 0.4 M . The micellar aggregate in this system is 20–27% ionized. For anionic soaps such as potassium oleate for which the coacervation has been observed at KCl concentrations of the order of 1.6 M , the micellar ionization is 20–30%² in salt free solutions.

There is an apparent lower limit of ionization of the micellar species below which coacervation is not observed in the soap systems investigated. In the system Hyamine 1622-NaI-H₂O flocculation

(23) U. P. Strauss and P. L. Wineman, *J. Am. Chem. Soc.*, **80**, 2366 (1958).

occurs at room temperature for NaI concentrations in excess of the stoichiometric concentration of the soap without a transition through a two solution phase region. The micellar charge density must be sufficient to maintain a potential barrier to coagulation in the entire range of electrolyte added to obtain two phase system. In a theoretical treatment of complex coacervation in mixtures of polycations and polyions Voorn²⁴ has suggested that there is a minimum charge for a given chain length before coacervation is possible. Increasing the chain length reduces the minimum charge necessary for coacervation.

Initial micellar formation and micellar growth with the addition of electrolyte are governed by two forces. The aggregating force is Van der Waal's association of the non-polar portion of the soap molecules. The balancing repulsive forces are the coulombic interactions of charged micellar sites of similar charge.

The addition of electrolyte may alter the coulombic interactions in three ways: (a) the intermicellar charge interactions may be screened; (b) the degree of ionization may be altered (no distinction is made here between bound counterions and ion pair formation); (c) where adjacent charge sites on the micelle are sufficiently separated, the intra-micellar coulombic interactions may be critically damped.

The properties of Hyamine 1622-NaCl solutions suggest that theta solvent properties ($>0.05 M$ NaCl) are associated with (a) inter-micellar screening effects, and the electrolyte transition range ($0.17-0.19 M$ NaCl) characterized by a large micellar growth is associated with (b) the ionization properties and (c) the intra-micellar charge screening effects. The large micellar growth with small electrolyte increments at high electrolyte concentrations is a further indication of the reduced role of intra-micellar coulombic interactions.

For electrolyte concentrations above the transition range, micellar shape is essentially governed by Van der Waal association, solvation of the bound ions and ionized polar heads, and steric effects related to the size and nature of the polar heads, with intra-micellar coulombic effects playing a very much reduced role. A cylindrical model of the micelle with polar heads and bound ions on the surface of the cylinder and the non-polar tails oriented toward the interior of the cylinder is consistent with the observations of the Hyamine 1622 solutions.

The observed temperature effects are consistent with the proposed model. At low fixed NaCl concentrations, intra-micellar charge effects are sufficiently operative so that small temperature increments produce relatively small changes in the system over the range of temperature investigated ($5-30^\circ$). For fixed NaCl concentrations at higher levels, close to the electrolyte transition range at room temperature, the large difference between the properties of these solutions at the lower and higher temperatures may be associated with the damping of the intra-micellar coulombic interactions at lower temperatures.

Michelli, Voorn and Overbeek¹³ have shown

(24) M. J. Voorn, *Rec. trav. chim.*, **75**, 317, 405, 925 (1956).

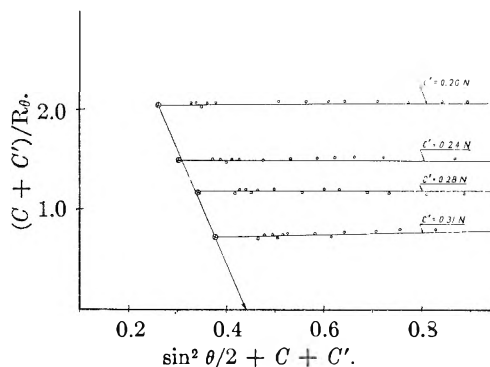


Fig. 3b.—Critical electrolyte concentration derived from the angular dependence of the modified reciprocal reduced intensity, Hyamine 1622-BaCl₂-H₂O system: C = Hyamine concn. = $0.0644 M$; C' = BaCl₂ concn. (normal); $T = 26^\circ$; $\lambda = 4360 \text{ \AA}$.

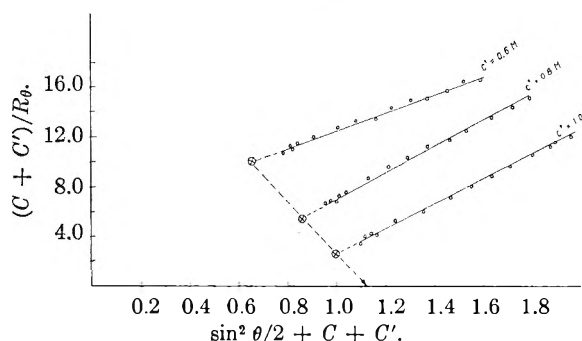


Fig. 3c.—Critical electrolyte concentration derived from the angular dependence of the modified reciprocal reduced intensity, Cetol-NaCl-H₂O system: C = molar concn. of Cetol = $0.005 M$; C' = molar concn. of NaCl; $T = 30^\circ$; $\lambda = 4360 \text{ \AA}$.

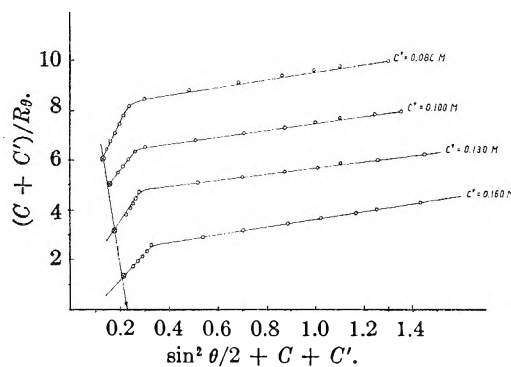


Fig. 3d.—Critical electrolyte concentration derived from the angular dependence of the modified reciprocal reduced intensity, HDTAB-KSCN-H₂O system: C = HDTAB concn. = $0.05487 M$; C' = KSCN concn.; $T = 29.0^\circ$.

that two solution phase formation in complex coacervate systems (polycation-polyanion mixtures) may be explained in terms of electrostatic interactions. The free energy of the system may be represented by an expression consisting of two terms, an electrostatic free energy term and an entropy of mixing term. The electrostatic free energy is independent of particle weight and may be expressed in terms of electrostatic free energy per unit volume of polyion. The entropy term shows an inverse dependence on the length of the polyion rod. For a system consisting of a rod-like assembly

of quasi independent charges of low electrostatic free energy favorable conditions for coacervation require a low entropy of mixing.

In the Hyamine 1622-NaCl solutions, assuming cylindrical micellar model, the large micellar growth that occurs prior to the onset of two phase formation, with small NaCl increments, results in a marked elongation of the cylinder. Hence, a sharp decrease in entropy of mixing ensues without a concurrent large change in the charge properties of the system. Where the entropy of mixing decreases sufficiently, coacervation will occur. The smaller charge effects are in the direction of reducing the micellar charge density. These are cooperative effects that favor coacervation. The mechanism of coacervation in cationic soap systems differs from complex coacervation in mixed poly-electrolyte systems. In the Voorn-Overbeek interpretation of the mechanism of complex coacervation, the primary effect is the reduction of the electrostatic free energy of the system resulting from the mixing of oppositely charged polyions.¹³

It has been previously reported¹ that the coacervate layer, *i.e.*, the soap-rich layer in a two phase system shrinks with further addition of electrolyte in excess of the c.e.c. A distinctive feature of the soap-rich phase is the apparent high degree of ordering of the micellar aggregates. Ordering is indicated by two effects: (a) the turbidity and (b) the dissymmetry of light scattering in the coacervate layer of Hyamine 1622

systems show a sharp decrease with added electrolyte. These effects may be related to destructive interference of the scattered radiation, characteristic of a system with high degree of order.

Current work in progress on viscosimetry, diffusion, flow birefringence and charge properties of cationic soap coacervate systems confirm the general character of the properties of the homogeneous systems indicated from the light scattering studies. The intrinsic viscosities for Hyamine 1622-NaCl-H₂O solutions exhibit no shear dependence for NaCl concentrations below the electrolyte transition range and are shear dependent for NaCl concentrations above the electrolyte transition range. The details of these studies will be published in a later paper.

Acknowledgment.—The authors wish to express their appreciation for support provided by the Department of Health, Education and Welfare, Public Health Service—Grant No. A-2300 (C1 and C2).

DISCUSSION

H. L. BOONJ (Leyden University).—Have you observed elasticity in your systems?

I. COHEN.—The viscous properties of the homogeneous phase of several cationic soap-electrolyte-H₂O systems have been detailed in the following paper of this group. These systems show essentially the same properties as the oleate-electrolyte-H₂O systems investigated by Bungenburg de Jong, *et al.* The term elasticity cannot properly be applied to these systems. The homogeneous phase of the soap-electrolyte-H₂O system at relatively high electrolyte concentration is a free flowing solution of high viscosity.

CRITICAL PHENOMENA IN AQUEOUS SOLUTIONS OF LONG CHAIN QUATERNARY AMMONIUM SALTS. III. VISCOSITY, DIFFUSION AND CHARGE PROPERTIES

By IRVING COHEN AND TONY VASSILIADES

Department of Chemistry, Polytechnic Institute of Brooklyn, Brooklyn, N. Y.

Received July 5, 1961

The viscosity of several aqueous quaternary ammonium salt solutions was studied as a function of added electrolyte and temperature. The intrinsic viscosities of coacervating systems (two solution phase formation) as a function of simple univalent electrolyte concentration show a discontinuity coincident with the electrolyte transition range previously determined from light scattering experiments. For the higher electrolyte concentrations, in excess of the transition electrolyte concentration, the intrinsic viscosity is a linear function of $M^{3/2}$ (micellar molecular weight) and $L/M^{3/2}$ (where L is the long dimension of the anisotropic micellar particle) derived from light scattering data. The temperature dependence and the electrolyte specificity of the electrolyte transition range was investigated by viscosimetry techniques. The self-diffusion coefficient of the cationic micellar soap system, Hyamine 1622, was studied as a function of added sodium chloride by means of the capillary technique, using a dye as an indicator. The electrolyte transition range is characterized by a sharp drop in the diffusion coefficient. The charge properties of coacervating and non-coacervating cationic soap systems were studied at low electrolyte concentration. There is a direct correlation between the charge properties of these systems and their subsequent behavior with further addition of electrolyte. The viscosity, diffusion and charge properties of the coacervating cationic soap systems are consistent with the micellar model previously proposed: at low electrolyte concentration the micelle is dimensionally isotropic and at high electrolyte concentrations the micelle is a cylindrical rod-shaped particle.

Introduction

The viscosity, diffusion and charge properties of dilute aqueous solutions of long chain quaternary ammonium salts have been studied as a function of added simple electrolytes. A number of the micellar systems behave as coacervates in that they separate into two solution phases with the addition of electrolyte. In the coacervating systems, for each electrolyte, at a constant tempera-

ture and constant soap concentration, there is a critical electrolyte concentration (CEC) necessary for two solution phase formation.

The electrolyte specificity and the light scattering properties of these systems have been reported previously.¹ From these studies of the coacervating systems, an electrolyte transition range (ETR) may be described, intermediate between zero elec-

(1) I. Cohen and T. Vassiliades, *J. Phys. Chem.*, **65**, 1774 (1961).

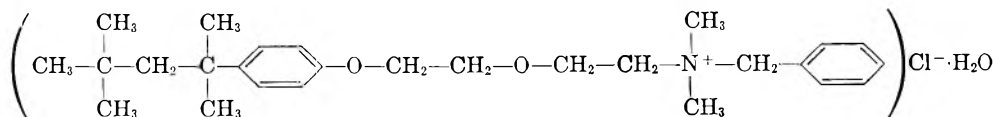
trolyte and the CEC which may be associated with the transition of the micellar solute aggregate from an essentially isotropic to an anisotropic particle. Non-coacervating quaternary ammonium salt solutions do not show this distinctive behavior. The present study is an attempt to further characterize the homogeneous phase of a coacervating aqueous cationic soap system, in terms of properties of the system which are sensitive to size and shape of the solute particles involved.

In addition, previous light scattering studies of the Hyamine 1622-NaCl-H₂O systems have shown unique charge properties. At low sodium chloride concentrations, this system showed a relatively low ionization as compared to a large number of soap systems previously investigated. The study of the ionization properties of aqueous cationic soap-electrolyte solutions has been extended to several related coacervating and non-coacervating systems.

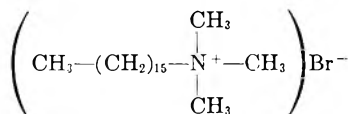
Experimental

Materials.—The following cationic soaps were used in this investigation:

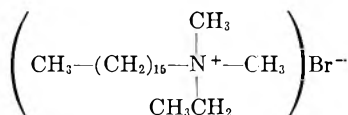
1-Hyamine 1622-di-isobutylphenoxyethoxyethyl dimethylbenzylammonium chloride monohydrate.



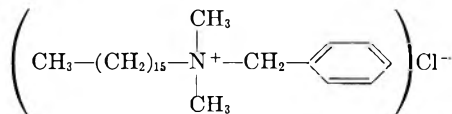
2-HDTAB.—Hexadecyltrimethylammonium bromide



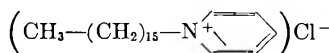
3-EHDDAB.—Ethylhexadecyldimethylammonium bromide



4-Cetol.—Hexadecyldimethylbenzylammonium chloride



5-CPC.—Cetylpyridinium chloride



Hyamine 1622 was obtained from Rohm and Haas and contained 1.5% H₂O as the only appreciable impurity. The hexadecyltrimethylammonium bromide (HDTAB) and the ethylhexadecyldimethylammonium bromide (EHDDAB) were obtained from Eastman Organic Chemicals, the cetylpyridinium chloride (CPC) from Mathe son Coleman and Bell, and the hexadecyldimethylbenzylammonium chloride (Cetol) from Fine Organics, Inc. All the soaps were of technical grade and no further purification was necessary. All inorganic electrolytes used in this investigation were of C.P. grade.

Apparatus and Experimental Techniques

Viscosity.—Viscosity measurements were performed in modified Ubbelohde viscometers as described by Immergut and Schurz.² Equation (1) was used to obtain the constants needed to calculate the kinetic energy corrections

$$\eta = A\rho t + B\rho/t \quad (1)$$

(2) E. Immergut and J. Schurz, *J. Polymer Sci.*, **9**, 279 (1952).

where η is the absolute viscosity, ρ is the density of the solvent at the temperature of the experiment, t is the time of flow through each bulb, and A and B are constants. The absolute viscosity of water at 30.0 and 40.0° is used to determine A and B for each of the bulbs of the viscometers used. Hence, the absolute viscosity in each bulb was first calculated according to equation (1) and from these values the relative, specific, reduced and intrinsic viscosities were determined in the usual manner. The volume of each bulb was measured by weighing the amount of mercury which each contained.

The average rate of shear (β) was calculated from the equation:

$$\beta = 8V/3\pi r^3 t \quad (2)$$

where r is the radius of the capillary, V is the volume of the bulb and t is the time of flow through the bulb being considered. The plots of reduced viscosities versus shear gradient were extrapolated to zero shear gradient.

Diffusion.—The diffusion measurements were carried out by the open-end capillary technique devised by Anderson and Saddington.³ The diffusion cells had an inside diameter of approximately 1 mm. and a height of approximately 5 cm. The diffusing species was labeled by means of a water-insoluble dye, azobenzene.⁴ Hyamine 1622-azobenzene solutions obey Beer's law and show a well-defined absorption peak at 320 m μ . The concentration measurements before and after diffusion were made spectrophotometrically. The diffusion cells were filled by means of a hypodermic needle with the colored material and lowered into a reservoir of

dye-free liquid. The dye-free liquid was maintained in a thermostated bath with a temperature control of $\pm 0.1^\circ$. Ten to fifteen minutes were allowed before diffusion runs were started, so that the diffusion cells could attain temperature equilibrium. Diffusion times ranged from 3 to 8 days.

The solution of Fick's law for the boundary conditions of these experiments is given by the equation

$$D = 0.93321 (L^2/t) \log 0.81055 (C_0/C_{av})$$

where D is the self-diffusion coefficient in sq. cm. per second, L is the length of the diffusion cell, t is the time in seconds and C_0 and C_{av} are the concentrations of the diffusing species in the cell before and after diffusion, respectively.

CMC Measurements.—Critical micelle concentrations were obtained by measuring the refractive index as a function of the soap concentration. The refractive index measurements were made by means of a Zeiss dipping refractometer, using a light source of wave length of 5820 Å.

Micellar Charge.—Micellar charges at low electrolyte concentrations were determined from light scattering data in the manner previously described.¹

Results and Discussion

Viscosity.—The intrinsic viscosity of aqueous Hyamine 1622 solutions as a function of added univalent electrolyte shows the following characteristics:

(a) The Hyamine 1622-NaAc-H₂O system at 30° is a non-coacervating system. From light scattering measurements, it has been determined that with increasing NaAc concentration the micellar aggregate for this system grows to a limiting molecular weight of approximately 54,000. The intrinsic viscosity of aqueous Hyamine 1622 solutions as a function of NaAc concentration (Fig. 1, curve a) shows a slight linear increase to a limiting value corresponding to the limiting micellar weight. The intrinsic viscosity shows no shear dependence for this system.

(3) L. S. Anderson and K. Saddington, *J. Chem. Soc.*, S381 (1949).

(4) H. W. Hoyer and K. J. Mysels, *J. Phys. Chem.*, **54**, 966 (1950).

(b) The Hyamine 1622-NaCl-H₂O system is a coacervating system. At the onset of two-phase formation, the micellar molecular weight increases to approximately 800,000. The plot of intrinsic viscosity *versus* NaCl concentration (Fig. 1, curve b) shows three distinct regions. At low electrolyte concentrations the intrinsic viscosity rises slowly and shows no shear dependence. In the ETR previously identified from light scattering measurements, the intrinsic viscosity rises sharply with small electrolyte increments. For NaCl concentration in excess of ETR, the intrinsic viscosity shows a relatively sharp linear rise with increasing NaCl concentration. In this region the intrinsic viscosity is shear dependent and the rate of shear increases sharply as the CEC of the system is approached.

(c) Temperature changes profoundly effect the ETR of the Hyamine 1622-NaCl-H₂O system. As the temperature is lowered from 36° to 30° and 12°, respectively (Fig. 1, curves c and d), the ETR is shifted to lower values and the increase in intrinsic viscosity in the ETR is more pronounced at the lower than at the higher temperatures. For a given temperature reduction the shift in the ETR to lower concentrations is comparable to the reduction of the CEC that accompanies the same temperature reduction.

(d) the effect of electrolyte specificity upon the intrinsic viscosity of the homogeneous phase of a coacervate system is illustrated by the Hyamine 1622-NaNO₃-H₂O system (Fig. 1, curve e.) NaNO₃ is a more effective coacervating agent in Hyamine 1622 solutions than NaCl.

The ETR for the NaNO₃ system occurs at lower concentration (~0.02 M NaNO₃) than the ETR of the NaCl system (0.17-0.19 M NaCl) at the same temperature (*T* is 30.0°).

Figures 2a and 2b show the relationship of the intrinsic viscosity of the Hyamine 1622-NaCl-H₂O system with micellar molecular weight and the length of the micellar particle derived from light-scattering measurements. For electrolyte concentrations higher than the NaCl transition range, these empirical relationships hold

$$[\eta] = KM^{3/2} \quad (\text{Fig. 2a})$$

and

$$[\eta] = K'L^{3/2}/M \quad (\text{Fig. 2b})$$

where *K* and *K'* are constants, *M* is the micellar molecular weight and *L* is the micellar particle length.

Figure 3 represents the viscosity properties of four C₁₆ long-chain cationic systems which span the whole spectrum of behavior of coacervating and non-coacervating systems of this type. Curve (a) is a plot of intrinsic viscosity of the CPC-NaCl-H₂O system as a function of NaCl concentration. This is a non-coacervating system showing a characteristic limiting micellar molecular weight of 46,000 for a spherically-shaped micelle.⁵ The intrinsic viscosity of this system shows a slight linear rise to a limiting value corresponding to the limiting micellar molecular weight.

Curve (b) is a plot of intrinsic viscosity of the

(5) E. W. Anacker, *J. Phys. Chem.*, **62**, 41 (1958).

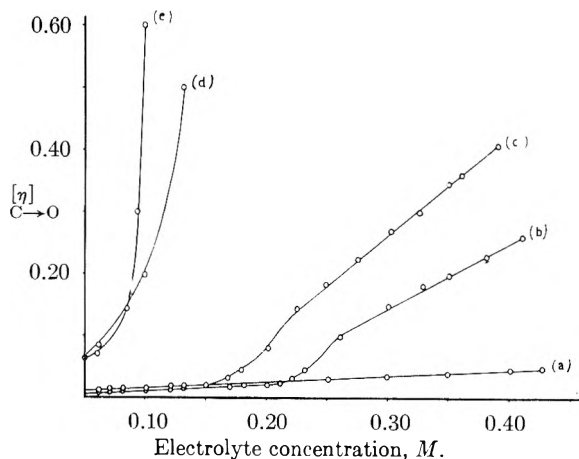


Fig. 1.—Effect of electrolyte and temperature on the intrinsic viscosity of aqueous Hyamine 1622 solutions: (a) Hyamine 1622-Na acetate, *T*, 30.0°; (b) Hyamine 1622-NaCl, *T*, 36.0°; (c) Hyamine 1622-NaCl, *T*, 30.0°; (d) Hyamine 1622-NaCl, *T*, 12.0°; (e) Hyamine 1622-NaNO₃, *T*, 30.0°.

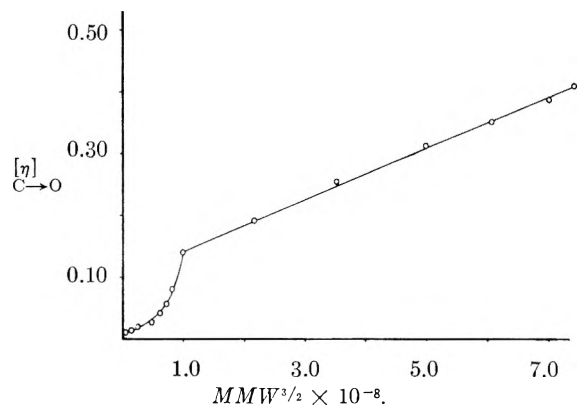


Fig. 2 (a).—Intrinsic viscosity at zero shear gradient *versus* *M*^{3/2} where *M* is the micellar molecular weight for the system Hyamine 1622-NaCl-H₂O.

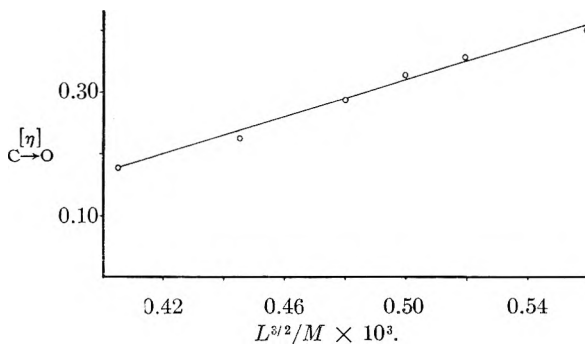


Fig. 2 (b).—Intrinsic viscosity at zero shear gradient *versus* *L*^{3/2}/*M* for the Hyamine 1622-NaCl-H₂O system; *L* is the micellar particle long dimension; *M* is the micellar molecular weight.

HDTAB-KBr-H₂O system as a function of KBr concentration. This is a non-coacervating system in saturated KBr solution. For KBr concentrations in excess of 0.17 *M*, the micellar particle shows a considerable dimensional anisotropy.⁶ The intrinsic viscosity of this system in a non-linear

(6) P. Debye and E. W. Anacker, *J. Phys. and Colloid Chem.*, **55** 644-655 (1951).

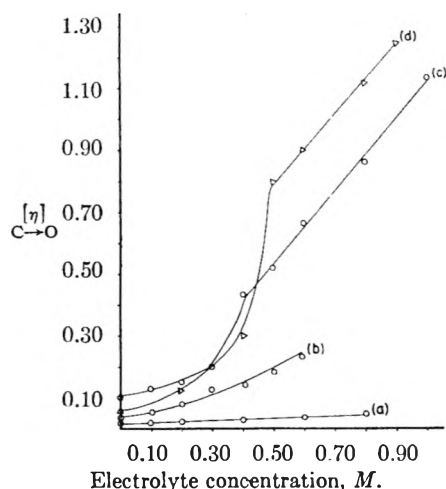


Fig. 3.—Variation of intrinsic viscosity at zero shear gradient with addition of electrolyte for soap-electrolyte- H_2O systems: (a) CPC-NaCl, T 30°; (b) HDTAB- NaNO_3 , T 30°; (c) Cetol-NaCl, T 35°; (d) EHDDAB- NaNO_3 , T 36.0°. The scale for the EHDDAB- NaNO_3 system has been reduced to fit the graph, the true scale being abscissa $\times 5$, ordinate $\times 10$.

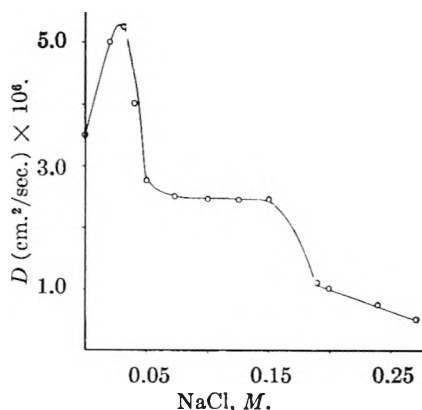


Fig. 4.—The self-diffusion coefficient of aqueous Hyamine 1622-NaCl solutions as a function of the molar concentration of NaCl at constant soap concentration (0.0644 M Hyamine 1622) and constant temperature (T 30°).

function of added KBr. However, there is no evidence of relatively sharp ETR for this system and the transformation of the micellar aggregate from an isotropic entity at low KBr concentration to an anisotropic entity at higher KBr concentration is much more gradual than with typical coacervating systems.

Curve (c) represents the intrinsic viscosity of the Cetol-NaCl- H_2O system as a function of added NaCl. This is a coacervating system showing a well defined ETR (0.3–0.4 M NaCl) and shear dependence of the intrinsic viscosity for higher NaCl concentrations ($>0.4 M$).

Curve (d) represents the EHDDAB- NaNO_3 - H_2O system. This system separates into two solution phases at extremely high NaNO_3 concentrations (the CEC for this system is $\sim 5.0 M$). At the onset of two phase formation, the system shows high dissymmetry of light scattering, in excess of 2.0, and a very high micellar molecular weight, of the order of 2.5 – 3.0×10^6 . The viscosity properties of this system show a typical pattern for a coacervating system, with the NaNO_3 transition

range occurring at high NaNO_3 concentration ($\sim 1.0 M$).

Diffusion.—The self-diffusion properties of the Hyamine 1622-NaCl- H_2O system at 30° and constant monomer concentration were studied in detail. Figure 4 is a plot of the self-diffusion coefficient *versus* NaCl concentration. The essential features of the diffusion properties of this system are the following: (a) At 0.02 M NaCl, the self-diffusion coefficient passes through a maximum value.

(b) Between 0.03–0.17 M NaCl there is a small linear decrease in the self-diffusion coefficient of the micellar species. The small decrease of the self-diffusion coefficient in this NaCl concentration region is consistent with a growing isotropic micellar model previously proposed from light scattering studies.

(c) In the electrolyte transition range, 0.17–0.19 M NaCl, a sharp drop in the self-diffusion coefficient occurs. This decrease in the self-diffusion coefficient cannot be accounted for in terms of micellar growth alone. In large measure, this decrease may be associated with the change in the entropy term of the free energy of activation for the diffusion process related to the transformation of the micellar aggregate from an isotropic to an anisotropic solute particle.

(d) The continued marked decrease of the self-diffusion coefficient for NaCl concentrations in excess of the electrolyte transition range may be associated with the growing anisotropic micellar aggregate.

Critical Micelle Concentration.—The reduction of the critical micelle concentration (CMC) for the Hyamine 1622 and HDTAB systems under the influence of added electrolyte was investigated. Winsor and others⁷ have reported that for anionic soap systems there is no apparent cation specificity associated with the lowering of the CMC. However, with the cationic systems investigated, anion specificity previously encountered for the CEC and the electrolyte transition range is observed in the lowering of the CMC under the influence of added electrolyte (Fig. 5). The upper set of curves represents the initial reduction of the CMC for aqueous Hyamine 1622 solutions with several univalent electrolytes. The more effective an anion is as a coacervating agent, the more pronounced is the initial lowering of the CMC with the addition of the anion to the system. The initial slope of the CMC *vs.* electrolyte concentration curve for the non-coacervating NaAc system as very much less (in absolute value) than the initial slopes for the coacervating electrolytes NaCl, NaNO_3 , NaBr and NaClO_3 . Qualitatively, an approximate critical initial negative slope for these curves may be defined, below which (in absolute value) the electrolyte does not coacervate the system and above which the electrolyte is capable of inducing two phase formation.

The lower set of curves of Fig. 5 are plots of CMC *vs.* electrolyte for the HDTAB system with a CMC in salt-free solution of approximately one-half that of the Hyamine 1622 system. With

⁷ P. A. Winsor, "Solvent Properties of Amphiphilic Compounds" Butterworths Scient. Publ., London, 1954, Ch. 2.

the exception of the NaSCN (curve h), these are all non-coacervating systems. The curves indicate electrolyte specificity and the initial slope of the curves for the non-coacervating electrolytes are comparable with the non-coacervating Hyamine 1622-NaAc-H₂O system.

There is an apparent direct correlation between the effectiveness of an electrolyte as a coacervating agent in an aqueous cationic soap system and its effectiveness in the initial lowering of the CMC of the system.

Micellar Charge Density.—Figure 6 represents plots of p/m micellar charge to soap monomer ratios, versus electrolyte concentration at low electrolyte concentration derived from light scattering data, for aqueous Hyamine 1622 solutions with (a) NaNO₃, (b) NaCl, and (c) NaAc. Curve (d) represents p/m vs. electrolyte for the EHDDAB-NaNO₃-H₂O system. Curve (e) represents the HDTAB-KBr-H₂O system.

The p/m ratio for the non-coacervating Hyamine 1622-NaAc-H₂O system (c) rises non-linearly to a limiting value of 0.24 at 0.07 M NaAc. This is similar to the charge pattern of CPC-NaCl-H₂O,⁴ which rises to a limiting value of 0.27 ± 0.02 .

For the Hyamine 1622-NaCl-H₂O system (b) the p/m ratio shows a maximum of 0.21 at 0.02 M NaCl and drops off to 0.10 at 0.04 M NaCl. The NaCl concentration corresponding to maximum p/m values is coincident with the NaCl concentration corresponding to the maximum self-diffusion coefficient of Fig. 4. The relationship between the charge properties and the diffusion coefficient maximum at low electrolyte concentrations may be considered to be the following: in the absence of added electrolyte, the diffusion rate of the isotropic micellar species is determined by the size of the micelle and the micellar charge density. Initially, the addition of electrolyte results in a small micellar growth, increased micellar ionization and an increase in the gegenion concentration with contributions from greater ionization and the added electrolyte. The initial increase in the rate of diffusion may be associated with two effects, (a) the partial screening of the intermicellar coulombic forces and (b) the effect of "drag" of the faster moving gegenions on the micelles to satisfy the requirement of electroneutrality throughout the solution. The suppression of micellar ionization resulting from the further addition of electrolyte depresses the latter effect and further suppresses the inter-micellar coulombic interactions. The resulting diffusion properties of this system for the NaCl concentration range 0.04–0.17 M are those of relatively non-interacting growing isotropic particles.

The Hyamine 1622-NaBr-H₂O and Hyamine 1622-NaNO₃ (curve a) systems show a common p/m maximum which occurs at lower electrolyte concentration than the NaCl system, 0.015 M NaBr or NaNO₃. The coincidence of the p/m versus electrolyte concentration curves for the NaBr and NaNO₃ systems is reported for other properties of the two systems. The lowering of the CMC, the minimum electrolyte required for theta solvent properties in the system, the ETR and the

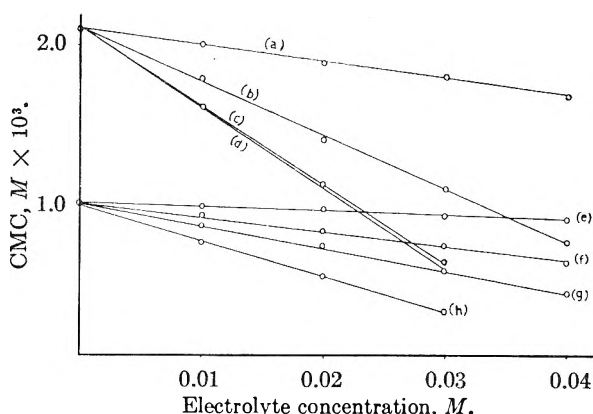


Fig. 5.—Reduction of critical micelle concentration with addition of electrolyte, T 30.0°: (a) Hyamine 1622-Na acetate; (b) Hyamine 1622-NaCl; (c) Hyamine 1622-NaNO₃; (d) Hyamine 1622-NaBr; (e) HDTAB-NaClO₄; (f) HDTAB-NaNO₃; (g) HDTAB-NaBr; (h) HDTAB-NaSCN.

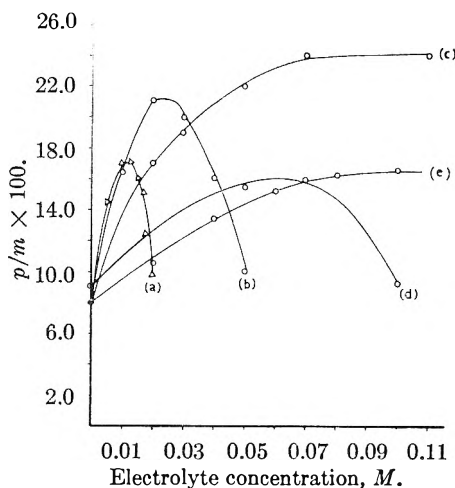


Fig. 6.—Variation of micellar charge density (p/m) with addition of simple univalent electrolyte: (a) Hyamine 1622-NaNO₃, T 30.0°; (b) Hyamine 1622-NaCl, T 30°; (c) Hyamine 1622-NaAc, T 30°; (d) EHDDAB-NaNO₃, T 36°; (e) HDTAB-KBr, T 30°. Micellar charges (p) and aggregation numbers (m) are derived from light scattering data.¹

CEC are substantially the same for the two systems.

Curve (d) for the EHDDAB-NaNO₃-H₂O system shows a broad p/m maximum at a relatively high NaNO₃ concentration, 0.7 M. This p/m maximum is associated with a high theta solvent NaNO₃ concentration of 0.7 M, an electrolyte transition range of 1.0 M NaNO₃ and CEC of 5.0 M NaNO₃.

Curve (e) for the HDTAB-KBr-H₂O system shows initial properties similar to the p/m pattern for the EHDDAB-NaNO₃-H₂O system. However, this curve does not exhibit an ionization maximum and levels off at 0.07 M KBr to a p/m value of 0.15. This limiting ionization is considerably lower than the ionization of the non-coacervating CPC-NaCl-H₂O and Hyamine 1622-NaAc-H₂O systems. This intermediate ionization pattern may account for the special properties of this system, *i.e.*, a relatively large rod-shaped micellar aggregate at high KBr concentrations in a non-coacervating system.

In all of the coacervating cationic soap systems investigated, a critical suppression of ionization of the micellar species with the addition of electrolyte was a precondition for the appearance of an ETR, the large growth of anisotropic aggregates and the subsequent separation of homogeneous solutions into two solution phases.

Conclusions

Viscosity, diffusion and charge properties of the cationic soap electrolyte-H₂O systems studied are consistent with the micellar model proposed from light scattering studies. In an electrolyte-free solution, the micelle is an isotropic entity. The addition of electrolyte induces micellar growth. Initially, there are two general ionization patterns observed in cationic soap systems with the addition of electrolyte. Each of these ionization patterns is associated with a distinctive set of subsequent properties of these systems. (a) For those systems in which micellar dissociation increases to a relatively high value with the addition of electrolyte as observed in Hyamine 1622-NaAc-H₂O and CPC-NaCl-H₂O solutions, the micelle grows to a limiting value and the light scattering and viscosity data are consistent with a spherical model of the micellar aggregate. (b) For those systems in which the micellar dissociation is critically suppressed with small additions of electrolyte, further addition of electrolyte induces an ETR. This ETR is characterized by a micellar transformation from an isotropic to an anisotropic particle. In a comparison of the effect of several electrolytes on a typical system of this type, Hyamine 1622-electrolyte-H₂O, the more pronounced the suppression of micellar dissociation, two subsidiary effects are observed: The ETR is shifted to lower concentrations and the change in the organization of the micelle is more pronounced in the electrolyte transition range. For electrolyte concentrations above the ETR, small electrolyte additions result in a large growth of the anisotropic micellar species with a subsequent separation of the homogeneous phase into two solution phases. The linear relationship of the intrinsic viscosity with $M^{3/2}$ and $L^{3/2}/M$ in this region of electrolyte concentration for the Hyamine 1622-NaCl-H₂O system is consistent with an approximate solvated rod-shaped micellar particle.⁸

A comparison of the non-coacervating HDTAB-

KBr-H₂O system and the EHDDAB-NaNO₃-H₂O coacervating system illustrates an effect of considerable theoretical importance. Debye⁶ has reported rod-shaped micelles for the former 1312 Å. in length at 0.233 *M* KBr. In this case, the intramicellar coulombic interactions are sufficiently depressed with the addition of KBr to permit a large growth of an anisotropic micellar particle while maintaining a sufficient micellar charge to inhibit coacervation even in saturated KBr solutions.

For the EHDDAB-NaNO₃-H₂O system, the ionization pattern shows a broad maximum at a relatively high NaNO₃. The micelle grows to a very large size before two-phase formation occurs. For this system, the very high dissymetry of light scattering indicates that at the onset of two phase formation, the micelle is a cylindrical rod greater than 2000 Å. in length.

Both of these systems show rod-shaped particles in the homogeneous phase which are approximately two times the length of the micellar particles of Hyamine 1622 systems at the onset of two-phase formation. The primary difference between the HDTAB-KBr-H₂O and the EHDDAB-NaNO₃-H₂O systems may be related to their charge properties.

The coacervating EHDDAB-NaNO₃-H₂O system is one of apparent lower charge density than the non-coacervating HDTAB-KBr-H₂O system. The divergent properties of these systems and the properties of coacervating Hyamine 1622-systems may be explained in terms of the Michaeli-Voorn⁹ mechanisms originally proposed for coacervation in polyanion-polycation systems, *i.e.*, coacervation in extended polyelectrolyte systems occurs in low charge density systems and for a given charge density there is a minimum particle length necessary for two phase formation. An examination of the homogeneous phase of several cationic soap-electrolyte-H₂O systems by light scattering, viscosity and diffusion techniques indicates that the initial ionization character of each of these systems at low electrolyte concentrations is the pivotal property to which all subsequent behavior of the micellar system may be qualitatively correlated.

Acknowledgment.—The authors wish to express their appreciation for support provided by the Department of Health, Education and Welfare, Public Health Service Grant No. A-2300 (C1 and C2).

(8) J. J. Hermans, "Flow Properties of Disperse Systems," Interscience Publishers, Inc., New York, N. Y., 1953, Ch. 5.

(9) J. Michaeli, M. J. Voorn and J. Th. G. Overbeck, *J. Polymer Sci.*, **23**, 449 (1957).

ULTRACENTRIFUGAL DETERMINATION OF THE MICELLAR CHARACTER OF NON-IONIC DETERGENT SOLUTIONS. II¹

BY C. W. DWIGGINS, JR., AND R. J. BOLEN

Petroleum Research Center, Bureau of Mines, Bartlesville, Oklahoma

Received March 7, 1961

An analytical ultracentrifuge was used to determine the temperature dependence of the anhydrous, weight-average, micellar molecular weight of a polyoxyethylated nonylphenol in aqueous solutions. Micellar molecular weights were determined several times under different conditions at each temperature. Partial specific volumes were determined at each temperature. The micellar molecular weight of this detergent increased at a rate of 2217 (± 66) molecular weight units per degree in the temperature range of 10.5 to 35.0°.

Introduction

Micelle formation is one of the factors that affect the cleaning efficiency of detergents, and studies of this phenomenon should lead to a more complete understanding of detergency action. Among other applications non-ionic detergents have been used by the petroleum industry as water additives² to increase the production of petroleum.

Both light scattering³⁻⁵ and ultracentrifuge studies⁶ of non-ionic detergents in aqueous solutions have shown that micellar molecular weights are highly dependent on structures of the detergents, but the temperature dependence of micellar molecular weight requires investigation. The analytical ultracentrifuge previously was used to determine anhydrous, weight-average, micellar molecular weights of four non-ionic detergents in aqueous solutions.⁶ This instrument allows control over a wide range of temperatures and is well suited for a study of the temperature dependence of micellar molecular weights.

Theoretical

The transient-state method of determining molecular weights in the analytical ultracentrifuge may be used to avoid independent determinations of diffusion coefficients,^{7,8} and synthetic boundary methods may be used to determine relative optical concentrations without independent determinations of specific refractive increments.⁹ The treatment of the data obtained from the Schlieren optics analytical ultracentrifuge for non-ionic detergents has been given in detail⁶ and will not be repeated here.

The micellar molecular weights of non-ionic detergents in aqueous solutions are expected to change with temperature. Phase separation at the cloud-point temperatures of the detergents suggests, but does not prove, that a significant temperature effect is present.

Although qualitative and semiquantitative treatments of micelle formation have been proposed,

a good quantitative theory is not available. The statistical mechanical treatment of micelle formation¹⁰ is perhaps the most complete theory that has been proposed. However, it would be very difficult to calculate micellar molecular weights or their temperature dependence using this theory. Many of the parameters required for solving the equations would be difficult to determine with the necessary accuracy. In addition, because of the complexity of micelle formation, several assumptions are necessary, and the theory is semi-quantitative at present. The statistical mechanical theory does include a temperature term, suggesting that a temperature dependence of micellar molecular weight is likely.

The molecules of the detergent studied contain varying numbers of oxyethylene groups, and the number of molecules of varying size should be represented by Poisson's distribution formula.¹¹

Fortunately, the transient-state ultracentrifuge methods used allow determination of weight-average, anhydrous, micellar molecular weights.⁶⁻⁸ A chain-length distribution is not necessarily a disadvantage since nearly all commercially available non-ionic detergents are of this type. Studies of detergents having a narrow or no chain-length distribution would be of interest also, but such polyoxyethylene detergents are difficult to obtain.

Experimental

A Spinco Model E analytical ultracentrifuge, equipped with Schlieren optics including a phase-plate diaphragm was used. A rotor temperature indicator control (RTIC) was used, and temperature control to 0.05° was obtained. Double-sector, 12-mm., cells were used for all of the work. The experimental conditions, equipment and techniques have been described.⁶

The detergent studied is a polyoxyethylated nonylphenol and is more than 99% pure surfactant.⁶ This detergent is manufactured under the trade name of Igepal CO-710 by the General Aniline and Film Company.

Solutions of the detergent had to be kept for several days for the numerous studies at various temperatures. It had been noted previously that molds grew in several stock detergent solutions after several days of storage at room temperature.⁶ During early experiments, good reproducibility became difficult, especially in the temperature range of 20 to 30°. Investigation of this problem revealed at least one type of prolific mold growth as well as several classes of bacteria in stored solutions of the detergent. Immediately before use all surfaces in contact with detergent solutions were treated with alcohol and dried to eliminate problems caused by biological contamination. In addition to sterilization of equipment, refrigeration of stored detergent solutions and use of freshly redistilled water were required before satisfactory experimental results could be obtained. In

(1) Presented before the 35th National Colloid Symposium, Rochester, N. Y., June 15-16, 1961.

(2) H. N. Dunning, H. J. Gustafson and R. T. Johansen, *Ind. Eng. Chem.*, **46**, 591 (1954).

(3) A. M. Mankowich, *J. Phys. Chem.*, **58**, 1027 (1954).

(4) P. Debye, *J. Appl. Phys.*, **15**, 338 (1944).

(5) P. Debye, *J. Phys. Chem.*, **51**, 18 (1947).

(6) C. W. Dwiggin, Jr., R. J. Bolen and H. N. Dunning, *ibid.*, **64**, 1175 (1960).

(7) W. J. Archibald, *ibid.*, **51**, 1204 (1947).

(8) H. K. Schachman, "Ultracentrifugation in Biochemistry," Academic Press, New York, N. Y., 1959, pp. 181-199.

(9) S. M. Klainer and G. Kegeles, *J. Phys. Chem.*, **59**, 952 (1955).

(10) C. A. J. Hoeve and G. C. Benson, *ibid.*, **61**, 1149 (1957).

(11) P. J. Flory, *J. Am. Chem. Soc.* **62**, 1561 (1940).

some of the experiments biological contaminants caused non-reproducible results with an apparent reduction of as much as 20,000 molecular weight units after 3 to 5 days of mold growth. As would be expected, the most prolific mold growth occurred at or near room temperature and was, in all probability, some function of seasonal environment. The apparent reduction in micellar molecular weights may have been caused by waste products of the mold changing the refractive indices of the solutions, making the synthetic boundary and transient-state experiments incompatible because of differences in contamination for the two runs. Similar problems also might be met in light-scattering studies.

Occasionally disturbances of the centrifuge produced convection, especially near the lower and upper temperature limits studied. At one time, non-reproducible results were traced to convection caused by sudden, large, line-voltage variations and by sudden changes in room temperature during a period when photographs were not being taken. Convection peaks often had disappeared when photographs for molecular weight determination were taken, but the data gave erroneous results. It was found desirable to make many photographs with the automatic camera during the complete time interval of centrifugation to check for possible convection. Also, temperature was monitored with a bridge circuit and a recorder to check for possible temperature changes. If either convection peaks or temperature variations greater than 0.05° were detected during centrifugation, the data were discarded and the experiment was repeated. Precession should be minimized, because it may give non-reproducible results. An occasional standardization check with a substance of known molecular weight, such as digitonin, proved helpful.

Partial specific volumes were obtained from pycnometric measurements of solution densities at each temperature of interest as previously described.⁶ Bicapillary pycnometers were used for maximum accuracy. The temperature of the pycnometer water-bath was maintained constant to within 0.005° . The densities were converted to specific volume at each temperature. It was found that specific volume varied linearly with composition within experimental error, up to a few per cent. detergent solution as was observed previously.⁶ An equation was fitted to the specific volume *vs.* composition data by the method of least squares for each temperature, and deviations were found to be randomly distributed. The average deviation of individual specific volume data from the lines fitted by least squares ranged from 0.00001 to 0.00005 for the various temperatures. Values of partial specific volume (ml. g.^{-1}) as a function of temperature are given in Table I.

Results and Conclusions

Results of transient-state molecular-weight determinations for a variety of conditions at each temperature are given in Table I. The following straight line was fitted to the means of the weight-average, anhydrous, micellar molecular weight at each temperature *vs.* temperature by the method of least squares

$$M = 2217^\circ + 23,996 \text{ where}$$

$$M = \text{micellar molecular weight}$$

The slope of the straight line, 2,217, represents the increase in micellar molecular weight per degree and has a standard deviation of 66, as determined from the least squares calculations. As would be expected, individual points depart from the line to the largest extent near the temperature extremes studied. Because a high temperature attachment was not available, studies at temperatures above 35° could not be made. The curve should not be extrapolated to temperatures much higher than 35° because abnormal behavior is likely to occur near the cloud-point temperature of the detergent. Furthermore, the temperature-dependence of micellar

TABLE I
PROPERTIES OF IGEPAL CO-710 NON-IONIC DETERGENT SOLUTIONS AND MICELLES AS A FUNCTION OF TEMPERATURE

Temp., $^\circ\text{C.}$	Initial concn., wt. %	Time of run, min.	Micellar mol. wt., ^a $\times 10^{-4}$	Partial specific vol., ml. g.^{-1}
10.5	0.7171	1896	4.98	.893
..	0.7171	2885	4.73	...
..	1.0240	2140	4.91	...
..	1.0240	2740	5.00	...
..	1.6478	1469	5.06	...
..	1.6478	2729	4.86	...
15.0	1.0431	1440	5.38	.902
..	1.0431	1804	5.51	...
..	1.0431	2800	5.33	...
..	1.0469	1080	5.76	...
..	1.0469	2060	5.51	...
20.0	1.0469	1020	6.78	.907
..	1.0469	1380	7.02	...
..	1.0469	1440	6.72	...
22.5	1.0469	480	7.20	.909
..	1.0469	1322	7.48	...
..	1.0469	1442	7.57	...
25.0	0.9870	1440	8.13	.910
..	1.0469	300	7.92	...
..	1.0469	962	7.83	...
27.5	1.0469	450	8.51	.912
..	1.0469	1080	8.43	...
..	1.0469	1440	8.34	...
30.0	1.0469	300	8.96	.913
..	1.0469	960	8.97	...
..	1.0469	1440	8.97	...
35.0	1.0469	422	10.08	.914
..	1.0469	1080	10.32	...
..	1.0469	1440	10.45	...
Schlieren angle— 60°	R.p.m.—9341	Cell thickness—12.00 mm.		

^a Weight-average, anhydrous, micellar molecular weights.

molecular weight may be slightly different for different batches of Igepal CO-710 if the batches differ slightly in average chain-length distribution of oxyethylene groups. The micellar molecular weight determined at 25° was slightly lower than that previously reported for this detergent,⁶ and if significant, this fact suggests such an effect.

DISCUSSION

E. D. GODDARD (Lever Brothers Company).—Dr. Dwiggins might be interested to know that values of micellar weight for various nonylphenol ethylene oxide condensates reported by Schick and Eirich (ACS meeting, St. Louis, April, 1961) are in quite good agreement with his values at 25° —for E. O. contents of 15 to 30, values were around 70,000. An interesting feature about the nonylphenol condensates is that, as in the case of most ionic detergents, any change brought about in the system to decrease the critical micellar concentration leads to an increase in micellar weight, *e.g.*, addition of salt or decrease of E. O. chain length. In the system discussed here, where increased temperature presumably has the effect of lowering the CMC, the same pattern may be seen. Has the variation of CMC with temperature been measured?

C. W. DWIGGINS.—The variation of CMC with temperature was not measured. However, the detergent studied had a CMC of the order of $10^{-4} M$ at 25° .

COLLOIDAL ALUMINA—THE CHEMISTRY AND MORPHOLOGY OF COLLOIDAL BOEHMITE

By JOHN BUGOSH

Industrial and Biochemicals Department, E. I. du Pont de Nemours & Co., Inc., Experimental Station, Wilmington, Delaware

Received March 7, 1961

This will be the first of a series of papers on a new type of film-forming colloidal alumina consisting of fibrillar boehmite particles. Tactoidal structures are formed in the sols, which also show streaming birefringence. Separation of sols into two liquid phases, one of which is paracrystalline, showing permanent birefringence, has been observed for the first time in an alumina dispersion. Such alumina sols can be made by autoclaving an aqueous solution of basic aluminum chloride. Factors such as anion type, anion concentration, alumina concentration, time and temperature of heating are important in obtaining a fibrillar product. The constitution of these alumina sols will be discussed, as well as the methods used for studying their size and shape, and the ionic species present in the sols. Quantitative analytical techniques applied for the first time in the study of alumina sols, such as rate of dissolution in acid and streaming birefringence, will also be outlined. The unique film-forming characteristics of this colloidal alumina will be discussed.

Introduction

Since Gay-Lussac's pioneering work in 1810,¹ various procedures have been available for preparing colloidal alumina sols and gels. Intensive examination of these preparations by the author as well as others²⁻⁷ has shown that, in general, they contain mixtures of particles with different crystalline types and shapes as well as widely varying particle sizes. In addition, the alumina sols often either gel, precipitate slowly or otherwise markedly "age" on standing.

Previous investigators have concentrated on characterizing either the dispersed alumina particle phase by X-ray, electron diffraction or electron microscope^{6,7} or characterizing the primarily ionic intermicellar liquid by conventional physical chemical techniques.⁸⁻¹⁰ In recent years the newer physical methods have been used more extensively than the older classical chemical methods have been.

It is the purpose of this paper to show that colloidal boehmite, AlOOH , can be produced as a fibrous colloid by hydrolysis of basic aluminum chloride or nitrate in water at high temperature. The boehmite so produced consists of stable colloidal fibrils, about 50 Å. in diameter, which are physically analogous to linear, high molecular weight organic molecules. This type of alumina forms sols which are highly viscous, show streaming

birefringence, and can be dried to clear, coherent films.¹¹

Experimental

Starting Materials. Basic Aluminum Chloride.—Basic aluminum chloride solution with an atomic ratio of aluminum to chloride of 2/1 is also called a 5/6 basic solution, and formulas such as $\text{Al}_2(\text{OH})_5\text{Cl}$ are also used, with the understanding that they refer only to stoichiometric relationships and not to the molecular structures of the salts in solution. The ratio may also be expressed in this case as $\text{Al}_2\text{O}_3/\text{Cl} = 1.0/1.0$.

The method used for making basic aluminum chlorides is described by Huehn, *et al.*¹² and Denk.¹³ The method consists of adding one mole of the normal aluminum chloride hexahydrate salt (Mallinckrodt, C.P.) to one liter of water at 60–70°, and then adding aluminum metal powder (Merck) in small increments with good agitation. If an excessive amount of aluminum metal is added to the mixture before the previously added metal has reacted, there is a tendency to form a very viscous, translucent, hard, intractable mass. By varying the amount of aluminum metal added, the basicity of the final product can be easily controlled. For example, to obtain a basic aluminum chloride with an atomic ratio of aluminum to chloride of 1 or 3/3, two moles of aluminum metal would be added to the solution of aluminum chloride described above.

In an attempt to prepare basic aluminum chloride solutions with ratios of Al/Cl greater than 2.0/1, difficulty was encountered, since upon addition of the aluminum metal after passing $\text{Al}/\text{Cl} = 2.0/1$, the products became very viscous and set up to hard, grey masses.

A commercial basic aluminum chloride,¹⁴ "Chlorhydrol," supplied by the Reheis Company, Berkeley Heights, N. J., has also been used. A typical analysis of the dry product was 45.72% Al_2O_3 , 33.27% volatile matter, and 16.58% Cl, corresponding to $\text{Al}/\text{Cl} = 1.98$; supplied as a water solution, the product contained 23.5% Al_2O_3 , 8.18% Cl, corresponding to $\text{Al}/\text{Cl} = 2.0/1$.

Reaction Conditions.—The synthesis conditions which principally affect the character of the product obtained are: (1) acids used, (2) concentration of Al_2O_3 , (3) concentration of acid, (4) ratio of Al_2O_3 to acid, (5) operating temperature, and (6) temperature-time relation.

The acid radicals which have been used are those of strong mono-basic acids which have a dissociation constant greater than 0.1 at 25°, such as hydrochloric, nitric or perchloric.

The concentration of alumina as Al_2O_3 can be widely varied without greatly modifying the character of the products produced. The upper limit on the alumina concentration is fixed by the excessive, irreversible aggregation of the product. If a concentration of more than about 1.6 M Al_2O_3 is used at temperatures below about 250°, the products may be badly and irreversibly aggregated. We obtained good results with the concentration of alumina varied between 0.05 and 1.6 moles per liter when temperatures below 250° were used.

- (1) Gay-Lussac, *Ann. chim. phys.*, **74**, 193 (1810).
- (2) L. Gmelin, "Handbuch der anorganische Chemie," 8th Ed., 35B-Aluminum, Leipzig, 1934, pp. 98–123.
- (3) R. Fricke and G. F. Huttig, "Handbuch der allgemeinen Chemie," IX, Hydroxyde and Oxyhydrate, Leipzig, Section 12, 1937, pp. 57–113.
- (4) A. S. Russell, *et al.*, "Alumina Properties," Technical Paper No. 10 (Revised), Aluminum Co. of America, Pittsburgh, Pa., 1956.
- (5) F. J. Shipko and R. M. Haag, AEC R and D Report KAPL-1740, General Electric Co., July 10, 1957.
- (6) H. B. Weiser, "Inorganic Colloid Chemistry," Vol. II "The Hydrous Oxides and Hydroxides," John Wiley and Sons, Inc., New York, N. Y., 1935, Chapter III.
- (7) P. Souza Santos, A. Vellejo-Freire and H. L. Souza Santos, *Kolloid-Z.*, **133**, 101 (1953); J. H. L. Watson, J. Parsons, A. Vellejo-Freire and P. Souza Santos, *ibid.*, **140**, 102 (1955); Sho Suzuki, *ibid.*, **156**, 67 (1958); Z. Y. Berestneva, *et al.*, *Kolloid Zhur.*, **13**, 323 (1951).
- (8) R. B. Dean, "Modern Colloids," D. Van Nostrand, New York, N. Y., 1948, Chapter II.
- (9) A. W. Thomas, "Colloid Chemistry," McGraw-Hill Book Co., New York, N. Y., 1934, Chapter VII.
- (10) W. Pauli and E. Valko, "Elektrochemie der Kolloide," J. Springer, Wien, 1929, pp. 540–546.

- (11) J. Bugosh, U. S. Patent 2,915,475, Dec. 1, 1959 (du Pont).
- (12) H. Huehn, *et al.*, U. S. Patent 2,196,016, April 2, 1940.
- (13) G. Denk and J. Alt, *Z. anorg. allgem. Chem.*, **269**, 244 (1952).
- (14) Manufacturers' literature, "Chlorhydrol, 1958."

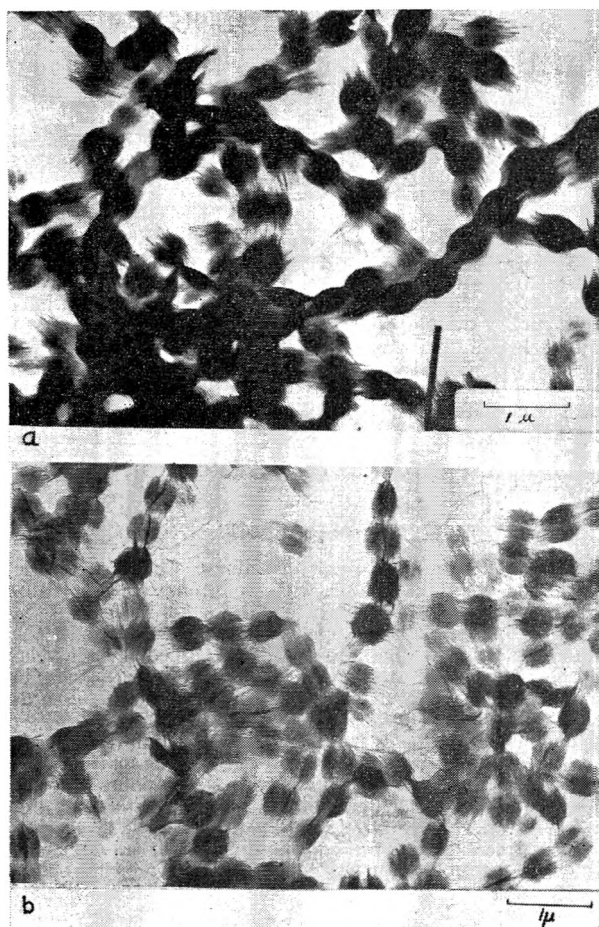


Fig. 1.—Electron micrograph of precipitated tactoids of fibrous colloidal boehmite.

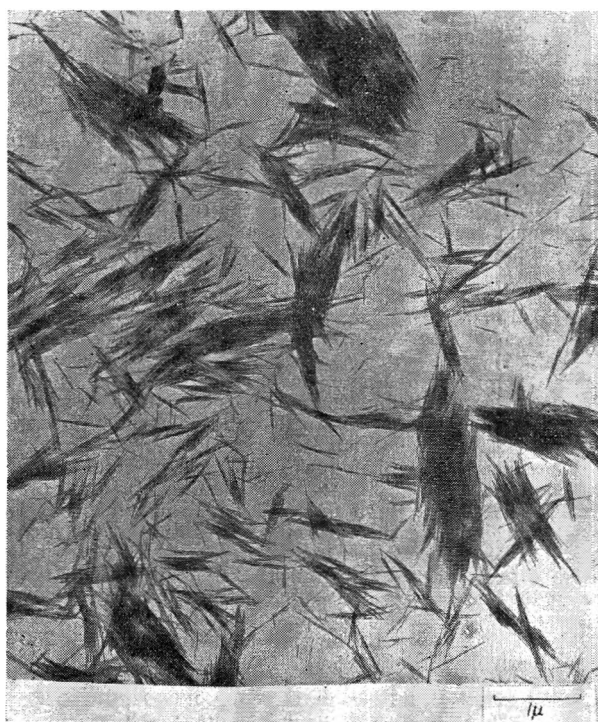


Fig. 2.—Electron micrograph of less aggregated tactoids of fibrous colloidal boehmite.

Our results also indicate that the upper limit of the acid anion concentration should not exceed 4.2 *M*, and should preferably not be below 0.05 *M*.

The relative proportions of alumina to acid radical can be varied, but an aqueous dispersion in which the molarity of the acid radical is from 0.5 (Al_2O_3) to $(\text{Al}_2\text{O}_3) + 0.2$, where (Al_2O_3) is the alumina molarity in the aqueous dispersion calculated on the basis of Al_2O_3 has given reproducible results.

The higher the reaction temperature, the shorter the time required to effect formation of a fibril of a given character. In general, if a temperature around 220° is used, heating for a few minutes up to an hour or so will be sufficient, while at about 160°, fibrils of increasing length are obtained with times from, say, about one-half hour to about one day.

If a typical aqueous solution containing 2% Al_2O_3 , supplied as basic aluminum chloride, and having an Al_2O_3 :chloride ion mole ratio of 1:1 is heated at 160° for four hours a viscous translucent sol will be obtained.

If the concentration of alumina is increased, a very thixotropic but still opalescent gel will be obtained with concentrations of Al_2O_3 of 3 and 4%. As the concentration is raised above about 4 or 5%, the products become more aggregated.

Typical Preparations of Fibrous Colloidal Boehmite.—(A) A typical preparation of fibrous colloidal boehmite as a precipitate is as follows:

A basic aluminum chloride with a molar ratio of $\text{Al}_2\text{O}_3/\text{Cl} = 2/3$ prepared by the method described above showed that it contained, on a weight basis, 15.4% Al_2O_3 and 8.05% Cl which corresponds to a molar ratio $\text{Al}_2\text{O}_3/\text{Cl}$ of 0.67/1.00, and an alumina molarity of 1.86.

Five volumes of this solution were diluted up to a total of 100 volumes with distilled water and the mixture shaken. The concentration of alumina in this solution was 0.093 *M* (as Al_2O_3) while the chloride molarity was 0.140. This water clear solution had a pH of 4.08. It was then placed in a sealed glass container and autoclaved for five hours at 160°. Upon cooling, the material removed from the autoclave contained a white precipitate which, upon electron microscopic examination and X-ray diffraction examination was shown to contain very long hair-like fibrils of alumina monohydrate having the boehmite crystal lattice. Practically all of these fibrils of boehmite alumina had formed "tactoids" by a sidewise parallel alignment, and these small tactoids had, in addition, aligned themselves in an end-to-end fashion to produce very long fiber bundles of boehmite alumina. Two preparations of this type are shown in Fig. 1.

(B) The colloid may be prepared in less marked tactoidal form as follows:

A basic aluminum chloride solution was made as described above, containing by analysis 8.00% Al_2O_3 and 8.43% Cl. After 10-fold dilution the solution had an alumina content equivalent to 0.09 *M* as Al_2O_3 , and a molarity of the acid radical, chloride, of 0.271.

The solution was heated in a sealed glass container at 160° for 16 hours. During this heating, fibrous boehmite precipitated in the initially water clear solution. The fibrous boehmite was readily dispersed upon gentle shaking, and in an electron micrograph appeared as in Fig. 2.

(C) Fibrous boehmite as a sol rather than as a precipitate is obtained as follows. A basic aluminum chloride solution containing 24% Al_2O_3 and an Al_2O_3 :Cl atomic ratio of 1:1 was diluted to 3% Al_2O_3 and this water-clear solution was placed into a Pyrex autoclave reactor fitted with a spiral vented capillary top. The autoclave reactor was surrounded with water and the combination was heated up in 4 hours to 160° and held at that temperature for 3.75 hours. The autoclave and contents were then cooled to about 58°.

The product was a semi-rigid gelatinous mass which readily liquefied upon agitation, and became pourable. The sol showed flow birefringence between crossed "Polaroid" sheets and the electron micrograph, as shown in Fig. 3, shows micron-long fibrous particles were slightly aggregated in a side-to-side fashion.

Methods of Characterization. Specific Surface Area.—The specific surface areas of dry powders were measured by using the Brunauer-Emmett-Teller (BET) method of nitrogen adsorption. To obtain a dry powder, the sols or gels were mixed with several volumes of *n*-butanol or *n*-propanol, fully dehydrated by azeotropic distillation, and then heated in an autoclave to 300° and the alcohol slowly vented. After being cooled in the closed autoclave, the powder was then vacuum dried at 110°. ¹¹

X-Ray Diffraction.—The X-ray diffraction patterns were determined on a North American Phillips Co. wide range goniometer equipped with a Geiger tube and Brown recorder.

Electron Photomicrographs.—For routine examination of samples, a water dispersion of the alumina is diluted to a concentration of about 0.01–0.1 and then part of a drop dried on a microscope screen. Formvar or silica supports have commonly been used with either an RCA EMU-2 or an EMT electron microscope.

Rate of Solution in Acid.—Fibrous colloidal boehmite displays considerable resistance to acid attack.

The stability of fibrous colloidal alumina can be examined by measuring the rate at which the product dissolves in strong acid. The rate is expressed as the time in minutes, Θ , required to dissolve half of the product in acid.

The Θ value can be determined as follows. An amount of the alumina sample equivalent to 4.8 g. of Al_2O_3 is weighed out. One hundred and eleven milliliters of 5.0 N HCl is heated to 98°. The mole ratio of acid to alumina is thus 12:1. Distilled water sufficient with the alumina and acid to make a total of 200 g. is measured out. The water is added to the alumina sample and the mixture is heated to 98°. The diluted alumina sample and acid are mixed, stirred and transferred to a stoppered bottle and placed in a controlled temperature bath held at 98°. If the alumina sample is a sol or dispersion which is not stable or which is not readily prepared at a concentration such that 4.8 g. as Al_2O_3 can be contained in the amount of water involved in this technique, then the amounts of acid and alumina can be reduced but maintained in the ratio of 12:1 moles as above.

Ten gram samples are taken at intervals. Each is diluted to 100 g. with distilled water and quenched to 25° to arrest depolymerization. Each is titrated immediately with 0.5 N sodium hydroxide.

One sample is taken immediately and others are taken at measured time intervals of about, say, three to five minutes. If it is found that the sample is rapidly depolymerized then a special effort can be made to effect titration as soon as possible after adding the acid to the alumina and as frequently as possible thereafter. If the sample is more slowly depolymerized then the time intervals can be extended.

The results of the titration are interpreted as in the determination of the concentration of a weak acid in the presence of a stronger one. As the base is added to the system any excess of the unreacted hydrochloric acid is first neutralized with the base until the pH rises rather rapidly to about pH 3.5. The aluminum chloride, or other aluminum salt, acts as a buffer and the pH does not rise further until it has been neutralized. The titration is continued until the pH rises to about 8. More precisely the inflection point is reached at 7.25. The moles of sodium hydroxide used to effect neutralization between pH 3.5 and 7.25 is then divided by 3 to give moles of aluminum ion in the system. This type of titration is discussed in greater detail by Treadwell, *et al.*¹⁵

The sols comprise various amounts of alumina in three states of polymerization. There will usually be some unpolymerized alumina, some partially polymerized "nuclei," and of course, the fully polymerized product. A complex plot is obtained when the per cent. of soluble alumina is plotted against time. The plot for a sol such as sample C is shown in Fig. 4.

Two factors should be noted: (1) The intercept at zero time, point *x*, on the per cent. alumina axis is not equal to zero; (2) the relationship is not linear.

The curved nature of this plot results from the fact that the dissolution of the colloidal particle is a surface reaction. A correction must therefore be applied to the per cent. of alumina dissolved which will compensate for the apparent slowing down of the reaction as the particle dissolves, and the available surface for reaction gradually decreases. It can be shown from theoretical considerations that in the case of fibers this correction is given by the expression

$$F = (100 - \% \text{ Al}_2\text{O}_3 \text{ dissolved})^{1/2}$$

where *F* is the fraction of the initial surface area remaining at the time that the dissolved alumina was determined by titration. Figure 5 illustrates the application of this correction, and in this figure the per cent. of alumina has been divided by *F*. It will be noted that the line is now essentially straight.

(15) Treadwell, *et al.*, *Helv. Chim. Acta*, **15**, 980 (1932).

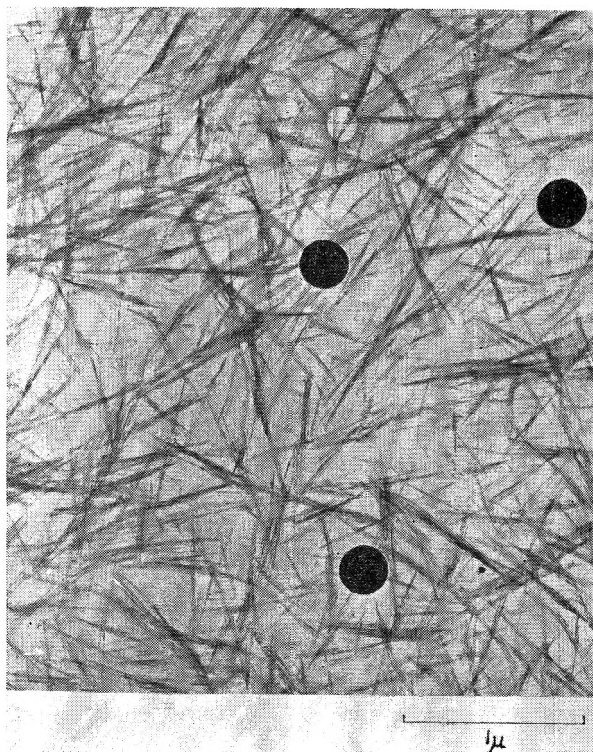


Fig. 3.—Electron micrograph of fibrous colloidal boehmite from a thixotropic sol. Black spheres are standard latex particles 280 m μ in diameter.

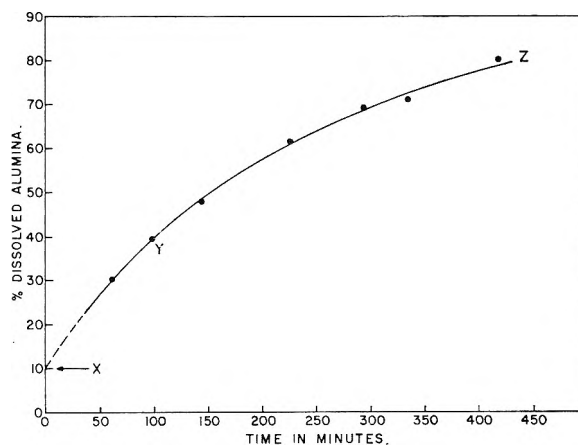


Fig. 4.—Rate of dissolution of fibrous colloidal boehmite in acid.

As mentioned above, various amounts of unpolymerized alumina may remain at the completion of the autoclaving step. It is for this reason that the per cent. alumina dissolved does not equal zero at zero time. The unpolymerized alumina present at the beginning of the titration appears as such even before any of the product has depolymerized.

If this alumina is subtracted from that determined at all other times, a plot similar to that shown in Fig. 6, having a slightly different slope, will result. The value for Θ for this sample is 180.

Properties of Fibrous Colloidal Boehmite.—The characteristics and properties of a typical preparation were as follows.

Specific Surface Area.—To determine the specific surface area, a portion of the sol was transferred azeotropically to 1-butanol and heated to 300° and vented. The dry white product contained 81.08% Al_2O_3 , 1.56% chloride, and 5.2% carbon and had a nitrogen surface area of 318 m²/g. An electron micrograph showed that the fibrillar nature of the material was unchanged.

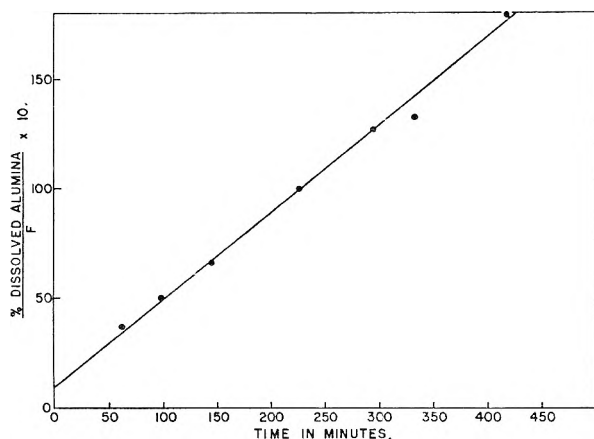


Fig. 5.—Data of Fig. 4 corrected for effect of progressively lowered surface area.

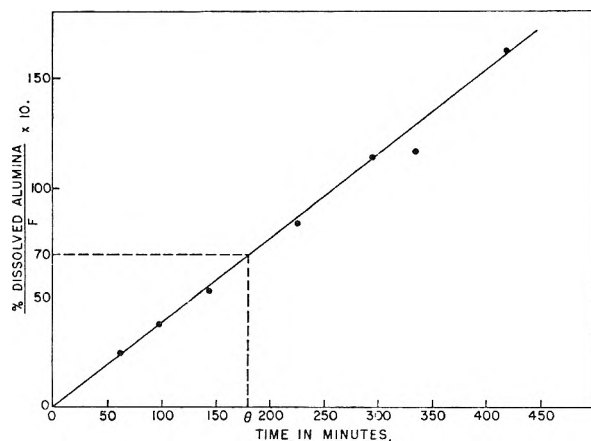


Fig. 6.—Rate of dissolution of colloidal boehmite showing determination of value of "theta."

X-Ray Diffraction.—As shown in Table I, the diffraction lines of fibrous colloidal boehmite are comparable with those of macroscopically crystalline boehmite except for the broadening of the lines characteristic of a colloid. The smallest average particle dimension calculated from line broadening is of the same order as the fibril width estimated from electron micrographs and also calculated from specific surface area, *viz.*, 4 to 7 μ .

TABLE I

X-RAY DIFFRACTION DATA—FIBROUS COLLOIDAL BOEHMITE

d (\AA)	Line width at half max. intensity (degrees 2θ) ^a	I/I_0
6.23	2.24	100
3.17	2.80	20
2.35	1.68	34
1.86	1.40	41
1.85	1.44	41
1.435	1.44	15
1.38	1.68	9

^a Line width for 5 to 20 μ α -quartz ranged from 0.20 at 4.27 \AA . to 0.30 at 1.54 \AA .

Streaming Birefringence.—Suspensions and sols of fibrous colloidal boehmite have the property of streaming birefringence. When a sol of one or two per cent. concentration is agitated, while viewed between crossed polarizers, orientation of the fibrillar particles due to velocity gradients is readily observed. Procedures have been described elsewhere,¹¹ for measuring quantitatively the flow-birefringence of sols and thence calculating fiber length. In Sample C the length measured by flow birefringence was 1200 μ .

The Separation of the Paracrystalline Phase.—When excess chloride is removed from a thixotropic sol such as

Preparation C, with an ion-exchange resin, *e.g.*, according to the procedure described by Dalton, *et al.*,¹⁶ and then allowed to stand undisturbed for a few hours, a distinct liquid layer separates on the bottom of the vessel. The phase boundary is as sharp as between a non-polar oil and water, and can be readily seen between crossed polarizing sheets, since the bottom layer is permanently birefringent while the upper phase is birefringent only upon flow. This effect is independent of the particular method used to deionize a sol, but in addition to ionic content, the effect also depends upon concentration of alumina, particle length and the state of aggregation of fibers.

Although this phenomenon has been observed before for fibrous particles such as tobacco mosaic virus,¹⁷ vanadium pentoxide sol,¹⁸ and platelet particles such as bentonite,¹⁹ it is believed that this was the first time such a phase separation was observed for a colloidal alumina.

The essentially transparent upper and lower phases are in equilibrium, and the ratio of concentrations of alumina in the lower to the upper phase is about 1.5:1.0. When portions of the lower phase, *e.g.*, containing 4.25% solids, are removed and progressively diluted with water containing the same acid anion and pH as the sol, the volume of lower phase progressively diminishes and that of the upper phase increases, as shown in Table II. The samples are viewed between sheets of crossed "Polaroid" so that the lower, permanently birefringent phase can be seen.

TABLE II

PROGRESSIVE DILUTION OF PARACRYSTALLINE LIQUID PHASE

Total % solids	4.3	3.7	3.0	2.6	2.3
Volume % lower phase	100	92	86	81	69
Total % solids	1.8	1.5	1.3	1.0	0.8
Volume % lower phase	47	22	3	1	0

P. J. Flory²⁰ calculated that for very long particles the ratio of concentrations in lower to upper phases should be about 1.56. Characteristics of the paracrystalline phase and conditions necessary for its separation will be discussed in a further communication.

Some Properties of Fibrous Boehmite Sols. Viscosity and Thixotropy.—As prepared, a sol such as Sample C is semigelled, but becomes quite fluid when stirred or shaken. On standing, gelling again occurs. Liquefaction by stirring and gelling upon standing can be repeated indefinitely. Deionization of this sol reduces the apparent viscosity and increases the thixotropic gel-time. A high degree of thixotropy, with shorter gel time, can again be obtained with the sol if the pH is adjusted to 5-6.5. Raising the pH to 7-8 immediately yields a gel. This neutral gel is a thixotropic paste, which retains a stable consistency, becoming fluid when stirred but solidifying immediately when at rest.

The sols are viscous when made, and therefore difficult to concentrate by evaporating water. However, they can be concentrated if they are first deionized, so that the thixotropic viscosity is reduced. However, in any case, viscosity becomes very high and gelling occurs when the concentration exceeds 10 or 15% Al_2O_3 .

Films.—When a fibrous boehmite alumina dispersion is dried on a surface, a clear coherent film is formed. This film-forming characteristic is a direct consequence of the fibrous nature of the ultimate particles. Presumably there is a considerable amount of interparticle association through the hydroxyl groups on the surface. In spite of the fact that the film is transparent, the ultimate fibrillar nature can still be seen by electron micrographic examination.

Films several mils thick are readily prepared by casting a dilute sol onto a glass surface coated with a parting agent such as a thin film of silicone grease. Translucent to transparent films have been made which remain coherent and transparent to 95°. This result was unexpected since the boehmite originally in the film is first transformed to almost

(16) Dalton, *et al.*, U. S. Patent 2,733,205, January 31, 1956.

(17) G. Oster, *J. Gen. Physiol.*, **33**, 445 (1950).

(18) H. Zocher and D. Goldstein, *Anais Assoc. Brasil. Quim.*, **8**, 20 (1949).

(19) A. Isihara, *J. Chem. Phys.*, **19**, 1142 (1951); L. Langmuir, *ibid.*, **6**, 873 (1938).

(20) P. J. Flory, *Proc. Roy. Soc. (London)*, **234A**, 73 (1956).

anhydrous γ -alumina at about 400° and to Θ -alumina at about 950°. The result is understandable, since fibrous boehmite alumina powder was heated at these same temperatures and examined with the electron microscope; both heated samples had retained the fibrous character of the original boehmite.

Fibrous boehmite films when air-dried are water sensitive, *i.e.*, are softened and partially reprecipitated. Under these conditions there are apparently very few Al-O-Al bonds formed between the particles to promote insolubility. Insoluble, harder, as well as chemically non-reactive films are

obtained, however, after baking for a few minutes at 350–400°. Such films are very insoluble in water and dissolve only very slowly in warm concentrated hydrochloric acid.

Acknowledgments.—The writer would like to express his appreciation to R. Fisher, J. F. Godlewski and V. H. Keirstead for preparing the electron micrographs and to A. F. Biddle and O. E. Schupp for aid with electron diffraction and X-ray studies.

CASEIN INTERACTIONS AND MICELLE FORMATION¹

BY DAVID F. WAUGH

Department of Biology, Massachusetts Institute of Technology, Cambridge, Mass.

Received March 7, 1961

The colloidal particles of milk, the calcium caseinate micelles, are thoroughly familiar to us through everyday contact, ready accessibility, and abundance, the rate of production and consumption in the United States being measured in millions of kilos of micelles per day. As familiarity with the micelle system increases there develops an appreciation of the complexity of the properties of the system and of the structures and interactions of the constituent components which, it turns out, number upwards of eight if one includes only casein proteins² and calcium ion.

Information concerning the number and properties of all of the individual components is far from complete. This is due in large part to the fact

that, even in the absence of calcium or other divalent cations, most of the major protein components interact strongly with each other, the structure, stability, and composition of the interaction product being dependent on the number and concentrations of the interacting components, adjustable conditions such as pH, ionic strength and temperature, and on the past history of the preparation (for example, acidification increases the stability of some interaction products). Certain stable association products behave as single components. Our chief concern here will be not with the properties of the individual components but primarily with the specific interactions which are a prerequisite for micelle formation: namely the interactions between α_2 -caseins, κ -casein and divalent cations. Attention will be given to β -casein since the manner in which β -casein enters the micelle structure suggests a secondary specific interaction. We take, until quantitative data are available, the relative abundances of the major components as 55% α_2 -caseins, 15% κ -casein and 35% β -casein, noting that these are estimated to account for about 80% of the total caseins.

The properties of the micelles in milk are an unusual group combination. First, the micelles are in rapid equilibrium with their constituent components and complexes in solution; second, certain combinations of individual components such as the α_2 -caseins and calcium ion are only slightly soluble; third, the micelle population may have a broad size range depending on the concentrations and relative abundances of the components³; and fourth, an enzymatic alteration in κ -casein alone is sufficient to produce the phenomena associated with clotting.

Equilibrium properties of the micelle system may be studied conveniently by subjecting an aliquot to high field centrifugation (140,000 $\times g$, 50 min.) with subsequent determination of the distribution of casein protein between centrifugable and non-centrifugable forms. Using this technique it was found some time ago (see ref. 6) that (a) the addition of calcium ion progressively decreased the amount of non-centrifugable caseins; (b) dilution with physiological saline progressively increased the non-centrifugable casein, and (c)

(1) Carried out under research grants from the Molecular Biology Program of the National Science Foundation and the Division of Research Grants, National Institutes of Health, Department of Health, Education and Welfare.

(2) Procedures for the isolation of certain specific major casein components; namely α_1 -casein, α_2 -casein, κ -casein and β -casein will be described elsewhere. These components have been prepared in pure form according to evidence derived from starch gel electrophoresis, amino acid end group analyses, analyses for specific chemical groupings such as disulfide (present only in κ -casein), and behavior on diethylaminoethyl cellulose columns. The preliminary fractionation procedure was based on the work of von Hippel and Waugh⁴ and Waugh and von Hippel⁵ and utilized the instability of α_2 - κ -complexes at low temperatures and the relative solubilities of α_2 -caseins, β -casein, and κ -casein in the presence of calcium ion at 2 and 37°. Subsequent fractionations utilized ultracentrifugation and DEAE columns run in the presence of urea to dissociate complexes. These procedures, and some of the properties of the resulting products, have been worked out at the Massachusetts Institute of Technology in collaboration with Dr. J. Morton Gillespie (Commonwealth Scientific and Industrial Research Organization, Wool Research Laboratories, Division of Protein Chemistry, Victoria, Australia); Dr. Jean Garnier (Ministere de l'Agriculture, Station Centrale Jouy-en-Josas, Republique Francais); Mrs. Elizabeth S. Kleiner (M.S. from M.I.T. in 1959); Dr. Martha Ludwig (Research Associate, Department of Biology, M.I.T.); and Dr. Paul Dreizen (National Research Council Fellow, Research Associate, Department of Biology, M.I.T.). The interactions of the caseins are strong and varied. We have felt that no one component could be described with assurance until all major components had been characterized adequately. Since this now has been accomplished, descriptions of methods for isolation and the characteristics of the major casein components will be prepared shortly. Preliminary data on fractionation and characterization have been referred to previously.⁶

(3) P. H. von Hippel and D. F. Waugh, *J. Am. Chem. Soc.*, **77**, 4311 (1955).

(4) D. F. Waugh and P. H. von Hippel, *ibid.*, **78**, 4576 (1956).

(5) H. Nitschmann, *Helv. Chim. Acta*, **32**, 1258 (1949).

(6) H. Nitschmann, *ibid.*, **32**, 1258 (1949). The micelle range is given as 400–2800 Å. in diameter.

(7) D. F. Waugh, *Discussions Faraday Soc.*, **25**, 186 (1958).

the addition of inorganic phosphate or other ions such as oxalate or citrate, which sequester calcium, progressively increased the amount of non-centrifugable caseins. Indeed, micelles may be harvested by centrifugation, brought into solution with, for example, citrate and the resulting clear solution dialysed against saline or distilled water to remove calcium citrate and excess citrate, yielding a casein solution which has been called first cycle casein. Ultracentrifugation of this material at low temperatures⁴ reveals two peaks at 1.3S and 7.5S, which have been identified as representing primarily β -casein and the stoichiometric complexes of α_s -caseins and κ -caseins. It should be noted that the α_s - κ -complexes are present in the absence of calcium, at temperatures of 1°, and at pH 7 where all components carry a net negative charge.

At a temperature of 25° in the absence of calcium, as before, the pattern of first cycle casein alters considerably, all but a few per cent. of the protein present now giving rise to a symmetrical peak having a corrected sedimentation coefficient of 7.8S at 1% protein concentration, pH 7.0 and 0.15 ionic strength. The peak shows little boundary spreading, which suggests that the product of interaction is a monodisperse complex. Remembering the components present in first cycle casein it is apparent that this complex must contain most, if not all, members of the casein family. It may be considered provisionally as an α_s - κ - β -m-casein complex; possibly primarily as an α_s - κ - β -complex. These interaction complexes are to be compared with the interaction products obtained with other possible combinations.

Techniques for accomplishing a separation which yields crude fractions, one of which contains largely α_s -caseins and β -casein (second cycle casein) and the other κ -casein and minor components (Fraction S) have been described.^{3,4} Studies of these materials revealed several interesting polymers. At 4° second cycle casein gives an ultracentrifuge pattern having two peaks: one at 1.3S and a second at 4.4S. These have been identified as arising mainly from monomer β -casein and polymeric α_s -caseins. As the temperature is increased β -casein progressively interacts with the α_s -casein polymers until at ~20° it is absent. The sedimentation coefficient of the interaction product progressively increases with temperature. Heterogeneity is evident since the faster peaks are skewed, the velocity of the maximum ordinate increase with centrifugation time, and there is considerable boundary spreading.³ Evidently α_s - and β -caseins do not form stoichiometric interaction products, although interaction is evident. On ultracentrifugation of Fraction S,⁴ two peaks are observed, one at 1.3S, largely minor casein components, and a second, largely κ -casein polymers, at 13.5S.

On mixing second cycle casein and Fraction S in the correct proportions α_s - κ -complexes are reformed immediately, giving an ultracentrifuge pattern characteristic of first cycle casein. It is noted now that the formation of α_s - κ -complexes can be accomplished with pure α_s -caseins and κ -casein. This point will be emphasized later in considering the minimum requirements for micelle

formation. The point to be made is that studies with purified components confirm results obtained with studies of impure fractions, namely, that the α_s - κ -complexes are stoichiometric interaction products involving by weight approximately 4 parts of α_s -caseins and 1 part of κ -casein. In the studies referred to⁴ it was shown that an excess of α_s -caseins leads, on the addition of calcium ion, to a calcium α_s -caseinate precipitate plus micelles while the presence of excess κ -casein leads, in the absence of calcium ion, to an ultracentrifuge pattern having a well-defined peak at 16S as well as a peak at 7.5S, the latter characteristic of α_s - κ -complexes. When β -casein is present a peak at 1.3S is seen with low temperature centrifugation.

Minimum Requirements for Micelle Formation with Calcium Ion.—Interactions in the presence of calcium have been examined by noting the conditions under which the addition of calcium to protein mixtures leads to the spontaneous formation of stable micelles. Calcium concentrations of 0.005, 0.01, 0.02, 0.03, and 0.05 *M* have been used at pH 6.8–6.9 in the presence of 0.01 *M* sodium or potassium chloride and at protein concentrations of 1–1.5% (see Table I).

TABLE I

- I. Skim milk brought into solution with potassium citrate and dialysed *vs.* 0.01 *M* sodium chloride (contains all of the caseins and whey proteins).
- II. First cycle casein dialysed *vs.* 0.01 *M* sodium chloride (contains all of the caseins and traces of other proteins).
- III. Dialysed whey protein.
- IV. α_s -caseins, β -casein, κ -casein (purified, see 2).
- V. Minor components other than α_s -caseins, β -casein and κ -casein.

These materials have been mixed in various sequences and proportions at an ionic strength of 0.01⁷ and tested by adding calcium.

Before examining these tests the solubilities of the individual components should be noted, as summarized in Table II.

TABLE II

Component	Solubility, g./l. in 0.03 <i>M</i> calcium ion	
	0–4°	25–37°
α_s -Caseins	0.03	0.17
β -Casein	sol.	0.2
κ -Casein	sol.	sol.
Minor components	sol.	sol.
Whey proteins	sol.	sol.

First cycle casein and dialysed skim milk (I and II of Table I) are first examined since these are expected to contain all casein components in near normal ratios of abundances. The addition of calcium ion at 37° and pH 6.5–7.0 to levels near 0.005 *M* leads to no noticeable increase in turbidity, the solution remaining clear. As the calcium concentration is increased the solution develops micelles over a narrow concentration range, the micelle system being stable over a broader concentration range. The micelle range cannot be specified exactly except for a specific preparation of first cycle casein or dialysed skim milk. As

(7) A decreased complex and micelle stability often is observed at higher ionic strengths. This is true even of skim milk of the type shown in Table I. This is a factor to be taken into account in examining the equilibria discussed later in the text.

will be seen this undoubtedly results from the fact that different milks do not have the same casein composition. Most first cycle caseins give stable micelles at 0.03 *M* Ca and most will show trace precipitate formation at 0.05 *M* Ca. As the calcium concentration is increased beyond 0.05 *M*, increasing amounts of precipitate form, the amount being maximum at about 0.25 *M*. This precipitate consists largely of α_s -caseins.⁴

Summarized now are the results obtained by using mixtures of the materials shown in Table I. Two procedures have been used in testing for micelle development. In the first of these calcium is added to the mixture at 2° and in the second calcium is added, using a quick mixing technique, at 37° after incubating mixtures for 10 minutes at 37°. In both cases any precipitate which formed was harvested by centrifuging at 200 *g* for 0.5 minute, after allowing a 10-minute reaction time.

One general conclusion is drawn immediately from the results: micelles will not form in any system which does not contain α_s - and κ -caseins. In such systems precipitates form in accord with the solubility characteristics shown in Table II. The temperature at which calcium ion is added makes no difference.

When α_s -caseins and κ -casein are present the result depends upon the pH, the concentration of added calcium, the temperature at addition, the relative proportions of these caseins, and the ionic strength.⁷ At 37° and a weight ratio of 4(α_s/κ), the addition of calcium to 0.03 *M* leads immediately to the formation of a stable suspension of micelles. When excess α_s -caseins are present, the excess forms a precipitate leaving stable micelles in suspension. When excess κ -casein is present, the opacity of the micelle suspension is decreased, suggesting that the average micelle size is diminished. Sufficient κ -casein may, in fact, be introduced so that the system, even at 0.05 *M* calcium ion, becomes only opalescent.

At 2° entirely different results are obtained. As the calcium ion concentration is increased, at the α_s/κ weight ratio present in first cycle casein, increasing amounts of α_s -caseins precipitate leaving essentially a supernatant containing the remaining caseins in micelles or in solution. These precipitates are not pure α_s -caseins but contain other caseins as contaminants. In addition, the efficiency of the precipitation of α_s -caseins may be increased up to levels of 0.17–0.25 *M* calcium beyond which levels increasing amounts of α_s -caseins appear in solution. Previously we noted that α_s - κ -complexes are present in first cycle casein at 2°. It is evident now that at 2° these complexes are unstable in the presence of calcium ion with respect to the solubility of Ca- α_s -caseinates. Further insight into this relationship may be obtained by progressively increasing the κ -casein content of first cycle casein. As this is done the amount of α_s -caseins which precipitate at 2° is reduced until at a weight ratio of about unity and at 0.03–0.05 *M* calcium ion no precipitate forms.

Two further significant general observations should be noted. The first of these is that whey

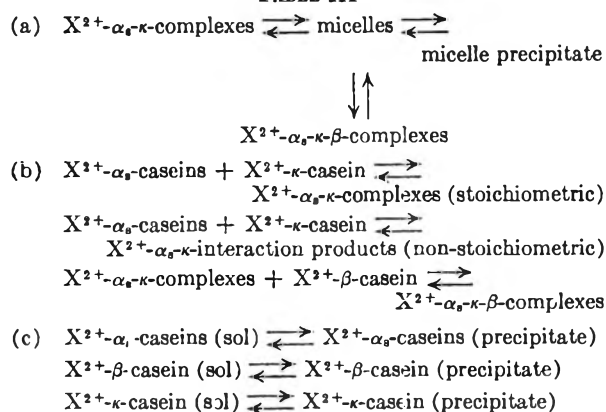
protein, preparation III, reduces the amount of precipitate when added to first cycle casein. We suspect that this may be due partly to the presence of κ -casein in "whey protein" but the matter requires further study. The second general observation has a direct bearing on whether or not the micelle system represents a true equilibrium. This second general observation has been derived from studies of skim milk, first cycle casein, and mixtures of α_s -caseins and κ -casein. First cycle casein is taken as an example. Calcium is added at 2° to first cycle casein to give a concentration of about 0.03 *M*, the exact level being chosen so that a copious precipitate of α_s -caseins forms. After the precipitate has settled the temperature of the entire aliquot is raised to 37°. With time a suspension of stable micelles forms. If this suspension, or a fresh suspension made at 37°, is cooled to 2° a precipitate will again form but the length of time required for precipitate formation is several orders of magnitude greater than the time required for precipitation when calcium is added at 2°. The time element was not fully appreciated when experiments of this type were first described.⁶ Evidently the structure of α_s - κ -complexes is temperature sensitive so that calcium ions can fit into the structure at 37°, produce intra-complex ion bridges and lead to a stability which is only slowly reversed. At 2° the structure will not accept calcium in the same way and a rapid splitting of the complexes occurs. This view and a scheme for the structure of the complex have been given previously.⁶ It was suggested also that at 37°, interaction with calcium leads to an intra-complex saturation of strong binding sites for calcium making them unavailable for inter-complex association.

Micelles form only if α_s -caseins and κ -caseins are present simultaneously. There remains the question as to whether or not the presence of α_s - and κ -caseins alone is sufficient for micelle formation. The answer to this question, obtained in recent experiments using purified preparations, is that at the correct weight ratio of 4, stable micelles are obtained on adding calcium at 37° (0.02–0.03 *M*). The two α_s -caseins, which differ significantly in phosphorus content, have been tested individually. The interesting result, in addition to the fact that each forms α_s - κ -complexes and micelles, is that the two types of micelles are different in structure and dissociation properties. These caseins are both designated α_s -caseins since both interact with κ -casein. They will be differentiated as α_{s1} - and α_{s2} -caseins.

Equilibria.—From the data summarized in the previous section we conclude that the state of a casein system in the presence of divalent cations is determined by the result of a set of equilibrium reactions, some of the more important being shown in Table III where X^{2+} represents a divalent cation. Only α_s -caseins, β -casein and κ -casein have been used in constructing Table III. At some time in the future minor-casein components probably must be included as well as a variety of obvious interaction products which have been omitted. Table III is important because it allows us to focus at-

tention on the central positions occupied by κ -casein and the α_s - κ -complexes and to raise the possibility that a micelle precipitate and an X^{2+} κ -casein precipitate, etc., might be important considerations when ions other than calcium are used, as is actually the case.

TABLE III



With respect to calcium we have not observed either micelle precipitates or precipitates of κ -casein or minor casein components at 2° or 37°. The ultracentrifuge patterns of first cycle casein suggest that there is little excess κ -casein (absence of a peak at 16S, see ref. 4). The distribution of components leads to stable micelles at 37° using 0.02–0.03 *M* Ca ion. The concentrations of Ca- α_s -caseinates in solution are thus less than those required for precipitate formation. If the same first cycle casein is cooled to 2°, the stability of the complex is reduced and dissociation takes place, increasing the concentrations of Ca- α_s -caseinates and Ca- κ -caseinate in solution. The former increases sufficiently to produce a precipitate while Ca- κ -caseinate remains in solution. There results then the formation of non-stoichiometric interaction products of Ca- α_s - κ -caseinates which are soluble. Dissociation, precipitation and the formation of non-stoichiometric Ca- α_s - κ -caseinates take place until the levels of Ca- α_s -caseinates in solution are just in equilibrium with Ca- α_s -caseinate precipitates. As pointed out previously, sufficient κ -casein may be added to α_s -caseins so that calcium addition produces little or no change in turbidity.

Of great interest are β -casein and the minor casein components in this scheme. As noted, stable micelles will form using α_s -caseins and κ -casein alone. At 37° β -casein seems to be incorporated in micelles at least to the extent that it is present in first cycle casein, although at 37° β -casein is almost as insoluble as the α_s -caseins. Observations of this type and the fact that essentially a single peak is observed on centrifuging first cycle casein at 25°, suggest that a second specific interaction be added to that leading to the formation of α_s - κ -complexes. This interaction would lead to the formation of α_s - κ - β -complexes and would be one in which the reactive (phosphorus) groups of β -casein are masked on an intracomplex basis, possibly in a manner similar to that in which the reactive (phosphorus) groups of α_s -

caseins are utilized after interactions with κ -casein. The properties of the micelle system suggest that other specific interdependent reactions are to be anticipated.

Divalent Ions.—All divalent cations so far examined, with the exception of magnesium, will form micelles under appropriate conditions. The list includes copper (0.03 *M*), calcium, strontium, barium (0.03 *M*), zinc, cadmium (0.007 and 0.015 *M*), manganese (0.015 *M*), cobalt and nickel (0.03 *M*). Depending on the particular cation the pH used is between 6.5 and 7.0. The parentheses indicate the approximate median of the concentration range for micelle formation at 37°.

The results may be summarized and interpreted with the help of Table III. According to this table, the micelle system degenerates as a result either of the instability of α_s - κ -complexes, the equilibrium levels of α_s -caseins for the complexes being greater than those for the formation of an ion-caseinate precipitate, or an instability of the micelles, the larger ones growing at the expense of the smaller ones until a micelle precipitate forms. Possibly, of course, micelles coalesce as such to give a precipitate.

With all divalent cations so far examined a sufficiently low ion concentration may be chosen so that at 0–37° the casein solution (first cycle casein or solubilized skim) remains clear with no noticeable increase in turbidity. Complex stabilization is assumed to be taking place with the free ion concentration remaining below that which can promote complex association. There follows then for all ions but magnesium a range of ion concentration over which micelles progressively form; the micelle range starts with the appearance of opalescence and ends with the formation of traces of precipitate. As noted just above this precipitate may be a micelle precipitate or if the complex is unstable, splitting occurs and the precipitate will contain largely α_s -caseins (low temperatures) or α_s - and β -caseins (higher temperatures).

If attention is centered on the micelle forming range, these ion groups are apparent: (1) Mg does not form micelles; nor does it precipitate α_s - or κ -caseins. It will antagonize micelle formation with Ca. (2) Ca, Sr, and Ba behave similarly. The micelle forming range is narrow at 2° and is terminated by splitting. At 37° the micelle forming range is broad and is terminated by splitting. Splitting requires long periods of time at the higher temperature. (3) Cu, Ni, Co, Mn, Cd and Zn are characterized by the stability which they give to the α_s - κ -complexes. The range of ion concentration producing stable micelles, which decreases from Cu to Zn, is terminated for Co, Mn, Cd, and Zn by the formation of micelle precipitates. The micelle concentration range is in all cases greater at 0° than at 37°. Cu and Ni were not used in high enough concentrations to produce micelle precipitates. Co, Mn, Cd and Zn are particularly interesting from the standpoint of α_s - κ -complexes for the solubilities of their X^{2+} - α_s -caseinates are low at 0 or 37°, particularly for the last three members of the series, and the last member, Zn, also precipitates κ -casein.

Of interest also from the standpoint of the structure of α' - κ -complexes is the fact that all micelle systems will, on the addition of the enzyme rennin, clot in a similar way. A model of the complex⁶ has been proposed in which part of the κ -casein molecule is represented as being exposed and thus readily available. This would allow an attack on part of this component in an otherwise structurally stable association.

At least one ion of the last named group, Mn, has been used to take an additional step toward an understanding of α_s - κ -complex and micelle formation. This has involved studies using the electron microscope.⁸ Since Mn produces complexes of unusual stability we felt that a system containing complexes and micelles formed at higher protein concentrations might be diluted in the presence of low concentrations of Mn without leading to dissociation as typically occurs exten-

(8) Mr. Robert Noble has undertaken these studies under the thesis requirements for the Ph.D.

sively with ions such as Ca. Pure components of κ -casein, α_{s1} -casein and α_{s2} -casein have been used. In both cases the complexes and micelles exhibit the expected stability. The resulting electron micrographs reveal structural and stability differences, micelles formed with α_{s1} - κ -casein complexes being the more stable.

The purpose of the present discussion has been to focus attention on the interaction of α_s -caseins and κ -casein in initiating the series of interactions leading to micelle formation and to draw attention to a second interaction; namely that between α_s - κ -casein complexes and β -casein. With the recent availability of pure components these interactions and equilibria may be approached on a quantitative basis. These are, of course, recognized as steps leading to an understanding of micelle formation. The central problem of micelles remains: since they are large and have a wide distribution of size, why do the larger ones not grow at the expense of the smaller ones and produce a precipitate?

PHASE SEPARATION IN POLYELECTROLYTE SOLUTIONS.

II. INTERACTION EFFECTS

BY ARTHUR VEIS

*Department of Biochemistry, Northwestern University Medical School, Chicago, Illinois**Received March 9, 1961*

The Voorn-Overbeek equations for complex coacervation were modified to include a term to account for a non-zero heat of mixing. The resulting equations were applied to an analysis of previously reported coacervation data on gelatin-gelatin systems. The (non-electrostatic) interaction parameter, χ_{12} , was evaluated from these data and was found to be a function of both the temperature and the initial mixing concentration. χ_{12} was not proportional to T^{-1} . The electrostatic free energy term of the Voorn equation, in which $(\partial F_c/\partial n_1)$ is a function of the polyion volume fraction, ϕ_2 , to the 3/2 power, was not compatible with these data. A more general electrostatic term, $f_1(\sigma, \phi)$, was devised, evaluated and found to be a more nearly linear function of ϕ_2^1 , the solute volume fraction in the dilute phase. The function $f_1(\sigma, \phi)$ was negative at low mixing concentrations and approached zero at high mixing concentrations. These data were interpreted as indicating the formation of stable aggregates of low configurational entropy in the original mixture. The coacervation is then driven by the gain in configurational entropy on the formation of the randomly mixed concentrated gelatin phase and the dilution of the non-random aggregate phase. The deviations from the Voorn-Overbeek equations can be considered as indicating a standard state entropy change when the polyions are mixed.

Biological systems contain, in general, mixtures of macromolecules dissolved or suspended in a common solvent, water. One may, therefore, approach an understanding of the behavior of certain of these systems from the point of view of the properties of mixtures of polymers. When two chemically distinct polymers are mixed in a common solvent three events are possible: (1) two phases appear, each phase rich in one of the two polymers; (2) two phases appear, one very concentrated, the other very dilute, but each containing nearly equivalent amounts of both polymers; or (3) the solution mixture remains as a homogeneous single phase.

The first situation is typical of mixtures of non-ionic polymers, the second of mixtures of oppositely charged macropolyions, while the third is typical of mixtures of polymers which exhibit strong interactions with the solvent. Relatively simple theories have been developed to describe the phase separation in each of the first two cases. The treatment of non-ionic polymers has been reviewed in detail by Flory.¹ Voorn² and Overbeek and Voorn³ have developed the theory for polyelectrolytes. Voorn's experimental verification of the polyelectrolyte theory was based on the interaction of polyions of quite different character.² In the previous paper in this series Veis and Aranyi⁴ studied the phase separation in mixtures of very similar proteins under conditions that seemed to adhere rather more closely to the theoretical requirements of the Voorn treatment. This investigation suggested that the basic treatment was deficient in two respects. In Voorn's theory² it was assumed that the solutions were athermal so that the heat of mixing, ΔH_M , was zero. Second, it was assumed that both phases in the equilibrium two phase system were composed of independent random coils, that is, there were no specific interactions between macromolecules. The gelatin-gelatin system⁴ seemed to be governed principally by these interaction effects.

tin system⁴ seemed to be governed principally by these interaction effects.

This paper is concerned with an analysis of the coacervation equilibria, especially those concerning protein mixtures, taking these interactions into account. The terminology and symbols used are the same as those used by Voorn² so that the final results may be compared directly.

I. The Effect of Solvent-Solute Interactions on the Coacervation Phase Equilibria. A. General Considerations.—In its most general form Flory^{1,5,6} and Huggins⁷⁻⁹ have shown the free energy of mixing of a non-ionic polymer with solvent to be given by equations 1. In equation 1b

$$\Delta F_M = \Delta H_M - T\Delta S_M \quad (1a)$$

$$\Delta F_M = kT[n_1 \ln \phi_1 + n_2 \ln \phi_2 + \chi_{12} n_1 \phi_2] \quad (1b)$$

n_1 and n_2 are the numbers of molecules of solvent and solute, respectively, ϕ_1 and ϕ_2 their volume fractions. χ_{12} is a dimensionless quantity that characterizes the solvent-solute interaction energy per solvent molecule divided by kT . For a multi-component system the equation for ΔF_m becomes

$$\Delta F_m = kT \sum_i n_i \ln \phi_i + kT \sum_{\substack{\text{all } i-j \text{ pairs} \\ i < j}} \chi_{ij} n_i \phi_j \quad (2)$$

in which χ_{ij} now represents the interaction per kinetic unit i -kinetic unit j pair divided by kT .

If the polymer chain bears electrically charged groups then there is also a contribution to the free energy of forming the solution, a term corresponding to the work of charging up the polymers, an electrostatic free energy, ΔF_e . The essential feature of Voorn's treatment is that the polyions are treated as the sum of single charges, and that these charges may be distributed throughout the solution without regard to the fact that they reside on polymer chains. In this case the electrical work involved is just that of charging each ion at the final ionic strength and is given by the Debye-Hückel limiting law as

(1) P. J. Flory, "Principles of Polymer Chemistry," Cornell Univ. Press, Ithaca, N. Y., 1953.

(2) M. J. Voorn, *Fortschr. Hochpolym.-Forsch.*, **1**, 192 (1959); *Rec. trav. chim.* **75**, 317, 405, 427, 925, 1021 (1956).

(3) M. J. Voorn and J. Th. G. Overbeek, *J. Cellular Comp. Physiol.*, **49**, Suppl. 1, 7 (1957).

(4) A. Veis and C. Aranyi, *J. Phys. Chem.*, **64**, 1203 (1960).

(5) P. J. Flory, *J. Chem. Phys.*, **9**, 660 (1941).

(6) P. J. Flory, *ibid.*, **10**, 51 (1942).

(7) M. L. Huggins, *ibid.*, **9**, 440 (1941).

(8) M. L. Huggins, *J. Phys. Chem.*, **46**, 151 (1942).

(9) M. L. Huggins, *Ann. N. Y. Acad. Sci.*, **43**, 1 (1942); **44**, 431 (1943).

$$F_e = -\frac{\epsilon^2 K}{3D} \sum_i N_i Z_i^2 \quad (3)$$

where N_i is the concentration of ions species i and charge Z_i . K is the Debye constant, ϵ the electronic charge, and D the dielectric constant. Voorn reduced this expression to

$$F_e = -\alpha k T N_r \left(\sum_i \sigma_i \phi_i \right)^{3/2} \quad (4)$$

In equation 4, N_r is the total number of lattice sites of volume v in the solution, ϕ_i is the volume fraction of component k and σ_i is the net charge density per polyion i . The electrostatic interaction parameter α is defined by equation 5

$$\alpha = \frac{\epsilon^2}{3D} \left(\frac{4\pi\epsilon^2}{DkTv} \right)^{1/2} \left(\frac{1}{kT} \right) \quad (5)$$

If r_i is the number of lattice sites occupied by i in a total volume V , the following useful relationships may be developed

$$N_r = \sum_i r_i \quad (6)$$

$$V = v N_r \quad (7)$$

$$\phi_i = \frac{n_i r_i}{N_r} = \frac{n_i r_i v}{V} \quad (8)$$

$$N_i = \sum_i n_i Z_i \quad (9)$$

The complete expression for the free energy of forming a polyion solution is

$$\Delta F_T = kT \sum_i n_i \ln \phi_i + kT \sum_{i < j}^{ij} \chi_{ij} n_i n_j \phi_i + \Delta F_e \quad (10)$$

and, with Voorn's electrostatic term

$$\Delta F_T = kT \sum_i n_i \ln \phi_i + kT \sum_{i < j}^{ij} \chi_{ij} n_i n_j \phi_i - \alpha k T N_r \left(\sum_i \sigma_i \phi_i \right)^{3/2} \quad (11)$$

The discussion will now be restricted to the symmetrical case of a mixture containing a polycation P^+ , an equivalent amount of polyanion Q^- , and solvent. No other ions will be presumed to be present. At equilibrium, assuming that coacervation takes place, this system will consist of two phases. By convention the dilute phase will be designated by the superscript I, the concentrated coacervate phase by superscript II. The subscript 1 will designate the solvent, 2 and 3, P^+ and Q^- , respectively. We shall consider only those systems in which P^+ and Q^- are of identical molecular weight and, hence, equivalent weight and charge density. Finally, we assume that the kinetic units of each polymer chain are of the same size. These assumptions may appear restrictive but they correspond to the situation readily realizable with gelatin-gelatin systems.

To preserve electroneutrality at equilibrium

$$\begin{aligned} \phi_2^I &= \phi_3^I \\ \phi_2^{II} &= \phi_3^{II} \end{aligned} \quad (11)$$

and the electrochemical potentials must be equal in each phase. As long as diffusible small ions are absent, the potential differences will be zero for this symmetrical system,² and the equilibrium conditions require only that the chemical potential, μ , of each component be the same in each phase

$$\left(\frac{\mu_1 - \mu_1^0}{RT} \right)^I = \left(\frac{\mu_1 - \mu_1^0}{RT} \right)^{II} \quad (12,a)$$

$$\left(\frac{\mu_2 - \mu_2^0}{RT} \right)^I = \left(\frac{\mu_2 - \mu_2^0}{RT} \right)^{II} \quad (12,b)$$

$$\left(\frac{\mu_3 - \mu_3^0}{RT} \right)^I = \left(\frac{\mu_3 - \mu_3^0}{RT} \right)^{II} \quad (12,c)$$

The differentiation of equation 10 yields

$$\begin{aligned} \frac{\mu_1 - \mu_1^0}{RT} &= \ln \phi_1 + (1 - \phi_1) - \phi_2 \left(\frac{r_1}{r_2} \right) - \phi_3 \left(\frac{r_1}{r_3} \right) + \\ &(\chi_{12}\phi_2 + \chi_{13}\phi_3)(\phi_2 + \phi_3) - \chi_{23} \left(\frac{r_1}{r_2} \right) \phi_2 \phi_3 + \frac{1}{RT} \left(\frac{\partial F_e}{\partial n_1} \right)_{P,T,n_2} \quad (12) \end{aligned}$$

$$\begin{aligned} \frac{\mu_2 - \mu_2^0}{RT} &= \ln \phi_2 + (1 - \phi_2) - \phi_1 \left(\frac{r_2}{r_1} \right) - \phi_3 \left(\frac{r_2}{r_3} \right) + \\ &(\chi_{12}\phi_1 + \chi_{23}\phi_3)(\phi_1 + \phi_3) - \chi_{13} \left(\frac{r_2}{r_1} \right) \phi_1 \phi_3 + \frac{1}{RT} \left(\frac{\partial F_e}{\partial n_2} \right)_{P,T,n_1} \quad (13) \end{aligned}$$

$$\begin{aligned} \frac{\mu_3 - \mu_3^0}{RT} &= \ln \phi_3 + (1 - \phi_3) - \phi_1 \left(\frac{r_3}{r_1} \right) - \phi_2 \left(\frac{r_3}{r_2} \right) + \\ &(\chi_{31}\phi_1 + \chi_{32}\phi_2)(\phi_1 + \phi_2) - \chi_{12} \left(\frac{r_3}{r_1} \right) \phi_1 \phi_2 + \frac{1}{RT} \left(\frac{\partial F_e}{\partial n_3} \right)_{P,T,n_1} \quad (14) \end{aligned}$$

For the specific case under consideration, the following simplifications can be made: $\phi_2 = \phi_3$, $r_2 = r_3$, $\sigma_1 = 0$, $\sigma_2 = -\sigma_3$, r_1 is set equal to 1 and $r_2 \gg 1$. It is also assumed that the polymer backbone chains are chemically similar so that $\chi_{12} = \chi_{13}$; $\chi_{23} = \chi_{32}$. With these conditions, and the use of Voorn's formulation of the electrostatic free energy (equation 4), equation 12 reduces to equation 15, and equation 13 to equation 16.

$$\begin{aligned} \frac{\mu_1 - \mu_1^0}{RT} &= \ln \phi_1 + (1 - \phi_1) + \\ &1.414\alpha (\sigma_2 \phi_2)^{3/2} + 4\chi_{12}\phi_2^2 \quad (15) \end{aligned}$$

$$\begin{aligned} \frac{\mu_2 - \mu_2^0}{RT} &= \ln \phi_2 + \phi_1 + \chi_{12} + (\chi_{23} - 3\chi_{21})\phi_2 + \\ &2(\chi_{21} - \chi_{23})\phi_2^2 + r_2 [2 - \chi_{12})\phi_2 + 2\chi_{12}\phi_2^2 + \\ &1.414\alpha (\sigma_2 \phi_2)^{3/2} - 2.12\alpha \sigma_2 (\sigma_2 \phi_2)^{1/2} - 1] \quad (16) \end{aligned}$$

At equilibrium we find the relationships

$$\begin{aligned} \ln \frac{\phi_1^I}{\phi_1^{II}} - (\phi_1^I - \phi_1^{II}) &= 4\chi_{12} [(\phi_2^{II})^2 - (\phi_2^I)^2] + \\ &1.414\alpha [(\sigma_2 \phi_2^{II})^{3/2} - (\sigma_2 \phi_2^I)^{3/2}] \quad (17) \end{aligned}$$

and

$$\begin{aligned} \ln \frac{\phi_2^{II}}{\phi_2^I} + 2\chi_{12} [(\phi_2^{II})^2 - (\phi_2^I)^2] - (2 + 3\chi_{12})[\phi_2^{II} - \phi_2^I] &= \\ r_2 \{ (\chi_{12} - 2)(\phi_2^{II} - \phi_2^I) - 2\chi_{12} [(\phi_2^{II})^2 - (\phi_2^I)^2] - \\ &1.414\alpha [(\sigma_2 \phi_2^{II})^{3/2} - (\sigma_2 \phi_2^I)^{3/2}] + \\ &2.12\alpha \sigma_2 [(\sigma_2 \phi_2^{II})^{1/2} - (\sigma_2 \phi_2^I)^{1/2}] \} \quad (18) \end{aligned}$$

The terms containing ϕ_1 and ϕ_2 in these equations are experimentally directly accessible. The constant α can be calculated from equation 5 at each temperature. Hence, the parameters χ , σ and r can be determined from measurements of the intensity of coacervation. Equation 17 is particularly well suited for the evaluation of the χ_{12} and σ_2 because of its simple form.

B. Coacervation in the Non-gelling Region ($T = 40^\circ$).—The experimental data on gelatin-gelatin salt free mixtures reported in the previous paper⁴ were used for the following analysis. The smoothed curve values for the coacervate concentration, C_c (Fig. 1, ref. 4), and the corresponding values of the equilibrium liquid concentration,

TABLE I
ANALYSIS OF EQUATION 17 AT $T = 40^\circ$ ($\alpha = 4.236$)

1	2	3	4	5	6	7	8	9	10	11	12
C_T , g./cc. $\times 10^3$	C_L , g./cc. $\times 10^3$	C_c , g./cc. $\times 10^3$	ϕ_1^I	ϕ_1^{II}	ϕ_2^I $\times 10^2$	ϕ_2^{II} $\times 10^2$	Left side eq. 17	$(\phi_2^{II})^2$ $\times 10^4$	$(\phi_2^I)^2$ $\times 10^4$	1.414α $[(\phi_2^{II})^2 -$ $(\phi_2^I)^2]$ $\times 10^8$	f_1 (σ, ϕ) $\times 10^8$
2	1.82	7.66	0.99818	0.9234	0.091	3.83	3.00	14.67	0.008	44.7	
3	2.80	6.42	.99720	.9358	.140	3.21	2.15	10.30	.019	34.14	
4	3.67	5.48	.99633	.9452	.183	2.74	1.57	7.51	.034	26.71	-0.30
5.1	4.61	4.85	.99539	.9515	.230	2.425	1.19	5.88	.053	21.92	-0.04
6.0	5.44	4.60	.99456	.9540	.272	2.30	1.07	5.29	.074	20.07	+0.26
7.0	6.42	4.49	.99358	.9551	.321	2.245	1.04	5.04	.103	19.05	+0.56
8.0	7.44	4.40	.99256	.9560	.372	2.20	1.02	4.84	.138	18.15	+0.85
9.0	8.39	4.03	.99161	.9597	.419	2.015	0.76	4.06	.175	15.37	+0.02
10.1	9.21	2.92	.99079	.9708	.460	1.46	0.40	2.13	.216	8.68	+0.01

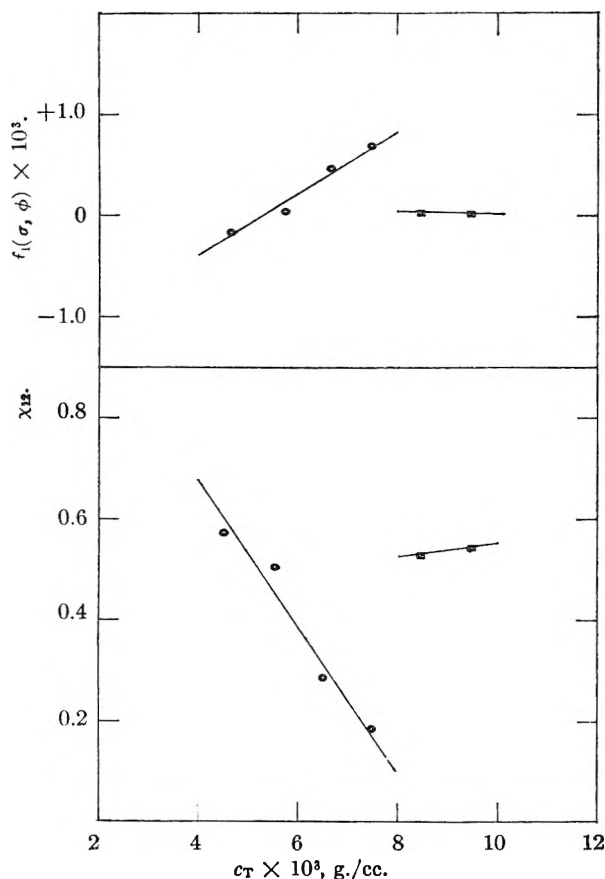


Fig. 1.—The dependence of the solvent-solute and electrostatic interaction parameters on the mixing concentration, gelatin-gelatin system at 40° , analysis of the data according to equation 19.

C_L , were tabulated as a function of the initial mixing concentration C_T , at the temperatures 50, 40, 25.5 and 15° . The volume fractions ϕ_1 and ϕ_2 were computed, assuming unit density for the gelatins and $\phi_2 = \phi_1$. The appropriate computations were carried out for substitution into equation 17. The values for the case of 40° are given in Table I.

These data are given in detail in Table I to emphasize the relative importance of the terms in ϕ , ϕ^2 and $\phi^{3/2}$ in each phase. Column 10 is the numerical value of the left hand side of equation 17. Column 13 is the multiplier of χ_{12} and column 14 the multiplier of $(\sigma_2)^{3/2}$. In polymer systems it is frequently found that χ_{12} is a function of polymer concentration. Therefore, since it seemed likely

that σ_2 , the polyion charge density, would be relatively constant, reasonable values of σ_2 were assumed and χ_{12} was calculated first. A value of χ_{12} was calculated for each C_T in Table I at $\sigma_2 = 10^{-1}$ to 10^{-3} .⁴ The values obtained, using the difference term in the $3/2$ power of the phase concentrations, were completely erratic and a semblance of order was found only if σ_2 was set equal to zero.

A second alternative was to abandon the formulation of ΔF_e given by equation 4 and merely modify equation 17 to include a more general function of the concentration and charge density, to yield equation 19. Assuming next that both χ_{12} and

$$\ln \frac{\phi_1^I}{\phi_1^{II}} - (\phi_1^I - \phi_1^{II}) = 4[(\phi_2^{II})^2 - (\phi_2^I)^2] \chi_{12} + f_1(\sigma, \phi) \quad (19)$$

$f_1(\sigma, \phi)$ would vary uniformly with C_T over small ranges in C_T , adjacent sets of the data were solved simultaneously to yield average values of $f_1(\sigma, \phi)$ and χ_{12} . The values of these parameters calculated in this fashion are plotted as C_T in Fig. 1. Both $f_1(\sigma, \phi)$ and χ_{12} were found to vary linearly with C_T but two ranges and a sharp discontinuity in each were evident. This discontinuity coincides with the inflection point of a plot of C_C vs. C_T (Fig. 1, ref. 4) and the abrupt change noted earlier in ρ , the fraction of the total protein found in the coacervate phase (Fig. 2, ref. 4).

Examination of equation 12 shows that $f_1(\sigma, \phi)$ is the difference between the partial molar electrostatic free energy of the solvent in each phase, as represented in equation 20

$$f_1(\sigma, \phi) = \frac{1}{RT} [(\bar{F}_{e,1})^{II} - (\bar{F}_{e,1})^I] \quad (20)$$

At high values of C_T these partial molar electrostatic free energy terms must have nearly the same value since $f_1(\sigma, \phi)$ becomes negligibly small. It is also probable that $(\bar{F}_{e,1})^{II}$ is relatively constant because the coacervate concentration varies only to a small extent over the range from $C_T = 4 \times 10^{-3}$ to 10×10^{-3} g. ml. Therefore, the observed variation in $f_1(\sigma, \phi)$ at low C_T must be due to the manner in which $(\bar{F}_{e,1})^I$, the partial molar free energy of the solvent in the dilute phase, depends on C_T . $(\bar{F}_{e,1})^I$ appears to be a linear, or nearly linear, function of ϕ_2^I rather than a function of $(\phi_2^I)^{3/2}$. Working back through equation 19 it can be seen that positive values of $f_1(\sigma, \phi)$ would increase the ratio ϕ_1^I/ϕ_1^{II} , enhancing coacervation.

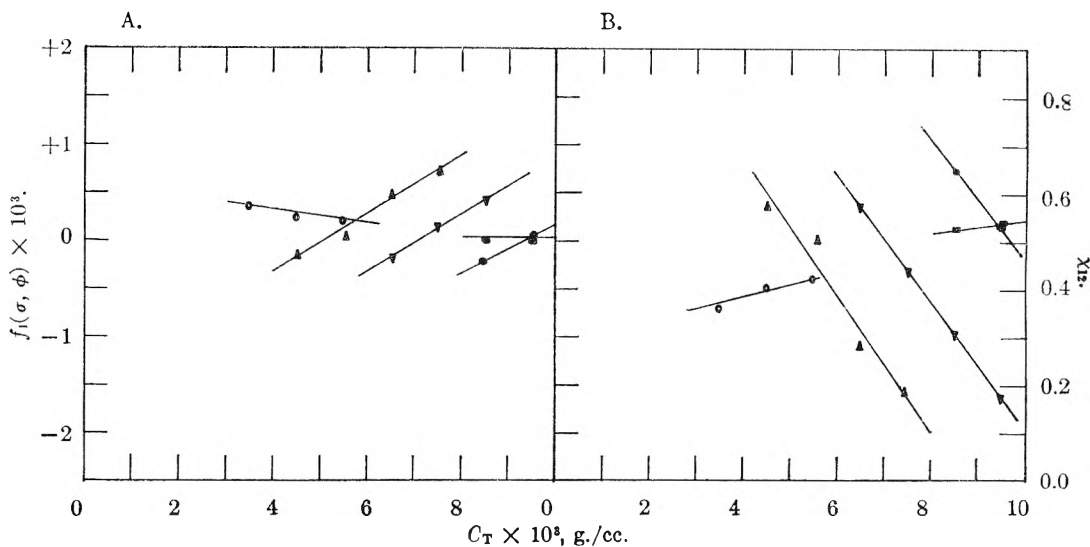


Fig. 2.—The effect of temperature on the interaction parameter-mixing concentration relationships: \circ , 50° ; \triangle , 40° ; ∇ , 25.5° ; \bullet , 15° .

C. The Effect of Temperature on χ_{12} and $f_1(\sigma, \phi)$.—The coacervation data reported in the previous paper⁴ for the systems at 15, 25.5 and 50° were analyzed in the fashion outlined above according to equation 19. It was found that at each temperature there was a range in C_T where χ_{12} and $f_1(\sigma, \phi)$ corresponded to one or both of the branches of the χ_{12} (or $f_1(\sigma, \phi)$) vs. C_T plots at 40° . This is shown in Fig. 2.

The principal effect of changing the temperature is to shift the C_T range over which a given χ_{12} - C_T relationship applies. For example, only the upper branches of the χ_{12} and $f_1(\sigma, \phi)$ plots are evident at 50° , and these are located at a lower range in C_T than the upper branches of the 40° plots. On the other hand, in the C_T range examined only the lower branches of the 25.5 and 15° plots were found, located at progressively higher C_T values (Fig. 2).

II. The Role of Solute Aggregation in Coacervating Systems.—From the discussion of the preceding section it is evident that solute-solvent interactions play an important role in regulating the coacervation phenomena. It is equally pertinent to inquire about the significance of specific solute-solute interaction and aggregation. This should be of special importance in gelatin systems as a result of the well known tendency of gelatin to form three dimensional network aggregates at temperatures below 40° . Ideally, such an examination of aggregation could be made through the use of equations 13 and 18 in which r_2 , the molecular size, is an important factor. However, there are two factors that negate the feasibility of analyzing equation 13 at this time.

It is apparent that the Voorn approximation for the term $1/RT(\partial F_e/\partial n_2)_{P,T,n_1}$ is not appropriate and that a term similar to equation 20 should be substituted for the last two terms of equation 18. Because of the symmetry of the polyions, the mixture could be considered as a binary system of H_2O and PQ and the Gibbs-Duhem relationship applied so that $\bar{F}_{e,2}$ could be calculated from $\bar{F}_{e,1}$.

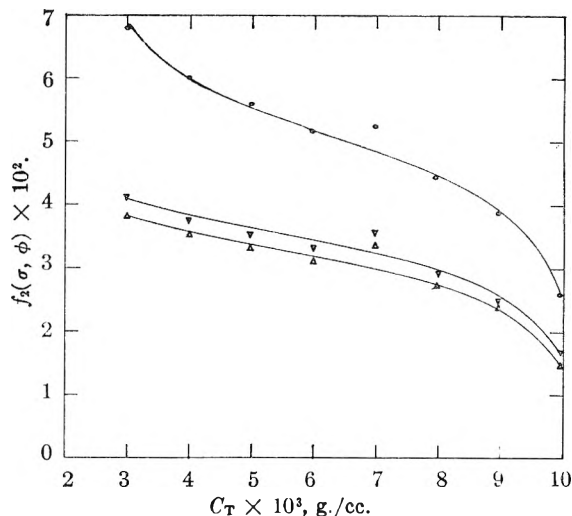


Fig. 3.—The variation of $f_2(\sigma, \phi)$ with C_T at various values of r_2 : \circ , $r_2 = 10^2$; ∇ , $r_2 = 10^3$; \triangle , $r_2 = 10^4$ and all higher values.

$$n_1 d\bar{F}_{e,1} = -n_2 d\bar{F}_{e,2} \quad (21)$$

$$\bar{F}_{e,2} - \bar{F}_{e,2}^0 = - \int_0^{n_2} \frac{n_1}{n_2} d\bar{F}_{e,1} \quad (22)$$

Unfortunately, it is not possible to evaluate $\bar{F}_{e,2}^0$ with the limited data available.

Even without a knowledge of the exact composition of $\bar{F}_{e,2}$, however, it can be seen that $\bar{F}_{e,2}$ is a linear function of r_2 since

$$\frac{n_1}{n_2} = \frac{r_2 \phi_1}{r_1 \phi_2} = r_2 \left(\frac{\phi_1}{\phi_2} \right) \quad (23)$$

Thus, the right-hand side of equation 18, after modification of the electrostatic term, can still be factored into the product of r_2 and a difference term which is close to zero. Representing the electrostatic term as $r_2 f_2(\sigma, \phi)$, the value of $f_2(\sigma, \phi)$ at 40° can be estimated from the data of Table I for various assumed values of r_2 . Plots of $f_2(\sigma, \phi)$ vs. C_T are illustrated in Fig. 3. When $r_2 > 10^3$ $f_2(\sigma, \phi)$ becomes relatively insensitive to the value of r_2 . Very precise values of each term would be

required to obtain significant information about the effect of variation in r_2 through aggregation.

III. Discussion and Interpretation.—The Flory-Huggins theory for the free energy of mixing, as expressed in equation 1b, assumes that the configurational entropy represents the total entropy change on mixing and that ΔF_M refers to the process of forming the solution from pure, disoriented polymer and pure solvent. Any interaction between polymer and solvent is considered to give rise to a heat of mixing ΔH_M , proportional to χ_{12} and this is the interpretation used above. However, Flory points out that, in general, there may also be a contribution to the entropy from these and other possible interactions. This interaction entropy can be characterized as a standard state entropy change and is proportional to the number of interacting polymer segments in the same manner as ΔH_M . Hence, the form of the interaction term in equation 1b does not need to be changed, one has only to realize that χ_{12} contains an entropy as well as an enthalpy contribution. If there is no standard state entropy change χ_{12} will be proportional to $1/T$; if χ_{12} is dependent on T in a more complicated way, then the interaction is equivalent to introducing a change in standard state. In the present case, χ_{12} is not proportional to $1/T$.

TABLE II
EVALUATION OF ΔH_M AND $\Delta S_M'$ FROM χ_{12}

$T, ^\circ\text{C.}$	$\frac{(\chi_{12})}{C_T} = 8 \times 10^{-4}$	$\frac{\Delta\chi_{12}}{\Delta T}$	$\frac{\Delta H_M}{\text{kcal./mole solvent-solute segment contacts}}$	$\frac{\Delta S_M'}{\text{e.u./mole solvent-solute segment contacts}}$
40	0.09	-0.020	3.7	+5.85
25.5	.38	-0.033	5.6	+9.1
15	.71			

From the definition of χ_{12} the following standard thermodynamic relationships can be deduced

$$\Delta H = -RT^2 n_1 \phi_2 \left(\frac{\partial \chi_{12}}{\partial T} \right) \quad (24)$$

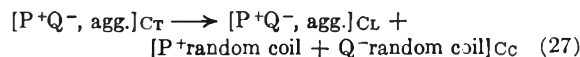
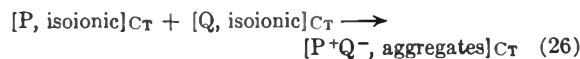
$$\Delta S' = -R n_1 \phi_2 \left(\frac{\partial(\chi_{12} T)}{\partial T} \right) \quad (25)$$

$\Delta S'$ is the entropy in excess of the configurational entropy or the standard state entropy change from the completely random pure polymer system. The χ_{12} plots at $T = 40, 25.5$ and 15° all extend through $C_T = 8 \times 10^{-3}$ g./cc. At this concentration the values of ΔH_M and $\Delta S'$ have been computed using equations 24 and 25. These values are listed in Table II in terms of the enthalpy and entropy per mole of water-gelatin segment contacts. The magnitude of ΔH_M , which corresponds to the integral heat of mixing, is appropriate for protein systems. The variations in ΔH_M and $\Delta S'$ with temperature are also in the direction that one might predict. One must put more energy into the system to form the solutions at low temperature, and the formation of the solution is accompanied by a greater increase in relative disorder.

As mentioned earlier χ_{12} is usually found to be a function of the polymer concentration. However, the dramatic variation in χ_{12} with C_T at low $C_T(40^\circ)$ is much greater than usual, and very different from the situation existing in solutions

of either gelatin by itself. The second virial coefficient of each gelatin in salt solutions at 40° has been found to be $0-3.7 \times 10^{-4}$ cc. mole/g.² by light scattering.¹⁰ Osmotic pressure measurements on a lower molecular weight gelatin in 2.0 M KCNS also yielded the value of 3.0×10^{-4} cc. mole/g.².¹¹ Both investigations covered the same concentration range as in this coacervation study. These comparisons emphasize the importance of the initial mixing concentration and suggest that, in analogy with the standard state entropy change brought about by solvent-solute interactions, there is a comparable interaction between P^+ and Q^- that depends on C_T and contributes to $\Delta S'$.

Veis and Aranyi⁴ proposed the following sequence of reactions to account qualitatively for their data on the gelatin-gelatin system. The



first reaction, the mutual titration of the isoionic protein molecules and the formation of aggregates takes place instantaneously. The phase separation occurs more slowly, and therefore is necessarily controlled by the nature of the P^+Q^- aggregate. This scheme for the coacervation reactions would also apply to mixtures of polyions each bearing only a single type of charged group, at low ionic strength. The formation of specific P^+Q^- aggregates fits readily into the above interpretation of the variation in χ_{12} with C_T if one assumes that the aggregate size and stability is influenced by interaggregate interactions.

Positive values of χ_{12} indicate a preference for solvent-solvent and solute-solute segment interactions, or from the standard state entropy point of view, the imposition of order. The negative slope of the plot of χ_{12} vs. C_T in the low C_T range is consistent with a relative decrease in aggregate order and/or the increased availability of hydrophilic protein groups to the solvent upon increasing the initial mixing concentration. The fact that a plot of $f_1(\sigma, \phi)$ vs. C_T has a positive slope in this C_T range, and that $f_1(\sigma, \phi)$ is negative at low C_T , shows that the interactions leading to aggregation are of electrostatic origin and are most pronounced the more dilute the initial mixing concentration. Negative values of $f_1(\sigma, \phi)$ mean that $\Delta F_e > 0$ for the phase transition, *i.e.*, work is being done on the system to separate the components of the P^+Q^- aggregates. The net negative value of ΔF_T therefore, must arise from the fact that ΔS_M is also positive for the phase separation. The reaction described by equation 27 provides this positive ΔS_M , the aggregates of low configurational entropy are diluted while the concentrated phase can be thought of as a typical solution of random chain polymers of high configurational entropy.

Voorn² and Voorn and Overbeek³ were careful to point out that the use of the unmodified Flory-Huggins equation for ΔS_M and the assumption of uniform charge distribution would be least likely

(10) A. Veis and J. Cohen, *J. Polymer Sci.*, **26**, 113 (1957).

(11) H. Boedtker and P. Doty, *J. Am. Chem. Soc.*, **78**, 4267 (1956).

to apply to very dilute mixtures or, at any time, in the dilute equilibrium phase. The variations in χ_{12} and $f_1(\sigma, \phi)$ describe the deviations from these assumptions and the discontinuity in each function can be considered as marking the concentration at which the transition from the "dilute solution model" to the "concentrated solution model" takes place. For the particular gelatins investigated this occurs at $C_T = 7 \times 10^{-3}$ g./cc. at 40° .

From a mechanistic point of view, a concentrated polyion solution is one in which the domains of each polymer molecule overlap so that segments from different molecules may occupy adjacent volume elements as frequently as may different segments of the same molecule. In this region, the electrically charged groups can be distributed uniformly without regard to their residence on the polymer chains and the Flory-Huggins equation applies. Under these conditions Voorn's treatment leads to the conclusion that the electrostatic free energy change on phase separation is favorable for coacervation and that the change in entropy is positive, but minimal. In this connection it is interesting to see that $f_1(\sigma, \phi)$, on the upper branches of the 40° and 50° plots, is a small slowly decreasing function of C_T , and that, at 40° , it is practically equal to zero. On the other hand, in this same concentration range at 40° , $\chi_{12} > 0.50$. For a binary polymer system (polymer + solvent) the critical value of χ_{12} above which phase separation occurs is 0.5. Thus, one may conclude that in this particular gelatin-gelatin system at 40° , the coacervation observed at $C_T > 7 \times 10^{-3}$ g./cc. is due to the fact that enough solute-solute interaction remains so that water is not a very good solvent for the $P^+ Q^-$ mixture, rather than to the fact that the electrostatic free energy is lowered appreciably by further concentration of the mixture. Raising the temperature to 50° makes water a better solvent, lowering χ_{12} below 0.5; consequently, the coacervation intensity drops. Coacervation takes place at 50° in the lower C_T region where $f_1(\sigma, \phi)$ is positive and ΔF_e can be made more negative by increasing the polyion concentration. However, at the higher concentrations where the Voorn model would be expected to apply $f_1(\sigma, \phi)$ drops to zero and, since $\chi_{12} < 0.5$, the mixtures remain completely miscible with water.

It is known that a partial regeneration of the peptide chain configuration characteristic of native collagen accompanies the gelation of gelatin. This reorganization begins to be significant when the temperature is dropped below 35° . The low temperature measurements ($T \leq 35^\circ$) were carried out in such a fashion as to minimize this effect. That is,⁴ the solutions were prepared at 40° and mixed at that temperature, then equilibrated at the final lower temperature. In this way, all of the solutions initially contained randomly dispersed gelatins. There is no evidence to suggest that the electrostatic aggregation discussed above raises the tem-

perature at which the reorganized chain segments might be stable. If such organized chain segments and gel-like aggregates were present at 40° and 50° they would be favored in the concentrated phase. This would lead to conclusions in regard to ΔF_e similar to those postulated by Voorn. As we have seen this behavior is not that which was observed.

IV. Conclusions.—When solutions of oppositely charged polyions are mixed, at low polyion charge density and low ionic strength, intermolecular complexes or aggregates are formed. These aggregates form immediately, are stable, and are crucial in regulating the subsequent coacervation equilibria. Thermodynamically the aggregate formation is equivalent to introducing a change in standard state from the model of random, non-interacting pure polymer.

The analysis of the gelatin-gelatin complex coacervation data described above emphasizes that the formation of the coacervate phase from the aggregates takes place with only a small, and not always favorable change in ΔF_e . The phase separation is, in effect, driven by the gain in configurational entropy on the formation of an amorphous randomly mixed concentrated phase and the dilution of the non-random aggregate phase.

The Voorn-Overbeek model is appropriate only for calculating the thermodynamic properties of the concentrated phase formed from relatively concentrated initial mixtures. One may include a concentration dependent interaction term in the basic equation for ΔF_T . The resulting equations can be used to examine a given set of data but are too complex in form to be useful in making predictions on new systems.

Other interactions may take the place of electrostatic factors to enhance aggregate formation, but only those which are distributive in nature (*e.g.*, gelation) can lead to coacervation. Specific site interactions bring about coprecipitation. From this point of view, one can also conclude that coacervation due to electrostatic interactions will also be limited to systems of relatively low charge density unless the ionic strength is high. One should find precipitates at low ionic strength in these cases.

This research was supported in part by Research Grant RG-8114 from the United States Public Health Service, National Institutes of Health.

DISCUSSION

I. COHEN (Polytechnic Institute of Brooklyn).—Is there any experimental evidence of order in the coacervate phase?

A. VEIS.—There is no direct evidence for order in the coacervate phase when the coacervation system is composed of random coil polyelectrolytes. However, it can be observed that the coacervates are frequently less turbid than their equilibrium liquids. Further, in the gelatin system we have noted that coacervates of nearly the same concentration, but formed at different initial mixing concentrations, do not have the same turbidity. These observations would indicate some departure from completely random mixing in the coacervate. We are presently concerned with an experimental approach to this problem.

SOME COLLOIDAL PROPERTIES OF DECYL- AND DODECYLTRIMETHYLAMMONIUM DODECYL SULFATE

BY HORST W. HOYER, ANNE MARMO AND MARGARET ZOELLNER

Chemistry Department, Hunter College of the City University of New York, New York 21, N. Y.

Received June 27, 1960

Solutions of decyl and dodecyltrimethylammonium dodecyl sulfate were prepared by mixing solutions of equivalent amounts of decyl or dodecyltrimethylammonium hydroxide and dodecyl hydrogen sulfate. Dilute solutions are stable in a limited concentration range up to and slightly above the c.m.c., then pass through a region in which coacervation occurs, and are again stable in concentrated solutions. The dodecyl solutions show surface tension lowering, with increasing concentration, to 30 dynes/cm. at a concentration of $3.0 \times 10^{-5} M$, at which concentration micelle formation occurs. For the decyl compound the c.m.c. is at $1.9 \times 10^{-4} M$. Electrophoretic mobility determinations of the micelles of the latter compound gave a value of $1.09 \pm 0.02 \times 10^{-4} \text{ cm.}^2/\text{volt-sec.}$ Addition of excess dodecyl hydrogen sulfate causes the mobility to rise rapidly to a maximum of $10 \times 10^{-4} \text{ cm.}^2/\text{volt-sec.}$ when a 100% excess is present and then to decrease slowly as more is added. The initial rapid rise is interpreted as due to the incorporation of the dodecyl sulfate ion into the micelle with a resulting increase in micellar charge. The gradual decline from the maximum value is a result of the normal repression of the ionic atmosphere with increasing ionic concentration.

Introduction

During the course of some exploratory work on the critical micelle concentrations and electrophoretic mobilities of colloidal electrolytes it was decided to examine the behavior of mixtures of dodecyltrimethylammonium chloride and sodium dodecyl sulfate. The work soon was expanded to include solutions consisting of the corresponding hydroxide and acid and also the decyltrimethylammonium chloride and hydroxide. Apparently little previous work has been undertaken with these alkyl sulfate salts of the quaternary ammonium bases. Bolle and Bourgeois¹ have prepared several of these compounds from the sulfate esters but had not reported upon their properties. Anacker² studied the light scattering of solutions of the related compounds, octyltrimethylammonium octane sulfonate and the corresponding decane sulfonate.

Experimental

The preparation of the decyl- and dodecyltrimethylammonium chloride is described in the following paper.³ The sodium dodecyl sulfate was supplied by Professor K. J. Mysels and also has been described previously.⁴ The decyl- and dodecyltrimethylammonium dodecyl sulfate solutions normally were prepared by converting the corresponding quaternary salts to the hydroxides and the dodecyl sulfate to the acid form by passage through appropriate ion exchange columns. Each solution then was standardized against HCl or NaOH and equivalent amounts of each were mixed as needed. No changes were observed in the standard solutions during the series of experiments. For the surface tension work a stable concentrated solution, 0.0685 *M*, was diluted for the different measurements. A second set of measurements was taken on mixtures of equivalent amounts of the sulfate and quaternary salts.

Dye solubilization determinations and electrophoretic mobility measurements were made by the procedure recently described.³ Surface tension measurements were made with a Du Nouy tensiometer at $25 \pm 1^\circ$.

Results

Stability of Solutions.—One of the several unusual properties of solutions of decyl- and dodecyltrimethylammonium dodecyl sulfate is the apparent stability of highly concentrated solutions, the instability of relatively dilute solutions, and

the stability of very dilute solutions. One of the first solutions of dodecyltrimethylammonium dodecyl sulfate prepared was 0.0685 *M* and has been sitting without any sign of instability for five months. Dilution of this solution with tap or deionized water causes separation of a flocculent precipitate. The rate of precipitation increases as the solution is made progressively more dilute. Dilution to $1 \times 10^{-3} M$ causes separation of a precipitate within 3 to 4 days. Dilution to $6 \times 10^{-5} M$ will produce a precipitate within approximately 30 minutes. Dilution to $1 \times 10^{-5} M$ or less does not produce any precipitate. The volume of precipitate is greater for the more concentrated solutions.

For initial concentrations less than that of approximately $1 \times 10^{-4} M$ the precipitate can be made to dissolve by heating the solution to 60–80°. If the hot solution is permitted to cool undisturbed to room temperature, the precipitate will reappear as a ring of coacervate floating half way up in the solution and with a radius half that of the beaker. Using different size beakers changes the diameter of the ring. The formation of these coacervate rings was observed for solutions of the decyl and dodecyl compounds in the concentration range of $5 \times 10^{-4} M$ to $5 \times 10^{-3} M$ with or without an excess of either the quaternary compound or the dodecyl sulfate. If some water-insoluble dye such as Sudan IV is solubilized in the hot solution then most of it will appear in the coacervate, coloring the ring a deep red. A photograph of one such ring has been published.⁵

Surface Tension and C.M.C. Determinations.—The time lag in the formation of the precipitate permits determination of the surface tension of these solutions. Figure 1 shows the results obtained upon dilution of the concentrated (0.0685 *M*) solution of dodecyltrimethylammonium dodecyl sulfate. Low values of approximately 30 dynes per cm. were obtained in solutions as dilute as $3 \times 10^{-5} M$. As a check, separate determinations on dodecyltrimethylammonium chloride and sodium dodecyl sulfate solutions were made and then on mixtures of these two solutions. These results are indicated by the x's on the graph. These solutions are not identical with the first series since

(1) J. Bolle and L. Bourgeois, *Mem. serv. chim. etat (Paris)*, **38**, 159 (1953).

(2) E. W. Anacker, *J. Colloid Sci.*, **8**, 402 (1953).

(3) H. W. Hoyer and A. Marmo, *J. Phys. Chem.*, **65**, 1807 (1961).

(4) R. J. Williams, J. N. Phillips and K. J. Mysels, *Trans. Faraday Soc.*, **51**, 728 (1955).

(5) *Chem. Eng. News*, **38**, 104, July 4, 1960.

they contain an equivalent amount of NaCl due to the manner in which they were prepared. This additional NaCl depresses the surface tension below that of the solution of the pure compound.

†. This type of surface tension curve is typical of colloidal electrolytes. In dilute solutions the simple ions exist, and with increasing concentration the surface tension decreases to a minimum value. This minimum has generally been interpreted as the concentration range in which micelle formation occurs. Our surface tension data would require a c.m.c. for the dodecyl compound at approximately $3 \times 10^{-5} M$. To check this we attempted both dye absorption and dye solubilization determinations. Both proved inadequate for the dodecyl compound and we then prepared the decyltrimethylammonium dodecyl sulfate. A spectral change was observed with the dye absorption method but the apparently low micelle concentration made detection of the precise concentration region at which this occurred extremely difficult. Fortunately the dye solubilization technique proved adequate and gave a value of the c.m.c. of $1.9 \times 10^{-4} M$ for the decyl compound. Surface tension measurements on this compound also gave values in this region. We concluded that the surface tension minimum of approximately $3 \times 10^{-5} M$ for dodecyltrimethylammonium dodecyl sulfate does represent the c.m.c. for this compound even though this could not be confirmed by dye solubilization or absorption for this compound.

Micelle Mobilities.—Since the preceding clearly demonstrated the existence of micelles at concentrations considerably below those previously reported for colloidal electrolytes, we decided to investigate the electrophoretic mobility of these micelles. Since the compound is formed from equivalent amounts of an anionic and a cationic detergent, one expects the formation of a neutral micelle with little or no electrophoretic mobility. On the other hand, the extremely low ionic strength of the solution should enhance the mobility of any ionic micelle which might form. Because of the higher stability of the decyltrimethylammonium dodecyl sulfate solution, we decided to work with it rather than with the dodecyl compound. As an additional precaution against precipitation we made our mobility determinations at 35° . Prior work⁶ had shown that temperature effects on the mobility of micelles are slight, the increased mobility at higher temperatures being readily accounted for by the increased fluidity of the water.

Four determinations were made at concentrations of $2.5 \times 10^{-4} M$. Two of these were on solutions prepared by mixing equivalent amounts of decyltrimethylammonium hydroxide and dodecyl hydrogen sulfate and two by mixing equivalent amounts of the corresponding chloride and sodium salts. In each case the micelle had a negative charge as shown by the direction of migration in the electrophoresis apparatus. The four determinations gave values of mobility equal to $1.09 \pm 0.02 \times 10^{-4} \text{ cm.}^2 \text{ per volt-sec.}$ The mobilities then were determined in the presence of

(6) H. W. Hoyer and A. Greenfield, *J. Phys. Chem.*, **61**, 735 (1957).

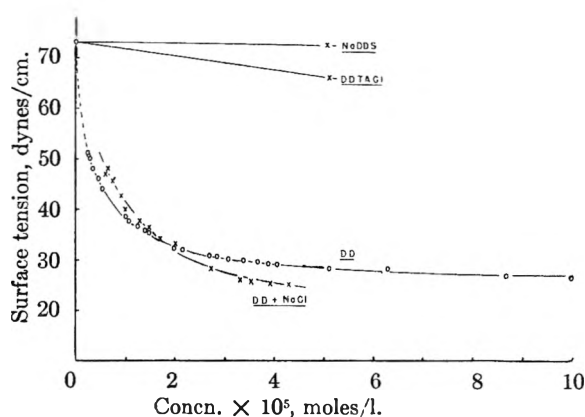


Fig. 1.—Surface tension measurements of dodecyltrimethylammonium dodecyl sulfate (DD) without and with an equivalent amount of NaCl: NaDDS = sodium dodecyl sulfate, DDTACl = dodecyl trimethylammonium chloride.

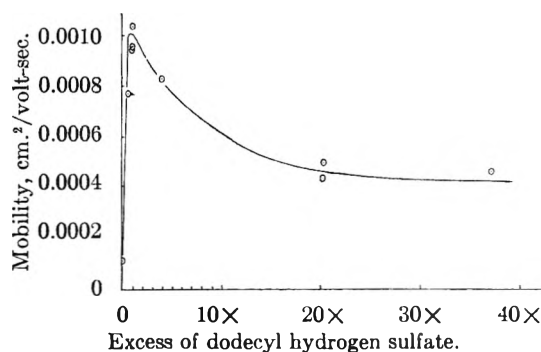


Fig. 2.—Electrophoretic mobility of the decyltrimethylammonium dodecyl sulfate micelle in the presence of an excess of dodecyl hydrogen sulfate. The concentration of decyltrimethylammonium dodecyl sulfate is $2.5 \times 10^{-4} M$.

an excess of dodecyl hydrogen sulfate. The resulting data are shown in Fig. 2 along with the average value obtained for the four determinations mentioned above. The mobility rises rapidly and reaches a maximum value of $0.001 \text{ cm.}^2 \text{ per volt-sec.}$ when approximately a 100% excess of the sulfate is present and then falls slowly as more of the dodecyl hydrogen sulfate is added.

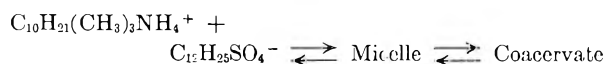
An attempt to reproduce this behavior with varying excesses of decyltrimethylammonium hydroxide proved impossible since solutions with a 50% excess of this compound were unstable even at elevated temperatures. However, a solution with a 25% excess proved stable. Mobility measurements show that in this case the micelle was now positively charged and had a mobility of $3.9 \times 10^{-4} \text{ cm.}^2 \text{ per volt-sec.}$

Discussion

The discovery of the micellar nature of this class of compounds extends the phenomenon of micelle formation to extremely dilute concentration. The majority of association colloids so far studied have critical micelle concentrations in the range of 10^{-2} to $10^{-3} M$.⁷ We have found that the decyltrimethylammonium dodecyl sulfate micelle exists above concentrations of $3 \times 10^{-5} M$. However, at the slightly higher concentrations of approximately $6 \times 10^{-5} M$, the micelle exists

(7) H. B. Klevena, *J. Am. Oil Chemists' Soc.*, **30**, 74 (1953).

in equilibrium with a colloid-rich coacervate. The micellar range of the corresponding decyltrimethylammonium dodecyl sulfate is somewhat greater, extending from $1.9 \times 10^{-4} M$ to approximately $5 \times 10^{-4} M$. The equilibria existing in these solutions may be written



Surface tension, electrical conductivity, dye solubilization and dye adsorption determinations support this view.

The formation of the coacervate rings upon cooling presented an interesting problem. Apparently they are produced by the convection currents generated as the solution cools. These will be downward near the glass wall and upward in the center of the beaker. They would thus tend to sweep any material with a density close to that of water into a ring shaped region half way up the solution and with a radius half that of the beaker. These conditions were observed with containers of different sizes. An analogous phenomenon is the manner in which a precipitate collects in the center of the bottom of a beaker when the liquid in the beaker is swirled.

The surface tension behavior of these solutions, while unusual insofar as low values are obtained at concentrations approximately 1/100 as large as those usually observed for the surface active agents, is still explainable in terms of the action of such agents. It would appear that this group of compounds affords a transition from the soluble surface active compounds to the "insoluble" surface film-forming substances. It might be expected that these substances will possess unusual emulsifying properties. Preliminary studies show that they form oil in water emulsions of high stability and water in oil emulsions of moderate stability.

The mobility measurements raise a number of theoretical questions, only some of which can be answered at this time. Why did the apparently

neutral micelle possess such a high mobility? We are inclined to believe that a number of factors, including the low ionic strength of the solution, the size of the micelle and the high surface activity of the decyltrimethylammonium hydroxide, are responsible. The mobility rises so rapidly with addition of dodecyl hydrogen sulfate that adsorption of a small fraction of the highly dilute quaternary compound on the surface of the glass could readily produce a negatively charged micelle with a slight excess of the dodecyl sulfate. The observed formation of a negatively charged micelle upon addition of a known excess of dodecyl hydrogen sulfate and of a positively charged micelle with an excess of the quaternary compound is in agreement with this point of view.

It is well established that addition of hydrocarbons or long chain alcohols to solutions of association colloids results in their incorporation into the micelle. The present work demonstrates that this is also true for amphipathic ions and shows that such a process can produce marked changes in the electrical properties of the micelle. Upon the continued addition of an excess of hydrogen dodecyl sulfate to a micellar solution of decyltrimethylammonium dodecyl sulfate the electrophoretic mobility increases rapidly to a maximum of $10 \times 10^{-4} \text{ cm.}^2$ per volt-sec. and then decreases gradually. The initial rapid increase can only be due to the incorporation of the dodecyl sulfate ion into the micelle. This results in a gradual increase in the negative charge on the micelle. Eventually the micellar charge becomes great enough to prevent the further incorporation of the dodecyl sulfate into the micelle. Continued addition of the dodecyl hydrogen sulfate then decreases the mobility due to the repression of the ionic atmosphere by the added electrolyte.

Acknowledgment.—We are indebted to the National Science Foundation for the financial support which made this work possible and to Professor Karol J. Mysels for making available the high purity sodium dodecyl sulfate.

THE ELECTROPHORETIC MOBILITIES AND CRITICAL MICELLE CONCENTRATIONS OF THE DECYL-, DODECYL- AND TETRADECYLTRIMETHYLAMMONIUM CHLORIDE MICELLES AND THEIR MIXTURES

BY HORST W. HOYER AND ANNE MARMO

Chemistry Department, Hunter College of the City University of New York, New York 21, N. Y.

Received June 27, 1960

The electrophoretic mobilities of the decyl-, dodecyl- and tetradecyltrimethylammonium chloride micelles were studied at 25° as functions of their concentrations in aqueous solution. The values obtained were 2.78, 3.50 and 5.06×10^{-4} cm.² per volt-sec., respectively, at the corresponding critical micelle concentrations. The mobilities of mixtures of the dodecyl and tetradecyl quaternary compounds, but not the corresponding critical micelle concentrations, were found to be linear functions of the mole fractions of the two substances. Addition of dodecyl alcohol to the dodecyltrimethylammonium chloride solution gave values of the mobility essentially that of the pure quaternary amine salt at its critical micelle concentration. The data require that 74% of the gegenions surround the micelle in a compact double layer while the remaining 26% constitute the diffuse double layer, the potential of which is essentially that given by the zeta potential.

Introduction

The present investigation was undertaken to extend our experimental information concerning the electrophoretic mobility of colloidal electrolytes, specifically that of the micelles of the alkyl trimethylammonium chlorides and their mixtures. Previous work had been concerned with the mobilities of the sodium lauryl sulfate micelles¹ and that of the micelles of the decyl-, dodecyl- and tetradecylamine hydrochlorides.² Included with the latter was a study of the effect of temperature on the mobility of the dodecylamine hydrochloride micelle. In the present work we wished to study the mobility of the decyl-, dodecyl- and tetradecyltrimethylammonium chloride micelles and the micelles produced by mixtures of these substances with one another. Included in our study was an evaluation of the effect of dodecyl alcohol on the mobility of the dodecyltrimethylammonium chloride micelle.

Experimental

Preparation of Quaternary Ammonium Salts.—The decyl-, dodecyl- and tetradecyltrimethylammonium chlorides were prepared using essentially the procedure of Reck, Harwood and Ralston³ except that, in the absence of a high pressure reaction vessel, the corresponding iodides were first formed and then converted to the chlorides by exchange reaction with a saturated solution of silver chloride. The more insoluble silver iodide is precipitated and the quaternary ammonium chloride remains in solution. The procedure for decyltrimethylammonium chloride is given.

To a mixture of 62.9 g. of decylamine,⁴ 48 ml. of water and 400 ml. ethanol was added dropwise 55 ml. of 80–90% formic acid. The temperature rose to 37°. Then 80 ml. of 36% formaldehyde was added and the temperature was raised slowly to 60°. The solution was maintained between 60 and 80° for approximately three hours at which time the evolution of carbon dioxide had ceased. It then was made alkaline with sodium hydroxide and the tertiary amine separated and dried over sodium carbonate. The amine was vacuum distilled through a one-meter vacuum-jacketed column and 22.6 g. of decyldimethylamine, coming over at 176–178° and 172 mm. pressure, was obtained. To the cold amine was added 34 ml. of methyl iodide. The resulting crystals of decyltrimethylammonium iodide were

separated and recrystallized from acetone. These were converted as needed to solutions of the corresponding chloride by letting a solution of the iodide stand overnight, with agitation, in contact with silver chloride. Evaporation of a sample of the solution to dryness, sodium fusion of the residue, and a resulting negative iodide test served to indicate completion of the exchange reaction. It was necessary to resort to sodium fusion of the residue in order to destroy the amine since it interferes if the iodide test is run on the solution.

The procedure for the preparation of the dodecyl- and tetradecyltrimethylammonium chloride is similar to the above. The dodecyldimethylamine distilled over at 132–134° at 13 mm. pressure and the tetradecyldimethylamine came over at 141–143° at 6 mm. Because of the lower solubility of the iodides of these compounds the exchange reaction with silver chloride required several days for completion.

Dodecyl Alcohol.—The dodecyl alcohol was Eastman Kodak grade and was used as received. A solution of the alcohol was prepared by adding sufficient dodecyl alcohol to 0.0732 *M* dodecyltrimethylammonium chloride solution so that the solutes consisted of 6.09 mole % dodecyl alcohol and 93.91 mole % quaternary ammonium chloride. Since the alcohol does not dissolve readily, it was necessary to heat the mixture to 65° for one hour with occasional shaking to effect solution.

Mobility and C.M.C. Determinations.—Electrophoretic mobilities were determined by the open tube,¹ dye solubilization⁵ method used with the hydrogen ion coulometer.⁶ Purified Sudan IV was used as the solubilized dye.

Critical micelle concentrations were determined by conductivity measurements and by dye solubilization determinations.⁷ The former proved inadequate for mixtures of the different quaternary salts in that the transition regions were not abrupt enough for precise determination of the critical micelle concentrations. However, solubilization of Sudan IV in solutions consisting of different concentrations of the quaternary salts permitted extrapolation to a concentration of the salt at which no dye would be solubilized. The undissolved dye may be separated by filtration or by centrifugation. In spite of the objections leveled against the former procedure for removing undissolved dye, we could find no differences in the critical micelle concentrations determined by these two methods and therefore, because of its much greater convenience, used the filtration procedure. It is possible to prepare the solubilized dye by either heating the dye with the detergent for 2 to 3 hours at 60–75° and then letting the solution stand at room temperature for 3 or 4 days or by shaking the dye with the solution at room temperature for 3 or 4 days. Almost identical values were obtained by these two methods for several different quaternary amine solutions. Because of the convenience of the heating method, it was adopted as our procedure for the determination of the c.m.c.

(1) (a) H. W. Hoyer, K. J. Mysels and D. Stigter, *J. Phys. Chem.*, **58**, 385 (1954); (b) D. Stigter and K. J. Mysels, *ibid.*, **59**, 45 (1955).

(2) H. W. Hoyer and A. Greenfield, *ibid.*, **61**, 735 (1957).

(3) R. A. Reck, H. J. Harwood and A. W. Ralston, *J. Org. Chem.*, **12**, 517 (1947).

(4) Distilled decyl-, dodecyl- and tetradecylamines were supplied by the Research Division of Armour and Co.

(5) H. W. Hoyer and K. J. Mysels, *J. Phys. Chem.*, **54**, 966 (1950).

(6) H. W. Hoyer, *ibid.*, **60**, 372 (1956).

(7) A discussion of these and other methods for determining critical micelle concentrations may be found in the paper by R. J. Williams, J. N. Phillips and K. J. Mysels, *Trans. Faraday Soc.*, **51**, 728 (1955).

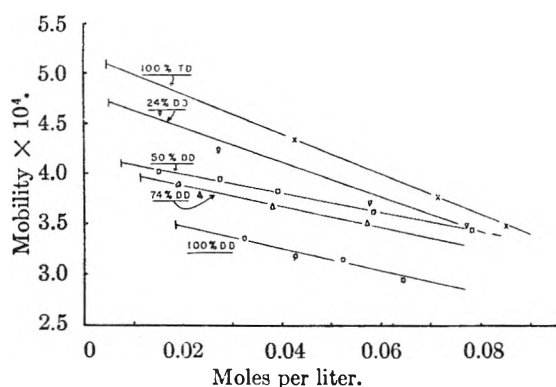


Fig. 1.—The electrophoretic mobilities of dodecyltrimethylammonium chloride (DD), tetradecyltrimethylammonium chloride (TD) and their mixtures at 25°; mobility in cm.^2 per volt-sec.

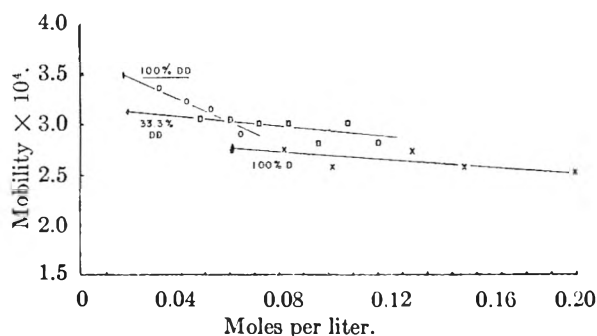


Fig. 2.—The electrophoretic mobilities of decyltrimethylammonium chloride (D) and dodecyltrimethylammonium chloride (DD) and of a mixture of the two; mobilities in cm.^2 per volt-sec.

Results

Decyl-, Dodecyl- and Tetradecyltrimethylammonium Chlorides and their Mixtures.—Figure 1 shows the values obtained for the mobilities of the dodecyl- and the tetradecyltrimethylammonium chloride micelles and of the micelles formed from mixtures consisting of 24, 50 and 74 mole % of the dodecyl compound. The data for each mixture are extrapolated to the critical micelle concentration which is indicated by a small vertical dash at the left end of each curve in the different figures. Figure 2 gives the experimental data for the mobilities of the decyltrimethylammonium chloride, the corresponding dodecyl compound, and a mixture containing 66.7 mole % of the decyl compound. The extrapolated values at the c.m.c. are particularly significant since these represent mobilities at the concentrations at which the micelles are first formed from solutions of the monomer ions. These are listed in Table I along with the corresponding c.m.c. values.

Dodecyltrimethylammonium Chloride and Dodecyl Alcohol.—In order to investigate the effect of a solubilized long chain alcohol on the mobility of the micelle a solution of dodecyl alcohol and dodecyltrimethylammonium chloride in a mole ratio of 6.09 to 93.91 was prepared. Mobilities were determined on this solution and on dilutions of this solution in which the same ratio of alcohol to quaternary salt was maintained. These results are shown in Fig. 3. The data for the dodecyltrimethylammonium chloride are again plotted on the same scale for purposes of comparison. The

TABLE I
CRITICAL MICELLE CONCENTRATIONS AND ELECTROPHORETIC MOBILITIES AT THE C.M.C. FOR DECYL-, DODECYL- AND TETRADECYLTRIMETHYLAMMONIUM CHLORIDES

Decyl	Moles Dodecyl	Tetradecyl	C.M.C. (moles/l.)	Mobility at c.m.c. ($\text{cm.}^2/\text{volt-sec.}$)
0	1	0	0.0172	3.50×10^{-4}
0	2.86	1	.0114	3.97×10^{-4}
0	1	1	.00747	4.20×10^{-4}
0	1	3.15	.00501	4.72×10^{-4}
0	0	1	.00447	5.06×10^{-4}
1	0	0	.0611	2.78×10^{-4}
2	1	0	.0196	3.12×10^{-4}

average value of $3.42 \times 10^{-4} \text{ cm.}^2$ per volt-sec. is within the experimental accuracy of the value 3.50×10^{-4} obtained by extrapolation of the mobilities of the pure dodecyl solution to its c.m.c.

Discussion

In previous work on the mobilities of the aliphatic amine hydrochloride micelles⁸ it had been observed that a linear relationship exists between the log of the micelle mobility and the log of the total gegenion concentration. As a special case of this, the log of the mobility at the c.m.c. must also be proportional to the log of the c.m.c. We have observed that this latter special case is true for the quaternary ammonium salts studied. On such a plot the values for the quaternary salts fall on a line with a slightly greater slope, and with a small displacement toward lower mobility values than do the values for the amine hydrochloride micelles. This supports the conclusion reached in the earlier work that the ionic strength of the solution is one of the more important factors influencing micelle mobility. The small differences observed for the two homologous series imply that structural factors are also important.

That such factors are important is shown in Fig. 4 in which the mobilities and c.m.c.'s of the micelles of dodecyl and tetradecyltrimethylammonium chloride and of their mixtures are plotted against the mole fraction of dodecyl compound. The linear relation observed for the mobilities implies that, in the mixture, the mobility is given by an equation of the form

$$u = N_1u_1 + N_2u_2 \quad (1)$$

where the u 's refer to the electrophoretic mobilities and the N 's to the mole fractions of compounds 1 and 2.

In recent years the theory of electrophoresis has been developed extensively, particularly by Booth⁸ and by Overbeek.⁹ Stigter and Mysels^{1b} have used the results of these workers to determine the zeta potentials and charges on the sodium dodecyl sulfate micelles, simplifying the calculations by using inverted forms of Booth's original series. Using these inverted series we have calculated zeta potentials and charges for the decyl-, dodecyl and tetradecyltrimethylammonium chloride micelles and their mixtures. The results are given in Table II.

(8) F. Booth, *Proc. Roy. Soc. (London)*, **A203**, 514 (1950).

(9) J. Th. G. Overbeek, *Kolloid-Beih.*, **54**, 316 (1943).

TABLE II
ZETA POTENTIALS AND CHARGES FOR ALIPHATIC
QUATERNARY AMMONIUM CHLORIDE MICELLES AT THEIR
CRITICAL MICELLE CONCENTRATIONS

Mole fraction of quaternary ammonium chloride			Zeta potential (m.v.)	Charge per micelle	Charge per molecule
C-10	C-12	C-14			
1.00	0.00	0.00	53.5	11.5	.28
0.67	0.33	.00	65.3	11.1	.28
.00	1.00	.00	75.0	13.4	.24
.00	0.74	.26	87.1	15.7	.26
.00	.50	.50	93.8	16.4	.25
.00	.24	.76	103.8	19.0	.26
.00	.00	1.00	115.0	20.7	.25

In making these calculations it was necessary to know the radii of the corresponding micelles. We have averaged the values reported by Debye¹⁰ and Trap and Hermans¹¹ from light scattering experiments on the bromides, recalculated these to values for the chlorides, and used them along with interpolated values for the mixed micelles.

It is interesting to observe that, while the zeta potentials and the charges on the micelles increase as the micellar molecular weight increases, all seven micelles show the same per cent. ionization, $26 \pm 1\%$. This, however, is not to be interpreted to mean that only 26% of the molecules are ionized. Since electrovalent compounds such as these quaternary ammonium chlorides are always ionized, it is necessary to regard the surface of the micelle as composed of completely ionized groups. Around the micelle, and traveling with it, there will be a layer of solution containing a definite concentration of gegenions. The outer boundary of this layer is the surface of shear and determines the zeta potential of the micelle. Even though the actual micellar charges vary from 11.5 to 20.7 all seven micelles studied have 74% of their gegenions within this surface. The remaining 26% of these gegenions constitute the ionic atmosphere. This result carries with it the important consequence that the ratio of chloride ion to quaternary ion in the micelles is constant and therefore the consequence that the activities of these ions in the micelle are also constant.

It is well established that colloidal electrolytes in aqueous solutions are surrounded by a diffuse ionic layer determined by the gegenions. The unusual aspect of the zeta potential of these micelles is that it acts as if it were the total diffuse ionic potential. The justification for this remark will be given.

For an equilibrium system involving micelle and solution the electrochemical potential of the chloride gegenion must be identical throughout. We therefore write

$$\mu_{\text{Cl}}^s + ze\phi^s = \mu_{\text{Cl}}^m + ze\phi^m \quad (1)$$

where μ is the chemical potential, ϕ the galvanic potential deep within each region, e the electronic charge, z the chloride ion charge and where the superscripts s and m refer to solution and micelle, respectively. We also may write

(10) P. Debye, *J. Phys. Chem.*, **53**, 1 (1949).

(11) H. J. L. Trap and J. J. Hermans, *Proc. Koninkl. Ned. Akad. Wetenschap.*, **58B**, 97 (1955).

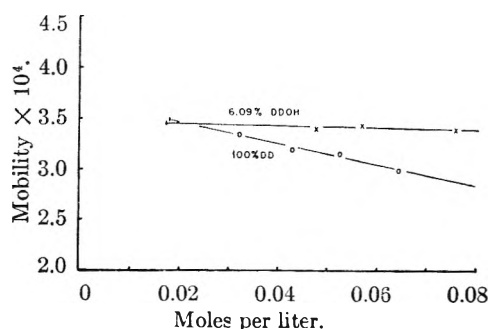


Fig. 3.—The electrophoretic mobilities of dodecyltrimethylammonium chloride and of a solution of it containing 6.09% dodecyl alcohol; mobilities in cm^2 per volt-sec.

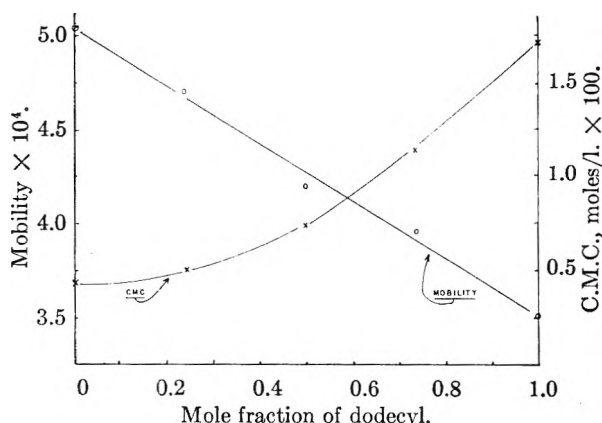


Fig. 4.—Mobilities and c.m.c.'s of mixtures of dodecyl- and tetradecyltrimethylammonium chlorides, mobilities in $\text{cm}^2/\text{volt-sec}$.

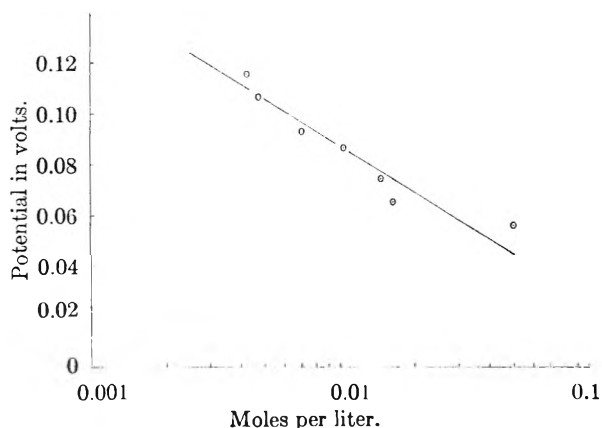


Fig. 5.—The zeta potential *versus* activity plot for the decyl-, dodecyl- and tetradecyltrimethylammonium chloride micelles and their mixtures at their critical micelle concentrations.

$$\mu_{\text{Cl}}^s = \mu_{\text{Cl}}^m + kT \ln a \quad (2)$$

where a is the activity of the chloride gegenions in the equilibrium solution. By analogy we write for the chemical potential of the chloride ion in the micellar region

$$\mu_{\text{Cl}}^m - \mu_{\text{Cl}}^s = kT \ln a^m = \text{constant} \quad (3)$$

The last equality of equation 3 follows from the requirement that the activities of quaternary and chloride ions in the micelle are constant. Substituting (2) and (3) into (1) gives

$$\phi^m - \phi^s = \text{constant} + \frac{kT}{ze} \ln a \quad (4)$$

This difference in galvanic potential normally is divided into two parts,¹² the χ potential connected with the polarization and orientation of neutral molecules at the interface, and the diffuse ionic potential, D , from the distribution of free charges in the solution around the particle. If the χ potential is assumed to be independent of the distribution of the ionic charges near the interface then the diffuse potential must vary with the ionic concentration in a manner similar to that of the galvanic potential difference

$$D = \phi^m - \phi^s - \chi = \text{constant} + \frac{RT}{zF} \ln a \quad (5)$$

R and F are the gas and faraday constants.

If it were possible to plot the diffuse ionic potential as a function of the gegenion activity a semi-log plot according to equation 5 would give a slope of -0.059 . Although diffuse ionic potentials cannot be measured it is possible to calculate zeta potentials according to Booth's theory. The values obtained for these quaternary ammonium chloride micelles are tabulated in Table II and plotted in Fig. 5. The slope of the best straight line, as found by the least squares method, is -0.061 . The activity of the chloride ion was taken to be the

(12) See, for example, J. Th. G. Overbeek and J. Lyklema, "Electrical Potentials in Colloidal Systems" in "Electrophoresis," edited by M. Bier, Academic Press, New York, N. Y., 1959.

same as that of the mean activity coefficient in sodium chloride solutions of the same concentration. While this is an unproven assumption it may be pointed out that the use of concentrations rather than activities results in only a small change in the slope.

The close agreement between the experimental slope for the zeta potentials and the theoretical slope for the diffuse potential suggests that, within the limits of present day experimental technique, the zeta potential in systems of thermodynamically stable colloidal electrolytes is essentially equal to the total diffuse ionic potential. Physically this is equivalent to asserting that the micelle is surrounded by a compact portion of the double layer which includes a fixed fraction, 74% for the systems studied, of the gegenions necessary to "neutralize" the micelle. The remainder of the gegenions are distributed in a diffuse double layer. The compact inner portion of the double layer is relatively unresponsive to changes in equilibrium electrolyte concentration, that is, to changed critical micelle concentrations. Such effects are reflected by changes in the zeta potential of the outer diffuse layer.

Acknowledgment.—The authors gratefully acknowledge financial support furnished for this work by the National Science Foundation. Drs. Karol and Estella Mysels offered constructive criticism during the writing of this paper.

WATER SORPTION BY DEXTRANS AND WHEAT STARCH AT HIGH HUMIDITIES

BY N. W. TAYLOR, J. E. CLUSKEY AND F. R. SENTI

Northern Regional Research Laboratory,¹ Peoria, Illinois

Received October 22, 1950

Water absorption and desorption isotherms of amorphous dextran, partially crystallized dextran, and wheat starch were determined at relative humidities between 74 and 99.7%. Water sorption of NRRL B-512 dextran was followed before, during and after crystallization. Results, interpreted according to the Flory-Huggins polymer solution theory, indicate that at water contents of 33% and higher, the amorphous dextrans behave as randomly coiled polymers in solution, apparently free of complications due to physical structure. The water absorptions of the partially crystallized dextran, and also of the starch, were interpreted by comparison with amorphous dextrans in terms of current concepts of effects of crystallinity and elastic network.

It was shown previously that water absorption by dextrans is influenced by the presence of crystallinity and that in amorphous dextrans the water adsorption is only slightly dependent upon chemical structure,² if at all.

High water absorption at high relative humidity (RH) and disappearance of hysteresis suggest that in this region water absorption is essentially a solution process. The mechanism of water absorption at high RH by such amorphous dextrans appears to be relatively simple compared to that by starch, for example. For this reason dextrans may serve as model substances with which to compare absorp-

tion by starch. In this work, water absorptions of wheat starch and several dextrans have been determined in the RH range approaching saturation.

At RH higher than ordinary atmospheric conditions, the additional water absorbed by biological polymers generally is assumed to be in a state similar to liquid water or water in solution or, in certain cases, to be in part pure water in capillary pores. Both these ideas evolved fairly early^{3,4} and are applicable in individual cases. Because there appear to be few, if any, distinct pores in starch,⁵ the possibility of pore absorption was not considered. Since the advent of the polymer solu-

(1) This is a laboratory of the Northern Utilization Research and Development Division, Agricultural Research Service, U. S. Department of Agriculture.

(2) N. W. Taylor, H. F. Zobel, N. N. Hellman and F. R. Senti, *J. Phys. Chem.*, **63**, 599 (1959).

(3) J. J. Hedges, *Trans. Faraday Soc.*, **22**, 178 (1926).

(4) J. R. Katz, *ibid.*, **29**, 279 (1933).

(5) N. N. Hellman and E. H. Melvin, *J. Am. Chem. Soc.*, **72**, 5186 (1950).

tion theory developed by Flory⁶ and by Huggins,⁷ the meaning of absorption of solvents by polymers as a solution process has been clarified. The theory is a good description particularly of the solution behavior of randomly coiled, non-polar polymers. Reviews of this theory^{8,9} and of water absorption by polymers¹⁰⁻¹³ have appeared. It has been suggested that the theory also may adequately describe water absorption by proteins and other biological polymers.^{14,15}

Superimposed on water sorption as a solution process are the effects of physical structure on sorption. Water absorption is limited by the crystalline phase present in some polymers. In cellulose, for example, water uptake is proportional at intermediate RH to the fraction of amorphous material, as distinct from crystalline. The proportion of amorphous material, however, does not account for all variation in water sorption observed in cellulose samples, particularly at higher RH.¹⁶

Another structure which limits water absorption is the cross-linked network such as has been postulated in wool¹⁷ and other insoluble polymers. The effects of chemically cross-linked structures on solvent absorption by synthetic polymers¹⁸ have been investigated and provide further reference systems to which water absorption by starch may be compared.

In a crystalline polymer, the amorphous material may be constrained by an elastic network composed of molecular chains running between different crystalline regions. Because the amount of crystallinity and other physical structures is only partly known in polymers such as starch, their relation to water sorption is still unresolved.

Experimental

Materials.—Wheat starch was prepared in the pilot-plant by washing flour dough with cold tap water. Defatted wheat starch was prepared by refluxing wheat starch 4 times with 85% methanol, according to Schoch.¹⁹

NRRL B-1398 dextran was native dextran prepared in this Laboratory by Jeanes, *et al.*²⁰ NRRL B-512 dextran, an unhydrolyzed preparation synthesized enzymatically in the pilot plant,²¹ had a molecular weight of about 2 million as determined by light scattering. Both dextrans, as prepared, had amorphous X-ray diffraction patterns.

Methods.—The sorption of water was determined by

measuring the weight of water in the sample at a controlled RH. The apparatus consisted essentially of a sample flask, a flask of water as a humidity source, and a precision mercury manometer, interconnected by a manifold. The apparatus was built around a standard vacuum line with a mercury diffusion pump backed by a mechanical pump. High-vacuum grade stopcocks were used throughout. The sample and water flasks were in separate water-baths at temperatures controlled within about 0.01° or about 0.02° on overnight runs. Relative humidity (RH, *i.e.*, water vapor pressure, as the percentage of vapor pressure of water at the temperature of the sample) over the sample was controlled by the temperature of the water flask. The sample flask was controlled at 25.10°. Thermometers were calibrated by comparison with thermometers calibrated by the National Bureau of Standards. One thermometer was further calibrated occasionally by determining its reading at the sodium sulfate decahydrate transition point.²² It appeared that the temperatures measured were accurate within about 0.01°.

The sample was contained in a vacuum flask with a right-angle high-vacuum stopcock having a rim for a mercury seal (Eck and Krebs 5050).²³ The rim prevented loss of grease in handling. The flask was attached to the manifold section by means of a 10/30 standard taper joint. The flask was evacuated and weighed against a tare which displaced the same volume of air, within 1 m. After the flask and tare sat on the balance at least half an hour, weighings were reproducible within a few tenths of 1 mg. The dry weight of a sample in the flask was determined by evacuating the flask to constant weight and subtracting the weight of the empty evacuated flask, with corrections for the known weights of stopcock grease. Drying was accomplished by evacuation and heating to 60 or 70° with a light bulb in a chimney. At room temperature a sample of starch dried to the same weight but slower. Dry weights of samples were reproducible within 0.3 mg. Reproducibility of sorbed water weights was consistent with the precision of temperature control and pressure measurement.

Weights of water absorbed in the samples were corrected for the weight of water vapor in the flask. The weight of vapor was proportional to pressure up to 98% RH, and agreed with tabulated density of water vapor when extrapolated to 100% RH. Above 98% the experimental vapor weight increased abruptly, *e.g.*, to 4.7 mg. instead of 3.9 mg. at 99.7% RH, owing to adsorption on the glass.

Water vapor pressure was read in a 25-mm. wide manometer viewed with a cathetometer composed of a telescope in a Gaertner comparator mounted on a rotating cathetometer stand. The telescope objective was about 5 inches from the manometer tubes. At this distance an NBS calibrated meter bar could be measured correctly within a few microns. Vapor pressure readings on water, reproducible within about 0.01 mm. or occasionally 0.02 mm., agreed with E. W. Washburn's values.²⁴ No meniscus correction was necessary.²⁵ Zero pressure read about 0.01 mm. of negative pressure, even though both sides of the manometer could be exhausted.

The pressure of residual air in the system was measured in a section composed of a Pirani gage and a small cold trap to which a solid CO₂ freezing mixture could be applied. In preliminary experiments pressures greater than 10 μ of non-condensable gas slowed considerably the rate of approach to equilibrium. Therefore, pressure was kept below 5 μ in general; in a few cases where pressure of air rose above 10 μ experimental data were rejected. To maintain this low air pressure without resorting to long periods of evacuation, it was necessary to flush with water vapor all glass which had been exposed to air. Three successive admissions of vapor, each followed by 10-minute evacuations, were sufficient. Condensation was prevented in the parts of the apparatus not in the water-baths by heating with light bulbs and resistance wire wound around the glass tubing. Where the flasks entered the baths, plastic shields were slipped over the necks to prevent evaporation and cooling on the outside.

- (6) P. J. Flory, *J. Chem. Phys.*, **10**, 51 (1942).
- (7) M. L. Huggins, *Ann. N. Y. Acad. Sci.*, **43**, 1 (1942).
- (8) M. L. Huggins, *ibid.*, **44**, 431 (1943).
- (9) P. J. Flory, "Principles of Polymer Chemistry," Cornell Univ. Press, Ithaca, N. Y., 1953, pp. 495-540.
- (10) M. Dole, *Ann. N. Y. Acad. Sci.*, **51**, 705 (1949).
- (11) A. D. McLaren and J. W. Rowen, *J. Polymer Sci.*, **7**, 289 (1951).
- (12) H. J. White and H. Eyring, *Textile Research J.*, **17**, 523 (1947).
- (13) John A. Howson, "Structure-Sorption Relationships," Part I, 2nd edition, E. Ott, H. M. Spurlin, and M. W. Grafflin, Eds., Interscience Publ. Inc., New York, N. Y., 1954, p. 393.
- (14) J. W. Rowan and R. Simha, *J. Phys. Colloid Chem.*, **53**, 921 (1949).
- (15) J. A. Cutler and A. D. McLaren, *J. Polymer Sci.*, **3**, 792 (1948).
- (16) P. H. Hermans, "Contribution to the Physics of Cellulose Fibres," Elsevier, Amsterdam, 1946.
- (17) A. B. D. Cassie, *Trans. Faraday Soc.*, **41**, 458 (1945).
- (18) P. Doty and H. S. Zable, Paper 4 in "High Polymer Physics," Part III, H. A. Robinson, ed., Remsen Press, New York, N. Y., 1948.
- (19) T. J. Schoch, *J. Am. Chem. Soc.*, **64**, 2054 (1942).
- (20) A. Jeanes, *et al.*, *ibid.*, **76**, 5041 (1954).
- (21) V. E. Sohns, S. P. Rogovin, H. F. Conway and C. T. Langford, U. S. Agricultural Research Service, AIC-372 (1954).

(22) J. Hole, *Chem. Met. Eng.*, **52**, 115 (1945).

(23) The use of trade names in this article is for identification only and implies no endorsement by the U. S. Department of Agriculture.

(24) "International Critical Tables of Numerical Data, Physics, Chemistry and Technology," Vol. III, McGraw-Hill Book Co., New York, N. Y., 1928, p. 211.

(25) F. A. Gould and T. Vickers, *J. Sci. Instr.*, **29**, 85 (1952).

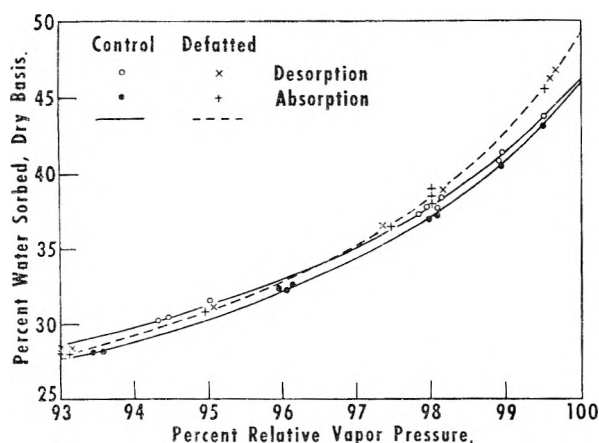


Fig. 1.—Water sorption isotherms of wheat starch at 25°.

Care was taken to obtain equilibria on the main absorption and desorption isotherms. Absorption equilibrium always was approached starting with an initially dry sample, and usually a series of ascending RH was investigated. Desorption equilibrium always was approached with an initially saturated sample (or water content over 100% of dry weight in the B-1398 dextran), and usually a series of descending RH was investigated.

Samples were distributed as thinly as possible around the inside of the sample flask. Thin sample layers and very low residual air pressures seemed to be the main factors favoring rapid attainment of equilibrium.

Results

Water Sorption of Wheat Starch.—Water absorption and desorption experiments on the wheat starch samples disclosed that equilibria were achieved in 4 hours in absorption experiments; subsequent 16-hour equilibration produced little change. In desorption experiments the water contents after 4 hours were sometimes appreciably higher than the values attained after 16 or more, but further equilibrations resulted in no significant change in water contents. Therefore 1-day or longer equilibrations were made on desorption.

No significant change occurred in the starch samples during the long series of experiments at high RH. Experiments performed at the end of the series, after five absorption-desorption cycles, agreed with earlier experiments at the same RH. The data thus accurately characterize the particular defatted wheat starch samples.

Water absorption and desorption experiments on the control wheat starch which was not defatted (Fig. 1) show that water sorption hysteresis exists, and the loop closes at saturated humidity.

In the absorption-desorption isotherm of defatted wheat starch (Fig. 1), remarkably little hysteresis was found in the RH region examined here. In other experiments at RH less than 85%, however, no significant difference from the control starch occurred. The isotherm for the defatted sample rises above the control isotherms shown in Fig. 1 as RH increases. The close agreement at 95% RH indicates that some mechanism may be involved other than removal of inert fatty material. A few data on a separately defatted sample showed that this isotherm fell between the absorption isotherms of the control and defatted samples in Fig. 1. Hence, the defatting procedure may influence water sorption somewhat.

Water Sorption of Dextran NRRL B-1398.—In general, in absorption experiments on B-1398 dextran (Table I), water contents attained in 4 hours and after 16 more hours agreed at RH below 99%.

TABLE I
WATER SORPTION OF DEXTRAN NRRL B-1398

RH, 100 p/p_0	Water content on absorption, dry basis, %	Water content on desorption, dry basis, %
99.7	192	213
99.2	144	
98.1	98.6 ± 0.4	100
88.8	40.3 ± .1	
80.0	27.7 ± .0	
74.0	23.0 ± .1	23.1 ± 0.1

In one experiment, a discrepancy in the values at these two times was attributed to the fact that the sample had formed a solution and collected at the bottom of the flask. After this experiment, excess water was added, and the sample was redistributed around the flask, frozen and dried. Subsequent 4-hour and longer equilibrated pairs at the same RH showed better agreement. The experiments at RH higher than 99% showed considerable drift in water content with further equilibration. When the large amount of water to be transferred per humidity increment at this RH is considered, a slower approach to equilibrium is expected. Desorption experiments required more than 4 hours to achieve equilibrium, as for the starch. The values in Table I are those after at least 16 hours of equilibration. Standard deviations are given where two or three observations were made.

There appeared to be no significant hysteresis of water content in B-1398 dextran at RH higher than 74%. There was a small difference in absorption and desorption results at 98.1%, and a substantial difference at 99.7%, but this last can be attributed to a slower approach to equilibrium as a result of the larger amounts of water to be transferred at the highest RH. If absorption and desorption results at the longest times are averaged, it appears that 205% of water is held at 99.7% RH.

Water Sorption of NRRL B-512 Dextran.—Fig. 2 shows the effect of aging at high RH on the water absorption of two B-512 dextran samples. In the first series of experiments, a dissolved sample after freeze-drying in the flask was equilibrated at 92.5% RH. The water content was constant for about 1 day, after which it decreased and a haze appeared as a result of crystallization which was anticipated in this dextran at high RH.² At point C, the RH was increased to 98.1%, and the water content shown at point D was observed 2 hours later. This point is to be contrasted with the results in the second series of experiments: A sample of amorphous dextran was equilibrated at 98.1% RH, and after 1 day the equilibrium water content appeared to be about 104% water. The longer time to reach equilibrium can be attributed to a relatively thick mass of sample. The constant water content is evidence of no crystallization in 3 days. When the humidity was dropped to 92.5% RH at point B, water content fell and a haze appeared after a day, indicating the onset of crystallization.

The dotted portion of the curve is the course of water sorption estimated by analogy with the first experiment. At the end of the experiments, sample 1 had an L-1 plus L-3 type X-ray diffraction pattern, and sample 2 had an L-3 type pattern.²⁶ Both patterns were rather weak compared to a typical granular starch pattern or crystalline dextran.

When the third amorphous B-512 dextran sample was equilibrated at 95.4% RH, the fall in water content began after 2 days (Fig. 3). Other RH values were explored later as indicated in the figure. The sample was dried twice after 10 days, but the drying times are not included in the time axis since the samples should be stable when dry.

In the fourth series, a short exploratory sequence, 99.3, 95.4 and 92.4% RH was run to re-examine the behavior of the amorphous B-512 dextran (Fig. 4). The sample evidently began crystallizing the second day at 92.4% RH, so further investigation was made on the crystalline sample. As before, when the sample was dried the drying time was omitted from the time axis in Fig. 4.

In summary, the results of these four experimental series indicate that the water absorption by amorphous B-512 dextran can be determined before crystallization occurs. Water sorption drops upon crystallization of the dextran. The lag period before the drop in water content is greater at 95.4% RH than at 92.5% RH, while at 98.1% RH the lag period is at least 3 days and crystallization may not occur at all. Comparison of the equilibria at 92.4% RH shows that the sample crystallized at 95.4% RH sorbs definitely more water; consequently, the sorption appears dependent on sample history.

Density of Concentrated Dextran Solution.—

The density of a concentrated B-512 dextran solution was determined by placing about 2 g. each of B-512 dextran and water in a 25-ml. pycnometer with a 3-mm. neck. Weights were determined within a milligram. After the solution stood overnight in an evacuated desiccator, it was clear and free of bubbles. The volume of the solution was measured by filling the pycnometer at 25.0° with water-saturated toluene of known density. In a single determination, the density of a 48.30% by weight dextran solution was 1.230 compared to the predicted value of 1.233, calculated from the partial specific volume, 0.606 ml./g. for B-512 dextran at 25°, determined from unpublished solution density data of D. Macmillan and E. H. Melvin of this Laboratory. Essentially the same partial volume is found with Snyder's data at 20°.²⁷

The partial specific volume of B-512 dextran in solution is essentially constant up to 50% dextran by weight.

Discussion

Amorphous Dextran.—Water absorption data were obtained on two dextrans in the amorphous state. NRRL B-1398 dextran was chosen because it showed little tendency to crystallize even on long

(26) A. Jeanes, N. C. Schielts and C. A. Wilham, *J. Biol. Chem.*, **176**, 617 (1948).

(27) C. F. Snyder, *et al.*, *J. Research Natl. Bur. Standards*, **53**, 131 (1954).

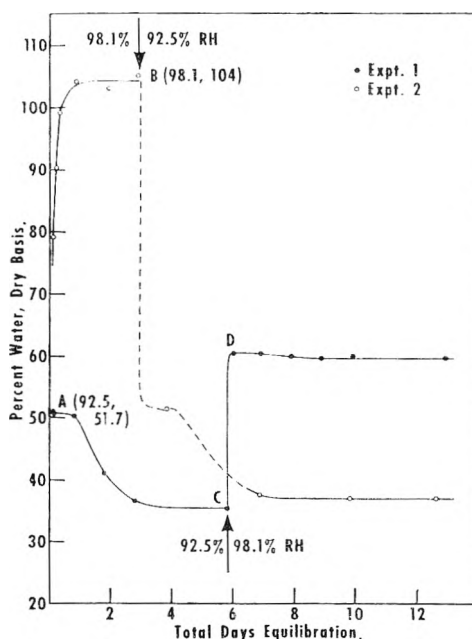


Fig. 2.—Water sorption sequences of two B-512 dextran samples. In each case the humidity was changed at the arrow as indicated.

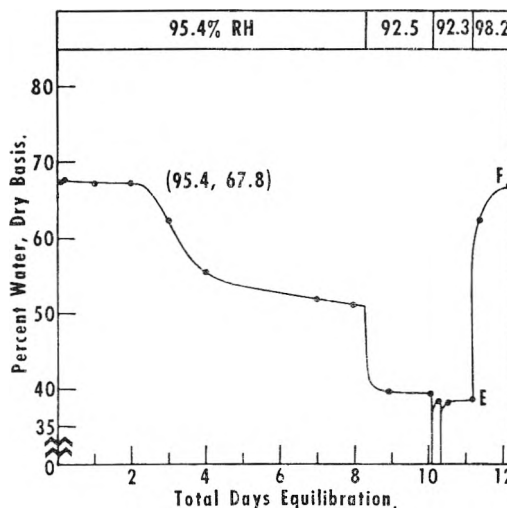


Fig. 3.—Water sorption of the third B-512 dextran sample during the humidity sequence indicated at the top of the figure. The vertical lines to the bottom of the figure indicate the sample was dried.

standing at high RH. Although NRRL B-512 tended to crystallize, it was possible to measure its sorption in the amorphous state by rapid attainment of equilibrium. These systems were analyzed in terms of the theory of solutions of randomly coiled polymers developed by Flory⁶ and Huggins.⁷ In one form the theory is reduced to the equation

$$\ln p/p_0 = \ln v_1 + (1 - \bar{V}_1/\bar{V}_2)v_2 + \mu v_2^2 \quad (1)$$

in which p/p_0 is RH/100; v is the volume fraction; \bar{V} is the partial molal volume; subscripts 1 and 2 refer to solvent and solute, respectively; and μ is best regarded as an arbitrary constant.⁶ For solutes of high molecular weights in the high concentrations found in sorption experiments, the partial molal volume ratio disappears

$$\ln p/p_0 = \ln v_1 + v_2 + \mu v_2^2 \quad (2)$$

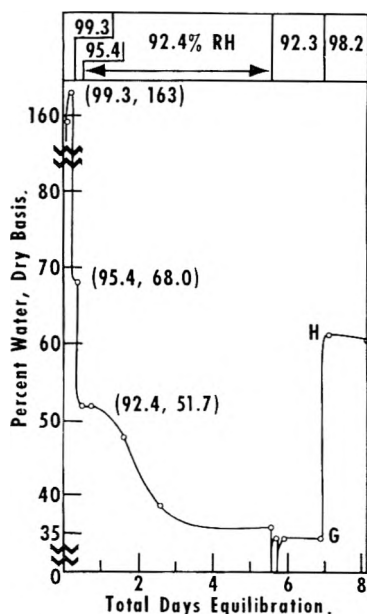


Fig. 4.—Water sorption sequence of the fourth B-512 dextran sample. The vertical lines to the bottom of the figure indicate the sample was dried.

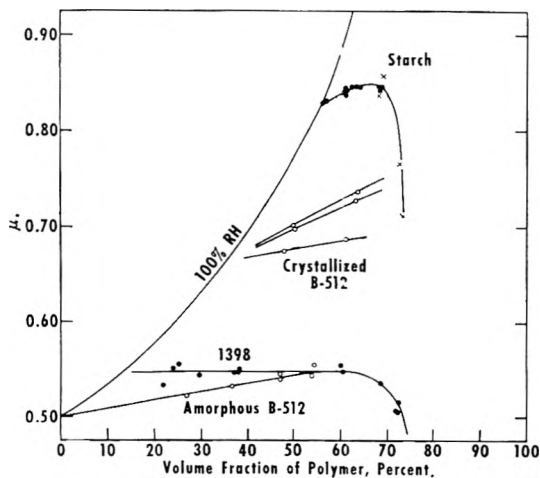


Fig. 5.—Water sorption isotherms of dextrans and starch plotted as values of μ and v_2 , the volume fraction of polymer. See text under Discussion.

In practice, many randomly coiled polymers are found to behave according to the equations with nearly constant values of μ , at least over a limited concentration range.²⁸ The water sorption data of B-1398 dextran are shown in Fig. 5 converted to values of v_2 and μ by means of equation 2 using the partial specific volume of B-512 dextran. The sorption isotherm maintains a constant value of μ , 0.548, up to about 65% dextran by volume, after which a sharp decline in μ occurs. It appears that B-1398 dextran obeys the Flory-Huggins theory at water contents higher than 33% dry basis, *i.e.*, where $v_2 = 65\%$.

The region above the curved 100% RH line in Fig. 5 corresponds to RH greater than saturation for very high molecular weight polymers. The isotherm of B-1398 dextran extrapolated toward $v_2 = 0$ reaches 100% RH at finite polymer concentration; therefore, a restricted water uptake is

predicted. Since B-1398 dextran has been reported to be water-soluble,²⁰ this restricted water uptake likely is the result of a trace amount of crystallinity which developed in early experiments. It was found in other work that B-1398 dextran does develop a trace of crystalline X-ray diffraction pattern when exposed to high RH. In addition, this sample absorbed less water than the amorphous B-512 sample.

The data for amorphous B-512 dextran, also shown in Fig. 5, fit a line which is extrapolated to $\mu = 0.5$ at $v_2 = 0$. Unlimited water sorption at saturation is predicted. The value of μ at $v_2 = 0$ also can be calculated from the second virial coefficient determined from light scattering data. Theoretical treatments of concentrated and dilute solutions are not identical²⁹ but a comparison is possible. Values of μ , calculated from data reported by Senti, *et al.*,³⁰ on hydrolyzed dextran B-512, increase with increasing molecular weight, and at higher molecular weights are approximately 0.50 (*i.e.*, the second virial coefficients became vanishingly small on the scale of observations used). Evidently, the isotherm drawn in Fig. 5 correctly describes the entire solution and high-RH-sorption behavior of amorphous B-512 dextran below about $v_2 = 65\%$ or above 33% water sorption.

In this high RH region the Flory-Huggins theory seems to be a good model for amorphous B-512 dextran. This dextran is established as a randomly coiled, branched polymer in dilute solution. The continuous linear isotherm up to $v_2 = 65\%$ implies that this solution behavior is not drastically altered in this concentration range. The gradual change in μ is no greater than that found for some other randomly coiled polymer-solvent systems,²⁸ and thus is no indication of physical structure such as aggregation. Other evidence favors a solution model: gradual flow was observed in dextran preparations containing as little as 28% water; also, water sorption hysteresis is negligible at water contents greater than 20% water.² Therefore, evidence supports the view that the B-512 dextran-water system exhibits essentially polymer solution behavior at high water contents, apparently free of effects due to physical structure.

At lower RH, a different interpretation is warranted. When the entire intermediate and high RH sorption isotherm is considered,² a number of changes in character appear at about $v_2 = 65$ or 33% water content, and 85% RH, which indicate a change in sorption mechanism at this point. These changes include the sharp decrease in μ , as well as the occurrence of hysteresis, at lower water contents. These observations apply to the B-1398 dextran, but the absorption isotherm of the B-512 dextran previously was shown to be identical; consequently, the ideas apply equally well to amorphous dextrans in general.

The decrease in μ denotes relatively more water absorbed than the Flory-Huggins isotherm would predict. The site-bound water which, in theory, occurs at low RH offers a well-established mech-

(29) P. J. Flory, *J. Chem. Phys.*, **13**, 453 (1945).

(30) F. R. Senti, *et al.*, *J. Polymer Sci.*, **17**, 527 (1955).

anism to increase water sorption and amounts to roughly 10 to 15% water for dextrans.² By comparison, the maximum excess of observed water content over the isotherm corresponding to a constant $\mu = 0.56$ was calculated to be about 6% of dry weight for absorption and 10% for desorption; it occurs in the region of 40% RH. The complete isotherm may be interpreted as site absorption followed by solution absorption.

The interpretation presumes strong binding sites at low RH, but no evidence favoring binding sites is observed at high RH. Furthermore, the upward trend of μ to higher dextran concentrations in the solution region favors absence of a strong hydrate. This apparent anomaly invites speculation that at water contents lower than 33%, which corresponds to about 3 water molecules per glucose residue, the dextran hydroxyls are rather poorly bonded together. The polymer chains are too bulky and close together to allow the freedom of position and orientation required for complete hydrogen bonding. These weakly bonded hydroxyls strongly bind water molecules, until in excess water the dextran and water hydroxyls are nearly equivalent in strength. An analogous but converse argument has been used to explain the lack of a sigmoid isotherm (*i.e.*, indicating no binding sites) in polyvinyl alcohol, in which the hydroxyl groups are situated so as to be easily hydrogen bonded with groups adjacent in the chain.^{21,32}

If sorption on sites does occur at 33% water and lower, then according to Dole¹⁰ the curve p/p_0N vs. p/p_0 should have a positive slope in this region. N is the water content per g. of dry solid. When this plot was made, the curve had a maximum at about 75% RH, and 22% water content. The positive slopes at lower humidities, both for absorption and desorption, agree with our postulated site absorption.³³ The analysis is equivalent to accepting the concave downward portion of the sorption isotherm as indicating site absorption.

The Flory-Huggins theory has been criticized on theoretical grounds, and alternative approaches are possible. One such is Zimm's clustering function.^{35,34} An isotherm in terms of this function focuses attention on the extent to which the solvent molecules tend to cluster together. The Flory-Huggins isotherm predicts increasingly large values of the clustering function at high humidity, and the data for the amorphous dextrans behave accordingly at volume fractions of water greater than 0.45. The interesting aspect of the clustering function for the amorphous dextrans is that in the region $v_1 = 0.25$ to 0.35 it drops precipitously with decreasing v_1 . Then, at v_1 less than 0.25, both absorption and desorption isotherms drift slowly downward with decreasing v_1 , toward the value -4 . The break in this isotherm between $v_1 = 0.25$ and $v_1 = 0.35$ is another suggestion of a change in mechanism.

(31) P. M. Hauser and A. D. McLaren, *Ind. Eng. Chem.*, **40**, 112 (1948).

(32) I. Sakurada, A. Nakajima and H. Fujiwara, *J. Polymer Sci.*, **35**, 497 (1959).

(33) The authors are indebted to one of the journal reviewers for this suggestion.

(34) B. H. Zimm and J. L. Lundberg, *J. Phys. Chem.*, **60**, 425 (1956).

Crystalline Dextrans.—Figures 2, 3 and 4 show the decline in water contents of B-512 dextran samples at various RH values, as the samples crystallized. The observations after crystallization, C and D, G and H, and also E and F, show the water contents of each of three samples at two values of RH and define parts of the sorption isotherms of these crystalline samples. The data from these three crystallized dextran B-512 samples are shown in Fig. 5. Their lesser water absorptions are reflected by the higher values of μ . If the isotherms are linear, their extrapolations to lower v_2 cross the saturation line; therefore, limited water absorptions are predicted. The samples were, in fact, not completely soluble at the end of the experiments. Such depressed sorption and insolubility are features generally shown by other crystalline polymers.

In an analysis of sorption by such crystalline polymer systems, Kawai³⁵ has shown that in principle both the non-absorbing crystalline fraction and also the effective cross-linking network must be considered. Such a model has been used to characterize cellulose. No data on extent of crystallinity in the three crystalline dextrans were obtained, but the extent of crystallinity was estimated by assuming that the elastic network was completely relaxed and had no effect on sorption at about 75% RH, the point of transition from solution absorption to site absorption in amorphous dextran. The difference in water absorbed by a completely amorphous sample and the partially crystalline sample at this humidity then can be attributed to the non-absorbing crystalline fractions, which were 20 to 30% for the three crystalline dextrans.

With these values of crystallinity, the network in the amorphous material can be estimated by the procedure devised by Flory³⁶ for cross-linked polymers. Effective chain lengths were found to be about 10 glucose residues long. While these figures are subject to large errors, the values obtained show that the assumed model for a partly crystalline polymer is not unreasonable in describing water sorption by crystalline dextrans.

Starch.—The sorption isotherms of defatted wheat starch also are plotted in Fig. 5. Partial specific volume was assumed to be 0.60, the value in dilute solution.³⁷ Some data are included which were obtained in other studies at lower RH. Granular starch is partly crystalline and oriented within the granule, and the amorphous material may not be randomly arranged, but the isotherm is similar to that of the crystalline dextrans.

The water sorption isotherm of starch can be compared to these dextrans if water absorption of amorphous starch is identical with that of amorphous dextran. Evidence in favor of this point is the finding that amylose behaves as a randomly coiled polymer in water solution as does dextran, and that the second virial coefficient of amylose is negligible in aqueous KCl solution.³⁸ In dilute molecularly

(35) T. Kawai, *J. Polymer Sci.*, **37**, 181 (1959).

(36) P. J. Flory, *ref. 9*, p. 577.

(37) O. Lamm, *Kolloid-Z.*, **69**, 44 (1934).

(38) W. W. Everett and J. F. Foster, *J. Am. Chem. Soc.*, **81**, 3464 (1959).

dispersed solution, μ is about 0.50, as it is for dextran B-512.

The crystalline fraction and network properties were calculated as with crystalline dextrans. A crystallinity of 54% and an amorphous network two glucose residues long were obtained. These figures rather strain the model, but suggest a greatly associated, closely knit structure. The results do not favor as a model for granular starch a few strong cross-linking regions holding together a relatively large amount of randomly coiled, unassociated material.

Acknowledgments.—The authors gratefully acknowledge the help of Allene Jeanes, who supplied dextran NRRL-1398; F. Castle, who constructed the glass apparatus; L. Bair, who constructed part of the cathetometer; R. Tobin, who determined the light-scattering molecular weights; and H. Zobel, who determined the X-ray diffraction patterns. We also wish to thank Dr. Eugene Melvin and Dr. Duncan Macmillan for the use of their unpublished measurements of dextran solution densities.

DEUTERIUM EXCHANGE IN STARCHES AND AMYLOSE

BY N. W. TAYLOR, H. F. ZOBEL, MILFORD WHITE AND F. R. SENTI

Northern Regional Research Laboratory,¹ Peoria, Illinois

Received January 13, 1961

In all starch and amylose preparations examined, the hydroxyl hydrogens were shown by weight change to be completely exchangeable with liquid D₂O, within an experimental error of 1 or 2%. Samples examined were defatted wheat starch, potato starch, high-amylose corn starch, acid hydrolyzates of amylose with both A and B X-ray patterns, a palmitic acid complex of amylose in helical configuration and retrograded amylose preparations. Some of the retrograded preparations were soluble in boiling water, and some were insoluble. The insoluble preparations retained their B X-ray diffraction patterns. Deuterated wheat starch was completely exchangeable with water vapor at low relative humidity, and also with liquid methanol, but was not completely exchangeable with liquid ethanol. Inaccessibility to this last solvent was ascribed to lack of penetration. Complete exchange found in all other cases indicates that the A, B and helical crystal structures have exchangeable hydroxyls and that all or nearly all hydrogen bonds in starch are relatively weak. It appears that association in retrograded amylose and resistance to redispersion in hot water are mainly effected by the crystalline regions, which would afford the necessary cooperative strength.

Molecular association is commonly accepted as playing an important role in the behavior of starch—either in the granule or during retrogradation after gelatinization.²⁻⁷ Such evidence as the relative solubility of starch preparations in hydrogen bond-breaking solvents, development of crystalline X-ray diffraction patterns during aging of pastes, and variability in gelatinization behavior after heat-moisture or other treatments leaves little doubt that molecular association as effected by hydrogen bonds is a most significant feature of starch chemistry. But even though there is good evidence in favor of associative phenomena, the precise mechanisms involved, as well as the extent of association, are unsolved problems because quantitative description of such association is not available. Exchange of hydrogen and deuterium in the hydroxyl groups of starch was investigated to study these problems.

When D₂O is mixed with a substance containing hydrogen-bonding radicals such as hydroxyl, the H and D should freely exchange, provided that the D₂O can penetrate the substance and further that there is no resistance structure present. Resistance of hydrogen-bonding groups to exchange has been interpreted as a reflection of special

structures in proteins⁸⁻¹² and polypeptides¹³ and as a reflection of crystallinity in cellulose,¹⁴⁻¹⁶ wool¹⁷ and polyvinyl alcohol.¹⁸ The work reported here was undertaken to determine whether some of the known properties of starch might be ascribed to resistant structures, indicated by inaccessibility of some of the hydroxyl hydrogens to exchange. Although none were found, the absence of such structures of itself appears to be helpful in interpreting starch structure.

Materials and Methods.—The wheat and high-amylose corn starches were pilot-plant preparations. Wheat starch was washed from a flour-water dough with cold tap water. High-amylose corn was steeped in distilled water containing 0.25% SO₂, and the starch was isolated by a standard wet-milling procedure.¹⁹ It contained 68% amylose by iodine potentiometry and 1.0% protein by Kjeldahl. Potato starch was a laboratory preparation isolated by the method of Maywald, *et al.*²⁰ The starches were defatted by extract-

(1) This is a laboratory of the Northern Utilization Research and Development Division, Agricultural Research Service, U. S. Department of Agriculture.

(2) K. H. Meyer, *J. Phys. & Colloid Chem.*, **53**, 319 (1949).

(3) G. V. Caesar and M. L. Cushing, *ibid.*, **45**, 776 (1941).

(4) M. Samec, *Dis Stärks*, **5**, 105 (1953).

(5) N. P. Badenhuizen, *Protoplasmatologia*, **11**, B2bδ (1959).

(6) M. Samec, *J. Polymer Sci.*, **23**, 801 (1957).

(7) H. W. Leach, L. D. McCowen and T. J. Schoch, *Cereal Chem.*, **36**, 534 (1959).

(8) A. Hvidt and K. Linderstrøm-Lang, *Biochim. Biophys. Acta*, **14**, 574 (1954).

(9) A. Hvidt, *ibid.*, **18**, 306 (1955).

(10) R. D. B. Fraser and T. P. MacRae, *J. Chem. Phys.*, **28**, 1120 (1958).

(11) G. H. Haggis, *Biochim. Biophys. Acta*, **19**, 545 (1956).

(12) P. E. Wilcox, *ibid.*, **34**, 602 (1959).

(13) A. Elliott and W. E. Hanby, *Nature*, **182**, 654 (1958).

(14) V. J. Frillette, J. Hanle and H. Mark, *J. Am. Chem. Soc.*, **70**, 1107 (1948).

(15) H. J. Marrinan and J. Mann, *J. Appl. Chem. (London)*, **4**, 204 (1954).

(16) J. Mann and H. J. Marrinan, *Trans. Faraday Soc.*, **52**, 481, 487 (1956).

(17) R. W. Burley, C. H. Nicholls and J. B. Speakman, *J. Textile Inst.*, **46**, T427 (1955).

(18) H. Tadokoro, S. Seki and I. Nitta, *J. Polymer Sci.*, **22**, 563 (1956).

(19) R. L. Zipf, R. A. Anderson and R. L. Slotter, *Cereal Chem.*, **27**, 463 (1950).

ing with 85% methanol (v./v.) overnight in a Soxhlet extractor. Corn amylose P was prepared in the pilot plant by Schoch's procedure.²¹ The samples showing highly crystalline A and B patterns were acid hydrolyzates of corn amylose P. Corn amylose L was a laboratory preparation from defatted corn starch, separated by Schoch's procedure and recrystallized twice from butanol-water: the iodine sorption was 196 mg./g.

Several retrograded amylose preparations were used. Prep. I was corn amylose P retrograded by slurring with water and holding overnight at room temperature. Prep. II, containing only traces of material having a degree of polymerization less than 20, was a corn amylose P hydrolyzate which was retrograded under water 19 days in a refrigerator. Prep. III was amylose L dissolved with butanol in hot water to make a clear solution; the butanol was boiled off, and the amylose retrograded by precipitation in a refrigerator. Prep. IV was amylose L humidified 2 days at 97% RH, ground to pass 60 mesh, held 20 hours under water at room temperature, dried, ground to pass 60 mesh, held again under water 20 hours and dried. Preps. I, III and IV had the rather diffuse B X-ray patterns²² of retrograded amylose, while Prep. II had a relatively strong, sharp B pattern.

The palmitic acid complex was made by a method similar to that of MacMasters, *et al.*²³ A slurry of 2 g. of amylose L in butanol was poured into boiling water to make a clear solution; 0.2 g. of palmitic acid was added in butanol, and the butanol was boiled off; the suspension was autoclaved 1 hour at 15 p.s.i. and stirred 2 days at 93°. On the second day, more 1-butanol was added and distilled off and by the third day, a white, crystalline precipitate had appeared. The suspension was cooled, the excess palmitic acid was skimmed off the top and the crystals were removed by centrifuging, washed with boiling water and freeze-dried. The palmitic acid content was 4.0% based on weight of material removed by Soxhlet extraction with 85% methanol.

Deuterium oxide was from the Liquid Carbonic Co.,²⁴ reported to be 99.5% D; this value was confirmed by density measurement. Methanol was J. T. Baker analyzed, reported assay 99.9%. Ethanol was 200-proof, $d = 0.7799$ g./ml. at 30.5° and was distilled *in vacuo*; the middle third was taken.

X-Ray patterns were taken with Cu K α radiation using an X-ray diffractometer or a flat cassette powder camera.

Liquids were handled and transferred in the vacuum line used previously in water-sorption experiments²⁵ and were distilled *in vacuo* by cooling the receiving flask in ethanol-solid CO₂ mixtures. The samples generally weighed about 1 g. They and the contacting liquids were weighed in a vacuum flask with tare of equal air displacement. Samples wet with H₂O or D₂O were dried with vacuum pumps to constant weight within about 0.2 mg. in 1 day. After several hours of drying the samples were heated to about 60°, except as otherwise noted, to speed up the drying procedure. Samples wet with ethanol required 3 or 4 days of drying to reach constant weight; samples wet with methanol did not reach constant weight after 5 days of drying. Dry weights were determined by plotting daily weights against reciprocal of time and then extrapolating to infinite time.

In the back exchange with water vapor, relative humidity was maintained at 19.3% by holding the water source at 0° and the sample flask at 25°.

Results

Calculation of Percentage Exchangeable H.—If it is assumed that the equilibrium constant is unity for hydrogen and deuterium when they are exchanged between water and accessible starch hydroxyl groups, then the total exchangeable hydrogen and deuterium in the starch hydroxyls can be represented by the equation

$$H_1^S + D_1^S = D_2^S \left(\frac{H_1^L + D_1^L}{D_1^S - D_2^S + D_1^L} \right) \quad (1)$$

where H is the number of equivalents of hydrogen and D of deuterium, either in the sample as denoted by superscript S or in the liquid as denoted by superscript L. Subscript 1 denotes the quantities before contacting the sample with liquid and subscript 2, after contacting. If the sample contains only hydrogen on hydroxyls and contacts pure D₂O liquid, the equation reduces to

$$H_1^S = \frac{D_2^S \times D_1^L}{D_1^L - D_2^S} \quad (2)$$

Here D_1^L and D_2^S are calculated from the weight of D₂O added and from the change in weight of the dried sample, respectively. Then the amount of exchangeable H initially present, H_1^S , can be calculated. The percentage of H exchangeable is 100 H_1^S divided by the total equivalents of sample hydroxyl H calculated from the weight of sample.

The equations are based on the further assumption that there is no fractionation during distillation of the liquid from the sample. There should be some departure from the assumptions, but the error involved appears to be small, as the results reported will show.

Exchange between Wheat Starch and Water.—

The complete exchangeability of the hydroxyls in defatted wheat starch with D₂O is shown by the results (Table I) of the exchange of starch with heavy water and the back exchange of the deuterated starch with water vapor at low humidity. The same starch sample was used successively in the three experiments. In Experiments 2 and 3 the deuterated starch was first rehydrogenated with water. The initial weights of the original and rehydrogenated sample are identical, showing that in Experiments 2 and 3 the samples had in fact been completely rehydrogenated. In Experiments 1 and 2, a single exchange was achieved by contacting the sample for 1 hour with a known amount of D₂O, resulting in the deuterium contents shown in row 3, expressed as percentage of the calculated number of hydroxyls in the starch. In Experiment 3, the starch was saturated with deuterium by four successive applications of D₂O, each followed by drying. The sample then was completely deuterated. The deviation from 100% exchange is about the same as the amount of impurities (ash, protein, etc.) typically present in starch and is not an indication of resistant hydroxyls in the starch. For each experiment the percentage of exchangeable hydrogen in the original sample was calculated from the data. In all cases the hydroxyl groups in the wheat starch were completely exchangeable within experimental error. As the first two experiments agree closely with the third, it appears that different behavior between H and D is of minor importance in these experiments. The slightly higher values of exchangeable H found in Experiments 1 and 2 may be the result of fractionation during distillation from the sample, or non-unity equilibrium constant, but these and other data show the effect to be small.

Granule swelling occurs in an excess of water

(20) E. Maywald, R. Christensen and T. J. Schoch, *J. Agr. Food Chem.*, **3**, 521 (1955).

(21) T. J. Schoch, *J. Am. Chem. Soc.*, **64**, 2957 (1942).

(22) R. S. Bear and D. French, *ibid.*, **63**, 2298 (1941).

(23) M. M. MacMasters, C. W. Bice and G. E. Hilbert, Northern Regional Research Laboratory report, unpublished, 1944.

(24) The use of trade names in this article is for identification only and implies no endorsement by the U. S. Department of Agriculture.

(25) N. W. Taylor, J. E. Cluskey and F. R. Senti, *J. Phys. Chem.*, **65**, 1810 (1961).

TABLE I
 DEUTERIUM EXCHANGE AND LOW HUMIDITY REHYDROGENATION OF WHEAT STARCH

Row	Treatment	Experiments		
		1	2	3
1	Initial sample weight, g.	0.99905	0.99910	0.99910
2	D ₂ O added, g.	2.295	2.211	4X contacted
3	D in hydroxyl, % of hydroxyl	91.9	90.9	98.0
4	Exchangeable H, % of hydroxyl	100	99	98
5	Water absorbed, % dry basis	7.8	8.3	7.9
6	D in hydroxyl after H ₂ O, % of hydroxyl	63	61	67
7	Hydroxyl exchangeable at low RH, % of hydroxyl	104	106	92

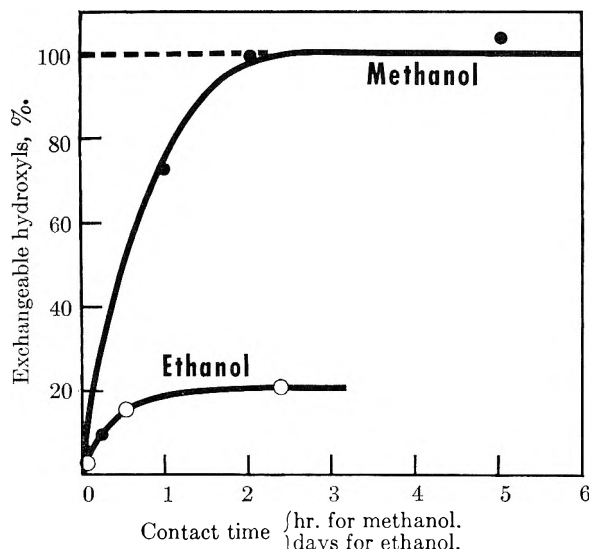


Fig. 1.—Calculated percentage of exchangeable hydroxyls in deuterated wheat starch contacted with alcohols.

and might influence exchangeability; hence, exchange at low swelling was tested. For this purpose the deuterated samples just described were exposed to water vapor at 19% relative humidity (RH) for $\frac{1}{2}$ hour. The water absorbed is shown in row 5 of Table I. The values are identical within experimental error with the equilibrium value of approximately 8% absorbed at 19% RH. Then, after an additional $\frac{1}{2}$ -hour contact time with the flask closed, the samples were dried and weighed. The calculated deuterium content remaining is shown in row 6. To calculate the percentage of hydroxyl exchangeable with the water at low RH, it was assumed that the exchangeable hydroxyl initially present contained the same D-H ratio as all the hydroxyls. This assumption is reasonable because during the introduction of deuterium all the hydroxyls were freely exchangeable with the liquid D₂O added; hence, the D is randomly arranged on the hydroxyls. The calculated percentages of hydroxyl exchangeable at low humidity are shown in row 7. Because of the small quantities exchanged, these experiments are not as sensitive as the previous ones, but the calculations show that the hydroxyls (*i.e.*, OH and OD radicals) seem to be all freely exchangeable with water vapor at low humidity as well as in liquid D₂O. Apparently, granule swelling, which occurs on adding excess water, is not necessary for accessibility of the hydroxyl groups.

Exchange of Wheat Starch and Alcohols.—Exchange of deuterated defatted wheat starch with

alcohols was examined to determine whether these relatively poor solvents would afford a limited exchange. The sample to be treated with methanol had 97.2% of the hydroxyl H replaced by D after 3 contacts with D₂O. The sample to be treated with ethanol had 98.9% replacement with D after 4 contacts with D₂O. Essentially these samples were completely deuterated. The alcohols were distilled into the starch samples, allowed to stand a specified time and distilled off at room temperature. The last trace of solvent then was removed on the vacuum line. To obtain a further contact time, the same sample of alcohol again was distilled into the starch sample. In Fig. 1, the total contact time is plotted *vs.* percentage exchangeable hydroxyl found in the starch. The starch hydroxyl was completely exchangeable with methanol in a few hours, but complete exchange was not achieved with ethanol in eight days.

Deuteration of Other Starches and Fractions.—

Results of treating other samples with D₂O are shown in Table II. Essentially complete exchangeability was observed not only for the granular starches, but also for the various amylose preparations. Data were rejected on several samples which were not defatted. They were later proved to contain volatile material which vitiated the results.

TABLE II

DEUTERIUM EXCHANGEABILITY OF STARCHES AND FRACTIONS

Material	Exchangeable H, % of theor.
High-amylose corn starch	101
High-amylose corn starch completely deuterated	100
Potato starch	99
Highly crystalline A (overheated)	97
Highly crystalline B (Prep. I)	101
Highly crystalline B (Prep. II)	103
Palmitic acid complex with amylose	100 ^a
Retrograded amylose I	98
Retrograded amylose II	102
Retrograded amylose III	101
Retrograded amylose IV	96
Retrograded amylose IV completely deuterated	100

^a The theoretical hydroxyl content was calculated with allowances for the content of palmitic acid.

The samples with highly crystalline A and B patterns, both acid hydrolyzates of corn amylose, gave sharp X-ray diffraction lines. The sample with highly crystalline A pattern was heated to 160° by mistake during drying and was slightly discolored. Thus the 97% exchangeability is very likely too low because of some degradative

loss of weight. The data show that both A and B crystalline structures are exchangeable.

The interpretation of the results of exchange in terms of accessibility of crystalline regions is complicated by the disappearance of X-ray crystallinity on drying, as was done before adding D_2O to the sample. Figure 2 shows the X-ray pattern before and after vacuum drying the sample which gave a good crystalline B pattern. The sample with highly crystalline A pattern behaved similarly although several broad peaks appeared in the pattern after drying.

Solubility and X-Ray Diffraction Patterns of Retrograded Amyloses.—The deuterated retrograded amylose samples in Table II were boiled in water for 16 hours to test their solubilities. Preps. I and IV remained largely insoluble and retained their tough, horny appearance as well as the crystalline B X-ray patterns; II, a hydrolyzate, dissolved immediately on warming; and III, retrograded in the cold, dissolved except for about 2% which retained a B X-ray pattern.

The X-ray diffraction patterns of Preps. III and IV were recorded after humidification overnight at 98 and 85% RH (Fig. 3). The cold retrograded Prep. III appears somewhat less crystalline, but the diffraction peaks also appear wider. The widths at half maximum intensity of the 16 Å. diffraction peaks were measured. This peak was chosen because it is relatively well resolved from adjacent peaks. From these widths, the crystal size was calculated, using the Scherrer equation.²⁶ After equilibration of wetted samples at 98% RH, the apparent crystal size in Prep. III was 51 Å. and in Prep. IV, 70 Å. After equilibration of the wetted samples at 85% RH, the apparent crystal size in Prep. III was 47 Å. and in Prep. IV, 62 Å. Measurements on replicate patterns were in good agreement. The cold retrograded preparation, dispersible in hot water, had smaller apparent size of the crystalline regions.

Discussion

Exchange in Starch Granules.—Results show that the hydroxyl hydrogens in all three kinds of granular starch examined were completely exchangeable with liquid D_2O . Further, the wheat starch was completely exchangeable at low humidity, within a larger experimental error. Apparently hydroxyl hydrogens in the crystalline regions are exchangeable, both in the A crystalline structures of wheat starch and the B crystalline structures of potato and high-amylose corn starches.

The disappearance or diminishing of the X-ray diffraction pattern on completely dehydrating starches is well known. Because D_2O was added to dried starch samples, the results may not be a direct test of accessibility of hydroxyls in the original crystalline regions. However, the conclusion that the crystalline regions are completely accessible appears justified. If the starch crystalline regions reformed rapidly when D_2O was added and were resistant to exchange, these regions should have contained a lower proportion of D at the termi-

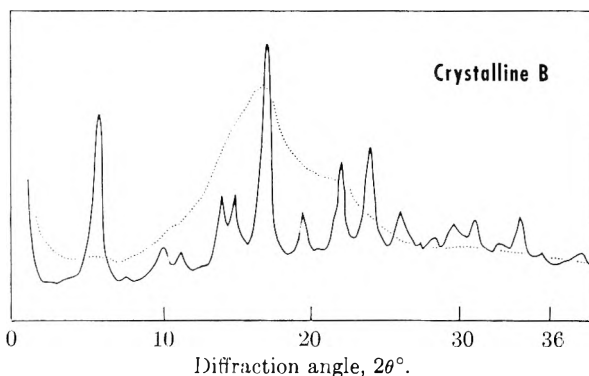


Fig. 2.—X-Ray diffraction pattern of an amylose hydrolyzate with B crystallinity. The solid curve is taken after the preparation was dried in room atmosphere and the dotted curve, after drying *in vacuo*.

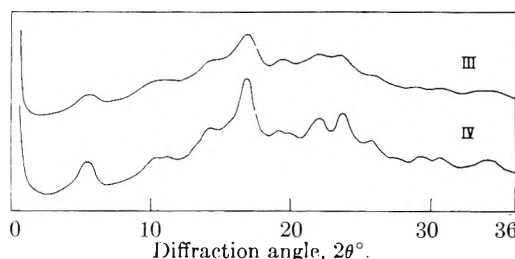


Fig. 3.—X-Ray diffraction patterns of retrograded amylose preparations III (cold) and IV (room temperature) at 35% RH.

nation of the experiment than the accessible regions. Even if recrystallization was not sufficiently rapid, it is difficult to conceive of a crystalline structure that would be resistant to exchange and yet so easily disrupted by drying. This argument would apply especially to the highly crystalline samples in which swelling stresses should be smaller as a result of the reduced molecular weight.

A crystalline hydrate has been postulated to account for the crystal structure deduced from the B X-ray pattern.^{27,28} The diminished X-ray patterns of dehydrated starches tend to confirm the existence of such a hydrate. The complete accessibility observed in this study is a consequence to be expected of a hydrated crystal lattice, although exchange could occur in the absence of a hydrate by transfer of H and D along neighboring hydroxyl groups. Thus, several lines of evidence rather favor the existence of hydrates in the crystal lattice.

Complete exchange of wheat starch with methanol also was achieved, but at a measurably slow rate. Complete exchange with ethanol was not achieved, and at best the reaction proceeded very slowly. The rates of exchange seen here are similar to the rates of approach to equilibrium for apparent densities of starch granules in these solvents.²⁹ In water, the equilibrium density was achieved immediately; in methanol, in several hours; and in ethanol, equilibrium took a month or more. Bushuk and Winkler³⁰ showed that the sorption

(27) D. R. Krieger, *Biochim. Biophys. Acta*, **6**, 406 (1951).

(28) R. E. Rundle, L. Daasch and D. French, *J. Am. Chem. Soc.*, **66**, 130 (1944).

(29) C. A. Glass, Northern Regional Research Laboratory report, unpublished.

(30) W. Bushuk and C. A. Winkler, *Cereal Chem.*, **34**, 87 (1957).

(26) H. P. Klug and L. E. Alexander, "X-Ray Diffraction Procedures for Polycrystalline and Amorphous Materials," John Wiley and Sons, Inc., New York, N. Y., 1954, p. 491.

isotherms and rates of sorption for the three sorbates decreased in the series water > methanol > ethanol. They noted sorption varied inversely with molecular volume. It seems that the exchange with ethanol was limited, not because of a specific resistant structure in the starch, but because the starch was impenetrable by ethanol.

Helical Form of Amylose.—An additional known crystal structure was studied in the palmitic acid complex of amylose. Its V X-ray pattern indicates the amylose to be in a helical configuration.^{31,32} This crystallized complex is insoluble and stable in water, in contrast to a butanol-complexed amylose. The sample was completely exchangeable. Polypeptides, on the other hand, are resistant to exchange in the helical configuration.¹³

Stability of a crystal may depend on the cooperative action of many hydrogen bonds. If the helix exists in solution, however, the opportunity for cooperative action is reduced to interaction between hydroxyls on neighboring turns. Because of the limited interaction possible, the complete exchangeability observed indicates that features other than hydrogen bonds probably are more important in stabilizing this helical structure. The hydrocarbon-like complexing agent is one stabilizing factor. This conclusion was reached by Mikus, Hixon and Rundle on other evidence.³³ However, there is some evidence that other amylose complexes may involve hydrogen bonding.³⁴⁻³⁶

Retrograded Amylose Preparations.—These are amylose-water systems that have become insoluble in water. Usually they are not easily soluble even in hot water. They have B X-ray patterns, but because some preparations with B structure may be dispersed easily in hot water, other structures or great variations in structures may exist in retrograded preparations. The data in Table II show that no structures were detected with hydroxyls resistant to exchange, although as in all these experiments a very small content, e.g., 1 or 2%, of resistant hydroxyls is not ruled out.

Our results with retrograded amylose contradict the report by Čeh and Hadži³⁷ that potato amylose and amylopectin were resistant to exchange after appropriate treatments. They used a different type of starch and different conditions than we did, but neither of these factors seems sufficient to explain the opposing results. An alternative explanation of their results is offered. Čeh and Hadži show that amylose aged in cold water is more resistant to exchange than freshly prepared amylose. Figure 4 of their paper shows that in one experiment their aged amylose exchanged slower than fresh amylose and, in fact, had not reached equilibrium in the several hours allotted for exchange. Likely,

in their exchange experiments equilibrium had not been achieved, and the observed resistance to deuteration was rather a reflection of slowed exchange in less penetrable material. Further, because equilibrium with flowing gas is not easily achieved under these circumstances, complete replacement of H by D may not have occurred even in several half-hour equilibrations. Their test for equilibrium was approximate constancy of weight in one more treatment after four treatments. This test would not be a sensitive measure of equilibrium during a slow reaction. Because of these considerations, it cannot be concluded that resistant hydroxyls have been demonstrated in their work.

In view of the resistance of retrograded amylose to dispersion in water, the essentially complete accessibility of the hydroxyl hydrogens to deuterium exchange might seem anomalous. One mechanism seems particularly attractive, however. The crystalline regions are one type of association which might have the necessary stability. Since all hydroxyl groups are exchangeable with D₂O, it can be inferred that any hydrogen bond in a wet preparation would exist only a fraction of the time. In the crystalline regions, however, a considerable collective action of a number of hydrogen bonds could occur that would be permanent enough to have the resistance observed. It seems reasonable to postulate that only association with this collective action is important in retrograded amylose preparations. This association would include crystalline regions observable by X-ray diffraction, as well as the beginnings of association of molecular chains to form a regular structure. Association at random points between chains should not be a significant contribution in wet preparations of purified retrograded amylose.

Effects of pretreatments on the dispersibility of starches have been observed^{2,38,39} and interpreted as an effect on the size of the crystalline regions.⁴⁰ Direct evidence that the crystalline regions can be highly variable is shown by the results of characterization of our retrograded amylose samples. Preps. III and IV were prepared from the same sample of highly purified amylose and should differ only in their state of retrogradation. Prep. III, retrograded in the cold, was soluble in the 16-hour boiling treatment, in contrast to Prep. IV, and had smaller apparent crystallite sizes. Preps. I and IV not only remained insoluble under the boiling treatment but retained their B X-ray patterns as well.

This discussion reinforces the concept of K. Meyer² and of others that the crystalline regions are the outstanding form of association in starches and that the size, form and amount of crystalline regions as well as X-ray type importantly affect starch properties. Both the complete accessibility of all samples tested and the evidence on dispersibility of the retrograded amyloses favor this view.

(31) R. S. Bear, *J. Am. Chem. Soc.*, **64**, 1388 (1942).

(32) R. E. Rundle and D. French, *ibid.*, **65**, 558 (1943).

(33) F. F. Mikus, R. M. Hixon and R. E. Rundle, *ibid.*, **68**, 1115 (1946).

(34) R. L. Whistler and G. E. Hilbert, *ibid.*, **67**, 1161 (1949).

(35) J. Holló and J. Szejtli, *Die Stärke*, **10**, 248 (1958).

(36) Hazel Rossotti, *J. Polymer Sci.*, **36**, E57 (1959).

(37) M. Čeh and D. Hadži, *Die Stärke*, **10**, 99 (1958).

(38) N. P. Badenhuizen, ref. 5, p. 18.

(39) L. Sair and W. R. Fetzer, *Ind. Eng. Chem.*, **36**, 205 (1944).

(40) L. Mandelkern, *Chem. Revs.*, **66**, 903 (1956).

KINETICS OF ION EXCHANGE IN A CHELATING RESIN

BY RICHARD TURSE AND WM. RIEMAN III

Ralph G. Wright Chemical Laboratory, Rutgers, The State University, New Brunswick, New Jersey

Received January 30, 1961

Failure to obtain satisfactory chromatographic separations of metals with a chelating cation-exchange resin, Dowex A-1, led to a study of the kinetics of ion exchange with this resin. A modification of the limited-bath technique of Kressman and Kitchener was used. The experimental results can be explained only by the assumption that the chemical exchange reaction (not diffusion) is the slow step.

An investigation of chromatographic separation of metals with the chelating resin Dowex A-1 was undertaken in this Laboratory. The resin¹ consists of the well-known crosslinked polystyrene matrix with $-\text{CH}_2\text{N}(\text{CH}_2\text{COOH})_2$ as the functional group. The behavior of this resin in elutions of non-chelating cations is fairly similar to that of Dowex 50. For example, the elution of ammonium chloride with 0.5 *M* potassium chloride as eluent at a flow rate of 0.3 cm. per min. gave a nearly Gaussian graph with an average of 18 plates per cm. On the other hand, the elution of magnesium chloride with 1 *M* sodium chloride at a comparable flow rate gave a badly tailing graph with calculated plate numbers of 16 and 2.0 per cm. on the ascending and descending slopes, respectively. Cations that chelate with the iminodiacetate group more strongly than magnesium gave even worse graphs. Separations of such metals by elution chromatography were entirely unsatisfactory. Attempts to separate such metals by displacement chromatography were equally unsuccessful.

This led to the suspicion that the rates of ion exchange of chelating metals with this resin were abnormally slow, and a study of the kinetics was undertaken.

There is ample evidence in the literature to indicate that the rate of ion exchange, where chelation is not involved, is governed by the diffusion of the ions either within the resin particle (usually for solutions above 0.1 *M*) or in the film of solution surrounding the resin particles (usually for solutions below 0.001 *M*). At intermediate concentrations both processes exert an influence. Boyd, *et al.*,² investigated ion-exchange kinetics by the "shallow-bed" technique. They passed a rapid stream of electrolyte solution through a shallow bed of resin for a controlled length of time. Thus the concentration of the solution remained essentially constant during the process.

Kressman and Kitchener,³ on the other hand, used the "limited-bath" technique. They lowered a rotating, platinum-gauze cage containing a measured quantity of resin into a solution containing an exactly equivalent quantity of the exchanging cation. They stopped the reaction by simply removing and rinsing the cage. Since the two groups of investigators applied different conditions their equations are different; neverthe-

less, their conclusions are in complete agreement.

The kinetic equation for an exchange controlled by particle diffusion under the limited-bath conditions³ is

$$\frac{Q_t}{Q_\infty} = \frac{6}{\tau} \frac{Q_0}{Q_0 - Q_\infty} \sqrt{\frac{Dt}{\pi}} \quad (1)$$

Q_t is the amount of exchange in time t ; Q_∞ is the amount of exchange at equilibrium; Q_0 is the amount of resin (and of solute) taken in the experiment (all quantities in milliequivalents); r is the radius of the resin beads in centimeters; and D is the coefficient of diffusion inside the resin bead. Thus a plot of Q_t/Q_∞ vs. \sqrt{t} should be a straight line for exchanges controlled by bead diffusion. The diffusion coefficient of the ions concerned can be calculated from the equation for the slope

$$S = \frac{6}{\tau} \frac{Q_0}{Q_0 - Q_\infty} \sqrt{\frac{D}{\pi}} \quad (2)$$

An approximation introduced in the derivation of equation 1 causes deviations from linearity when Q_t/Q_∞ exceeds about 0.6.

The kinetic equation for an exchange controlled by a second-order chemical reaction in the limited-bath method^{4,5} is

$$\ln Z = 2kQ_0(Q_0 - Q_\infty)t/Q_\infty \quad (3)$$

where

$$Z = \frac{Q_t(Q_0 - 2Q_\infty) + Q_0Q_\infty}{Q_0(Q_\infty - Q_t)}$$

Here the Q 's have the dimensions of equivalents per liter, and k is the second-order rate constant. A plot of $\log Z$ vs. t should be linear for a chemically controlled exchange. The rate constant can be calculated from the slope of such a plot

$$S = 2kQ_0(Q_0 - Q_\infty)/2.30Q_\infty \quad (4)$$

Another very useful method of identifying the slow step in an ion-exchange process is to study the kinetics of the process in two experiments performed under identical conditions except for a difference in the particle size of the resin. According to equation 1, the rate of a diffusion-controlled process is accelerated by a decrease in particle size. On the other hand, equation 3 indicates that the rate of a chemically controlled exchange is independent of the particle size of the resin.

Still another method of identifying the slow step is to conduct two kinetic experiments under identical conditions except for a change in concentration.

(1) "Dowex Chelating Resin A-1," The Dow Chemical Co., 1959, p. 2.

(2) G. E. Boyd, A. W. Adamson and L. S. Meyers, Jr., *J. Am. Chem. Soc.*, **69**, 2836 (1947).

(3) T. R. E. Kressman and J. A. Kitchener, *Discussions Faraday Soc.*, **7**, 90 (1949).

(4) A. A. Frost and R. G. Pearson, "Kinetics and Mechanism," John Wiley and Sons, Inc., New York, N. Y., 1953, p. 174.

(5) R. Turse, thesis, Rutgers, The State University, New Brunswick, N. J., 1960.

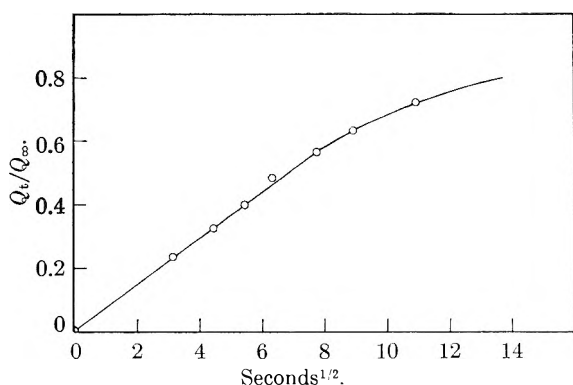


Fig. 1.—Particle-diffusion plot for Dowex 50-X8: reaction $MgR_2 + Ca^{++}$ at 25° .

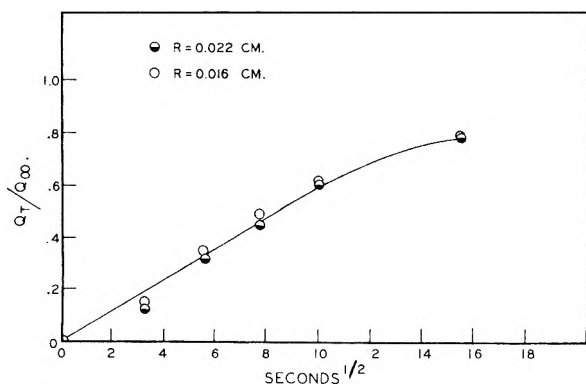


Fig. 2.—Particle-diffusion plot for Dowex A-1: reaction $2NaR + Ca^{++}$ at 25° .

Provided that the change in concentration is not so great as to exceed the limits within which diffusion in the resin is the slow step, the change should have no effect on a process controlled by resin diffusion. On the other hand, an exchange controlled by a second-order chemical reaction should be markedly affected by a change in concentration.

Experimental Work

Resins.—Dowex Chelating Resin A-1 was supplied by The Dow Chemical Company as spherical beads, mostly of 40-50 mesh. It consists of a crosslinked polystyrene matrix with iminodiacetate groups. For purposes of comparison, some kinetic experiments also were performed with Dowex 50-X8, a sulfonated, crosslinked polystyrene. The very fine particles were removed from both resins by slurring the resin in deionized water, allowing the main portion to settle and decanting the suspension of the fines.

Portions of each resin in the sodium form were wet-sieved to obtain fractions in each of three ranges of mesh size. Twenty randomly selected spheres from each of the six fractions then were examined with a micrometer microscope to find the mean diameter of each fraction.

To convert Dowex A-1 to any desired form, the usual procedure was as follows: The resin (unless in the sodium form) was converted to the hydrogen form by treatment with hydrochloric acid in a column, then to the sodium form by slurring with excess sodium hydroxide in a beaker, and finally to the desired form by treatment in a column with the appropriate salt. Both column treatments were continued until the effluent had the same composition as the influent. A simple column treatment sufficed to convert Dowex 50 into any desired form.

The exchange capacities of the sodium forms of the dry resins were determined by drying the resin for 20 hours *in vacuo* at 60° , putting a weighed portion into a column, passing a sufficient quantity of 0.1 *M* hydrochloric acid through the column, and finally determining both hydrogen and chloride ions in the total effluent. The difference is

the quantity (milliequivalents) of sodium in the resin. The exchange capacities of other forms of the resins were calculated from those of the sodium form and the appropriate equivalent weights.

Kinetic Experiments.—A modification of the limited-bath technique was used. One-hundred ml. of a standard solution of the electrolyte, about 0.1 *M* in all cases, was placed in a 250-ml. beaker and stirred at a constant, rapid rate in a thermostat controlled to 0.01° . After thermal equilibrium was attained, a quantity of dry resin, exactly equivalent to the cation in solution, was added rapidly. After the desired time interval, an adequate portion of the solution was transferred rapidly with suction from the beaker through a sintered-glass filter into a flask. A suitable volume of the solution in the flask was subjected to analysis to determine the extent to which the ion-exchange reaction had occurred. The procedure was repeated at other time intervals with fresh portions of solution and resin. In experiments at 37.5 and 50° for long time intervals, excessive evaporation from the beaker was avoided by covering it with a metal foil provided with a hole for the stirrer shaft.

The determination of ammonium ion was accomplished by titration with sodium hydroxide in the presence of formaldehyde.⁶ Nickel, magnesium, cobalt, calcium, cadmium, manganese and copper were determined by titration with ethylenediaminetetraacetate.⁷ Hydrogen ion was determined by titration with sodium hydroxide.

Results and Interpretation

Dowex 50.—In the case of Dowex 50, plots of Q_t/Q_∞ vs. \sqrt{t} are linear, indicating that these exchanges are controlled by diffusion within the resin beads. Figure 1 is typical of these plots. It is linear to about the same value of Q_t/Q_∞ as found by Kressman and Kitchener.

Table I presents the results of these exchanges.

A comparison of experiments 3 and 4 shows that the reaction was more rapid (larger *S*) with the finer resin particles. Furthermore, the two experiments yielded the same value of *D*, as is to be expected in diffusion-controlled kinetics. A comparison of experiments 5 and 6 confirms these findings.

Dowex A-1.—In the reaction between the sodium form of Dowex A-1 and ammonium ion, good linear plots of Q_t/Q_∞ vs. \sqrt{t} also were obtained. Furthermore, identical values of $D = 18 \times 10^{-8}$ were calculated from experiments at 25° with resins of different average radii, 0.019 and 0.021 cm. These observations indicate that bead diffusion is the slow step in this exchange reaction.

The exchange of the sodium form of Dowex A-1 with calcium ion (numbers 1 and 2 in Table II) was studied. The plots of Q_t/Q_∞ are shown in Fig. 2. Although the approximate linearity of the graph supports the hypothesis that diffusion inside the resin is the slow step, the fact that resins of different particle sizes gave identical graphs is very strong evidence that neither bead diffusion nor film diffusion is the slow step. The same data are plotted as $\log Z$ vs. *t* in Fig. 3. Both the linearity and the coincidence of the graphs support the hypothesis that the second-order chemical reaction is the slow step.

Even more striking evidence for a chemically controlled exchange reaction with Dowex A-1 is

(6) W. Riemann, J. D. Neuss and B. Naiman, "Quantitative Analysis," Third Edition, McGraw-Hill Book Co., New York, N. Y., 1951, p. 166.

(7) F. J. Welcher, "The Analytical Uses of Ethylenediaminetetraacetic Acid," D. Van Nostrand Co., New York, N. Y., 1958.

TABLE I
KINETIC EXPERIMENTS WITH DOWEX 50-X8

No.	Reagents	Mean r , cm.	Temp., °C.	Q_0	Q_∞	S	$D \times 10^4$
1	NaR + NH ₄ ⁺	0.031	25	0.0970	0.0448	0.135	45
2	2NaR + Ca ⁺⁺	.031	25	.0926	.0750	.082	2.0
3	MgR ₂ + Ca ⁺⁺	.031 ^a	25	.0896	.0548	.073	6.8
4	MgR ₂ + Ca ⁺⁺	.027 ^a	25	.0920	.0564	.083	6.8
5	MgR ₂ + Ca ⁺⁺	.031 ^a	50	.0936	.0570	.106	15
6	MgR ₂ + Ca ⁺⁺	.027 ^a	50	.0936	.0570	.120	14

^a The beads of magnesium resin were assumed to have the same radii as the beads of the sodium resin because the actual difference in the radii is less than the standard deviation of the measurements.

TABLE II
SECOND-ORDER RATE CONSTANTS

No.	Reaction	r , cm.	Temp., °C.	Q_0	Q_∞	$S \times 10^3$	$k \times 10^3$
1	2NaR + Ca ⁺⁺	0.022	25	0.0924	0.0902	3.68	18.8
2	2NaR + Ca ⁺⁺	.019	25	.0924	.0902	3.68	18.8
3	2NaR + Ca ⁺⁺	.022	37.5	.0936	.0912	4.85	22.8
4	2NaR + Ca ⁺⁺	.022	50	.0936	.0912	7.46	34.8
5	MgR ₂ + 2H ⁺	.022	25	.1130	.0974	4.25	2.70
6	MgR ₂ + 2H ⁺	.016	25	.1051	.0921	3.63	2.81
7	MgR ₂ + 2H ⁺	.022	37.5	.0945	.0862	6.10	7.76
8	MgR ₂ + 2H ⁺	.022	50	.0934	.0846	13.3	15.7
9	MgR ₂ + Ca ⁺⁺	.016	25	.0936	.0544	2.36	0.403
10	MgR ₂ + Ca ⁺⁺	.022	37.5	.0936	.0548	2.82	.490
11	MgR ₂ + Ca ⁺⁺	.022	50	.0936	.0550	3.46	.593
12	MgR ₂ + Ca ⁺⁺	.016	50	.0936	.0550	3.40	.593
13	CaR ₂ + Mg ^{++a}	.016	25	.0936	^a		
14	CoR ₂ + 2H ⁺	.022	25	.0935	.0853	1.18	1.51
15	NiR ₂ + 2H ⁺	.022	25	.0871	.0727	0.678	0.453
16	MnR ₂ + 2H ^{+b}	.019	25	.0886	.0880	0.366	6.96
17	MnR ₂ + 2H ^{+c}	.019	25	.1172	.1022	1.34	0.90
18	CdR ₂ + 2H ⁺	.022	25	.0835	.0760	0.269	0.376
19	CuR ₂ + 2H ⁺	.022	25	.0840	.0448	^d	
20	HR + NH ₃	.022	25	.0980	.0914	2.41	3.92
21	2HR + Ba(OH) ₂	.022	25	.0900	.0817	0.106	0.134

^a This reaction failed to reach equilibrium in 26 hours. ^b This reaction was run with 0.1 N HCl as the acid. ^c This reaction was run with 0.1 N HClO₄ as the acid. ^d This reaction failed to exhibit a straight line in the second-order plot.

furnished by a comparison of experiments 5 and 6 of Table II. If bead diffusion controls the rate, no. 6 should be the faster; and if the chemical reaction controls the rate, no. 5 should be faster. The plots, shown in Fig. 4 and 5, indicate unequivocally that the chemical reaction is the rate-controlling step. It is to be noted that the slopes of the graphs of $\log Z$ vs. t are different because of the values of Q_0 . However, the two graphs yield closely checking values of k (Table II). It should also be noted that the plots of Q_t/Q_∞ are not linear.

Experiments 11 and 12 of Table II done with two different particle sizes (0.016 and 0.022 cm.) but with identical values of Q_0 yielded graphs that coincided very closely.

Table II lists all the exchange reactions of Dowex A-1 that were studied except that between sodium resin and ammonium ion. Each experiment of Table II gave excellent linear plots of $\log Z$ vs. t , similar to those of Fig. 2 and 4, except where noted.

The results of exchange experiments with Dowex A-1 involving one or two ions capable of complexing strongly with this resin can be explained only by assuming that the chemical exchange is the slow step in the over-all process. Strongly complexing cations include the alkaline earths and hydrogen but not the alkalis or ammonium.

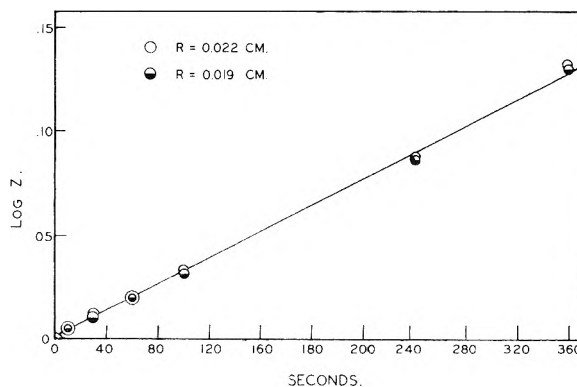


Fig. 3.—Second-order plot for Dowex A-1: reaction $2\text{NaR}_2 + \text{Ca}^{++}$ at 25°.

The data for experiments 9, 10, 11 and 12 were obtained from determinations of the magnesium in solution and gave good linear graphs of $\log Z$ vs. t . However, when calcium concentrations in the solution also were determined in experiment 9, it was found that during the first one-half minute more calcium entered the resin than the quantity of magnesium which left the resin. Titrations of chloride ions during this interval revealed that chloride was entering the resin in

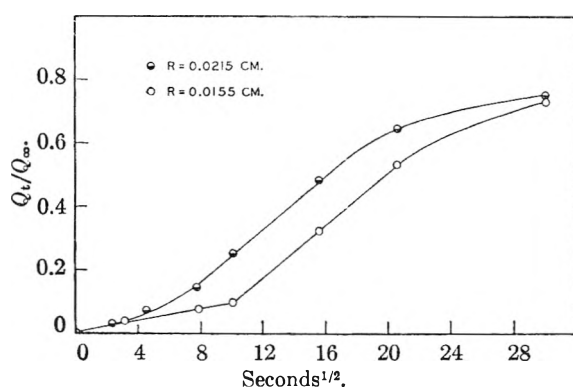


Fig. 4.—Particle-diffusion plot for Dowex A-1: reaction $\text{MgR}_2 + 2\text{H}^+$ at 25° .

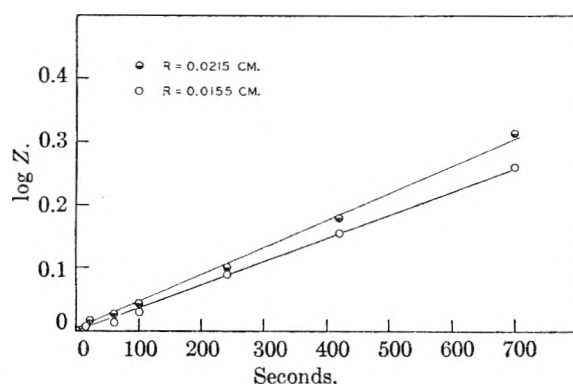


Fig. 5.—Second-order plot for Dowex A-1: reaction $\text{MgR}_2 + \text{Ca}^{++}$ at 25° .

significant quantities, as required by electroneutrality. During the second one-half minute, both the chloride and calcium concentrations in the solution increased. After the end of the first minute, the concentration of calcium in solution decreased normally, and the concentration of chloride remained constant. Microscopic observations of a single bead of magnesium-form Dowex A-1 immersed in 0.1 *M* calcium chloride revealed that it swelled markedly for 30 seconds, shrank for the next 40 seconds and then remained constant in volume. Further details of this abnormal behavior and a possible explanation are given elsewhere.⁵

Although the concept of a reaction-controlled exchange seems iconoclastic to some, a survey of the pertinent literature indicates that chemical control is not at all surprising when the exchange involves the making and/or breaking of chelate bonds. Some chelation reactions are slow even

in aqueous solution. For example, the titrations of aluminum, chromium(III), iron(III) and manganese(II) with ethylenediaminetetraacetate are done at high temperature⁷ to hasten the reaction. Also, the exchange between the nickel complex of this ligand and radioactive free nickel ion is less than 5% complete in 24 hours.⁸ These authors also give many other examples of slow chelation reactions in aqueous systems.

Furthermore, reactions that are rapid in aqueous solution may be very slow when one of the reagents is incorporated in a polymer. For example, a resin has been prepared⁹ which has both ion-exchange and oxidation-reduction properties, arising from sulfonated benzene rings and hydroquinone rings, respectively. Although the kinetics of the reactions of the resin have not been studied in detail, column experiments indicated a normally rapid exchange process and a very slow oxidation-reduction reaction. Oxidation of the reduced resin required 16 hours for completion. The rapid exchange reactions indicate that diffusion within this resin is not much slower than in ordinary ion-exchange reactions. Therefore the slow oxidation of the reduced form must be due to the slow chemical change from the reduced (hydroquinone) form to the oxidized (quinone) form. It is well known that the oxidation of monomeric hydroquinone occurs rapidly in aqueous solution. Incorporation of this monomer in a resin greatly decreases the velocity of its reaction with oxidizing agents. Therefore it is not surprising that even those metals which chelate rapidly with methyliminodiacetate or ethylenediaminetetraacetate react slowly when this chelating group is incorporated in a resin.

Conclusions.—Exchange reactions of Dowex A-1 that involve one or two strongly chelating cations are controlled by a second-order chemical reaction, not by diffusion. This statement is based on the following observations made with 0.1 *M* solutions: (1) Plots of $\log Z$ vs. t are linear as required for a second-order reaction. (2) The exchange rate is independent of the particle size of the resin. (3) The exchange rate is dependent on the concentration of the solution as required by the equation for second-order kinetics.

Acknowledgment.—The authors wish to express their gratitude to The Dow Chemical Company for financial support of the study and the supply of the resins used.

(8) F. Basolo and R. Pearson, "Mechanisms of Inorganic Reactions," John Wiley and Sons, Inc., New York, N. Y., 1958.

(9) L. Lutinger and H. G. Cassidy, *J. Polymer Sci.*, **20**, 417 (1956).

THE STARCH-IODINE-IODIDE INTERACTION. PART II. POTENTIOMETRIC INVESTIGATIONS¹

BY JOHN A. THOMA² AND DEXTER FRENCH

Department of Chemistry, Iowa State University, Ames, Iowa

Received February 25, 1961

Contrary to previous belief, starch oligosaccharides in the range maltotetraose-maltopentadecase form I_3^- complexes, as evidenced by potentiometric titration. Maltodecaose and higher oligosaccharides bind additional iodine. The logarithms of the formation constants plotted against the number of glucose units per oligosaccharide molecule give essentially straight lines. However, a distinct break between maltohexaose and maltoheptaose is suggestive of a "loop" to "helix" transition in the configuration of the complex. The formation constant for the maltohexaose- I_3^- complex is lower than for the cyclic α -Schardinger dextrin I_3^- complex by a factor of about 10^3 . This difference stems not only from the unfavorable conformational entropy change (random coil to loop) but also from a relatively lower $-\Delta H$ of complex formation for the open chain compound.

Introduction

In the preceding paper of this series,³ some semi-quantitative observations were made concerning the effect of chain length on the starch-iodine complex. In order to formulate a more quantitative analysis of the effect of the chain length on the stoichiometry of the starch-iodine complex, isolated starch oligosaccharides in the range maltotetraose (G_4) to maltopentadecase (G_{15}) were studied by the electrometric methods developed by Bates and co-workers.⁴

Materials and Apparatus.—The reagents used were described in the preceding paper.³ The titration vessel was a micro three-neck flask. An eye dropper with rubber bulb, which served as a stirrer, was fitted into one neck and a platinum electrode was sealed through the side of the stirrer to make contact with the solution to be titrated. The tip of an "Agla" micrometer syringe (Burroughs Wellcome and Co., London), capable of delivering 0.5 ml. \pm 0.5 μ l., was placed into another neck and an agar bridge was placed into the third neck. The agar bridge consisted of a glass tube drawn out so that the orifice was about 0.1 mm. in diameter. To avoid contaminating the iodine electrode vessel with chloride or other foreign ions, it was filled with a hot 2% solution of agar (Bacto-agar, Difco) of the same KI concentration as that used in titrating the dextrans, and allowed to gel. The space above the agar in the bridge then was filled with saturated KCl and the orifice of a calomel half-cell dipped into it. The potential of the system was measured with a Leeds and Northrup Type K potentiometer in conjunction with a suspension galvanometer capable of detecting differences of 0.02 mv.

Agar bridges were prepared daily and stored in the same concentration of KI as that used to titrate the dextrans. With duplicate titrations, the average deviation, for the points used to plot the standard I_2 curves, was generally within 0.1 mv. when measured with bridges prepared simultaneously. However, the average deviation for the points used to plot the standard I_2 curves was as much as 0.4 mv. when measured with bridges prepared on different days. The average difference between duplicates in the oligosaccharide-iodine e.m.f. measurements ranged from 0.7 mv. at low iodine levels to 0.1 mv. at high iodine levels.

Methods.—The method outlined by Bates⁴ but modified to a micro scale was used. To obtain reproducible e.m.f.'s, it was necessary to take readings while the solutions were agitated gently by alternately squeezing and releasing the bulb of the eye dropper.

The reliability of the micro method was tested by titrating cyclohexanamylose (α) with I_2 -KI. The apparent formation constant in 0.1 M KI for the αI_3^- complex determined by

the micro method was 1.7×10^6 , consistent with that obtained by Dube.⁵ Possible hysteresis in these systems was tested for and excluded by noting the exact agreement in the amount of bound iodine in the "forward" and "backward" titration of an oligosaccharide mixture.

Weighed samples of the air-dried dextrans (which assayed between 87 and 92% carbohydrate) were dissolved in 1.20 ml. of 0.25 or 0.75 M KI solution to give approximately 0.8 to 1% dextrin solutions. Then 0.50 ml. of each dextrin solution was pipetted into the micro three-neck flask and titrated with 2.00×10^{-2} M I_2 in 0.25 or 0.75 M KI. E.m.f. measurements on duplicate samples were in good agreement. Titrations were conducted in 0.25 M KI at $0.2 \pm 0.1^\circ$ and $25.2 \pm 0.1^\circ$ and in 0.75 M KI at $25.2 \pm 0.1^\circ$.

The maximum concentration of I_2 which could be measured accurately was about 10^{-2} M. At higher concentrations, the standard I_2 curves (e.m.f. vs. $\log [I_2]$) demonstrated marked deviations from linearity and the measuring system became rather insensitive to changes of I_2 concentration. These effects may have been caused by a reaction of I_2 with the agar bridge or the formation of polyiodine complexes⁶ at the high concentrations of I_2 .

Results

The absence of hysteresis during the forward and backward titration of an amylopectin hydrolysate (from which the individual saccharides were isolated³) with I_2 -KI and $Na_2S_2O_3$ -KI demonstrated that complex formation is rapid and reversible. This conclusion also was supported by the fact that the e.m.f. values with the individual saccharides were stable immediately after thorough mixing of iodine and dextrin.

Titration data for G_4 through G_9 in 0.25 M KI at 25.2° are plotted in Fig. 1. Each experimental point is the average of closely agreeing duplicates but the curves were drawn from a template calculated for a 1:1 reaction and fitted to the experimental points (see the Discussion).

When the maltodextrans larger than G_9 were titrated, the amount of iodine which could be bound at high iodine concentration exceeded the calculated amount for a 1:1 complex, indicating that a second mole of iodine (as I_2 or I_3^-) was being bound. The data for G_{10} through G_{15} were handled by the method of Bjerrum⁷ (Fig. 2) which verified the existence of a second complex and gave the numerical values of both the first and second formation constants.

A logarithmic plot of the apparent formation

(1) Journal Paper No. J-4025 of the Iowa Agricultural and Home Economics Experiment Stations, Ames, Iowa. Proj. 1116. Supported in part by grants from the Corn Industries Research Foundation and General Foods, Inc.

(2) Union Carbide and Carbon Fellow 1957-1958.

(3) J. A. Thoma and D. French, *J. Am. Chem. Soc.*, **82**, 4144 (1960).

(4) F. L. Bates, D. French and R. E. Rundle, *ibid.*, **65**, 142 (1943).

(5) H. Dube, Ph.D. dissertation, Iowa State University, Ames, Iowa, 1947.

(6) M. Davies and E. Gwynne, *J. Am. Chem. Soc.*, **74**, 2748 (1952).

(7) J. Bjerrum, "Metal Ammine Formation in Aqueous Solution," P. Haase and Son, Copenhagen, 1941.

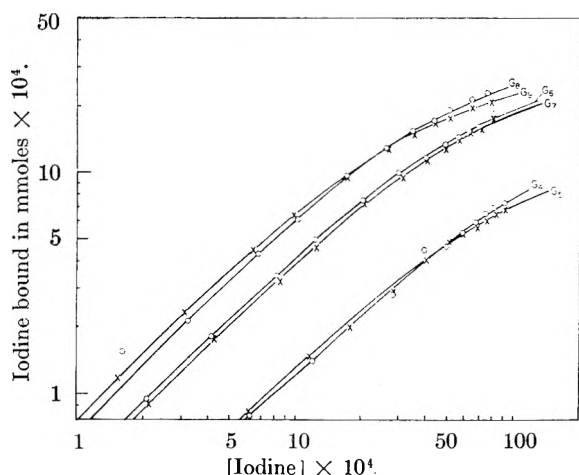


Fig. 1.—Double logarithmic plots for G_4 – G_9 at 25° , $0.25 M$ KI: The continuous curves are drawn from a template calculated for a 1:1 reaction between oligosaccharide and iodine. The vertical irregularity of the curves results from variation in the size of sample taken for titration.

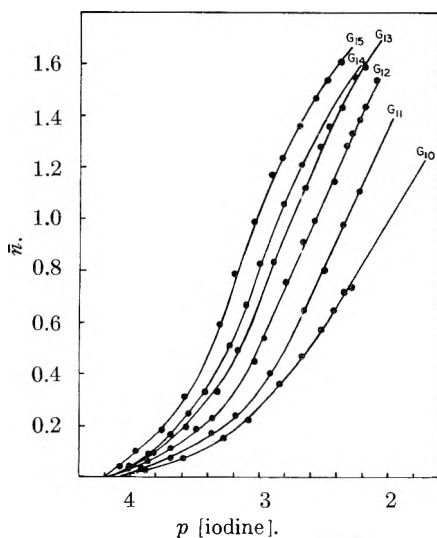


Fig. 2.—Bjerrum plots for G_{10} – G_{15} : \bar{n} is the average number of molecules of bound iodine per molecule of carbohydrate.

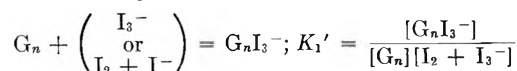
constants in $0.25 M$ KI at 25.2° for G_4 through G_{15} as a function of n (the number of glucose residues per molecule) (Fig. 3, curves A, B, C) reveals a discontinuity between $n = 6$ and $n = 7$. To be sure that this discontinuity was not simply an experimental error, the formation constants were also determined at 0° . At this lower temperature, experimental errors were reduced because the higher binding affinities of the dextrans enabled bound iodine to be calculated more accurately. The apparent formation constants for G_4 through G_9 at 0.2° in $0.25 M$ KI reported in Fig. 3 were determined from the titration curves of the dextrans plotted in Fig. 4 (theoretical template fitted to the experimental points).

The molecularity of I^- in the complexes was determined by titration of G_{13} and G_{14} at 25.2° in $0.75 M$ KI and comparison of the apparent resultant equilibrium constants with those obtained at 25.2° in $0.25 M$ KI. The titration characteristics of G_{13} and G_{14} in $0.75 M$ KI at 25.2°

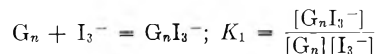
are recorded in Fig. 5 and the equilibrium constants are reported in Fig. 3.

Discussion

In determining the "bound iodine" by potentiometric titration, it is impossible to distinguish experimentally between I_2 and I_3^- because these measurements were conducted in a large excess of I^- . However, for practical purposes, the total free iodine was considered to be I_3^- . Using the formation constant of I_3^- , $K_1 = 768$,⁶ it can be calculated that in $0.25 M$ KI considerably less than 1% of the total iodine exists as I_2 . The first apparent formation constants (K_1') determined potentiometrically for the reaction



are related to the real formation constants for the reaction



by the equation

$$K_1 = K_1' \left(1 + \frac{1}{K_1 [I^-]} \right)$$

Similarly, the second apparent formation constants are related to the real formation constants by the equation

$$K_2 = K_2' \left(1 + \frac{1}{K_1 [I^-]} \right)$$

If dextrin and iodine react to form a 1:1 complex, then the *shape* but not the *position*, of a plot of the \log [iodine] bound *vs.* the \log [iodine] free will be independent of both the equilibrium constant and the maximum amount of iodine which can be bound. The apparent formation constant is equal to the reciprocal of the concentration of the iodine free when $1/2$ of the dextrin is complexed and can be evaluated by fitting a calculated template to the experimental points. The molecularity of iodine in the complexes may be noted from the initial slopes of the curves. For G_4 through G_9 , the initial slopes indicated that one molecule of iodine (undoubtedly as I_3^-) is bound in the complex. One additional piece of information can be gleaned from this graphical analysis: the maximum amount of iodine which can be bound. This value should correspond to the amount of saccharide titrated and furnished an additional check on the experimental results.

When the maximum amount of iodine which could be bound, determined from the template, was compared with the total dextrin concentration, the values agreed within experimental error for G_8 and G_9 but considerably exceeded the dextrin concentrations for G_{10} and G_{11} . Furthermore, it was noted that the $\log K'$ values determined by the template method (above G_9) no longer increased linearly with n , the number of residues per molecule. At this point, it appeared that polyiodide complex formation was becoming measurable and that the second apparent formation constants were within an order or two of magnitude of the first apparent formation constants. To establish values for the successive apparent formation con-

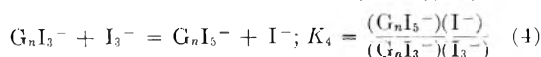
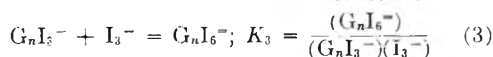
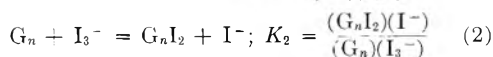
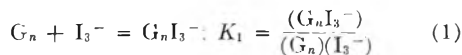
stants for the saccharides having n greater than nine, the method outlined by Bjerrum⁷ and extended by Irving and Rossotti⁸ was employed. In this method, \bar{n} (moles of iodine bound per mole of added dextrin) is plotted against the negative logarithm of the total "free" iodine ($I_2 + I_3^-$) concentration. The pK' values for the two associations are obtained by the use of the graphical method of Irving and Rossotti.⁸ With G_9 and G_{10} the attainable iodine levels do not permit the second complex to be formed sufficiently to allow a very accurate evaluation of K_2' . With the higher saccharides the Bjerrum plots were reasonably symmetrical about $\bar{n} = 1$, a requirement for a reaction bimolecular in iodine (Figs. 2 and 5).

The logarithms of the equilibrium constants determined for the dextrans G_{10} and above by the method of Bjerrum again follow a linear relationship when plotted against n . Furthermore, the first equilibrium constants determined for G_{10} and G_{11} by the template method (using the initial points where polyiodine formation could be considered insignificant and taking the maximum iodine which could be bound in the first complex equivalent to the total dextrin concentration) agree within experimental error with those determined by the treatment of Bjerrum.

The maximum amount of iodine which could be bound by saccharides composed of seven or less glucose units was less than one mole per mole of dextrin. This would be reasonable if the reactions are polymolecular with respect to dextrin, or if the dextrans are contaminated by an inert impurity. Further work needs to be done in order to resolve this discrepancy.

Although iodine binding by G_3 at 25.2° and by G_3 and even G_2 at 0.2° could be detected, the scatter in the experimental points was too great to permit a determination of the equilibrium constants. The e.m.f. values obtained when glucose was titrated were identical with blanks within experimental error. Therefore, it could not be conclusively established whether or not glucose exhibited any affinity for iodine although this would be predicted by extrapolation of the data in Fig. 3.

At constant KI levels, no information can be gained about the molecularity of I^- in the complexes from I_2 titrations. For example, it is impossible to differentiate between the equilibria (1) and (2) or between (3) and (4)



However, by varying the I^- levels one can readily differentiate between the first and second sets and third and fourth sets of equilibria. In a large excess of I^- , K' , the measured apparent formation constants, will either equal K_2/I^- and K_4/I^- and show dependence on I^- , or will equal K_1 and

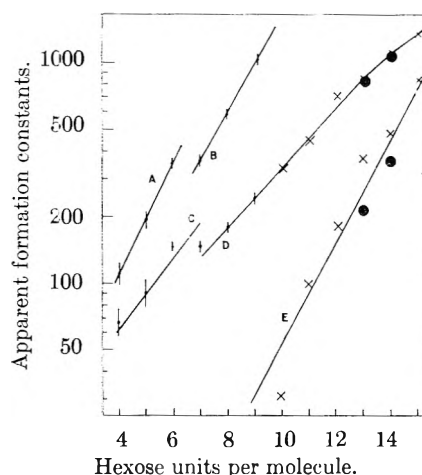


Fig. 3.—Apparent formation constants for oligosaccharide-iodine complexes: A, B, K_1' values at 0°, 0.25 M KI; C, D, K_1' values at 25°, 0.25 M KI; E, K_2' values at 25°; ●, K_1' and K_2' values for G_{13} and G_{14} at 25°, 0.75 M KI; all values for G_{10} – G_{15} were determined from Bjerrum plots.

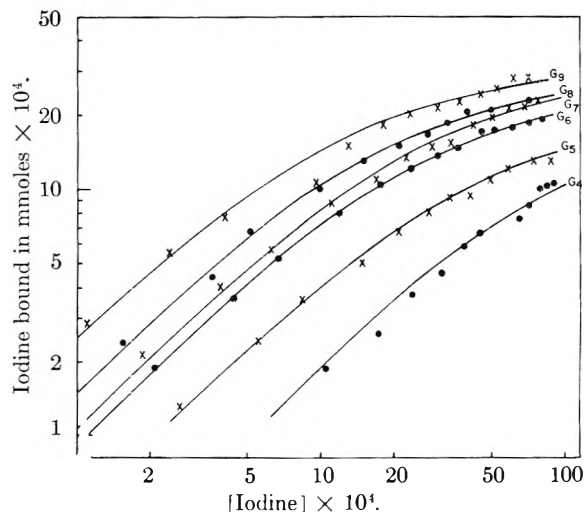


Fig. 4.—Double logarithmic plots for G_4 – G_9 at 0°, 0.25 M KI.

K_3 and be independent of I^- . When the equilibrium constants for G_{13} and G_{14} determined in 0.75 M KI were compared with the equilibrium constants determined in 0.25 M KI (see Fig. 3), they were considered to be equal. This result indicated the correctness of equations 1 and 3. It must be remembered, however, that these experiments were conducted in solutions of very high KI concentrations, and that the stoichiometry of I^- in the complexes may well be different at lower KI concentrations or with other chain lengths.

Considering the ratios of the equilibrium constants for analogous reactions in the G_6 and α - I_2 -KI systems to be approximately equal and considering the orders of magnitude of the formation constants for αI_3^- , αI_2 ,⁹ and αI^- ,⁵ it appears extremely likely that $G_6 I_2$ and $G_6 I^-$ complexes would remain below the limits of experimental detectability.

Figure 6 illustrates idealized hypothetical steps

(8) H. Irving and H. S. Rossotti, *J. Chem. Soc.*, 3397 (1953).

(9) J. A. Thoma and D. French, *J. Phys. Chem.*, **62**, 1603 (1958).

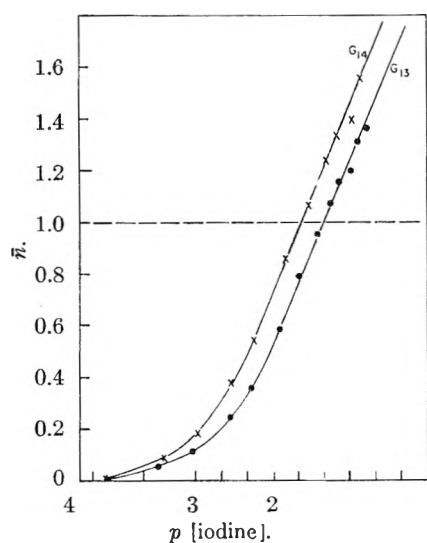


Fig. 5.—Bjerrum plots for G_{13} , G_{14} at 25° , $0.75 M KI$.

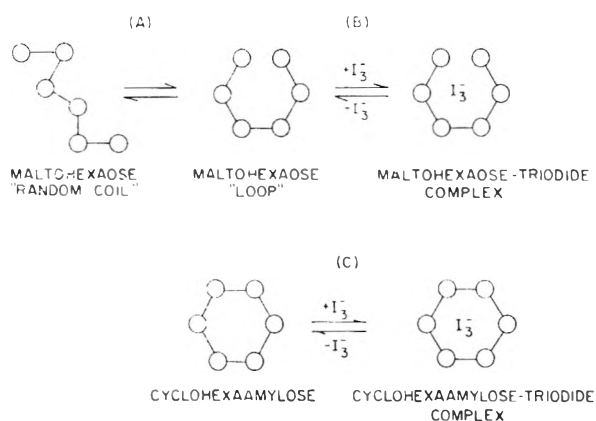


Fig. 6.—Iodine complex formation with maltohexaose (G_6) and cyclohexaamylose (α): The configuration of G_6 in solution is probably a "random coil" and is transformed in part into a "loop" in the I_3^- complex; with α the molecule is initially in a suitable form for complex formation and therefore reacts more avidly with I_3^- .

in the reaction of G_6 (random coil) to form a "loop" which then reacts with I_3^- to form a complex. The second step may be considered to be analogous with the α - I_3^- reaction. However, preliminary results indicate that $-\Delta H$ for the G_6 reaction is much less than for α , so that the large difference in I_3^- complex formation constants between α and G_6 cannot be ascribed wholly to entropy of coiling.

It is reasonable that the standard free energy of the reaction of G_n to form an I_3^- complex can be represented by the equation

$$\Delta F_n^0 = n \Delta F_a^0 + \Delta F_b^0 \quad (5)$$

Here n is the number of glucose units in the polymer, ΔF_a^0 is the increase in standard free energy of the reaction per glucose unit, and ΔF_b^0 is a constant. This treatment has neglected stabilization of the helix by hydrogen bonding, which is most likely insignificant if the chain is too short to form more than one or two turns of the helix, but may be an important factor for a large molecule like amylose.

According to equation 5, a plot of the log of the

apparent formation constants against n should be linear if each monomer has equal "accessibility" to the bound iodine. The constant ΔF_b^0 , the intercept, will represent the end effects. Figure 3 is in harmony with this hypothesis.

The discontinuity in the plot of the first apparent formation constants between G_6 and G_7 readily can be interpreted as a configurational transformation from a "loop" to a helical arrangement. This argument is also supported by the large difference of the ratios of the binding affinities of G_6 and G_7 and the corresponding cyclic Schardinger dextrans, cyclohexaamylose (α) and cycloheptaamylose (β). Dube⁵ reported that the I_3^- binding affinity of α was 100 times larger than that of β . If the G_7 - I_3^- complex existed in a loop rather than in a helical configuration, the apparent formation constants for G_6 and G_7 would be expected to differ by a factor of approximately 100, while the measured values were the same within experimental error.

The values for the first apparent formation constants appeared to be leveling off in the neighborhood of 2 to $2\frac{1}{2}$ turns of the helix. This result would be expected when the length of the helix becomes much larger than the length of the I_3^- ion. The values for the second apparent formation constants became steadily larger in the region tested; however, they too may eventually "plateau." It appears that as n increases, the stability of the polyiodine complexes increases more rapidly than the stability of the I_3^- complexes, and a value of n finally will be reached when the second apparent formation constants will become larger than the first apparent formation constants. This pattern may be reasonably expected to repeat itself for higher complexes as the maltodextrin series is ascended. Whether this cooperative effect represents principally a potential energy effect (entering iodine reinforces existing dipole moment¹⁰) or an entropy effect (since the second iodine enters a partially coiled dextrin) or a combination of them is a moot question.

For many years it has been tacitly assumed that maltodextrins with less than 6 glucose units (a complete turn of the helix) would not bind iodine. However, from the results of this investigation, it is apparent that this assumption is entirely erroneous. Furthermore, it appears from the free energy relationship in Fig. 3 that there is no qualitative but only a quantitative difference in the binding of iodine by dextrans of varying chain length, except in the loop to coil transition at G_7 . Therefore, it may be small uncoiled or partially coiled chain segments which are responsible for the second phase of iodine absorption by starch, frequently referred to as "adsorption." If, because of steric factors, there are a number of uncoiled segments with varying affinities for iodine it is reasonable that absorption of iodine by starch would follow a Freundlich adsorption isotherm after the large helical segments are filled.

Acknowledgment.—The authors wish to thank Prof. R. S. Hansen for enlightening discussions regarding the interpretation of the data.

(10) R. S. Stein and R. E. Rundle, *J. Chem. Phys.*, **16**, 195 (1948).

SOLVENTS HAVING HIGH DIELECTRIC CONSTANTS. XI. ELECTROMOTIVE FORCE MEASUREMENTS OF THE CELL Pt, H₂; HCl (*m*); AgCl-Ag IN N-METHYLACETAMIDE AT 40°^{1,2}

BY LYLE R. DAWSON, RICHARD C. SHERIDAN AND HARTLEY C. ECKSTROM

Department of Chemistry, University of Kentucky, Lexington, Kentucky

Received March 13, 1961

The e.m.f. of the cell Pt, H₂; HCl(*m*); AgCl-Ag in N-methylacetamide has been measured at 40°. The standard potential of the silver-silver chloride electrode was found to be 0.20573 ± 0.00035 volts. Activity coefficients of HCl solutions in N-methylacetamide at 40° have been calculated for concentrations ranging from 0.002 to 0.1 molal.

Studies of platinum-hydrogen and silver-silver chloride electrodes have been made in aqueous and non-aqueous solutions by many investigators. However, the only electromotive force studies in a solvent having a dielectric constant greater than that of water were made in formamide by Mandel and Decroly³ with a silver-silver chloride electrode and by Pavolopoulos and Strelow⁴ with a cadmium-cadmium chloride electrode. Although the electrical conductivities of more than seventy electrolytes in N-methylacetamide have been studied in detail in this Laboratory by Dawson and co-workers during the last decade, no measurements leading to a knowledge of thermodynamic properties of these solutions have been made. It was the purpose of this investigation to study the reproducibility of the platinum-hydrogen and silver-silver chloride electrodes in N-methylacetamide solutions of HCl and to initiate studies of the thermodynamic properties of systems involving solvents having high dielectric constants. (Dielectric constant of N-methylacetamide at 40° is 165.5.)

Experimental

Materials.—N-Methylacetamide was prepared by the method described by Dawson, Wilhoit and Sears.⁵ The final purification was accomplished by several fractional freezings under an atmosphere of dry nitrogen in which a uniform, gradual freezing technique gave a material with a conductivity of 2.5×10^{-8} ohm⁻¹ cm.⁻¹ at 40°, a density of 0.9414 g./ml. at 40° and a melting point of 30.2°. (This freezing point is higher than any recorded previously for this compound.)

Hydrogen chloride gas was obtained by dropping concentrated H₂SO₄ onto warm reagent grade KCl and then passing the gas through a trap at Dry Ice temperatures. The white crystalline compound HCl·2(CH₃CONHCH₃) which was used in preparing the solutions for the electromotive force studies was obtained from the dry HCl gas and the purified N-methylacetamide by the method of Blicke and Burckhalter.⁶ This compound was prepared, purified and stored under an atmosphere of dry nitrogen.

Silver oxide was precipitated from a solution of reagent grade AgNO₃ in conductivity water by the addition of a solution of reagent grade NaOH. The customary precautions in preparation were followed by a large number of washings.⁷

The chloride solution used for chloridizing the silver electrodes was free of bromide impurities. A 1 molar HCl solution was prepared with conductivity water by diluting in an all-glass apparatus the middle portion of the second distillation of the constant boiling mixture of reagent grade HCl.

Electrolytic H₂ was passed through a Deoxo catalytic purifier and traps containing Ascarite and Drierite and finally just before entering the e.m.f. cell was passed over anhydrous magnesium perchlorate.

The HCl solutions in N-methylacetamide were prepared by dissolving a weighed quantity of HCl·2(CH₃CONHCH₃) in a weighed amount of N-methylacetamide. The concentration of the solution in the e.m.f. cell was increased when desired by adding enough stock solution directly to the cell to give the desired concentration change.

Electrodes.—The hydrogen electrode consisted of platinum foil 1.0 cm. by 1.5 cm. attached to No. 18 B and S gage platinum wire fused into a soft glass standard taper ground joint unit. Electrical contact was made with the electrodes by means of a copper wire dipping in mercury contained inside the glass support. The electrodes were cleaned in 50% aqua regia and plated with platinum black by the customary electrolysis in a 3% solution of chloroplatinic acid in 1 M HCl. The electrolysis was continued in 10% H₂SO₄ to remove impurities and to saturate the platinum black with H₂. The electrode was thoroughly rinsed in distilled water and soaked in conductivity water. Finally, the electrode was rinsed in N-methylacetamide several times and stored in a dilute solution of HCl in N-methylacetamide until ready for use.

The silver-silver chloride electrodes were of the thermal-electrolytic type and were prepared according to the method of Harned,⁸ Bates⁷ and Taniguchi and Janz.⁹ The electrode bases were 2 mm. by 8 mm. spirals of about six turns of No. 26 B and S gage platinum wire. These were fused into soft glass standard taper ground joint units similar to those used for the hydrogen electrode and with similar electrical contact. After completion, the electrodes were stored in a 0.05 M HCl aqueous solution for 10–20 hours and then rinsed several times in N-methylacetamide. The electrodes were soaked in a dilute solution of HCl in N-methylacetamide for several hours and then rinsed three times in the cell solution before use.

Apparatus.—The electromotive force cell was an all-glass type of the design recommended by Harned and Morrison¹⁰ for use in non-aqueous solvents.

Electromotive force measurements were made with a type K-2 Leeds and Northrup potentiometer. A General Electric galvanometer was used in conjunction with the potentiometer; with very dilute solutions the sensitivity was ± 0.0001 volt, and with more concentrated solutions the sensitivity was ± 0.00002 volt. A Weston unsaturated type standard cell was used as reference. This cell was calibrated against a cell of similar quality which had been certified by the National Bureau of Standards. The customary shielding was provided to guard against potential leaks.

All measurements were made in a mineral oil-bath thermostated to 40.00 ± 0.03°. Adequate agitation was given all parts of the bath by mechanical stirring.

Procedure.—After careful washing and drying, the cell

(1) Taken from a M.S. thesis submitted by R. C. Sheridan.

(2) This work was supported in part by a research grant from the U. S. Atomic Energy Commission.

(3) M. Mandel and P. Decroly, *Nature*, **182**, 794 (1958); *Trans. Faraday Soc.*, **56**, 29 (1960).

(4) T. Pavolopoulos and H. Strelow, *Z. physik Chem. (Frankfurt)*, **2**, 89 (1954).

(5) L. R. Dawson, E. D. Wilhoit and P. G. Sears, *J. Am. Chem. Soc.*, **78**, 1589 (1956).

(6) F. F. Blicke and J. H. Burckhalter, *ibid.*, **64**, 451 (1942).

(7) R. G. Bates, "Electrometric pH Determinations," John Wiley and Sons, Inc., New York, N. Y., 1954, p. 200.

(8) H. S. Harned, *J. Am. Chem. Soc.*, **51**, 416 (1929).

(9) H. Taniguchi and G. J. Janz, *J. Electrochem. Soc.*, **104**, 123 (1957).

(10) H. S. Harned and J. O. Morrison, *Am. J. Sci.*, **33**, 161 (1937).

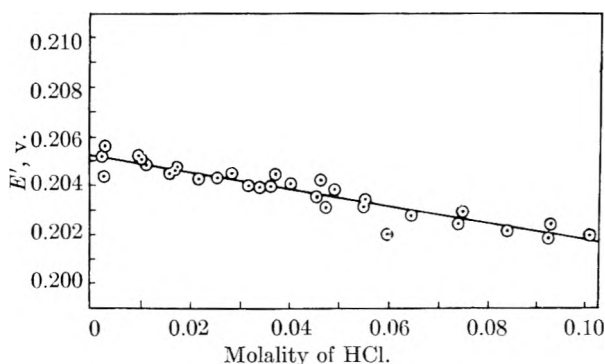


Fig. 1.—Plot of E' as a function of molality for hydrogen chloride in N-methylacetamide at 40° .

unit was purged with N_2 . About 10 ml. of initial starting solution was placed in each saturator, and 28–30 ml. of this solution was added to the U-tube from a weighing buret. This was sufficient to cover the electrodes completely. The depth of the hydrogen jet varied from 4.5 to 5.5 cm. The initial starting solution was used also in the hydrogen exit trap where the gas bubbled through approximately 10 mm. of solution before escaping to the atmosphere. The electrodes were placed in position after being rinsed in three test-tubes containing the initial starting solution. The cell then was placed in position in the oil-bath, and prepurified N_2 was bubbled rapidly through the cell for at least 15 minutes before starting the H_2 flow and adjusting it to a flow rate of 1 to 2 bubbles per second.

The first e.m.f. reading was taken 20–30 minutes after starting the H_2 flow. Readings were taken at 30 minute intervals until the potential became constant. Equilibrium was assumed to have been obtained when there was no detectable change in potential for 2 to 4 hours.

After equilibrium was reached, the concentration of HCl in the cell was increased by the addition of a given amount of concentrated stock solution of HCl in N-methylacetamide from a weighing buret. Ten to 20 hours were required for the cell to regain equilibrium after increasing the concentration.

The resistance of the potentiometer was adjusted against the standard cell before each measurement and checked again after the measurement. The positive lead from the potentiometer was connected to the Ag–AgCl electrode. All measurements were reduced to 760 mm. pressure of H_2 . The barometric pressure had been recorded during the potential measurements; the vapor pressure of N-methylacetamide at 40° was estimated to be 0.2 mm. and the correction for the depth effect of the hydrogen jet was in accordance with Hills and Ives.¹¹

Repeat determinations over the same concentration range were performed using new stock solutions and newly prepared platinum and Ag–AgCl electrodes.

Results

The e.m.f. values, corrected to 760 mm. of pressure, are given in Table I as a function of HCl molality for three independent series of measurements. Values of E' were calculated from the equation¹²

$$E + 0.124264 \log m - 0.019217 \sqrt{m} = E^0_{Ag-AgCl} - 0.124264 \beta m \quad (1)$$

where the symbols have their usual meaning and E' is used to represent the value of the left side of the above equation.

(11) G. J. Hills and D. J. G. Ives, *Nature*, **163**, 997 (1949).

(12) This is the expression resulting from $\mathcal{E} = E^0 - 4.606 RT/F \log m - 4.606 RT/F \log \gamma_{\pm}$ where $\log \gamma_{\pm}$ is assumed to be equal to $(-\alpha \sqrt{m} + \beta m)$. The Debye–Hückel constant α has been evaluated for N-methylacetamide at 40° and is equal to 0.15465 (for $\log \gamma_{\pm}$ to the base 10).

TABLE I
E.M.F. DATA FOR HCl IN N-METHYLACETAMIDE AT 40°
(COR. TO 760 MM.)

m_{HCl}	E_{cell}	γ_{\pm}
	Run 1	
0.002757	0.5248	0.982
.01659	.4286	.969
.01770	.42543	.964
.02631	.40421	.961
.03500	.38889	.959
.04869	.37107	.959
.06115	.35855	.963
	Run 2	
0.00300	0.5194	0.996
.01087	.4515	.967
.01787	.42495	.963
.02927	.39888	.953
.03804	.38518	.945
.04631	.37398	.956
.04719	.37382	.941
.05638	.36344	.954
.06619	.35493	.952
.07588	.34748	.953
.08543	.34109	.953
.09411	.33594	.952
.10225	.33175	.947
	Run 3	
0.00301	0.5205	0.973
.01009	.45562	.967
.01155	.44818	.969
.02240	.41262	.966
.03223	.39330	.960
.03723	.38576	.956
.04141	.38033	.950
.05040	.36997	.946
.05688	.36326	.949
.07624	.34765	.946
.09450	.33612	.945

Discussion

In Fig. 1, the values for E' are plotted against the corresponding values for m . Extrapolation of E' values to zero concentration by the method of least squares gave a value for the standard potential of the Ag–AgCl electrode in N-methylacetamide at 40°

$$E^0 = 0.20573 \pm 0.00035 \text{ volt}$$

The “best” fit of the data corresponds to a straight line with a slope of -0.033267 . The value of β in eq. 1 is 0.26771.

In water at 40° , $E^0_{Ag-AgCl} = 0.21208$ volt,¹³ and in formamide at 40° , $E^0_{Ag-AgCl} = 0.181$ volt.³

Utilizing the value of E^0 , the mean molal activity coefficients, γ_{\pm} , of HCl in N-methylacetamide at 40° were calculated by the equation given in footnote 12. These values are listed in Table I. The experimental results approach the values given by the Debye–Hückel limiting equation at the lower concentrations. The activity coefficients of HCl in N-methylacetamide decrease with increasing molality much less than in aqueous solutions. For example

(13) R. G. Bates and V. E. Bower, *J. Research Natl. Bur. Standards*, **53**, 283 (1954).

	N-Methyl- acetamide 40°	Water ¹³ 40°	Ethanol ¹⁴ 25°
<i>m</i>	0.01	0.01	0.01
γ_{\pm}	.967	.903	.490
<i>m</i>	.10	.10	.10
γ_{\pm}	.947	.793	.232

(14) H. Taniguchi and G. J. Janz, *J. Phys. Chem.*, **61**, 688 (1957).

The values for HCl in ethanol at 25° are given for comparison since no data are available at 40°.

The properties of the cell Pt, H₂; HCl(*m*); AgCl-Ag in N-methylacetamide are being studied in this Laboratory as a function of temperature and these studies are being extended to other solvent systems of high dielectric constant.

DEUTERIUM ISOTOPE EFFECTS IN THE GAS PHASE OXIDATION OF FORMALDEHYDE BY NITROGEN DIOXIDE

By DONALD BARTON¹

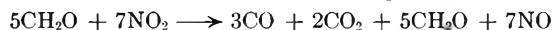
Department of Chemistry, University of Michigan, Ann Arbor, Michigan

Received March 26, 1961

Deuterium isotope effects in the kinetics of the gas phase oxidation of formaldehyde by nitrogen dioxide are reported at 126°. The competitive isotope effect for 1% CD₂O is approximately 3.0. No exchange reaction forming CHDO is detectable under the conditions of the competitive experiments. By means of separate experiments with CH₂O and CD₂O the ratio of second-order rate constants is found to be 13.5 ± 1.5. The CO:CO₂ ratio in the products decreases when CD₂O is substituted for CH₂O. The kinetic and stoichiometric observations for 2:1 initial NO₂:CH₂O ratios agree substantially with those in the literature. However, when the ratio NO₂:CH₂O is reduced the stoichiometric relationships change, favoring CO. A chain mechanism, in which hydrogen abstraction reactions are important, accounts for most of the observations.

Introduction

Previous studies² of the oxidation of CH₂O by NO₂ revealed second-order kinetics when the initial ratio of NO₂:CH₂O was 2:1. A constant ratio of CO:CO₂ was observed in the products. At 2:1 initial NO₂:CH₂O ratios the reactant proportions were represented by the equation



For this and similar reactions,³ rate-controlling bimolecular association reactions have been proposed. Rate-controlling hydrogen abstraction reactions also have been proposed.⁴ Both suggested mechanisms utilize a rate-controlling reaction between CH₂O and NO₂ followed by rapid destruction of the intermediates to give the required products. There appeared to be a significant probability that the "elementary reaction" between NO₂ and CH₂O was accessible for an isotope study.

Experimental

A conventional vacuum apparatus was used. The procedure for storage and transfer of formaldehyde and nitrogen dioxide was similar to that described in reference 2. The pressure in the reaction vessel was measured by means of a quartz spiral manometer and an external mercury manometer. The reaction vessel (133 ml., S/V ratio 2 cm.⁻¹) was constructed of Pyrex and surrounded by an aluminum cylinder inside controlled heaters. At the end of a reaction, when complete product analysis was carried out, the products were passed through a trap at -210° condensing all gases except CO. Nitric oxide, in excess of that forming N₂O₂ when NO₂ was present, was removed at -160°. If no NO₂ was present the CO₂ was removed at -78° after the trap and contents were allowed to stand overnight to permit polymerization of formaldehyde. If NO and NO₂ are present the CO₂ so removed is contaminated by NO. This may be removed by cycling the -78° fraction through

a trap at -163°, removing the NO. Some of the CO fractions were examined for nitrogen and hydrogen by oxidation with CuO followed by examination for gas not oxidized by CuO (N₂) and condensed at -78° (H₂O). CO₂ fractions were examined for N₂O by shaking with KOH solution. The gases mentioned were not detected by the described methods and are considered not to constitute greater than 2% of their respective fractions.

Hydrogen from the residual formaldehyde was obtained by two methods.

(1) Oxidation by H₂O₂ in alkaline solution.⁵

The following procedure is typical. After collection of all gases removable at -78° the residue (presumably formaldehyde and water, and some NO₂ when this reagent was in excess) was distilled to a bulb at the bottom of a U-trap. Hydrogen peroxide (1.5 ml. of 6% H₂O₂ in H₂O) and potassium hydroxide (3 ml. of 1 N) were added from a side arm to the cold bulb and the bulb was immersed in a 60° bath for about 10 minutes. A number of preliminary experiments allowed quantitative removal of hydrogen (one-half the total) with little oxygen, but in all cases of regular experiments considerable oxygen was evolved. Mass spectrometric analyses were carried out in the presence of oxygen. In most cases the peroxide-base solution was tested at the completion of the reaction for excess reagent by adding formaldehyde solution and observing gas evolution.

(2) Isolation of residual formaldehyde, oxidation and reduction of the water.

This procedure is subject to some manipulative error, but is not empirical. The residual formaldehyde and water were collected and distilled through a Spence and Wild⁶ apparatus to obtain liquid formaldehyde. The procedure causes a loss of formaldehyde and a slight depletion of deuterium in the collected sample. The low initial deuterium concentrations (Fig. 1, upper line) represent total samples passed

(5) The reaction 2HCHO + H₂O₂ + 2NaOH → 2HCOONa + 2HOH + H₂ is known to be suitable for quantitative analysis of CH₂O.⁶ It is also known that no solvent hydrogen appears in the hydrogen gas produced.⁷ This was confirmed during the course of the present study. It was predicted that the deuterium content of the evolved hydrogen would be identical with that of the formaldehyde. However, it was found to be approximately one-half that of the formaldehyde. The method produced self-consistent results when applied to the residual formaldehyde, but must be considered as an empirical method.

(6) J. F. Walker, "Formaldehyde," Reinhold Publ. Corp., New York, N. Y., 1953, p. 384.

(7) K. Wirtz and K. F. Bonhoeffer, *Z. physik. Chem.*, **32B**, 108 (1936).

(8) R. Spence and W. Wild, *J. Chem. Soc.*, 338 (1935).

(1) Department of Chemistry and Chemical Engineering, University of Illinois, Urbana, Illinois.

(2) F. H. Pollard and R. M. H. Wyatt, *Trans. Faraday Soc.*, **45**, 760 (1949).

(3) (a) F. H. Pollard and K. A. Holbrook, *Nature*, **177**, 799 (1956);

(b) A. D. Walsh, *Fuel*, **33**, 243 (1954).

(4) J. H. Thomas, *Trans. Faraday Soc.*, **49**, 630 (1953).

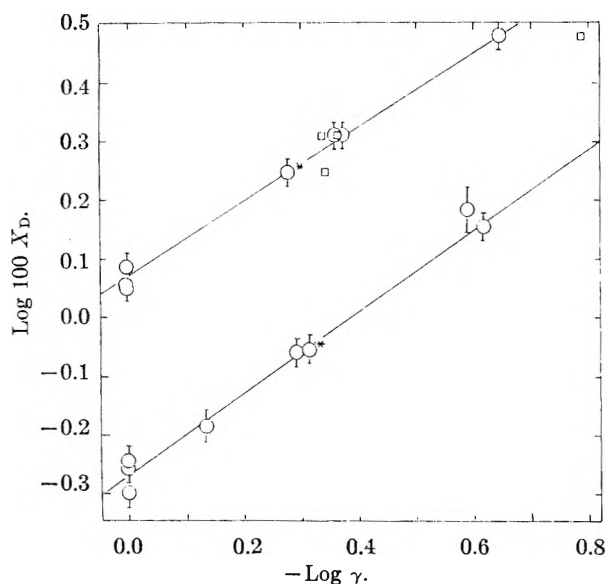


Fig. 1.—Competitive isotope effect. Upper line by method 2, lower line by method 1. Circles, pressure change method for fraction reacted; squares, carbon analyses for fraction reacted; *, experiment with excess NO_2 .

through a separation procedure analogous to that required for a reaction. The upper initial samples were not subjected to the Spence and Wild distillation. All initial points were weighted equally, but the low values should receive more consideration. The liquid formaldehyde obtained was oxidized by NO_2 and the water was collected and reduced, using zinc.

Note that the methods yield similar results for the NO_2 : CH_2O competitive isotope effect.

Mass spectrometric analyses were carried out by means of a Nier type isotope ratio mass spectrometer.

Normal formaldehyde was obtained by distillation of para-formaldehyde prepared by evaporation of Merck Reagent 40% water solution of formaldehyde. Formaldehyde- d_2 was obtained by distillation of CD_2O polymer obtained from Merck and Company, Canada. Tracer (1%) formaldehyde was prepared by mixing CD_2O polymer with normal formaldehyde and distilling together by the Spence and Wild method. Matheson nitrogen dioxide was passed through P_2O_5 and distilled.

Most of the tracer concentration experiments were carried out by using an excess of formaldehyde over NO_2 and allowing the reaction to proceed essentially to completion. The absence of NO_2 simplifies the separation procedure. Typical starting pressures may be seen in Table II. The enrichment of CD_2O in the residue as a function of the fraction of the formaldehyde remaining was found to be not largely affected by the initial reagent ratio. The present experiments, however, do not exclude a moderate dependence on starting reagent ratio. Notice subsequently that the kinetics vary with the starting ratio. Experiments with excess NO_2 are marked in Fig. 1.

The quantity of formaldehyde reacted was equated to the pressure change for the experiments utilizing analytical methods 1 and 2. The quantity reacted also was calculated by means of the carbon oxides produced for the experiments utilizing analytical method 2. The two methods of calculating the fraction of reaction yield results differing by a few per cent. at most. For consistency the pressure change method is used for plotting. The points using carbon balance, which are somewhat scattered, are shown in Fig. 1. The results should of course be identical if the stoichiometry is exactly as shown.

It is necessary to demonstrate the absence of the exchange reaction $\text{CH}_2\text{O} + \text{CD}_2\text{O} \rightleftharpoons 2\text{CHDO}$ and the absence of deuterium-hydrogen exchange between water and formaldehyde. An approximately 1:1 mixture of CH_2O and CD_2O was prepared and distilled by the Spence and Wild method. This was oxidized with less than the stoichiometric amount of NO_2 and allowed to remain in the reactor overnight. The residual formaldehyde was collected and purified by distillation and scanned by the mass spectrometer. This is

Experiment 15, Table II. While the CD_2O increased from about 44% to about 62% of the total formaldehyde, the mass 31 height indicated that the proportion of CHDO had changed by less than 1% of the total (from about 2%). This experiment demonstrates the absence of appreciable hydrogen exchange among the formaldehyde species and also between formaldehyde and water. In addition, incidentally, the absence of exchange during the distillation is shown.

Results

The data were treated by conventional methods.⁹ Beginning with the expression

$$\frac{d[\text{CH}_2\text{O}]}{d[\text{CD}_2\text{O}]} = \frac{k_b}{k_d} \frac{[\text{CH}_2\text{O}]}{[\text{CD}_2\text{O}]}$$

the expression

$$\log X_d = \frac{\alpha - 1}{\alpha} (-\log \gamma) + \log X_d(t = 0)$$

may be derived for low CD_2O concentrations. X_d is the mole fraction of deuterium in residual formaldehyde; $X_d(t = 0)$ the mole fraction of deuterium in formaldehyde (initially), $\alpha = k_b/k_d$; and γ the fraction of total formaldehyde remaining. The results are shown in Fig. 1. The least squares slopes with 95% confidence limits are: method 1, 0.69 ± 0.07 , $\alpha = 3.2$; method 2, 0.63 ± 0.06 , $\alpha = 2.7$. Note the great sensitivity of the calculated α to the accuracy of the slope measurement.

A number of kinetic experiments were carried out using CH_2O and CD_2O separately. For 2:1 initial NO_2 /formaldehyde ratios reasonable second-order plots are obtained. For CH_2O the second-order rate constant obtained from an integrated plot was $0.076 \text{ l. mole}^{-1} \text{ sec.}^{-1}$ (cf. the value 0.060 for ref. 2). The value for k_b/k_d obtained by integrated plots is 12.6. By measuring slopes of pressure-time curves (those reported are initial slopes), a value for $d[\text{CH}_2\text{O}]/d[\text{CD}_2\text{O}]$ may be approximated.

TABLE I

RATE CONSTANTS AS MEASURED BY INITIAL SLOPES					
Initial NO_2 pressure, cm.	Initial CH_2O pressure, cm.	Rate constant, cm. sec. $\times 10^4$	Initial NO_2 pressure, cm.	Initial CD_2O pressure	Rate constant cm. sec. $\times 10^4$
13.19	10.25	4.02	20.50	10.10	0.242
10.17	20.30	4.46	20.42	10.16	.236
20.46	10.11	3.42	13.22	10.38	.309
13.21	10.26	4.17	10.28	20.50	.374
20.56	10.11	3.72	10.10	20.45	.348

When all conditions are identical (*i.e.*, initial pressures) except the substitution of D for H, the following ratio of initial slopes is obtained

$$\frac{d[\text{CH}_2\text{O}]}{d[\text{CD}_2\text{O}]} = 13.5 \pm 1.5$$

The range covers all cases measured. However, when a "second-order rate constant" is calculated, using the definition

$$k = \frac{\text{Initial slope}}{P_{if} \times P_{in}}$$

P_{if} being the initial formaldehyde pressure and P_{in} the initial NO_2 pressure, a trend is observed in the rate constant, as a function of the initial ratio of reagents. The kinetics are not completely described by second-order behavior.

(9) A. M. Downes and G. M. Harris, *J. Chem. Phys.*, **20**, 196 (1952); R. B. Bernstein, *J. Phys. Chem.*, **56**, 893 (1952).

TABLE II
CARBON MONOXIDE: CARBON DIOXIDE RATIOS IN THE PRODUCTS

	Initial pressure, cm.		Ratio NO ₂ /CH ₂ O or CD ₂ O	Ratio CO/CO ₂
	CH ₂ O	NO ₂		
1 ^a	20.78	14.02	0.68	2.36
2 ^a	20.79	14.04	0.68	2.53
3 ^a	20.87	21.70	1.03	2.39
4	10.25	13.19	1.28	2.14
5 ^a	10.32	16.38	1.58	1.79
6 ^a	10.27	17.08	1.67	1.77
7 ^a	10.35	20.28	1.96	1.50
8	10.11	20.46	2.02	1.6
9 ^{a,b}	20.68	14.03	0.68	2.17
	CD ₂ O			
10	20.45	10.10	0.49	1.90
11	20.50	10.28	0.50	1.91
12	10.38	13.22	1.27	1.25
13	10.10	20.50	2.02	0.95
	CH ₂ O/CD ₂ O 6:4			
14	20.58	9.00	0.44	2.22
15	20.35	10.33	0.51	2.14

^a Contains 1% CD₂O. ^b NO₂ completely reacted except in No. 9.

In addition to the above two kinetic isotope effects it was observed that the stoichiometry is affected when D is substituted for H. Over a wide range of initial reagent ratios the CO:CO₂ ratio is given by

$$\frac{([CO])}{([CO_2])}_{CH_2O} / \frac{([CO])}{([CO_2])}_{CD_2O} \cong 1.5$$

See Table II.

It also was observed (see Table II) that as the initial NO₂:CH₂O ratio is reduced below 2 (results at a ratio of 2 compare with those of ref. 2) then the CO:CO₂ ratio is increased in both CH₂O and CD₂O reactions. This change in proportions with initial reagent concentrations implies a change with extent of reaction. This should be detectable at low NO₂ concentrations, when the NO₂ concentration is changing rapidly. This aspect has not been fully treated. Preliminary evidence is shown by no. 2 and 9, Table II. Experiment 2 is a complete reaction; experiment 9 is a partial reaction.

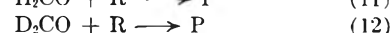
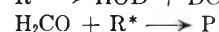
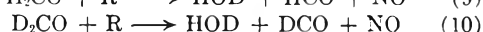
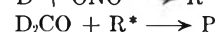
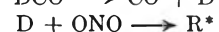
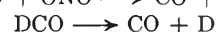
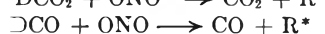
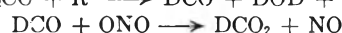
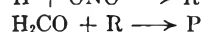
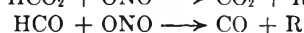
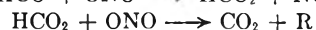
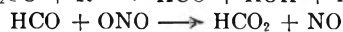
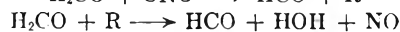
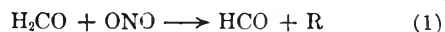
Discussion of Results

The variation in the ratio of carbon oxides with reagent ratio and with the substitution of deuterium for hydrogen indicates that (a) some fraction of the CO is formed from an intermediate without reaction of the intermediate with NO₂ and (b) H abstraction is more important in the reaction controlling the rate of formation of CO than in the reaction controlling the rate of formation of CO₂.

The large separate isotope effect and the small competitive effect has led to the suggestion that the large effect is due to a compounding of two or more elementary isotope effects. This might occur, for example, if chain initiation and propagation were H abstraction reactions and H abstraction were not important in chain breaking.

Although a detailed mechanism must be based upon more evidence, a provisional scheme, which

incorporates the above ideas, is presented. The chain carriers R and R* are not identified but in the mechanism given have the composition HNO₂ and DNO₂, respectively. The products P of the chain breaking steps also are not identified. These will be present in small amounts if the chains are long.



The application of the steady-state method with long chains ($k_2 \gg k_3$) yields for CH₂O

$$\frac{d[CH_2O]}{dt} = \frac{2k_1k_2}{k_3} [CH_2O][NO_2]$$

and for CD₂O, separately

$$\frac{d[CD_2O]}{dt} = \frac{2k_1'k_2'}{k_3'} [CD_2O][NO_2]$$

If H abstraction is not important in the chain-breaking reaction, *i.e.*, $k_3 \cong k_3'$

$$\frac{d[CH_2O]}{d[CD_2O]} = \frac{k_1k_2}{k_1'k_2'} \frac{[CH_2O]}{[CD_2O]}$$

A suitable combination of elementary isotope effects such as

$$\frac{k_1}{k_1'} = \frac{k_2}{k_2'} = 3.7$$

leads to the large experimental effect, 13.5. For low CD₂O concentrations in competitive reactions, the approximation has been made that $[R^*] \ll [R]$. If rate constants for all termination reactions are equal, the competitive isotope effect results from the ratio of two elementary rate constants

$$\frac{d[CH_2O]}{d[CD_2O]} = \frac{k_2}{k_{10}} \frac{[CH_2O]}{[CD_2O]}$$

The ratio of rate of formation of CO to that of CO₂ is

$$\frac{d[CO]}{d[CO_2]} = \frac{k_5 + k_6/[NO_2]}{k_3}$$

This is qualitatively consistent with the variation in stoichiometry with reagent ratio.

The effect of replacing H with D on the formation of carbon oxides is given by the expression

$$\frac{\left(\frac{d[CO]}{d[CO_2]}\right)_{CH_2O}}{\left(\frac{d[CO]}{d[CO_2]}\right)_{CD_2O}} = \frac{k_5/k_3 + k_6/k_3[NO_2]}{k_5'/k_3' + k_6'/k_3'[NO_2]}$$

Since k_3, k_3' refer to oxygen transfer reactions, the

deuterium isotope effect would be small. The expression then would reduce to approximately

$$\frac{k_5 + k_6/[\text{NO}_2]}{k_5' + k_6'/[\text{NO}_2]}, k_5' < k_3, k_6' < k_6$$

not inconsistent with the observed stoichiometry.

The effect of NO_2 concentration on the quantities of CO and CO_2 produced is not necessarily inconsistent with the observations of ref. 2, for if $k_6/k_3[\text{NO}_2]$ is sufficiently smaller than k_5/k_3 , as $[\text{NO}_2]$ is increased the ratio CO/CO_2 becomes decreasingly sensitive to extent of reaction and to NO_2 concentration. More data are required on the changing stoichiometry with extent of reaction at low NO_2 concentrations.

The mechanism presented does not account for the variation in "second-order rate constant" with reagent ratio (Table II).

Mechanism steps similar to 1, 3 and 5 in the above mechanism were proposed by Thomas.⁴ A chain mechanism for the oxidation of CH_2O by O_2 has been proposed by Scheer.¹⁰ Some thermodynamic quantities appropriate to the mechanism may be found in ref. 11 and 12.

Acknowledgments.—The author wishes to acknowledge the advice and suggestions of Professor R. B. Bernstein throughout this work. The financial support from the Alfred P. Sloan Foundation and the U.S.A.E.C., Division of Research, is appreciated. The author thanks Leslie B. Sims for criticisms.

(10) M. D. Scheer, "Fifth Symposium (International) on Combustion," Reinhold Publ. Corp., New York, N. Y., 1955, p. 435.

(11) National Bureau of Standards, Circular 500, 1952.

(12) W. A. Rosser, Jr., and H. Wise, *J. Chem. Phys.* **26**, 571 (1957)

THE SOLUTION CONDUCTANCE OF CYANOCARBON SALTS¹

BY RICHARD H. BOYD

Contribution No. 687 from the Central Research Department, Experimental Station, E. I. du Pont de Nemours and Company, Wilmington, Delaware

Received March 29, 1961

The conductances of sodium salts of tricyanovinyl alcohol, 1,1,2,3,3-pentacyanopropene, bis-(tricyanovinyl)-amine and 1,1,2,6,6,7-hexacyano-1,3,5-heptatriene have been measured in water and those of the tetramethylammonium salts in acetonitrile and in acetone-carbon tetrachloride mixtures. The tetramethylammonium salt of pentacyanopropene also was studied in nitrobenzene-carbon tetrachloride mixtures. Sodium hexacyanoheptatrienide undergoes reversible dimerization in water as evidenced by the conductance curves and also by its electronic absorption spectrum. All of the salts exhibit normal behavior in acetonitrile with very slight ion-pairing. Ion-pair formation for the cyanocarbon salts in acetone-carbon tetrachloride mixtures is somewhat less pronounced than for comparable salts and solvents reported on in the literature. The ion-pair distance parameters derived from the dielectric constant dependence of the association constants reflect charge delocalization in the anions. Ion pairing has no appreciable influence on the optical spectrum of pentacyanopropenide. The variation of the Walden product (Δ_{07}) with dielectric constant is very slight but noticeable in acetone-carbon tetrachloride mixtures. The variation for pentacyanopropenide in nitrobenzene-carbon tetrachloride mixtures is comparable to that found previously for other salts. Simplified Hückel-type molecular orbital calculations of the negative charge distribution in three of the anions were made and show extensive charge delocalization.

Introduction

The synthesis of tetracyanoethylene and a number of its percyano derivatives recently has been reported.² A number of these compounds have the interesting property of being acids and forming salts.³ The purpose of this paper is to report the physical behavior of some of these cyanocarbon anions in solution. These ions should be particularly interesting since they form a new class in which the negative charge appears to be highly delocalized over the molecular surface.

Measurement of electrolytic conductance was chosen as the principal experimental means of investigation in view of its generality, precision and theoretical foundation. Measurements in water and a number of organic solvents were made. Salts of tricyanovinyl alcohol (TCV alcohol), 1,1,2,3,3-pentacyanopropene (PCP), bis-(tricyanovinyl)-amine [bis-(TCV)-amine] and 1,1,2,6,6,7-hexacyano-1,3,5-heptatriene (HCHT) were chosen as a series representative of the various cyanocarbon anions, covering a range of sizes and type.

Their structures are shown in Fig. 1. Sodium salts were studied in water because of their high solubility. Tetramethylammonium (TMA) salts were studied in acetonitrile, nitrobenzene-carbon tetrachloride mixtures, and acetone-carbon tetrachloride mixtures.

Fuoss⁴ recently has published a summary of the final version of the Fuoss-Onsager theory of the conductance of symmetrical charge type electrolytes. The conductance measurements reported here are analyzed in terms of that theory. The physical processes that occur then will be discussed in terms of the parameters calculated from the fitting of the theory to the data.

Experimental Details

The conductance bridge consisted of a Leeds and Northrup Co. shielded ratio box (Cat. No. 1553) and a calibrated General Radio Corp. decade resistance box (Type 1432-N) (together with single 10 k./step and 100 k./step decade resistances to extend the range). A Leeds and Northrup Co. (No. 1185) air capacitor was used for the capacitance balance. A Hewlett-Packard Corp. audio oscillator (Type 200AB) and a DuMont oscilloscope (Type 350-R) (together with a Ballentine Laboratories a.c. voltmeter as a preamplifier) were used as signal source and detector, respectively.

Two conductance cells of the design of Mukerjee, *et al.*,⁵

(1) Paper XXI in the series Cyanocarbon Chemistry.

(2) T. L. Cairns, *et al.*, *J. Am. Chem. Soc.*, **80**, 2775 (1958).

(3) (a) W. J. Middleton, E. L. Little, D. D. Coffman and V. A. Engelhardt, *ibid.*, **80**, 2795 (1958); (b) D. W. Wiley, J. K. Williams and B. C. McKusick, to be published.

(4) R. M. Fuoss, *ibid.*, **81**, 2659 (1959).

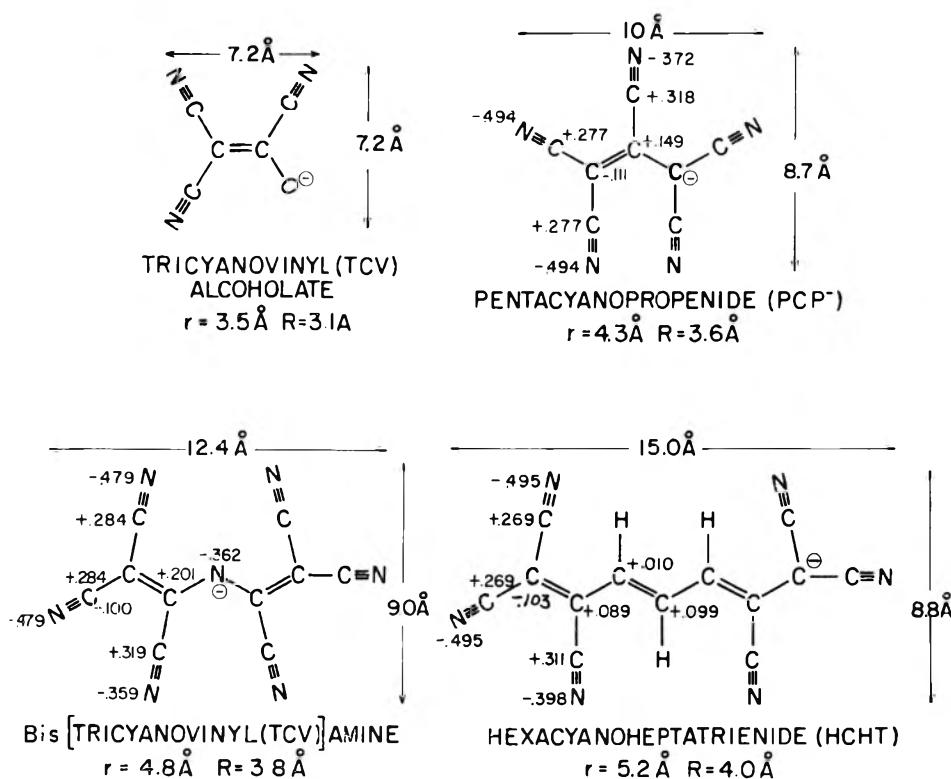


Fig. 1.—Structures of anions studied. Effective charge distributions from simple LCAO-MO calculations are shown for three of the anions. r = radius of equivalent disk and R = radius of equivalent sphere from measurements on Stuart-Briegleb models.

were used. A cell consists of two bright platinum electrodes sealed into a Florence flask and contains a "Teflon" polytetrafluoroethylene covered magnetic stirring bar. The volumes and cell constants are 1 liter and 0.07092 and 250 ml. and 0.15050. They were calibrated with potassium chloride over the useful concentration range using the conductance data of Shedlovsky, *et al.*⁶ The same volume of liquid was used in all experiments with the smaller cell to avoid changes of cell constant with cell content. The stirring motor can be immersed directly in the oil-bath, a convenience deserving of use in other experiments. The bath was set at 25° and controlled to $\pm 0.01^\circ$.

TMA⁺/TCV alcoholate⁻ and tetraethylammonium bis-(TCV)-amine were obtained as laboratory samples that had been prepared by the methods of Middleton, *et al.*³ and were purified by recrystallization from ethanol. TMA⁺/PCP⁻ and NH₄⁺/HCHT⁻ were prepared for us by the methods of reference 3, respectively.

Aqueous solutions of sodium salts were prepared by making solutions of the acids by ion exchange by the method of Middleton, *et al.*³ The acids then were titrated potentiometrically with 0.1 N NaOH solution. This served both to prepare the salt and to determine its amount. The conductance measurements were made by adding increments of the fairly concentrated solution from the titration to the 1-liter conductance cell by means of a weight pipet.

TMA⁺/bis-(TCV)-amine⁻ and TMA⁺/HCHT⁻ were prepared from aqueous solutions of the sodium salts by adding an excess of TMA⁺/Br⁻. The precipitated salts were purified by several recrystallizations from hot water.

TMA salts were added to the 250-ml. conductance cell dry by dropping in the sample in a small "Teflon" cup. The samples were weighed to $\pm 1 \mu\text{g.}$ on a microbalance.

Distilled water in equilibrium with air was used for conductance measurements and had a specific conductance (κ) of $\sim 1.5 \times 10^{-6} (\Omega\text{-cm.})^{-1}$. Eastman (yellow label) acetonitrile was redistilled several times from phosphorus pentoxide and had a κ of $\sim 1 \times 10^{-7} (\Omega\text{-cm.})^{-1}$.

Acetone (Baker and Adamson, ACS specification) was dried over calcium chloride and distilled from alumina according to the directions of Reynolds and Kraus.⁷ It had a $\kappa \approx 7 \times 10^{-8} (\Omega\text{-cm.})^{-1}$.

Merck reagent grade carbon tetrachloride was found to have the same dielectric constant and density before and after distillation, in good agreement with literature values (see Table I), and so was used directly from the bottle. The conductivity was too low to measure.

Nitrobenzene was purified and distilled at 60° according to the directions of Witschonke and Kraus⁸ ($\kappa \approx 6 \times 10^{-9}$). TMA⁺/PCP⁻ was soluble in nitrobenzene-carbon tetrachloride mixtures, but the rate of solution was slow, and this system was not very convenient to work with.

The dielectric constant, viscosity and density of the acetone-carbon tetrachloride mixtures were required, but no data are available in the literature on these properties, and consequently, they were measured. The dielectric constant was difficult to measure because the conductivity was relatively high and increased rapidly with time in a stainless steel dielectric cell. Apparently a reaction catalyzed by the metal surface of the cell takes place. However, the conductivity of freshly distilled acetone remained constant in a platinum cell. The cell consists of two concentric platinum tubes ($\frac{3}{8}$ " and $\frac{1}{4}$ " o.d.) spaced by "Teflon" bushings. Holes drilled through the tubes near each end permitted filling when the cell was placed in a graduated cylinder containing the liquid to be measured. Platinum leads were spotwelded to the tubes and connected to binding posts where the bridge connections were made. A Wayne-Kerr Co. Universal Bridge (B221) was used to measure the capacitance. This bridge has the advantage of permitting accurate capacitance measurements at relatively high conductivities. Benzene was used to calibrate the cell, which has an empty capacitance of 33.23 $\mu\text{mf.}$ The dielectric constant found for pure acetone (20.61) is in agreement with the value 20.7 reported by Maryott and Smith.⁹

(5) P. Mukerjee, K. Mysels and C. I. Dulin, *J. Phys. Chem.*, **62**, 1390 (1958).

(6) T. Shedlovsky, A. S. Brown and D. A. MacInnes, *Trans. Electrochem. Soc.*, **66**, 165 (1934).

(7) M. B. Reynolds and C. A. Kraus, *J. Am. Chem. Soc.*, **70**, 1709 (1948).

(8) C. R. Witschonke and C. A. Kraus, *ibid.*, **69**, 2472 (1947).

Viscosities were determined in an Ostwald viscometer calibrated with water (using η water = 0.8900 centipoise).¹⁰ Densities were determined by weighing the solvents in a calibrated volumetric flask.

The solvent properties determined are listed in Table I.

TABLE I

PROPERTIES OF ACETONE-CARBON TETRACHLORIDE MIXTURES, 25°

Compn. (wt. fraction acetone)	Density (g./ml.)	Dielectric constant	Viscosity (centipoise)
1.0000	0.7844 (0.7850) ^a	20.61 (20.7) ^b	0.3056 (0.3075) ^a
0.5979	0.9966	15.18	0.3918
.4978	1.0528	13.47	.4208
.4264	1.1090	12.19	.4506
.3314	1.1858	10.31	.4971
0	1.5842 (1.58452) ^a	2.228 (2.228) ^b	.8976

^a J. Timmermans, "Physico-Chemical Constants of Pure Organic Compounds," Elsevier Pub. Co., New York, N. Y., 1950. ^b A. A. Maryott and E. R. Smith, ref. 9.

The visible and ultraviolet spectra were measured in a Cary Model 14 recording spectrophotometer.

The experimental values of equivalent conductances and concentrations in the various systems are listed in Table II.

Discussion of Results

1. Behavior of Sodium Salts in Water.—The equivalent conductance data are plotted against the square root of the concentration in Fig. 2. It is immediately apparent for Na⁺/HCHT⁻ that the conductance behavior in water is anomalous for either a completely or incompletely dissociated electrolyte. The equivalent conductance actually increases with concentration. The behavior of the other salts (Fig. 2) is nearly normal, but comparison with the complete Fuoss-Onsager theory⁴ indicates the possibility of a slight abnormality here also. The conductance function for a completely dissociated 1:1 electrolyte (ignoring the effect of solute on the solvent viscosity) is given by

$$\Lambda = \Lambda_0 - Sc^{1/2} + Ec \log c + Jc \quad (1)$$

where

Λ = equivalent conductance; Λ_0 , its value at infinite dilution

$S = \alpha + \Lambda_0\beta$ ("Onsager" slope)

$E = E_1\Lambda_0 - E_2$

$J = \sigma_1\Lambda_0 + \sigma_2$

c = molar concentration

TABLE II

EQUIVALENT CONDUCTANCE DATA, 25°

TCV alcoholate		PCP		Bis-(TCV)-amine		HCHT	
$C \times 10^4$	Λ	$C \times 10^4$	Λ	$C \times 10^4$	Λ	$C \times 10^4$	Λ
Sodium salts: Water							
						0.58138	78.236
						0.89235	78.264
						1.4517	78.542
2.0164	90.10	2.0463	84.63	2.3129	80.01	2.8676	78.968
2.9813	89.88	2.9057	84.46	4.6224	79.60	4.2948	79.298
4.9491	89.57	4.9445	84.15	6.7834	79.38	6.8602	79.782
6.8271	89.30	6.9129	83.91	8.6547	79.21	9.3537	80.169
9.6976	88.98	9.9605	83.56	10.999	78.97	11.6995	80.448
20.176	88.09	16.147	83.04	13.858	78.71	15.456	80.816
		21.430	82.66				
Tetramethylammonium salts: Acetonitrile, Dielectric constant 36.0							
				1.2725	162.93	0.8962	152.93
1.1520	188.00	1.1389	175.12	2.6193	161.25	1.8106	151.59
2.3379	185.59	2.4147	173.64	3.9495	160.18	2.7693	150.90
3.5620	184.55	3.5845	172.44	6.5158	158.15	4.4116	149.56
5.9609	182.62	5.7592	170.59	9.1241	156.54	6.2227	148.30
8.3559	180.94	7.8148	169.26	13.014	154.65	8.6607	147.02
11.896	179.07	11.610	167.14				
Acetone-carbon tetrachloride mixtures, Dielectric constant 20.61 (pure)							
		0.9588	183.65	1.2888	169.22	1.0609	159.83
2.0849	197.56	2.0013	181.01	2.6062	166.16	2.0987	157.24
3.2445	193.97	2.9767	178.78	3.8516	163.84	3.1338	155.38
5.3897	189.48	4.8997	175.72	6.4297	160.21	5.1726	151.89
7.5299	185.93	7.0363	172.93	9.0427	157.29	7.2142	149.57
10.7440	181.63	9.9047	169.76	12.932	154.41	10.258	146.56
Dielectric constant 15.18 (wt. fraction 0.5979 acetone)							
1.1680	149.31	1.0044	140.82				
2.2780	143.72	2.0260	136.69				
3.3994	139.13	3.0143	133.29				
5.5919	132.60	4.9932	128.57				
7.7904	127.88	6.9811	124.67				
11.171	122.22	9.9890	120.24				

(9) A. A. Maryott and E. R. Smith, Natl. Bur. Standards Circular 514, U. S. Department of Commerce.

(10) J. F. Swindella, J. R. Coe and T. B. Godfrey, *J. Research Natl. Bur. Standards*, **48**, 1 (1952); R. C. Hardy and R. L. Cottingham, *ibid.*, **42**, 573 (1949).

α , β , E_1 and E_2 are known constants depending on the dielectric constant and viscosity of the solvent and the temperature. σ_1 and σ_2 are constants depending on these properties and also a_j , the

Dielectric constant 13.47 (wt. fraction 0.4978 acetone)							
1.0965	134.13	1.0411	125.19	1.3053	117.56	1.2043	109.70
2.1940	126.44	2.0651	121.02	2.5895	112.39	2.4159	105.39
3.2877	121.09	3.0840	117.24	3.8669	108.66	3.6268	102.26
5.4682	113.62	5.1280	111.75	6.4411	103.26	6.0449	97.76
7.6610	108.11	7.1476	107.50	9.0385	99.38	8.4655	94.58
11.045	101.81	10.165	102.89	12.934	95.00	12.093	90.95
Dielectric constant 12.19 (wt. fraction 0.4264 acetone)							
0.99944	114.44	1.3100	105.89				
1.9933	108.27	2.6207	99.64				
2.9959	103.64	3.9321	95.82				
4.9993	97.04	6.5599	89.80				
7.0019	92.36	9.1935	85.58				
10.008	87.29	13.124	81.04				
Dielectric constant 10.31 (wt. fraction 0.3314 acetone)							
1.1166	89.49	0.9989	92.91	1.3837	85.242	1.0027	84.607
2.1039	78.63	1.9949	83.59	2.7612	77.342	2.0360	77.384
3.1469	71.65	3.0226	77.72	4.1356	72.364	3.0047	73.931
5.2431	63.32	5.0135	70.48	6.9249	65.810	4.9731	68.638
7.2462	58.31	7.0233	65.62	9.6556	61.660	7.0345	64.310
10.451	52.88	1.0030	60.69	13.777	57.370	10.100	60.573
TMA ⁺ /PCP ⁻ : Nitrobenzene-carbon tetrachloride							
W_2^a	0	0.4676		0.5596		0.6241	
Dielectric constant	34.69	18.90		15.80		13.68	
$C \times 10^4$	Λ	$C \times 10^4$	Λ	$C \times 10^4$	Λ	$C \times 10^4$	Λ
1.0947	34.645	2.0093	38.166	0.9588	39.529	1.0798	37.832
2.2887	34.273	4.0978	36.644	1.9061	37.941	2.2246	35.388
3.4450	34.015	6.1600	35.527	2.8537	36.757	3.4976	33.482
5.6956	33.612	10.5810	33.777	4.7507	34.997	5.9497	30.897
7.9073	33.299	14.4684	32.624	6.6402	33.675	7.8757	29.448
11.263	32.892	20.6157	31.217	9.4884	32.130	11.0295	27.649

^a W_2 = wt. fraction carbon tetrachloride.

center-to-center contact distance between oppositely charged ions. As Fuoss⁴ points out, a plot of $\Lambda' = \Lambda + Sc^{1/2} - Ec \log c = \Lambda_0 + Jc$ against c should be a straight line, the slope of which determines J and hence allows a_T to be calculated. Figure 3 shows such a plot for Na⁺/TCV alcoholate⁻, Na⁺/PCP⁻, and Na⁺/bis-(TCV)-amine⁻. It is apparent that there is curvature at low concentration for these salts. However, this is where the solvent correction is quite large (~7% at $2 \times 10^{-4} M$) and adsorption could be important, so the effect may well be spurious. The KCl calibration showed no such behavior in the same concentration range, so the effect appears to be related to the nature of cyanocarbon salts and apparently increases with the size of the anion. We have assumed that the straight line portions drawn indicate normal behavior and have computed J and a_T values from the slopes.¹¹ These are listed in Table III. Λ_0 values are listed in Table V. Thus, Na⁺HCHT⁻ is characterized by a conductance considerably greater than normal and the other salts probably behave normally.

A reasonable explanation for the anomalous behavior of Na⁺HCHT⁻ is a reversible dimerization equilibrium between the anions. This phenomenon has been previously proposed to explain

the conductance results for aqueous solutions of soaps, such as lauryl sulfate.^{5,12} The authors of references 5 and 12 review arguments for believing that dimerization is the only reasonable type of ion association to account for conductance greater than expected for a normal electrolyte. Furthermore, aqueous solutions of ionic dyes are believed to undergo extensive dimerization and higher aggregation.¹³ Naturally the effects of this behavior on the optical absorption have been more thoroughly studied in these compounds than on the electrolytic conductance. However, equivalent conductance behavior similar to that of Na⁺HCHT⁻ has been found in aqueous solutions of several dyes.¹⁴

Further evidence for dimerization comes from the electronic spectrum of Na⁺HCHT⁻. This shows the presence of a band at intermediate concentration ($\sim 10^{-3} M$) not present in very dilute solution ($\sim 10^{-5} M$) (see Fig. 4). Na⁺HCHT⁻ shows deviations from Beer's law for the principal absorption at 635 m μ that can be explained by a dimerization equilibrium. With the assumption that only the monomer absorbs at this wave length and that its concentration is controlled by the

(12) P. Mukerjee, *J. Phys. Chem.*, **62**, 1404 (1958).

(11) After this work was completed J. E. Lind, Jr., and R. M. Fuoss made available to us a manuscript now published, *J. Am. Chem. Soc.*, **83**, 1828 (1961), describing measurements on tetraethylammonium salts of PCP and bis-(TCV)-amine. TEA⁺/PCP⁻ was measured in water and showed normal behavior over the concentration range ~ 0.7 to $2 \times 10^{-4} M$.

(13) There is an extensive literature on this phenomenon. We will cite only the excellent early study of E. Rabinowitch and L. F. Epstein [*J. Am. Chem. Soc.*, **63**, 69 (1941)]. See also T. Förster, *Ann. Rev. Phys. Chem.*, 1957, Annual Reviews, Inc., Palo Alto, Calif., for recent work.

(14) C. Robinson and H. E. Garrett, *Trans. Faraday Soc.*, **35**, 771 (1939).

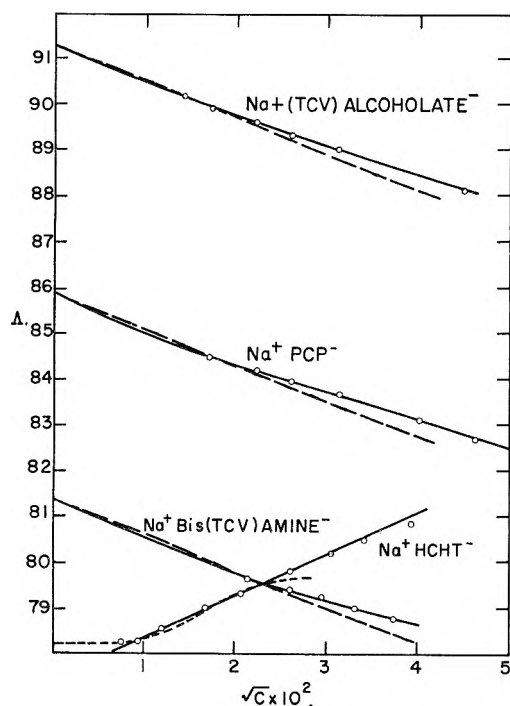


Fig. 2.—Equivalent conductances of sodium salts of cyanocarbon anions [tricyanovinyl (TCV) alcoholate, pentacyanopropenide (PCP⁻), bis-tricyanovinyl-(TCV)-amine and hexacyanoheptatrienide (HCHT⁻)] in water at 25.00° plotted against square root of concentration (mole/l.). Short dashed curve is a calculated curve allowing for presence of dimerization. Long dashed lines show Onsager slopes.

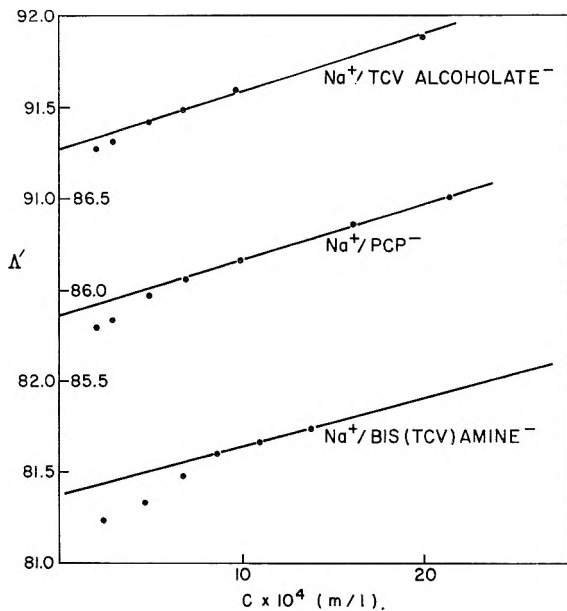
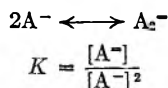


Fig. 3.— $\Lambda' = \Lambda + Sc^{1/2} - Ec \log c$ plotted against square root of concentration (mole/l.) for Na⁺/tricyanovinyl (TCV) alcoholate⁻, Na⁺/pentacyanopropenide (PCP⁻) and Na⁺/bis-tricyanovinyl-(TCV)-amine.

equilibrium



where A⁻ is the anion monomer and A₂⁻ is the

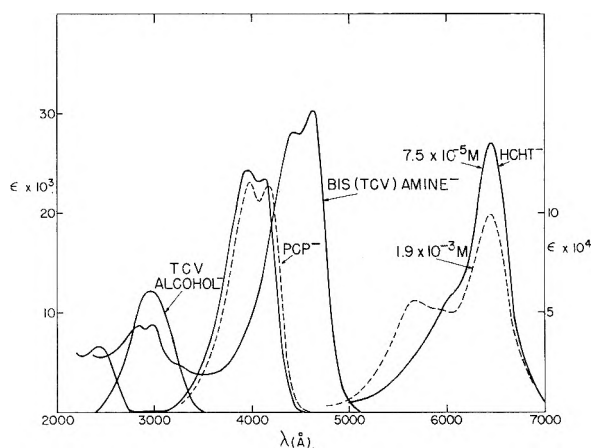


Fig. 4.—Visible ultraviolet spectra for cyanocarbon anions [tricyanovinyl (TCV) alcoholate, pentacyanopropenide (PCP⁻), bis-tricyanovinyl-(TCV)-amine and hexacyanoheptatrienide (HCHT⁻)] in water. Molar extinction coefficient, ϵ , of HCHT⁻ is plotted on scale at right, others on left. Dashed line for PCP⁻ is for acetone-carbon tetrachloride mixture. Dielectric constant was 10.31.

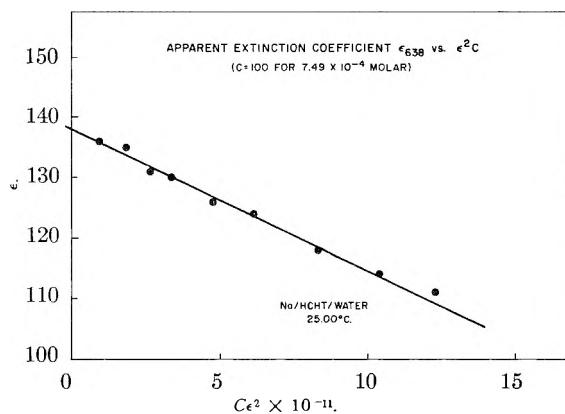


Fig. 5.—Determination of anion dimerization constant for hexacyanoheptatrienide (HCHT⁻) from plot of ϵ vs. ϵ^2c , ϵ = apparent extinction coefficient at 635 m μ and c = stoichiometric concentration (mole/l.).

anion dimer, it can be shown that

$$\epsilon = \epsilon^0 - \left(\frac{2K}{\epsilon^0}\right) \epsilon^2c$$

where

ϵ is the apparent extinction coefficient at 635 m μ
 ϵ^0 is the true one for monomer
 c is concn., moles/l.

A plot of ϵ^2c vs. ϵ should be a straight line of slope $2K/\epsilon^0$ and intercept ϵ^0 . It is seen in Fig. 5 that such a plot does give a good straight line. K is found to be 217 l./mole and $\epsilon^0 = 138,000$. The dimer band at 568 m μ is poorly resolved, and analysis of the absorption at that wave length involves much greater error. However, analysis correcting for monomer absorption at 568 m μ indicates an equilibrium constant of ~ 500 l./mole and ϵ (dimer) = 104,000 is indicated. The difference in K 's from the two bands probably is due to the assumption of no dimer absorption at 635 m μ . Allowance for some dimer absorption here would result in a higher K and still give a straight plot.

An attempt was made to calculate the conductance behavior of Na⁺HCHT⁻ from the measured

K in the manner of Mukerjee, *et al.*⁵ The simple Onsager theory was used, and suitable values for the equivalent conductance of the monomeric and dimeric anions were chosen. Figure 2 shows (dotted line) a calculated curve using $\lambda_0^- = 28.1$, $\lambda_0^+ = 1.47 \lambda_0^-$ and $K = 500$. This somewhat higher value for K than found from the Beer's law deviation of the monomer was required. Even so, the calculated conductance does not continue to rise as fast as the experimental curve.

No effects on the electronic spectra of the other salts were noticed, *i.e.*, they obey Beer's law and no additional bands were found. This is consistent with the normal conductances.

The cause of the dimerization is interesting to speculate on. Apparently it is an example of the type of dimerization taking place in ionic dye solutions. It is the result of unusually high intermolecular forces (van der Waals in nature) that exist in molecules that are also very strong absorbers in the ultraviolet and visible regions. The high dielectric constant of water results in a rather moderate electrostatic repulsion energy so that stable dimers can form. The three anions that show no dimerization are moderately strong absorbers (see Fig. 4). HCHT⁻ is a very strong absorber (Fig. 4), and it shows pronounced dimerization. The dimer band at 568 μ apparently is an example of an "H" band as described by West and Carroll.¹⁵ The dimer absorbs at a different frequency due to resonance interaction between excited and unexcited molecules in the dimer.

The cyanocarbon salts thus provide a striking demonstration of the correlation between electronic absorption and aggregation. The salts studied are similar in chemical structure and size and shape. But only the very strong absorber, HCHT⁻, shows pronounced dimerization.

2. Behavior of Tetramethylammonium Salts in Acetonitrile.—The tetramethylammonium salts in acetonitrile behave normally, and the Λ' plots are straight lines giving reasonable values of the distance parameter a_J (see Table III). However, the a_J (except for HCHT) are somewhat smaller than indicated by the behavior in the other organic solvents indicating some slight association is probably present (see the end of Sec. 3). Thus, in a solvent like acetonitrile ($D = 36.0$) the dielectric constant is low enough that anion dimerization is effectively prevented through increased electrostatic repulsion. The dielectric constant is high enough, however, that ion pairing between anion and cation is very slight. The Λ_0 values are listed in Table V and are discussed separately under 4. Lind and Fuoss¹¹ find negligible association for TEthylA⁺/PCP⁻ and bis-(TCV)-amine in acetonitrile which is consistent with our results assuming the larger size of the TEthylA⁺ ion reduces the association from very slight to negligible.

3. The Behavior of Tetramethylammonium Salts in Acetone-Carbon Tetrachloride and Nitrobenzene-Carbon Tetrachloride Mixtures. Ion Pairing.—The conductance data in acetone and nitrobenzene mixtures with carbon tetrachloride were fitted by the Fuoss-Onsager equation includ-

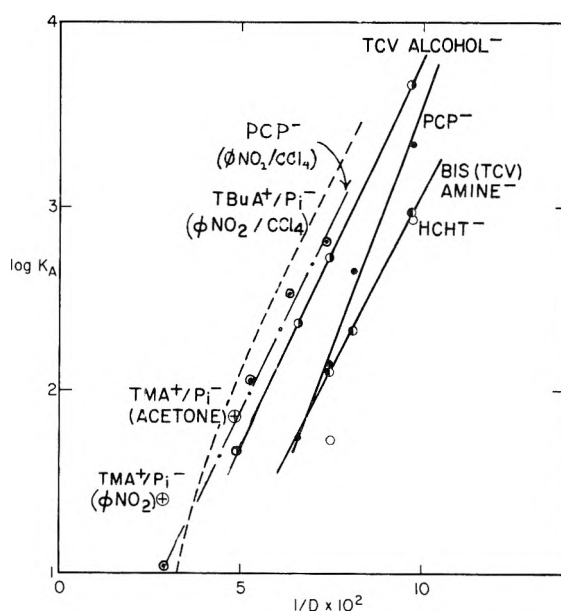


Fig. 6.—The logarithm of the ion-pair association constant, K_a , plotted against the reciprocal of the dielectric constant, D (25.00°), tetramethylammonium (TMA) salts of: \circ , hexacyanoheptatrienide (HCHT⁻); \bullet , bis-tricyanovinyl-(TCV)-amine; \bullet , pentacyanopropenide (PCP⁻), \circ , tricyanovinyl (TCV) alcoholate (all in acetone-carbon tetrachloride mixtures). -----, TBuA⁺/Picrate⁻(Pi⁻) in nitrobenzene-carbon tetrachloride mixtures. Single points also are plotted for TMA⁺/Pi⁻ in acetone and nitrobenzene — \oplus . ----- \circ — TMA⁺/PCP⁻ in nitrobenzene-carbon tetrachloride mixtures.

ing ion-pair equilibrium effects. The curve fitting was accomplished by a least-squares method with an IBM 650 computer. Many of the curves were also fitted by hand with the Fuoss "y - x" method.⁴ The agreement between the methods was good. No correction was made for the effect of solute on solvent viscosity. The distance parameter in the Debye-Hückel activity coefficient term was taken *a priori* to be 6 Å. In pure acetone the ion-pair association constant K_a was found to be slightly negative for the salts, except TMA⁺/TCV alcoholate⁻. Therefore, the results were recomputed with K_a constrained to be zero. The results for TMA⁺/TCV alcoholate⁻ in pure acetone and TMA⁺/PCP⁻ in pure nitrobenzene were calculated by hand assuming a_J to be fixed at 6.5 Å, a value inferred from the results at lower dielectric constant where the association is more pronounced and both K_a and a_J can be calculated with higher accuracy. This procedure seems justified as the K_a values as calculated agree well with extrapolation of K_a from lower dielectric constant mixtures. The association constants, K_a , and the J parameter (along with a_J) are listed in Table III. The values of the limiting conductances, Λ_0 , are listed in Table V and are discussed in the next section.

We are interested in the influence of the cyanocarbon anion structure on ion-pair association. The anion charge is expected to be highly delocalized, resulting in decreased electrostatic attraction between anion and cation at a given distance. However, the expected flat structures would make close approach distances possible, resulting in rather high electrostatic attraction.

(15) W. West and B. H. Carroll, *J. Chem. Phys.*, **19**, 417 (1951).

TABLE III
 ION PAIR ASSOCIATION CONSTANTS AND ION SIZE FROM $J(a)$, 25°

D	TCV alcoholate			PCP			Bis-(TCV)-amine			HCHT		
	K_a	$J \times 10^{-4}$	$a_J(\text{Å})$	K_a	$J \times 10^{-4}$	$a_J(\text{Å})$	K_a	$J \times 10^{-4}$	$a_J(\text{Å})$	K_a	$J \times 10^{-4}$	$a_J(\text{Å})$
	Sodium salts: Water											
...	0.0315	7.2	...	0.025	6.0	...	0.0270	7.3
	Tetramethylammonium salts: Acetone-carbon tetrachloride mixtures											
20.61	(47.2)	(1.553)	(6.5)	...	1.423	6.5	...	1.317	6.5	...	1.182	6.0
15.18	234.7	2.931	6.5	54.8	2.475	5.5
13.47	533.1	4.012	7.1	137.4	3.360	5.9	124.3	3.246	6.2	53.0	3.031	6.4
12.19	442.9	4.468	6.6	214.7	4.009	6.2
10.31	4633	8.467	9.7	2179	7.434	8.4	945.5	6.091	6.8	863	6.082	7.6
	Acetonitrile ^a											
36.0	...	0.221	4.1	...	0.203	3.9	...	0.205	4.4	...	0.264	6.8
	Nitrobenzene-carbon tetrachloride mixtures ^b											
34.69	(10.7)	(0.0660)	(6.5)
18.90	106.1	0.3060	5.6
15.80	331.3	0.7311	7.4
13.69	631.8	1.030	6.4

^a The values of dielectric constant, viscosity and density used in the computations are those reported by F. Accascina, S. Petrucci and R. M. Fuoss, *J. Am. Chem. Soc.*, **81**, 1301 (1960). ^b The values of dielectric constant, viscosity and density used in computation were interpolated from data reported by H. Sadek and R. M. Fuoss, *ibid.*, **76**, 5905 (1954). The parameters enclosed in parentheses indicate calculations made with a fixed value of a_J .

By means of $\log K_a$ vs. $1/D$ (D = dielectric constant) plots and comparison with other systems, some conclusions can be made. Figure 6 shows such a plot. Appropriate data for comparison are not plentiful, but the picrate ion (Pi^-) has been studied. It is similar in size and shape, although not necessarily in charge distribution, to the cyanocarbon anions PCP^- and bis-(TCV)-amine $^-$. Values of K_a for TMA^+/Pi^- in pure acetone¹⁶ and pure nitrobenzene¹⁷ are shown in the figure. Tetrabutylammonium picrate (TBA^+/Pi^-) has been studied in nitrobenzene-carbon tetrachloride mixtures,¹⁸ and the results also are shown. Presumably for TMA^+/Pi^- in nitrobenzene-carbon tetrachloride mixtures the curve would be similar but lying above the TBA^+/Pi^- ($\text{C}_6\text{H}_5\text{NO}_2\text{-CCl}_4$) curve by an amount suggested by the single measurement in pure nitrobenzene shown. The picrate ion behaves similarly to ions such as bromide, iodide and nitrate.¹⁸ Thus it may be seen that association in the cyanocarbon solutions is somewhat less pronounced than for other ions that have been studied. However, it is seen that the lower K_a values for cyanocarbons are not simply a matter of lower slopes. $\text{TMA}^+/\text{PCP}^-$ in acetone-carbon tetrachloride, for instance, has a higher slope in the same dielectric constant range than TBA^+/Pi^- but a lower K . It may also be noticed that the K_a values for $\text{TMA}^+/\text{PCP}^-$ are higher in nitrobenzene-carbon tetrachloride than in acetone-carbon tetrachloride and the slopes are slightly different. The K_a values for the four cyanocarbon salts in the same solvent are in the order expected on the basis of size, but the slopes of the $\log K_a$ vs. $1/D$ plots do not appear to behave in a simple manner.

Table IV shows the a_K (ion pair contact distance)

(16) M. J. McDowell and C. A. Kraus, *J. Am. Chem. Soc.*, **73**, 3293 (1951). Their data were recalculated using the complete Onsager-Fuoss theory with the computer. The new K_a value is 71.2 vs. 89 calculated by them.

(17) E. G. Taylor and C. A. Kraus, *ibid.*, **69**, 1731 (1947).

(18) E. Hirsch and R. M. Fuoss, *ibid.*, **82**, 1018 (1960).

values calculated from the slopes of the $\log K_a$ vs. $1/D$ plots, and the relation slope = $\epsilon^2/2.303a_KkT$ which holds for spherical ions in a continuous medium. It is not immediately clear to what molecular distance this should be compared for a flat ion such as a cyanocarbon. One extreme would be to compare it with the radius of the TMA ion plus the radius calculated from $(3/4\pi V)^{1/3}$, where V is the molecular volume found from models (Stuart-Briegleb). The other extreme would be to use the contact distance of the TMA ion against a point on a flat face of the anion (that is, 3.5 Å., the radius of $\text{TMA}^+ + 1.6$ Å., the half thickness of π electron orbitals or less). Distances calculated by these two methods also are listed in Table IV. Calculations likewise are included for TBA^+/Pi^- ($\text{C}_6\text{H}_5\text{NO}_2\text{-CCl}_4$). It seems physically unreasonable to identify the distance a_K calculated from the slopes with contact at a point since the a_K are comparable to or larger than the contact distance (≤ 5.1 Å.). Work on other ions has given distances from slopes that are consistently smaller than those found from models.¹⁸⁻²⁰ Thus, it is fair to conclude that the ion-pair configuration is not one of contact of the cation at a point of localized charge on the anion. This conclusion is, of course, consistent with the supposed delocalized charge in these anions. The first approach above (average distances from volumes) gives distances which at least in the case of PCP^- seem to be too large in comparison with a_K .

An alternative method of calculating the pair distance, instead of assuming point charges in spherical ions (a_K), would be to assume an idealized model where the cation is a sphere with a point charge at the center but on the axis of the center of a thin circular disk that is uniformly charged. Distances (a'_K) can be calculated by equating the electrostatic attraction energy of this configura-

(19) H. Sadek and R. M. Fuoss, *ibid.*, **81**, 4507 (1959).

(20) D. S. Berns and R. M. Fuoss, *ibid.*, **82**, 5585 (1960).

tion with $2.303kT \times \frac{1}{D}$ (slope of the $\log K_a$ vs. $1/D$ plot). The distances calculated in this way (a'_K) are listed in Table IV. This model seems more physically reasonable than the one with contact at a point with localized charge since it gives distances that are either comparable to or less than the contact distance from models (5.1 Å.).

TABLE IV
ION PAIR DISTANCE PARAMETERS^a (IN Å.)

Salt	Acetone-carbon tetrachloride mixtures			
	a_K	a_{es}	a_{con}	a'_K
TMA ⁺ /TCV alcoholate ⁻	5.78	6.6	<5.1	5.3
TMA ⁺ /PCP ⁻	4.53	7.1	<5.1	3.5
TMA ⁺ /bis-(TCV)-amine ⁻	6.21	7.3	<5.1	5.3
Nitrobenzene-carbon tetrachloride mixtures				
TMA ⁺ /PCP ⁻	5.84	7.1	<5.1	4.5
TBA ⁺ /Pi ⁻	5.91	8.9	<6.9	4.6

^a a_K = distance calculated from slope of $\log K_a$ vs. $1/D$ assuming slope = $e^2/2.303a_KkT$. a_{es} = structural distance assuming sums of radii of equivalent spheres (from measurements on Stuart-Briegleb models). a_{con} = structural distance assuming contact of TMA⁺ with anion at a point. a'_K = distance calculated from slope of $\log K$ vs. $1/D$ assuming slope = $W/2.303kT$, where W is electrostatic energy of attraction of a spherical cation (TMA⁺) on axis of a uniformly charged thin circular disk.

In order to see if ion pairing has an appreciable influence on the electronic structure of the anion, the ultraviolet absorption spectrum was measured as a function of concentration for TMA⁺/PCP⁻ in the lowest dielectric constant acetone-carbon tetrachloride mixture studied ($D = 10.31$). The spectrum was very similar to that in water (see Fig. 4), and no deviation from Beer's law was found. A similar conclusion has been reached by Lind and Fuoss.¹¹

Distance parameters derived from the $J(a)$ term, a_j , are listed in Table III. They seem consistent and are reasonably independent of composition in the mixtures. Somewhat higher values were found in the lowest dielectric constant acetone-carbon tetrachloride mixture ($D = 10.31$). The a_j values for TMA⁺/PCP⁻ in acetone-carbon tetrachloride and nitrobenzene-carbon tetrachloride are in agreement. The agreement of the a_j values for PCP⁻ and TCV alcoholate⁻ and bis-(TCV)-amine⁻ in water with the a_j in the above solvents is good also (Na⁺ and TMA⁺ have similar sizes in water, $\lambda_0^+ = 50.10$ and 44.92 , respectively). The lower values in acetonitrile probably reflect slight association there. K_a 's in the range of 5-10 would give a_j values in agreement with those in the other solvents. There does not seem to be a variation of a_j with the size of the ion in a given solvent as might be expected. Perhaps this is a reflection of the non-spherical shape of the anions.

4. Mobility Behavior.—Single ion conductances for the cyanocarbon anions can be calculated directly only for water, where accurate values of λ_0^+ for sodium ion are known.²¹ Estimates in acetone can be made from the measurements of Reynolds and Kraus⁷ on triphenyl fluoroborides, which give λ_0^+ as 98.0 for the TMA cation. In

(21) See for instance R. A. Robinson and R. H. Stokes, "Electrolyte Solutions," Appendix 6, 2nd Ed., Academic Press, New York, N. Y., 1959.

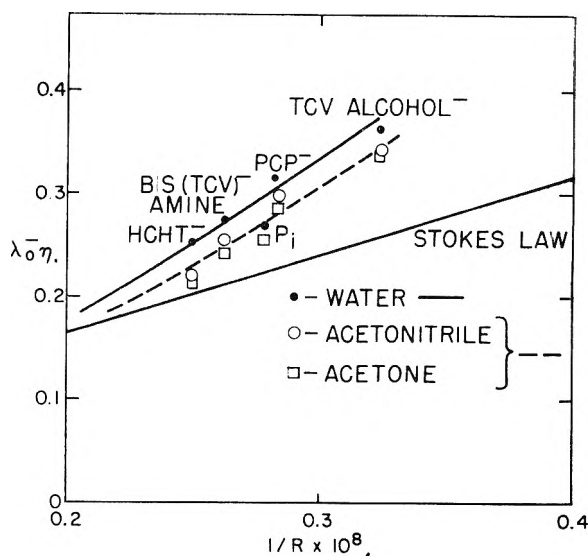


Fig. 7.—Walden product ($\lambda_0^- \eta$) for cyanocarbon anions [tricyanovinyl (TCV) alcoholate, pentacyanopropenide (PCP⁻), bis-tricyanovinyl-(TCV)-amine, and hexacyanoheptatrienide (HCHT⁻)] plotted against reciprocal of the radius of the equivalent sphere (from measurements on Stuart-Briegleb models). Also shown is Stokes law line $\lambda_0^- \eta = 0.8194/R_-(\text{Å.})$ (25.00°).

acetonitrile Berns and Fuoss²⁰ have given λ_0^+ for TMA⁺ as 92.5 from measurements on tetraphenyl borides.

Figure 7 shows $\lambda_0^- \eta$ plotted against $r = (3/4 \pi V)^{1/3}$, where V is the molecular volume calculated from Stuart-Briegleb models. Also shown is the Stokes' law line $\lambda_0^- \eta = 0.8194/R_-$ for macroscopic spheres. It is felt that the deviation from spherical shape of the anions probably does not influence the mobility behavior greatly, at least from a direct hydrodynamic viewpoint. For instance, the calculations of Perrin²² on the friction constant of ellipsoids show little effect of distortion at moderate values of the axial ratios. The deviations from Stokes' law have been generally thought of as arising from two sources, solvation type interactions and a breakdown of continuum hydrodynamics on a molecular scale.²³ The deviations from Stokes' law found for the cyanocarbon anions are similar to those found for other ions. The mobility behavior is quite similar in the solvents shown, indicating no special solvation effects.

Recently, Fuoss²⁴ has noticed that the Walden product ($\lambda_0^\pm \eta$) in solvent mixtures decreases with dielectric constant. This effect may be seen in the $\lambda_0 \eta$ values presented in Table V. He suggests that this variation is due to dielectric relaxation in the solvent induced by the ions' motion and that this effect can be represented by an equation of the form

$$\lambda_0^\pm = \frac{0.8194 \times 10^{-8}}{R_\infty + S/D}$$

In Fig. 8 are plotted values of

$$R = \frac{0.8194 \times 10^{-8}}{\lambda_0^- \eta} \text{ vs. } 1/D$$

(22) F. Perrin, *J. phys. radium*, [7] **7**, 1 (1936).

(23) See for instance Robinson and Stokes, ref. 21, Chapter 6.

(24) R. M. Fuoss, *Proc. Natl. Acad. Sci. U. S.*, **45**, 807 (1959). See also refs. 18, 19 and 20.

TABLE V

D	LIMITING EQUIVALENT CONDUCTANCE, 25°									
	TCV alcoholate $\eta \times 10^2$	Λ_0	$\Lambda_{0\eta}$	PCP		Bis-(TCV)-amine		HCHT		
				Λ_0	$\Lambda_{0\eta}$	Λ_0	$\Lambda_{0\eta}$	Λ_0	$\Lambda_{0\eta}$	
	Sodium salts: Water									
	0.8903	91.26	0.8125	85.85	0.7643	81.37	0.7244	78.2°	0.696	
	Tetramethylammonium salts: Acetone-carbon tetrachloride mixtures									
20.61	0.3056	209.8	0.6411	191.0	0.5837	176.7	0.5400	166.9	0.5100	
15.18	.3918	161.8	.6339	150.0	.5877					
13.47	.4208	149.3	.6283	136.7	.5752	128.9	.5424	119.3	.5020	
12.19	.4506			127.6	.5750	118.5	.5340			
10.31	.4981	123.5	.6139	114.6	.5697	103.5	.5145	98.6	.4901	
	Acetonitrile									
36.0	0.3438	191.7	0.6519	179.3	0.6164	167.0	0.5741	156.3	0.5374	
	Nitrobenzene-carbon tetrachloride mixtures									
34.69	1.839			35.43	0.6516					
18.90	1.329			41.33	.5493					
15.80	1.240			42.68	.5292					
13.69	1.180			42.58	.5024					

^a Estimated by curve fitting using dimerization constant determined spectroscopically.

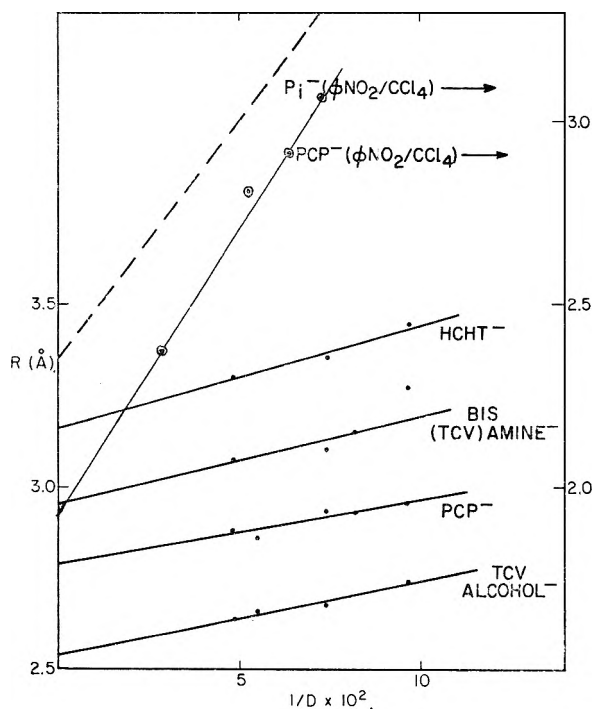


Fig. 8.—The Stokes law radii ($\bar{r}(\text{Å}) = 0.8194/\lambda_0^- \eta$) for cyanocarbon anions [tricyanovinyl (TCV) alcoholate, pentacyanopropenide (PCP⁻), bis-tricyanovinyl-(TCV)-amine, and hexacyanoheptatrienide (HCHT⁻)] plotted against reciprocal of dielectric constant, D . Solid points and full lines are for acetone-carbon tetrachloride mixtures (25.00°) and are plotted on scale at left. PCP⁻ in nitrobenzene-carbon tetrachloride mixtures is shown as \odot and full lines and is plotted on scale at right. Picrate (Pi⁻) in nitrobenzene-carbon tetrachloride is shown as dashed line, plotted on scale at right.

for our data in the acetone- and nitrobenzene-carbon tetrachloride mixtures. The λ_0^- values were calculated assuming the transference numbers are independent of composition in the mixtures and using the λ_0^+ value for tetramethylammonium ion in acetone given above. For nitrobenzene-carbon tetrachloride the values were calculated using the

Hirsch and Fuoss^{18,25} value of $\lambda_0^- = 16.66$ for picrate and the Taylor and Kraus¹⁷ value of $\Lambda_0 = 33.3$ for TMA⁺/Pi⁻ in nitrobenzene to arrive at λ_0^+ for TMA⁺ as 16.6.

The variation of λ_0^- with dielectric constant is just noticeable in the acetone-carbon tetrachloride mixtures with the slopes about $1/2$ to $1/3$ as large as those observed for tetraalkyl tetraphenyl borides in acetonitrile-carbon tetrachloride mixtures²⁰ and of the order of one-tenth as large as those for tetrabutylammonium bromide in nitrobenzene-carbon tetrachloride mixtures.¹⁹ For PCP⁻ in nitrobenzene-carbon tetrachloride, the variation is very similar to that found for other ions in this system (see Fig. 8 for comparison with Pi⁻). Thus, we conclude that the slope of such plots is sensitive to the particular solvent system but not to the type of ion. It should be noticed that the values of the intercepts (R_∞) for PCP⁻ in acetone-carbon tetrachloride and in nitrobenzene-carbon tetrachloride do not agree very well (2.79 vs. 1.95 Å., respectively).

5. Molecular Orbital Calculations.—The stability and structure of the cyanocarbon anions suggest that there is a great deal of resonance with consequent delocalization of the negative charge over the molecule. Simplified Hückel-type LCAO-MO calculations were made on three of the anions in order to get an idea of this charge distribution. Planar structures were assumed with sp^2 hybridization of the carbons. The out-of-plane p orbitals of the nitrogens were used along with those of the carbons to form the molecular orbitals. The resonance integral β_{n-c} was taken as $1.2\beta_{c-c}$.²⁶ The coulomb integral α_n was taken as $\alpha_c + \beta_{c-c}$.²⁶ The resulting effective charge distributions (indicated in Fig. 1) confirm the supposed charge delocalization with the nitrogens actually being the most negative atoms.

Acknowledgments.—The author is indebted to

(25) R. M. Fuoss and E. Hirsch, *J. Am. Chem. Soc.*, **82**, 1013 (1960).

(26) L. E. Orgel, T. L. Cottrell, W. Dick and L. E. Sutton, *Trans. Faraday Soc.*, **47**, 113 (1951).

many colleagues in this Laboratory for discussions regarding this work and for providing samples. Dr. R. E. Merrifield was particularly helpful in discussing the origin of the dimerization of cyano-carbon anions. Dr. D. W. Wiley was especially helpful in synthesizing a number of the compounds studied, and this assistance is very gratefully

acknowledged. The author is indebted to Mr. D. W. Marquardt and Miss A. Sheldon of the Engineering Research Laboratory, du Pont Experimental Station, who very skillfully carried out the computer calculations. He is also grateful to Professor Fuoss and Dr. Lind for making their manuscript available to us prior to publication.

THE KINETICS AND MECHANISM OF THE THERMAL DECOMPOSITION OF PLUTONIUM HEXAFLUORIDE¹

BY J. FISCHER, L. TREVORROW AND W. SHINN

Chemical Engineering Division, Argonne National Laboratory, Argonne, Illinois

Received March 30, 1961

The kinetics and mechanism of the decomposition of plutonium hexafluoride have been investigated, and the rate of decomposition has been formulated as a concurrent first and zero-order reaction with respect to plutonium hexafluoride pressure. It has been inferred that the decomposition, in the temperature range studied, proceeds by both a homogeneous and heterogeneous unimolecular decomposition. The heterogeneous decomposition occurs on the surface of plutonium tetrafluoride.

Introduction

Plutonium hexafluoride undergoes thermal decomposition to plutonium tetrafluoride and fluorine. Both the stoichiometry and the equilibria involved in the decomposition of plutonium hexafluoride have been investigated previously.² In the present work, the rate of thermal decomposition of plutonium hexafluoride vapor has been studied by a static method at initial pressures of 14 to 100 cm. and at temperatures of 140, 161 and 173°.

Experimental

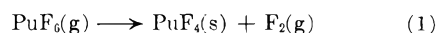
The physical and chemical properties of plutonium hexafluoride are such that special apparatus and techniques must be employed in experimentation with this compound. The triple point of plutonium hexafluoride is 51.59°, 533.0 mm., and the boiling point is 62.16°.³ Plutonium hexafluoride is a very strong fluorinating agent that reacts vigorously with many chemicals and must be handled in closed systems under anhydrous conditions. The radioactive decay of plutonium presents some very serious hazards to the laboratory worker. Decay of plutonium-239, the most prevalent isotope, is accompanied by the emission of highly energetic α -particles. The 239 isotope has a high specific activity and a long biological half-life. It is extremely toxic. The maximum permissible body burden has been set at 10^{-7} g. There is an additional radiation hazard associated with the fluorides of plutonium-239. The α -particles emitted by the plutonium isotope react with the fluorine nucleus to produce fast neutrons. This neutron hazard must be seriously considered by the experimenter when dealing with plutonium fluoride samples weighing more than 10 g. It is clear that special precautions in the way of equipment and procedure are necessary to protect the laboratory worker from ingestion of this isotope. The study of plutonium hexafluoride chemistry in our laboratories has been carried out in metal systems contained in glove boxes.

Materials.—Commercial fluorine of high purity was used in preparing plutonium hexafluoride. The plutonium hexafluoride used in the decomposition rate studies was prepared by reacting fluorine, at 500 to 550°, with plutonium dioxide or plutonium tetrafluoride, obtained from AEC sources. Fluorine, at a pressure of about one atmosphere, was circulated through the preparation equipment by means

of a magnetic piston pump. The fluorine flowed through a nickel preheater at 500°. Hot fluorine flowed from the preheater through a tubular nickel reaction furnace in which it passed across the surface of powdered plutonium tetrafluoride or plutonium dioxide contained in a nickel boat. This resulted in a mixture of plutonium hexafluoride, fluorine and oxygen, when the oxide was used, from which the plutonium hexafluoride was condensed in nickel traps cooled with Dry Ice. Volatile impurities were removed from the plutonium hexafluoride by cyclic sublimation, condensation and vacuum distillation.

Equipment.—All parts of the equipment, exposed to fluorine and plutonium compounds, were constructed with nickel and Monel. Component parts of the apparatus were connected by manifold systems to a high vacuum system consisting of mechanical and oil diffusion pumps, to a helium supply, to a fluorine supply, and to pressure measuring devices such as Bourdon gages and diaphragm pressure transmitters. Nickel valves, flare fittings, silver soldered and welded joints served to connect the various components of the apparatus. All of the equipment was pretreated with fluorine before use.

Experimental Procedure.—There is no change in the number of gas molecules during the thermal decomposition of plutonium hexafluoride vapor according to equation 1



Therefore, it is not possible to follow the rate of decomposition of the vapor by pressure measurements in a static system. The deposition of plutonium tetrafluoride would interfere with measurement of the partial pressure of plutonium hexafluoride by many of the common physical methods. Thus a number of physical measurements which might be used to follow the reaction continuously are rendered inapplicable.

Rates of decomposition were obtained from initial and final compositions after heating a sample of plutonium hexafluoride for a given period. Prior to each experiment the storage vessel containing the plutonium hexafluoride was evacuated to a pressure of about 2×10^{-4} mm. at -196° to remove fluorine accumulated from radiation decomposition. The plutonium hexafluoride then was transferred by vacuum distillation to a supply vessel where it was condensed, and any remaining fluorine was removed by evacuation at -196° . The 50-ml. supply vessel was connected by a manifold to a 50-ml. decomposition vessel which had been weighed previously. The supply vessel and associated lines were heated to about 70 to 80°, at which temperature the rate of decomposition was extremely low, in order to aid the transfer of adequate quantities of plutonium hexafluoride. The vessel was preheated to the experimental temperature in a thermostated aluminum block wound with Nichrome wire. The temperature of the decomposition

(1) This work was performed under the auspices of the U. S. Atomic Energy Commission.

(2) L. E. Trevorrow, W. A. Shinn and R. K. Steunenberg, *J. Phys. Chem.*, **65**, 398 (1961).

(3) B. Weinstock, E. E. Weaver and J. G. Malm, *J. Inorg. & Nuclear Chem.*, **11**, 104 (1959).

vessel was held constant to $\pm 0.2^\circ$. An experiment was initiated by opening the valve to the evacuated decomposition vessel, and allowing the warm plutonium hexafluoride to expand into it. The approximate amount of plutonium hexafluoride transferred to the reaction vessel was controlled by *PVT* measurements. When the expansion was complete, the valve on the reaction vessel was closed, and the decomposition of plutonium hexafluoride was allowed to proceed, isothermally, for a measured time interval.

At the end of the experiment the furnace was lowered, and the decomposition vessel was quenched in liquid nitrogen. The vessel was cooled rapidly to approximately 100° in one minute and to room temperature in two minutes. Thus, the error introduced by decomposition during the quenching period was small since the quenching period was short. The rate of fluorination of plutonium tetrafluoride has been shown to be relatively slow at temperatures below 170° .⁴ Thus, during the quenching period the composition of the gas mixture was not sufficiently altered by changes in the rates of either the forward or the reverse reaction to cause a significant error in the results. After quenching, the decomposition vessel was warmed to room temperature, and weighed to determine the starting amount of plutonium hexafluoride. The vessel then was evacuated at 25° to remove plutonium hexafluoride and the fluorine formed during the reaction. The vessel was weighed again to find the weight of plutonium tetrafluoride formed. The weights were used to calculate the amount of plutonium hexafluoride which had decomposed. Partial pressures of plutonium hexafluoride were calculated from the weights using the ideal gas law. A single reaction vessel was used for several consecutive experiments. Therefore, each experiment was carried out in the vessel containing plutonium tetrafluoride which had accumulated from previous experiments. A small correction was made of the volume of the vessel to account for the accumulation of plutonium tetrafluoride.

Results and Discussion

The values of the equilibrium constants for equation 1 are quite small.² At 140° the equilibrium constant, $(\text{PuF}_6)/(\text{F}_2)$, is 3.18×10^{-4} ; at 170° the equilibrium constant is 5.26×10^{-4} . From consideration of the equilibrium constants and the extent of displacement from equilibrium in these experiments, it is concluded that the rate of fluorination is negligible compared to the rate of decomposition of plutonium hexafluoride. In the interpretation of the results on the rate of decomposition of plutonium hexafluoride, the effect of the reverse reaction was considered to be unimportant.

The rate of decomposition of plutonium hexafluoride was studied by the static method in two types of vessels at 161° . The volumes of the vessels were almost equal, but the ratios of surface to volume were different. In one case the vessel was packed with nickel wool to increase the specific area. For the non-packed vessel, the surface to volume ratio was 1.8 cm^{-1} and the volume was 52 ml. For the packed vessel, the surface to volume ratio was 14 cm^{-1} and the volume was 51 ml. The surface to volume ratios are values based on geometric measurements.

The first few experiments in both vessels yielded very low decomposition rates. The rates increased rapidly in the first few experiments for the non-packed vessel, and then remained almost constant in subsequent experiments. In the packed vessel the rates increased to a value much greater than those in the non-packed vessel containing about the same amount of plutonium tetrafluoride. In

the packed vessel the plutonium tetrafluoride probably was deposited over a greater area on the surface and in the interstices of the nickel wool. It was concluded that the rate of decomposition of plutonium hexafluoride is dependent upon the surface area of plutonium tetrafluoride.

One of the reaction vessels was cut open and the plutonium tetrafluoride was found as a coating on the walls of the vessel and as pieces on the bottom of the vessel. The distribution of the plutonium tetrafluoride was not uniform.

After the deposition of a small quantity of plutonium tetrafluoride, in the non-packed vessel, the rates appeared to be independent of the quantity of plutonium tetrafluoride in the vessel. This was true when the quantity of plutonium tetrafluoride in the vessel varied from about 1 to 3 grams. Because of the manner in which plutonium tetrafluoride accumulated in the vessel, the active surface area of plutonium tetrafluoride did not increase linearly with the weight of plutonium tetrafluoride. It is assumed that for this reason the active solid surface area did not increase significantly throughout the set of experiments in the non-packed vessel reported here. Thus it was possible to obtain a set of consistent results even though the weight of PuF_6 in the reaction vessel was different for each experiment in the set. The results of the rate experiments at 140 , 161 and 173° in the non-packed vessel are shown in Table I. The rate was found to be dependent on the pressure of plutonium hexafluoride in the non-packed vessel.

The experimental results can be expressed by a rate equation which is of concurrent first and zero orders with respect to plutonium hexafluoride pressure

$$-dp/dt = k_0 + k_1 p \quad (2)$$

The experimental procedure used in this work yields integrated rates of decomposition; therefore, the integrated form of the rate equation was used to correlate the data obtained. The integrated form of equation 2 is

$$p = e^{-k_1 t} p_0 + e^{-k_1 t} (k_0/k_1) - k_0/k_1 \quad (3)$$

where p_0 = initial pressure

p = partial pressure after reaction time, t

Each experiment yielded values of p and p_0 . If the reaction times are held constant for a set of experiments, then equation 3 shows that p is a linear function of p_0 . Therefore, most of the experiments at a given temperature were carried out for the same reaction time but at various initial pressures. The use of constant reaction times permitted the values of k_0 and k_1 to be calculated conveniently. The values of k_1 and k_0 for equation 3 were calculated from the data of Table I by using the method of least squares. The rate constants obtained in this manner are listed in Table II.

The Arrhenius equation and the method of least squares were used to correlate the rate constants with temperature. The equations obtained are

$$\log k_0 = 7.124 - \frac{3.469 \times 10^3}{T(^{\circ}\text{K.})} \quad (4)$$

and

$$\log k_1 = 7.260 - \frac{4.292 \times 10^3}{T(^{\circ}\text{K.})} \quad (5)$$

(4) M. J. Steindler, D. V. Steidl and R. K. Steunenberg, *Nuclear Sci. and Eng.*, **6**, 333 (1959).

TABLE I
RATE OF DECOMPOSITION OF PLUTONIUM HEXAFLUORIDE
VAPOR

Static technique; initial volume of reaction vessel, 52.0 ml.; non-packed reaction vessel.

Reaction time (min.)	Initial pressure PuF ₆ (cm.)	Obsd. final press. PuF ₆ (cm.)	Obsd. integral rate (cm./hr.)	Calcd. ^a final press. PuF ₆ (cm.)	Dev. (cm.)
Temp. 140.1°					
120	101.8	86.8	7.5	86.9	+0.1
120	99.5	85.6	7.0	84.8	- .8
120	86.7	73.6	6.6	73.1	- .5
120	76.3	62.2	7.1	63.6	+1.4
120	70.0	56.1	7.0	55.9	-0.2
120	64.0	52.2	5.9	52.3	+ .1
120	56.4	45.7	5.4	45.3	- .4
120	48.5	37.4	5.6	38.1	+ .7
120	41.4	30.9	5.1	31.3	+ .4
120	14.0	7.1	3.4	6.4	- .7
Av. dev.					±0.4
Temp. 160.6°					
90	98.1	70.4	18.5	69.2	-1.2
90	59.6	37.9	14.5	38.6	+0.7
90	51.2	31.5	13.1	31.9	+0.4
90	32.6	16.5	10.7	17.1	+0.6
90	16.8	5.9	7.3	4.5	-1.4
Av. dev.					±0.9
Temp. 173.1°					
60	108.7	74.2	34.5	71.7	-2.5
60	92.8	59.9	32.9	59.3	-0.6
60	75.5	43.8	31.7	45.9	+2.1
60	75.4	46.3	29.1	45.8	-0.5
60	68.9	39.8	29.1	40.7	+0.9
60	63.7	35.4	28.3	36.7	+1.3
60	53.0	27.0	26.0	28.4	+1.4
60	44.9	20.0	24.9	22.1	+2.1
60	31.2	13.1	18.1	11.4	-1.7
60	25.7	8.3	17.4	7.2	-1.1
60	22.2	6.0	16.2	4.5	-1.5
Av. dev.					±1.4
Temp. 150.3°					
120	102.5	77.9	12.3	78.9	+1.0
120	49.8	31.9	8.9	33.0	+1.1
90	14.3	6.0	5.5	5.4	-0.6
90	14.0	6.1	5.3	5.1	-1.0
Av. dev.					±0.9

^a Calculated from the equation $p = p_0 e^{-k_1 t} + e^{-k_2 t}$ (k_0/k_1) - k_0/k_1 , using: $\log k_0 = 7.124 - (3.469 \times 10^3)/T(^{\circ}\text{K.})$ $\log k_1 = 7.260 - (4.292 \times 10^3)/T(^{\circ}\text{K.})$.

TABLE II
RATE CONSTANTS FOR THE THERMAL DECOMPOSITION OF
PLUTONIUM HEXAFLUORIDE

The reaction surface area of the experimental vessel is implicit in the constant k_0 . The uncertainty values are calculated probable errors.

Temp. (°C.)	k_0 (cm. min. ⁻¹)	k_1 (min. ⁻¹)
140.1	$5.58 \pm 0.36 \times 10^{-2}$	$7.25 \pm 0.53 \times 10^{-4}$
160.6	$10.9 \pm 0.94 \times 10^{-2}$	$25.0 \pm 1.8 \times 10^{-4}$
173.1	$24.2 \pm 1.6 \times 10^{-2}$	$41.9 \pm 2.8 \times 10^{-4}$

The experimental activation energies are 15.9 ± 1.5 kcal./mole for the zero-order reaction, and 19.6 ± 0.7 kcal./mole for the first-order reaction.

A few experiments were carried out at 150.3°. The rate constants at 150.3°, calculated from equations 4 and 5, were used to calculate the final pressures at 150.3° using the initial pressures. The observed and calculated final pressures were in agreement as shown in Table I.

The rate constant for the zero-order reaction is dependent on the surface to volume ratio. Since measurements of absolute surface areas were not obtained in the present work, the values for k_0 derived from the experimental results must be considered to hold true only for the particular surface to volume ratio of the reaction vessel used in these experiments.

The results of experiments in the packed reaction vessel are listed in Table III. The rates obtained in the packed vessel at 161° increased with the weight of plutonium tetrafluoride in the vessel. The rate constant, k_1 for the homogeneous reaction, derived from experiments in the non-packed vessel at 161°, was assumed to hold for the rates in both the packed and non-packed vessels. The value of k_1 then was used together with the results obtained in the packed vessel and equation 3 to calculate values of k_0 for the rates in the packed vessel. The values of k_0 thus calculated were not constant, but increased in order of the average weight of plutonium tetrafluoride present during an experiment. This relationship can be seen from the data in the last two columns of Table III.

TABLE III
RATE OF DECOMPOSITION OF PLUTONIUM HEXAFLUORIDE
VAPOR

Static technique; initial volume of vessel, 51.1 ml.; vessel packed with nickel wool; temperature, 160.6°.

Reaction time (min.)	Initial press. PuF ₆ (cm.)	Final press. PuF ₆ (cm.)	Av. wt. PuF ₆ in vessel (g.)	Calcd. ^a k_0 (cm. min. ⁻¹) $\times 10^2$
360	84.8	0.8	0.26	14
90	22.8	0.02	0.58	22
90	89.6	43.0	0.79	35
120	74.3	4.6	1.13	49
30	22.9	6.0	1.39	53
180	103.0	0.7	1.74	45
30	22.3	2.8	2.10	62
90	89.5	3.8	2.41	83
30	69.3	31.9	2.78	111
30	32.9	6.7	2.96	83

^a Calculated by substituting the value of k_1 at 161° from Table II in equation 3.

Since the surface area of plutonium tetrafluoride increases as more solid is deposited in the packed vessel, this datum serves to demonstrate that the rate of decomposition increases with increase in surface area.

The concurrent zero and first-order dependence of the rate on reactant pressure is similar to that reported for the decomposition of germanium tetrahydride.⁵ The first-order dependence can be attributed to the unimolecular, homogeneous de-

(5) K. Tamaru, M. Boudart and H. Taylor, *J. Phys. Chem.*, **69**, 801 (1955).

composition of plutonium hexafluoride in the gas phase, and the zero-order dependence can be attributed to the simultaneous, heterogeneous decom-

position of plutonium hexafluoride on the surface of plutonium tetrafluoride saturated by the chemically adsorbed gas.

THE HEATS OF COMBUSTION OF NIOBIUM CARBIDES¹

BY ELMER J. HUBER, JR., EARL L. HEAD, CHARLES E. HOLLEY, JR., E. K. STORMS AND
N. H. KRİKORIAN

University of California, Los Alamos Scientific Laboratory, Los Alamos, New Mexico

Received April 1, 1961

A series of niobium carbides, NbC_x, has been burned in an oxygen bomb calorimeter. The carbides covered a range from $x = 0.489$ to $x = 0.984$. Extrapolation of the curve, $\Delta H = 6.60 - 70.95x + 30.75x^2$, obtained for eight compositions (NbC_{0.686} through NbC_{0.984}) to $x = 1$ gave -33.6 ± 0.6 kcal./mole as the heat of formation of NbC. The heat of formation of Nb₂C was -46.6 ± 1.2 kcal./mole. Combustion of powdered Nb metal gave a heat of formation of -454.4 ± 1.6 kcal./mole for Nb₂O₅. A comparison of these values with those of other workers is made.

Introduction

The increased utilization of the transition metal compounds, especially for high temperature applications, has necessitated the investigation of their thermochemical properties. Because many of these compounds exist over a range of composition, their properties depend on the particular composition. Many times the form of this relationship also is important. For example, during previous work² the preparation of niobium carbides of various compositions became increasingly difficult as stoichiometric NbC was approached. Such behavior suggests that perhaps the free-energy of the NbC phase was becoming essentially constant even before NbC_{1.00} was reached. If this is indeed the case, several other properties of this system may be correlated. This work was undertaken to obtain the major contribution to the free energy values for NbC by measuring the heat of formation.

Present values for the heats of formation of niobium carbides consist of widely scattered estimates³⁻⁵ and two experimentally determined values.^{6,7}

This paper describes the determination of the heat evolved from the combustion of weighed samples of NbC_x, where x varied from 0.489 to 0.984. The method, using a bomb calorimeter at a known initial pressure of oxygen, has been described.⁸ The energy equivalent of the calorimeter was 9988.0 ± 3.3 j./° as determined by the combustion of standard benzoic acid.

Niobium Carbides.—In Table I are listed the analyses of the niobium carbides, which were prepared in this Laboratory. The method of

preparation has been described⁹ and the niobium-niobium carbide system has been discussed.² Niobium metal also is included.

TABLE I

ANALYSES OF NIOBIUM CARBIDES AND METAL, WEIGHT %

x in NbC _x	Nb	C, total	C, free	N	O	H	Fe
Metal	99.45	0.016	..	0.094	0.430	0.004	0.005
0.489	93.86	5.81	..	.081	.180	.004	.03
.500	93.84	6.00	..	.100	.06
.686	91.91	8.0801
.699	91.74	8.2501
.786	90.68	9.20022	..	.01
.861	89.98	10.01	..	.005	.002
.889	89.64	10.24	..	.021	.024	.004	..
.935	89.18	10.72	..	.005	.046	.001	.005
.979	89.56	10.33	..	.021	.024	.047	..
.984	87.05	12.92	1.87	.024

The niobium metal powder used was -325 mesh which probably accounts for the relatively large oxygen impurity. Metal powder from the same batch was used to make the carbides. The oxygen in each of the samples was determined by a diffusion-extraction method.¹⁰ The free carbon in the NbC_{0.984} material was determined chemically and also was seen in the X-ray pattern. Vanadium and zirconium were detected in two of the samples in very small amounts. At the temperature of preparation of the carbides, the iron impurity in the niobium should have been removed by volatilization. It is therefore assumed that the iron impurity in the carbides was introduced as metallic iron when the carbides were ground to a powder for the combustion experiments.

Combustion of the Niobium Carbides.—Each sample, including the niobium metal, was burned in oxygen at 25 atm. pressure on sintered discs of β -Nb₂O₅. Ignition was made by passing an electrical current through a 10 mil diameter niobium fuse wire. Although each material was in a finely divided form, no weight increase was found upon exposure to oxygen for one hour. The average

(9) E. K. Storms and N. H. Krikorian, *J. Phys. Chem.*, **63**, 1747 (1959).

(10) W. R. Hansen and M. W. Mallett, *Anal. Chem.*, **29**, 1868 (1957).

(1) This work was done under the auspices of the Atomic Energy Commission.

(2) E. K. Storms and N. H. Krikorian, *J. Phys. Chem.*, **64**, 1471 (1960).

(3) O. H. Krikorian, "High Temperature Studies. Part II. Thermodynamic Properties of the Carbides," Univ. of California Radiation Laboratory Report, UCRL-2888, April, 1955.

(4) G. V. Samsonov, *J. Phys. Chem. (U.S.S.R.)*, **30**, 2057 (1956).

(5) B. F. Ormont, *ibid.*, **33**, 1455 (1959).

(6) A. D. Mah and B. J. Boyle, *J. Am. Chem. Soc.*, **77**, 6512 (1955).

(7) F. G. Kusenko and P. V. Gel'd, *Izvest. Sibir. Otdel. Akad. Nauk S.S.S.R.*, **2**, 46 (1960).

(8) E. J. Huber, Jr., C. O. Matthews and C. E. Holley, Jr., *J. Am. Chem. Soc.*, **77**, 6493 (1955).

initial temperature was 25.2° and the average temperature rise 1.1431°.

Each solid combustion product was heated to constant weight in oxygen at 1,000° to determine the amount of unburned material. The CO₂ evolved was collected and the change in weight of the sample noted. Thus, it was possible to distinguish between CO₂ adsorbed on the disc material and combustion product and CO₂ from unburned carbide. Combustion varied from 98.78 to 100% of completion. Occasionally a check was made on the combustion gases, but no CO was found.

Only the β-form of Nb₂O₅ was found in the combustion products. Its specific heat was taken as 0.477 j./g./°. From six to eight runs were made on each material. They are summarized in Table II.

Calculations.—Listed in the first column of Table III are the formulas of the materials burned, including the uncertainties in those formulas which were derived from the uncertainties in the analyses.

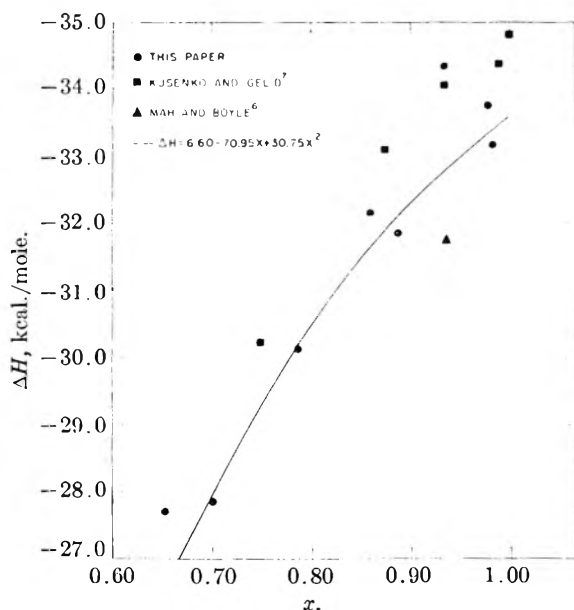
TABLE II

THE HEATS OF COMBUSTION OF Nb AND NbC_x

Mass burned, g.	Wt. Nb fuse, wire, mg.	Wt. Nb ₂ O ₅ , g.	Energy equiv. joules/deg. total	ΔT, °K.	Energy from Fir- ing, j.	NbC _x , j./g.	Dev. from mean
Nb Metal							
1.2440		29.9	10015.9	1.2503	17.8	10052	38
1.1947		58.2	10029.4	1.1956	16.1	10024	9
1.1674		43.5	10022.3	1.1656	19.2	9990	24
1.1825		43.9	10022.5	1.1820	15.9	10005	9
1.1837		43.6	10022.4	1.1826	15.7	10000	14
1.1794		43.6	10022.4	1.1723	14.6	9950	65
1.1931		43.5	10022.3	1.2056	17.0	10113	99
1.1789		43.5	10022.3	1.1758	17.6	9981	33
						10014	36
						Stand. dev.	18
NbC_{0.489}							
1.0095	32.45	33.0	10017.3	1.0945	15.9	10517	25
1.0336	32.71	33.8	10017.7	1.1174	15.2	10492	49
1.0541	33.10	33.5	10017.6	1.1477	15.4	10572	30
1.0646	33.86	33.5	10017.6	1.1531	20.1	10507	35
1.0648	31.98	33.6	10017.6	1.1564	15.2	10558	17
1.0718	32.32	33.9	10017.8	1.1633	15.4	10551	9
1.0549	31.80	33.9	10017.8	1.1537	14.8	10634	93
1.0110	32.01	31.5	10016.6	1.0939	13.5	10501	40
						10542	37
						Stand. dev.	17
NbC_{0.500}							
1.0173	33.17	30.9	10016.3	1.1106	17.2	10585	41
1.0163	31.95	32.1	10016.9	1.1071	16.3	10575	31
1.0276	32.82	32.3	10017.0	1.1137	16.7	10514	30
1.0063	31.61	32.6	10017.2	1.0899	16.3	10512	32
1.0525	31.37	32.5	10017.1	1.1417	16.1	10546	2
1.0247	31.83	31.8	10016.8	1.1126	14.5	10545	1
0.9762	32.93	31.7	10016.7	1.0617	16.5	10543	1
1.0142	32.17	28.9	10015.4	1.1013	19.6	10532	12
						10544	19
						Stand. dev.	9
NbC_{0.686}							
0.9954	31.59	29.0	10015.5	1.1161	15.6	10890	1
1.0090	35.37	29.4	10015.7	1.1354	16.7	10896	5
1.0018	34.63	29.0	10015.5	1.1255	18.5	10881	10
1.0081	31.01	29.0	10015.5	1.1305	16.8	10901	10
1.0010	32.53	37.0	10019.3	1.1234	17.6	10895	4
1.0040	31.88	37.1	10019.4	1.1247	15.2	10884	7
						10891	6
						Stand. dev.	3

NbC_{0.699}							
1.0001	31.72	36.7	10019.2	1.1229	18.7	10907	13
1.0076	31.80	36.5	10019.1	1.1348	16.3	10945	20
1.0069	32.54	36.6	10019.2	1.1334	19.6	10928	3
1.0178	29.08	36.2	10019.0	1.1403	17.0	10916	4
1.0071	29.43	35.6	10018.7	1.1303	15.9	10930	5
1.0184	31.07	36.0	10018.9	1.1433	16.8	10920	5
1.0165	29.94	36.3	10019.0	1.1411	16.5	10930	5
						10925	3
						Stand. dev.	5
NbC_{0.786}							
0.9786	33.05	28.3	10015.2	1.1177	9.4	11083	33
.9940	32.34	27.8	10015.0	1.1316	9.2	11059	15
.9913	32.88	34.5	10018.2	1.1231	9.7	11000	44
.9650	32.64	33.9	10017.9	1.0994	10.5	11077	33
1.0047	31.54	34.2	10018.0	1.1539	9.5	11196	152
1.0114	32.96	34.1	10018.0	1.1299	9.8	10947	97
1.0089	32.99	34.2	10018.0	1.1414	8.9	10996	43
1.0183	32.43	34.1	10018.0	1.1515	9.8	10995	43
						11044	60
						Stand. dev.	27
NbC_{0.801}							
1.0430	31.84	22.4	10012.3	1.1993	10.5	11183	15
0.9801	31.78	27.7	10014.9	1.1310	9.6	11208	40
1.0133	31.96	26.1	10014.1	1.1658	10.2	11181	13
0.9965	33.10	30.1	10016.1	1.1444	10.1	11145	23
1.0175	31.45	25.6	10013.9	1.1697	9.2	11180	12
1.0164	31.54	25.8	10014.0	1.1659	8.3	11155	13
1.0234	32.19	26.0	10014.1	1.1710	7.6	11124	44
1.0178	32.78	26.2	10014.2	1.1705	8.6	11172	4
						11168	20
						Stand. dev.	9
NbC_{0.859}							
0.9353	32.57	34.3	10016.9	1.0845	11.5	11237	5
0.9920	32.38	28.1	10014.0	1.1462	9.3	11220	12
1.0100	30.95	28.8	10014.3	1.1676	8.7	11248	16
1.0118	33.33	28.5	10014.2	1.1712	13.3	11231	1
0.9918	30.83	30.1	10015.2	1.1459	9.7	11236	4
1.0388	32.92	34.5	10017.0	1.1994	11.1	11223	9
						11232	8
						Stand. dev.	4
NbC_{0.935}							
0.9530	30.74	34.1	10018.0	1.1102	10.9	11320	80
.9447	32.31	34.6	10018.2	1.0990	10.1	11286	46
.9566	25.95	34.7	10018.3	1.1015	8.9	11242	2
.9453	32.37	33.9	10017.9	1.0859	8.7	11141	99
.9801	32.58	34.4	10018.1	1.1333	11.7	11233	17
.9485	34.00	33.6	10017.7	1.0994	9.8	11227	13
						11240	43
						Stand. dev.	25
NbC_{0.979}							
0.9719	33.11	41.4	10020.3	1.1406	9.3	11394	5
.9777	30.83	41.2	10020.3	1.1442	9.2	11387	12
.9910	31.71	40.7	10019.9	1.1623	10.3	11406	8
.9877	32.05	40.5	10019.8	1.1587	9.4	11406	7
.9817	30.41	40.4	10019.8	1.1500	9.2	11404	5
1.0079	31.75	40.5	10019.8	1.1801	10.5	11391	8
0.9871	32.02	41.8	10020.4	1.1576	8.7	11403	4
						11399	7
						Stand. dev.	3
NbC_{0.984}							
0.9770	31.52	36.1	10018.9	1.1865	9.4	11820	10
.9749	31.95	35.7	10018.7	1.1853	9.0	11829	1
.9854	29.93	35.8	10018.8	1.1955	9.0	11828	2
.9671	31.33	33.8	10017.8	1.1747	9.8	11819	11
.9767	29.46	29.1	10015.7	1.1857	8.2	11835	5
.9788	30.24	29.0	10015.6	1.1901	9.0	11845	15
.9845	29.82	29.3	10015.8	1.1955	9.4	11836	6
						11830	7
						Stand. dev.	3.5

The average value for the heat of combustion under bomb conditions is recorded in the second

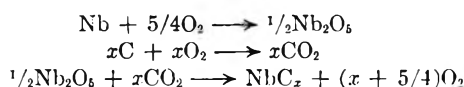
Fig. 1.—The heats of formation of NbC_x vs. x .

column, and the value corrected for the presence of the impurities in the third column. To make these corrections it was necessary to assume that (1) nitrogen, where present, was in the form of NbN which burned to Nb_2O_5 and NO_2 with a heat of 6580 j./g.; (2) oxygen existed as NbO with a heat of combustion of 4880 j./g.; (3) hydrogen was combined as NbH which evolved 10490 j./g.; (4) iron burned with a heat of 7325 j./g.; (5) free carbon gave 33000 j./g. In addition, since both $\text{NbC}_{0.686}$ and $\text{NbC}_{0.699}$ are in the two-phase region,⁹ corrections had to be made for an estimated 2 mole % Nb_2C in the $\text{NbC}_{0.686}$ and an estimated 1 mole % Nb_2C in the $\text{NbC}_{0.699}$. These preparations lie to the left of the phase boundary at the temperature of preparation. The amounts of Nb_2C impurity were estimated from the X-ray patterns. The corrected compositions agree with the estimated position of the phase boundary within the limits of error of the analyses. The large negative correction for the $\text{NbC}_{0.984}$ arises, of course, from the presence of free carbon in this material.

TABLE III
HEATS OF COMBUSTION, NbC_x , j./g.

x	Uncorr.	Corr. for impur.	% Change
Metal	10014	10194	+1.80
0.489 ± 0.001	10542	10642	+0.95
.500 ± .003	10544	10598	+ .51
.686 ± .004	10891	10906	+ .14
.699 ± .004	10925	10933	+ .07
.786 ± .001	11044	11064	+ .18
.861 ± .009	11168	11172	+ .04
.889 ± .008	11232	11252	+ .18
.935 ± .002	11240	11268	+ .25
.979 ± .001	11399	11398	- .01
.984 ± .003	11830	11436	-3.33

The values for the heats of formation of the niobium carbides are listed in Table IV. They are derived from the addition of the heats of the reactions



The uncertainties attached to the ΔH values include the uncertainty in the determination of the energy equivalent of the calorimeter, the uncertainties found in the calorimetric measurements, and the uncertainty in the value for the heat of formation of Nb_2O_5 , all expressed as twice the standard deviation, plus an estimated uncertainty in the correction for impurities, combined according to standard methods for the propagation of errors. Humphrey's value¹¹ of $\Delta H = -455.2 \pm 0.6$ kcal./mole for Nb_2O_5 was used rather than the value obtained in this paper (454.4 ± 1.6 kcal./mole) because strips of niobium were used in his work and they probably had less surface contamination than the fine powder used in these experiments. Agreement of the two values is, however, good. The NBS value for the heat of formation of CO_2 was used.¹²

Reduction to unit fugacity of oxygen was made using the value $(\partial E/\partial P)_{25} = -1.574$ cal./atm./mole. For CO_2 - O_2 mixtures this value was modified by the factor $1 + 1.69N(1 + N)$, where N is the mole fraction of CO_2 .¹³

The conversion to a constant pressure process was made by the relationship $\Delta H = \Delta E + \Delta nRT$. The 1955 International Atomic Weights were used.¹⁴

TABLE IV
HEATS OF FORMATION, NbC_x , KCAL./MOLE

x	$-\Delta H_F$
0.489 ± 0.001	21.55 ± 0.85
.500 ± .003 ($1/2 \text{Nb}_2\text{C}$)	23.3 ± .6
.686 ± .004	27.7 ± .4
.699 ± .004	27.85 ± .4
.786 ± .001	30.1 ± 1.4
.861 ± .009	32.15 ± 0.6
.889 ± .003	31.85 ± 0.4
.935 ± .002	34.35 ± 1.3
.979 ± .001	33.75 ± 0.4
.984 ± .003	33.15 ± .35
1.00 (NbC, extrapolated)	33.6 ± .6
Nb_2O_5	454.4 ± 1.6

The values for the heats of formation for the eight compositions ($\text{NbC}_{0.686}$ through $\text{NbC}_{0.984}$) were fitted to a quadratic equation by the method of least squares, using an IBM 704 computer. Each value was weighted inversely proportionately to the square of its uncertainty. The resulting equation is

$$\Delta H = 6.60 - 70.95x + 30.75x^2$$

Although this curve appears to fit the points, the large error in the points makes it possible to choose a straight line without making a statistically significant difference. Nevertheless, it is felt that a curve, not necessarily a quadratic, should

(11) G. L. Humphrey, *J. Am. Chem. Soc.*, **76**, 978 (1954).

(12) Natl. Bur. Standards, Circ. 500, p. 99, 1952.

(13) W. N. Hubbard, D. W. Scott and G. Waddington, "Experimental Thermochemistry," F. D. Rossini, Editor, Interscience Publishers, Inc., New York, N. Y., 1956, pp. 98, 101.

(14) E. Wichers, *J. Am. Chem. Soc.*, **80**, 4122 (1958).

represent the data better than a straight line. If this equation is extrapolated to $x = 1$, stoichiometric NbC is found to have a heat of formation of -33.6 ± 0.6 kcal./mole. This value, however, is only of academic interest because stoichiometric NbC cannot be made under ordinary conditions, if at all.

The values obtained by Mah and Boyle⁶ and Kusenko and Gel'd⁷ are compared to this work in Fig. 1.

Nb₂C also has a range of homogeneity but one that is very narrow. At the temperature of preparation the samples NbC_{0.489} and NbC_{0.500} probably bracketed this region very closely.

Therefore, a value of -43.1 ± 1.7 kcal./mole is the value of ΔH for Nb₂C in equilibrium with Nb, and -46.6 ± 1.2 kcal./mole is the value of ΔH for Nb₂C in equilibrium with NbC. The form of the relationship between these extremes is unknown. These values can only be compared with O. H. Krikorian's estimate³ of -40 ± 8 kcal./mole.

Acknowledgments.—Valuable assistance was rendered by F. H. Ellinger, X-ray analysis; J. A. Mariner, spectrochemical analysis; and G. C. Heasley and L. Gritzco, chemical analysis. Thanks are due R. K. Zeigler for programming the data for the IBM 704 computer.

KINETICS OF THE REACTION OF SULFUR TETRAFLUORIDE WITH URANIUM TRIOXIDE AND URANYL FLUORIDE¹

BY CARL E. JOHNSON AND JACK FISCHER

Chemical Engineering Division, Argonne National Laboratory, Argonne, Illinois

Received April 1, 1961

The reactions between sulfur tetrafluoride and uranium trioxide and sulfur tetrafluoride and uranyl fluoride have been studied between 255 and 370° by following the change in weight of the solid phase using a thermobalance. The rate of production of uranium hexafluoride is in agreement with the kinetics expected for reaction between a gas and a solid at a continuously diminishing spherical interface. The rate of reaction is temperature dependent. The activation energies for reaction of sulfur tetrafluoride with uranium trioxide and uranyl fluoride are, respectively, 6.0 and 32.0 kcal./mole. The rate of reaction with uranyl fluoride is dependent upon the partial pressure of sulfur tetrafluoride. A 1.55 exponent was found. A minimum gas velocity was found above which the reaction rate is independent of the velocity of gaseous reactant past the solid.

Introduction

A study of the rates of reaction between gaseous fluorinating agents and uranium and its compounds provides information about the kinetics and mechanisms of the reaction of gases with solid surfaces. In the majority of cases the end product is volatile uranium hexafluoride and even though intermediate compounds may be produced, the reaction proceeds on a reactive surface at all times. Thus the rates are governed primarily by the processes at the gas-solid interface and do not depend on diffusion through a layer of condensed product, as is the case in many oxidation reactions.

An extensive amount of research has been done on gas-solid reactions for which the end products are solids. Kinetic studies are more limited for the case in which the products of reactions are gaseous. They include work on the C-H₂O,²⁻⁴ C-CO₂,^{5,6} and C-O₂,^{7,8} systems, the UF₄-F₂,⁹ UF₄-ClF₃¹⁰ and Ni-Cl₂¹¹ systems.

(1) Work performed under the auspices of the U. S. Atomic Energy Commission.

(2) G. S. Scott, *Ind. Eng. Chem.*, **33**, 1279 (1941).

(3) J. Gadsby, C. Hinshelwood and K. W. Sykes, *Proc. Roy. Soc. (London)*, **A189**, 129 (1946).

(4) F. J. Long and K. W. Sykes, *ibid.*, **A193**, 377 (1948).

(5) L. J. Jolly and A. Poll, *J. Inst. Fuel*, **26**, 33 (1953).

(6) J. Gadsby, F. J. Long, D. Sleightholm and K. W. Sykes, *Proc. Roy. Soc. (London)*, **A193**, 357 (1948).

(7) P. L. Walker, R. J. Foresti and C. C. Wright, *Ind. Eng. Chem.*, **45**, 1703 (1953).

(8) F. J. Long and K. W. Sykes, *J. Chem. Phys.*, **47**, 361 (1950).

(9) V. Y. Labaton and K. D. B. Johnson, *J. Inorg. & Nuclear Chem.*, **10**, 74 (1959).

(10) V. Y. Labaton, *ibid.*, **10**, 86 (1959).

(11) J. D. McKinley, Jr., and K. E. Shuler, *J. Chem. Phys.*, **28**, 1207 (1958).

The factors which govern the kinetic laws for gas-solid reactions are: the chemical reactions at the phase boundary, the diffusion rates of reactants and the rates of nucleation and crystallization of solids. A reaction taking place at a surface may in general be separated into five steps¹²

- (1) Transport of the reacting gas to the surface
- (2) Chemisorption of the gas
- (3) Chemical reaction at the surface
- (4) Desorption of the reactant product
- (5) Transport of the reaction product away from the surface

Transport of the reacting gas to the surface of the solid and transport of the reaction product away from the surface are ordinary diffusion processes. Diffusion in the gaseous state is considered to be fast involving little or no activation energy and is therefore not expected to limit the reaction in any way. The processes of chemisorption of the gas and desorption of the reaction product are much more likely to be the slow steps in heterogeneous reactions since both may involve appreciable energies of activation. In practice, however, it is not always convenient to separate the chemical reaction at the surface from the process involved in desorption of the reaction product, because of insufficient knowledge about the desorption process. Therefore, what is generally done is to consider the reaction at the surface, giving rise to gaseous products, as a single step.

In this paper further work is reported on the reactions of gaseous sulfur tetrafluoride with uranium

(12) S. Glasstone, K. J. Laidler and H. Eyring, "Theory of Rate Processes," McGraw-Hill Book Co., New York, N. Y., 1941.

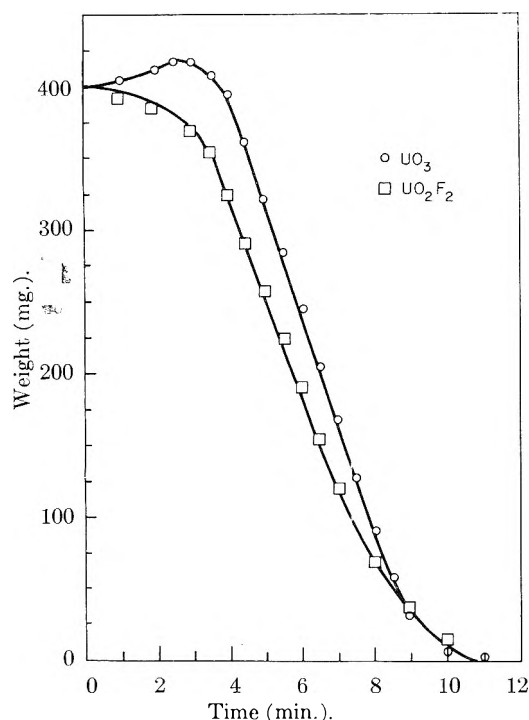


Fig. 1.—Rate of fluorination of UO_3 and UO_2F_2 at 335° .

trioxide and uranyl fluoride, the stoichiometry of this reaction having previously been investigated.¹³ The present work was undertaken to elucidate the kinetics and the mechanism of this gas-solid reaction.

Experimental

Materials.—The uranium trioxide, uranyl fluoride and sulfur tetrafluoride referred to in this article are the same commercial products used in the previously reported¹³ study.

Apparatus.—A Sartorius Selecta thermobalance was used for the kinetic rate studies. A continuous record of weight change *versus* time is obtained on a Bristol Dynamaster recording potentiometer. The sample pan is suspended from the stirrup of the balance by a nickel chain directly into the reaction chamber located immediately below the balance. The reaction chamber is fabricated from a 2-inch nickel pipe and is heated by a resistance-wound furnace. Hot convection currents from the furnace are kept out of the balance by a baffle and gas blanket arrangement. The Sartorius balance is protected from attack by corrosive gases by keeping a small positive pressure of argon in the balance at all times.

A gas distribution manifold attached to the reaction chamber allows choice of reaction gas whose flow rate was measured with a calibrated thermal flow meter. All gases passed through a preheat furnace prior to entering the reaction furnace. The sample temperature is measured by a calibrated thermocouple positioned directly beneath the sample pan. A record of the sample temperature *versus* time is obtained on a multipoint recording potentiometer. In addition the temperature of the preheat furnace, reaction furnace and the output of the thermal flow meter are monitored continuously.

Procedure.—In a typical experiment 400.0 mg. of a $-200 + 230$ mesh fraction of either uranium trioxide or uranyl fluoride was placed on a tared platinum pan and then lowered into the preheated reaction chamber. The weight of sample plus pan was checked on the Sartorius balance while temperature equilibrium between gas and solid was being attained. During this period argon was purged through the reaction chamber. When temperature equilibrium had been achieved the purge gas was shut off and

sulfur tetrafluoride was allowed to flow through the reaction chamber at a flow rate of about 150–200 cm.³/min.

Each experiment was performed under conditions of constant temperature and constant total flow of reacting gas. The gas manifold connected to the reaction chamber is equipped with a 14-liter ballast tank which was charged with various mixtures of nitrogen and sulfur tetrafluoride. The gas mixture then was allowed to pass over the sample at atmospheric pressure at a constant flow rate. For a particular partial pressure study the ballast tank was charged with a gas mixture at least 24 hours prior to use to allow gaseous equilibrium to take place.

Discussion of Results

If the reaction between a solid and a gas is one in which the active sites of the surface of a solid is saturated with gas molecules, the rate of the reaction should be zero order with respect to the pressure of the reactant gas. If this is not the case then the rate will be fractional or higher order. At constant pressure the rate of such a process then will be proportional to the area of the interface at any time during the reaction. A system of solid and gas may be idealized by assuming the solid to consist of spherical particles (of uniform size) with reaction starting at $t = 0$ on all particles. In such a reaction the following relationship can be deduced.¹⁴

If the initial mass of a solid particle $M_0 = 4/3 \cdot \pi r_0^3 \rho$, where r_0 = initial radius and ρ = bulk density then the rate of reduction in mass at a given temperature is assumed to be proportional to the surface area of the particle

$$-\frac{dM}{dt} = k4\pi r^2 \quad (1)$$

where r is the radius of the particle at time t and k is the constant for a given temperature and partial pressure of reactant gas.

The fraction of reaction F that has taken place in time t is given by

$$F = \frac{M_0 - M}{M_0} = 1 - \left(\frac{r}{r_0}\right)^3$$

when substituted in equation 1 becomes

$$\begin{aligned} \frac{dM}{dt} &= -k4\pi r_0^2 (1 - F)^{2/3} \\ \frac{dF}{dt} &= \frac{1}{M_0} \frac{dM}{dt} = \frac{3k}{r_0 \rho} (1 - F)^{2/3} \end{aligned} \quad (2)$$

Integrating expression 2 we obtain

$$(1 - F)^{1/3} = 1 - k't \quad (3)$$

where $k' = k/r_0 \rho$.

When the quantity $(1 - F)^{1/3}$ is plotted against time for a typical experiment, the points lie on a straight line in agreement with the equation. There is some deviation at the beginning and the end of the reaction. Experimental conditions used govern the deviations at the beginning of each experiment. The reaction chamber is full of argon at the start of each experiment; therefore it is felt that at least five minutes are needed for displacement of argon by sulfur tetrafluoride to take place. Consequently the rates will be abnormally low at the beginning of each run.

Deviation from the expected kinetics at the end of the reaction may be caused by a number of variables not the least of which is the small amount

(13) C. E. Johnson, J. Fischer and M. J. Steindler, *J. Am. Chem. Soc.*, **83**, 1620 (1961).

(14) J. S. Anderson, *Bull. Soc. Chim.*, **20**, 781 (1953).

of sample remaining. Chemisorption of sulfur tetrafluoride on the surface of the remaining solid may contribute significantly to the final weight of the sample thereby biasing the results.

The results of a typical reaction of sulfur tetrafluoride with uranium trioxide are shown in Fig. 1. The initial increase in weight at the start of the reaction is attributed to the formation of uranyl fluoride. In several experiments when the reaction was stopped before completion, it was noted that the material remaining in the pan was made up of two distinct phases. The top 60% was pale yellow in color; the lower material, orange. Chemical analysis confirmed an uptake of fluorine. X-Ray diffraction analysis indicated the yellow material to be anhydrous uranyl fluoride and the orange material to be unreacted uranium trioxide.

Thermobalance data on the reaction of sulfur tetrafluoride with uranyl fluoride, also shown in Fig. 1, gave no indication of uptake or increase in weight prior to formation of volatile uranium hexafluoride. If an intermediate such as UOF_4 does form it evidently reacts too fast for the anticipated weight increase to be observed.

Early experiments had shown that uranyl fluoride was a product of the first step in the reaction of uranium trioxide and sulfur tetrafluoride, therefore, subsequent work was done using anhydrous uranyl fluoride as the starting material.

The variations of the reaction rate constants, k' of equation 3, with temperature for the reactions of sulfur tetrafluoride at one atmosphere with uranium trioxide and uranyl fluoride are given in Fig. 2. The logarithm of the reaction rate constant k' is plotted against the reciprocal of the absolute temperature from which the activation energy for the reaction of uranyl fluoride with sulfur tetrafluoride was calculated to be 32.0 kcal./mole. Surface reactions in general have activation energies of the order of 30 kcal./mole.¹² The reaction of uranium trioxide with sulfur tetrafluoride has an activation energy of the order of 6.0 kcal.

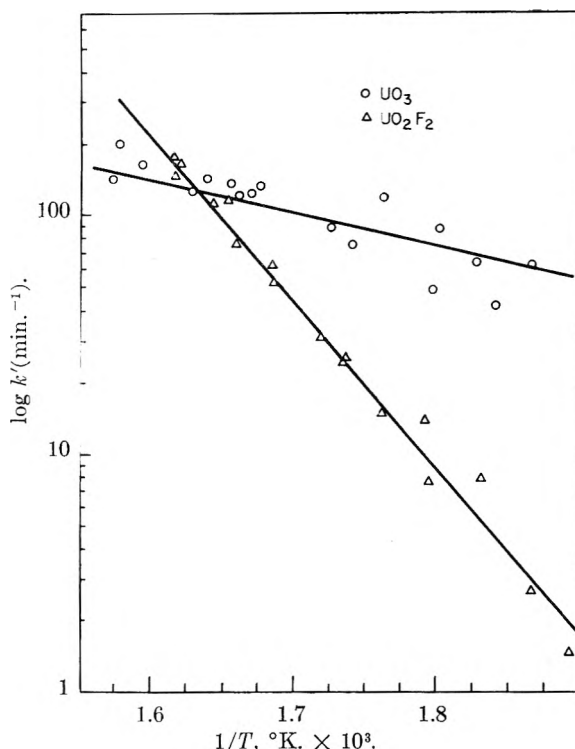
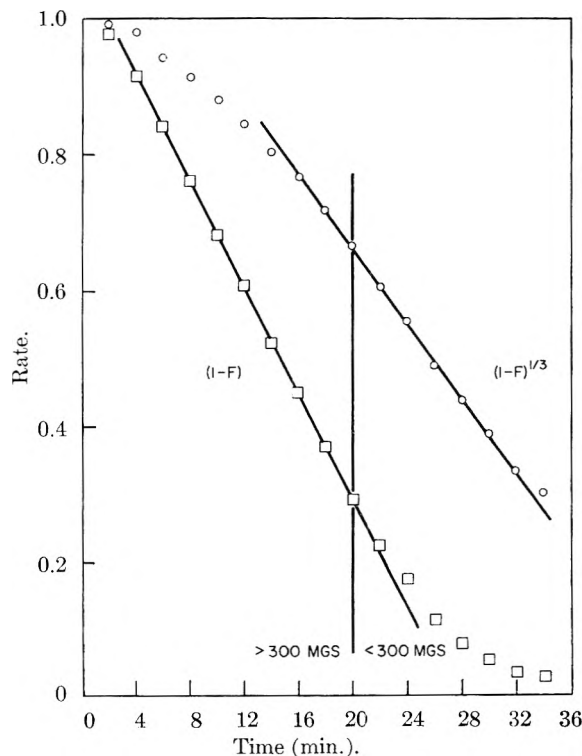
TABLE I

EFFECT OF PARTIAL PRESSURE OF SULFUR TETRAFLUORIDE ON THE RATE CONSTANT AT 333°
Total pressure, 750 ± 10 mm.

Partial pressure of sulfur tetrafluoride (atm.)	Flow rate of SF_4 (cc./min.)	k (min. ⁻¹)
1.0	200	0.0920
0.8	160	.0435
.6	120	.0225
.3	60	.00867 ^a
.2	40	.00505

^a Interpolated value.

The greatest portion of the experimental work was carried out at one atmosphere pressure of sulfur tetrafluoride. In several experiments, however, the partial pressure of sulfur tetrafluoride was varied keeping temperature and gas flow rate constant. This was done by charging the 14-liter ballast tank with various mixtures of sulfur tetrafluoride and nitrogen. Each gas mixture then was passed over the sample at atmospheric pressure at a constant rate. These data are given in Table I. A slope of 1.55 obtained from a graph

Fig. 2.—Arrhenius plot for UO_3 and UO_2F_2 .Fig. 3.—Effect of bed depth on rate of fluorination of UO_3 by SF_4 .

of the logarithm of the rate constant *versus* the partial pressure of sulfur tetrafluoride in atmospheres illustrates the pressure dependence of the reaction rate constant.

To ascertain whether the pressure dependence of the rate constant was not a dilution effect additional experiments were run keeping temperature

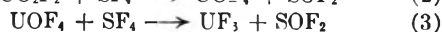
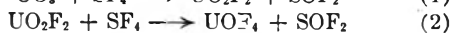
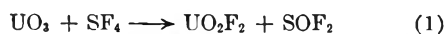
and partial pressure of sulfur tetrafluoride constant and varying the flow rate of gas. These data are given in Table II. It is evident that if the sulfur tetrafluoride flow rate is greater than 30 cc./min. the rate constant at a fixed temperature and fixed partial pressure of sulfur tetrafluoride becomes independent of flow rate. In all of the experimental work the flow rate of sulfur tetrafluoride varied between 40 and 200 cc./min.

TABLE II
EFFECT OF GAS FLOW RATE ON RATE CONSTANT

Total flow rate, cc./min.	SF ₄ flow rate, cc./min.	Temp., °C.	Partial pressure of SF ₄ (atm.)	k (min. ⁻¹)
36	21.6	362	0.60	0.0202
76	45.6	362	.60	.0747
162	97.3	362	.60	.0765
240	144	362	.60	.0757
57	18.8	360	.33	.0151
82	27.1	360	.33	.0244
180	59.4	360	.33	.0295
278	91.8	360	.33	.0268
110	22.0	365	.20	.0088
165	33.0	365	.20	.0168
266	53.2	365	.20	.0172

The rate of fluorination of uranyl fluoride of high surface area from a bed of material about 5 mm. deep is shown in Fig. 3. In this graph the rate constant is plotted as a linear function of $(1 - F)$ and a diminishing sphere rate function of $(1 - F)^{1/2}$. The conversion of uranium trioxide to uranyl fluoride takes place in a relatively thin layer ($\sim 150 \mu$ in depth) of material. It appears that this same effect holds for deep beds of uranyl fluoride. As this reaction zone proceeds downward through the bed the rate of reaction appears linear with time. When the amount of reactant in the pan is 350 mg. or less, about one particle layer of thickness, the rate of reaction reverts to a diminishing sphere model.

In considering the total reaction of uranium trioxide with sulfur tetrafluoride the following mechanism is suggested



The first step in this mechanism has been demonstrated by chemical analysis and X-ray diffraction of reaction products. The reaction is apparently one of solid phase conversion of uranium trioxide to uranyl fluoride. Unsuccessful attempts were made to observe the reaction boundary between uranium trioxide and uranyl fluoride using large particles of uranium trioxide.

At this time the second and third steps in the mechanism can only be deduced considering steric effects on the reaction which have yet to be established experimentally. Stoichiometry studies indicated two moles of sulfur tetrafluoride are needed for each mole of UO_2F_2 converted to UF_6 . In all the experiments for which infrared data were compiled the only gaseous sulfur product found was thionyl fluoride. Molecular structure evidence^{15,16} indicates the sulfur tetrafluoride molecules to have a trigonal bipyramid configuration with one of the three equatorial positions unoccupied (point group (C_{2v})). The molecular configuration of thionyl fluoride¹⁷ is thought to be either pyramidal (C_3) or trigonal bipyramid (C_{2v}) in nature. Assuming that the C_{2v} structure predominates in the product, it is easily seen that each sulfur tetrafluoride molecule contributes only two of its fluorines to the solid. This further suggests that, in order for steps (2) and (3) of the reaction mechanism to take place in a single step, two molecules of sulfur tetrafluoride must simultaneously reside on an active site on the surface of the uranyl fluoride for fluorine-oxygen exchange to take place. Because bimolecular gas-solid reactions of this type are extremely rare some credence is given to the existence of UOF_4 as a reaction intermediate. Attempts at the preparation and isolation of UOF_4 have up to now been unsuccessful. However, the formation of UOF_4 as a reaction intermediate cannot be completely ruled out.

Acknowledgment.—The authors wish to acknowledge the assistance of J. Stockbar in the experimental work and of M. Homa and R. Schablaske for X-ray diffraction analyses.

(15) R. E. Dodd, L. A. Woodward and H. L. Roberts, *Trans. Faraday Soc.*, **52**, 1052 (1956).

(16) F. A. Cotton, J. W. George and J. S. Waugh, *J. Chem. Phys.*, **28**, 994 (1958).

(17) J. K. O'Loane and M. K. Wilson, *ibid.*, **23**, 1313 (1955).

CATION HYDRATION EFFECTS ON THE THERMODYNAMICS OF WATER ADSORPTION BY KAOLINITE¹

By J. J. JURINAK AND D. H. VOLMAN

Department of Soils and Plant Nutrition and Department of Chemistry, University of California, Davis, California

Received April 1, 1961

The isosteric ΔH and differential ΔS values are calculated for the adsorption of water on Ca- and Ba-kaolinite and compared with similar functions for water adsorption by Li-kaolinite, which is regarded free from cation hydration effects. In the coverage range studied water interaction with Ca- and Ba-kaolinite was thermodynamically similar. The effect of hydration was noted throughout the monolayer region. The apparent heat of cation hydration suggests that forces emanating from the kaolinite surface do not extend much beyond the monolayer.

Introduction

Previous studies in this Laboratory have indicated that water adsorbed on Li-kaolinite at low coverages does not react with sorbed lithium ions. This lack of reactivity permits Li-kaolinite to be regarded as a kaolinite surface free from exchangeable cation hydration effects.² Thermodynamic data³ of water adsorbed on Li-kaolinite have indicated that adsorbed water molecules attract each other and form a structural surface network which reduces the entropy of the adsorbed water molecules to a value that is similar to the entropy of ice at 0°. Prior to adsorbate interaction, water molecules appear to be mobile, although localized adsorption with a high degree of vibration cannot be precluded.⁴ The entropy of adsorbed water ($S_{298}^0 - \Delta S_{ads}$), with no configurational correction, is less than that of liquid water between W/W_m values of about 0.30 and 0.70. No data were obtained for W/W_m less than 0.15. These differential thermodynamic data are in fair agreement with those reported by Martin.⁵ He concluded that sorbed water on Li-kaolinite and Na-kaolinite was more random than liquid water because adsorbate interaction only occurred over a relatively small P/P_0 range and integral entropy calculations of sorbed water resulted in values that exceeded those of liquid water. Since water adsorption on Li-kaolinite is considered free from cation hydration, the study reported here is an attempt to ascertain the effect of cation hydration on the adsorption of water by kaolinite.

Experimental Methods.—The kaolinite used was from Dry Branch, Georgia, and donated by the Georgia Kaolinite Co. The exchange capacity was determined as 1.5 meq./100 g. with regard to lithium and sodium ions and 2.0 meq./100 g. with regard to calcium and barium ions. The kaolinite was made monoionic by washing the clay several times with a normal chloride solution of a given cation then washing free of chloride with 95% alcohol. The clay was air-dried, crushed, and the 0.5–1.0 mm. aggregate fraction retained as the adsorbent. Prior to adsorption all samples were degassed at 68–70° for 24 hours, at 1×10^{-6} mm. pressure. Water was found to be reversibly adsorbed on Li-kaolinite when outgassed at this temperature.² In regards to Ca-kaolinite the choice of this outgassing temperature is rather arbitrary. Previous studies suggested that at 70° adsorption of water is at an apparent maximum, but because of the complicating factors of particle coalescence and possible dehydroxylation of the mineral at higher tem-

peratures the exact hydrated state of the calcium ion cannot be fully defined. For purposes of comparison, the outgassing temperature of Ba-kaolinite also was chosen at 70°.

The adsorption apparatus and technique have been previously described.² Isotherms were obtained at $29.45 \pm 0.05^\circ$ and $15.30 \pm .15^\circ$. The adsorption data for a given monoionic sample at each temperature represent the composite of data for 3 or 4 independent adsorption cycles.

Calculations.—The differential free energy, enthalpy and entropy of adsorption are calculated for an isothermal transfer of one mole of adsorbate from its standard state, at 760 mm., to a surface which exists at various coverages.^{6,7} The Clausius-Clapeyron equation was used to calculate the differential (isosteric) heat, ΔH ; the differential entropy, ΔS , of adsorption is calculated by its well known relation to ΔF and ΔH . An attempt to separate the ΔH of cation hydration from the energetics of surface adsorption was made by handling the adsorption data in a novel manner. At a given temperature and equilibrium pressure the amount of water adsorbed by lithium kaolinite was subtracted from the water adsorbed by a hydrated system, *i.e.*, Ca- or Ba-kaolinite. The water adsorption difference was found at the two adsorption temperatures and the Clausius-Clapeyron equation was applied holding the water adsorption difference constant. The differential enthalpies calculated in this manner are plotted against W/W_m , and can be compared with the ΔH of adsorption.

Results

Figure 1 shows the adsorption of water by the monoionic systems at the two temperatures used in the study. It was noted that at low pressures the adsorption of water by Ca- and Ba-kaolinite was similar. Figures 2 and 3 show the ΔH and ΔS values for the adsorption of water by the monoionic kaolinites. The thermodynamics values refer to the defined process and are plotted relative to the reference Li-kaolinite surface. The apparent heats of hydration of adsorbed Ba and Ca ions are shown in Fig. 4 and also are plotted against surface coverage relative to Li-kaolinite.

Discussion

Data in Fig. 1 show the cation effect on the adsorption of water by Ca and Ba systems. As the relative pressure reached approximately 0.04 the cation effect became evident in the expected manner. Assuming that Li-kaolinite can be re-

(1) Support of this work by a grant (NSF-G10228) from the National Science Foundation is gratefully acknowledged.

(2) J. J. Jurinak, *J. Phys. Chem.*, **65**, 62 (1961).

(3) J. J. Jurinak and D. H. Volman, *ibid.*, **65**, 150 (1961).

(4) J. W. Ross and R. J. Good, *ibid.*, **60**, 1167 (1956).

(5) R. T. Martin, Paper presented at 8th National Clay Conference, Norman, Oklahoma, 1959.

(6) C. Kimball and E. K. Rideal, *Proc. Roy. Soc. (London)*, **A187**, 53 (1946).

(7) D. H. Everett, *Trans. Faraday Soc.*, **46**, 942 (1950).

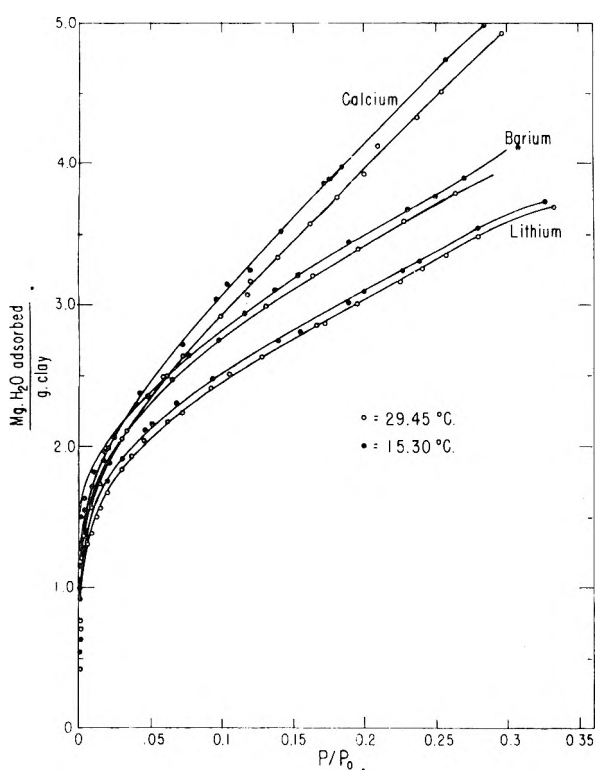


Fig. 1.—The adsorption of water vapor by monoionic kaolinite at the designated temperatures. The Li-kaolinite data have been reported previously.³

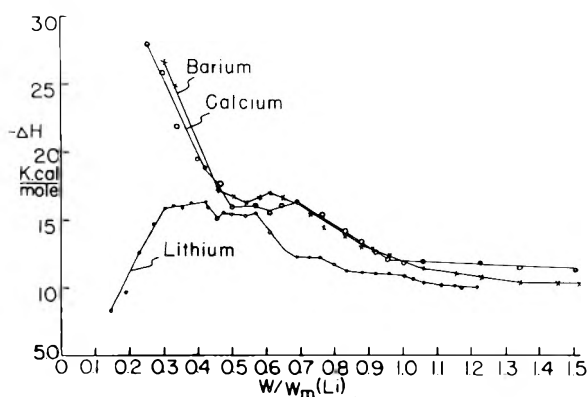


Fig. 2.—The ΔH of water adsorption by Ca- and Ba-kaolinite, at $T = 296^\circ\text{K}$., using Li-kaolinite as the reference surface. The Li-kaolinite data have been reported³ previously.

garded as a reference surface and that the exchangeable cation does not alter the surface area^{8,9} during the adsorption of water, the amount of water associated with each cation was calculated by using the BET equation and subtracting the water adsorbed by Li-kaolinite. The calculations indicate that in the completion of the monolayer each calcium ion coordinated 6.5 water molecules while each barium ion coordinated 2.7 molecules. The interaction of 6.5 water molecules with each Ca ion is in fair agreement with the data of Hendricks, Nelson and Alexander¹⁰ and Mering¹¹ who

(8) A. G. Keenan, R. W. Mooney and L. A. Wood, *J. Phys. Colloid Chem.*, **55**, 1462 (1951).

(9) J. J. Jurinak and D. H. Volman, *ibid.*, **63**, 1373 (1959).

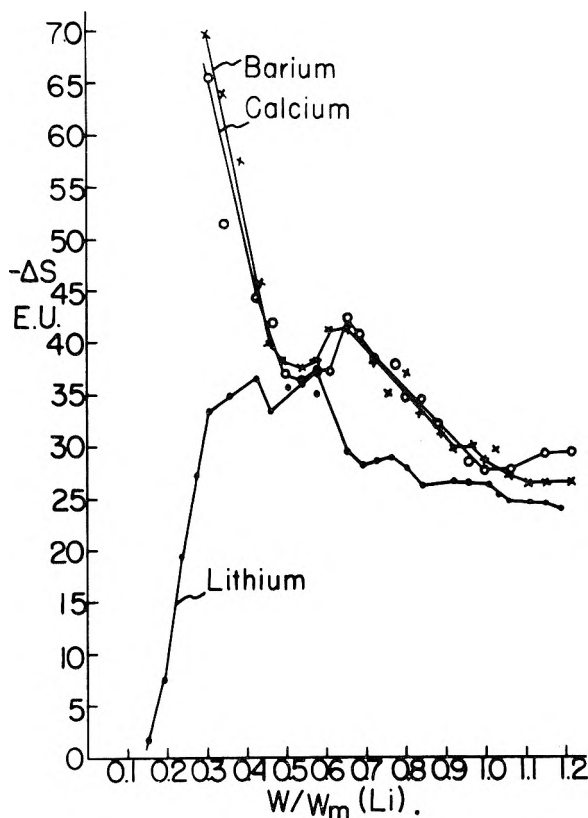


Fig. 3.—The ΔS of water adsorption by Ca- and Ba-kaolinite at $T = 296^\circ\text{K}$., using Li-kaolinite as the reference surface. The Li-kaolinite data have been reported previously.³

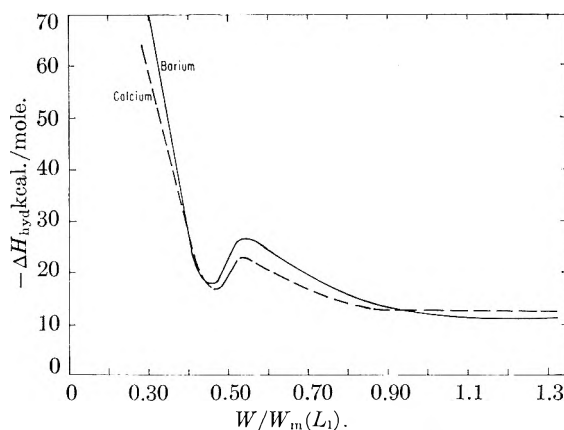


Fig. 4.—The apparent differential enthalpy of adsorbed Ba and Ca ion hydration calculated from adsorption data as described.

both using different techniques estimated that each Ca ion adsorbed on montmorillonite was initially associated with 6 water molecules. Considerable disagreement is found with the data of Keenan, Mooney and Wood⁸ who reported that at the formation of the water monolayer on kaolinite an average of 10 water molecules were associated with each exchangeable Ca ion and 4.7 molecules associated with each Ba ion. However, if the ratio of water oriented by Ca to the water

(10) S. B. Hendricks, R. A. Nelson and L. T. Alexander, *J. Am. Chem. Soc.*, **62**, 1457 (1940).

(11) J. Mering, *Trans. Faraday Soc.*, **42B**, 205 (1946).

oriented by Ba can be used as an index of relative attracting strength, their data result in a ratio value of 2.2, which is close to the ratio of 2.4 calculated from the data of the present study.

The differential enthalpies and entropies of water adsorption by Ca- and Ba-kaolinite are compared with Li-kaolinite in Fig. 2 and 3. All functions are plotted against W/W_m where W_m is based on the amount of adsorbate required for the development of the monolayer on Li-kaolinite. All curves are thus plotted relative to the defined reference surface. It should be noted that if the convention were allowed to plot the ΔH and ΔS values for Ca- and Ba-kaolinite against their respective W_m values the thermodynamic values for all monoionic systems studied would be very similar over the major portion of the monolayer region. The hydration effect would be restricted mainly to the coverage region <0.30 . The use of the W_m of Li-kaolinite as the base amplifies the cation hydration effect since the data are compared to a kaolinite surface apparently free from cation hydration effects. Using $W_m(\text{Li})$ as the base a marked effect of cation hydration on the energetics of water adsorption is noted at all coverages but particularly at $W/W_m(\text{Li})$ less than 0.40. The ΔH and ΔS curves of calcium and barium kaolinite over most of the surface are coincident and the differences observed between the two hydrated cations in the initial portions of the ΔH and ΔS curves are considered mainly due to the lack of precision in the low pressure region. Thus the expected initial difference in water affinity between Ba and Ca ions must be manifested in the $W/W_m(\text{Li})$ region below 0.30.

Thermodynamic data of *n*-butane adsorption by Li-kaolinite³ showed heterogeneity effects occurring over the initial 10% of the surface and it appears reasonable to assume that this effect is mainly the result of adsorption on the edges of kaolinite particles. All thermodynamic data for water adsorption are thus regarded as being primarily the result of adsorption on the planar surfaces of the clay.

Although a mechanistic interpretation based on thermodynamic data is limited, the present data allow speculation concerning the effect of cation hydration on the 2-dimensional orientation which is observed during the adsorption of water by Li-kaolinite. Since edges have been shown to represent only about 10% of the total surface of the kaolinite used, the dominating effect of hydration on the thermodynamic data throughout the monolayer region suggests that cation exchange sites could well exist both on the planar surfaces as well as edges, thus supporting the contention of isomorphous substitution in the kaolinite lattice.¹² The question as to whether the 2-dimensional network adsorbed water, noted on Li-kaolinite,³ is disrupted as the cations orient water molecules or whether the cations serve to tighten up the surface network cannot be resolved definitely from the data obtained. The ΔS values only suggest that the surface water configuration in the presence of a hy-

dratable cation is more ordered than the configuration based on water interaction alone. Comparison of the initial experimental ΔS values of 65–70 e.u. for the Ca and Ba systems with the third law entropy, $S_{298}^0 = 45.1$ e.u.¹³ of water suggests chemisorption. The initial ΔH values of approximately 30 kcal. support this view. Indeed, $W/W_m(\text{Li})$ has to increase to 0.80 or 0.90 before the ΔS values decrease to 34.5 e.u., the translational contribution to the total entropy of water, as calculated by the Sackur–Tetrode equation. The limited ΔS and ΔH data obtained beyond the monolayer region do provide some differentiation between the Ca and Ba ions. Comparing the ΔS values with $\Delta S_{\text{vap}}^0 = 28.4$ e.u. at 298°K.,¹⁴ it is observed that the water associated with the Ca ion is more restricted whereas the water associated with the Ba ion is less restricted than liquid water. These data suggest that the Ca ion exerts its influence through a greater thickness of adsorbed water, a result which is not unexpected because of the stronger hydration tendencies of calcium. Another possible explanation is suggested by the ion hydration concepts of Frank and Wen.¹⁵ Using their approach, the ionic size of Ba would be considered large enough to produce a zone of structure breaking beyond the initial zone of water orientation, thus resulting in an increase in entropy as the film thickens. This concept also predicts that the calcium ion is small enough to be considered a net structure-former, hence, the lower entropy of adsorbed water in the calcium system as the film thickens. The ionic radii of Ba and Ca ions are 1.35 and 0.99 Å.,¹⁶ respectively.

Figure 4 shows the apparent heat of hydration, ΔH_{hyd} of Ba and Ca adsorbed on kaolinite. This calculation is based on water-ion interaction after surface effects are removed from the data. The ΔH_{hyd} values may be regarded as the maximum value one may obtain for the ΔH of water adsorption in the systems studied. Since the exchangeable cation also satisfies the charge deficiency of the clay, the ΔH of adsorption is expected to be lower than ΔH_{hyd} , as the data indicated. Because of the similarity in adsorptive characteristics of the Ba and Ca systems, the ΔH_{hyd} values are also parallel. The heat of hydration of Ca and Ba ions, assuming a coordination number of six, according to Bernal and Fowler¹⁷ is 410 and 350 kcal./g. ion. If these values are converted to a mole of water basis as are the adsorption data, the heats of hydration are about 68 and 60 kcal./g. ion for Ca and Ba, respectively. Thus the apparent ΔH_{hyd} values at low coverages result in reasonable values if ion hydration is the major mechanism. It is interesting to note that beyond the monolayer the ΔH_{hyd} of both Ca- and Ba-kaolinite closely approaches the experimental ΔH of adsorption values. These data suggest that forces emanating from the kao-

(13) A. R. Gordon, *J. Chem. Phys.*, **2**, 65 (1934).

(14) D. D. Wagman, J. E. Kilpatrick, W. J. Taylor, K. S. Pitzer and F. D. Rossini, *J. Research Natl. Bur. Standards*, **34**, 1-3 (1945).

(15) H. S. Frank and Wen-Yang Wen, *Discussions Faraday Soc.*, **24**, 133 (1957).

(16) L. Pauling, "The Nature of the Chemical Bond," Cornell University Press, Ithaca, N. Y., 1948, p. 346.

(17) J. D. Bernal and R. H. Fowler, *J. Chem. Phys.*, **1**, 515 (1933).

(12) G. H. Cashen, *Trans. Faraday Soc.*, **55**, 477 (1959).

linate surface do not extend much beyond the monolayer and that the adsorbed cation plays the dominate role in influencing water interaction as the water film thickens.

ACTINIDE(IV) CHLORIDE SPECIES ABSORBED BY ANION EXCHANGE RESINS FROM CHLORIDE SOLUTIONS¹

By J. L. RYAN

Hanford Laboratories Operation, General Electric Company, Richland, Washington

Received April 10, 1961

Spectrophotometric studies of anion-exchange resins, of solid crystalline salts, and of non-aqueous solutions were used to identify the tetravalent actinide chloride species absorbed by anion-exchange resins. The absorbed species were found to be UCl_6^- , NpCl_6^- and PuCl_6^- when the resin was loaded from either hydrochloric acid or lithium chloride solutions. An attempt was made to determine the degree of formation of the hexachloro complexes in concentrated hydrochloric acid.

Anion-exchange resins have been shown to absorb uranium(IV), neptunium(IV), and plutonium(IV) from concentrated hydrochloric acid solutions,²⁻⁴ and this absorption has been used as the basis for various separation procedures. Previous work has shown that the complex anion species absorbed by anion-exchange resins can be identified by spectrophotometric studies of the resin phase and of non-aqueous solutions and solid crystalline salts of the complex anions.^{5,6} Uranium(IV) and plutonium(IV) are known to form salts of the type M_2UCl_6 and M_2PuCl_6 , respectively, where M is a large monovalent cation. The salts Cs_2UCl_6 , $[(\text{CH}_3)_4\text{N}]_2\text{UCl}_6$ and $[(\text{C}_2\text{H}_5)_4\text{N}]_2\text{UCl}_6$ were reported by Dieke and Duncan.⁷ Anderson prepared and identified Cs_2PuCl_6 , $[(\text{CH}_3)_4\text{N}]_2\text{PuCl}_6$ and others.⁸ Ferraro has reviewed the preparation of the cesium, tetramethylammonium and tetraethylammonium U(IV) salts and has shown that they do not form hydrates.⁵ Crystallographic studies of Cs_2PuCl_6 ,¹⁰ Cs_2UCl_6 ,¹¹ and of the tetramethylammonium and tetraethylammonium salts of U(IV) and Pu(IV)¹² have shown that the actinide ions are octahedrally coordinated to six chlorides in the crystal. The purpose of this paper is to compare the absorption spectra of crystalline salts known to contain the hexachloro anion and the absorption spectra of non-aqueous solutions of some of these salts with the absorption spectra of anion-exchange resins loaded with the quadrivalent actinides from chloride media, and thus identify the species absorbed by the anion-exchange resins.

(1) This paper is based on work performed under Contract No. AT(45-1)-1350 for the United States Atomic Energy Commission.

(2) K. A. Kraus and F. Nelson, "Proc. Intern. Conf. Peaceful Uses Atomic Energy, Geneva, 1955," Vol. VII, p. 113, 1956.

(3) L. Wish, *Anal. Chem.*, **31**, 326 (1959).

(4) F. Nelson, K. A. Kraus, H. O. Phillips and Y. Marcus, in Oak Ridge National Laboratory Chemistry Division Annual Progress Report, ORNL-2584, Period ending June 20, 1958, pp. 58-60.

(5) J. L. Ryan, *J. Phys. Chem.*, **64**, 1375 (1960).

(6) J. L. Ryan, *ibid.*, **65**, 1099 (1961).

(7) G. H. Dieke and A. B. F. Duncan, "Spectroscopic Properties of Uranium Compounds," McGraw-Hill Book Co., Inc., New York, N. Y., 1949, pp. 147-148.

(8) H. H. Anderson, "The Transuranium Elements," Division IV, Vol. 14B, paper 6.13, McGraw-Hill Book Co., Inc., New York, N. Y., 1949, p. 793.

(9) J. R. Ferraro, *J. Inorg. & Nuclear Chem.*, **4**, 283 (1957).

(10) W. H. Zachariasen, *Acta Cryst.*, **1**, 268 (1948).

(11) S. Siegel, *ibid.*, **9**, 827 (1956).

(12) E. Staritzky and J. Singer, *ibid.*, **5**, 536 (1952).

Experimental

Preparation of Actinide(IV) Chloride Stock Solutions.—Uranium trioxide, which had been prepared by ignition of uranyl nitrate, was used as source material for preparation of uranium(IV) chloride solutions. The trioxide was dissolved in concentrated hydrochloric acid, taken to dryness, and redissolved in concentrated hydrochloric acid. The uranium then was reduced to the (IV) state with aluminum metal. Aluminum was chosen since it does not yield double chlorides with cesium or quaternary ammonium chlorides and does not absorb on anion-exchange resin from hydrochloric acid. After reduction with aluminum the uranium was loaded onto a column of Dowex 1, X-4 (50 to 100 mesh) anion-exchange resin. The column was washed with 12 M HCl to remove aluminum and the U(IV) then was eluted with 4 M HCl. At this concentration U(VI) is still rather strongly held by the resin.² Uranium(IV) solutions were made up in this manner immediately before using to minimize air oxidation.

Anion-exchange purified plutonium nitrate^{13,14} and neptunium nitrate¹⁵ were used as source materials for the preparation of plutonium(IV) and neptunium(IV) chloride solutions. The neptunium was isotopically pure Np^{237} and contained about 0.01 weight % plutonium. Both the neptunium and plutonium could be expected from past experience^{13,14} to contain other impurities to the extent of less than 100 parts per million parts of plutonium or neptunium.

Plutonium(IV) nitrate was loaded onto anion-exchange resin at 60° from 7 M HNO_3 . The resin then was washed extensively with 12 M HCl at 25°, completely converting the green $\text{Pu}(\text{NO}_3)_6^-$ ion on the resin to the yellow chloro complex. During elution with 0.5 M HCl, considerable disproportionation of Pu(IV) occurs. This is due to the fact that both Pu(IV) and Pu(VI) absorb on the resin from hydrochloric acid and Pu(III) does not, thus allowing the Pu(VI) and Pu(III) to form separate elution bands. The product was adjusted to about 6 M HCl to promote re-conversion to Pu(IV).

Neptunium nitrate was loaded onto anion-exchange resin from 7 M HNO_3 -0.1 M semicarbazide.¹⁴ During conversion to the chloride form by washing with 12 M HCl-0.2 M semicarbazide at 25°, considerable gassing occurred while the bulk of the nitrate was being removed. After conversion to the chloride form, the column was washed with 12 M HCl to remove semicarbazide and was eluted with 2 M HCl. The product was spectrophotometrically pure Np(IV).

Preparation of Quaternary Ammonium Chlorides.—Tetraethylammonium chloride was prepared from Eastman tetraethylammonium bromide by conversion to the hy-

(13) J. L. Ryan and E. J. Wheelwright, *Ind. Eng. Chem.*, **51**, 60 (1958).

(14) J. L. Ryan and E. J. Wheelwright, Atomic Energy Commission Research and Development Report, HW-55893 (Hanford Laboratories), Jan. 2, 1959.

(15) J. L. Ryan, Atomic Energy Commission Research and Development Report, HW-59193 REV (Hanford Laboratories), Sept. 3, 1959.

droxide by anion exchange followed by neutralization of the hydroxide with hydrochloric acid. The solution was thermally evaporated and the salt finally dried at 90° and 20 mm. pressure. Tetra-*n*-propylammonium chloride was prepared in the same manner from Eastman tetra-*n*-propylammonium iodide but was not dried.

Preparation of Hexachloro Actinide(IV) Salts.—The salts $[(C_2H_5)_4N]_2UCl_6$, $[(C_2H_5)_4N]_2NpCl_6$ and $[(C_2H_5)_4N]_2PuCl_6$ were prepared by adding tetraethylammonium chloride in 12 *M* HCl to the respective actinide(IV) stock solutions adjusted to 8–12 *M* HCl. The salts were normally dried over solid sodium hydroxide and magnesium perchlorate but also could be washed with acetone and dried under a heat lamp. No tendency toward oxidation of the uranium salt was observed either during drying or upon long exposure of the dry salt to air. Although both $[(C_2H_5)_4N]_2UCl_6$ and $[(C_2H_5)_4N]_2PuCl_6$ were reported previously,^{7,12} analyses were performed on all three salts. Metal analyses were in all cases by controlled potential coulometric titration.

Anal. Calcd. for $[(C_2H_5)_4N]_2UCl_6$: U, 33.5; Cl, 29.9. Found: U, 33.6; Cl, 29.4.

Anal. Calcd. for $[(C_2H_5)_4N]_2NpCl_6$: Np, 33.4. Found: Np, 33.0.

Anal. Calcd. for $[(C_2H_5)_4N]_2PuCl_6$: Pu, 33.6. Found: Pu, 32.9.

The salts Cs_2UCl_6 , $[(CH_3)_4N]_2UCl_6$, $[(C_2H_7)_4N]_2UCl_6$ and $[(C_2H_7)_4N]_2PuCl_6$ also were prepared but were not analyzed. The first two of these have been previously reported⁷ and are well characterized.^{12,11,9}

Spectrophotometric Measurements.—Spectrophotometric measurements were made with a Cary Model 14 recording spectrophotometer with cell compartment thermostated at 25° using matched 1.00 cm. silica cells for all solution and resin spectra. Solid spectra were obtained on mulls of the powdered compounds in petrolatum using calcium carbonate in petrolatum as blank. Cells for the solid spectra were either 1.00 cm. silica cells with 0.90 cm. silica inserts, or were silica or glass plates held apart by spacers of the appropriate thickness (about 0.1 cm.). Slit width was variable within the following limits: solution spectra, 0.02–0.1 mm.; Dowex 1, X-1 (50 to 100 mesh) spectra, 0.2–0.7 mm.; and mull spectra, 0.4–1.2 mm.

Nitromethane was Eastman spectro grade and was dried with Drierite (anhydrous $CaSO_4$). Uranium was determined on all solutions used in spectrophotometric studies by controlled potential coulometric titration. Neptunium and plutonium solutions were analyzed by α -counting.

Results and Discussions

The absorption spectrum of anion-exchange resin loaded with U(IV) from and in contact with 12 *M* HCl is compared with the absorption spectrum of solid $[(C_2H_5)_4N]_2UCl_6$ and with the spectrum of a solution of this salt in nitromethane in Fig. 1. The absorption spectrum of U(IV) in 12 *M* HCl is included for comparison. The absorption spectra of single crystals of Cs_2UCl_6 and $[(CH_3)_4N]_2UCl_6$ have been published by Gruen¹⁶ and these are essentially identical to the spectrum of the mull of the tetraethylammonium salt of Fig. 1. The spectrum of $[(C_2H_5)_4N]_2UCl_6$ in nitromethane is almost but not completely identical to the spectrum of the solid salt, indicating that the nitromethane solution contains principally the hexachloro complex. Addition of excess $(C_2H_5)_4NCl$ to a nitromethane solution of this salt has no effect on the spectrum indicating that no dissociation of the complex occurs in nitromethane. The slight differences in the spectra of the solid and the nitromethane solution can therefore be attributed to the markedly different environment of the hexachloro ion in the solid crystal and in the solution.

(16) D. M. Gruen and R. L. McBeth, *J. Inorg. & Nuclear Chem.*, **9**, 290 (1959).

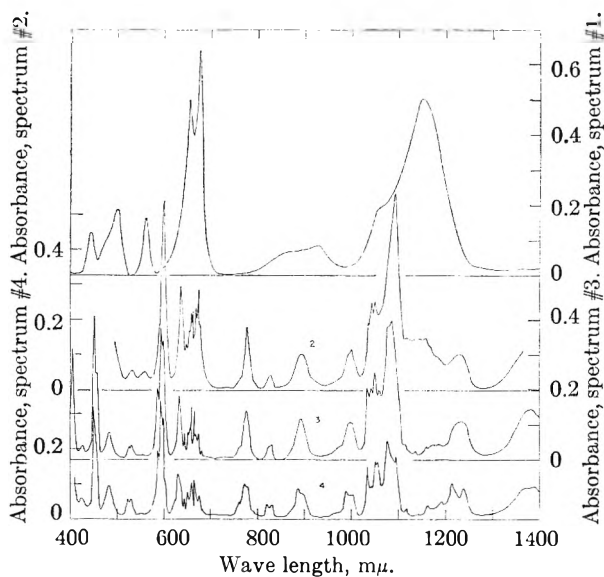


Fig. 1.—Absorption spectra of U(IV) chlorides: (1) 1.01×10^{-2} *M* U(IV) in 12 *M* HCl; (2) U(IV) loaded on Dowex 1, X-1 (50 to 100 mesh) anion-exchange resin from 12 *M* HCl; (3) 6.64×10^{-2} *M* $[(C_2H_5)_4N]_2UCl_6$ in nitromethane; (4) solid $[(C_2H_5)_4N]_2UCl_6$ mull in petrolatum.

Figure 1 shows that the absorption spectrum of U(IV) loaded on anion-exchange resin is that of the UCl_6^- ion. The somewhat high absorbance for the resin in the regions 640 to 680 $m\mu$ and 1100 to 1200 $m\mu$ compared to the spectrum of $[(C_2H_5)_4N]_2UCl_6$ is due to a small amount of U(IV) in the aqueous phase in equilibrium with the resin. (The molar extinction coefficients of U(IV) in 12 *M* HCl are in general much higher than those of the UCl_6^- ion, a fact particularly noticeable in the above noted wave length ranges.) Variation in resin crosslinkage, resin loading, and aqueous hydrochloric acid concentration had no effect on the resin spectrum when it was corrected for the contribution of the aqueous phase uranium. Resin loaded from lithium chloride has the same absorption spectrum as that loaded from hydrochloric acid. This indicates that in all cases UCl_6^- is the ion absorbed by the resin.

As seen in Fig. 1, the absorption spectrum of U(IV) in 12 *M* HCl differs markedly from that of the UCl_6^- ion. With the absorption spectrum of the pure UCl_6^- complex as obtained in nitromethane, it should be possible, by proper choice of wave lengths, to estimate the amount of hexachloro complex present in aqueous hydrochloric acid solutions of U(IV). This is seriously complicated, however, by the fact that the molar extinction coefficients of the hexachloro complex are generally much lower than those of U(IV) in hydrochloric acid. Thus in the range 400 to 1400 $m\mu$ the highest molar extinction coefficient for U(IV) in 12 *M* HCl is 10 times that for the highest molar extinction coefficient for UCl_6^- in this range. Because of this, it is only possible to set an upper limit for the amount of hexachloro complex in 12 *M* HCl. At 405 $m\mu$, U(IV) in concentrated hydrochloric has a relatively very low absorbance and the UCl_6^- ion has a relatively high absorption maximum. If it is assumed (1) that all of the absorbance in 12 *M*

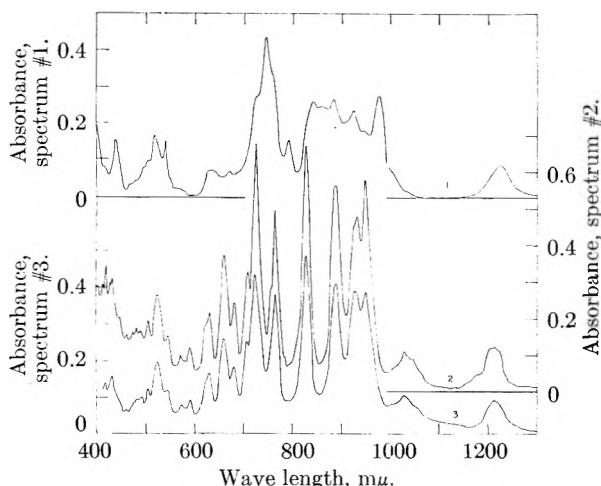


Fig. 2.—Absorption spectra of Np(IV) chlorides: (1) $6.58 \times 10^{-3} M$ Np(IV) in 12 *M* HCl; (2) $5.74 \times 10^{-2} M$ $[(C_2H_5)_4N]_2NpCl_6$ in nitromethane; (3) Np(IV) loaded on Dowex 1, X-1 (50 to 100 mesh) anion-exchange resin from 12 *M* HCl.

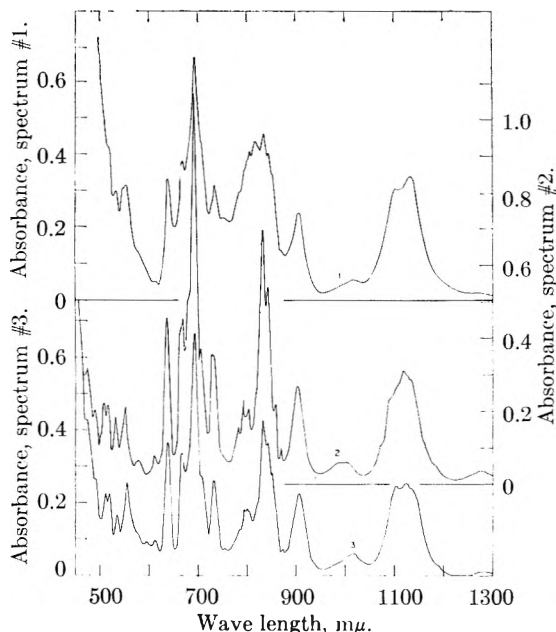


Fig. 3.—Absorption spectra of Pu(IV) chlorides: (1) $2.78 \times 10^{-2} M$ Pu(IV) in 12 *M* HCl; (2) $4.73 \times 10^{-2} M$ $[(C_2H_5)_4N]_2PuCl_6$ in nitromethane; (3) Pu(IV) loaded on Dowex 1, X-1 (50 to 100 mesh) anion-exchange resin from 12 *M* HCl.

HCl at this wave length is due to the hexachloro ion and (2) that the molar extinction coefficient of this complex at this wave length is the same as in nitromethane, then the upper limit for the amount of hexachloro complex present in 12 *M* HCl is about 13%. The amount actually present is probably considerably less.

Figure 2 shows the absorption spectra for Np(IV) loaded anion-exchange resin, Np(IV) in 12 *M* HCl, and $[(C_2H_5)_4N]_2NpCl_6$ in nitromethane. Figure 3 shows the corresponding spectra for Pu(IV). In both cases the resin absorbs the hexachloro complexes ($NpCl_6^-$ and $PuCl_6^-$). The absorption spectrum of solid $[(C_2H_5)_4N]_2NpCl_6$ was obtained and is essentially identical to the spectrum of this compound in nitromethane.

The same difficulty is encountered with neptunium as with uranium in attempting to calculate the amount of hexachloro complex present in hydrochloric acid solutions. In this system the highest molar extinction coefficient in the range 410–1400 $m\mu$ for Np(IV) in 12 *M* HCl is 5.6 times the highest value for $NpCl_6^-$ in nitromethane. The neptunium case is further complicated by the fact that no strong absorption occurs for $NpCl_6^-$ at any wave length where the absorbance of Np(IV) in concentrated hydrochloric acid is relatively weak. Examination of the 12 *M* HCl–Np(IV) spectrum at 827 $m\mu$, where the $NpCl_6^-$ ion has a strong absorption maximum, shows no evidence of a shoulder or inflection point. This would indicate a maximum of not more than 10 to 15% hexachloro complex present in 12 *M* HCl.

The spectrum of Pu(IV) in 12 *M* HCl shows considerable resemblance to that of $[(C_2H_5)_4N]_2PuCl_6$ in nitromethane. Also the maximum molar extinction coefficient in 12 *M* HCl in the range 500–1400 $m\mu$ is only about 5% higher than that of $PuCl_6^-$ in nitromethane, and occurs at the same wave length for both of these solutions. It thus appears that a considerable amount of the plutonium hexachloro complex may be present in 12 *M* HCl.

If the absorption spectra of solutions of Pu(IV) at lower hydrochloric acid concentrations are examined, it is found that the molar extinction coefficients increase at almost all wave lengths with decreasing hydrochloric acid concentration down to 8 *M* HCl. Thus no isosbestic points occur to indicate the number of species present.

The Pu(IV) hexachloro complex has an absorption maximum at 638 $m\mu$. This maximum is also found in solutions of plutonium(IV) in concentrated hydrochloric acid but decreases rapidly with decreasing acid concentration, disappearing completely at 8 *M* HCl. If it is assumed that the lower chloro complexes do not have absorption maxima at this wave length and that the molar extinction coefficient of the hexachloro complex is about the same in hydrochloric acid and nitromethane at this wave length, it is possible to estimate the amount of hexachloro complex present in hydrochloric acid solutions. Unfortunately, this estimate cannot be very accurate since the molar extinction coefficient or coefficients of lower species are not known. It appears, though, that in 12 *M* HCl, perhaps 75% of the Pu(IV) is present as the hexachloro complex and that in 9 *M* HCl only about 8% is present.

The greater tendency of Pu(IV) (as compared to U(IV) and Np(IV)) to form hexachloro complexes also is manifested in its higher distribution onto anion exchange resins from hydrochloric acid^{3,4} and in its higher distribution coefficients into tri-*n*-octylamine extractant than Np(IV) and U(IV).¹⁷

The solubilities of Cs_2UCl_6 and Cs_2PuCl_6 in varying hydrochloric acid concentrations have been reported.¹⁸ The solubility of Cs_2UCl_6 is 3.4 times as great in 12 *M* HCl as the solubility of Cs_2PuCl_6

(17) W. E. Keder, Hanford Laboratories, unpublished data.

(18) J. Kooi, E. Weisskopf and D. M. Gruen, *J. Inorg. & Nuclear Chem.*, **13**, 310 (1960).

and this difference becomes greater with decreasing hydrochloric acid concentration. If it is assumed that this difference is due mainly to the difference in the degree of complexing in the case of U(IV) and Pu(IV) and that the actual solubility products for the two salts are about the same, the amount of hexachloro complex in 12 *M* HCl would be about 40 times greater in the case of Pu(IV) than in the case of U(IV). This is in qualitative agreement with the spectrophotometric data presented here.

In lithium chloride the degree of chloride com-

plexing of Pu(IV) is considerably less than in hydrochloric acid. Thus in saturated lithium chloride (19.2 *m*) the same amount of chloro complexing (approximately 50% hexachloro) is observed as in 14 *m* HCl. Since for 19.2 *m* LiCl, $a_{\pm} = 1,100$ and for 14 *m* HCl, $a_{\pm} = 380$,¹⁹ the difference in chloro complexing in the two media cannot be explained by differences in mean ionic activity.

(19) R. A. Robinson and R. M. Stokes, "Electrolyte Solutions," Butterworth Scientific Publications, London, 1955.

ALUMINA: CATALYST AND SUPPORT. XII.¹ THE EFFECT OF INTRINSIC ACIDITY OF ALUMINAS UPON HYDROGEN-DEUTERIUM EXCHANGE

By HERMAN PINES AND JEAN RAVOIRE²

Ipatieff High Pressure and Catalytic Laboratory, Department of Chemistry, Northwestern University, Evanston, Ill.

Received April 17, 1961

The hydrogen-deuterium exchange on γ -alumina has been studied. The catalytic effect of the aluminas was correlated with the intrinsic acidity of the aluminas. Alumina prepared from aluminum isopropoxide and having relatively strong acid sites is about 60 times as active for the exchange reaction as an alumina catalyst prepared from sodium aluminate and containing less than 0.1% by weight of sodium. A mechanism for hydrogen-deuterium exchange is proposed.

Extensive studies carried out in our laboratory have revealed that alumina has intrinsic acidic properties, and that the strength of the acid sites depends upon the methods used for the preparation of the alumina.³ Alumina prepared by hydrolysis of aluminum isopropoxide catalyzed the isomerization of cyclohexene to methylcyclopentenes, whereas alumina prepared from potassium aluminate did not affect such isomerization. It also was demonstrated that aluminas of different intrinsic acidities exert a deep influence upon the isomerization of alkenes⁴ and dehydration of alcohols⁵; they also influence the catalytic properties of molybdena-alumina,⁶ chromia-alumina,^{7,8} and platinum-alumina⁹ catalysts.

The hydrogen-deuterium exchange over γ -aluminas has been reported by Holm and Blue¹⁰ and by Weller and Hindin.¹¹ These authors related the effects of pretreatments on the activity of aluminas for hydrogen-deuterium exchange. More recently Taylor and Kohn¹² have shown that ionizing radiations enhance the activity of γ -alumina for the same reaction. The purpose of the present paper is to determine the effect of the

intrinsic acidities of aluminas upon the rate of the exchange reaction between hydrogen and deuterium.

Experimental

1. **Apparatus and Procedure.**—The apparatus is similar to the one described by Hindin and Weller.¹¹ In the present system a magnetic pump was used for circulating the gases. The pump, as described by Watson,¹³ consists mainly of a glass piston (containing an iron core) moving forward and backward in a glass tube thanks to two selenoids energized by a d.c. current, switched electronically. The gas is drawn in and expelled through four valves. The reactants before reaching the catalyst passed through a coil which was made of one meter long tubing and which surrounded the chamber containing the catalyst. The reactor was surrounded either by a bath or by a furnace. The gases were circulated at a rate of about 40 cc. per second.

A mixture of hydrogen and deuterium was admitted into the reactor by expansion of the gases from a tube in which a certain pressure has been established by means of a mercury bulb. All the volumes being known, the pressure in the reactor could be established in a fraction of a second. The volume of the reactor was 176 cc. After the desired time about 4 cc. of gas at STP were withdrawn and analyzed by means of mass spectroscopy.

Before each set of experiments the reactor was filled with helium to about 200 mm. of pressure and kept in contact with the catalyst for about 0.5 hour, in order to bring the catalyst to the temperature of the bath or the furnace surrounding the reactor. Helium then was pumped out.

Electrolytic hydrogen was used, which was purified by passing it through a palladium catalyst, a liquid nitrogen trap, and finally through charcoal kept at liquid nitrogen temperature. Deuterium and helium used were of very high purity. Each of the gases was purified further by passing through activated charcoal maintained at the temperature of liquid nitrogen. An equimolar mixture of hydrogen and deuterium was used for the exchange studies.

2. **Catalysts.**—The catalysts were prepared according to the general method described previously.³

Catalyst A.—Aluminum isopropoxide was distilled twice and then hydrolyzed with distilled water. The precipitate of aluminum hydroxide was washed, filtered, dried at 120° for 72 hours, compressed and screened to obtain 8–10 mesh granules.

Catalyst B.—Aluminum turnings made from high purity

(1) For paper XI of this series see C. N. Pillai and H. Pines, *J. Am. Chem. Soc.*, **83**, 3274 (1961).

(2) Postdoctoral Fellow supported by a grant from the Petroleum Research Fund administered by the American Chemical Society. Grateful acknowledgment is hereby made to the donors of said Fund.

(3) H. Pines and W. O. Haag, *J. Am. Chem. Soc.*, **82**, 2471 (1960).

(4) W. O. Haag and H. Pines, *ibid.*, **82**, 2488 (1960).

(5) H. Pines and C. N. Pillai, *ibid.*, **82**, 2401 (1960).

(6) H. Pines and G. Benoy, *ibid.*, **82**, 2483 (1960).

(7) C. T. Chen, W. O. Haag and H. Pines, *Chem. and Ind. (London)*, 1374 (1959).

(8) H. Pines and C. T. Chen, *J. Org. Chem.*, **26**, 1057 (1961).

(9) H. Pines and T. W. Greenlee, *ibid.*, **26**, 1052 (1961).

(10) V. C. F. Holm and R. W. Blue, *Ind. Eng. Chem.*, **43**, 1506 (1951); **44**, 107 (1952).

(11) S. W. Weller and S. G. Hindin, *J. Phys. Chem.*, **60**, 1506 (1956).

(12) (a) E. H. Taylor and H. W. Kohn, *J. Am. Chem. Soc.*, **79**, 252 (1957); (b) H. W. Kohn and E. H. Taylor, *J. Phys. Chem.*, **63**, 500 (1959).

(13) J. S. Watson, *Can. J. Technol.*, **24**, 373 (1956).

aluminum bar, 99.99% pure, were dissolved in a solution of sodium hydroxide. The solution was neutralized with nitric acid, and alumina precipitated by passing carbon dioxide into the solution. The precipitate was washed eight times with distilled water, dried, compressed and screened, as indicated above.

Catalyst C.—The preparation was the same as that for B, but the precipitate was washed four times instead of eight times.

The catalysts were degassed and calcined under conditions specified in part C of Results.

The areas of the calcined catalysts as determined by adsorptions of nitrogen using the BET method were

Catalyst A, 304 m.²/g.; B, 280 m.²/g.; C, 283 m.²/g.

Results

a. **Definition of the Activity.**—The activity of the catalyst is given by the rate of exchange which can be correlated with the rate of formation of the HD molecules by the first-order law of isotopic exchange reactions.¹⁴ This relation takes the following form in the case of the reaction $H_2 + D_2 \rightleftharpoons 2HD$ (neglecting the kinetic isotope effect)

$$R = \frac{-\ln \left(1 - \frac{[HD]}{[HD]_{eq}} \right)}{2t}$$

in which R = rate of exchange; t = time; $[HD]$ = concentration in HD at the time t ; $[HD]_{eq}$ = concentration in HD at equilibrium.

The $[HD]_{eq}$ values at different temperatures were calculated from the reported data.¹⁵ It has been found more convenient to express the rate of exchange in atom-grams of hydrogen per gram of catalyst per minute multiplied by 10^5

$$k = R \frac{A}{W} 10^5$$

in which A is the number of moles of gas in the reactor; W is the weight of the catalyst.

It has been noticed that the activity of a freshly activated catalyst, tested by successive identical experiments, decreased with time, and then became constant. The ratio of k calculated from the first experiment to the k corresponding to the "steady state" was about 3 for catalyst A at -95° . At this temperature a time of contact of one minute was sufficient to reach a constant value of k . The deactivation effect decreased with increasing reaction temperature; at 300° with catalyst C the deactivation effect was not observed. The activity which will be reported in this paper will be the "Steady State" activity. Once the steady state is reached, the first-order law is always obeyed, which permits one to conclude that the circulation of the gas was not a rate-determining factor.

b. **Comparison of Catalytic Activity vs. Intrinsic Acidity.**—In line with observations reported by Weller and Hindin the activity of alumina catalysts depend upon the methods of pretreatment. It thus was found that catalyst A, which had been calcined at 700° for 4 hours, placed in contact with air at room temperature and then degassed at 280° for 16 hours at 10^{-3} mm. pressure, had a relative activity for hydrogen-deuterium exchange equal to $k = 1.4$ at C° and $p = 45$ mm.

(14) O. E. Myers and R. J. Prestwood, "Radioactivity Applied to Chemistry," ed. by A. C. Wahl and N. A. Bonner, John Wiley and Sons, Inc., 1951, New York, N. Y.

(15) H. C. Urey and D. Rittenberg, *J. Chem. Phys.*, **1**, 137 (1933).

pressure ($t = 2$ min., final $[HD] = 0.60$). The same catalyst however, degassed at 300° for 15 hours and then at 520° for 2 hours had an activity given by $k = 600$ at -95° ($t = 30''$, final $[HD] = 0.41$).

The difference in activity between catalyst A, which was prepared from aluminum isopropoxide and B and C, prepared from potassium aluminate is most striking. In the case of alumina A it was necessary to carry out the reaction at -95° in order to have a measurable rate with 0.176 g. of the catalyst; k was found to be equal to 600, as indicated above. Catalyst B and C were less active and therefore it was possible to measure the exchange reactions at 20° . The rates of reaction k , for catalysts B and C are given in Table I.

A comparison can be made between the activity of catalyst A and catalysts B and C by accepting $k = 30$ as an average value for catalysts B and C and by extrapolating k to -95° , taking 1 kcal. as the apparent activation energy. It thus was found that for catalysts B and C k is equal to 10 as compared with $k = 600$ for catalyst A.

No sharp differences can be detected between alumina B and C. The differences found are within an experimental error, the degassing not being a very reproducible operation.

TABLE I

RATE OF EXCHANGE BETWEEN HYDROGEN AND DEUTERIUM OVER ALUMINA B AND C

Hr. of degassing at				
$520^\circ, 10^{-3}$ mm.	24	46		
Alumina B: time, sec.	30	30		
Final [HD]	0.083	0.109		
k	19	26		
Alumina C: time, min.	1	30 sec.	1	3
Final [HD]	0.238	0.257	0.340	0.456
k	18	40	32	29

TABLE II

DETERMINATION OF THE ORDER OF HYDROGEN-DEUTERIUM EXCHANGE

Catalyst	Temp., °C.	Pressure, mm.	Time (" min.) (" sec.)	Final [HD]	k	n^a
A	-95	45	30"	0.41	600	0.6
			15"	0.19	1690	
			1'	.40	1640	
			30"	.40	550	
B	30	45	1'	.15	19	0.7
			30"	.07	16	
			40"	.05	95	
B	-23	45	2'	.19	14	0.6
			5'	.33	13	
			10'	.43	14	
			2'	.09	54	
			7'	.27	65	
			15'	.40	65	
			5'	.30	11	
C	300	45	10"	.25	101	0.7
			30"	.44	110	
			20"	.29	380	

^a n = order of reaction.

c. **Kinetic Data.**—The order of the exchange reaction between hydrogen and deuterium as a

function of pressure of 45 to 450 and 270 mm. has been found to be in the range between 0.6 and 0.7, regardless of whether catalysts A or B and C are used (Table II). The order with respect to the total pressure is defined by $k\alpha p^n$.

The activation energy at a pressure of 45 mm. had been found to be equal to 1.0 kcal./mole for alumina B between 25 and 100° and to 1.3 kcal./mole for alumina C between 26 and 300°. These values are lower than the 2.5 to 4.5 kcal./mole found by Weller and Hindin,¹ for an alumina prepared from aluminum isopropoxide and corresponding to our alumina A. This difference agrees with the compensation effect, catalyst B and C being less active.

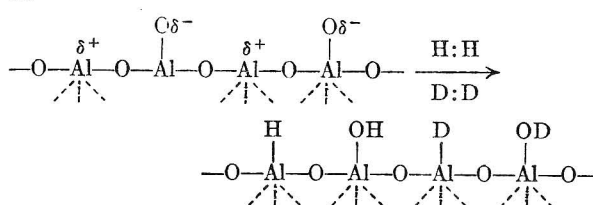
It should be noted however that our catalyst A is apparently more active than the one used by Hindin and Weller¹¹ since we can evaluate from their results (Table III, R , identical to their k , = 1,2), $k = 400$ at -78° and 380 mm. pressure, assuming that the weight of the catalyst is 0.2 g. This has to be compared with $k = 1640$ at -95° and 270 mm. pressure in the present work.

Discussion of Results

The experimental data show that there is a strong correlation between the activity of alumina for hydrogen-deuterium exchange and its intrinsic acidity. Alumina A which has the strongest acidic sites is 60 times as active as aluminas B and C in which some of the acidic sites were neutralized by sodium ions (0.1% wt. % of Na). It seems that Lewis acid sites are responsible for the catalytic action. It had been reported¹¹ that the exposure of the alumina to the action of traces of moisture lowers its catalytic activity. It also was shown² that exposure of alumina A to the humidity of the

atmosphere inhibits the development of color in the alumina to certain indicators like crystal violet leuko base or malachite green leuko base. All these phenomena give support to a heterolytic dissociation of hydrogen and deuterium gas, whereby a hydride ion is abstracted by the Lewis acid sites of the alumina.

The hydrogen-deuterium exchange on alumina can be presented schematically using for the surface of dehydrated alumina a model suggested by Hindin and Weller.¹⁶ The hydrogen and deuterium molecules would be dissociated heterolytically in a way for the hydride or deuteride to be adsorbed on the incompletely coordinated aluminum ions on the surface (Lewis acid sites), while the proton or deuteron will then be preferentially adsorbed on the oxygen. This can be presented as



The desorption of the gases from the catalyst surface would lead to the formation of H_2 , D_2 and HD .

Moisture acts as poison for the hydrogen-deuterium exchange because the acidic sites of the aluminum surface will be covered with the hydroxy groups and thus will prevent the hydrides and deuterides to be adsorbed on the catalyst. Sodium hydroxide exerts a similar effect.

(16) S. G. Hindin and S. W. Weller, *J. Phys. Chem.*, **60**, 1501 (1956).

ETHANE RADIOLYSIS AT VERY LOW CONVERSION

BY KANG YANG AND PRESTON L. GANT

Radiation Laboratory, Continental Oil Company, Ponca City, Oklahoma

Received April 20, 1961

The γ -radiolysis of ethane was investigated at 60 cm., about 25° and at very low conversion. The major products were H_2 , $n-C_4H_{10}$, and C_2H_4 with initial yields of, respectively, 8.8, 2.2 and ~ 2 (molecules per 100 e.v. absorbed). These yields decreased sharply with increasing conversion. Ethylene and nitric oxide reduced the rate of hydrogen formation to the same limiting value. This result was interpreted to mean that both scavengers removed thermalized radicals but had no measurable effects on the yields from non-radical processes; then one of the scavengers, nitric oxide, was used to distinguish radical reactions from non-radical ones. Radical processes, essentially the same as those occurring in the mercury-sensitized photolysis of ethane, were entirely responsible for the decrease in the yields of H_2 , $n-C_4H_{10}$ and C_2H_4 : $C_2H_6 \rightsquigarrow H$ (1); $C_2H_6 \rightsquigarrow C_2H_4$ (2); $H + C_2H_6 \rightarrow H_2 + C_2H_5$ (4); $H + C_2H_4 \rightarrow C_2H_5$ (6); $C_2H_5 + C_2H_6 \rightarrow C_4H_{10}$ (7); or $C_2H_4 + C_2H_6$ (8). From the rate curves for H_2 and C_2H_4 , the rate constant ratio, k_6/k_4 was estimated to be 4.0×10^4 . This estimate agrees fairly well with the value of 2.5×10^4 for the same ratio recently determined by Back in an investigation of the mercury-sensitized photolysis of ethane. "Hot" ethyl radicals formed in (6) may undergo (7) or (8) prior to complete thermalization. The decrease in n -butane yield at higher conversion was explained through this "hot" radical effect. Decompositions of excited ethane ions and subsequent ion-molecule reactions were sufficient to account for the contributions from non-radical processes to the yields of H_2 , CH_4 and CH_3 , thus confirming earlier correlations between mass spectra and radiolysis data by Dorfman and Sauer. In connection with gas phase dosimetry, it was shown that the hydrogen yields in ethylene and propylene radiolysis give good reproducibility without elaborate purification and that these yields are independent of conversion. The use of these systems as secondary dosimetric standards is recommended particularly for gas phase radiolysis work at very low conversion.

Introduction

Recent investigation¹ of the radiolysis of gaseous saturated hydrocarbons at very low conversion

(1) R. A. Back and N. Miller, *Trans. Faraday Soc.*, **55**, 911 (1959).

revealed important facts. The G -values, molecules/100 e.v., for both saturated and unsaturated products decrease with increasing conversion. The proposed mechanism is that unsaturated prod-

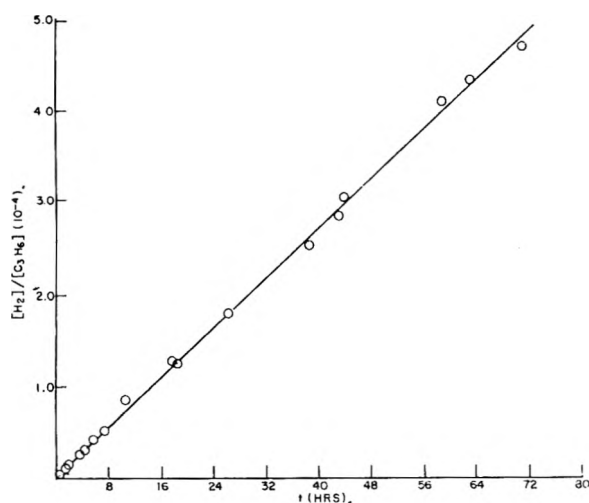


Fig. 1.—The formation of hydrogen in propylene radiolysis.

ucts disappear as a result of the scavenging of radicals that, otherwise, would end up as saturated products by undergoing hydrogen abstraction reactions.^{1,2}

In the case of ethane radiolysis, the initial value of $G(H_2)$ and the dependence of $G(H_2)$ on conversion have been reported previously.^{2,3} Corresponding data on other radiolysis products were needed to elucidate the mechanism of ethane radiolysis and also to ascertain the mechanism by which G -values decrease with increasing conversion, but such data were not available. The present investigation has provided this missing information together with more extensive data on the dependence of $G(H_2)$ on conversion.

Still another object of the present work was an experimental test of a prediction: If the decrease in G -values is totally attributable to the effect of the scavenging of radicals, then the molecular yields (the contribution to G -values from non-radical processes) should not depend on conversion. If so, various published results⁴ on the molecular yields measured at higher conversion can be relied upon as measuring the rates of primary processes. The present results on the systems $C_2H_6 + NO$, C_2H_4 and C_3H_6 confirm the prediction.

This work necessitated some improvement on conventional purification and analytical techniques. Bromine treatment together with low temperature gas-solid chromatography was required to obtain ethane with hydrocarbon impurities less than 10^{-4} mole %. For the determinations of very low concentrations of products ($\sim 10^{-3}$ mole %) a flame ionization detector with gas-solid chromatography was indispensable.

Experimental

Materials and Purification.—All hydrocarbons employed were Phillips' research grade. Nitric oxide with stated purity of 99% minimum was purchased from Matheson. Ethylene and propylene were degassed by repeated evacuation at liquid nitrogen temperature and then subjected to bulb-to-bulb distillations four times, each time retaining the middle third only. Nitric oxide was degassed similarly but subjected to the distillation only once.

The ethane contained about 10^{-3} mole % ethylene and methane not removable by the degassing and distillation. To eliminate the ethylene, Back's method was slightly modified.⁵ Ethane was allowed to stand for 24 hours at room temperature in a steel bomb containing activated charcoal treated with bromine. While the bomb was immersed in a Dry Ice-acetone bath, the ethane was transferred to an activated charcoal trap previously degassed by pumping for 24 hours at 450° . Liquid nitrogen was used for the transfer. By warming the trap, the ethane was allowed to distil very slowly. Head and tail portions of the distillate were discarded, and the middle third was retained. This bromine treatment reduced the concentration of ethylene to less than 10^{-4} mole %. To eliminate methane, a purification method based on low temperature selective adsorption was used. Molecular sieve (Linde, 13X, 30-60 mesh) in a spiral trap was degassed by pumping for 24 hours at 450° ; then the trap was saturated with the ethane at Dry Ice-acetone temperature and degassed by pumping for 10 minutes. The ethane recovered by warming up the column to room temperature contained less than 10^{-4} mole % methane.

The vacuum system employed in the purification of gases and the subsequent preparation of irradiation samples was completely free from mercury.

Dosimetry and Irradiation.—The γ -source was four spent fuel elements from the Materials Testing Reactor, Arco, Idaho. Relative amounts of energy absorption were measured with an air gap ionization chamber. In calibrating the ionization chamber, the methane dosimeter was not satisfactory because the $G(H_2)$ showed poor reproducibility. We have confirmed the presence of about 10^{-3} mole % ethylene in the methane purified by conventional degassing and distillation. This impurity seems to be the main reason for the lack of reproducibility.

In searching for a better secondary dosimeter that can be used in gas phase radiolysis at low conversion, we found that both ethylene and propylene give excellent results. Figure 1 shows that $G(H_2)$ in propylene radiolysis (60 cm.) is constant over a 100-fold change in irradiation time. An equally good straight line was obtained in ethylene radiolysis (60 cm. 0.5-48 hours). With the ethylene and propylene purified by the aforementioned method, the $G(H_2)$ values were reproducible with less than 2% average deviation. Ethylene and propylene purified by just degassing with no subsequent distillation gave essentially the same result.

For the present purpose, we assumed that $G(H_2)$ in ethylene radiolysis is 1.2^{6-8} and calculated energy absorption by irradiated samples on the basis of this value. It also was assumed that the energy absorbed by a molecule is proportional to the number of electrons in that molecule. In propylene radiolysis, the $G(H_2)$ was 1.1.

All irradiation data were obtained at a hydrocarbon pressure of 60 cm., at approximately 25° (the prevailing temperature of the pool water surrounding the γ -source), and at an energy input rate, \dot{E} , close to 3.95×10^{-4} e.v. per hour per molecule of ethane. When \dot{E} is expressed in this way, the rate of formation of a product in per cent. per hour divided by \dot{E} gives the G -value for that product directly. In some experiments, 6 cm. of nitric oxide were also added.

Analysis.—After irradiation, samples were connected to a chromatograph through breakoff seals. Chromatographic analyses were carried out under these conditions: H_2 determination; silica gel column, room temperature, argon carrier, thermistor detector as supplied from Perkin-Elmer modified by the addition of an amplifier to increase sensitivity about 20 times. CH_4 and C_2H_4 determinations; activated charcoal column, 125° , helium carrier, flame ionization detector. $n-C_4H_{10}$ determination; silica gel column, 78° , helium carrier, flame ionization detector.

For the determinations of H_2 , CH_4 and C_2H_4 , it was necessary to reverse the flow of the carrier gas at the end of each analysis, thus washing high boiling components out of the column; otherwise the retention times, hence the peak heights also, of the components changed in an uncontrollable manner. The charcoal column was well suited for the determination of low concentrations (10^{-3} mole %) of ethyl-

(5) R. A. Back, *Can. J. Chem.*, **37**, 1834 (1959).

(6) M. C. Sauer, Jr., and L. M. Dorfman, Abstracts, 137th Meeting Am. Chem. Soc., April 1, 1960.

(7) F. W. Lampe, *Radiation Research*, **10**, 691 (1959).

(8) We express our appreciation to the referee who informed us of this more recent value.

(2) R. A. Back, *J. Phys. Chem.*, **64**, 124 (1960).

(3) K. Yang, *Can. J. Chem.*, **38**, 1234 (1960).

(4) For example, see L. M. Dorfman and M. C. Sauer, Jr., *J. Chem. Phys.*, **32**, 1886 (1960).

ene in ethane. In this column ethylene comes off before ethane, and the large ethane peak does not interfere with ethylene determination. Methane and nitric oxide came off the charcoal column close together. The flame ionization detector, however, does not respond to nitric oxide; consequently the present analysis was much more accurate than the previous investigation in which a thermistor detector⁹ was employed.

For the calibration of the chromatographic apparatus, samples of ethane with known concentrations (10^{-3} – $10^{-2}\%$) of H_2 , CH_4 , C_2H_4 and C_4H_{10} were prepared by pressure measurements. In these concentration ranges, the responses of both thermistor and flame ionization detector were linear.

Results

Table I summarizes the G -values for H_2 , CH_4 , C_2H_4 and $n-C_4H_{10}$ determined from the initial rates. Except for $G(CH_4)$, all values are much higher than the values estimated at higher conversions.^{9,10} The high yield of ethylene (~ 2) is particularly noteworthy because the formation of this compound seemed negligible at higher conversions.

TABLE I

THE G -VALUES IN ETHANE RADIOLYSIS			
H_2	CH_4	$n-C_4H_{10}$	C_2H_4
8.8	0.39	2.5	~ 2 .

TABLE II

THE $G(H_2)$ VALUES IN ETHANE RADIOLYSIS				
	$G(H_2)$ Total	$G(H_2)$ Radical contribution	$G(H_2)$ Molecular contribution	Radical contribution, %
Back's ^a	8.9	5.6	3.3	63
Our's ^b	8.8	5.6	3.2	64

^a Ethylene as a scavenger. ^b Nitric oxide as a scavenger.

Acetylene (~ 0.2) and propane (~ 0.8) also were detected. For reasons not yet known, we could not reproduce the calibration factor for the acetylene chromatographic peak. The determination of propane was uncertain due to the tailing of the large ethane peak. Because of these difficulties and the fact that the information is not indispensable for the present purpose, we did not investigate further the formations of acetylene and propane.

In discussing the radiolysis mechanism, it is convenient to divide the G -values for H_2 , CH_4 and $n-C_4H_{10}$ into two parts: Molecular yields, $G(X)_M$, estimated from the rates in the presence of nitric oxide and radical yields, $G(X)_R$, which are equal to total yields minus molecular yields. In later discussion justification for these terms will be given.

Figure 2 shows the dependence of radical yields on conversion: $G(CH_4)_R$ did not decrease measurably, but radical yields for H_2 and $n-C_4H_{10}$ sharply decreased with increasing conversion. Figure 3 summarizes the molecular yields as functions of time and shows that all molecular yields were independent of conversion. In Fig. 4, the formation of ethylene in scavenger-free radiolysis is plotted for different irradiation times. The rate sharply decreases with conversion, and the concentration of ethylene rapidly approaches a steady state value of 2.3×10^{-3} mole %. In the inhibited system, nitric oxide prevents the removal of ethylene; and ethylene concentration increases linearly throughout the experiments (Figs. 3 and 4).

(9) K. Yang and P. J. Manno, *J. Am. Chem. Soc.*, **81**, 3507 (1959).

(10) For a review, see B. M. Tolbert and R. M. Lemmon, *Radiation Research*, **3**, 52 (1955).

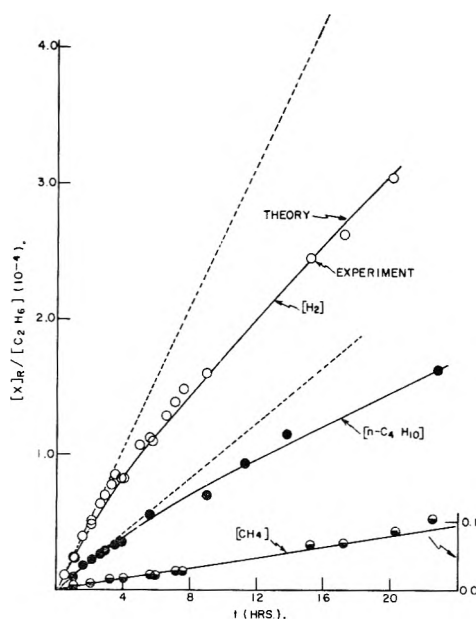


Fig. 2.—The formation of products by radical processes in ethane radiolysis.

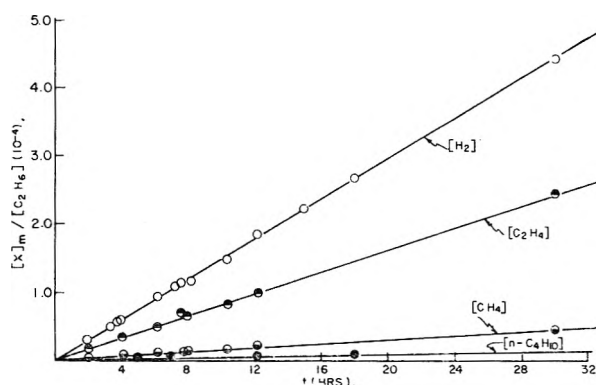


Fig. 3.—The formation of products by non-radical processes in ethane radiolysis.

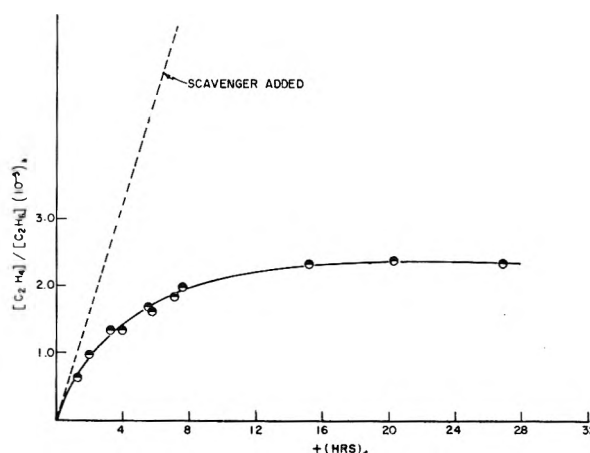


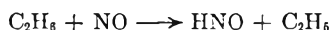
Fig. 4.—The formation of ethylene in the scavenger-free radiolysis of ethane.

The only published data that can be compared with the present result are those of Back² in which the formations of hydrogen in ethane and propane radiolyses were investigated at very low conversion and in the presence and absence of a scavenger,

ethylene. The two sets of data are compared in Table II. In preparing this table, Back's results, originally given as relative rates, were recalculated to give a $G(\text{H}_2)$ of 1.2 in ethylene radiolysis; and the $G(\text{H}_2)$ values in the $\text{NO} + \text{C}_2\text{H}_6$ system were calculated on the basis of 100 e.v. absorbed by ethane alone. The two sets of data agree very well.

Discussion

Molecular and Radical Processes.—As shown in Table II, nitric oxide and ethylene give the same $G(\text{H}_2)_M$. The same limiting rate with different scavengers has been observed also in the thermal decomposition of hydrocarbons.¹¹ This was interpreted as showing the molecular nature of the inhibited reaction. Recently, an alternative mechanism has been proposed showing how the reactions that proceed in the presence of adequate inhibitor and lead to the limiting values of the rate of hydrogen formation in thermal decomposition could still be radical reactions.¹² According to this mechanism, nitric oxide not only inhibits but also initiates radical reactions



The activation energy for the over-all process was estimated as 75 kcal. Isotope mixing in thermal decomposition in the system, $\text{C}_4\text{H}_{10} + \text{C}_4\text{D}_{10}$, seems not incompatible with the above mechanisms.¹³ If an attempt is made, however, to apply the mechanism to the present investigation, in which radiolysis was carried out at room temperature, one encounters a difficulty. Processes with activation energies of 75 kcal. are not likely to proceed with measurable rates at room temperature. To confirm this further, we prepared samples of $\text{NO} + \text{C}_2\text{H}_6$ and allowed them to stand for 7 days in the absence of a radiation field. Hydrogen was not detectable ($<10^{-3}\%$) in the resulting samples. One could assume that excited nitric oxide molecules (charged or neutral) were formed as a result of absorption of γ -energy or by the processes of energy transfer from ethane to nitric oxide and that the reactions involving these excited molecules might have lower activation energies. If so, one would obtain a rate depending both on the nature and the concentration of inhibitor, which is certainly not the case.¹⁴ We believe that the most probable explanation for the results in Table II is that both inhibitors prevent reactions in which thermalized radicals participate but have no measurable effect on the yields from non-radical processes. In the following, Figs. 1 and 2 are interpreted in the light of this conclusion.

Radical Processes.—For the mechanism for radical processes, we consider the reactions

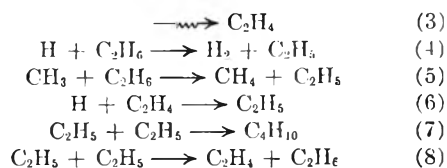


(11) F. J. Stubbs and C. Hinshelwood, *Proc. Roy. Soc. (London)*, **A200**, 458 (1950).

(12) B. W. Wojciechowski and K. J. Laidler, *Can. J. Chem.*, **38**, 1027 (1960).

(13) A. Kupperman and J. G. Larson, *J. Chem. Phys.*, **33**, 1264 (1960).

(14) For further discussion, see K. Yang, *J. Phys. Chem.*, **65**, 42 (1961).



With the exceptions of (2) and (5), these are essentially the same reactions that have been proposed in the mercury-sensitized photolysis⁵ of ethane. Ethane and ethylene compete for the hydrogen atoms resulting from (1), and the fraction of hydrogen atoms that undergoes reaction with ethane ends up as hydrogen molecules; hence

$$\frac{d}{dt} [\text{H}_2]_R = \frac{r_i}{1 + (k_6/k_4)([\text{C}_2\text{H}_4]/[\text{C}_2\text{H}_6])} \quad (\text{E-1})$$

The subscript R denotes the contribution of radical processes to the concentration; and r_i and k_i denote, respectively, the rate and rate constant of the i -th reaction. The r_i in (E-1) can be determined from the initial slope of the curve of $[\text{H}_2]_R$ vs. time (Fig. 2). To estimate k_6/k_4 , we consider the reactions at higher conversions in which both $d[\text{H}_2]_R/dt$ and $[\text{C}_2\text{H}_4]$ approach steady state values of, respectively, h and $[\text{C}_2\text{H}_4]_\infty$; then from (E-1)

$$\frac{k_6}{k_4} = \frac{[\text{C}_2\text{H}_6]}{[\text{C}_2\text{H}_4]_\infty} \frac{r_i - h}{h} \quad (\text{E-2})$$

From Figs. 2 and 4 and also using (E-2), we estimate $k_6/k_4 = 4.0 \times 10^4$. Back⁵ estimated the value 2.5×10^4 for the same ratio in the mercury-sensitized photolysis of ethane. The two values are probably in as good agreement as one can expect in such determinations. With the value 4.0×10^4 and also employing the experimental $[\text{C}_2\text{H}_4]$ as a function of time (Fig. 4), (E-1) was integrated (using an IBM 650 computer) to give a theoretical curve for $[\text{H}_2]_R$ vs. time. The experiment and theory are in good agreement, as shown in Fig. 4.

Available information^{15,16} on various rate constants suggests that, under the present experimental conditions, the reaction of methyl radicals with ethylene is negligible compared with (5); hence, in agreement with the experimental results, $G(\text{CH}_4)_R$ should not depend on conversion (Fig. 2).

It may appear that the decrease in $G(n\text{-C}_4\text{H}_{10})_R$ is due to the reaction



Using the recent value of $k_9/k_7^{1/2}$ reported by Lampe and Field,¹⁷ we estimated that under our experimental conditions the rate of (9) cannot exceed 6.7×10^{-4} times the rate of (7). Another possibility, that some ionic species attack n -butane, also can be eliminated, since the rate of formation of n -butane would then approach zero at high conversions in contradiction with the experimental results (Fig. 2).

As the most probable explanation, we consider a mechanism in which the "hot" ethyl radicals formed in (6) undergo recombination (7) and disproportionation (8) prior to complete thermalization. The ratio, k_8/k_7 , for the reactions with "hot"

(15) R. K. Brinton, *J. Chem. Phys.*, **29**, 781 (1958).

(16) A. F. Trotman-Dickenson, "Gas Kinetics," Butterworth's Scientific Publications, 1955.

(17) F. W. Lampe and F. H. Field, *Can. J. Chem.*, **37**, 995 (1959).

radicals is known to be higher than the ratio for the reactions involving only thermalized radicals.¹⁸ This "hot" radical effect persists to rather high pressure,¹⁸ and the high value of k_8/k_7 observed in the photolysis of ethane⁵ also was explained on this basis.

To establish the details of the proposed mechanism, we shall next consider the rate curves for H_2 , C_2H_4 and $n-C_4H_{10}$. The number of hydrogen molecules present in a sample after t hours of irradiation is equal to the number of hydrogen atoms formed by (1) minus the number that reacted with ethylene as shown in (6). The number of ethylene molecules removed from the system as a result of scavenging is equal to the number formed by (3) minus the number remaining in the system; hence

$$[H_2]_R = (r_1 - \alpha r_3)t + \alpha[C_2H_4] \quad (E-3)$$

The α in (E-3) is introduced to allow for the fact that some of the ethylene removed by scavenging is recovered by the disproportionation reaction (7). Let f be the fraction recovered; then clearly

$$\alpha = \frac{1}{1-f} \quad (E-4)$$

In general, α is a function of time; however, at higher conversions where $[C_2H_4]$ attains a steady-state value, $[C_2H_4]_\infty$, α may be considered as a constant also; (E-3) then suggests that the plot of $[H_2]_R$ vs. time should approach a straight line, the slope of which becomes $(r_1 - \alpha r_3)$, and the intercept at the $[H_2]_R$ axis equals $\alpha[C_2H_4]$. The slope and intercept gave, respectively, 1.6 and 1.8 for α . The average value, 1.7, is adopted in the subsequent discussion; hence f in (E-4) becomes 0.41; i.e., 41% of the ethylene is recovered by disproportionation.

According to the present mechanism, the number of ethylene molecules undergoing reaction (6) at high conversion is equal to the difference between $G(H_2)_R$ at low conversion and $G(H_2)_R$ at high conversion. The value estimated from Fig. 2 is 3.0 molecules per 100 e.v.; hence the number of ethylene molecules formed by disproportionation at high conversion becomes $3.0 \times 0.41 = 1.2$ molecules per 100 e.v. If we assumed that most of the reactions involving only thermalized ethyl radicals give n -butane (which seems to be a fair approximation¹⁸), then the above number should be about the same as the decrease in n -butane yield as ethane radiolysis proceeds from low to high conversion. The decrease in $G(n-C_4H_{10})_R$ estimated from Fig. 2 is 1.0 which agrees well with the value of 1.2 as estimated above; thus we conclude that the decrease in $G(n-C_4H_{10})_R$ with increasing conversion is explainable through the "hot" radical effect.

Molecular Processes.—Two processes that

(18) A. H. Turner and R. J. Cvetanovic, *Can. J. Chem.*, **37**, 1075 (1959).

should be considered in discussing molecular mechanisms are (a) decomposition of excited parent ion and (b) subsequent ion-molecule reactions.^{4,19,20} If one assumes that process (a) gives product ions, the relative intensities of which are exactly the same as the ones observed in ethane mass spectra, then one can calculate the molecular yields from known ethane mass spectra²¹ and the information on energy required to produce an ion pair in gaseous ethane (24.6 e.v.).²² The results are compared with the present experimental values in Table III. The calculated $G(H_2)_M$ and $G(CH_4)_M$ were taken from the paper by Dorfman and Sauer,⁴ while $G(CH_3)_M$ was calculated assuming that the only reaction responsible for the formation of methyl radical is



Table III shows that processes (a) and (b) are sufficient to explain the molecular yields of H_2 , CH_4 and CH_3 .²³ The same processes were, however, insufficient to account for the large yields of ethylene and hydrogen atoms. In these cases some other molecular processes, such as electron-ion recombination, seem to contribute the major parts.

TABLE III

THE OBSERVED AND CALCULATED MOLECULAR CONTRIBUTIONS TO G -VALUES IN ETHANE RADIOLYSIS

	H_2	CH_4	CH_3
Obsd.	3.2	0.3	0.08
Calcd.	3.3	0.6	0.08

Conclusion

The G -values for major products in ethane radiolysis decrease with increasing conversion; hence, for the determination of accurate initial values, one has to investigate the radiolysis at very low conversions (10⁻³%). Careful purification of the ethane is also essential. Free radical processes are entirely responsible for the observed decreases in the G -values. This part of the radiolysis mechanism closely resembles the photolysis mechanism. All molecular yields are independent of conversion. In this connection, it is noteworthy that the formation of hydrogen, presumably by molecular processes,^{6,14} in the radiolyses of ethylene and propylene is also independent of conversion.

Acknowledgment.—We express our appreciation to Dr. F. H. Dickey for his valuable discussion and Mr. J. D. Reedy and Mr. E. L. DeWitt for helping with the experimental work.

(19) L. M. Dorfman, *J. Phys. Chem.*, **62**, 29 (1958).

(20) J. H. Futrell, *J. Am. Chem. Soc.*, **81**, 5921 (1959).

(21) "Catalog of Mass Spectral Data," A.P.I. Project 44, Carnegie Institute of Technology, Pittsburgh, Series No. 2.

(22) W. P. Jesse and J. Sadauskis, *Phys. Rev.*, **97**, 1668 (1955).

(23) However, the possibility that excited neutral species may contribute to these yields is not ruled out; for example, see H. Okabe and J. R. McNesby, *J. Chem. Phys.*, **34**, 668 (1961).

ELECTROMOTIVE FORCE MEASUREMENTS IN THE SYSTEM AgNO_3 AND NaCl IN EQUIMOLAR NaNO_3 - KNO_3 MIXTURES AND THEIR COMPARISON WITH THE QUASI-LATTICE THEORY

BY D. G. HILL¹ AND M. BLANDER

Oak Ridge National Laboratory, P. O. Box X, Oak Ridge, Tennessee²

Received April 25, 1961

Electromotive force measurements in dilute solutions of Ag^+ and Cl^- ions in molten equimolar mixtures of NaNO_3 and KNO_3 demonstrate over the range of temperatures of 233–528° that the temperature coefficient of the association constant for the formation of the ion pair Ag^+Cl^- is, within the estimated experimental error, correctly given by the expression $Z(\exp(-\Delta E/RT) - 1)$ which has been derived from the quasi lattice model, where Z is the coordination number and ΔE is the energy of ion pair formation and is a constant. K_1 varies from 1050 (moles/mole solvent)⁻¹ at 233° to 133 (moles/mole solvent)⁻¹ at 528°. For possible values of $Z = 4, 5$ and 6 average values of $-\Delta E$ of 5.64, 5.36 and 5.12 kcal./mole, respectively, were calculated.

Introduction

In this paper are described measurements of the activity coefficients of AgNO_3 in dilute solutions of Ag^+ and Cl^- ions in molten equimolar mixtures of NaNO_3 and KNO_3 at five temperatures ranging from 233 to 528°. In previous papers, similar measurements in pure KNO_3 ^{3,4} and in pure NaNO_3 ^{5,6} have been made and compared to the results based on the quasi-lattice model.^{6,7} The comparison demonstrated that the temperature coefficient of the association constant K_1 , for the formation of the ion pair Ag^+Cl^- is correctly predicted by the expression derived from the theoretical calculations

$$K_1 = Z(\exp(-\Delta E/RT) - 1) = Z(\beta - 1) \quad (1)$$

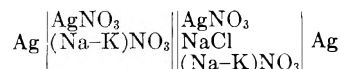
where Z is a coordination number, $\beta = \exp(-\Delta E/RT)$, and ΔE is the energy of ion pair formation and is a constant. K_1 was larger and ΔE was more negative by about 1 kcal. in the solvent KNO_3 than in NaNO_3 . The purpose of this paper is to demonstrate the validity of equation 1 and the constancy of ΔE over a larger range of temperatures than previously and to obtain information on the solvent effect in a mixed solvent.

Experimental

The apparatus, materials and procedure were the same as have been described previously. In some batches of molten reagent grade alkali nitrates a precipitate was observed upon addition of AgNO_3 . For the experiments particular batches from the manufacturers in which this precipitate was not observed were used. At 233 and 279° it was difficult to fabricate a reference electrode with a high enough conductance which did not leak. Consequently the galvanometer was somewhat sluggish and there was some scatter in the data at these temperatures. At 528° the reproducibility of the measurements was poorer than at the lower temperatures and was about ± 1 millivolt.

Results

As described previously,^{3,4} electromotive force measurements were made in the concentration cell



for low concentrations of Ag^+ and Cl^- ions. The addition of increments of NaCl to the right hand half cell at fixed concentrations of AgNO_3 in both half cells led to a change of e.m.f. from which the activity coefficient of AgNO_3 could be calculated

$$\Delta \text{e.m.f.} \cong \frac{2.303RT}{F} \log \gamma_{\text{AgNO}_3} \quad (2)$$

where $a_{\text{AgNO}_3} = N_{\text{Ag}^+}N_{\text{NO}_3^-}\gamma_{\text{AgNO}_3} \cong R_{\text{AgNO}_3}y_{\text{AgNO}_3}$ where the N are ion fractions and R_i is the mole ratio of the component i and

$$\frac{R_{\text{AgNO}_3}}{N_{\text{Ag}}} = 1 + R_{\text{NaCl}} + R_{\text{AgNO}_3}$$

which is close to unity in dilute solutions so that within the experimental precision, $y_{\text{AgNO}_3} = \gamma_{\text{AgNO}_3}$. The concentrations of ions for which data are reported are well below concentrations at which a precipitate was observed visually. Values of $-\log \gamma_{\text{AgNO}_3}$ are given in Table I for different values of R_{AgNO_3} and R_{NaCl} at 233, 278, 385, 479 and 528°. The experimental results at 385° are plotted in Fig. 1 for $R_{\text{AgNO}_3} = 0.2 \times 10^{-3}$ and 2.2×10^{-3} . The comparison in Fig. 1 of the concentration dependence of the experimental results with calculations based on the symmetric and the asymmetric approximations based on the quasi-lattice model indicates that the concentration dependence of the asymmetric approximation is closer to the experimental results. In Fig. 2 are plotted values of $-\log \gamma_{\text{AgNO}_3}$ versus R_{Cl} at $R_{\text{AgNO}_3} \cong 0.2 \times 10^{-3}$ at five temperatures ranging from 233 to 528°. The points at 233 and 278° represent points from four separate sets of measurements, at 385 and 479 from one and at 528 from three. One low set of measurements at 528° which was not plotted was rejected.

Discussion

The solid lines of Fig. 2 represent values of $-\log \gamma$ from the calculations based on the asymmetric approximation^{4,5} for the values of Z and ΔE listed in Table II where the range of values of 4 to 6 probably covers all reasonable values of Z . Within the estimated error of the measurements the values of ΔE for any given value of Z are constant at all temperatures at which measurements were made. *This demonstrates that over a*

(1) Duke University, Durham, North Carolina, Consultant, Reactor Chemistry Division, Oak Ridge National Laboratory, Summer 1960.

(2) Operated for the United States Atomic Energy Commission by the Union Carbide Corporation.

(3) M. Blander, F. F. Blankenship and R. F. Newton, *J. Phys. Chem.*, **63**, 1259 (1959).

(4) J. Braunstein and M. Blander, *ibid.*, **64**, 10 (1960).

(5) D. G. Hill, J. Braunstein and M. Blander, *ibid.*, **64**, 1038 (1960).

(6) M. Blander and J. Braunstein, *Ann. N. Y. Acad. Sci.*, **79**, 838 (1960).

(7) M. Blander, *J. Phys. Chem.*, **63**, 1262 (1959).

KNO_3 at 385° is made in Table III. The results at other temperatures are comparable. The value

TABLE III

COMPARISON OF THE VALUES OF K_1 AND ΔE IN NaNO_3 , NaNO_3 - KNO_3 (50-50 MOLE %), AND KNO_3 AT 385°

K_1 (mole/mole KNO_3) ⁻¹	Z	NaNO_3 - KNO_3 (50-50 mole %)		
		NaNO_3	KNO_3	KNO_3
$-\Delta E$ (kcal./mole)	$Z = 4$	5.17	5.67	6.18
	$Z = 5$	4.88	5.38	5.89
	$Z = 6$	4.65	5.15	5.68

of ΔE in the mixture is the average of the values in the pure NaNO_3 and KNO_3 and it appears that for any one value of Z ⁸

$$\Delta E_1(\text{NaNO}_3\text{-KNO}_3) = N_{\text{Na}}\Delta E_1(\text{NaNO}_3) + N_{\text{K}}\Delta E_1(\text{KNO}_3) \quad (3)$$

The linear relation derived from equations 3 for values of β appreciably greater than unity

$$\ln K_1(\text{NaNO}_3\text{-KNO}_3) \cong N_{\text{Na}} \ln K_1(\text{NaNO}_3) + N_{\text{K}} \ln K_1(\text{KNO}_3) \quad (4)$$

is suggested by the results. Equations 3 and 4 are

(8) Slightly different values of Z in these two pure molten nitrates should not make any effective difference.

of a type first suggested by Flood and co-workers.⁹

Differences between the solvents NaNO_3 and KNO_3 may be ascribed (a) to the differences in the "polarization" of electrons in $\text{Ag}^+\text{-Cl}^-$ pair "bonds" by the solvent cation⁶ or (b) to a coulombic effect, which in a mixture of two cations and two anions of different sizes, aside from contributions due to other types of interactions, will lead to a negative contribution to the energy of association of the small cation with the small anion (i.e., Ag^+ and Cl^- in KNO_3).¹⁰ This negative contribution will be greater for a given small anion and small cation pair the greater the differences in the sizes of the two cations or of the two anions. As both these effects are in the same direction they cannot be separated easily.

Acknowledgment.—The authors would like to thank Professor J. Braunstein of the University of Maine and Dr. R. F. Newton for many valuable discussions.

(9) See for example H. Flood, T. Forland and K. Griothheim, *Z. anorg. u. allgem. Chem.*, **276**, 289 (1954).

(10) If the interionic distance for $\text{Ag}^+\text{-Cl}^-$ is d_1 , for $\text{Ag}^+\text{-NO}_3^-$ d_2 , $\text{M}^+\text{-Cl}^-$ d_3 , and $\text{M}^+\text{-NO}_3^-$ d_4 it is easy to demonstrate the well known fact that if $d_1 > d_2$ and $d_3 > d_4$ then the coulombic term $-e^2(1/d_1 + 1/d_3 - 1/d_2 - 1/d_4)$ is negative if the d_i are additive sums of ionic radii so that $d_1 + d_3 = d_2 + d_4$.

SPECTROPHOTOMETRIC DETERMINATION OF THE DISSOCIATION CONSTANT OF SILVER CHLORIDE IN PYRIDINE¹

BY STANLEY BRUCKENSTEIN AND JIRO OSUGI²

School of Chemistry, University of Minnesota, Minneapolis, Minn.

Received May 10, 1961

A new spectrophotometric method for the determination of the dissociation constants for equilibria of the type $\text{AB} \rightleftharpoons \text{A} + \text{B}$ is described. The method yields $K = 8.4 \times 10^{-6}$ for the dissociation constant of silver chloride in anhydrous pyridine.

Introduction

Although the dissociation constants of approximately thirty compounds have been determined conductometrically³⁻⁵ using pyridine as a solvent, the dissociation constant of silver chloride has not been reported.

A spectrophotometric method has been developed for the determination of the dissociation constant of silver chloride in pyridine and is of interest because of its possible applications to other non-aqueous solvents. Previously described aqueous spectrophotometric methods for the determination of equilibrium constants normally involve media buffered with respect to one of the species produced on dissociation. For example, to determine the dissociation constant of an acid, (1) the pH at which the acid is half neutralized is determined spectrophotometrically,⁶ (2) the acid is placed in a

buffer of known pH and the ratio of the acid to its conjugate base determined from the known molar absorptivities,⁷ (3) the absorbance of the acid in three different buffers is measured and three simultaneous equations are solved to find K ,⁸ (4) a variation of the Benesi-Hildebrand plot⁹ is employed or (5) in salt solutions of constant ionic strength, the Type II plot is used.¹⁰

Such methods cannot be used in low dielectric constant solvents because of the formation of ion triplets, quadrupoles, etc., and the inability to make suitable estimates of ionic activity coefficients in any but the most dilute of solutions. The method described below is applicable to solutions containing only the solute, AB , which dissociates according to the scheme $\text{AB} \rightleftharpoons \text{A} + \text{B}$, and requires the determination at a suitable wave length of the absorbance as a function of the analytical concentration of AB . The restrictions of the method require

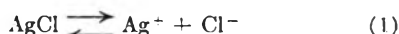
- (1) Sponsored by the Office of Ordnance Research, U. S. Army.
- (2) Department of Chemistry, Faculty of Science, Kyoto University, Kyoto, Japan.
- (3) M. M. Davies, *Trans. Faraday Soc.*, **31**, 1561 (1935).
- (4) W. F. Luder and C. A. Kraus, *J. Am. Chem. Soc.*, **69**, 2481 (1947).
- (5) D. S. Burgess and C. A. Kraus, *ibid.*, **70**, 706 (1948).
- (6) N. Bjerrum, *Samm. chem. chemische-tech. Vorträge*, **21**, 30 (1915).

- (7) L. Flexser, L. P. Hammett and A. Dingwall, *J. Am. Chem. Soc.*, **57**, 2103 (1935).
- (8) D. H. Rosenblatt, *J. Phys. Chem.*, **53**, 40 (1954).
- (9) H. A. Benesi and J. B. Hildebrand, *J. Am. Chem. Soc.*, **71**, 2703 (1949).
- (10) S. Bruckenstein and D. C. Nelson, *J. Chem. Eng. Data*, in press.

that (1) either A or B be non-absorbing at the wave length used, and (2) the molar absorptivity of one of the two remaining absorbing species be known if a graphical treatment of the data is employed.

Theory

Potentiometric studies of silver chloride solutions in pyridine¹¹ indicate that silver chloride is weakly dissociated according to



The spectrum of pyridine solutions of silver chloride in the range 300 to 400 $m\mu$ is markedly concentration dependent and the dissociation constant can be determined from the variation of the apparent molar absorptivity, ϵ_c , of silver chloride at 310.0 $m\mu$ with the analytical concentration of silver chloride, C . ϵ_c is defined as the ratio of the observed absorbance to the product of the cell path length and solute analytical concentration. Assuming there are only two absorbing species in solution, solvated silver ion and undissociated silver chloride

$$\epsilon_c = \epsilon_{\text{AgCl}}[\text{AgCl}]/C + \epsilon_{\text{Ag}^+}[\text{Ag}^+]/C \quad (2)$$

where the molar absorptivity of a species is indicated by ϵ with the appropriate subscript and equilibrium concentrations by brackets. The degree of dissociation, α , = $[\text{Ag}^+]/C$ = $[\text{Cl}^-]/C$ and $1 - \alpha$ = $[\text{AgCl}]/C$. Substituting these relationships into equation 2 yields

$$\alpha = \frac{\epsilon_c - \epsilon_{\text{AgCl}}}{\epsilon_{\text{Ag}^+} - \epsilon_{\text{AgCl}}} \quad (3a)$$

and

$$1 - \alpha = \frac{\epsilon_{\text{Ag}^+} - \epsilon_c}{\epsilon_{\text{Ag}^+} - \epsilon_{\text{AgCl}}} \quad (3b)$$

The dissociation constant for reaction 1 is

$$K = \frac{a_{\text{Ag}^+} a_{\text{Cl}^-}}{a_{\text{AgCl}}} = \frac{\alpha^2 C}{(1 - \alpha)} \frac{f_{\text{Ag}^+} f_{\text{Cl}^-}}{f_{\text{AgCl}}} \quad (4)$$

where f represents the activity coefficient of the species indicated in the subscript. In very dilute solutions it is a good approximation to assume that $f_{\text{AgCl}} = 1$ and $f_{\text{Ag}^+} = f_{\text{Cl}^-} = f$. Substituting equations 3a and 3b into equation 4 and rearranging yields

$$\epsilon_c = \epsilon_{\text{Ag}^+} - \frac{f^2[\epsilon_c - \epsilon_{\text{AgCl}}]^2 C}{(\epsilon_{\text{Ag}^+} - \epsilon_{\text{AgCl}})K} \quad (5)$$

In dilute pyridine solutions, the Debye-Hückel limiting law may be used to estimate f . Using 12.0 as the dielectric constant of pyridine yields equation 6

$$-\log f^2 = 17.04 \sqrt{\alpha C} = 17.04 \left[\frac{[\epsilon_c - \epsilon_{\text{AgCl}}] C}{\epsilon_{\text{Ag}^+} - \epsilon_{\text{AgCl}}} \right]^{1/2} \quad (6)$$

Thus, the thermodynamic dissociation constant of silver chloride can be calculated from the slope of the straight line which is obtained by plotting ϵ_c vs. $f^2[\epsilon_c - \epsilon_{\text{AgCl}}]^2 C$ provided ϵ_{Ag^+} and ϵ_{AgCl} are known. ϵ_{AgCl} can be determined experimentally, but a precise experimental value of ϵ_{Ag^+} could not be obtained because even at the lowest concentration of silver chloride studied complete dissociation did not occur. Instead, various values of ϵ_{Ag^+} were assumed, and plots made according to

(11) J. Osugi and S. Bruckenstein unpublished data.

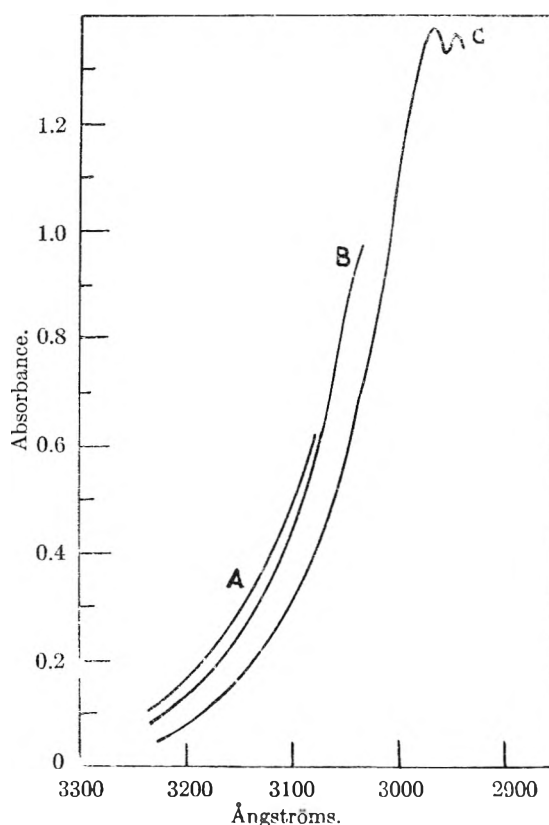


Fig. 1.—Spectra of silver chloride in pyridine: C, $C = 0.055 M$, cell length = 0.100 cm.; B, $C = 0.0055 M$, cell length = 1.00 cm.; A, $C = 0.0011 M$, cell length = 5.00 cm. Lowest wave length recorded corresponds to a slit width of 0.3 mm. All data were obtained with a slit width ≤ 0.3 mm.

equation 5. The assumed value of ϵ_{Ag^+} which yielded the same value as the intercept according to equation 5 was used to calculate K .

In principle, ϵ_{Ag^+} and ϵ_{AgCl} need not be determined in a separate experiment. These quantities and K could be obtained from the experimental data and equations 5 and 6 by the least squares treatment.

Davies, Otter and Prue¹² used equations 2 and 4 to determine the ion-pair dissociation constant of cupric sulfate in water. However, they determined α by combining equation 4 with the Debye-Hückel law to obtain a transcendental equation containing α and K . α was obtained from the latter expression by assuming a value of K and plotting a rearranged form of equation 2 which should yield a straight line when α is plotted vs. ϵ_c . Using a method of successive approximations, different values of K were chosen until the best straight line resulted. Their method involves considerably more numerical work than does the use of equation 5, but does not require prior determination of ϵ_{AgCl} .

Experimental

Chemicals.—Reagent grade pyridine from the J. T. Baker Co. was dried by passing through a Molecular Sieve column (Type 5A, Linde Co.) of 19 inch length and 20 mm. diameter, and then was fractionally distilled from fresh Molecular Sieves in a nitrogen atmosphere. The boiling point of the sample was constant at 115° (at 740 mm.)

(12) W. G. Davies, R. J. Otter and J. E. Prue, *Discussions Faraday Soc.*, **24**, 103 (1957).

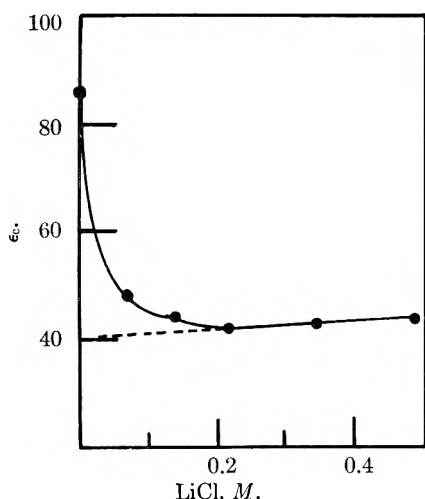


Fig. 2.—Effect of added lithium chloride on ϵ_c of silver chloride. $C = 0.0021 M$. Extrapolated value of $\epsilon_{AgCl} = 40$.

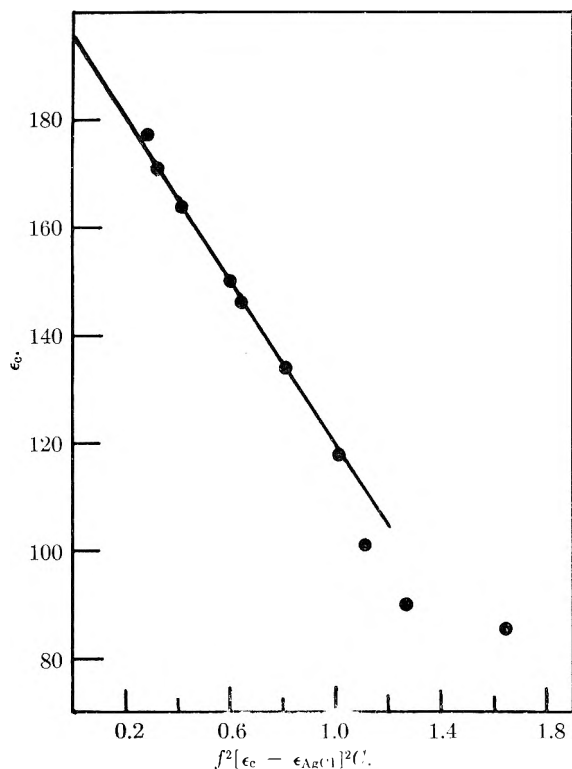


Fig. 3.—Plot of equation 5 for silver chloride: $\epsilon_{Ag^+} = 196$ and $\epsilon_{AgCl} = 40$.

throughout the distillation. The water content could not be detected by the Karl Fischer method and is assumed to be less than 0.001%. Pyridine was stored in Pyrex glass-stoppered bottles, using Quorn Teflon sleeves in place of grease as lubricant, and was dispensed from these bottles under a nitrogen atmosphere by introducing an automatic buret head.

Reagent grade silver chloride was dried in a vacuum oven at 120° and protected from light.

Reagent grade lithium chloride was dried *in vacuo* at 100° immediately before use.

Procedure.—A battery-operated Beckman Model DU spectrophotometer equipped with a photomultiplier attachment was used for all measurements, and the cell compartment was maintained at $25 \pm 0.1^\circ$. Calibrated cells were used and the cell calibrations verified by checking the constancy of the ratio of observed absorbance values for identical silver chloride solutions in cells of different length.

Results

Figure 1 presents the spectra of 0.055, 0.0055 and 0.0011 M silver chloride solutions in pyridine. In this experiment the product of the concentration of silver chloride and cell path length was held constant at 0.0055 M -cm. Table I gives the concentration dependence of the apparent molar absorptivity of silver chloride at 310.0 $m\mu$, while Fig. 2 shows the effect of adding lithium chloride to a 0.0021 M silver chloride solution.

TABLE I

APPARENT MOLAR ABSORPTIVITY OF SILVER CHLORIDE AT 3100 Å. AS A FUNCTION OF CONCENTRATION

C $M \times 10^2$	ϵ_c^a	f^2f	$f^2[\epsilon_c - \epsilon_{AgCl}]^2C$
0.00186	17, ^b	0.854	0.28 ₄
.00216	17, ^b	.848	.31 ₆
.00330	16, ^b	.818	.41 ₅
.00650	150 ^b	.767	.603
.00860	146 ^b	.741	.642
.0130	134, ^b 133 ^c	.707	.812
.0260	118 ^c	.639	1.011
.0518	101 ^c		
.1036	90.1 ^c		
.2070	86.0, ^c 87.6 ^d		
.518	78.5 ^d		
1.036	74.1 ^d		
1.727	69.6, ^d 71.1 ^e		
2.59	64.5 ^e		
3.45	61.9 ^e		
5.18	59.9 ^e		

^a A constant slit width of 0.2 mm. was used in all experiments. It was found that ϵ_c was independent of slit width provided the slit width did not exceed 0.2 mm. ^b Cell length = 10.00 cm. ^c Cell length = 5.00 cm. ^d Cell length = 1.000 cm. ^e Cell length = 0.100 cm. ^f Calculated from equation 6 using $\epsilon_{Ag^+} = 196$ and $\epsilon_{AgCl} = 40$.

Discussion

Aqueous solutions of pyridine undergo spectral changes on the addition of silver ion because of the formation of $AgPy^+$ and $AgPy_2^+$. These aqueous absorption bands occur below 280 $m\mu$, involve π - π^* transitions, and have peak molar absorptivities exceeding 10^3 . In pyridine as solvent, the silver absorption band is found at the edge of the solvent absorption band. It seems probable that perturbed solvent transitions occurring within pyridine molecules bound to silver ion and silver chloride are responsible for the observed absorption.

The spectra shown in Fig. 1 were interpreted using equilibrium 1 and assuming that the molar absorptivities of silver ion and undissociated silver chloride are different. It was established experimentally that chloride ion does not absorb in this region. A wave length of 310.0 $m\mu$ was chosen to study the concentration dependence of the ϵ_c because this wave length represented the best compromise of absorbance change with concentration and slit-width. At lower wave lengths, solvent absorption prevented the use of 10-cm. cell paths.

By adding a large excess of a non-absorbing chloride to a dilute solution of silver chloride, it was possible to repress completely the dissociation of silver chloride and thereby determine ϵ_{AgCl} .

The results of this experiment using lithium chloride are shown in Fig. 2. The addition of lithium chloride results in a rapid decrease to a minimum value of absorbance, followed by a linear increase in absorbance at higher lithium chloride concentrations. The reason for this increase is not clear, and may be due to higher chloro-complexes of silver. We have extrapolated this linear portion back to zero concentration of lithium chloride to obtain a value of $\epsilon_{\text{AgCl}} = 40$ liters mole⁻¹cm.⁻¹.

A plot of the data in Table I for the very dilute solutions of silver chloride shows that the apparent molar absorptivity rises rapidly as the silver chloride solution becomes more dilute, and that a limiting value in the vicinity of 200 liters mole⁻¹ cm.⁻¹ is approached.

Using the value $\epsilon_{\text{AgCl}} = 40$ and $\epsilon_{\text{Ag}^+} \sim 200$, a plot according to equation 5 was made. From the intercept of this plot, a second approximation to ϵ_{Ag^+} was obtained. The above procedure was repeated until the assumed value of ϵ_{Ag^+} agreed

with the value from the plot. Table I gives the detailed calculation for $\epsilon_{\text{Ag}^+} = 196$ and $\epsilon_{\text{AgCl}} = 40$, for which equation 5 yields a straight line of intercept 196 and slope -86.6 , as shown in Fig. 3. The calculated value of K_{AgCl} is 8.4×10^{-5} .

The dissociation constant of silver chloride in pyridine has not been determined by any other technique, but for comparison, the dissociation constants of silver nitrate, perchlorate and picrate were found by Luder and Kraus⁴ to be 9.3×10^{-4} , 19.1×10^{-4} , and 30.6×10^{-4} , respectively, using the Fuoss-Kraus method. They find that deviations from this plot occur when the concentration of silver salt is greater than $5 \times 10^{-4} M$. Deviations from equation 5 occur for silver chloride when the concentration is greater than $2.6 \times 10^{-4} M$. It seems likely that the failure of the conductance and of the spectrophotometric method at concentrations higher than 3 to $5 \times 10^{-4} M$ is caused by the use of the Debye-Hückel limiting law in estimating activity coefficients.

EXACT NUCLEAR MAGNETIC RESONANCE SHIELDING CONSTANTS FOR HYDRIDE, HELIUM, LITHIUM(I), OXYGEN(VI)¹

BY R. E. GLICK

Department of Chemistry, The Florida State University, Tallahassee, Florida

Received May 11, 1961

Exact nuclear magnetic resonance shielding constants have been computed from twenty term Hylleraas-type wave functions of Hart and Herzberg; $\sigma(\text{H}^-) = 2.4670 \times 10^{-5}$, $\sigma(\text{He}) = 5.9935 \times 10^{-6}$, $\sigma(\text{Li}^+) = 9.5459$ and $\sigma(\text{O}^{+6}) = 27.289$. These exact values were examined with reference to those obtained from wave functions of recent interest. In addition, the change in σ from that of a neutral atom to that of the monovalent negative ion has been determined to be of the order of 1×10^{-5} for O_2 to O^- with $\sigma(\text{O}^-) > \sigma(\text{O}_2)$. A similar but less than previously estimated effect would be expected for shielding in F_2 as compared to F^- .

Nuclear magnetic resonance shielding constants (σ) for certain two electron atoms can readily be obtained from exact wave functions² presently available. The shielding contribution parallels that associated with the diamagnetic term² in the computation of the magnetic susceptibility and requires knowledge of the ground state wave function alone. Thus

$$\sigma = -\frac{\Delta H}{H} = \frac{2e^2}{3mc^2} \alpha_0 \left\langle \frac{1}{r} \right\rangle_{\text{av}}$$

where

$$\left\langle \frac{1}{r} \right\rangle_{\text{av}} = \frac{1}{2} \int \psi \left(\frac{1}{r_1} + \frac{1}{r_2} \right) \psi d\tau$$

and the ψ 's employed are, in this instance, the twenty term Hylleraas' wave functions of Hart and Herzberg³

$$\psi = \eta e^{-(1/2)ks} (1 + \chi_{11}u + \chi_{22}t^2 + \chi_{33}s + \chi_{44}s^2 + \chi_{55}u^2 + \chi_{66}su + \chi_{77}t^2u + \chi_{88}t^3 + \chi_{99}t^2u^3 + \chi_{100}st^2 + \chi_{111}s^3 + \chi_{122}t^2u^4 + \chi_{133}ut^4 + \chi_{144}u^5 + \chi_{155}t^2u^3 + \chi_{166}st^2 + \chi_{177}st^4 + \chi_{188}st^2u + \chi_{199}t^6)$$

The variational coefficients (χ_i) and normalizing

factor (η) are given by Hart and Herzberg.³ The parameters $s = r_1 + r_2$, $t = r_2 - r_1$, $u = r_{12}$, are coördinates of the electrons from the nucleus and each other. In terms of Hylleraas' parameters

$$\left\langle \frac{1}{r} \right\rangle_{\text{av}} = 4\pi^2 \int_0^\infty \int_0^s \int_0^t \psi^2 su du dt ds$$

The individual integrals are easily evaluated, since

$$\int_0^\infty e^{-s^a} s^a ds \int_0^s t^b dt \int_0^t u^c du = \frac{(a+b+c+2)!}{(b+1)(b+c+2)}$$

In Table I are recorded σ values for hydride ion, helium, lithium ion and oxygen(VI) as well as for the hydrogen atom. In addition to those values computed in this study, values are included as calculated by Ormand and Matsen⁴ using wave functions of recent interest. The "quality" of the Hart and Herzberg-Hylleraas wave function in yielding $\langle 1/r \rangle_{\text{av}}$ can be seen by the equality between this value and that obtained using Pekeris'⁵ $\langle 1/r \rangle_{\text{av}}$ as obtained from a 1078 variation-parameter wave function which affords a non-relativistic energy supposedly accurate to 0.001 cm.⁻¹. This

(1) Support by a grant from the Petroleum Research Fund, American Chemical Society, is gratefully acknowledged.

(2) In general see N. F. Ramsey, in E. Segre, "Experimental Nuclear Physics," John Wiley and Sons, New York, N. Y., 1953, p. 428 and references therein.

(3) J. F. Hart and G. Herzberg, *Phys. Rev.*, **106**, 79 (1957).

(4) F. T. Ormand and F. A. Matsen, *J. Chem. Phys.*, **30**, 368 (1959).

(5) C. L. Pekeris, *Phys. Rev.*, **115**, 1218 (1959). Pekeris' value has converged to the required five place accuracy before his 252 parameter function.

value is entered in the last column, Table I. Corrections, due to relativistic and other effects, are well outside of the error, as limited by the constants employed, so that the values given in the second column of Table I may be taken to be exact.

It is of interest to compare $\langle 1/r \rangle_{av}$ of Ormand and Matsen⁴ with those determined in this investigation. The wave functions employed by Ormand and Matsen were: (i) different optimum orbital exponents with the same spacial description for equivalent electrons—open configuration⁵ (ii) same optimum orbital exponents and same spacial description—closed configuration (iii) same as (ii) using Slater exponents. Although (i) affords lower calculated energies⁶ than (ii), (ii) more nearly approximates $\langle 1/r \rangle_{av}$. (iii) appears considerably higher in every instance. These results can be interpreted in the same way as were results from intermediate wave functions of the Hylleraas type in effecting changes in the computed diamagnetic susceptibility⁷ where $\langle r^2 \rangle_{av}$ is required. Thus, it would seem that (i) tends to move electron density further from the nucleus, but must also, as lower energies are obtained, peak the probability density, whereas (ii) and, to a greater extent, (iii) could be described as behaving in the opposite sense.

A further area of interest is the contribution of the various electron levels in many electron atoms to diamagnetic shielding. Dickinson⁸ computed σ for all atoms using Hartree-Fock wave functions with interpolation, when necessary. Dickinson's value for He is 6.0×10^{-5} as compared to 6.0×10^{-5} as found here. His value for the oxygen atom; 39.5×10^{-5} , is probably correct to within a few per cent. If it is assumed that the outer electrons do not appreciably affect the contribution of the inner electrons, then, as is seen in Table

I, the two inner oxygen electrons contribute 27.3×10^{-5} , while the six outer electrons contribute 12.2×10^{-5} or about 2×10^{-4} /electron. As is seen in Table I, σ (H^e) increases by the equivalent of about 50% of one electron as compared to σ (H), therefore σ (O^-) should increase to $\sim 40.5 \times 10^{-5}$. A similar argument should apply for F and F^- and as often has been pointed out—although an estimate of 2.3 rather than 1×10^{-5} had been made for this contribution⁹—shielding for other than first row elements due to diamagnetic electron effects is generally unimportant compared to so-called "paramagnetic or orbital" effects.¹⁰

TABLE I
NUCLEAR MAGNETIC RESONANCE SHIELDING VALUES AS
DETERMINED FROM VARIOUS WAVE FUNCTIONS

Substance	a	$\sigma \times 10^5$ b_1	b_2	b_3	c
H	1.7750 ^d				
H ⁻	2.4670	2.3475	2.4409	2.4853	
He	5.9935 ^e	5.9856	5.9913	6.0357	5.9935
Li ⁺	9.5459	9.5396	9.5417	9.5861	
O ⁺⁸	27.289 ^f				

^a This study. ^b F. T. Ormand and F. A. Matsen, *J. Chem. Phys.*, **30**, 368 (1959). (1) Optimum orbital exponents, open configuration. (2) Optimum orbital exponents, closed configuration. (3) Slater orbital exponents, closed configuration. ^c C. L. Pekeris, *Phys. Rev.*, **115**, 1216 (1959). ^d ($e^2/3mc^2$) a_0 . Constants are due to Bearden and Thompson taken from C. D. Hodgman, Editor-in-Chief, "Handbook of Chemistry and Physics," Chemical Rubber Publishing Company, Cleveland, Ohio, 40th Ed., 1958. ^e Both ten and twenty term wave functions used. The ten term wave function employs the first ten terms of the twenty term function with coefficients given by S. Chandrasekhar and G. Herzberg, *Phys. Rev.*, **98**, 1050 (1955). ^f Only ten term wave function employed; see *e*, above.

(6) H. Shull and P.-O. Löwdin, *J. Chem. Phys.*, **25**, 1035 (1956).

(7) R. E. Glick, *J. Phys. Chem.*, **65**, 1552 (1961).

(8) W. C. Dickinson, *Phys. Rev.*, **80**, 563 (1950).

(9) See J. A. Pople, W. G. Schneider and H. J. Bernstein, "High Resolution Nuclear Magnetic Resonance," McGraw-Hill Book Co., Inc., New York, N. Y., 1959, p. 172.

(10) A. Saika and C. P. Slichter, *J. Chem. Phys.*, **22**, 26 (1954).

EXPLORATORY STUDIES ON THE SURFACE ACTIVITY OF POLYSOAPS¹

By HELMUTH E. JORGENSEN AND ULRICH P. STRAUSS

School of Chemistry, Rutgers, The State University, New Brunswick, New Jersey

Received May 15, 1961

The surface activity of several polysoaps was studied at air-water and water-hydrocarbon interfaces, both in the absence and presence of simple electrolyte. Among the materials studied were several polysoaps and a polyelectrolyte derived from poly-4-vinylpyridine by quaternization with ethyl and *n*-dodecyl bromides, a sulfonic acid polysoap and its sodium salt, and a polysoap prepared by quaternizing poly-2-vinylpyridine with 3-bromopropylbenzene. The poly-4-vinylpyridine polysoaps showed the following properties: (1) In the absence of simple electrolyte the surface activity was very small, which supports the conclusion that under similar conditions micelles of ordinary soaps and detergents are not significantly adsorbed at interfaces. (2) In the presence of KBr, the polysoaps depressed the surface and interfacial tensions markedly, but the polyelectrolyte did not. (3) Equilibrium was reached rapidly. (4) The *n*-dodecyl group content and the molecular weight of the polysoap had little effect on the surface activity. (5) Solubilization of diphenylmethane decreased the surface tension substantially. (6) The depressing effect of the polysoaps on the interfacial tension was considerably greater than on the surface tension. The sulfonic acid polysoap and its sodium salt had very little effect on the surface and interfacial tensions, even in the presence of simple electrolyte. In contrast to the other polysoaps, the poly-2-vinylpyridine polysoap depressed the surface tension significantly in the absence of simple electrolyte, and several hours were necessary to reach surface equilibrium.

The surface activity of soap² micelles³ has been the subject of much speculation. While it has been surmised that the micelles are not surface-active,^{4,5} this assumption could not be tested because of the inevitable presence of the highly surface-active free soap molecules.

With the availability of polysoaps⁶⁻⁹ which consist of polymer chains with chemically attached soap-like molecules, a test of the above assumption becomes possible. It has been shown that most polysoaps behave like prefabricated micelles in that they have a compact structure and solubilize hydrocarbons.⁶ Moreover, the micelles exist at the lowest concentrations, and no free soap molecules are present to compete for the surface.

In this paper we present results obtained from an exploratory study of the surface activity of several polysoaps at air-water and hydrocarbon-water interfaces both in the absence and presence of simple electrolyte. Among the materials studied were several polysoaps and one polyelectrolyte prepared from poly-4-vinylpyridine, one polysoap with sulfonate groups and one polysoap prepared from poly-2-vinylpyridine.

Experimental

Polysoaps Based on Poly-4-vinylpyridine.—Poly-4-vinylpyridine (J-1-77) was prepared in toluene according to the method of Strauss and Fuoss.¹⁰ Its intrinsic viscosity in 92.0 weight % ethanol was 0.190 dl./g. at 25°. This corresponds to a weight-average degree of polymerization of 300.¹¹ Four polysoaps were obtained by quaternizing 9.5, 20.3, 35.0 and 46.5% of the pyridine groups with *n*-dodecyl

bromide and the remainder with ethyl bromide, using 2,4-dimethyl-1,1-dioxytetrahydrothiophene (dimethylsulfolane) as solvent. A polyelectrolyte, poly-4-vinyl-N-ethylpyridinium bromide, was prepared similarly. The preparation, purification and analysis followed closely procedures previously described.⁷ A "13.6%" polysoap¹² previously prepared by Gershfeld⁷ (his sample No. G-147) also was employed. This polysoap differed from the others in that its degree of polymerization was about 4300, in that the parent poly-4-vinylpyridine was emulsion polymerized and in that the quaternization was carried out in nitroparaffin solvents.

Other Polysoaps.—A copolymer consisting of 20 mole % octylstyrene and 80 mole % styrenesulfonic acid with a degree of polymerization of approximately 1100 was prepared by Dickstein.⁹ This copolymer (D-178) will be denoted as the "sulfonic acid polysoap."

Polysoap A-1-141 was prepared by Ammondson⁸ by quaternizing poly-2-vinylpyridine with 3-bromopropylbenzene to the extent of 39.4%.

Hydrocarbons.—The following hydrocarbons were used as solubilizates or in the interfacial tension experiments: benzene (Eastman, white label, distilled, b.p. 79.7°); *n*-heptane (Phillips, pure grade 99 mole % minimum, distilled, b.p. 98.2°); diphenylmethane (Fischer, distilled at 107–109° at 3 mm.).

Electrolytes.—Potassium bromide and sodium chloride were C.P. products obtained from Matheson Coleman and Bell, while sulfuric acid, analytical reagent grade, was obtained from Mallinckrodt.

Water.—All solutions were made up with conductivity water which was tested periodically for its surface tension.

Foam Fractionation.—The polysoaps were purified by bubbling nitrogen through 1% solutions from a gas dispersion tube.¹³⁻¹⁵ The foam was allowed to drain and then discarded. The foaming was continued until a constant value of the surface tension was obtained. This took approximately three hours. The concentration of the foamed solutions was determined by conductivity measurements, using the original dried material as a standard. Three hours of foaming never lowered the concentrations by more than 4%.

Surface Tensions.—Most of the surface tensions reported here were measured at 20° by the drop-weight method with a Harkins drop-weight apparatus, (manufactured by the W. M. Welch Scientific Company) using the corrections of Harkins and Brown.¹⁶ About one minute was allowed for the formation of each drop.

Some surface tension measurements also were made by the double capillary method described by Sugden¹⁷ as modified

(1) This work was supported in part by the Office of Naval Research. The paper is based on a thesis presented by H. E. Jorgensen in partial fulfillment of the requirements for the Ph.D. degree, Rutgers, The State University, 1958. Presented at "Symposium on Micellar Solutions" before Division of Colloid and Surface Chemistry at 139th American Chemical Society Meeting, St. Louis, Missouri, March 29, 1961.

(2) The term "soap" is used in a general sense here, including anionic and cationic detergents.

(3) J. W. McBain, *Trans. Faraday Soc.*, **9**, 99 (1913).

(4) J. Powney, *ibid.*, **31**, 1510 (1935).

(5) N. K. Adam and H. L. Shute, *ibid.*, **34**, 758 (1938).

(6) U. P. Strauss and E. G. Jackson, *J. Polymer Sci.*, **6**, 649 (1951).

(7) U. P. Strauss and N. L. Gershfeld, *J. Phys. Chem.*, **58**, 747 (1954).

(8) C. J. Ammondson, Ph.D. thesis, Rutgers University, 1955.

(9) J. Dickstein, Ph.D. thesis, Rutgers University, 1958.

(10) U. P. Strauss and R. M. Fuoss, *J. Polymer Sci.*, **4**, 457 (1949).

(11) A. G. Boyes and U. P. Strauss, *ibid.*, **22**, 463 (1956).

(12) The percentage in quotation marks refers to the extent to which the pyridine groups were quaternized with *n*-dodecyl bromide.

(13) C. D. Miles and L. Shedlovsky, *J. Phys. Chem.*, **48**, 57 (1944).

(14) L. Shedlovsky, J. Ross and C. W. Jakob, *J. Colloid Sci.*, **4**, 25 (1949).

(15) A. P. Brady, *J. Phys. & Colloid Chem.*, **53**, 56 (1949).

(16) W. D. Harkins and F. E. Brown, *J. Am. Chem. Soc.*, **41**, 499 (1919).

(17) S. Sugden, *J. Chem. Soc.*, **119**, 1483 (1921).

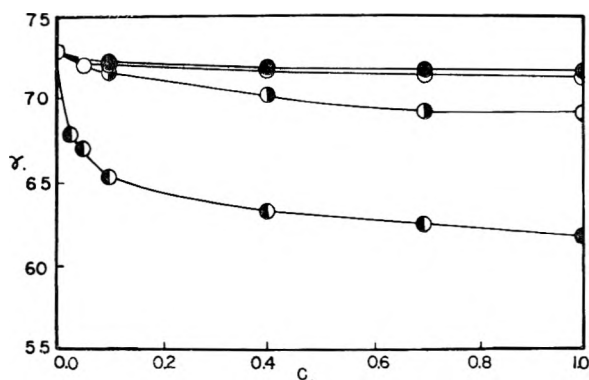


Fig. 1.—Surface tension of aqueous solutions of the "35.0%" polysoap at 20°. Molarity of KBr: ●, 0.00; ○, 0.01; ◐, 0.03; ●, 0.10.

by Ross and Epstein.¹⁸ This method made it possible to study cases where the attainment of surface equilibrium was very slow. Except for polysoap A-1-144, both methods yielded identical results.

Interfacial Tensions.—The interfacial tensions were measured by the drop-volume method with a Traube¹⁹ stalagmometer using the corrections of Harkins and Brown.¹⁶ Before measuring the interfacial tension, the solutions were saturated with the appropriate hydrocarbon by tumbling first at 45° for 48 hours and then at 20° for 24 hours.

Results and Discussion

Surface Tension with Poly-4-vinylpyridine Derivatives.—The effect of the "35.0%" polysoap on the surface tension of water and aqueous KBr solutions is shown in Fig. 1, where γ , the surface tension expressed in dynes per cm., is represented as a function of C , the polysoap concentration in g. per 100 ml. These surface tensions were measured by the drop-weight method. It was found that the other polysoaps derived from poly-4-vinylpyridine had similar effects on the surface tension as the "35.0%" polysoap.

The uppermost curve in Fig. 1 shows that in the absence of KBr the lowering of the surface tension is proportional to the polysoap concentration, amounting to about one dyne per concentration unit. This proportionality persists up to $C = 6$ g. per 100 ml., the highest concentration measured (not shown in Fig. 1). The small magnitude of the depression indicates that the polysoaps are only slightly adsorbed at the surface, thus furnishing strong evidence for the assumption that micelles of ordinary soaps and detergents are also not significantly surface-active.

The three lowest curves in Fig. 1 illustrate the effect of KBr, a typical simple electrolyte, on the surface activity of the polysoap. The shapes of the curves resemble those obtained with ordinary soaps and detergents, the surface tension decreasing rapidly at low polysoap concentrations and then levelling off. However, while the initial decrease pronounced with increasing KBr concentration, it never reaches the magnitude of the surface tension depressions observed with ordinary soaps.

According to Gibbs' adsorption equation²⁰ a decrease in the surface tension indicates that at least one of the components is adsorbed at the surface.

(18) J. Ross and M. B. Epstein, *J. Phys. Chem.*, **62**, 533 (1958).

(19) J. Traube, *Chem. Ber.*, **20**, 2644, 2824 (1887).

(20) J. W. Gibbs, *Trans. Conn. Acad. Sci.*, **3**, 391 (1876).

Some indirect evidence that it is the polysoap, and not the KBr, which is adsorbed, is furnished by the observation that the surface tension of solutions containing KBr and the polyelectrolyte, poly-4-vinyl-N-ethylpyridinium bromide, is very close to that of water—(within $1/2$ dyne when $(\text{KBr}) = 0.1 M$ and $C = 1$ g./100 ml.)—and is hardly affected by changes in the concentrations of either component.

More direct evidence may be obtained by the application of Gibbs' adsorption equation to our three-component system. If the surface excesses are defined in such a way that Γ_1 , the surface excess of solvent, vanishes,²¹ the Gibbs' equation leads to the following expressions for Γ_2 and Γ_3 , the surface concentrations of polysoap and KBr expressed in moles per square centimeter of surface, respectively

$$\Gamma_2 = \frac{a_{33} \frac{\partial \gamma}{\partial m_2} - a_{23} \frac{\partial \gamma}{\partial m_3}}{RT(a_{23}^2 - a_{22}a_{33})} \quad (1)$$

$$\Gamma_3 = \frac{a_{22} \frac{\partial \gamma}{\partial m_3} - a_{23} \frac{\partial \gamma}{\partial m_2}}{RT(a_{23}^2 - a_{22}a_{33})} \quad (2)$$

where $a_{ij} = (1/RT) \times (\partial \mu_i / \partial m_j)$, m_i = molarity and μ_i = chemical potential of component i . The values of a_{33} are calculated from published data for KBr solutions,²² the values of a_{23} are obtained from membrane equilibrium studies,²³ and the values of a_{22} are determined from light scattering results,²⁴ using a theoretical expression derived by Stockmayer.²⁵ For the particular H₂O-polysoap-KBr systems reported here, the magnitude of the parameters is such that equation 1 reduces to the familiar two-component system equation

$$\Gamma_2 = - \frac{1}{RT} \frac{d\gamma}{d \ln C} \quad (3)$$

The surface area available for a polysoap molecule, expressed in Å.² units, α , is then calculated by means of the equation

$$\alpha = \frac{10^{16}}{N_A \Gamma_2} \quad (4)$$

where N_A is Avogadro's number. Some representative values of Γ_2 and α are given in Table I.

The values of Γ_2 are about an order of magnitude smaller than those found for small surface-active molecules. However, since the molecular weight of the polysoaps is of the order of 10^5 , on a weight basis the surface excess is much larger for the polysoaps. The dependence of Γ_2 on the polymer concentration, which seems irregular on first sight, assumes some degree of regularity if we focus our attention on the maximum which appears with the "20.3%" polysoap in 0.1 M KBr. If we make the assumption that such a maximum exists in all our systems, but not necessarily within the range of measured polymer concentrations, we

(21) Ways of doing this are discussed by Adam and by Guggenheim. [N. K. Adam, "The Physics and Chemistry of Surfaces," 3rd ed., Oxford University Press, New York, N. Y., 1941, pp. 107-113, 404-409; E. A. Guggenheim, *Trans. Faraday Soc.*, **36**, 397-405 (1940)].

(22) G. Scatchard and S. S. Prentiss, *J. Am. Chem. Soc.*, **55**, 4355 (1933).

(23) D. Fraser, Ph.D. thesis, Rutgers University, 1950.

(24) U. P. Strauss and B. L. Williams, *J. Phys. Chem.*, **65**, 1390 (1961).

(25) W. H. Stockmayer, *J. Chem. Phys.*, **18**, 58 (1950).

TABLE I
 VALUES OF Γ_2 AND α

Polysoap	C	0.03 M KBr		0.1 M KBr		0.3 M KBr	
		Γ_2 $\times 10^{11}$, moles/ cm ² .	α , Å. ² / mole- cule	Γ_2 $\times 10^{11}$, moles/ cm ² .	α , Å. ² / mole- cule	Γ_2 $\times 10^{11}$, moles/ cm ² .	α , Å. ² / mole- cule
"9.5%" ($P_w = 300$)	0.0025	0.9	1900	3.0	570	9.4	180
	.025	1.7	1000	3.4	500	5.5	310
	.388	3.6	470	5.5	310	3.7	460
"20.3%" ($P_w = 300$)	.0025	1.1	1500	2.5	680	11.2	150
	.025	2.0	850	7.8	220	7.8	220
	.392	4.6	370	4.3	400	4.6	370
"35.0%" ($P_w = 300$)	.0024	0.3	5600	0.5	3400	5.3	320
	.024	1.0	1700	0.9	1900	5.6	300
	.384	1.4	1200	2.7	630	6.1	280
		0.04M KBr					
"13.6%" ($P_w = 4000$)	.05			9.4	180		
	.30			4.3	400		
	.75			4.3	400		

reach the not unreasonable conclusion that this maximum is displaced to lower polymer concentrations as the KBr molality is increased. The enhancement of the surface activity of polysoap by the KBr is due mainly to the fact that the KBr reduces the electrical charge of the polysoap.²⁶ This effect of electrical charge on the surface activity of macromolecules has been demonstrated previously for copolymers of 2-vinylpyridine and 4-vinylbenzoic acid.²⁷ In addition, the KBr reduces the solvent power of the water for the polysoap, which tends to bring the polysoap molecules into the surface.

The dodecyl group content of the polysoaps seems to have little effect on the surface activity; however, the "35.0%" polysoap appears to be somewhat less surface-active than the "9.5%" and the "20.3%" polysoaps. Possibly, there is more intramolecular association of the dodecyl groups in the case of the "35.0%" polysoap, so that fewer dodecyl groups are exposed to the aqueous medium. The results obtained with the "13.6%" polysoap, whose degree of polymerization was an order of magnitude larger than that of the other polysoaps, suggest that the surface activity is not sensitive to the molecular weight.

To obtain some idea of how the configuration of the polysoap molecules in the surface compares with the configuration in the bulk of the solution, the molecular dimensions in the solution were estimated from viscosity and light scattering results.²⁴ The values of the weight-average root-mean-square end-to-end distances of the three polysoaps with P_w equal to 300 ranged from 170 Å. for the "9.5%" polysoap in 0.02 M KBr to 60 Å. for the "35.0%" polysoap in 0.1 M KBr. The squares of these values, 29,000 and 3,600 Å.², are seen to be considerably larger than the values of α in the corresponding systems. Thus the polysoap molecules are either compressed or interpenetrate each other in the surface. To obtain a further measure of the configuration of the polysoap molecules in the surface, one may calculate the minimum thickness of the sur-

(26) U. P. Strauss, N. L. Gershfeld and H. Spiera, *J. Am. Chem. Soc.*, **76**, 5909 (1954).

(27) I. R. Miller and A. Katchalsky, *Proc. Sec. Intern. Congr. of Surface Activity, 2nd London*, **1**, 159 (1957).

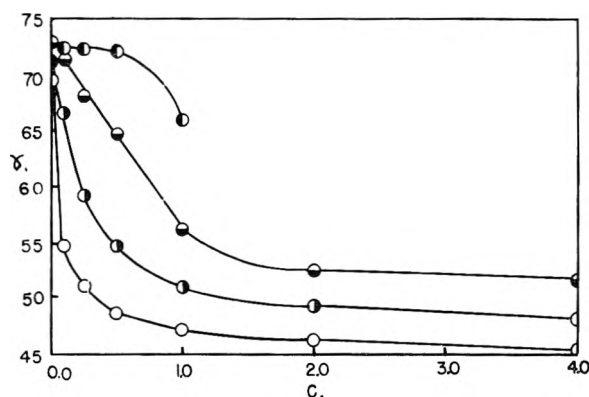


Fig. 2.—Surface tension of bromopropylbenzene addition product of poly-2-vinylpyridine. Drop-weight method: ●, 20°. Double capillary method: ◐, 20°; ◑, 30°; ○, 40°.

face layer in those solutions where α assumes its lowest value of about 200 Å.². To accommodate a completely unsolvated polysoap molecule of molecular weight equal to 7×10^4 and of density equal to unity in such a surface area, the polysoap molecule must extend 600 Å. into the solution. If the polysoap molecule is solvated, this distance would be even larger. The distance is obviously much larger than the mean molecular dimensions in the bulk of the solution.²⁸ Thus, these polysoaps behave differently from the polymethacrylic acid molecules studied by Katchalsky and Miller which had the same configuration in the surface and in the bulk of the solution.²⁹

Once Γ_2 has been calculated, it is easier to determine Γ_3 from equation

$$\Gamma_3 = - \left(\frac{1}{RT} \times \frac{1}{a_{33}} \times \frac{\partial \gamma}{\partial m_3} \right) - \left(\Gamma_2 \times \frac{a_{23}}{a_{33}} \right) \quad (5)$$

than from the equivalent equation 2. For our data, it then appears that the first term on the right hand side of equation 5 is always less than 15% of the second term, so that Γ_3 is essentially proportional to Γ_2 , but of opposite sign. Thus the salt is displaced from the surface in proportion to the amount of polysoap which is adsorbed.

Surface Tension with Sulfonic Acid Polysoap.—There were only very small effects on the surface tensions by the sulfonic acid polysoap in water and in 0.0486 M H₂SO₄ and by its sodium salt in water and in 0.1 M NaCl. Presumably the octyl groups are too short and/or there are not enough of them to make these polysoaps surface-active.

Surface Tension with Bromopropylbenzene Addition Product of Poly-2-vinylpyridine.—When the surface tension of aqueous solutions of the quaternization product of 3-bromopropylbenzene and poly-2-vinylpyridine was measured by the drop-weight method, the results depended on the time of holding the drops. Therefore no equilibrium values could be obtained by this method. The results obtained with ϵ one minute holding time at 20° are illustrated by the uppermost curve in Fig. 2. By

(28) The foregoing argument depends on the assumption that the material in the surface is representative of the material in the bulk and is not some low molecular weight or other species of higher surface activity. In view of the fact that the polysoaps were purified by foam fractionation, we believe this assumption to be valid.

(29) A. Katchalsky and I. Miller, *J. Phys. Chem.*, **55**, 1182 (1951).

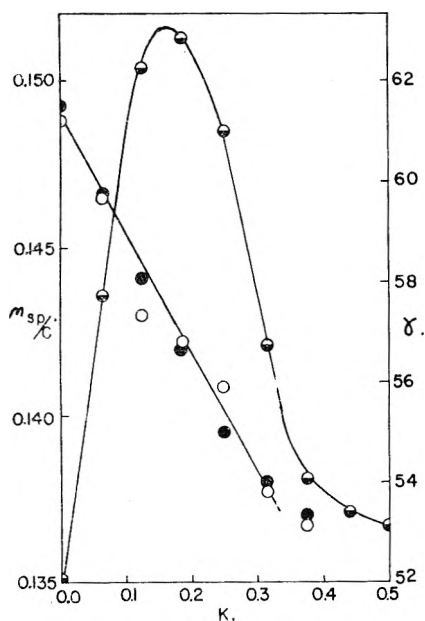


Fig. 3.—Effect of solubilized diphenylmethane on the reduced viscosity and the surface tension of the "35.0%" polysoap at 25°. \ominus , reduced viscosity; \circ , surface tension by drop-weight method; \bullet , surface tension by double capillary method.

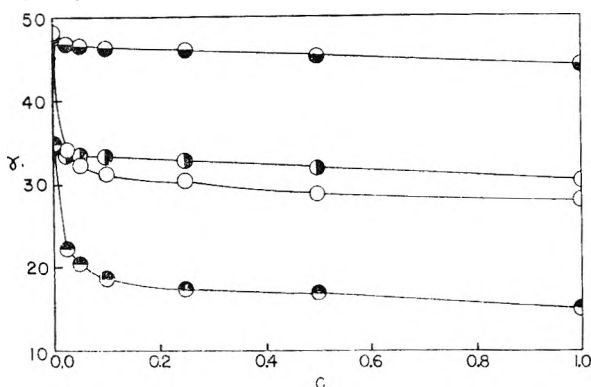


Fig. 4.—Interfacial tension of "35.0%" polysoap at 20°. Interfaces: \ominus , water-*n*-heptane; \circ , water-benzene; \circ , aqueous 0.1 *M* KBr-*n*-heptane; \bullet , aqueous 0.1 *M* KBr-benzene.

using the double capillary technique it was possible to let the solution surfaces equilibrate for the necessary periods of time (up to 12 hours) required. The results obtained with this method at 20, 30 and 40° are represented by the three lowest curves in Fig. 2. Unlike the other polysoaps studied, this polymer is surface active in water in the absence of simple electrolyte. Amundson had already observed that this polymer also differs from polysoaps prepared from poly-4-vinylpyridine in that it is a good emulsifying agent, that it does not solubilize hydrocarbons and that it has a high intrinsic viscosity, which implies a rather extended molecular structure.⁸ The extended molecular structure which causes the hydrophobic hydrocarbon side chains to be more exposed to the solvent and the lower degree of quaternization which reduces the solvent affinity may explain the high surface activity.

Correlation of Solubilization and Surface Tension.—The effect of solubilization on the vis-

cosity^{7,30,31} and the electrolytic conductance³² of polysoap solutions has been studied previously. Of especial interest was the maximum in the curves obtained when the reduced viscosity, η_{sp}/C , was plotted against *K*, the concentration in g./100 ml. of an aromatic solubilizate. Such a plot is shown in Fig. 3 for the solubilization of diphenylmethane in a 6% aqueous solution of the "35.0%" poly-4-vinylpyridine polysoap (half-shaded circles, ordinate on left). The surface tension results obtained by two independent methods with the same solutions used for the viscosity measurements also is shown in Fig. 3 (open and closed circles, ordinate on right). The surface tension is seen to decrease uniformly, while the reduced viscosity goes through its maximum. Therefore, the viscosity maximum cannot be ascribed to a corresponding maximum in the hydrophobicity of the polysoap molecules. A saturated aqueous solution of diphenylmethane had a surface tension of 71.1 dynes/cm., thus eliminating the possibility that the surface tension depression of the polysoap solution was caused by unsolubilized hydrocarbon. The surface tension then indicates that the solubilization enhances the surface activity of the polysoap molecules.

Interfacial Tension.—The effect of the "9.5%", "20.3%" and "35.0%" polysoaps on the interfacial tension of the following four solvent pairs was studied: (1) water, heptane; (2) water, benzene; (3) 0.1 *M* KBr, heptane; (4) 0.1 *M* KBr, benzene. The results for the "35.0%" polysoap which are very similar to those obtained with the other two polysoaps are given in Fig. 4. The depressions of the interfacial tension are seen to be considerably larger than the depressions of the surface tension, indicating that the hydrocarbon enhances the tendency of the polysoap to come to the interface. This can be demonstrated in a more quantitative way by examining the values of Γ_2 and α , calculated from the interfacial tension results by means of equations 3 and 4.³³ Depending only on the polysoap and KBr concentrations but very little on which of the three polysoaps or two hydrocarbons were used, the results for Γ_2 and α can best be summarized by presenting the average values, obtained at *C* = 0.0025, 0.025 and 0.25 g./dl., of the six polysoap-0.1 *M* KBr-hydrocarbon systems. The respective average values of Γ_2 are 21, 12 and 5×10^{-11} moles/cm.² those of α are 80, 140 and 330 Å.²/molecule, with the mean deviation from the individual values in each case close to 10%. By

(30) L. H. Layton, E. G. Jackson and U. P. Strauss, *J. Polymer Sci.*, **9**, 295 (1952).

(31) U. P. Strauss and L. H. Layton, *J. Phys. Chem.*, **57**, 352 (1953).

(32) U. P. Strauss and S. S. Slowata, *ibid.*, **61**, 411 (1957).

(33) It is assumed here that the solubilization does not affect the validity of equation 3. Since the polysoaps are insoluble in the liquid hydrocarbons, and since the chemical potential of the solubilized hydrocarbon is constant, the hydrocarbon component does not enter explicitly into the expression for Γ_2 . Therefore, in any case, equation 1 must be valid. However, the thermodynamic parameters a_{ij} may be altered by the solubilization, and since the necessary data for calculating these parameters are not available, we cannot be sure on theoretical grounds that the derivation of equation 3 from equation 1 is justified for this case. However, since equation 3 gives about the same results for Γ_2 for those systems where solubilization is known to be absent (see below) as in those where it is known to occur, we believe the above assumption to be valid.

comparing these results with those in Table I, we see that at the low polysoap concentrations the adsorption is substantially enhanced by the presence of the hydrocarbon layer, and, if the results for α are to be interpreted literally, that only a few hydrocarbon groups per adsorbed polysoap molecule can be accommodated in the interface.

While it has been shown that solubilization enhances the surface activity of polysoaps, this effect plays only a minor role in the interfacial tension depression. There are two pieces of evidence for this. First, while benzene is solubilized to a much

greater extent than heptane,^{7,30,31} the interfacial tension depressions with both hydrocarbons were about the same. Second, it is known that the "9.5%" polysoap does not solubilize heptane, while the "35.0%" polysoap does.⁷ Yet, under corresponding conditions, the "9.5%" polysoap was never the less effective of the two in depressing the interfacial tension in the heptane systems. It seems therefore more likely that the enhancement of the depression is due to the free energy of mixing of the liquid hydrocarbon with the paraffin side chains of the polysoap in the interface.

SEPARATION OF NITROGEN AND OXYGEN ISOTOPES BY EXCHANGE OF NITRIC OXIDE WITH NON-AQUEOUS SOLUTIONS OF NITRIC OXIDE COMPLEXES¹

By A. NARTEN AND T. I. TAYLOR

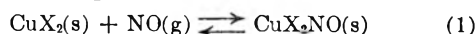
Department of Chemistry, Columbia University, New York, N. Y.

Received May 24, 1961

The distribution of the nitrogen and oxygen isotopes between gaseous NO and the CuCl_2 -complex in liquid methanol has been studied. The separation factor $\alpha(\text{N}^{14}/\text{N}^{15})$ has been determined by single stage equilibration: $\alpha(\text{N}^{14}/\text{N}^{15})$ varies from 1.017 at -20° to 1.012 at $+10^\circ$. The separation obtained in a 200 cm. column packed with 2×2 mm. silver mesh rings corresponds to stage heights of 2.2 and 3.0 cm. at interstage flows of 1.0 and 1.3 mM NO/cm^2 min. and temperatures $+14^\circ$ and -20° . From column experiments the separation factor for the oxygen isotopes has been estimated as $1.01 > \alpha(\text{O}^{16}/\text{O}^{18}) > 1.005$ at room temperature. The system can be refluxed thermally (exchange-distillation) and is attractive for N^{15} -enrichment. It is not feasible for O^{18} -enrichment due to side reactions in the column.

Introduction

Nitric oxide reacts with cupric halides in non-aqueous solutions forming a loose addition compound according to the reversible reaction

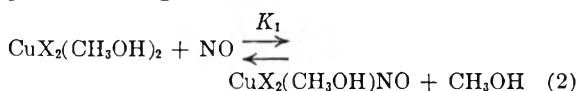


X being the anion Cl or Br, s being a great number of organic solvents, such as alcohols, ethers, esters, ketones, nitriles and carbonic acids. A maximum amount of 1 mole NO per mole CuX_2 can be absorbed by these solutions.² The addition compounds CuX_2NO can be obtained only in solution. They are intensely colored, ranging from deep blue to black violet. The color of the complex solutions is reported to vanish if an inert gas is bubbled through the liquid. The absorbed NO is also desorbed upon dilution with water.³ Aqueous solutions of cupric halides will absorb only traces of NO, and the nitric oxide complexes in non-aqueous CuX_2 -solutions are highly sensitive to water.⁴

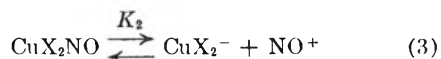
Methanol as a solvent for NO-complex forming cupric halides is commercially available at low cost; it can be dehydrated easily and dissolves the largest amount of CuX_2 . It is for these reasons that systems of CuX_2 in methanol with NO as the gas phase were investigated by us as a possible means for the separation of the isotopes of nitrogen and oxygen.

The deep blue color of the CuX_2NO -complexes

in methanol is due to the covalent CuX_2NO (probably solvated). The degree of association, $\beta = \text{moles NO/moles Cu}$ in solution, of the complex according to



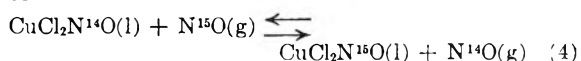
can be calculated from the equilibrium constant K_1 ⁵; at room temperature and atmospheric pressure the values are $\beta = 1$ for $\text{X} = \text{Br}$, and $\beta < 1$ for $\text{X} = \text{Cl}$. The CuX_2NO -complex in methanol dissociates⁵ into colorless ions



($K_2 \ll K_1$), and this has been responsible for erroneous structures suggested for the complexes.³

Separation Factors

The separation factor $\alpha(\text{N}^{14}/\text{N}^{15}) = [N(\text{N}^{15})/N(\text{N}^{14})]_{\text{l}}/[N(\text{N}^{15})/N(\text{N}^{14})]_{\text{g}}$, ($N = \text{mole fractions}$, l = liquid, g = gas), for the distribution of the nitrogen isotopes between gaseous nitric oxide and the CuCl_2NO -complex in methanol according to



was determined by single stage equilibration and subsequent analysis of the gas and liquid phases. The nitric oxide from both phases was completely

(1) Supported by a grant from the U. S. Atomic Energy Commission.

(2) W. Manchot, *Chem. Ber.*, **47**, 1601 (1914).

(3) V. Kohlschutter and M. Kutscheroff, *ibid.*, **37**, 3044 (1904).

(4) W. Manchot and E. Linkh, *ibid.*, **59**, 406 (1926).

(5) R. T. M. Frazer and W. E. Dament, *J. Am. Chem. Soc.*, **82**, 348 (1960); R. T. M. Frazer, private communication, to be published.

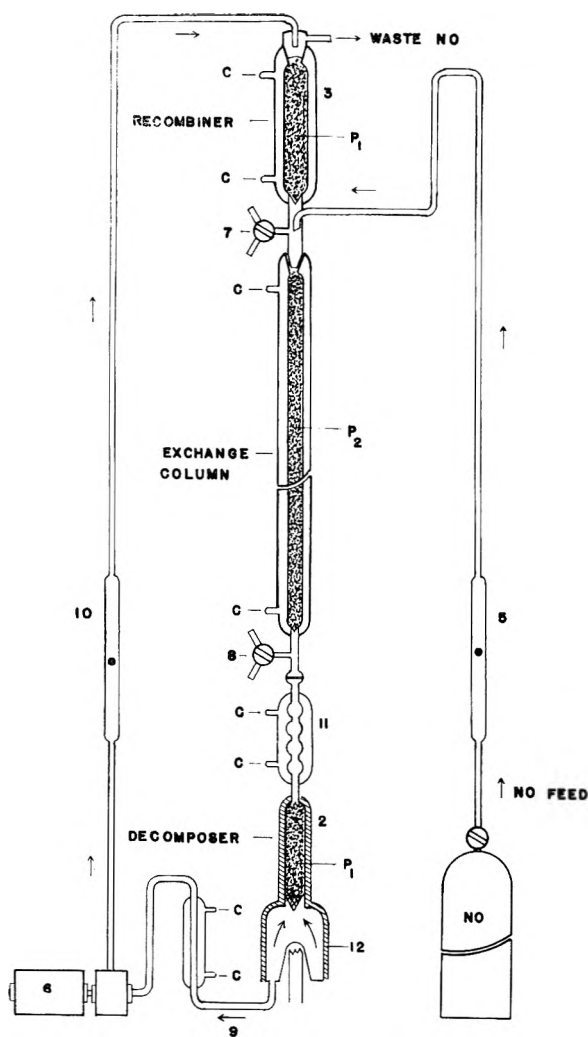
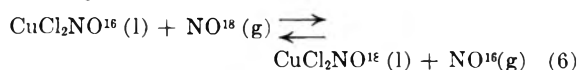


Fig. 1.—Column used for the determination of separation parameters.

separated by standard techniques and then reduced to nitrogen.⁶ Isotopic analysis was carried out in a CEC 21-201 dual collector mass spectrometer using the 29/28 ratio. At least three independent equilibrations each at temperatures between +10 and -20° and atmospheric pressure were carried out to obtain the equation

$$\log (N^{14}/N^{15}) = (4.80/T - 1.17 \times 10^{-2}) \pm 1.5 \times 10^{-3} \quad (5)$$

The separation factor $\alpha(O^{16}/O^{18})$ for the distribution of the oxygen isotopes between gaseous NO and the $CuCl_2NO$ -complex in methanol according to



was not determined. For the evaluation of single stage equilibration experiments it is necessary to assay the oxygen from the nitric oxide in both (or at least one of the) phases. With our present techniques we were unable to separate the NO-oxygen from the oxygen originating from reaction

(6) T. I. Taylor and W. Spindel, in "Proceedings of the International Symposium on Isotope Separation," North Holland Publishing Co., Amsterdam, 1958, p. 158.

products between NO and CH_3OH with the precision required for isotopic analysis. From column experiments we were able to estimate

$$\alpha(O^{16}/O^{18}) > 1.005 \quad (7)$$

at room temperature and atmospheric pressure.

No attempt was made to determine α for the CuB_2NO/NO -system (see next section).

The separation factors discussed in this section are summarized in Table I.

TABLE I
SUMMARY OF DATA ON EXCHANGE SYSTEMS BETWEEN GASEOUS NO AND $CuCl_2NO$ -COMPLEXES IN METHANOL AT ATMOSPHERIC PRESSURE

	+16°	+14°	-20°
Moles Cu/l	1.45	2.42	2.50
β	0.40	0.40	0.75
Moles NO/l.	0.58	.96	1.88
$\alpha(N^{14}/N^{15})$	1.012	1.012	1.017
$\alpha(O^{16}/O^{18})$	>1.005	>1.005	>1.005
H.E.T.P. (cm.) at	4.5 ^a	2.2 ^b	3.0 ^b
Optimum flow (mM NO/cm. ² min.)	2.8 ^a	1.0 ^b	1.3 ^b

Height of packed section 200 cm., 1 cm. i.d.; column packed with: ^a 1.6 mm. i.d. glass helices; ^b 2 × 2 mm. silver mesh rings, 1500 mesh/cm.².

Column Experiments

In order to utilize the exchange of nitrogen and oxygen isotopes between the gas and liquid phases of the CuX_2NO -NO systems according to (4) or (6) in an isotope separation process, the liquid and gas streams must be passed countercurrently in an exchange column with convenient reflux mechanisms on both ends. Since both N^{15} and O^{18} concentrate in the liquid phases of the system it is possible to produce the two heavy nuclides in the same separation unit.

Figure 1 shows the column which was used in the experiments. It consisted essentially of 3 sections: the exchange column (200 cm. long, 1 cm. i.d.) was packed with two different kinds of packing P_2 described below. Both the decomposer (40 cm. long, 2 cm. i.d.) and the recombiner (30 cm. long, 2 cm. i.d.) were packed with 3.2 mm. i.d. glass helices (Scientific Glass Co.). All three sections were kept at constant temperature by means of a circulating coolant C. Feed NO was introduced at a point between the column and the recombiner; in the experiments described, mixing of the feed gas with the upstreaming, depleted NO from the exchange column was allowed. The feed flow was adjusted so that the top concentration at 7 was near the natural isotopic abundance, and was controlled by the flow meter 5. The decomposer consisted of a still-pot, a rectifying section 2 and a condenser 11. The downstreaming liquid equilibrium mixture of CuX_2NO , CuX_2 and CH_3OH was warmed to some 60° by an upstream of methanol vapor which at the same time kept the NO-partial pressure in the rectifying section low. By the time the liquid reached the still-pot 12, the CuX_2NO complex was completely dissociated, and the pure CuX_2-CH_3OH solution was recycled to the top of the recombiner by means of a finger pump 6. The liquid flow was controlled by a flow meter 10. Methanol vapor from the decomposer was refluxed in the condenser 11. Top and bottom samples were taken from the gas phase through the three-way stopcocks 7 and 8, and were processed for mass spectrometer analysis as described before. Reflux of the two countercurrent phases was accomplished by absorbing the upstreaming NO in the re-cycled liquid CuX_2-CH_3OH solution in the recombiner. The CuX_2NO -complex in the downstreaming liquid was converted to gaseous NO in the thermal decomposer. To determine the reflux efficiency in the recombiner, samples of the liquid were taken at a point 9 (Fig. 1) and analyzed for nitric oxide. No NO could be detected in the liquid, even at very low boil-up rates in the pot of the decomposer. The only mechanical part in the whole system

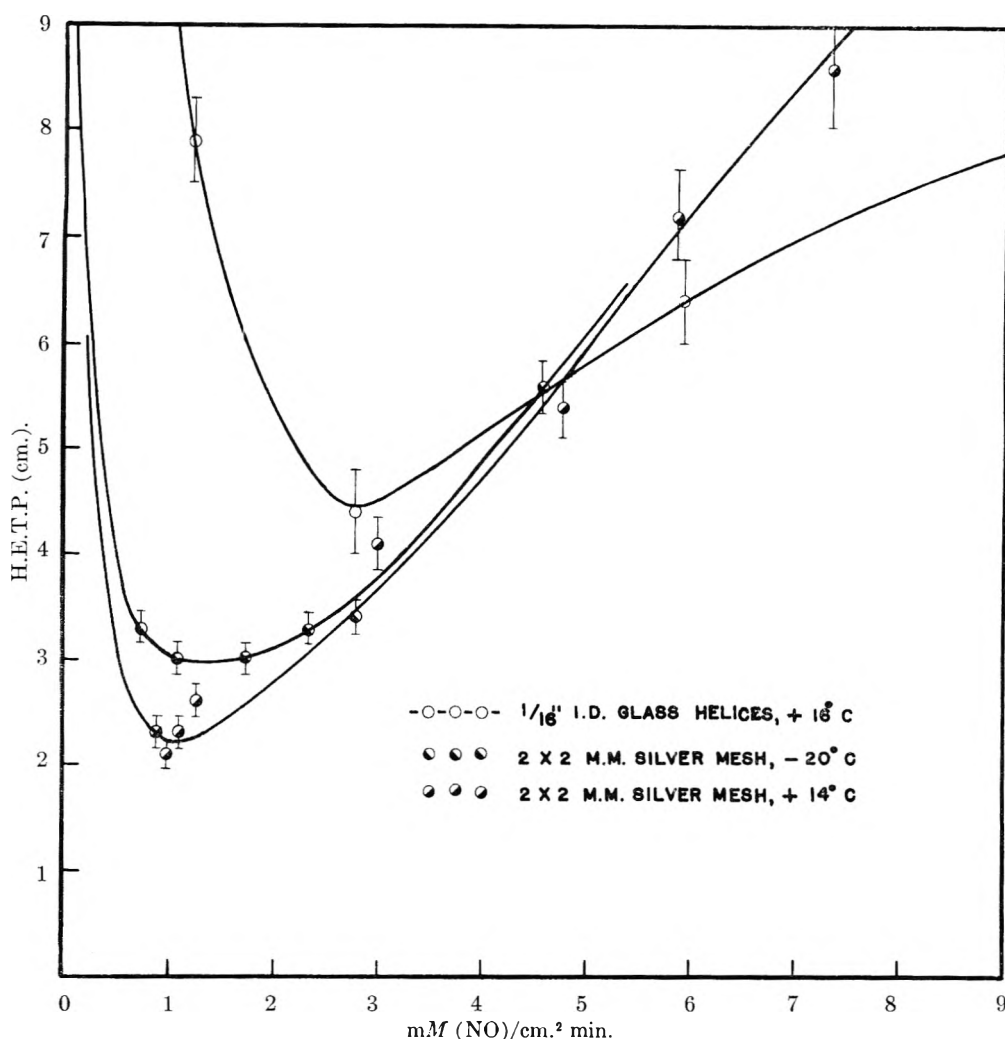


Fig. 2.—Flow dependence of the stage height (H.E.T.P.) for the NO-CuCl₂NO-CH₃OH system in a 200-cm. column, 1 cm. i.d.

was the finger pump which recycled the NO-free liquid phase. Thus, the operational stability of the entire unit was found to be excellent for CuCl₂, (with Br₂ see below). The column was operated for several weeks without continuous attention. Considerable difficulties had to be overcome because of the corrosiveness of the materials handled in the system. Glass was used where this was possible. In the finger pump, latex tubing was very satisfactory. Only glass and silver could be used as packing materials in the exchange column. All metals which are less noble than copper will reduce the Cu²⁺, giving CuX, which is insoluble in methanol. Among the materials tested were various stainless steels, Hastelloy B, and tantalum. Silver will form a compact coating of AgX in CuX-CH₃OH solution; a silver packing which has been conditioned for 7 days will not react with any component of the discussed systems. Packings used in the column experiments were 1.6 mm. i.d. glass helices (Scientific Glass Co.) and 2 × 2 silver mesh rings, 1500 mesh/cm.² (Eggmann and Co, Basel, Switzerland).

Due to the low NO-hold-up in the column, equilibrium was reached in less than 24 hours at all flow rates. From the measured over-all separation S_w , at infinite reflux, the stage height, λ_w , (HETP) was determined for the CuCl₂NO-NO system, using the well known relation

$$\lambda_w = L \frac{\ln \alpha}{\ln S_w} \quad (8)$$

L being the column length. The results are presented in Fig. 2.

The low value of $\lambda = 2$ cm. at room temperature clearly indicates that the rate of exchange is very fast. It is in fact determined by the rate of diffusion in the liquid phase;

comparable stage heights in a distillation column have been reported⁸ as $\lambda = 1$ cm. From an equation given by Kuhn,⁹ which relates the stage height with the various possible resistances to diffusion and interface mass transfer in a separation column, it can be shown⁷ that for exchange processes with a liquid carrier phase (if the concentrations of the substance to be separated in the liquid (C_L) and gas phase (C_g) is $C_L > 10C_g$) carried out in two different columns (1 and 2), or for a column operated at two different temperatures or (and) pressures (1 and 2)

$$\lambda_1/\lambda_2 = D_1/D_2 \left(\frac{\rho_1 \eta_2}{\rho_2 \eta_1} \right)^{1/3} \left(\frac{C_1}{C_2} \right)^{4/3} \cong \frac{T_1}{T_2} \left(\frac{\rho_1}{\rho_2} \right)^{1/3} \left(\frac{\eta_2 C_1}{\eta_1 C_2} \right)^{4/3} \quad (9)$$

D are the diffusion coefficients, ρ the specific weights, η the viscosities, T the kelvin temperatures, and C the concentrations in the liquid phase at the operating conditions 1 and 2; (9) gives a good approximation if the liquid and gas flows in the column under the conditions 1 and 2 are similar, i.e., if the interstage flow is the same. The stage height in an exchange column is necessarily higher than the one obtained in distillation columns under comparable conditions because of the fact that the concentration of the substance to be separated in the liquid phase is lower, even if the chemical exchange reaction as such is very fast.

(7) B. Stuke, *Z. Elektrochem.*, **57**, 655 (1953).

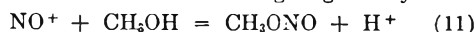
(8) M. Thuerkauf, A. Narter and W. Kuhn, *Helv. Chim. Acta*, **43**, 989 (1960).

(9) W. Kuhn, *ibid.*, **37**, 1416 (1954), equation 17.

In the case of isotopically double-labelled substances such as NO, the stage height at infinite reflux, λ_ω , is the same for both nuclides. It is therefore possible to determine $\alpha(O^{16}/O^{18})$ from the measured over-all separation $S_\omega(O^{16}/O^{18})$ and $S_\omega(N^{14}/N^{15})$, using the known values of λ_ω and $\alpha(N^{14}/N^{15})$, according to

$$\alpha(O^{16}/O^{18}) = \alpha(N^{14}/N^{15}) + S_\omega(O^{16}/O^{18})/S_\omega(N^{14}/N^{15}) \quad (10)$$

In the case of the $CuCl_2NO-NO$ system with methanol as the carrier phase, we found that $S(O^{16}/O^{18})/S(N^{14}/N^{15})$ depended on the flow in the column (at constant temperature). This can be explained only by the assumption that the column was not operating at total reflux. On the other hand, the parasitic production of the column was so small that it did not affect the separation of the nitrogen isotopes noticeably; the measured stage height $\lambda = 2$ cm. is in accord with (9). The possibility of an exchange of oxygen between NO and CH_3OH in the decomposer had to be eliminated, since we found no exchange upon equilibrating 1% NO^{18} with $CH_3OH-CuCl_2$ of natural oxygen abundance. In order to obtain a certain separation in an exchange column, it is necessary to operate the column at a reflux ratio $R > H$, H being the minimum reflux ratio, which is determined by the top and bottom concentrations and the separation factor. Both the top concentration and the separation factor are different for O^{16}/O^{18} and N^{14}/N^{15} . It is therefore conceivable that the parasitic production is such that for the nitrogen isotopes $H \ll R$, and therefore $\lambda \cong \lambda_\omega$, while for the oxygen isotopes $H \cong R$ and therefore $\lambda > \lambda_\omega$.¹⁰ A small constant withdrawal of nitric oxide at the bottom of the column thus can have quite different effects on the nitrogen or oxygen separation. Our measurements are consistent with the assumption of a small constant parasitic production and a separation factor $1.005 < \alpha(O^{16}/O^{18}) < 1.01$ at room temperature. Losses of NO at the product end of the column did not occur as a consequence of incomplete decomposition of the $CuCl_2NO$ -complex in the decomposer or liquid reaction products between NO and CH_3OH . Therefore, a gaseous product must be formed at the bottom end which leaves the column with the waste NO stream without exchanging its NO with the downstreaming liquid. Frazer⁵ has found that the CuX_2NO -complexes dissociate according to (3); the NO^+ ion thus formed does not remain as such in methanol (or other alcohols), instead, it reacts with methanol giving methyl nitrite



which is removed as parasitic product with the waste NO at a rate depending on the liquid and gas flows in the column and on the temperature both in the column and in the decomposer.

The major part of the experiments described in this section was carried out with $CuCl_2$ as the NO-complex forming halide in methanol. The $CuBr_2-NO$ system is inferior because $CuBr_2$ undergoes reduction in the presence of CH_3OH and NO, especially at the elevated temperature of the decomposer. The resulting $CuBr$ is almost insoluble in methanol, and will plug the column, thereby

decreasing the operational stability of the column greatly. The over-all separation $S_\omega(N^{14}/N^{15})$ for this system was found to be lower than with the $CuCl_2-NO$ system at comparable flow rates and temperatures. Therefore, no further attempts were made to determine the various parameters for the $CuBr_2-NO$ system.

Discussion

Systems consisting of CuX_2NO -complexes in methanol with NO as the gas phase have the desirable feature of not requiring chemical reflux. This makes it possible to use an exchange-distillation process for simultaneously concentrating both nitrogen-15 and oxygen-18. However undesirable side reactions in an exchange-distillation column which cannot be avoided without affecting other parameters in a way unfavorable to the separation characteristics of the systems, make the $CuBr_2-NO$ system not feasible for isotope separation at all and the $CuCl_2-NO$ system, for the concentration of oxygen-18 (although this is possible in principle).

However a system of $CuCl_2NO$ in methanol with NO as the gas phase is attractive for the concentration of nitrogen-15. The separation factor, stage height, reflux efficiency, and decomposition rate are favorable, and operation of the system is relatively simple and economical. As compared with other systems the only critical element involved in the scale-up of a $CuCl_2-NO$ cascade is the material of construction. Only glass, porcelain, or ceramic-lined metals appear to be feasible materials. Glass, ceramics, or silver will have to be used for the packing.

It is our opinion that the simultaneous concentration of nitrogen-15 and oxygen-18 (oxygen-17) by an exchange-distillation process using NO as the gas phase and solutions of NO-complex forming metal salts as the liquid phase would be very attractive. Experiments to find NO-complex forming metal salts which will permit the use of stainless steel or Hastelloy as construction and packing materials in a solvent which is capable of solvating the NO^+ ion without reacting with any component of the system so far have been unsuccessful.

Acknowledgment.—The authors are indebted to Professor W. Spindel of Rutgers University for use of his mass spectrometer in the single stage equilibration experiments, and to Dr. H. Hoever for stimulating discussions. The assistance of Mr. E. Fischbach was very helpful in the column experiments.

(10) W. Kuhn, P. Baertschi and M. Thuerkauf, *Chimica*, **8**, 109 (1954), equations 19, 20b, 20e. K. Cohen, "The Theory of Isotope Separation, National Nuclear Energy Series," III-1B, McGraw-Hill Book Co., New York, N. Y., 1951, p. 32, equation 2.13.

PROTON MAGNETIC RESONANCE STUDY OF THE BASICITY OF THE SILICON-OXYGEN BOND

By CHARLES M. HUGGINS

General Electric Research Laboratory, Schenectady, New York

Received May 26, 1961

The relative basicities of a series of siloxanes, alkoxy silanes and ethers were measured with respect to the proton donors ethanol, methanol and chloroform by the p.m.r. dilution shift of the acid proton. The magnitude of this shift in similar systems has been correlated with the extent of hydrogen bonding between the proton donor and the solvent molecule. P.m.r. shifts for chloroform of $\delta = -0.740$ were observed in the two ethers; the siloxanes caused shifts of less than $\delta = -0.057$, with the singular exception of hexamethylcyclotrisiloxane, $\delta = ca. -0.3$. The alkoxy silanes exhibited shifts intermediate between these two limits. It is argued that the normal siloxane linkage is essentially inert with respect to hydrogen bonding to chloroform due to the smaller effective electronegativity of silicon as compared to carbon. Essentially identical results were obtained using alcohols as proton donors, in which hexamethyldisiloxane compares closely with cyclohexane. These data, taken with previous work on siloxanes, demand consideration of bonding of a different type than in ethers. The implications of previously proposed $d\pi-p\pi$ dative bonding with respect to both the chemical and physical properties of siloxanes are discussed briefly.

Introduction

Of basic importance in the study of silicon chemistry is an understanding of the electron donating or withdrawing power of silicon. In a previous report,¹ it was shown that the substitution of silicon for carbon in chloroform considerably reduces both the acidity of the chloroform proton and the basicity of the over-all molecule. This effect was attributed to the decreased ionicity of the Si-H σ bond and to the formation of Si-Cl $d\pi-p\pi$ multiple bonds with the resultant decrease in ionicity.

It is, perhaps, of more importance to understand the character of the Si-O-Si bond, inasmuch as it forms the basic linkage of all higher silicone monomers and polymers. One measure of this bond character is its effective basicity as indicated by hydrogen-bonding interaction with proton donors. The magnitude of the interaction is a measure of the ionicity of the Si-O-Si bonding. The hydrogen-bonding of ethers (C-O-C) to a variety of proton donors has been studied in detail by various techniques. It is generally agreed that ethers form conventional hydrogen bonds to such proton donors as alcohols, phenols and chloroform.²⁻⁵ In a compilation of data on hydrogen-bonding systems, Tsuboi⁶ ranked the basicity of dithylether below acetone, water and methanol and above phenol, mesitylene and benzene.

The basicity of the direct silicon analogs of ethers, siloxanes, is just being investigated in detail. From first-order considerations of electronegativity, it would be expected that the Si-O-Si bond should be more ionic than C-O-C, hence more basic, and exhibit stronger hydrogen-bonding interactions with proton donors. However, arguments have been proposed to the effect that siloxanes are considerably less basic than the corresponding ethers. Qualitative measurements of heats of mixing of

siloxanes with chloroform indicate only minor interaction whereas the ether-chloroform system has a heat of mixing of about 700 cal./mole.⁷ In addition, solubility data for siloxanes in polar solvents indicate a lack of any strong specific interactions. A large series of siloxanes were investigated by West, Whatley and Lake,⁸ who measured infrared frequency shifts of the pyrrole and phenol acidic protons. Their results indicate a progressive decrease in basicity through the series, ether to alkoxy silane to siloxane. Because of the sometimes misleading nature of the infrared experiment³ the proton magnetic resonance (p.m.r.) frequency shift can serve as a definitive confirmation. The rather weak acid, chloroform, was chosen because of its single p.m.r. absorption peak, the small degree of self-association, and the quantity of previous work on chloroform in other solvents. Similar measurements using methanol and ethanol as test acids will demonstrate any marked steric effects or any reversals of form with respect to stronger acids.

Experimental

All spectra were obtained on a Varian Associates V-4300B High Resolution NMR spectrometer operating at a field strength of approximately 9400 gauss and a frequency of 40 megacycles. The chemical shifts were measured by techniques described by Tiers.⁹ In each case, the audio-frequency was measured to ± 0.1 c.p.s. and the chemical shift determined to ± 0.3 c.p.s. by the averaging of three or more separate measurements.

The shift of the chloroform proton was measured with respect to internal standards—cyclohexane, tetramethylsilane, or the trimethylsilyl group of the alkoxy silanes—depending on interference from solvent protons. Cyclohexane and tetramethylsilane have been widely used as internal standards for which it is assumed that the standard is subjected to no p.m.r. perturbations other than volume susceptibility changes. Since the unknown is being measured with respect to the internal standard in the same solution, this volume susceptibility shift cancels in the difference measurement. In these solutions, it is not expected that specific chemical interactions such as hydrogen bonding or complexing would be likely to effect shifts in the cyclohexane or trimethylsilane resonances—that is, the standards are considered to be "inert." However, it is becoming increasingly obvious that at least one other effect does influence the frequency of the internal reference. Evans¹⁰ found large

(1) C. M. Huggins and D. R. Carpenter, *J. Phys. Chem.*, **63**, 238 (1959).

(2) G. C. Pimentel and A. L. McClellan, "The Hydrogen Bond," W. H. Freeman & Co., San Francisco, Cal., 1960.

(3) C. M. Huggins and G. C. Pimentel, *J. Phys. Chem.*, **60**, 1615 (1956).

(4) R. C. Lord, B. Nolin and H. D. Stidham, *J. Am. Chem. Soc.*, **77**, 1364 (1955).

(5) G. J. Korinek and W. G. Schneider, *Can. J. Chem.*, **35**, 1157 (1957).

(6) M. Tsuboi, *Bull. Chem. Soc. Japan*, **25**, 60 (1952); *J. Chem. Soc. Japan*, **72**, 146 (1951).

(7) C. S. Marvel, N. J. Copley and E. Ginsberg, *J. Am. Chem. Soc.*, **62**, 3109 (1940).

(8) R. West, L. Whatley and K. J. Lake, *ibid.* **83**, 761 (1961).

(9) G. V. D. Tiers, *J. Phys. Chem.*, **62**, 1151 (1958).

(10) D. F. Evans, *Proc. Chem. Soc.*, 115 (1958).

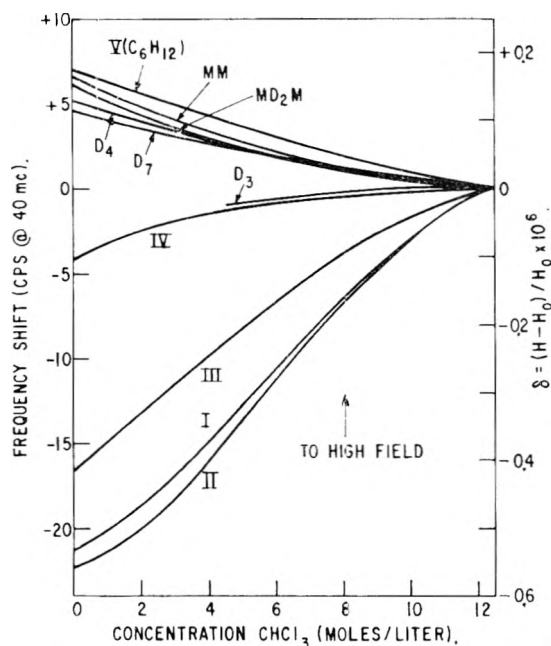


Fig. 1.—P.m.r. dilution shifts of CHCl_3 in various solvents (see text).

shifts in the fluorine resonance of benzotrifluoride in various solvents, the largest shifts being observed in solution with highly polarizable molecules such as methylene iodide and benzene. Similar effects, although much smaller in magnitude, have been observed in proton resonances. It may be said then that solvent effects other than hydrogen bonding or complexing may be important in determining the precise value of a proton resonance dilution shift.

The use of external references precludes this difficulty in measurement provided reliable susceptibility data are available. For many systems, including the silicon materials, such data are not generally available. Since it is more convenient to use internal reference materials, it is quite important to realize the nature of the assumptions involved. These experiments generally consist of studying the p.m.r. concentration dependences of a particular line of a solute molecule in a variety of solvents to which a trace of the reference material (e.g., cyclohexane) has been added. An ideal reference material would exhibit no p.m.r. shifts other than that due to volume susceptibility in any solvent; however, for comparative purposes, it is sufficient that any solvent polarization shifts be equivalent in the various solvents. This latter assumption is implicit in the measurements reported in this work. It is felt that the gross similarity of the several solvents makes this plausible.

The solvents used were either commercial, analytical grade reagents or laboratory stock available from previous preparations. The solvents were redistilled in a multiplate column. All liquids, including chloroform, were dried over Linde Molecular Sieve. All glassware was baked overnight at 120° and rinsed in the solvent to be used. Finally, all materials were scanned at maximum gain for any spurious p.m.r. absorptions with particular attention to the region in which water would be expected; none were found.

For the alcohol systems, the frequency shifts were measured with respect to internal standards: $(\text{CH}_3)_4\text{Si}$, 1% by volume, for the alcohol-cyclohexane and alcohol-ether systems, and the $(\text{CH}_3)_3\text{Si}$ -protons for alcohol-hexamethyldisiloxane systems. The measured shifts are sufficiently large to minimize the significance of observational errors introduced by the use of internal standards. Data for diethyl ether and ethyl alcohols were complicated by the strong interference of the methylene group. The concentration range of data for methanol-cyclohexane was severely limited by their relative immiscibility.

In mixtures involving "pure" alcohol, the hydroxyl proton resonances were split into the characteristic quartet for methanol and triplet for ethanol. Following common practice, a trace of HCl was added to exchange-narrow the hydroxyl band into a single line. Tests showed that up to

50 p.p.m. HCl could be used without causing noticeable shifts in the observed frequency—all samples contained 1–10 p.p.m. HCl added as a concentrated aqueous solution. Room temperature was maintained at $27 \pm 0.5^\circ$ for all measurements.

Results

The p.m.r. concentration dependence of chloroform was measured in ten solvents: two ethers, diethyl ether (I) and diisopropyl ether (II); two alkoxy silanes, trimethylethoxysilane (III) and trimethyl-*t*-butoxysilane (IV); five siloxanes, hexamethyldisiloxane (MM), decamethyltetrasiloxane (MD_2M), octamethylcyclotetrasiloxane (D_4), tetradecamethylcycloheptasiloxane (D_7), and hexamethylcyclotrisiloxane (D_3); and the assumed inert solvent, cyclohexane (V). The measurements as recorded are shown in Fig. 1. The measured shifts have been reduced to a common origin, $\delta = 0.0$, for concentrated chloroform. The concentration scale, moles/liter, rather than mole fraction, results in more directly comparable plots for these solvents of grossly varying molecular weights.

The top curve shown is for the chloroform-cyclohexane system; the others all show shifts to low field for the chloroform proton. This is consistent with expectations for hydrogen bonding to *n*-donor bases. The extrapolated value of the chemical shift for dilute chloroform is then a measure of the extent of complexing. These extrapolated values are listed in Table I. Since chloroform exhibits some self-association, the interpretation of any system requires correction for the dilution shift of chloroform itself. The data for the cyclohexane solutions are used as a basis for this correction. This assumption is, of course, subject to the reservations discussed earlier; that is, the measured shift includes any non-specific polarization shifts of chloroform and/or cyclohexane. However, since the data are only comparative, this effect will tend to be uniform over the solvents studied. Table I also includes the association shifts corrected by subtraction of $\delta = +6.8$ c.p.s.

TABLE I
P.M.R. SHIFTS OF CHCl_3 IN VARIOUS SOLVENTS

Solvent	$\Delta\delta$, obsd.	$\Delta\delta$, cor.
V C_6H_{12}	+0.170	(0)
MM $(\text{Me}_3\text{Si})_2\text{O}$	+ .155	-0.015
MD_2M $(\text{Me}_3\text{SiOSiMe}_2)_2\text{O}$	+ .145	- .025
D_4 $(\text{Me}_2\text{SiO})_4$	+ .122	- .048
D_7 $(\text{Me}_2\text{SiO})_7$	+ .113	- .057
D_3 $(\text{Me}_2\text{SiO})_3$	(- .1) ^a	(- .3) ^a
IV $\text{Me}_3\text{SiOCMe}_3$	- .105	- .275
III $\text{Me}_3\text{SiOCH}_2\text{Me}$	- .420	- .590
II $\text{Me}_2\text{HCOCHMe}_2$	- .535	- .705
I $\text{MeH}_2\text{COCH}_2\text{Me}$	- .570	- .740

$$\Delta\delta = \delta(\text{infinite dilution}) - \delta(\text{pure } \text{CHCl}_3)$$

$$\delta = (H - H_0)/H_0 \times 10^{-6}$$

^a Extrapolated.

At least two effects must be considered in correlating these shifts with chemical structure: the relative electronegativity of silicon *vs.* carbon and steric factors. It is obvious that the net association of two interacting groups depends both on their reactivities and upon the ease with which they can approach each other. It would be desirable to

compare only ethers and siloxanes having identical steric hindrances; such a comparison is, of course, impossible. Even if the two systems are similarly substituted, the molecular sizes and bond angles are grossly different. The larger bond angle (ca. 155°)¹¹ causes greater shielding for the Si-O-Si system; however, this is at least partially offset by the larger size of silicon. The effect of the reduced electronegativity of silicon can be seen readily by comparing the association shifts of the three groups: ethers, alkoxy-silanes and siloxanes. The two ethers, diethyl and diisopropyl, each show shifts of $\delta = -0.705$ and $\delta = -0.740$, indicating no appreciable difference in steric hindrance. The two alkoxy-silanes, trimethylethoxysilane and trimethyl-*t*-butoxysilane, show corrected shifts of $\delta = -0.590$ and $\delta = -0.275$, respectively. The smaller value for the *t*-butoxy compound is interpreted to be a measure of the relative steric hindrance compared to the ethoxy group. The smaller shift of the ethoxysilane compared to the ethers is considered to be the result of a decrease in basicity.

The siloxanes uniformly exhibit only negligible interaction with chloroform, with one exception (D_3). The maximum shift observed for the siloxanes (except D_3) is $\delta = -0.057$ for D_7 . It is interesting though that even these shifts are in the direction of quite weak bonding. The cyclic trisiloxane (m.p. 64°) was studied only over the limit of its solubility in chloroform at room temperature. The data over this range indicate a reasonably strong interaction of the same magnitude as trimethyl-*t*-butoxysilane. It is well known that D_3 possesses some ring strain,¹² thus it is prevented from forming normal Si-O-Si bond angles. The resultant forced bending of the bonds decreases the bond order and lowers the tendency to form dative multiple bonds. Hence, the ionicity should be greater than in the unperturbed bond.

A comparison of the p.m.r. data in Table I with the infrared data of West, *et al.*,⁸ is shown in Fig. 2. All the points, except D_3 , correlate within expectation. It should be noted that a lack of detailed correlation would not be unreasonable, since different effects are operative in the two measurements. The infrared shift is a measure of the hydrogen-bonding perturbation in the bound state; the measured p.m.r. shift represents only a lower limit since it is a weighted average of the bound and free states. The p.m.r. shift would show marked temperature dependence, whereas the infrared shift is only slightly temperature sensitive. However, the correlation as presented does lend credence to both sets of data.

The p.m.r. concentration dependences of the hydroxyl protons of methanol and ethanol were also measured in each of three solvents: cyclohexane, diethyl ether and hexamethyldisiloxane. The measurements are shown in Fig. 3, where, for comparative purposes, the data were reduced to a common origin, $\nu = \delta = 0$, for concentrated alcohol. All of the data are consistent with the interpretation that as alcohol is diluted the extent of hydrogen

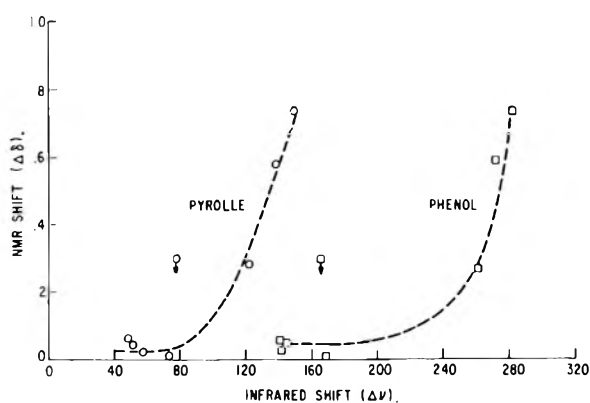


Fig. 2.—P.m.r. shift of chloroform at infinite dilution in solvent vs. infrared frequency shift of pyrrole and phenol in same solvent. The points with arrows are for D_3 , for which the n.m.r. shift is extrapolated and probably represents an upper limit. Infrared data from West, *et al.*⁸

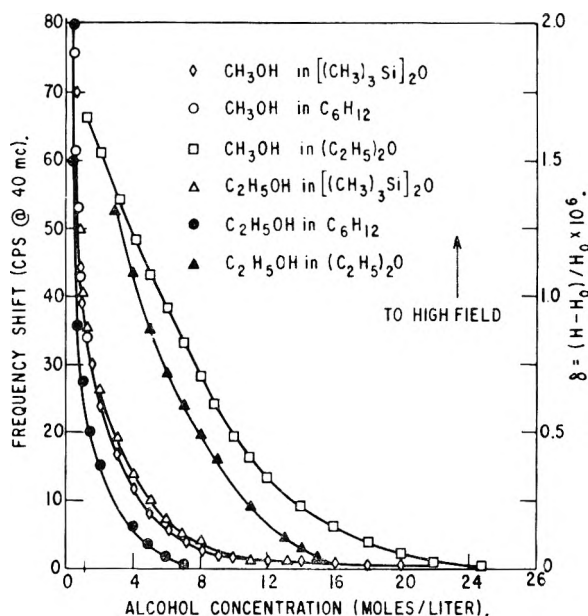


Fig. 3.—P.m.r. dilution shifts of methanol and ethanol in solvents as indicated.

bonding is generally decreased. The shape of the curves for alcohol-cyclohexane is characteristic of a strong hydrogen-bonding material which forms higher polymers (chain or cyclic) at finite concentrations and should be compared with the data of Becker and Liddell¹³ and Saunders and Hyne¹⁴ on methanol and ethanol in carbon tetrachloride solution, which show quite similar behavior. Detailed analyses of the concentration dependence of associated liquids in inert solvents have been made by Huggins, Pimentel and Shoolery¹⁵ and others^{13,14} who show that the data can be represented by a succession of hydrogen-bonding reactions, each accompanied by a characteristic p.m.r. shift. Later discussions of the quantitative significance of these measurements confirm the opinion that the reliability of the calculated equilibrium constants and p.m.r. shift parameters depends

(13) E. D. Becker and U. Liddell, *J. Mol. Spectr.*, **2**, 1 (1958).

(11) R. F. Curl, Jr., and K. S. Pitzer, *J. Am. Chem. Soc.*, **80**, 2371 (1958).

(14) M. Saunders and J. B. Hyne, *J. Chem. Phys.*, **29**, 1319 (1958).

(12) D. W. Scott, *ibid.*, **68**, 2294 (1946).

(15) C. M. Huggins, G. C. Pimentel and J. N. Shoolery, *J. Phys. Chem.*, **60**, 1311 (1956).

critically on the accuracy of shift measurements at extreme dilution and upon the purity of the materials used. A similar treatment of data for alcohol-ether appears hopeless at this stage. The simplest model must include the smaller alcohol-alcohol units and the perturbation of the monomers and "polymers" by the hydrogen-bonding basic solvent.

However, the qualitative features of the curves are evidence for the small basicity of the Si-O-Si system. As alcohol is diluted by a basic solvent, alcohol-alcohol polymers are dissociated by entropy and by the stabilization of the monomer in monomer-solvent complexes. The observed chemical shift will, then, reflect the shift due to breaking of alcohol-alcohol bonds less the reverse shift due to the formation of alcohol-solvent bonds. To first order, the differences among the chemical shift *vs.* concentration curves can be attributed to the effective basicities of the solvents. It is important to observe, however, that there is a loss of sensitivity due to the partially compensating effects; for example, a strong base will disproportionate a larger amount of alcohol-alcohol polymer, but at the same time forming a larger number of alcohol-solvent complexes and exhibiting a larger, compensating shift per complex formed. In this respect, the use of alcohol as a "test" acid suffers with respect to chloroform.

The behavior of the -OH p.m.r. shifts of methanol and ethanol is quite similar with respect to the three solvents. For both acids, the curves for hexamethyldisiloxane fall between the limits of cyclohexane and diethyl ether; in fact, they are considerably closer to inert. This correlation is in general agreement with the findings for CHCl_3 in siloxanes and ethers. Hence, it appears unlikely that steric effects are dominant in the comparison of ethers and siloxanes.

Conclusion

From these studies of the hydrogen-bonding basicity of the Si-O-Si linkage, it is evident that some type of bonding other than that in C-O-C bonds must be invoked. The predicted increase in ionic character due to the smaller electronegativity of silicon is not observed; but, rather, a significant decrease. It has been proposed that many of the unexpected properties of -Si-X bonds are due to the formation $d\pi-p\pi$ dative bonds involving the unshared p pairs from X and the overlapping, unfilled d orbitals of silicon. West^{8,16,17} correlates

(16) R. West and R. H. Baney, *J. Am. Chem. Soc.*, **81**, 6145 (1959).

(17) R. H. Baney, K. J. Lake, R. West and L. S. Whatley, *Chem. & Ind. (London)*, **36**, 1129 (1959).

his infrared measurements of hydrogen-bonding basicities with this type of bonding. Further, he proposes that bonding such as Si-O-C or Si-Cl involves only one p pair, whereas Si-O-Si for example, utilizes both unshared p pairs. This latter proposal makes it interesting to speculate about the bonding structure of $\text{N}(\text{SiH}_3)_3$, which has three silicon atoms competing for the one unshared pair from nitrogen.

While the chemical evidence for some kind of additional bonding in siloxanes is fairly complete, there remains the difficulty of correlating the existing spectral data. Dative bonding of the type discussed should influence the infrared stretching, bending and torsional force constant, but serious attempts to correlate the infrared frequencies and intensities are lacking. Wright and Hunter¹⁸ attributed the strong dipole change of the Si-O stretch to its high ionic character—at variance with the chemical evidence. It was tacitly assumed that the large value of $|d\mu/dq|$ for Si-O stretching implied a large bond moment. This assumption has been shown to be not general. Curl and Pitzer¹¹ made the most complete infrared assignment of $(\text{H}_3\text{Si})_2\text{O}$, but chose not to comment about the significance of their measurements with regard to bonding. They were not able to assign any observable band to the Si-O-Si bend, which they stated should have a large transition moment. Confirmation of the long-suspected low bending force constant of Si-O-Si came from the excellent work of Thorson and Nakagawa¹⁹ and Aronson, Lord and Robinson.²⁰ They were able to assign the group of infrared bands at 50-100 cm^{-1} as arising from mixed vibrational and rotational modes from the quasi-linear Si-O-Si system. It is felt that additional indirect chemical evidence will probably prove unfruitful in describing the nature of the bonding; but rather, detailed spectral measurements and their correlation with orbital theory are most likely to lead to a more complete understanding of the bonding between silicon and electronegative elements.

Acknowledgment.—The author is indebted to D. R. Carpenter previously at this Laboratory, for the detailed measurements leading to the data in this report and, further, to B. H. Zimm and S. W. Kantor for several fruitful discussions.

(18) N. Wright and M. J. Hunter, *J. Am. Chem. Soc.*, **69**, 803 (1947).

(19) W. R. Thorson and I. Nakagawa, *J. Chem. Phys.*, **33**, 994 (1960).

(20) J. R. Aronson, R. C. Lord and D. W. Robinson, *ibid.*, **33**, 1004 (1960).

CRITICAL COMPOSITION IN LIQUID MIXTURES OF COMPONENTS OF VERY DIFFERENT MOLAR VOLUMES

BY KŌZŌ SHINODA¹ AND JOEL H. HILDEBRAND

Department of Chemistry, University of California, Berkeley 4, California

Received May 29, 1961

Solubility-temperature curves have been determined for mixtures of pentaerythritol tetraerfluorobutyrate, $(C_3F_7COOCH_2)_4C$, with 5 other liquids. The critical temperatures, in °C., and critical compositions expressed as mole per cent. of the above compound are: CH_2Cl_2 , 38.5°, 5.7; $n-C_5H_{12}$, 62.1°, 13; $c-C_5H_{10}$, 80.8°, 10; $i-C_8H_{18}$, 78.80°, 17; $n-C_8H_{18}$, 119.4°, 16. These critical compositions are very unsymmetrical in accord with the large disparities in molal volume. They agree well with values calculated on the basis of the equation for regular solutions using ideal entropy instead of "Flory-Huggins" entropy.

Introduction

The extraordinarily large molal volume of pentaerythritol tetraerfluorobutyrate, "PETB," 541.5 cc. at 25°, makes this liquid exceptionally well suited for testing the relation between disparity of molal volumes and the asymmetry of liquid-liquid solubility-composition curves. We reported recently that the critical composition of solutions of chloroform and carbon tetrachloride with PETB show good agreement with theoretical values derived from the regular solution equation using ideal entropy of mixing rather than "Flory-Huggins" type entropy.² We also have shown that iodine solutions in both PETB and octamethylcyclotetrasiloxane^{3a} show no additional entropy of solution attributable to disparity in molal volume compared with solutions in other solvents with much smaller molal volumes.³ The present investigation was undertaken in order to test this conclusion in additional cases.

Experimental

Materials.—The PETB was obtained from the Minnesota Mining and Manufacturing Company through the kindness of Dr. N. W. Taylor. Its purification and physical properties were described in the paper referred to.² The dichloromethane, of "Spectro Grade," a product of Eastman Organic Chemicals, was used without further purification. The *n*-pentane, cyclopentane, *n*-octane (synthetic) were obtained from Matheson Company. The "isooctane" (2,2,2-trimethylpentane) was a Phillips "pure" product. These were dried over activated silica gel and fractionated in a vacuum-jacketed, 15-plate column at a reflux-ratio of 15:1. The boiling points corrected to 760 mm. were: *n*- C_5H_{12} , 34.5–34.7°; *c*- C_5H_{10} , 49.3°; *n*- C_8H_{18} , 125.8°; *i*- C_8H_{18} , 99.2°.

Procedure.—Various amounts of degassed PETB were weighed into tubes 6 mm. in diameter and 12 cm. long. The second liquid then was added, the contents frozen, evacuated, sealed and reweighed. Consolute temperatures were observed by repeated gradual heating and cooling, 0.01° per minute, while shaking the tubes. Successive observations agree within 0.02° near the top of the liquid-liquid curves, and within 0.1–0.2° on the sides. The thermometers used were calibrated against N.B.S. Standard thermometers. Corrections were made for the emerged stem.

Results

The results are shown in Table I and are plotted together with our earlier figures for $CHCl_3$ and CCl_4 in Fig. 1. The critical compositions and

temperatures, given in Table II, were obtained by aid of the rectilinear diameter relation.⁴ The curves for all liquid mixtures are so unsymmetrical that they offer a good test of the equations we have used for calculating the critical composition

$$RT \ln a_1 = RT \ln x_1 + v_1 \phi_2^2 (\delta_2 - \delta_1)^2 \quad (1)$$

where a_1 denotes the activity of component 1, x_1 its mole fraction, v_1 its molal volume, ϕ_2 the volume fraction of component 2, and the δ 's are the respective solubility parameters.⁴ The term, $R \ln x_1$, assumes that the partial molal entropy is

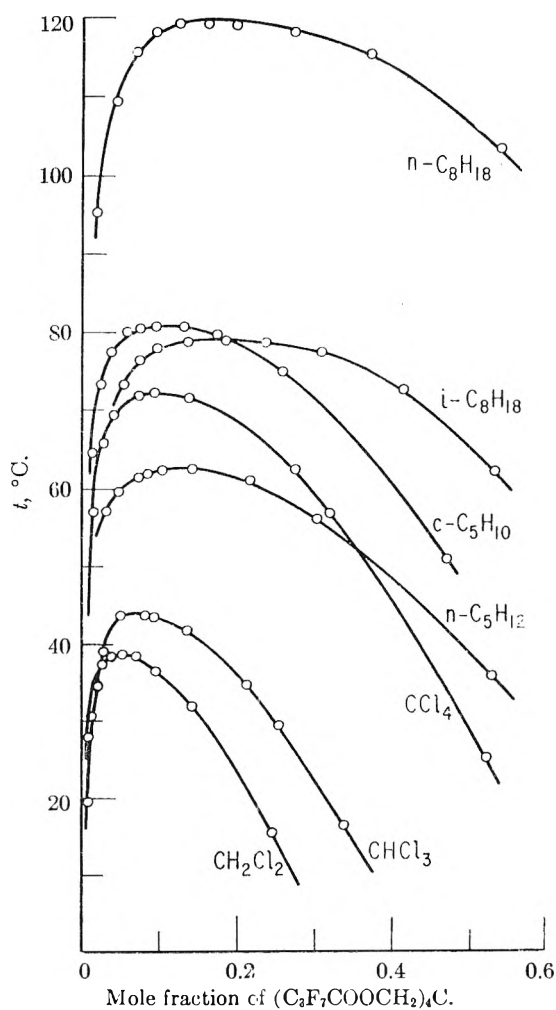


Fig. 1.

(1) Department of Chemistry, Yokohama National University, Minamiku, Yokohama, Japan.

(2) Kōzō Shinoda and J. H. Hildebrand, *J. Phys. Chem.*, **62**, 481 (1958).

(3) (a) Kōzō Shinoda and J. H. Hildebrand, *ibid.*, **62**, 292 (1958); (b) **61**, 789 (1957).

(4) J. H. Hildebrand and R. L. Scott, "Solubility of Non-electrolytes," Reinhold Publ. Corp., New York, N. Y., 1950.

TABLE I
 MOLE % OF (C₃F₇COOCH₂)₄C IN LIQUID MIXTURES

CH ₂ Cl ₂		n-C ₈ H ₁₈		c-C ₈ H ₁₆		i-C ₈ H ₁₈		n-C ₈ H ₁₈	
100x ₂	t, °C.	100x ₂	t, °C.	100x ₂	t, °C.	100x ₂	t, °C.	100x ₂	t, °C.
0.51	16.7	1.58	52.0	1.21	64.4	2.06	58.5	1.89	95
1.04	22.2	2.97	56.8	2.34	73.6	2.99	64.3	4.42	109.5
1.77	34.8	4.55	59.26	3.51	77.66	5.05	73.26	6.72	115.6
2.54	37.1	7.10	61.47	5.74	80.17	7.27	76.43	9.40	118.1
3.38	38.09	8.19	61.89	7.07	80.66	9.87	78.16	12.43	119.3
5.22	38.47	10.09	62.04	9.22	80.76	13.36	78.77	16.10	119.4
6.94	38.22	13.88	62.06	12.95	80.65	18.47	78.84	20.11	119.3
9.26	37.33	21.65	60.98	17.72	79.65	23.69	78.56	28.48	118.3
13.99	31.9	30.04	56.95	25.93	74.9	30.94	77.14	37.10	115.6
25.01	16.5	52.99	35.4	47.07	50.8	41.49	72.52	54.04	103.6
						62.02	53.0		

ideal. There has been, till recently, a question whether the non-ideal entropy of athermal solution of high polymers is to be attributed entirely to configurations of the polymer chain, or whether disparity in molal volumes of the component alone is accompanied by non-ideal entropy as formulated by Flory and by Huggins.

$$R[\ln\phi_1 - \phi_2(v_2 - v_1)/v_2] \quad (2)$$

Equations for the critical composition are derived by setting $\partial \ln a_1 / \partial \ln x_1 = 0$ and $\partial^2 \ln a_1 / \partial \ln x_1^2 = 0$. In this way we obtain for the critical composition

$$x_{1,c} = [v_1 + (v_2 - v_1 v_2)^{1/2}] / (v_2 - v_1) \quad (3)$$

from eq. 1 and

$$(x_1/x_2)_c = (v_2/v_1)^{1/2} \quad (4)$$

from eq. 2.

Table II gives (1) the critical temperatures; (2) the mole % of PETB at the critical point, x_1 , (3) the molal volumes of the pure liquids at the critical temperature; (4) the values of the experimental composition at the critical point; (5) the same calculated from eq. 3; (6) *ibid.* from eq. 4. The data for solutions with CHCl₃ and CCl₄ are added from the earlier paper.²

One sees that in every case eq. 3, based upon ideal entropy, gives much better agreement with the experimental value than does eq. 4, based upon "F-H" entropy.

There is one system,⁵ however, for which, significantly, the reverse is true, *i.e.*, stannic iodide and dicetyl, *n*-C₃₂H₆₆. The critical temperature is 193.5° and the critical composition close to 10 mole % of dicetyl. The molal volumes at this

(5) J. H. Hildebrand, *J. Am. Chem. Soc.*, **57**, 866 (1935).

TABLE II

COMPARISON OF EXPERIMENTAL CRITICAL COMPOSITIONS WITH THOSE CALCULATED BY EQUATIONS 3 AND 4

Liquid 1	t _c , °C.	v ₁	v ₂	x _{2,c}		
				Expt.	Eq. 3	Eq. 4
CH ₂ Cl ₂	38.5	65.7	549.5	0.057	0.061	0.040
CHCl ₃ ¹	43.5	82.6	553	.073	.077	.055
n-C ₈ H ₁₈	62.1	123.8	564	.13	.115	.093
CCl ₄ ¹	72.1	103	571	.09	.094	.079
i-C ₈ H ₁₈	78.8	178	573	.17	.164	.147
c-C ₈ H ₁₆	80.8	101	575	.10	.092	.069
n-C ₈ H ₁₈	119.4	185	603	.16	.162	.145

temperature are 174 and 615 cc., respectively. The critical mole fraction of dicetyl is 15, according to eq. 3, and 13 according to eq. 4. One may infer that the long, flexible chain of dicetyl slightly favors the "F-H" expression for entropy of mixing.

The foregoing calculations have neglected, as does eq. 1, the contribution of the unknown expansion to the entropy of mixing, therefore the evidence is not as complete as that afforded by the iodine solutions.

The critical temperatures are not consistent with the solubility parameters of the components, which is not strange, in view of the departures of these substances from spherical force-fields. We have here again⁶ evidence of exceptionally weak attraction between fluorocarbons and aliphatic hydrocarbons.

This work has been supported by the Atomic Energy Commission, under a contract administered by J. H. Hildebrand. We thank Dr. Nelson W. Taylor for the PETB and Dr. Berni J. Alder for criticism.

(6) Cf. J. H. Hildebrand, *J. Chem. Phys.*, **18**, 1337 (1950).

CATALYTIC ACTIVITY OF THE LANTHANIDE OXIDES FOR THE DEHYDROGENATION OF CYCLOHEXANE

By C. B. MCGOUGH AND G. HOUGHTON

Chemical Engineering Department, University of Pittsburgh, Pittsburgh, Penna.

Received June 5, 1961

A rising temperature flow reactor has been used to determine the activation energies, frequency factors and kinetics for the heterogeneous dehydrogenation of cyclohexane over La_2O_3 , CeO_2 , Pr_2O_3 , Nd_2O_3 and Sm_2O_3 . The effect of crystal structure was evaluated by preparing the oxides in their different crystal forms (A, B or C structures) and the effect of a support was investigated by depositing the oxides on alumina. Within the error of experiment, no effect of the support, crystal structure, paramagnetism or valence state could be detected, indicating perhaps that the catalytic activity of the lanthanide oxides is associated with outer electronic states.

Introduction

In a previous communication Bridges and Houghton¹ have evaluated the activities, for the dehydrogenation of cyclohexane, of certain transition metal oxides and compounds using a rising temperature flow reactor. In general the transition elements exhibit several valence states and their oxides are semiconductors that have a pronounced paramagnetism caused by holes in the d-band. In these respects the rare earth oxides provide a contrast since valence states other than trivalent are relatively uncommon and their paramagnetism arises from incomplete 4f orbitals which are screened from external influence by 5s and 5p electrons. Furthermore, three different crystal forms have been found in the rare-earth oxides, the most common being the A and C structures in which the coordination number of the metal ion is 7 and 6, respectively, and the B structure about which little is known. To evaluate the effects of paramagnetism, crystal structure and crystal field on catalytic activity, the present communication is concerned with the activity, for the dehydrogenation of cyclohexane, of the lanthanide series of rare-earth oxides in their various crystal forms. In this connection Komarewsky² has demonstrated that Nd_2O_3 and Sm_2O_3 show activity for the dehydrogenation of alcohols and cyclohexane as well as for the cyclization of *n*-heptane and 1-octene, while Taylor and Diamond³ have shown that the paramagnetic oxides Gd_2O_3 and Nd_2O_3 are more active in catalyzing the ortho-para hydrogen conversion than the non-paramagnetic La_2O_3 . Hopkins and Taebel⁴ have summarized the earlier work on the catalytic activity of the rare earths for oxidation, hydrogenation, decomposition and synthesis of organic compounds.

Experimental

Equipment.—The apparatus used to measure the catalytic activity of rare earth oxides for the dehydrogenation of cyclohexane was a modification of the rising temperature flow reactor previously described by Bridges and Houghton.¹

The major innovation in the present apparatus was that the gas leaving the reactor was analyzed continuously by a Sr-90 ionization detector of the Lovelock⁵ type (*cf.* Walter⁶)

instead of a thermal conductivity gauge. This method of continuous analysis was possible by virtue of the fact that the benzene-hydrogen-nitrogen mixture formed by complete dehydrogenation had an ionization considerably different from that of the cyclohexane-nitrogen feed mixture. The strength of the ionizing source was 10 milluries, giving a current changing with gas composition in the range 5×10^{-10} to 5×10^{-9} amp. at a potential of 300 volts applied between the central electrode and the wall of the ionization chamber, which had a free volume of 5.9 cc. The ionization current passed through a 2×10^8 ohm resistor, the voltage developed being converted to 0–10 mv. at an impedance of about 100 ohms for recording by means of a Leeds and Northrup chopper stabilized pH meter. Potentiometers were provided to adjust the 0 and 100% conversion points to be exactly 100 divisions apart for calibration purposes. Mass spectrometric analyses of the product gases showed that the recorder scale was linear within $\pm 1\%$ conversion in the range 0–100% and that thermal decomposition of cyclohexane by rare earth oxides was not appreciable below 610°.

In the present equipment the carrier stream of dry oxygen-free nitrogen was saturated with cyclohexane (Spectroscopic grade) in two bubblers maintained at $20.90 \pm 0.01^\circ$ and a constant pressure of 1090 mm. giving a feed composition of 7.2 mole % cyclohexane for nitrogen flow rates in the range 75–150 cc./min. The feed passed into a Vycor reactor of the design used previously¹ containing about 13 cc. of catalyst and then through capillary connecting tubing to the Sr-90 conversion detector. As in the previous apparatus the flow through the detector was maintained at a constant value, in this case 60 cc./min., by using a bubble type pressure regulator containing glycerol. Except for the mode of generation of the steadily changing reference voltage (*cf.* Redfield⁷), the temperature programming circuit was similar to that described earlier¹—in the present case the linearly varying reference voltage was obtained by applying a constant voltage to the input of an analog computer integrator. The catalyst temperature was measured by a Chromel-Alumel thermocouple in a stainless steel thermowell placed in the catalyst bed and the temperature was recorded to within $\pm 1^\circ$ by a 0–700° strip chart recorder running at the same chart speed (0.667 in./min.) as the conversion recorder.

The equipment was operated as described by Bridges and Houghton,¹ the final data being taken at constant activity with a temperature ramp of 2° per minute and a flow rate of 100 cc./min., when no significant difference was observable between the rising and falling temperature cycles.

In order to test the accuracy of the calibrations and to show that the time constants of the thermocouple, transport lines and detector were negligible, the conversion-temperature curves for a highly active fluorine-promoted Pt/ Al_2O_3 catalyst were determined at decreasing flow rates until the curves became identical and independent of flow rate, thus indicating that equilibrium had been reached. The resulting curves agreed, within experimental error ($\pm 1\%$ conversion), with curves calculated from the free energy data of Rossini.⁸ The standard free energy for cyclohexane dehydrogenation interpolated at 227° from the present work is 5.4 kcal./g.-

(1) J. M. Bridges and G. Houghton, *J. Am. Chem. Soc.*, **81**, 1334 (1959).

(2) V. I. Komarewsky, *Ind. Eng. Chem.*, **49**, 264 (1957).

(3) H. S. Taylor and H. Diamond, *J. Am. Chem. Soc.*, **57**, 1251 (1935).

(4) B. S. Hopkins and W. A. Taebel, *Trans. Electrochem. Soc.*, **71**, 397 (1934).

(5) J. E. Lovelock, *Nature*, **181**, 1460 (1958).

(6) J. F. Walter, M.S. Thesis, University of Pittsburgh, 1959.

(7) J. A. Redfield, M.S. Thesis, University of Pittsburgh, 1959.

(8) F. D. Rossini, *et al.*, "Selected Values of Physical and Thermodynamic Properties of Hydrocarbon and Related Compounds," Carnegie Press, Pittsburgh, Pennsylvania, 1953.

TABLE I
 SUMMARY OF EXPERIMENTAL DATA AND RESULTS

Symbol for figures	Catalyst	Crystal structure	Paramagnetic susceptibility, χ , at 570°C, cm. ³ /g. $\times 10^6$	Surface area, m. ² /g.		Temp. range, °C.	Kinetic data	
				Fresh	Used		E_a , kcal./g.-mole	B , g.-mole/min., m. ²
⬡	CeO ₂	Rutile	0	11.0	9.1	530-610	33.0 ± 2	40 + 30 - 20
○	Pr ₂ O ₃ -Pr ₆ O ₁₁	A + C	10.5-5.9 ^a	10.3	10.6	530-610	36.7 ± 2	570 + 400 - 300
◇	Nd ₂ O ₃	C	11.4	9.2	9.2	530-610	36.8 ± 2	450 + 400 - 200
□	Sm ₂ O ₃	C	5.5	13.1	13.1	530-610	35.1 ± 2	140 + 110 - 60
△	La ₂ O ₃	A	0	15.9	9.8	530-610	34.3 ± 2	110 + 90 - 50
●	Pr ₂ O ₃	A + C	10.5	8.5	9.7	530-610	37.9 ± 2	630 + 500 - 250
◆	Nd ₂ O ₃	A	11.4	2.7	3.1	560-625	39 ± 4 ^b	1650 + 3500 ^b - 1200
■	Sm ₂ O ₃	B	5.5	1.0	1.2	570-625	36 ± 4 ^b	405 + 600 ^b - 300
▲	La ₂ O ₃ -Al ₂ O ₃	..	0	181	167	490-610	37.0 ± 1	220 + 200 - 100
⬢	CeO ₂ -Al ₂ O ₃	..	0	..	157	490-610	39.9 ± 1	740 + 600 - 400
●	Pr ₂ O ₃ -Al ₂ O ₃	..	10.5-5.9 ^a	168	155	490-610	34.9 ± 1	45 + 40 - 20
◆	Nd ₂ O ₃ -Al ₂ O ₃	..	11.4	168	159	490-610	32.1 ± 1	9 + 7 - 4
■	Sm ₂ O ₃ -Al ₂ O ₃	..	5.5	196	168	490-610	32.9 ± 1	14 + 12 - 7
×	Al ₂ O ₃	..	0	195	193	550-625	43 ± 4 ^b	2620 + 2200 ^b - 1200

^a Paramagnetic susceptibility of 19.5×10^{-6} for Pr₂O₃ and 5.9×10^{-6} cm.³/g. for Pr₆O₁₁. The amount of Pr₆O₁₁ is unknown. ^b Appreciable correction for thermal decomposition was necessary. Calculations are based on zero-order kinetics.

mole, compared with the value of 5.17 calculated from the standard heats of formation of benzene and cyclohexane given by Rossini.⁸

The rare earth oxides used in the investigation were La₂O₃, CeO₂, Pr₂O₃, Nd₂O₃ and Sm₂O₃, with a minimum purity of 99.9%, obtained from Research Chemicals Incorporated, Burbank, California. Supported (on alumina) and unsupported oxides were used in the investigation.

Unsupported Rare Earth Oxides.—The unsupported oxide catalysts, with the exception of CeO₂, were prepared in their various crystal modifications by heat treatment as described by Iandelli.⁹

As received from Research Chemicals Incorporated, the oxides Nd₂O₃ and Sm₂O₃ showed the type C structure, which is a partial face-centered cubic structure of the Th₂O₃ type (cf. Iandelli⁹ and Wyckoff¹⁰). The type C structure occurs when the oxides are formed at low temperatures and is essentially a distorted fluorite structure in which trivalent rare earth ions replace calcium and three fourths of the fluorine positions are occupied by oxygen ions, the remaining positions being vacant. The praseodymium oxide, even after use in the reactor, was found to be a mixture of types A and C Pr₂O₃ together with some Pr₆O₁₁. In the case of La₂O₃ it was not possible to investigate the activity of the C structure, since the temperature of reaction was sufficient to convert this oxide completely into type A within the few hours necessary to reach a state of constant activity. This agrees with the observations of Iandelli,⁹ who found that temperatures in the range 500-600° were sufficient to convert type C La₂O₃ into type A, whereas temperatures above 800° were required for the other lanthanide oxides.

By heating the oxides at 1200° for 3 hours in an oxygen-free nitrogen atmosphere La₂O₃ and Nd₂O₃ were converted to the type A structure, Sm₂O₃ to the type B structure, while Pr₂O₃ provided a mixture of types A and C with no

Pr₆O₁₁. In order to ensure that no Pr₆O₁₁ was present before heat treating the oxide, it was first reduced at 600° for 3 hours. The type A structure is hexagonal and characterized by a complex 7-coordination of the metal ion (cf. Iandelli,⁹ Wyckoff¹⁰ and Pauling¹¹) while type B, although clearly distinct from types A and C, has not been positively classified, although Douglass and Staritzky¹² alternately describe it as pseudotrigonal, orthorhombic or monoclinic.

The CeO₂ oxide was not heat treated and the sample used was found to have the normal rutile structure in which the Ce⁴⁺ ion is 6-coordinated.

In order to convert the finely powdered oxides into a form that could be used in the flow reactor without incurring an excessive pressure drop, they were first pelleted at 12,000 lb./in.², using deionized water as a binder. The pellets then were sintered in nitrogen at 400° for 2-3 hours to remove water vapor. The sintering temperature was low enough to prevent any further changes in the crystal structure. The sintered pellets then were crushed and sized between 30-100 mesh screens. The resulting material had a surface area of about 10 m.²/g., the exact values for each oxide before and after use being reported in Table I as determined by the BET method using low temperature nitrogen adsorption.

The crystal structures of the unsupported oxides were identified after their use as catalysts by powder X-ray methods, using a General Electric XRD3 spectrometer with molybdenum radiation ($K\alpha = 0.07926$ Å.) and a zirconium filter.

Supported Rare Earth Oxides.—The lanthanide rare earth oxides were supported on 28-48 mesh Alcoa Fl alumina by first dissolving them in nitric acid, evaporating to dryness, dissolving the nitrate in enough water to fill the pore volume of the alumina (0.25 cc./g.) and then impregnating the support under vacuum. The impregnated alumina

(9) A. Iandelli, *Gazz. chim. ital.*, **77**, 312 (1947).

(10) R. W. G. Wyckoff, "Crystal Structures," Vol. II, Part V, Interscience Publishers, Inc., New York, N. Y., 1951.

(11) L. Pauling, *Z. Krist.*, **69**, 415 (1929).

(12) R. M. Douglass and E. Staritzky, *Anal. Chem.*, **28**, 552 (1956).

was dried at 150° for 3 hours and then sintered at 525° for 4 hours to decompose the nitrates. The final catalyst contained 15 wt. % of rare earth oxide in each case and had a BET surface area of about 150 m.²/g., the exact values before and after use being given in Table I.

Results

The activation energy E and frequency factor B in the Arrhenius equation for the velocity constant $k_n = B \exp(-E/RT)$ were determined from the experimental temperature-conversion curves by plotting $\log \phi_n$ versus $1/T$ as described previously by Bridges and Houghton.¹ For a certain amount of catalyst in the reactor the function ϕ_n depended only upon the conversion and the order of the reaction n , since the feed rate, feed composition and total pressure were the same for all the experiments. If $y = 0.072$ is the mole fraction of cyclohexane in the feed, x is the fractional conversion of cyclohexane to benzene and hydrogen and $\delta = 3$ is the increase in moles of the reacting system per mole of cyclohexane converted, then ϕ_0 and ϕ_1 for zero and first-order kinetics, respectively, are defined by the relations¹

$$\phi_0 = x \quad (1)$$

$$\phi_1 = -[y\delta x + (1 + y\delta) \ln(1 - x)] \quad (2)$$

In all cases the best line through the data was determined by least squares methods which also gave the indirect precision of E and B reported in Table I. In order to determine whether thermal decomposition was significant in the temperature range 490–610° over which the lanthanide oxides were active, the reactor was packed with Vycor wool and the thermal decomposition measured over a wide temperature range. Except in the cases of Al_2O_3 and heat treated Nd_2O_3 and Sm_2O_3 , any corrections for thermal decomposition below 610° were less than 4% conversion and did not appreciably affect the numerical values of E and B within the experimental error—furthermore, mass spectrometric analyses showed that the small amount of thermal cracking that did occur in the rare earths could be corrected for by using the data obtained with Vycor wool. However, in the cases of the heat treated Nd_2O_3 and Sm_2O_3 active in the range 560–625°, the surface areas of these oxides were low, so that a significant correction was required for thermal decomposition and the error of measurement of E and B has been adjusted accordingly in Table I. In addition, Table I and Figs. 2 and 3 show that although Al_2O_3 is considerably less active than either the supported or unsupported rare earths, it does possess some activity after correction for thermal decomposition that Innes¹³ has ascribed to the presence of trace quantities of iron or other impurities. In order to compare the present results for the rare earth oxides with those obtained for the transition metal oxides, the temperature-conversion curves shown in Fig. 3 were computed on the basis of the same feed rate per unit surface area of 0.0184 cc./min., m.² used by Bridges and Houghton.¹

Order of Reaction.—Figure 1 shows typical plots of $\log \phi_n$ versus $1/T$ for various supported and unsupported oxides in different crystal forms. The experimental data of Fig. 1 were obtained

(13) W. B. Innes, "Catalysis," Vol. 2, Reinhold Publ. Co., New York, N. Y., 1955.

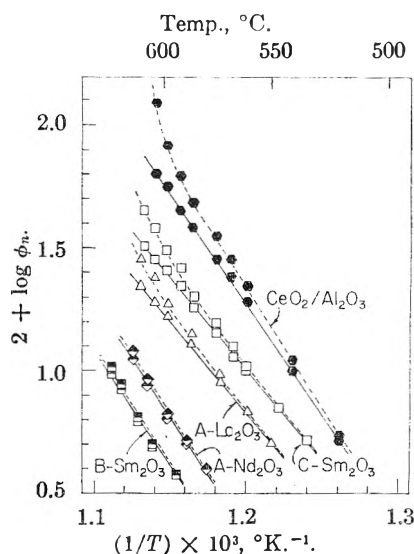


Fig. 1.—Plots of $\log \phi_n$ versus $1/T$ (cf. Table I for a list of symbols): —, zero-order kinetics; ----, first-order kinetics.

with roughly equal volumes of catalyst (12–14 cc.) and no attempt has been made to correct the data to either a fixed area or volume of catalyst, since the slopes and shapes of these curves are unaffected by the amount of catalyst, which is only important in computing the frequency factor, B . Plots similar to Fig. 1 were obtained for the other catalysts in Table I and an analysis of the slopes showed curvature in the first-order case but not in the zero-order case. That the reaction appears to be zero order indicates that the active surface is always covered by adsorbed reactant. However, in the cases of Al_2O_3 and heat treated Nd_2O_3 and Sm_2O_3 , the conversions after correction for thermal decomposition are low so that it is impossible to distinguish between zero and first-order kinetics, so that the data in Table I are reported for zero-order kinetics, the values for first-order kinetics being virtually the same for these oxides.

Activation Energies and Frequency Factors.—Table I summarizes the activation energies, E , and frequency factors, B , together with their accuracy. Since the reaction appears to be zero order, the values given in Table I are "true" activation energies and do not require correction for the heats of adsorption and desorption (cf. Hinshelwood¹⁴). All the catalysts, supported and unsupported, regardless of crystal structure, have activation energies in the narrow band 32–40 kcal./g.-mole, indicating that the surface and bulk characteristics of the solid have little influence on the energy barrier for dehydrogenation.

It is interesting to note that when $\log B$ was plotted against E/T , a straight line of slope 0.22 was obtained. Cremer¹⁵ has interpreted this linear relationship as due to quantum leakage of electrons on the catalyst surface by a "tunnel effect." However, Barrer¹⁶ has pointed out that the variation in velocity constant $k_n = B \exp(-E/RT)$ is often considerably less than the variation in

(14) C. N. Hinshelwood, "The Kinetics of Chemical Change," Oxford University Press, 1940.

(15) E. Cremer, *J. chim. phys.*, **47**, 439 (1950).

(16) R. M. Barrer, *ibid.*, **47**, 445 (1950).

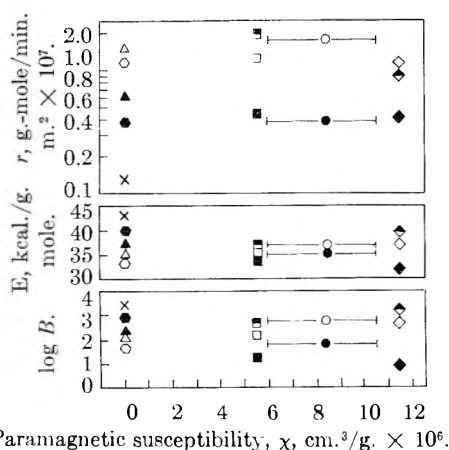


Fig. 2.—Effect of paramagnetic susceptibility and crystal structure on reaction rate, r (at 570°), activation energy, E , and frequency factor, B . (cf. Table I for a list of symbols and values of χ at 570° .)

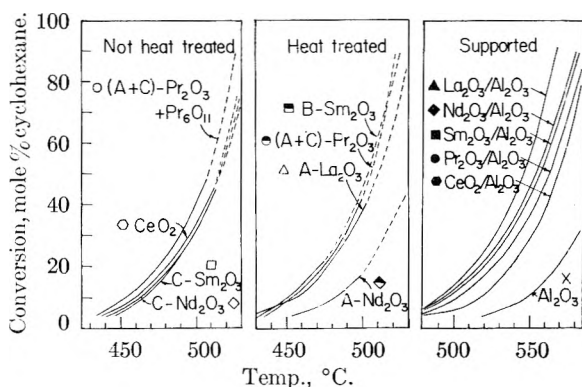


Fig. 3.—Conversion-temperature curves calculated at a feed rate per unit area of 0.0184 cc./min., $m.^2$ (cf. Table I for a list of symbols). —, calcd. from experimental temperature-conversion data below 610° ; ---, extrapolated using constants E and B in Table I.

$\exp(-E/RT)$, in which case $\log k_n$ may be taken as approximately constant when the slope of $\log B$ versus E/T is simply $1/2.303R = 0.22$. Hence in the present case, no physical significance can be attached to the linearity of the plots of $\log B$ versus E/T .

Discussion

It is now possible to discuss the influence of paramagnetism and crystal structure on the activity of the lanthanide oxides.

Effect of Paramagnetism.—Many investigations, particularly those of Selwood,¹⁷ have indicated that catalytic activity and paramagnetism are related in the transition elements. Figure 2 shows a plot of reaction rate, r , activation energy, E , and frequency factor, B , versus paramagnetic susceptibility for the rare earth oxides calculated at the temperature of 570° , using the susceptibility data of Selwood¹⁷ and Rabideau.¹⁸ In the case of Pr_6O_{11} the value of 5.9×10^{-6} cm.³/g. was estimated by assuming that the Curie-Weiss law was obeyed above 25° , as indicated by the data of Rabideau in the range -70 to 25° . It is evident from Fig. 2 that there appears to be little cor-

relation between paramagnetism and catalytic activity in the lanthanide oxides, suggesting that the unpaired 4f electrons do not participate in the mechanism. This might be expected, since the 4f electrons are effectively screened by the outer shells to such an extent that the paramagnetism is not influenced by crystal structure or the presence of a support (cf. Selwood¹⁷). That Taylor and Diamond³ have observed an effect of rare earth paramagnetism on the ortho-para hydrogen conversion is not contrary to the present measurements, since it is readily explained on the basis that spin isomerism does not necessitate electron exchange (cf. Kalckar and Teller¹⁹ and Selwood¹⁷), the only requirement being the existence of a magnetic field.

Inspection of Table I indicates that in the case of the unsupported oxides, the activation energy and frequency factor tend to reach a maximum at the point where the paramagnetic susceptibility is the largest in each series, the reverse being true for the supported oxides. However, the variations are on the borderline of the experimental error, so that if paramagnetism has any effect at all, it is small. Furthermore, if the specific reaction rate, r , is computed from E and B in Table I, then no apparent trend in this variable with paramagnetism can be detected (cf. Fig. 2).

Effect of Crystal Structure.—Figure 2 and Table I summarize the data for the effect of crystal structure on the activity of the unsupported lanthanide oxides. It is evident from these data that the effect of crystal structure is not significant. On the basis of a geometric model of catalysis this might be expected, since in the type C sesquioxides the metal-oxygen interionic distance lies between 2.34 and 2.44 Å., while in the type A oxides characterized by 7-coördination each metal ion has four oxygens at about 2.4 Å. and three at 2.7 Å., in no case a very large variation. However, if the hypothesis is introduced that crystal field splitting of bonding levels can have an effect on the activation energy, it might be expected that the difference between 7 and 6 coördination in structures A and C might have a significant effect on the activity, and furthermore that the B structure of Sm_2O_3 might show differences from the A and C structures. That no such differences were observed tends to indicate that the crystal field is not a significant contribution to the activity of the rare earth oxides.

Another interesting case is that of praseodymium oxide, which is a mixture of the A and C structures together with some Pr_6O_{11} in the sample that was not heat treated at 1200° . It might be expected that since the latter sample contained a mixture of valence states that impurity levels in the solid state sense might affect the surface kinetics; no such effects were observed. Furthermore, CeO_2 shows the same activation energy and kinetics as the sesquioxides, again indicating that the valence state of the metal ion is not an important criterion.

It would be erroneous to conclude from the above observations that crystal and defect structure had

(17) P. W. Selwood, "Magnetochemistry," Interscience Publishers, Inc., New York, N. Y., 1948.

(18) S. W. Rabideau, *J. Chem. Phys.*, **19**, 874 (1951).

(19) F. Kalckar and E. Teller, *Proc. Roy. Soc. (London)*, **A150**, 520 (1935).

no effect upon catalytic activity, since the surface structure of the solid may be quite different from that of the bulk as measured by X-ray spectroscopy. However, Schwab and Martin²⁰ have similarly found no effect of crystal structure in that the β and γ forms of KI have the same activity for the decomposition of ethanol, and in no case did they observe any significant change in catalytic activity for the decomposition of NH_3 and various organic compounds catalyzed by the different crystal forms of CuI , Ga_2O_3 , AgI , TlI and Na_2SO_4 .

Comparison of Activities.—Although the supported oxides were more active on an equal volume basis than the unsupported oxides, Fig. 3 shows that on an equal area basis the unsupported oxides are more active. At the same feed rate per unit area of 0.0184 cc./min., m^2 the supported oxides would be active in the temperature range 470–570°, while the unsupported oxides would be active in the range 430–530°. This result is not unexpected since the total surface area of the catalysts was used in the calculations and the BET method cannot distinguish between total surface area of the catalyst and the surface area of the deposited oxide. The present observations tend to lead to the conclusion that the surface area of the deposited oxide is lower than that of the unsupported oxide on the basis of an equal total area of catalyst and that the support has little effect on the activity. The solid region of the curves in Fig. 3 terminates at the temperature (610°) in the actual measurements, on an equal volume basis, above which thermal decomposition might affect the results. The broken line in Fig. 3 represents the extrapolation of the data using values of E and B obtained in the temperature region below 610°. In the case of the heat treated forms of Nd_2O_3 and Sm_2O_3 the solid curves in Fig. 3 are quite short, because the heat treatment of these oxides at 1200° caused pronounced sintering with consequent reduction of the surface area to 1–3 m^2/g ., as shown by Table I. It is evident from Table I that, with the exception of Nd_2O_3 and Sm_2O_3 , the lanthanide oxides are thermally quite stable.

A comparison now can be made of the lanthanide rare earth oxides and some transition metal oxides using the data of Bridges and Houghton.¹ For instance, on an equal area basis Cr_2O_3 is active in the temperature range 380–440° while the

lanthanide oxides are active in the range 430–540°, representing a lower specific activity in the latter case. In the case of 14.7% Cr_2O_3 on Al_2O_3 the temperature range is 340–470° for a water-washed sample and 400–540° for an unwashed sample, while the 15% lanthanide oxides on alumina are active in the range 450–590° on an equal total area basis, again indicating a lower activity. The activation energies for Cr_2O_3 and Cr_2O_3 - Al_2O_3 catalysts are in the range 20–30 kcal./g.-mole, while the supported and unsupported lanthanide oxides give activation energies in the range 32–40 kcal./g.-mole, representing a larger energy barrier for surface reaction in the rare earths.

Finally, it may perhaps be concluded from these experiments that the lanthanide rare earth oxides are uniformly active for the dehydrogenation of cyclohexane and that the catalytic activity is notably independent of crystal structure, paramagnetism and, in the case of praseodymium, independent of the valence state within experimental error. The lanthanide oxides are also less active than certain transition metal oxides and compounds. A possible explanation for these observations is that the activity of the rare earths is associated with bonding due to the outer 5s and 5p electrons, and that this bonding is localized to specific ions in the sense that it is relatively unaffected by defect structure and crystal field splitting arising from neighboring ions. In the case of the transition metal oxides, the bonding electrons also might be the electrons responsible for paramagnetism, so that catalytic activity and paramagnetism would be closely allied. The present observations tend to support those of Halpern²¹ who has shown that single ions in aqueous solution, such as Cu^{2+} , Ag^+ and Hg^{2+} , are active in catalyzing the homogeneous hydrogenation of other dissolved substances, suggesting that the activity is associated with the metal ion and is relatively independent of environment.

Acknowledgments.—The authors are grateful to the Gulf Research and Development Company for the mass spectrometric analyses, to Mr. R. L. Zanowick and Dr. W. E. Wallace of the University of Pittsburgh for obtaining the X-ray powder diffraction patterns, and one of us (C.B.M.) is indebted to the Westinghouse Corporation for a graduate fellowship.

(20) G. Schwab and H. H. Martin, *Z. Elektrochem.*, **43**, 610 (1937); **44**, 724 (1938).

(21) J. Halpern, "Advances in Catalysis," Vol. IX, Academic Press, Inc., New York, N. Y., 1957.

NOTES

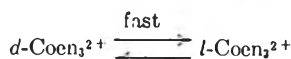
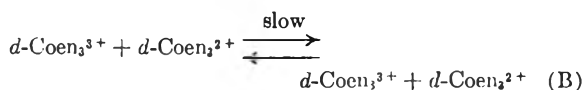
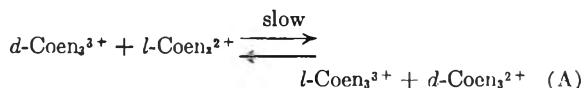
THE RATE OF ELECTRON TRANSFER
BETWEEN THE TRIS-
(ETHYLENEDIAMINE)-COBALT(II) AND
COBALT(III) IONS

BY FRANCIS P. DWYER AND ALAN M. SARGESON

Biological Inorganic Chemistry Section, John Curtin School of Medical
Research, Australian National University, Canberra, Australia

Received December 28, 1960

The rate of the slow electron transfer reaction between the tris-(ethylenediamine)-cobalt(II) and -cobalt(III) complex cations has been measured by the radio-isotope method.¹ Since the oxidized species in the reaction is optically stable, the reduced form optically labile, and the optical density of the mixed species in solution is not great, the rate of electron transfer can be measured conveniently by the racemization method, as suggested by Busch.² It will be evident that electron transfer proceeds through two reactions



Each act of electron transfer according to (A) leads to inversion of the Co(III) species, but electron transfer produces no rotational change in (B) and cannot be measured. It follows that the racemization rate is equivalent to twice the electron transfer rate, (A), since the racemization rate is twice the rate of inversion.

The dissociation of the tris-(ethylenediamine)-cobalt(II) ion in aqueous solution can be limited by using an excess of the free base but, as a result, a competing reaction is introduced, which also leads to racemization, but without electron transfer. The latter reaction involves the $\text{Co}^{\text{II}}\text{en}_3^{3+}$ ion and ethylenediamine in the activated³ state and not $\text{Co}^{\text{II}}\text{en}_3^{2+}$. A 7- or 8- covalent intermediate has been postulated in the reaction between *d,l*-tris-(ethylenediamine)-cobalt(III) salts and anhydrous ethylenediamine at 110°, which yields the cobalt(II) complex almost quantitatively.⁴

Experimental

Dextro-tris-(ethylenediamine)-cobalt(III) chloride *d*-tartrate 5-hydrate prepared by the method of Dwyer and Broomhead⁵ was twice recrystallized from water, then transformed

(1) W. B. Lewis, C. D. Coryell and J. W. Irvine, *J. Chem. Soc.*, Supplement issue, No. 2, 386 (1949).

(2) D. H. Busch, *J. Am. Chem. Soc.*, **77**, 2747 (1955).

(3) W. H. Gehman and W. C. Fernelius, *J. Inorg. Nuclear Chem.*, **9**, 71 (1959).

(4) F. P. Dwyer and A. M. Sargeson, *J. Am. Chem. Soc.*, **81**, 5269 (1959); *Nature*, **487**, 1022 (1960).

(5) F. P. Dwyer and J. A. Broomhead, "Inorganic Syntheses," Vol. VI, Ed. E. Rochow, in press.

to the chloride with concentrated hydrochloric acid, and crystallized by the addition of alcohol. The chloride was twice recrystallized from aqueous alcohol containing a little hydrochloric acid and air dried. The pure material gave $[\alpha]_D + 154^\circ$, (1 dm. tube.). *Anal.* Calcd. for $[\text{Coen}_3]\text{Cl}_3 \cdot \text{H}_2\text{O}$: C, 19.82; H, 7.21; N, 23.12. Found: C, 19.82; H, 7.19; N, 22.90.

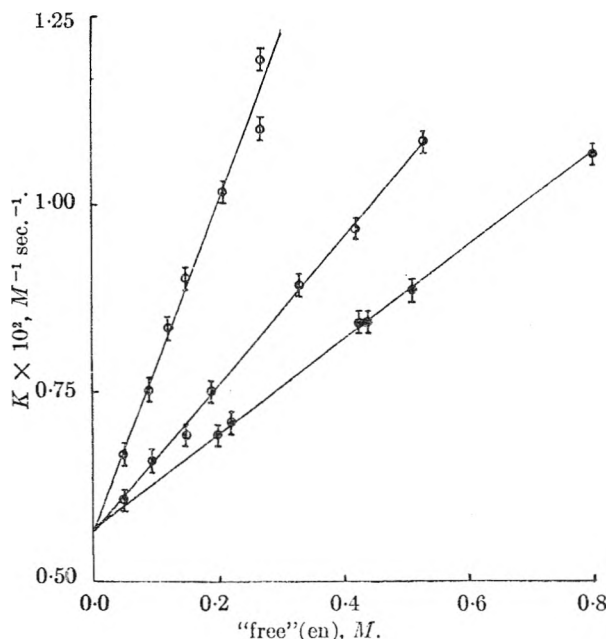


Fig. 1.—The dependence of the rate constant K on ethylenediamine and cobalt(II) concentration for $[\text{Co(III)}] = 0.0551 M$, $\mu = 0.45$, $T = 98^\circ$, \odot , $0.0309 M$ Co(II); \circ , $0.0103 M$ Co(II); \circ , $0.0206 M$ Co(II).

The reaction mixture, prepared from solutions of the appropriate concentration of pure *d*- $[\text{Coen}_3]\text{Cl}_3 \cdot \text{H}_2\text{O}$, Analar cobalt(II) chloride 6-hydrate and potassium chloride, was freed from traces of oxygen by continuous flow of "oxygen free" nitrogen. The nitrogen first was passed through another solution of the same composition, maintained at the same temperature, in order to avoid loss of water and ethylenediamine. Pure ethylenediamine (15 *M*, oxygen free) was added subsequently to start the reaction by forming the cobalt(II) complex *in situ*. Constant reaction rates were obtained within 15–20 minutes at 98°, and within 1 hr. at 25 and 50°. Dissolved oxygen not only catalyzed the reaction, an effect observed previously,¹ but oxidized some of the cobalt(II) complex. Samples were expelled at intervals from the reaction vessel using the nitrogen pressure and collected in a vessel cooled in ice. A 10-ml. portion of the quickly cooled mixture was added to sufficient concentrated hydrochloric acid to neutralize the ethylenediamine and decompose the cobalt(II) complex, the sample diluted to 20 ml., and the rotation measured in a 1 dm. tube. The ionic strength was controlled by the use of potassium chloride or, in a few runs, with potassium sulfate. The total Co(II) complex was estimated spectrophotometrically in a large proportion of the runs, and found to be constant over the time of reaction. Similarly, the Co(II) concentration estimated as the blue triphenylmethylarsonium tetra-(thiocyanato)-cobaltate(II),⁶ was found to be constant.

Results and Discussion

The rate constants were calculated from the polarimetric data in the usual way, using initially the expression:

(6) F. P. Dwyer and N. A. Gibson, *Anal. Chim. Acta*, **9**, 275 (1953).

TABLE I

$T, ^\circ\text{C.}$	$[\text{Co(en)}_3]^{3+}$	$[\text{Co(en)}_2]^{2+}$	$[\text{en}]$	$[\text{en}]$ "Free"	μ KCl	$K \times 10^2$	$k \times 10^3$ l. moles ⁻¹ sec. ⁻¹	$k' \times 10^3$ l. moles ⁻¹ sec. ⁻¹
98 ± 0.2	0.0551	0.0309	0.295	0.202	0.45	0.69	0.56	0.040
	.0551	.0206	.210	.148	.45	.69	.56	.038
	.0551	.0103	.085	.054	.45	.67	.56	.042
	.0551	.0309	.295	.202	.98	1.09	.94	.042
	.0551	.0309	.295	.202	1.48	1.45	1.32	.042
	.0551	.0309	.295	.202	1.98	1.84	1.70	.042
	.0551	.0309	.295	.202	0.98 ^a	1.13		.042
	.0551	.0309	.295	.202	.98 ^b	1.17		.042
	.0551	.0309	.295	.202	.50	0.72		
	.0441	.0309	.295	.202	.50	0.72		
50 ± 0.05	.0661	.0309	.295	.202	.50	0.71		
	.0551	.0309	.441		.98		0.054	
25 ± 0.05	.0551	.0491	.735		.98		.0077	
	.0551	.0639	.735		.98		.0077	
	.0551	.0737	.735		.98		.0075	
	.0551	.0491	.735		.48		.0048	
	.0551	.0491	.735		1.84		.0128	
98 ± 0.2	.0551		.333		.33			.043
80 ± 0.2	.0551		.300		.33			.0045
98 ± 0.2	.0551		.300		.98			.0043

^a $\mu = 0.98$ includes KOH 0.0105 M . ^b $\mu = 0.98$ K_2SO_4 .

$$R = K[\text{Co(III)}][\text{Co(II)}] \quad (1)$$

in which $[\text{Co(III)}]$ and $[\text{Co(II)}]$ refer to the concentrations of the complex species, and R is the rate of inversion. The results obtained at 98° are shown in Fig. 1, in which the rate constants calculated from (1) are plotted against the free ethylenediamine concentration. It will be seen that the racemization rate is dependent both on the concentration of the Co(II) complex and the free ethylenediamine concentration. The electron transfer racemization was separated from the secondary reaction by extrapolating the plots in Fig. 1 to zero free ethylenediamine concentration. This gave the electron transfer racemization rate constant $k = 0.56 \times 10^{-2}$ l. moles⁻¹ sec.⁻¹ at 98° . However, both reactions could be accounted for in the rate expression

$$R' = k[\text{Co(III)}][\text{Co(II)}] + k'[\text{Co(III)}][\text{en}] \quad (2)$$

whence $k = 0.56 \pm 0.02 \times 10^{-2}$ l. mole⁻¹ sec.⁻¹, and $k' = 0.042 \pm 0.004$ l. moles⁻¹ sec.⁻¹, in which k and k' are, respectively, the rate constants for the electron transfer racemization, and the reactions between tris-(ethylenediamine)-cobalt(III) ion and ethylenediamine. K (expression 1) is related to k and k' by the expression $K[\text{Co(II)}] = k[\text{Co(II)}] + k'[\text{en}]$.

The electron transfer reaction was dependent on both Co(II) and Co(III) concentration to the first power. Lewis, *et al.*,¹ found fractional exponents for the Co(III) dependence, though over a wider range of concentrations.

The rate of the secondary reaction was measured in the absence of Co(II) complex at 98 and 80° (Table I), and gave $k = 0.043 \pm 0.004 \times 10^{-2}$ and 0.0045 ± 0.0004 l. mole⁻¹ sec.⁻¹, respectively, with $E_a = 32$ kcal./g. mole and $\Delta S^\ddagger = +12$ e.u. This reaction rate was measured by Gehman and Fernelius³ who found the value $E_a = 24.6$ kcal./g. mole in the temperature range 74 – 85° for the pseudo first-order reaction occurring in the presence of 94 moles of free ethylenediamine.

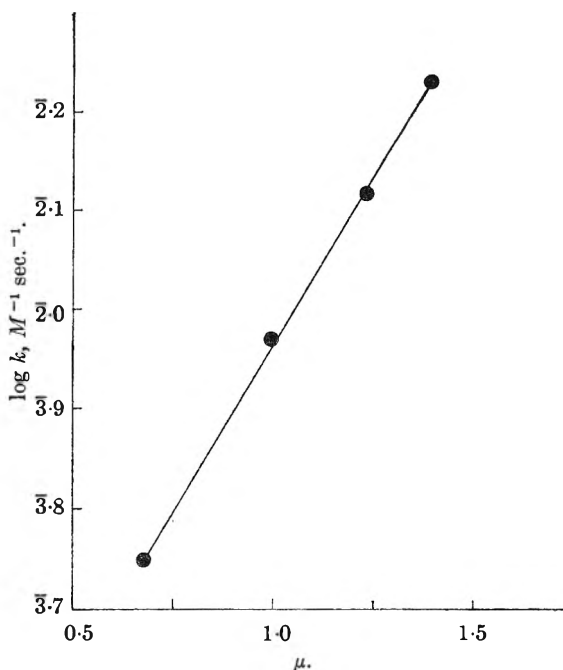


Fig. 2.— $\log k$ (electron transfer) vs. $\sqrt{\mu}$ at 98° ; $[\text{Co(III)}] = 0.0551 M$; $[\text{Co(II)}] = 0.0309 M$, $[\text{en}] = 0.295 M$.

The 7- and 8-covalent intermediate postulated, which is consistent with the exchange of C^{14} -labelled ligand,³ also may decompose with reduction to Co(II) complex. However, under the conditions used in this work, and those reported by the workers above,³ traces only of Co(II) complex were formed, insufficient in amount, probably, for the electron-transfer reaction to make any significant contribution to the rate.

At 25 and 50° the electron-transfer reaction rate was independent of the free ethylenediamine concentration. The first-order dependence on the Co(II) and Co(III) complex concentrations is shown in Table I. $\log k$ increased linearly with ionic strength, μ , Fig. 2 and there was no specific

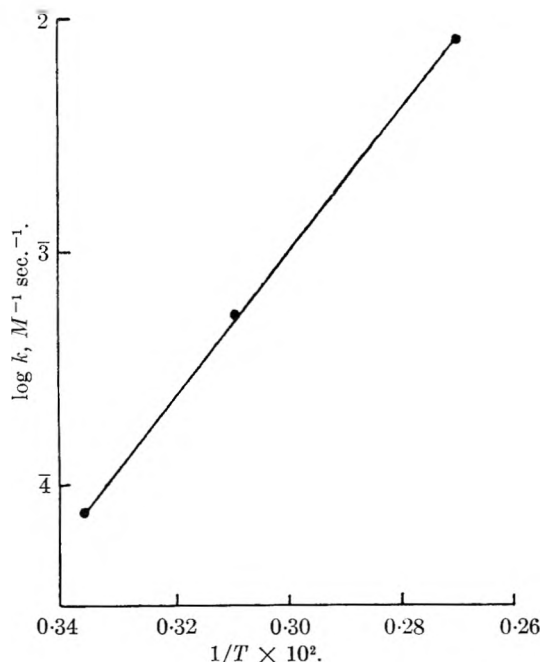


Fig. 3.— $\log k$ vs. $1/T$ for the electron transfer at $\mu = 0.98$. anion dependence, e.g., chloride compared with sulfate.

The electron transfer rate constants at 98° and at varying ionic strength have been separated from the secondary reaction involving ethylenediamine, which has been found to be independent of ionic strength (Table I). $\log k$ was a linear function of $1/T$ from 25 to 98° at $\mu = 0.98$ (Fig. 3). The rate constant $k_{25} = 0.77 \times 10^{-4}$ l. moles $^{-1}$ sec. $^{-1}$ and $E_a = 14.1 \pm 0.2$ kcal./g. mole, and $\Delta S^* = -32$ e.u. at $\mu = 0.98$ agree with the values ($k_{25} = 0.52 \times 10^{-4}$ l. moles $^{-1}$ sec. $^{-1}$, $E_a = 14.2$ kcal./g. mole, $\Delta S^* = -32$ e.u.) calculated from the data of Lewis, *et al.*

The rate of electron transfer was independent of hydroxyl ion concentration at 98° (Table I), an observation also made previously 1 at 25° . There was neither any catalysis due to ethylenediamine nor due to anions, as opposed to ionic strength effects. It would seem, therefore, that hydrogen atom transfer across the conjugate base forms of the cobalt complexes, ethylenediamine or anion bridging is not involved in the electron transfer.

CONFORMATION OF FLUORINATED CYCLOHEXANES

By J. FEENEY AND L. H. SUTCLIFFE

Department of Inorganic and Physical Chemistry, Liverpool University, Liverpool, England

Received January 27, 1951

Recently, a series of fluorinated cyclohexane derivatives has been examined by n.m.r. spectroscopy. 1 The ^{19}F spectra obtained at 40.00 Mc./sec. were assigned by selecting pairs of non-equivalent geminal fluorine atoms and by formulating a set of empirical rules based on neighbor interaction both through the bonds and through space. In

(1) J. Feeny and L. H. Sutcliffe, *Trans. Faraday Soc.*, **56**, 1559 (1960).

most cases it was possible to decide whether a given derivative is fixed or interconverting at room temperature from the number and intensity of AB quartets occurring in the spectra. 2

The more recent low temperature n.m.r. study by Tiers 3 on perfluorocyclohexane confirms the rather large value of the geminal fluorine coupling constant ~ 290 c./sec. and also provides a value for the chemical shift difference between these two atoms of 728 ± 2 c./sec. at 40.00 Mc./sec. The determination of the latter value now enables unequivocal assignments to be made about the conformational states of some of the fluorinated cyclohexane derivatives which were previously uncertain. 1 Since geminal fluorine atoms which are not appreciably affected by substituents will have a chemical shift difference of 728 c./sec. at 40.00 Mc./sec. its presence in a ^{19}F spectrum should be good evidence for a fixed conformer. The ^{19}F spectra of monochloro- and trifluoromethylundecafluorocyclohexane contain a chemical shift difference for the 4e and 4a fluorine atoms of ~ 730 c./sec., thus confirming the original conclusion that these molecules are fixed at room temperature. 1 This chemical shift is absent from the spectrum of undecafluorocyclohexane, hence the molecule is probably rapidly interconverting at room temperature. Of the decafluorocyclohexane derivatives, only the ^{19}F spectrum of the *trans* 1H/2H isomer has a pair of doublets separated by a chemical shift difference of ~ 730 c./sec., thus confirming that this molecule is fixed at room temperature. However, the two hydrogen atoms must be in equatorial positions in the fixed conformer and not in the axial positions as was originally stated. 1 It is still not possible to assign unequivocally the 1H:3H *cis* isomer to a fixed or rapidly interconverting conformation: however, the structure to which it was originally assigned, 1 having both hydrogen atoms in equatorial positions in a fixed molecule is inconsistent with the ^{19}F spectrum since such a molecule would give rise to geminal fluorine atoms which would have a chemical shift difference of ~ 730 c./sec.

It is intended to study the spectra of the compounds at low temperatures in order to determine the conformational states of the molecules where they are still uncertain.

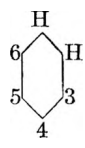
The large chemical shift difference found between axial and equatorial fluorine atoms in the low temperature spectrum of perfluorocyclohexane necessitates some modification of the ^{19}F shielding rules for fluorinated cyclohexanes given in ref. 1. Since all inductive effects will operate equally on the fluorine atoms in perfluorocyclohexane, the large shielding differences must be due to spatial shielding effects of one fluorine atom on another. Hydrogen substitution in the equatorial positions causes the geminal fluorine atoms in a neighboring CF_2 group to be shielded equally in a fixed molecule as can be seen from examination of the environment of the relevant fluorine atoms in the 1H/2H *trans* isomer given in Table III of ref. 1, part of which is reproduced below in Table I. The four

(2) H. J. Bernstein, J. A. Pople and W. G. Schneider, "High Resolution Nuclear Magnetic Resonance," McGraw-Hill Book Co., Inc., New York, N. Y., 1959, p. 119.

(3) G. V. D. Tiers, *Proc. Chem. Soc.*, 391 (1960).

immediate neighbors of each fluorine atom both through the bonds and through space are given and hydrogen atom neighbors are distinguished from the others by use of parentheses.

TABLE I
THE ENVIRONMENT OF FLUORINE ATOMS IN 1H/2H *trans*-DECAFLUOROCYCLOHEXANE

Compound	F atom position	Nearest neighbor through space	Nearest neighbor through bonds
	3e	(2e) 2a 4e 4a	(2e) 2a 4e 4a
	3a	(2e) 1a 4e 5a	(2e) 2a 4e 4a
	4e	3e 3a 5e 5a	3e 3a 5e 5a
	4a	3e 2a 5e 6a	3e 3a 5e 5a
	5e	4e 4a 6e 6a	4e 4a 6e 6a
	5a	4e 1a 6e 3a	4e 4a 6e 6a
	6e	(1e) 1a 5e 5a	(1e) 1a 5e 5a
	6a	(1e) 2a 5e 4a	(1e) 1a 5e 5a

Hence, the fluorine atoms in positions 4e, 4a, 5e and 5a give rise to two AB doublets separated by a chemical shift difference of 710 c./sec. at 40.00 Mc./sec. and those at positions 3e, 3a, 6e and 6a result in a single absorption band. It appears that the spatial effect is only operative when all the immediate neighbors of a fluorine atom are themselves fluorine atoms.

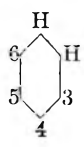
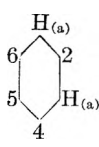
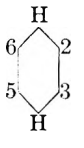
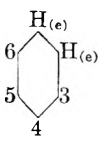
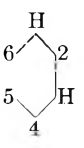
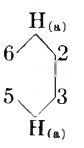
Table II gives the modified assignments for the dihydrodecafluorocyclohexanes. The absence of the ~730 c./s. chemical shift difference in the spectrum of the *trans* 1H/3H isomer cannot be taken as evidence for the presence of rapid conformational interconversion since a fixed isomer would not contain a pair of geminal fluorine atoms shielded similarly to those in perfluorocyclohexane. However, the low field absorption bands extend over a much smaller range than would be expected of a fixed conformer (the low field absorption bands of the rapidly interconverting *cis* 1H:4H molecule involve a chemical shift spread of only 300 c./s.). The assignment of this compound is somewhat speculative since it is almost certainly a mixture of the *trans* 1H/3H and 1H/4H isomers (these compounds can be separated only with difficulty⁴).

The assignments for *cis* 1H:2H and 1H:3H given in Table II are derived from suggestions made by Musher.⁵ These have been deduced from the recurrent chemical shifts found in the ¹⁹F resonance spectra of the *cis* 1H:2H, 1H:3H and 1H:4H isomers. From these assignments it can be seen that proximity to hydrogen atoms through bonds has a deshielding effect on the fluorine atoms in a neighboring CF₂ group.

From a ¹⁹F n.m.r. investigation of *cis* and *trans* perfluorodecalin Thomas⁶ has assigned the low field doublet of the low temperature ¹⁹F spectrum of perfluorocyclohexane to the axial fluorine atoms. The conclusions of Thomas are based on the assumption that spin-spin interaction between *trans* fluorine atoms on adjacent carbon atoms is greater than that between *cis* fluorine atoms in a cyclohexane ring. The results of Tiers and Thomas and the suggestions made by Musher all have been used

(4) R. P. Smith and J. C. Tatlow, *J. Chem. Soc.*, 2505 (1957).
(5) J. I. Musher, private communication.
(6) J. Homer and L. F. Thomas, *Proc. Chem. Soc.*, 139 (1961)

TABLE II
ASSIGNMENTS FOR THE 40 MC./S. ¹⁹F N.M.R. SPECTRA OF SOME DIHYDRODECAFLUOROCYCLOHEXANES AT ROOM TEMPERATURE

Compound	Assignment	Band	Chemical Shift (c./s.)
<i>cis</i> 1H:2H, b.p. ¹ 90.8° 	3,3',6,6' ^a 4,4',5,5' impurity? 1,2	1	1680
		2	1950
		3	2035
		4	2250
		5	5610
		6	5780
		7	5820
<i>cis</i> 1H:3H, b.p. 90.9° 	impurity? 2e,2a 4a,6a 4e,6e 5e,5a impurity? 1e,3e	1	1265
		2	1570
		4	1790
		3	1650
		5	1930
		6	2050
		8	2330
		7	2250
		9	5550
		10	5730
		11	5770
<i>cis</i> 1H:4H, b.p. ^b 85.4° 	2,2',3,3' 5,5',6,6' 1,4	1	1670
		2	1950
		3	2080
		4	2370
		5	5940
		6	5980
<i>trans</i> 1H/2H, b.p. 70° 	4a,5a 3e,3a,6e,6a 4e,5e 1a,2a	1	1790
		3	2070
		2	1860
		4	2155
		5	2420
		6	2550
		7	2840
		8	5850
		9	5900
Mixture of <i>trans</i> 1H/3H and <i>trans</i> 1H/4H, b.p. 79° 	2,2' 4,4',6,6' 5,5' 1,3	1	1815
		2	2010
		3	2085
		5	2255
		6	5860
		7	5905
	2e,2a,3e,3a 5e,5a,6e,6a 1e,4e	4	2100
		4	2100
		8	6120
		9	6165

^a Atoms marked with a prime are *trans* to the nearest hydrogen atom *via* the bonds in an interconverting molecule.

^b The boiling points quoted in the paper by P. Johncock, W. K. Musgrave, J. Feeney and L. H. Sutcliffe, *Chem. and Ind.*, 1314 (1959), require interchanging.

in obtaining the modified set of assignments for the dihydrodecafluorocyclohexane given in Table II.

DIASTEREOAZEOTROPES AS A MEANS OF RESOLUTION

BY CLIFFORD J. MCGINN

Department of Chemistry, Le Moyne College, Syracuse, N. Y.

Received February 27, 1961

This is the report of an attempt to resolve a racemic mixture by means of the fractional distillation of the mixture of its diastereoazeotropes. If each of the enantiomers d_1 and l_1 forms an azeotrope with a third optically active substance, d_2 , the two diastereoazeotropes may differ sufficiently in boiling point to permit resolution by fractional distillation, particularly if the ternary system d_1 - l_1 - d_2 should itself not contain a ternary azeotrope. If the system does form such a ternary azeotrope the possible resolution will thereby be restricted, the more so the more nearly equal are the concentrations of d_1 and l_1 in the azeotrope.

The specific resolution attempted was that of d,l -2-octanol (= d_1 and l_1) using d -limonene as the third component (= d_2). Several different solutions, varying in mole fraction of d_2 from 0.1 to 0.9, were fractionally distilled at several different temperatures and pressures. The fractions were analyzed for the optically active component d -limonene by means of infrared, and its contribution to the optical rotation was subtracted from the observed rotation. No positive evidence that resolution had occurred could be found. The fractionating column consisted of a three-necked round-bottom flask inside a heating mantle which was electrically controlled. Mounted on this was a three-foot column, packed with Raschig rings, wound with nichrome wire, and jacketed with asbestos one inch thick. Its temperature was controlled independently of the pot. On top of this was a distilling head containing a cold finger. The apparatus as described was equivalent to 20 theoretical plates.

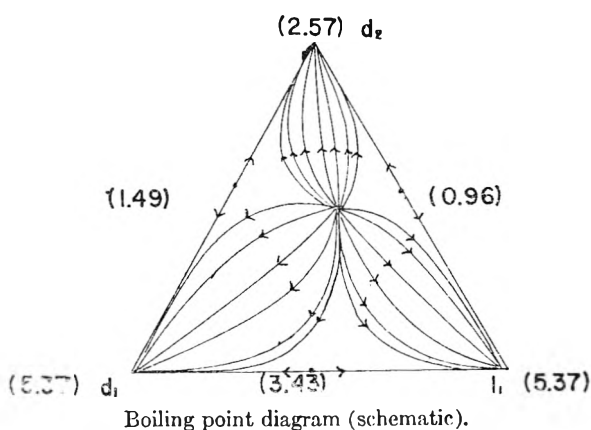
To determine why resolution had not occurred the d_1 - l_1 pair was resolved by conventional methods and the physical properties of the following systems were studied: d_1 , l_1 , d_1 - l_1 , d_1 - d_2 , l_1 - d_2 and d_1 - l_1 - d_2 . The actual systems were formed from d -2-octanol (d_1), l -2-octanol (l_1) and d -limonene (d_2). The physical properties measured were the boiling point, refractive index, density, and where applicable the temperature change on mixing. The above physical properties were determined simply to show the degree of non-ideality of the systems studied. The results are shown in Table I.

TABLE I¹

Sys-tem	Sp. gr. (27.6°)	B.p. (relative)	n_D (27.6°)	dt mix. (27.6°)
d_1	0.8111	5.37	1.4232
l_1	.8115	5.37	1.4232
d_1 - l_1	.8170	3.43	1.4246	-0.618
d_2	.8380	2.53	1.4711
d_1 - d_2	.8303	1.49	1.4466	-1.380
l_1 - d_2	.8284	0.96	1.4472
d_1 - l_1 - d_2	.8282	0.62	1.4460	-1.085

The systems d_1 - d_2 , l_1 - d_2 and d_1 - l_1 - d_2 were all 55.0% in d -limonene (the approximate composition of the ternary azeotrope d_1 - l_1 - d_2). Since the

(1) H. Mauser, *Ber.*, **90**, 299 (1959).



differences in the boiling points were expected to be small the actual boiling points were not taken. The recorded values are those taken with a Beckmann thermometer which was adjusted to the anticipated ranges for the systems studied.

The very fact that the racemic d_1 - l_1 solution is azeotropic, and hence non-ideal, is noteworthy. The expectation has been expressed (1) that such mixtures should be strictly ideal, whereas these data show the d,l -2-octanol mixture to deviate from strict additivity in all the properties measured. There seems to be no theoretical reason, however, for expecting strict ideality and strict additivity. The deviation in the properties will probably always be small, but varying in degree from system to system.

In the present considerations we are concerned with the boiling point diagram of the ternary system d_1 - l_1 - d_2 . The binary system d_1 - l_1 would be expected to be azeotropic, as observed, and of course symmetrical. The rest of the ternary diagram, however, must be asymmetric, as it seems to be from consideration of the boiling points: 1.49° for the d_1 - d_2 azeotrope, and 0.96° for the l_1 - d_2 azeotrope. The d_2 content of these two azeotropes should not be the same. While the results showed the compositions to be different, the differences unfortunately were within the limits of experimental error. The observed minimum ternary azeotropic boiling point (0.62°) is consistent with the existence of the three binary minimum azeotropes of the system. The composition of the ternary azeotrope is expected to be somewhat on the l_1 side of the system.

The boiling point diagram, then, with arrows indicating the course of the composition of the liquid residue during boiling, is of the following type (schematic). According to these relations, some resolution by fractional distillation should be possible. The actual failure of the resolution then means that either the asymmetry of the system is not sufficient for the fractionating technique used, or that the analytical procedure was not sufficiently sensitive to detect differences. It should be pointed out that the 2-octanol was recovered as sodium *sec*-octyl phthalate. It had no observable rotation.

The author is at present investigating the availability of fractionating columns with an efficiency sufficient to effect a possible resolution.

Acknowledgment.—This work is being supported by the American Chemical Society Petroleum Research Fund.

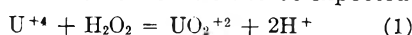
THE REACTION BETWEEN URANIUM(IV) AND HYDROGEN PEROXIDE¹

BY F. B. BAKER AND T. W. NEWTON

University of California Los Alamos Scientific Laboratory, Los Alamos, New Mexico

Received March 20, 1961

The purpose of this note is to describe some experiments which were done to help understand the reaction between U(IV) and H₂O₂ in aqueous HClO₄ solutions. The pertinent oxidation potentials are such that the net reaction to be expected is



The results to be given here show that the reaction does not proceed directly by this simple reaction but that it is in part, at least, a chain reaction and that it is accompanied by a small amount of H₂O₂ decomposition.

Experimental

Solutions of U(VI), U(IV), HClO₄, NaClO₄, and LiClO₄ were prepared as before.² Other U(IV) solutions were made by the reduction of U(VI) with metallic Zn or Pb. U(IV) made in all three ways showed essentially the same rate behavior. The H₂O₂ was from two sources, 30% solution from the Mallinckrodt Chemical Co. and 90% solution from the Becco Chemical Division of the Food Machinery and Chemical Corp. Both of these solutions were further purified by distillation under reduced pressure and gave essentially the same kinetic results. The second fraction from the 30% solution had a disagreeable odor and gave slightly higher rates; so subsequent runs were made with diluted 90% material. Cu(ClO₄)₂ was made by fuming Cu(NO₃)₂ with HClO₄ and then crystallizing from concentrated HClO₄. The other perchlorate salts were from the G. F. Smith Chemical Co. and were used without further purification, except for Co(ClO₄)₂ which was recrystallized.

The U(IV) solutions were analyzed by titration using standard Ce(IV) sulfate. H₂O₂ was analyzed as an oxidizing agent against standard Fe(II) and as a reducing agent against standard Ce(IV) with the same results. Mixtures of U(IV) and H₂O₂ were analyzed for the difference in their concentrations by adding aliquots to excess standard Fe(II) and back titrating with standard Ce(IV).

The rate runs were made spectrophotometrically by following the absorbance at 6478 Å. where U(IV) absorbs relatively strongly. The apparatus and general procedure have been described previously.²

Results

Stoichiometry.—The stoichiometry of the reaction was examined closely since it is known³ that the reaction between Fe(II) and H₂O₂ is quantitative when Fe(II) is in excess but that a large amount of extra H₂O₂ is consumed when H₂O₂ is in excess. The stoichiometry of reaction 1 was studied by analyzing known mixtures after reaction either for [H₂O₂] or for the [U(IV)]-[H₂O₂] difference. The results of some typical determinations of the number of moles of H₂O₂ consumed for each mole of U(IV) which reacted (consumption ratio) are given in Table I. The data show that, unlike the case of Fe(II), there is a small amount of H₂O₂

decomposition over the whole range of reactant concentrations studied. Similar determinations in 0.5 M HClO₄ or in solutions containing up to 0.006 M Na₂SO₄, 0.006 M HCl, 0.008 M Co(II) or 0.009 M U(VI), or at a temperature of 2.4° gave consumption ratios in the range of those listed in Table I.

TABLE I

MOLES OF H₂O₂ CONSUMED FOR EACH MOLE OF U(IV) REACTED (CONSUMPTION RATIO)

Conditions: 2M HClO₄, 23-25°, solutions deaerated with Ar

Initial values		Consumption ratio	Approximate rate constant, M ⁻¹ min. ⁻¹
[U(IV)], M × 10 ³	[H ₂ O ₂]/[U(IV)]		
3.04	0.54	1.024	48
3.08	.55	0.997	49
3.03	.55	1.017	47
1.54	1.1	1.014	57
2.76	1.1	1.010	68
1.35	2.5	1.023	95
2.69	2.5	1.033	111
1.35	5.0	1.062	114
1.48	8.3	1.035	..
1.48	10.8	1.029	..
1.48	13.8	1.019	..
1.48	18.0	1.029	..

Reaction Rates.—Preliminary runs made at 25° in air-saturated 2 M HClO₄ showed good reproducibility and were in accord with a rate law which was first order in U(IV) and in H₂O₂. Best values for the rate constants for these runs were determined by the use of a non-linear least squares program⁴ which minimized the sum of the differences between the observed and calculated absorbance values. The average second-order rate constant was found to be 56.8 with a standard deviation of 1.85 and a maximum deviation of 2.9 M⁻¹ min.⁻¹. The second-order rate law fit the experimental data quite well; the average difference between the calculated and observed absorbance values was only 0.002. The HClO₄ used in some of these runs was prepared by vacuum distillation, but no significant differences were observed. Similarly, the water used in some of the runs had been distilled but once, giving no detectable effect.

Although oxygen in the air reacts with U(IV) at an insignificant rate⁵ at room temperature in 2 M HClO₄, it has been found that it has a significant effect on the kinetics of the U(IV)-H₂O₂ reaction. Four additional runs were made in which the solutions were deaerated with argon; these gave average second-order rate constants ranging between 38 and 44 M⁻¹ min.⁻¹. Two additional runs using air-saturated solutions gave 53 and 54 M⁻¹ min.⁻¹ in agreement with the previous series. Two runs made using O₂ saturated solutions gave apparent second-order rate constants of 56 and 61 M⁻¹ min.⁻¹. The data from the solutions which had

(4) We are indebted to R. H. Moore and Ivan Cherry of the Theoretical Division of this Laboratory for computations involving the IBM-704 Computer: the former for modifying existing least square programs for our purpose (see R. H. Moore and R. K. Zeigler, LA-2367) and the latter for slope calculations.

(5) J. Halpern and J. G. Smith, *Can. J. Chem.*, **34**, 1419 (1956), report $-d[U(IV)]/dt = k[U(IV)][O_2]/[H^+]$ and show that in 0.5 M HClO₄ at 30° and 0.96 atm. of O₂ the half-time for the oxidation of U(IV) is about 120 min.

(1) This work was done under the auspices of the U. S. Atomic Energy Commission.

(2) T. W. Newton, *J. Phys. Chem.*, **63**, 1493 (1959).

(3) J. H. Baxendale, in "Advances in Catalysis," Vol. IV, Academic Press, Inc., New York, N. Y., 1952, p. 46 ff.

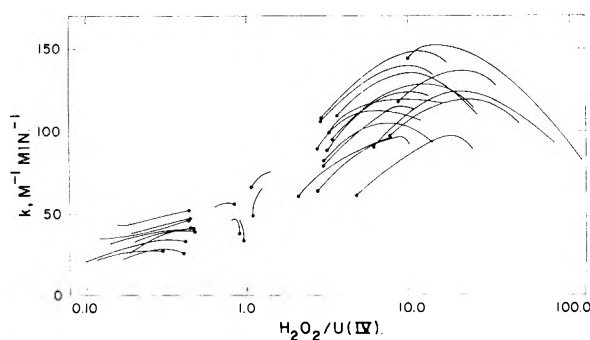


Fig. 1.

been deaerated with argon fit a second-order rate law much less well than those from the air saturated solutions mentioned above. Apparent second-order rate constants were computed from the slopes of the absorbance *versus* time functions⁴; these rate constants were found to decrease uniformly during the course of the run, having dropped about 20% by the time the reaction was 75% complete. It thus appears that oxygen in the solutions increases the rate and allows better adherence to a second-order rate law. Consumption ratio determinations showed that there is a small amount of induced oxygen reaction during the U(IV)-H₂O₂ reaction.

The data obtained in all the runs made at 25° in deaerated 2 M HClO₄ are summarized in Fig. 1. In order to make the data more readily comparable, the observed rates have been divided by the concentration product [U(IV)][H₂O₂] to give *k*, the apparent second-order rate constant, and plotted against *R*, the [H₂O₂]/[U(IV)] ratio. The individual runs are shown as separate lines. Although there is considerable scatter among the various runs, it is clear that the apparent second-order rate constants are larger in the high H₂O₂ region.

At constant *R* values there is no correlation between the apparent rate constants and the reactant concentrations. For example, when *R* = 5, the H₂O₂ concentrations for the runs shown from top to bottom in Fig. 1 were 3.9, 3.9, 5.0, 2.3, 1.9, 5.0, 2.5, 2.5, 3.6, 1.4, 1.9 and 4.5 mmoles per liter.

Experiments done at 25° with *R*₀, the initial value of *R*, equal to 0.5 showed that decreasing the HClO₄ concentration from 2 to 0.5 M (ionic strength held at 2 by the use of LiClO₄ or NaClO₄) increased the rate by a factor between 2 and 3.

Some rates were measured at 2.4, 9.8 and 34.2° as well as at 25°. The temperature coefficients of the apparent second-order rate constants made it possible to estimate the over-all activation energy for the reaction under various conditions. In 2 M HClO₄ with *R*₀ = 0.57 the activation energy was found to be 17 kcal./mole and with *R*₀ = 5 the corresponding value was 16 kcal./mole. In 0.5 M HClO₄ with *R* = 0.5, the activation energy was found to be 19 kcal./mole. Due to the known scatter of the data these activation energies are uncertain by at least 1 kcal./mole and it is not possible to attach any significance to the differences among the values.

The catalytic effect of several cations was investigated; in 2 M HClO₄ solutions with *R*₀ = 0.5,

0.01 M U(VI), 0.004 M Hg(II) and 0.003 M Pb(II) were without significant effect. The rate was roughly tripled by 0.005 M Ag(I) and by 0.01 M Mn(II) while 0.0002 M Fe(II) increased the rate about sixfold. The ions of Cu(II) and Co(II) were found to inhibit the reaction. The decreases in rate observed with these ions are summarized in Table II. It is to be noted that small amounts of Co(II) cause less inhibition when *R*₀ = 2 than when *R*₀ = 0.5, but that this effect is reversed at higher Co(II) concentrations.

TABLE II

EFFECT OF Cu(II) AND Co(II) ON THE RATE OF THE U(IV)-H₂O₂ REACTION

Conditions: 25°, 2M HClO₄. The tabulated values are the fractions of the corresponding uninhibited rates.

Inhibitor	<i>R</i> ₀	Inhibitor concn., <i>M</i>			
		10 ⁻⁴	10 ⁻³	10 ⁻²	10 ⁻¹
Cu(II)	0.5	0.85	0.73	0.60	..
Co(II)	0.5	..	.83	.56	0.33
Co(II)	2.0	..	.95	.50	.18

The effect of *R*₀ on the rates becomes smaller as the Co(II) concentration is increased; however, in 0.1 M solutions the rate is about 35% greater in solutions with the higher *R*₀.

Small amounts of sulfate did not affect the reaction rate but 1.4 × 10⁻³ M HCl in 2 M HClO₄ increased the rate by a factor of about 1.7.

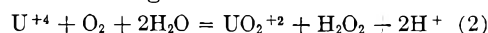
That the reaction is not catalyzed by glass surface was shown in an experiment in which the surface area was tripled by the use of a coiled Pyrex rod placed in the reaction vessel. For these runs the reaction was followed by removing aliquots at definite times and quenching them in excess Ce(IV).

Photochemical effects are unimportant since the rate was not increased significantly when the light from a 100 W tungsten lamp was focussed onto the reaction vessel.

The possibility of the formation of peroxide complexes has been considered. Although U(VI) does not form peroxide complexes in acid solution⁶ the existence of Pu(IV)-peroxide complexes⁷ makes U(IV)-peroxide complexes plausible. A study of such complexes is difficult because of the rapidity of reaction 1. Preliminary experiments were made in 0.5 M HClO₄ at 2.4° in which absorbances observed at 6478 Å. were extrapolated to the time of mixing. At a constant U(IV) concentration of 2.6 × 10⁻³ M the extrapolated absorbances were found to be a nearly linear function of the H₂O₂ concentration. A H₂O₂ concentration of 4.6 × 10⁻³ M gave an extrapolated absorbance which was 95% of its value in the absence of H₂O₂. This indicates that some complexing occurs but the effect is too small to make even a qualitative estimate of its extent.

Discussion

In their study of the reaction between U(IV) and dissolved oxygen, Halpern and Smith⁵ found that the reaction proceeds in two stages, the first a chain process leading to the net reaction



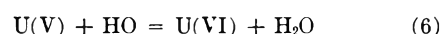
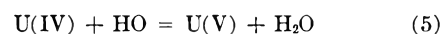
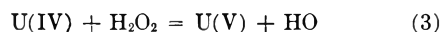
(6) J. Corpel, *Bull. soc. chim. France*, 752 (1953).

(7) R. E. Connick and W. H. McVey, *J. Am. Chem. Soc.*, **71**, 1534 (1949).

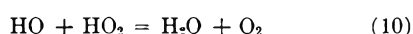
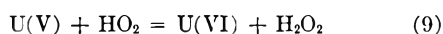
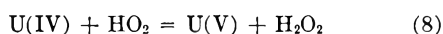
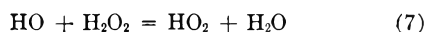
and the second reaction 1, which they found to be instantaneous. The chain carriers which were proposed for reaction 2 are U(V) and HO₂. Our experiments indicate that reaction 1 also is a chain process and that its rate is conveniently measurable.⁸ The discrepancy in the reported rates of (1) is probably due to the fact that Halpern and Smith used higher reactant and lower hydrogen ion concentration.

The principal evidence that reaction 1 proceeds by a chain is the fact that it is strongly inhibited by Co(II) and Cu(II). This conclusion is supported by the lack of reproducibility which was encountered in the rate measurements. It is interesting to note that the ions Mn(II) and Co(II) which had no effect on reaction 2⁵ were found in the present work to catalyze and inhibit reaction 1, respectively. Also the ions of Fe(II), Ag(I), Cu(II) and Cl⁻ show the opposite effect in the two reactions. These results imply that at least one of the radicals involved in reaction 1 is different from those involved in reaction 2.

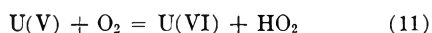
It is plausible that the chain carriers in reaction 1 are U(V) and HO and that in the absence of catalysts or inhibitors the most important reactions are



The mechanism given by reactions 3-6 does not show all that happens since it fails to account for deviations from a second-order rate law, the slight lack of stoichiometry, and the increase in the apparent second-order rate constant at high H₂O₂ concentrations. These complications might be explained by the additional reactions



Since Co(II) does not affect HO₂ radicals, their postulated existence in solutions with large *R* values is consistent with the observation that small concentrations of Co(II) have very small inhibiting effects in such solutions. The effect of oxygen may derive from the reaction



Acknowledgment.—The authors wish to thank Helen D. Cowan for technical assistance in the rate measurements. They also acknowledge many helpful discussions with Prof. Henry Taube, Dr. C. E. Holley, Jr., and especially with Dr. J. F. Lemons under whose general direction this work was done.

(8) A recent Russian report describes some preliminary experiments made in H₂SO₄ solutions: E. A. Kanevsky and L. A. Federova; *Radiokhimiya*, **2**, 559 (1960).

TETRACHLOROPHTHALIC ANHYDRIDE-AZAHYDROCARBON COMPLEXES

BY MIHIR CHOWDHURY¹

University College of Science & Technology, 92, Upper Circular Road
Calcutta-9, India

Received March 21, 1961

It was reported in a previous paper² that there was close correspondence between λ_{max} of T.C.P.A. complexes of hydrocarbons and those of corresponding azahydrocarbons. This suggested that the electron involved in the spectral jump came from the π -orbital of the azahydrocarbon. This does not however necessarily mean that the stability of the complex is also due to π - π interaction alone. In order to see whether the stabilities also are close to each other, we have determined the equilibrium constants of T.C.P.A. complexes of three azahydrocarbons by following a modified Benesi-Hildebrand relation. The data are summarized in Table I and the plots are given in Fig. 1. It has not been possible to extend the study to other aza-compounds because of incipient precipitation.

TABLE I
EQUILIBRIUM CONSTANTS OF CHARGE-TRANSFER COMPLEXES

Donor	Concn. of T.C.P.A., moles/l. $\times 10^4$	Inverse of concn. of donor (1/ <i>C</i>), l./mole	Wave length, μ	$\frac{1}{E - E_s} \times 10^2$	K_1 , mole ⁻¹ l.
Quinoline	3.670	9.711	355	1.015	26
		11.653		1.080	
		14.567		1.152	
		16.648		1.211	
		19.423		1.265	
α -Methylquinoline	3.177	10.502	355	0.790	15
		12.602		.887	
		15.753		.978	
		18.004		1.068	
		21.004		1.137	
7,8-Benzoquinoline	2.819	24.400	375	0.759	18
		29.270		.865	
		36.590		.975	
		48.780		1.182	
		58.550		1.376	

The equilibrium constants of azahydrocarbon complexes are somewhat higher than those of corresponding hydrocarbon complexes.² This indicates that in addition to π - π interaction there occurs some specific interaction with nitrogen non-bonding electrons. This also explains why the stabilities of complexes of methylquinoline and 7,8-benzoquinoline are less than that of quinoline in spite of the higher π -ionization potential of quinoline. Substituents in quinoline possibly offer hindrance to the localized interaction, thereby decreasing the stability.

It should be noted that the equilibrium constants of T.C.P.A.-hydrocarbon and T.C.P.A.-azahydrocarbon complexes are closer to one another than the case of I₂-hydrocarbon³ and I₂-azahydrocarbon complexes.⁴ In the case of I₂-complexes of aza-compounds, where *n*-electrons are supposed to be in-

(1) Whitmore Chemical Laboratory, Pennsylvania State University, University Park, Pennsylvania.

(2) M. Chowdhury and S. Basu, *Trans. Faraday Soc.*, **56**, 335 (1960).

(3) R. Bhattacharya and S. Basu, *ibid.*, **54**, 1286 (1958).

(4) J. Nag Chaudhuri and S. Basu, *ibid.*, **55**, 898 (1959).

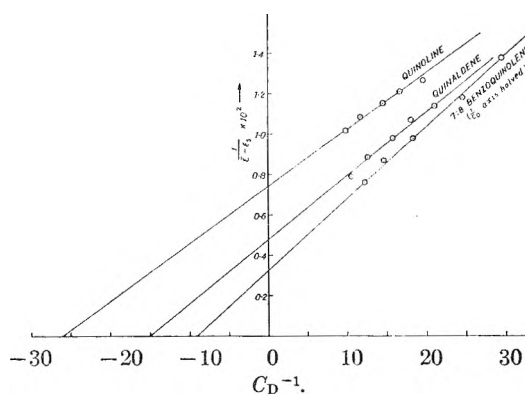


Fig. 1.

volved in bonding, the equilibrium constant is of different order from that of I_2 -hydrocarbon complexes. In the present case the aza-complexes and hydrocarbon complexes approach each other in stability more closely. It seems that both $n-\pi$ and $\pi-\pi$ interaction play their part in the formation of aza-complexes, the contribution of $\pi-\pi$ interaction being more in the present case than for I_2 -complexes.

For the determination of equilibrium constants, we have used the modified Benesi-Hildebrand relation, *i.e.*

$$\frac{1}{\bar{E} - E_s} = \frac{1}{E_c - E_s} \frac{1}{K} \frac{1}{C_D} + \frac{1}{E_c - E_s} \quad (1)$$

where

E_c, E_s = extinction coefficients of complex and acceptor substrate, resp.

$$\bar{E} = \frac{\text{Optical density of mixture (A)}}{\text{Optical path length (l)} \times \text{added initial concn. of acceptor } (C_s^0)}$$

C_D = concentration of donor

The plot of $1/(\bar{E} - E_s)$ against $1/C_D$ gives a straight line, the intercept of which on the $1/(\bar{E} - E_s)$ axis gives $1/(E_c - E_s)$ and slope of which gives $1/K(E_c - E_s)$. Recently Nash⁵ criticized the Benesi-Hildebrand relation on the ground that an auxiliary quantity, the molar absorptivity of the complex, need be determined before the object of primary interest, the equilibrium constant, can be determined. We have avoided this difficulty by determining K directly from the intercept on the $1/C_D$ axis. Nash's equation⁵ can, however, be derived very easily by simple algebraic transformation of the above equation.

Thanks are due to Professor S. Basu for helpful discussions.

(5) C. P. Nash, *J. Phys. Chem.*, **64**, 950 (1960).

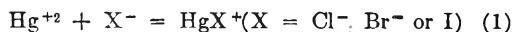
ENTHALPIES AND ENTROPIES OF FORMATION OF MERCURY(II)-HALIDE 1:1 COMPLEX IONS

By G. N. MALCOLM, H. N. PARTON AND I. D. WATSON

University of Otago, Dunedin, New Zealand

Received April 3, 1961

Although the equilibrium quotients for the reactions



have been determined at 25° on several occasions, there is very little information available about the enthalpy changes of these reactions. Gallagher and King¹ recently have reported enthalpy results determined calorimetrically for the case with chloride ions. We present here similar results for the reactions with chloride, bromide and iodide ions, all at 25°.

The results were obtained by measuring the heat effects produced by the dilution of small amounts of potassium halide solution with large volumes of acidified mercuric perchlorate solutions. The details of the method have been described previously.² The ionic strengths of the various final solutions were between 0.10 and 0.14. In all cases the concentration of the species HgX^+ was between twenty and a hundred times greater than that of the species HgX_2 , and the concentrations of the higher complexes were negligibly small.

Experimental

Apparatus.—The calorimeter has been described already.² In each experiment 10 ml. of potassium halide solution was diluted with 990 ml. of mercuric perchlorate solution. The calorimeter was calibrated again on two separate occasions during the course of this work by measuring the heats of the one-hundredfold dilution of two different sodium chloride solutions. The average values obtained for these heats of dilution at 25° (with the corresponding literature³ values shown in brackets) were 302 (297) and 316 (326) cal. mole⁻¹ of sodium chloride for solutions with initial concentrations 2.50 and 2.73 molal. The calorimeter was immersed in a thermostat at 25 ± 0.01°.

Materials.—A.R. Chemicals were used throughout the work. All stock solutions were made up by weight. A stock solution of mercuric perchlorate was prepared by dissolving a known weight of mercuric oxide in an excess of 60% perchloric acid. The pH of the solution was measured and the concentration of mercuric ion was checked by analysis. The concentrations of mercuric ion in the solutions used for the dilution of the potassium halide solutions ranged from 0.032 to 0.050 molal.

Results

The results of the dilution experiments are shown in Table I.

The concentrations of the ions in each solution were calculated from the total concentrations of mercuric and halide ions given in Table I and the association constants of the complex ions. The association constants used were those determined by Marcus⁴ at 25° and ionic strength 0.50, and were corrected to the particular ionic strengths of the solutions by the equation of Davies.⁵ The relation between the heat of association of reaction 1 at zero ionic strength and at any other ionic strength for which the association constant is K' is given by the formula⁶

$$\Delta H' = \Delta H^0 - \frac{3RT^2}{2} \left(\frac{1}{D} \times \frac{dD}{dT} + \frac{1}{T} \right) \ln \frac{K'}{K^0} \quad (2)$$

The calculated values of ΔH^0 for the three associa-

(1) P. K. Gallagher and E. L. King, *J. Am. Chem. Soc.*, **82**, 3510 (1960).

(2) D. W. Anderson, G. N. Malcolm and H. N. Parton, *J. Phys. Chem.*, **64**, 494 (1960).

(3) "Selected Values of Chemical Thermodynamic Properties," Natl. Bur. Standards Circ. No. 500, 1952.

(4) Y. Marcus, *Acta Chem. Scand.*, **11**, 599 (1957).

(5) C. W. Davies, *J. Chem. Soc.*, 2093 (1938).

(6) J. M. Austin, R. A. Matheson and H. N. Parton, "The Structure of Electrolytic Solutions," edited by W. J. Hamer, John Wiley and Sons, New York, N. Y., 1959.

TABLE I
THE HEAT (Q) OF THE REACTION

$$\text{KX}(m) \xrightarrow[\text{Hg}(\text{ClO}_4)_2(m')]{\text{diluted with}} \text{KX}(0.01 m)$$

m	Moles of $\text{KI} \times 10^3$	m'	Q , cal.	Ionic strength of final soln.
X = Cl				
1.00	10.11	0.047	-57.07	0.13
	10.00		-57.07	
	9.97		-57.09	
0.50	4.74	.047	-29.3	.13
	4.72		-29.2	
	4.69		-28.1	
0.25	2.48	.046	-13.4	.13
	2.48		-13.0	
	2.48		-13.0	
X = Br				
1.00	10.88	0.046	-96.6	0.13
	10.79		-95.9	
	10.80		-96.0	
0.50	4.74	.032	-48.5	.09
	4.73		-48.1	
	4.75		-48.4	
0.25	2.28	.032	-25.0	.09
	2.29		-24.6	
	2.25		-24.0	
X = I				
1.00	10.90	0.042	-184.7	0.12
	11.10		-181.1	
	11.0		-177.8	
0.50	5.41	.050	-89.7	.15
	5.28		-89.8	
	5.42		-92.5	
0.25	2.70	.050	-49.2	.15
	2.73		-52.3	
	2.74		-55.1	
0.10	0.94	.042	-19.7	.12
	0.92		-18.4	
	0.92		-19.2	

tion reactions involving the mercury(II)-halide complex ions are shown in Table II. The standard free energies of association calculated from the association constants at zero ionic strength, and the standard entropies of association calculated from the free energies and enthalpies are shown in the same table.

TABLE II
THERMODYNAMIC FUNCTIONS FOR THE REACTIONS

$$\text{Hg}^{+2} + \text{X}^- = \text{HgX}^+ \text{ at } 25^\circ$$

X	ΔG° , kcal. mole ⁻¹	ΔH° , kcal. mole ⁻¹	ΔS° expt., e.u. mole ⁻¹	ΔS° calc., e.u. mole ⁻¹
Cl	-10.0	-4.8 ± 0.5	17 ± 3	17
Br	-13.3	-10.6 ± .5	9 ± 3	11
I	-18.4	-17.6 ± .5	3 ± 3	4

Discussion

Errors.—This method of determining enthalpies of association of complex ions depends for its success on a knowledge of the corresponding association constants at the appropriate ionic strengths. In the present case the association constants are known only at ionic strength 0.5

whereas their values are required at ionic strengths 0.1 and zero. In the absence of more reliable information the Davies equation was used to extrapolate the association constant values from ionic strength 0.5 to zero. The reliability of this equation at ionic strengths greater than 0.1 is not known. Nevertheless it is of interest that Vanderzee and Dawson⁷ have used an equation very similar to the Davies equation to fit association constant values for CdCl^+ measured at ionic strengths 3, 2, 1 and 0.5, and obtained an extrapolated value at zero ionic strength in good agreement with an independent determination by Harned and Fitzgerald.⁸

In all the final solutions the halide ion is present predominantly as HgX^+ so that the values of ΔH do not depend to any great extent on the values of the association constants. The correction of the enthalpy values to zero ionic strength involves the use of the Davies equation. The magnitude of this correction is never more than 0.4 kcal. mole⁻¹. It is probable therefore that the uncertainty in the standard enthalpy values is within ± 0.5 kcal. mole⁻¹. The standard entropies of association will be in error by ± 2 e.u. mole⁻¹ from this cause. If the uncertainty in the free energy values arising from the use of the Davies equation is taken into account, the error in the standard entropy figures rises to as much as ± 3 e.u. mole⁻¹.

Gallagher and King¹ obtained a value for the enthalpy of association of HgCl^+ of -5.9 kcal. mole⁻¹ at ionic strength 0.5. Correction of this figure to zero ionic strength by means of equation 2 gives a value of -5.4 kcal. mole⁻¹. The agreement between the two results for $\Delta H^\circ(\text{HgCl}^+)$ is not close, but is within the combined experimental uncertainties.

Entropies of Association.—Comparison of the results in Table II with those for the corresponding reactions with cadmium(II) and lead(II) ions⁹ reveals that the entropy changes for the association of each cation with a given halide anion are the same within the experimental error, but the corresponding enthalpies of association are markedly different. For example, for the reactions involving the formation of HgBr^+ , CdBr^+ and PbBr^+ , the entropies of association are all about 9 e.u. mole⁻¹ but the enthalpies of association are -10.6, -0.3 and +0.3 kcal. mole⁻¹, respectively. These results are consistent with the view that the species HgX^+ , CdX^+ and PbX^+ are complex ions with direct contact between the cation and the anion, so that their formation involves a change in hydration structure of the ions. For a given anion the strengths of the various cation-anion bonds will influence the enthalpies of the association reactions but need have little effect on the entropies of association if these are largely determined by the change of hydration of the ions on association. George¹⁰ has shown that the entropies of a number of cation-anion association reactions can be represented by the equation

(7) C. E. Vanderzee and H. J. Dawson, *J. Am. Chem. Soc.*, **75**, 5659 (1953).

(8) H. S. Harned and M. E. Fitzgerald, *ibid.*, **58**, 2624 (1936).

(9) G. H. Nancollas, *Quart. Revs. (London)*, **14**, 402 (1960).

(10) J. D. B. George, *J. Am. Chem. Soc.*, **81**, 5530 (1959).

$$\Delta S^0 = \Delta S (\text{hydration of anion}) + \text{constant} \quad (3)$$

The entropy results for the mercury(II)-, cadmium(II)- and lead(II)-halide systems conform to this pattern with constants -9, -10 and -9, respectively. The implication of these results according to George is that these association reactions involve the loss of water of hydration. An equation for the entropy of association has been derived by Matheson⁶ based on an entropy cycle involving the replacement of one water molecule in the hydration shell of the cation by the anion. The form of the equation for water at 25° is

$$\Delta S^0 = 19.6 \left[\frac{Z_1^2 - Z_2^2}{2(\tau^+ + 1.5)} \right] + \overline{S_{\text{H}_2\text{O}}^0} - \overline{S_{\text{X}^-}^0} + 2.5 \quad (4)$$

where Z_1 and Z_2 are the charges on the central cation and the complex ion, respectively, and τ^+ is the crystal radius of the cation in ångströms. $\overline{S_{\text{H}_2\text{O}}^0}$ and $\overline{S_{\text{X}^-}^0}$ are the standard partial molar entropies of the water molecule and the anion in aqueous solution.¹¹ When the value of τ^+ for the mercury(II) cation is taken as 1.10 Å,¹² equation 4 leads to the entropy values shown in the fifth column of Table II. Although the equation involves several approximations there is good agreement between calculated and observed values. Similar agreement was found when the entropies of association calculated by equation 4 were compared with the observed values for the 1:1 complex halides of cadmium and lead.⁶

(11) R. E. Powell and W. M. Latimer *J. Chem. Phys.*, **19**, 1139 (1951).

(12) R. A. Robinson and R. H. Stokes, "Electrolyte Solutions," Butterworths, London, 1959.

PROTON MAGNETIC RESONANCE OF GLYCYLGLYCINATE, GLYCINEAMIDE, AND THEIR METAL COMPLEXES

By NORMAN C. LI, LEROY JOHNSON AND JAMES SHOOLERY

Varian Associates, Palo Alto, Calif., and Duquesne University
Pittsburgh, Pa.

Received April 18, 1961

Several papers^{1,2} have appeared recently dealing with proton resonance studies of dipeptides. Takeda and Jardetzky¹ found that in glycyglycine there are two peaks from the two CH₂ groups, indicating that they are non-equivalent. It would be of interest to continue such studies of dipeptides and determine the effect of chelating metal ions on the chemical shifts of these two CH₂ groups. A Varian Associates Model A-60 NMR spectrometer which operates at 60 Mc. was used.

Solutions containing 1.2 *M* concentrations of each constituent in 99.8% D₂O were placed in 3 mm. i.d., 4 mm. o.d. precision Pyrex tubes and the tubes were filled to a depth of about 40 mm. Pure tetramethylsilane in a 5 mm. o.d. annular cell was used as an external reference compound. The accuracy in measuring the peak positions is estimated to be ±0.01 p.p.m. The resonance signal of the protons being measured occurs at lower field than that of the reference, that is, $H < H_r$, and the

(1) M. Takeda and O. Jardetzky, *J. Chem. Phys.*, **26**, 1346 (1957).
(2) F. A. Bovey and G. V. D. Tiers, *J. Am. Chem. Soc.*, **81**, 2870 (1959).

downfield chemical shift is taken to be positive, in accord with the definition

$$\delta = 10^6 (H_r - H)/H_r$$

where H_r and H are the resonant fields for the reference substance and the sample, respectively.

TABLE I
PROTON CHEMICAL SHIFTS DUE TO THE PRESENCE OF METAL IONS

Sample	Volume susceptibility, $-\chi_v \times 10^6$	CH ₂ chemical shifts, p.p.m., (values in parentheses corrected to χ_v for GG ⁻)	
Sodium glycyglycinate, GG ⁻	0.756	4.25(4.25)	3.84(3.84)
ZnCl ₂ + GG ⁻	.785	4.42(4.36)	4.20(4.14)
MgCl ₂ + GG ⁻	.768	4.35(4.33)	4.00(3.98)
Glycineamide, GA	.749	3.80(3.82)	
ZnCl ₂ + GA	.766	4.20(4.18)	

Since an external reference is used, bulk-diamagnetic susceptibility corrections must be applied.³ For a cylinder of length large compared with the radius, the equation applicable here is

$$\delta_{\text{corr.}} = \delta_{\text{obsd.}} + 2\pi/3(\chi_v - \chi_{v,r})$$

where χ_v and $\chi_{v,r}$ are the volume magnetic susceptibilities of the sample and reference, respectively. The volume susceptibility of each of the solutions was determined immediately after the n.m.r. spectrum was taken, using the same spectrometer, following the method of Reilly, *et al.*,⁴ based on the use of the non-rotating concentric cell.⁵ The sample whose susceptibility was to be determined was placed in the inner cylindrical space and a substance with a single sharp line (in this case tetramethylsilane) was placed in the annulus. The resonance from the material in the annulus displays two maxima whose separation (n c.p.s.) is a linear function of the volume susceptibility of the liquid in the inner cell. The values of n for three pure liquids: chloroform, carbon tetrachloride, methanol (at room temperature, $-\chi_v = 0.735$,⁶ 0.684,³ 0.530,⁷ respectively) were determined and a linear plot of n vs. χ_v was obtained for the three liquids. From this graph, and from the values of n obtained for the solutions, the magnetic susceptibilities of the latter were obtained. These are included in Table I. The use of an n.m.r. spectrometer for determining magnetic susceptibilities consumes much less time than the use of the conventional Gouy method, and is recommended for routine susceptibility measurements.

In Table I, the two lines in GG⁻ are due to the two non-equivalent CH₂ groups and the downfield chemical shifts are increased by 0.11 and 0.30 p.p.m., respectively, in the presence of 1.2 *M* ZnCl₂. When ZnCl₂ is added to a solution of sodium glycyglycinate in D₂O, a chelate is formed, and there is either a reduction of electron density

(3) J. A. Pople, W. G. Schneider and H. J. Bernstein, "High Resolution Nuclear Magnetic Resonance," McGraw-Hill Book Co., New York, N. Y., 1959.

(4) C. R. Reilly, H. M. McConnell and R. C. Meisenheimer, *Phys. Rev.*, **98**, 264A (1955).

(5) Wilmad Glass Company.

(6) A. A. Rothner-By and R. E. Glick, *J. Chem. Phys.*, **26**, 1652 (1957).

(7) S. Broersma, *ibid.*, **17**, 873 (1949).

on the CH_2 which would reduce the shielding, or the presence of positively charged zinc ion distorts the bonding electron orbitals about the CH_2 protons and generates a paramagnetic shift which is in the direction of decreasing field. Li, *et al.*,⁸ have shown that the coordination sites in GG^- toward zinc are the terminal amino group and the peptide oxygen in the immediately adjacent amide group. Since in GG^- one of the CH_2 groups is situated between the two coordination sites, one might expect unequal shifts upon formation of a chelate and this corresponds to the observations.

From Table I it also is seen that when MgCl_2 is added to GG^- the corrected downfield chemical shifts produced are 0.08 and 0.14 p.p.m. The Mg chelate of glycylglycinate is less stable than the Zn chelate ($\log k_1 = 3.4$ and 1.3 ,⁹ respectively, for Zn and Mg chelates with GG^-). The weaker binding by Mg is reflected in the smaller chemical shift of the two CH_2 frequencies when MgCl_2 replaces ZnCl_2 .

It is seen from Table I that in going from GG^- to ZnGG and to MgGG , the effect on the chemical shift for the second CH_2 is greater than for the first CH_2 . From the above discussion regarding binding sites in GG^- toward the metal ions, we come to the conclusion that of the two CH_2 frequencies in GG^- , the signal at $\delta = 4.25$ comes from the CH_2 adjacent to the carboxylate group, while the signal at $\delta = 3.84$ comes from the CH_2 which is adjacent to the amino group.

In glycineamide there is one CH_2 group, hence only one CH_2 frequency. The change in δ , after susceptibility correction is applied, amounts to 0.36 p.p.m. when ZnCl_2 is added. This is in line with the finding that Zn chelates strongly to glycineamide ($\log k_1 = 3.3$).⁹

The proton magnetic resonance shift measurements alone do not provide unequivocal evidence for complex formation. The n.m.r. spectra do, however, support the evidence derived from other types of measurements, for instance, pH titrations. High resolution n.m.r. spectroscopy therefore represents an additional approach to the study of complex formation, analogous to the measurement of shifts in the infrared absorption bands.¹⁰

This research was supported in part by a grant from the National Science Foundation (Grant No. NSF G7447) to Duquesne University. Dr. D. E. O'Reilly of Gulf Research and Development Laboratories carried out preliminary experiments on n.m.r. shifts, for which we are indebted.

(8) N. C. Li, E. Doody and J. M. White, *J. Am. Chem. Soc.*, **79**, 5859 (1957).

(9) N. C. Li and M. C. M. Chen, *ibid.*, **80**, 5678 (1958).

(10) R. B. Penland, S. Mizushima, C. Curran and J. V. Quagliano, *ibid.*, **79**, 1575 (1957).

THE ELECTRIC MOMENTS OF SOME NITRATE ESTERS¹

BY A. R. LAWRENCE AND A. J. MATUSZKO

Research and Development Department, U. S. Naval Propellant Plant, Indian Head, Maryland

Received April 13, 1961

In connection with studies on plasticization and plasticizing agents, interest was developed in the

electric dipole moments of nitrate esters. Cowley and Partington² and de Kreuk³ measured the moments of several nitrate esters, but, apparently, there is no published work on an extended series of dinitrate esters. Measurements were made, therefore, on benzene solutions of several dinitrate esters.

Experimental

Materials.—Ethyl nitrate (Eastman Kodak) was purified by distillation through a 20-cm. column packed with glass helices. All other esters were obtained from the research laboratories of this Station. 2,2-Bis-(nitroxymethyl)-3-nitroxy-1-propanol was purified by chromatography on silica gel. The other nitrate esters were purified by distillation at reduced pressure. All of the nitrate esters were stored over silica gel in stoppered flasks. Solutions were prepared with thiophene-free benzene⁴ which was dried with calcium hydride.⁵

Apparatus and Procedure.—Electric moments were determined from benzene solutions at 25°. Dielectric constants were measured by a heterodyne beat method with a crystal controlled oscillator similar in design to the apparatus described by Hudson and Hobbs.⁶ The cell consisted of two concentric gold-plated brass tubes to which glass tubes were soldered at either end. The space between the tubes was provided with inlet and outlet tubes which permitted connection to increased or diminished pressure. A calibrated precision condenser, General Radio Type 722-D, was used in parallel with the cell and the low capacitance range of 25 to 100 $\mu\text{f.}$ was employed. Purified benzene was used to calibrate the cell. Temperature was controlled by means of a thermostat jacket on the outside of the cell. Densities were measured with a modified Ostwald pycnometer⁷ and refractive indices with an Abbe refractometer.

Measurements were made on a series of five or six solutions ranging from 0.01 to 0.10 *M.* Dielectric constants and specific volumes were plotted against weight fraction of solute and solute values for these quantities were obtained by the method of least squares. Molar refractions, R_2 , were calculated from the solution refractive index data. Solute polarizations at infinite dilution, P_∞ , were calculated from the Halverstadt and Kumler relationship,⁸ and dipole moments from the Debye equation

$$\mu = 0.01281 \times 10^{-18} ((P_\infty - R_2)T)^{1/2} \quad (1)$$

where T is the absolute temperature. The calculated data are presented in Table I. The probable error in the molar polarizations is ± 0.03 and the probable error in the dipole moments is $\pm 0.03 D$.

Discussion and Results

The electric moment obtained for ethyl nitrate ($\mu = 2.96 D$) is in agreement with the value found by Cowley and Partington² ($\mu = 2.91 D$) for the same compound.

For polymethylene compounds of the type $\text{X}-(\text{CH}_2)_n-\text{X}$ where X is a polar group, the moment increases, in general, as n increases.⁹ For large values of n ($n = 10$), the moments of the polymethylene compounds reach a limiting value equal to $2^{1/2} \mu_1$, where μ_1 is the limiting value reached when the corresponding simple aliphatic series is ascended.⁸ The limiting value for the series of

(1) Published with the permission of the Bureau of Naval Weapons, Navy Department. The opinions and conclusions are those of the authors.

(2) E. G. Cowley and J. R. Partington, *J. Chem. Soc.*, 1252 (1933).

(3) L. J. de Kreuk, *Rec. trav. chim.*, **61**, 819 (1942).

(4) A. I. Vogel, "A Textbook of Practical Organic Chemistry," 3rd Edition, Longmans, Green and Co., London, 1957, p. 173.

(5) A. S. Brown, P. M. Levin and E. W. Abrahamson, *J. Chem. Phys.*, **19**, 1226 (1951).

(6) B. E. Hudson and M. E. Hobbs, *Rev. Sci. Instr.*, **13**, 140 (1942).

(7) G. R. Robertson, *Ind. Eng. Chem., Anal. Ed.*, **11**, 464 (1936).

(8) I. F. Halverstadt and W. D. Kumler, *J. Am. Chem. Soc.*, **64**, 2988 (1942).

(9) J. R. Partington, "Advanced Treatise on Physical Chemistry," Vol. 5, Longmans, Green and Co., London, 1954, p. 497.

TABLE I
 EMPIRICAL CONSTANTS AND MOLAR POLARIZATIONS IN BENZENE SOLUTION AT 25°

Compound	ϵ_p	ν_p	a	b	P_∞	B_2 (obsd.)	μ (obsd.)	μ (lit.)
Ethyl nitrate	2.2584	1.14494	10.06	-0.19	199.3	20.4	2.96	2.91 ¹
1,2-Dinitroxyethane	2.2524	1.14474	8.91	- .47	287.6	26.4	3.58	3.28 ²
1,3-Dinitroxypropane	2.2019	1.15254	7.77	- .52	282.7	30.0	3.52	3.14 ²
1,4-Dinitroxybutane	2.2133	1.14450	7.38	- .39	296.4	35.2	3.58	
1,5-Dinitroxy-pentane	2.2397	1.14537	7.48	- .36	322.2	39.9	3.72	
1,6-Dinitroxyhexane	2.2519	1.14509	7.15	- .33	332.8	44.0	3.76	
1,2-Dinitroxypropane	2.2469	1.14375	9.92	- .40	349.6	30.8	3.95	3.72 ²
1,2-Dinitroxy-pentane	2.2727	1.14524	9.26	- .36	384.8	41.7	4.10	
Nitroglycerin	2.2597	1.14558	5.33	- .51	272.0	39.1	3.38	3.16 ³
2,2-Bis-(nitroxymethyl)- 1-nitroxypropane	2.2673	1.14531	4.76	- .46	281.5	47.1	3.39	
2,2-Bis-(nitroxymethyl)- 3-nitroxy-1-propanol	2.2690	1.14609	5.57	- .49	337.6	48.4	3.76	

normal aliphatic mononitrate esters occurs at *n*-propyl nitrate ($\mu = 2.98 D$).¹⁰ This would give a limiting value for the polymethylene series as $\mu = 4.1 D$. Table I, based on the present study, shows the observed increase for the series $O_2NO-(CH_2)_n-ONO_2$, as *n* goes from 2 to 6.

A second general trend is noticed among the dipole moments of the compounds: 1,2-dinitroxyethane ($\mu = 3.58 D$), 1,2-dinitroxypropane ($\mu = 3.95 D$) and 1,2-dinitroxy-pentane ($\mu = 4.10 D$). Here, evidently, the dipole moments increase as the size of the attached chain increases. De Kreuk² measured the dipole moment of 2,3-dinitroxybutane at 20° and found a value of $\mu = 4.12 D$. This lends some support to the simple assumption that increased side-chain size is accompanied by an increased dipole moment. This effect has been observed also with aliphatic dihalides.^{11,12}

The dipole moments of nitroglycerin, 2,2-bis-(nitroxymethyl)-1-nitroxypropane and 2,2-bis-(nitroxymethyl)-3-nitroxy-1-propanol were calculated by assuming free rotation,¹³ a nitroxy group moment of 2.73,² a C-O bond moment of 1.14, and a NOC bond angle of 110°. The respective values of 4.78, 4.74 and 5.06 indicate considerable restriction of free rotation in these compounds.

(10) C. P. Smyth, "Dielectric Behavior and Structure," McGraw-Hill Book Co., Inc., New York, N. Y., 1955, p. 288.

(11) M. L. Sherrill, M. E. Smith and D. D. Thompson, *J. Am. Chem. Soc.*, **56**, 611 (1934).

(12) A. A. Maryott, M. E. Hobbs and P. M. Gross, *ibid.*, **63**, 659 (1941).

(13) H. Eyring, *Phys. Rev.*, **39**, 746 (1932).

HYDRATED AND ANHYDROUS BIETHYLENEDIAMINE-COPPER(II) SULFATE

BY L. V. GREGOR, J. J. FRITZ AND P. E. FIELD

Publication No. 120 from the Cryogenic Laboratory, College of Chemistry and Physics, The Pennsylvania State University, University Park, Penna.

Received April 14, 1961

The complex ion bisethylenediamine-copper(II), abbreviated to $Cu(en)_2^{++}$, is quite stable in aqueous solution, and many of its salts have been prepared and studied.¹ However, there have been inconsis-

(1) N. V. Sidgwick, "The Chemical Elements and Their Compounds," Vol. 1, Oxford, 1950, pp. 163-164, A. Martell and M. Calvin, "Chemistry of the Metal Chelate Compounds," Prentice-Hall, New York, N. Y., 1952, p. 286.

encies in the literature concerning the possible hydrates of $Cu(en)_2SO_4$. Werner² prepared $Cu(en)_2SO_4$ by decomposing the ion formed when excess ethylenediamine was added to aqueous copper sulfate: he considered this ion to be $Cu(en)_3^{++}$. Upon dilution of this solution and addition of excess ethanol, a violet crystalline solid was formed which was assigned the composition $Cu(en)_2SO_4 \cdot 2H_2O$ by Werner. Johnson and Bryant³ observed that addition of ethanol to an aqueous solution of ethylenediamine and copper sulfate gave a violet crystalline substance which they analysed to be $Cu(en)_2SO_4 \cdot 4\frac{1}{2}H_2O$. This substance slowly effloresced to give the anhydrous salt at room temperature. In addition, both workers found that the other solids of various blue colors were obtained by the addition of ethanol under various conditions, among which was a material to which Johnson and Bryant ascribed the composition of $Cu(en)_2SO_4 \cdot 2H_2O$.

Some time ago there were reported⁴ the magnetic properties at low temperatures of $Cu(en)_2SO_4$ and its stable hydrate, which we found to be $Cu(en)_2SO_4 \cdot 4H_2O$. More recently Gordon and Birdwhistell⁵ reported a study of the complexes of copper with ethylenediamine, in which they stated that they were unable to obtain a stable hydrate of $Cu(en)_2SO_4$. In view of the uncertainty about the existence of this hydrate, we are reporting its preparation and properties in detail. We take this opportunity also to present further observations on the interesting magnetic properties of the anhydrous material.

Preparation of Bisethylenediamine-copper(II) Sulfate.—The hydrate of $Cu(en)_2SO_4$ was prepared from an aqueous solution containing reagent grade copper sulfate pentahydrate and redistilled ethylenediamine (b.p. 116.9°, lit. 118.0°) in a 1:2 mole ratio. A typical preparation involved 2.5 moles of copper sulfate pentahydrate and 5.0 moles of ethylenediamine in 700 ml. of H_2O . After evaporation on a steam-bath to about 100 ml., the solution was cooled in ice for several hours, resulting in the formation of several hundred grams of large blue-violet crystals. These crystals were filtered on a Buchner funnel by suction, pressed dry with filter paper, and dried further by shaking in a box lined with absorbent paper. Although stable in a stoppered

(2) A. Werner, *Z. anorg. u. allgem. Chem.*, **21**, 201 (1899).

(3) C. H. Johnson and S. A. Bryant, *J. Chem. Soc.*, 1783 (1934).

(4) J. J. Fritz, R. V. G. Rao and S. Seki, *J. Phys. Chem.*, **62**, 703 (1958).

(5) G. Gordon and R. Birdwhistell, *J. Am. Chem. Soc.*, **81**, 3567 (1959).

bottle, the crystals lost water in dry air, giving the anhydrous $\text{Cu}(\text{en})_2\text{SO}_4$, a violet-blue solid. (Note: While the colors of the two solids were clearly distinguishable, both were between blue and violet, as just indicated. For convenience the color near blue will hereafter be designated simply "blue" and that near violet as "violet.") The violet and blue forms were reversibly interconvertible by passing dry or water-saturated air or nitrogen over the solid.

Anhydrous $\text{Cu}(\text{en})_2\text{SO}_4$ was prepared by allowing the hydrate to dry either in a desiccator for a few days or in an oven at 105° for several hours.

Both the hydrate and the anhydrous compound were extremely soluble in water to give intensely colored violet solutions. The solution of the anhydrous salt in water, after evaporating and cooling in ice, gave back the violet crystals of the hydrate. Both forms were insoluble in ethylenediamine, pyridine, aniline, ethanol, ethyl ether, and aliphatic or aromatic hydrocarbons.

Attempts to precipitate $\text{Cu}(\text{en})_2\text{SO}_4$ from solution by addition of absolute ethanol resulted in a lustrous pale-blue solid whose solubility in water was considerably less than that of the hydrate of anhydrous material: moreover, the solutions were of a different color. Occasionally, dark sludges were formed which could not be recrystallized. It thus appeared that the evaporation method was distinctly more reliable for preparation of anhydrous material than the ethanol precipitation.

Analytical Results.—The determination of Cu was carried out electrolytically,⁶ by using a Fisher Electroanalyzer and platinum electrodes. The difficulty of drying the hydrate completely without decomposition caused the percentage of Cu in this material to vary over a much wider limit than would be expected for such a relatively accurate determination. The results are given in Table I.

TABLE I

Compound	Exp. % Cu	Calcd. % Cu	No. of detns.
$\text{Cu}(\text{en})_2\text{SO}_4$	22.55 ± 0.10	22.79	4
$\text{Cu}(\text{en})_2\text{SO}_4 \cdot 4\text{H}_2\text{O}$	17.89 ± 0.20	18.07	11

Loss of water on heating in an oven at 105° or decomposition into a vacuum gave an average of 20.7% H_2O (calcd. for $\text{Cu}(\text{en})_2\text{SO}_4 \cdot 4\text{H}_2\text{O}$ 20.48%). It was not found possible to obtain a sharp endpoint in a potentiometric titration (against HCl) for ethylenediamine, but the amount of the amine was found to be about 36% (calculated value 34%).

Phase Behavior.—In order to establish clearly the composition and range of stability of the hydrated salt, a phase study was made of the system $\text{Cu}(\text{en})_2\text{SO}_4\text{-H}_2\text{O}$ between 0 and 25° . This investigation consisted of three parts:

1. A specimen of anhydrous $\text{Cu}(\text{en})_2\text{SO}_4$ was thoroughly dried on a vacuum line and then "titrated" with water at 24.90° . The vapor pressure of the system was observed after each of 13 small increments of water had been distilled in. The observations covered the range of 0 to 4.5 moles water per mole of salt; the amounts added were observed volumetrically, and checked by weighing at 1.86, 3.88 and 4.45 moles per mole of salt, with volumetric observations used only for interpolation. The vapor pressure of the system remained constant from the first addition to 4.0 (± 0.05) moles of water per mole of salt, then rose sharply to a second plateau where it again remained constant as solution was formed.

2. A reverse titration was made at 0° in which the water content was reduced in five steps to 3.84 moles of water per mole of salt. Above 4.0 moles of water the vapor pressure was 3.9 mm.; below this composition it fell sharply to 2.4 mm.

3. The vapor pressures of a mixture containing 4.45 moles water/mole salt (tetrahydrate-solution) and of a mixture containing 3.85 moles water/mole salt (anhydrous-tetrahydrate) were measured at five points between 0 and 25° .

In both titrations and the vapor pressure measurement it was found necessary to wait at least an hour for equilibrium after each addition of water or change of temperature. In all cases the pressures were observed for at least three hours to ensure equilibrium.

The vapor pressures of the anhydrous-tetrahydrate system obeyed the linear equation $\log P \text{ mm.} = -2685/T + 10.214$ within their expected accuracy (0.1 to 0.2 mm.), with only random deviations. From this we conclude that the heat of dehydration is about 49,200 cal. per mole of tetrahydrate (12,300 cal. per mole of water) and that the entropy change of the dehydration reaction is about 33 gibbs per mole of water. (Since the vapor pressures were measured primarily to establish the nature of the phases present, they were not measured as accurately as possible, we estimate the uncertainty of the heat of dehydration as about 3% and that of the entropy change as 5%.) The vapor pressure at 25° , from the $\log P-1/T$ plot, is 16.3 ± 0.3 mm.

The vapor pressures of the tetrahydrate-saturated solution system also fitted a $\log p$ vs. $1/T$ plot and corresponded within 0.1 mm. to the equation $\log P \text{ mm.} = -2267/T + 8.899$. Comparison of the two vapor pressure equations indicates that the tetrahydrate should become unstable with respect to anhydrous material and saturated solution somewhat below 45° . Cooling curves on a mixture of salt and saturated solution established the transition point as 42.8° .

Discussion

The vapor pressure investigation described above indicates clearly that $\text{Cu}(\text{en})_2\text{SO}_4 \cdot 4\text{H}_2\text{O}$ is the stable hydrated phase of $\text{Cu}(\text{en})_2\text{SO}_4$ at ordinary temperatures, and that the water can be added or removed readily and reversibly. The nature of the results gives hints as to why other investigators of this system have obtained negative or ambiguous results in their efforts to obtain hydrates. In the first place, the relatively low decomposition temperature of the tetrahydrate (about 50°) will prevent getting the hydrate by evaporation of solutions above this temperature. Second, the vapor pressure of the tetrahydrate (16.8 mm.) at 25° is rather high. (The vapor pressure of pure water at this temperature is only 23.8 mm.) Consequently the addition of a material such as ethanol to precipitate the salt at room temperature is quite likely to reduce the activity of water below that required for the hydrate. Finally, the extreme solubility of the salt makes it difficult to prepare the hydrate from solution. We could do so only by chilling a solution previously concentrated by evaporation. We have

(6) H. H. Willard and N. H. Furman, "Elementary Quantitative Analysis," 3rd Ed., D. Van Nostrand Co., New York, N. Y., 1940, p. 431.

observed, but not reported, similar behavior previously⁷ with $\text{Cu}(\text{NH}_3)_4\text{SO}_4 \cdot \text{H}_2\text{O}$. In this case we found that ethanol precipitation of the complex resulted in material either uncertain in composition or too finely divided for our purposes, whereas chilling of a solution previously concentrated by evaporation gave excellent yields of large crystals of the desired material. It is ironical that the hydrate which is so difficult to prepare directly for the reaction mixture can be made easily by hydration of the anhydrous material, provided that a sufficiently high partial pressure of water vapor is provided.

Magnetic Properties of the Complex Salt.—In previously reported measurements⁴ of the low temperature magnetic properties of $\text{Cu}(\text{en})_2\text{SO}_4$ and $\text{Cu}(\text{en})_2\text{SO}_4 \cdot 4\text{H}_2\text{O}$, we observed that the hydrate was relatively ideal magnetically even below 4.2°K., whereas the anhydrous material had a maximum in its magnetic susceptibility somewhere between 4 and 10°K. At that time it appeared possible that the decrease in susceptibility at and below 4° might have been due to relaxation effects in the dynamic (400 cycle) susceptibility we observed, rather than a decrease in the static zero-frequency susceptibility. We have since repeated these measurements, confirming previous measurements at 400 cycles, and found no dependence of susceptibility on frequency up to 1000 cycles. Thus the observed maximum in susceptibility cannot be due to relaxation effects. It is probably caused by strong exchange interactions between copper ions, such as those previously adduced by Eisenstein⁸ to explain our observations on $\text{Cu}(\text{NH}_3)_4\text{SO}_4 \cdot \text{H}_2\text{O}$.

The magnetic behavior of the two $\text{Cu}(\text{en})_2^{++}$ compounds offers additional indirect evidence on the nature of the hydrated material. The magnetic anomalies displayed by the anhydrous material are greater than those shown by $\text{Cu}(\text{NH}_3)_4\text{SO}_4 \cdot \text{H}_2\text{O}$. This is not surprising since the ethylenediamine groups could well be more effective in promoting exchange interactions between copper atoms than are ammonia molecules. The fact that the hydrate $\text{Cu}(\text{en})_2\text{SO}_4 \cdot 4\text{H}_2\text{O}$ shows nearly ideal behavior (about as ideal as $\text{CuSO}_4 \cdot 5\text{H}_2\text{O}$, in fact) indicates that the water of hydration interferes with these interactions either by a specific chemical effect or possibly just by dilution. Additional ethylenediamine, as in Gordon and Birdwhistell's compound $\text{Cu}(\text{en})_3\text{SO}_4 \cdot \text{H}_2\text{O}$, should render the substance as anomalous or more anomalous than anhydrous $\text{Cu}(\text{en})_2\text{SO}_4$. Thus the magnetic evidence also strongly supports the composition assigned to the hydrated material: it was in fact one of the clues which led us to complete the identification of the material as a hydrate.

(7) J. J. Fritz and H. L. Pinch, *J. Am. Chem. Soc.*, **79**, 3644 (1957).

(8) J. E. Eisenstein, *J. Chem. Phys.*, **28**, 323 (1958).

THE EFFECT OF COPPER ALKANOATES ON OXIDIZING OLEFINS

By P. W. ALLEN

The Natural Rubber Producers' Research Association, Welwyn Garden City, Herts., England

Received April 18, 1961

Compounds of the transition elements can catalyze the autoxidation of a variety of substrates, including tetralin,¹ cumene,² cyclohexene,³ aldehydes⁴ and methyl linoleate.⁵ It has been generally supposed that catalysis results from the accelerated decomposition of the hydroperoxides which initiate these reactions. In the course of some experiments which were planned to demonstrate the reactivity of cupric compounds toward oxidizing isoprenoid substrates in aqueous dispersions, it became apparent that the interaction between $\text{Cu}(\text{II})$ and substrate was far more complex than could be accounted for by any simple mechanism. Two series of experiments are described in this Note: (i) the effect of copper alkanates on the oxidation of aqueous dispersions of olefins; (ii) the effect of cupric heptanoate on the oxidation of homogeneous solutions of olefins.

Experimental

Rates of oxygen absorption were measured using an apparatus which has been described previously.⁶ For some of the later experiments an automatic device⁷ was used. Reaction vessels were carefully cleaned by washing five times each with (i) nitric acid-alcohol, (ii) demineralized water, (iii) 0.5% aqueous EDTA, (iv) water, and (v) acetone. Materials were purified by conventional methods, except for squalene which was obtained from "90% squalene" (Eastman Kodak) by passing a petroleum ether solution (5%) successively through charcoal and alumina columns. The cupric alkanates solutions were prepared by titrating 0.1 N solutions of the fatty acids (from acetic to hexanoic) with potassium hydroxide to pH 5.0 and adding cupric nitrate to make the solution 5×10^{-4} molar in copper.

Results

For all runs results were obtained as plots of rate vs. extent of oxidation. The first series of experiments was planned with the intention of finding out whether the oxidation rate of olefins dispersed in water could be influenced by the presence of copper compounds in the aqueous phase. In the absence of copper compounds the autoxidation rates of ethyl linoleate at 65° and squalene at 55° were little affected by dispersion into water with shaking speeds ca. 300/min. at a ratio of water to olefin equal to 1:1. The introduction of cupric nitrate into the aqueous phase (up to 2×10^{-3} molar) did not alter oxidation rates. When, instead of cupric nitrate, cupric alkanates were introduced, considerable changes in oxidation rate were noted. Figure 1 shows the relative rates of oxidation (slope of rate/extent plots with copper relative to those without copper). As the carbon number of the fatty acid increases, so the oxidation rate, in the case of ethyl linoleate, is enhanced. Rough measurements of the partition coefficients of the cupric alkanates between non-polar solvents and water showed that there was a steady increase along the same series. By contrast, the data for squalene show a progressive reduction in oxidation rate.

The effects of Fig. 1 reflect the increasing solu-

(1) F. George and A. Robertson, *Trans. Faraday Soc.*, **42**, 217 (1946).

(2) H. S. Blanchard, *J. Am. Chem. Soc.*, **82**, 2014 (1960).

(3) A. J. Chalk and J. F. Smith, *Trans. Faraday Soc.*, **53**, 1214 (1957).

(4) C. E. H. Bawn, *J. Oil & Colour Chemists' Assoc.*, **36**, 443 (1953).

(5) W. Kern and H. Willersinn, *Makromol. Chem.*, **15**, 36 (1955).

(6) J. L. Bolland, *Proc. Roy. Soc. (London)*, **A186**, 218 (1946).

(7) J. Scanlan and J. R. Dunn, *J. Sci. Instr.*, **38**, 28 (1961).

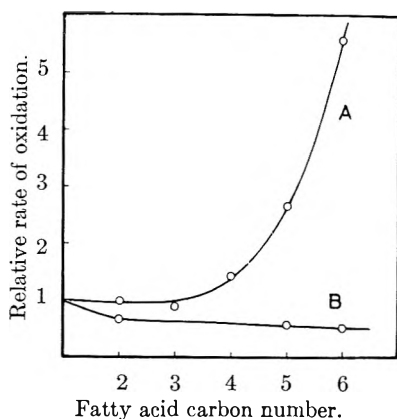


Fig. 1.—Relative rates of oxidation of ethyl linoleate at 65° (A) and squalene at 55° (B) dispersed in aqueous solutions of cupric alkanooates (5×10^{-4} molar).

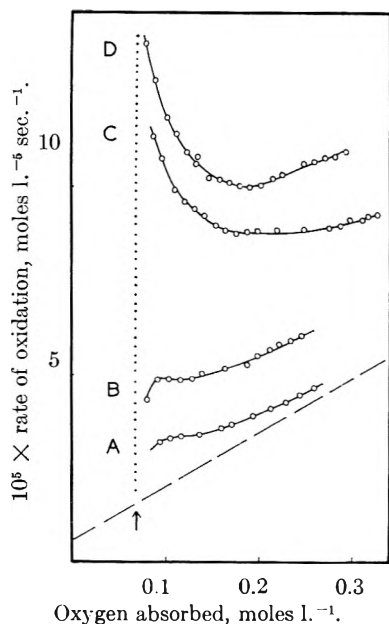


Fig. 2.—Rate of oxidation of ethyl linoleate in chlorobenzene solution at 65°, catalyzed by cupric heptanoate at concentrations of 0.7 (A), 4.4 (B), 14.4 (C) and 29.1 (D) $\times 10^{-3}$ moles/l. The point of addition of copper is indicated by the arrow and dotted line. The broken line shows the course of the substrate reaction.

bility in the olefin phase of cupric alkanooates as the carbon number increases. While the result for ethyl linoleate is the expected one, the effect noted with squalene is unusual. It was considered to be necessary to establish that this effect was not associated with the presence of an aqueous phase. The second series of experiments, therefore, was conducted in homogeneous solution with chlorobenzene as solvent and cupric heptanoate³ as the copper compound. The experiments were arranged so that cupric heptanoate could be added to the oxidizing olefin at some chosen extent of reaction. Figure 2 shows some data for ethyl linoleate (1.5 molar at 65°). As the amount of copper added is increased, so the initial abrupt catalysis is enhanced, after which the rate falls off before resuming a course parallel to that of the substrate reaction. With squalene as substrate (Fig. 3) there is an initial (but not very pronounced)

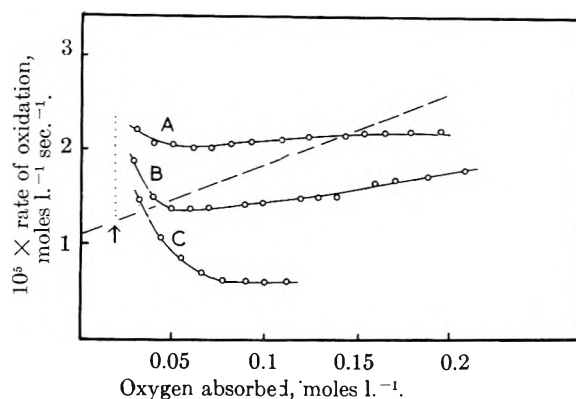


Fig. 3.—Rate of oxidation of squalene in chlorobenzene solution at 55°, catalyzed by cupric heptanoate at concentrations of 1.9 (A), 4.0 (B) and 42.8 (C) $\times 10^{-5}$ moles/l. Other symbols are as for Fig. 3.

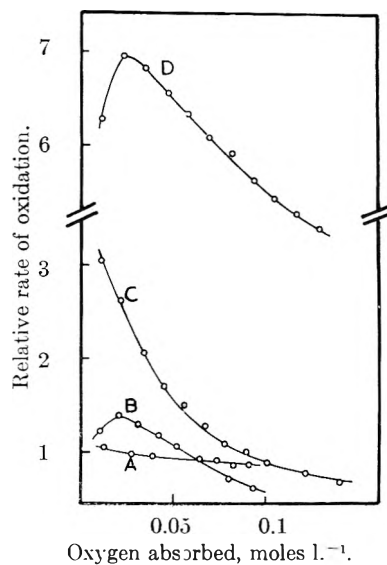


Fig. 4.—Relative rates of oxidation of gutta percha at 75° (A), squalene at 55° (B), 2,6-dimethylocta-2,6-diene at 65° (C) and ethyl linoleate at 65° (D) in chlorobenzene solution in the presence of cupric heptanoate (9×10^{-4} moles/l.).

rate increase followed by a rapid decline to rates below those for the substrate reaction. As the concentration of copper is increased, so the catalysis is suppressed and a retarded reaction sets in. This parallels the data of Fig. 1 and shows that the difference between ethyl linoleate and squalene is not confined to aqueous dispersions.

A further series of experiments studied the relative rates of oxidation with and without a fixed concentration of cupric heptanoate with four olefins as substrates in chlorobenzene (Fig. 4). Temperatures were chosen to give comparable substrate rates. There is a close similarity between all the curves, whether the reaction is catalyzed (relative rate >1) or retarded.

It was further noted that changing the reaction temperature from 50–70° did not increase or diminish the retardation shown by squalene. The over-all activation energy of the retarded reaction (18 kcal./mole) is close to that (19.4 kcal./mole) for the substrate reaction.

Discussion

Cupric heptanoate does not exhibit simple catalytic behavior toward the autoxidation of the four olefins examined. Even for the case where there is marked catalysis (ethyl linoleate in Figs. 2 and 4) the shape of the rate/extent curve indicates that there is an accompanying retarding effect. In the case of squalene the balance is reversed and the retardation is predominant. The simplest explanation of a fall-off in rate during a catalyzed reaction is that the concentration of one or more of the reactants (metal compound or olefin hydroperoxide, for example) becomes depleted. In fact, hydroperoxide yields were found to be unaffected by the addition of the copper compound. Depletion of the metal compound cannot account for reaction rates which are lower than the substrate reaction rate, unless the depletion reaction produces a retarding species. No plausible mechanism can be offered yet for the effects observed. Examination of the effect of cupric heptanoate on the decomposition rates of simple hydroperoxides has shown that the behavior is complex.⁸ It seems likely that metal compounds which exhibit variable valency may interact with almost any species present during an autoxidation chain reaction, and the effect of adding metal compounds to oxidizing olefins cannot therefore be predicted.

(8) C. L. M. Bell, unpublished work.

PHOTOCHROMISM

BY CARL A. HELLER, DWIGHT A. FINE AND
RONALD A. HENRY

Chemistry Division, U. S. Naval Ordnance Test Station, China Lake, Cal.

Received April 21, 1961

The compound investigated was 1,3,3-trimethylindolino-6'-nitrobenzopyrrolospiran (B) which has been prepared and studied previously.¹ Photochromism has been studied in several spirans^{2a} and some other compounds^{2b} which apparently exist in two forms, one of which is colored. Ultraviolet irradiation will change solutions from almost colorless to strongly colored. The colored form, so made, will fade to give the thermal equilibrium mixture.

General Observations.—When a saturated, colorless, hexane solution of B was irradiated the solution rapidly became dark-blue (almost black) and a dark-purple, crystalline solid separated. Since the analyses³ on this latter compound were the same as those for the starting compound, and since a benzene solution of this purple solid rapidly changed from the blue to colorless in the dark, it is concluded that the purple solid is the colored state C. In benzene no precipitation of purple solid occurred, although the solution developed the typical blue color; after long irradiation a yellow-orange solid, m.p. 185–187° dec., crystallized.⁴

(1) E. Berman, R. F. Fox and F. D. Thomson, *J. Am. Chem. Soc.*, **81**, 5605 (1959).

(2) (a) R. Heiligman-Rim, Y. Hirschberg and E. Fisher, *J. Chem. Soc.*, 156 (1961); (b) R. Hardwick, H. S. Mosher and R. Passailaigue, *Trans. Faraday Soc.*, **56**, 44 (1960).

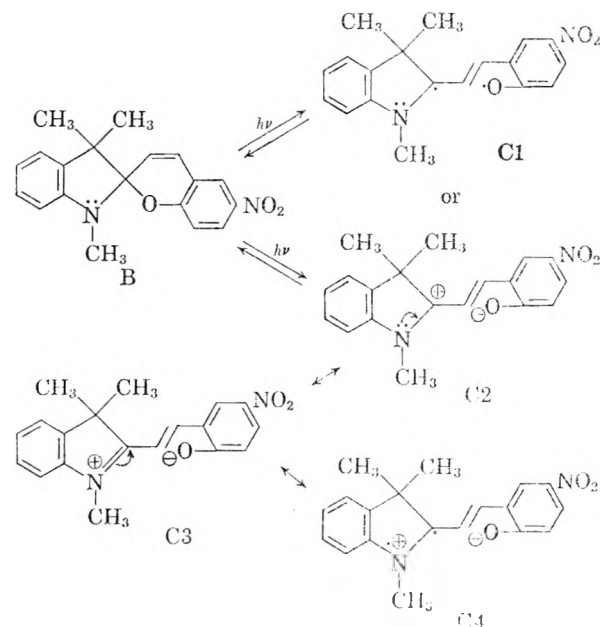
(3) Calculated for $C_{19}H_{18}N_2O_4$: C, 70.78; H, 5.68; N, 8.69. Found: C, 70.39; H, 5.35; N, 8.95. In contrast to the starting compound which melted 179–180°, this compound partially melted about 150°, resolidified, changed from purple to pink, and finally melted about 175°. When plunged into a hot bath at 160–165° this colored form melted completely, then resolidified.

Apparently, compound C is soluble in benzene and a photostationary equilibrium is established; however, in hexane compound C is only very sparingly soluble, it precipitates in a stable crystalline form, and the reaction goes almost to completion. On standing in room light the purple solid (C) gradually reverted to a greenish solid, similar in appearance to the starting compound (B). If stored in the dark, the colored form did not change appearance during several months.

It also was possible to recover the highly colored form (m.p. about 100°) by irradiating hexane solutions of 1,3,3-trimethylindolino-6'-nitro-8'-methoxybenzopyrrolospiran (m.p. about 155°).

Although previous workers^{1,5} have postulated a heterolytic photochemical cleavage of a bond to give the ionic "open form" shown as C2, electron spin resonance studies on the solid colored state (C) reveal a weak to medium absorption which indicates an unpaired electron ($g = 2.004 \pm 0.002$; $H = 20.4 \pm 4$ gauss). Hence this colored form might be a stable biradical (C1) formed by a homolytic cleavage of a bond or an ionic free radical (C4) similar to that in Wurster's salt.

Quantum Yields.—The number of quanta was measured by an RCA 935 phototube using the specifications in the RCA Tube Handbook. These checked with the output specifications for the Hanovia S100 lamp and with two runs with uranyl oxalate.⁷ A Cary Model 14 spectrophotometer was used to measure the change from non-colored (B) to colored (C) form. A 1 cm. path quartz cell was used for most of the studies.



The major problem was to find the extinction coefficient for form C at 5400 Å., where it has a broad peak as reported in ref. 1. A peak at 2650 Å. due to the form B decreases as form C increases. This 2650 Å. peak could, by high intensity irradiation, be decreased to 49% of its original value. The concentration of colored form must lie between 51 and 100% of the prepared molarity of the compound. This gives an extinction coefficient between 4.68 and 2.40

(4) The structure and nature of this product have not been determined; however, the analyses correspond approximately to those required for the reaction of two molecules of oxygen with each molecule of the starting compound.

Calcd. for $C_{19}H_{18}N_2O_4 \cdot 2O_2$: C, 59.06; H, 4.70; N, 7.25. Found: C, 60.37, 60.45; H, 4.60, 4.71; N, 6.97, 7.13.

(5) Y. Hirschberg, *J. Am. Chem. Soc.*, **78**, 2304 (1956).

(6) The parent compound (B), as a solid, shows an exceedingly weak absorption, probably because of contamination by a small amount of the colored form.

(7) W. A. Noyes, Jr., and P. A. Leighton, "The Photochemistry of Gases," Reinhold Publ. Corp., New York, N. Y., 1941.

$\times 10^4$ l. mole⁻¹ cm.⁻¹. The mean value of 3.54×10^4 cm.² mole⁻¹ was used to get quantum yields.

The Hanovia S-100 lamp was used with Corning 7-54 and 0.52 filters to isolate the 3660 Å. light. A compound filter with single crystal salt slices⁸ was used to isolate the 3130 Å. line.

Short exposures were used to produce form C which was measured in the spectrophotometer. Thermal fading of form C during exposure and before measurement was insignificant for this compound. From the light absorbed and the amount of colored form produced the quantum yield was calculated.

$$\phi = \frac{(A_f - A_i)V}{\epsilon \times t \times 1.11 \times \Delta i/S}$$

where

A = absorbance = $\log I_0/I$.

A_f and A_i = final and initial absorbance

ϵ = 3.54×10^4 l. mole⁻¹ cm.⁻¹

t = time in sec.

Δi = current change (μ amp.) for spiran soln. in cell

S = phototube sensitivity $10.9 \times 10^9 \mu$ amp. sec. einstein⁻¹

V = 3.14×10^{-3} l.

1.11 = corr. for light beam area on cathode

Values were obtained for 3130 and 3660 Å. and for solutions 0.3977 and 0.03977 millimolar at 26.5° and typical data are shown in the table.

TABLE OF TYPICAL RUNS

Concn. millimolarity	λ , Å.	Time, sec.	Phototube current, μ amp.		Absorbance change	ϕ
			Initial	Decrease		
0.0	3130	10.8	1.0	...	
.03977	3130	60.09	11.2	5.3	0.055	0.15
.3977	3130	100.07	10.65	9.2	.140	.13
.03977	3660	60.08	14.7	5.1	.045	.13
.3977	3660	80.12	15.6	13.4	.122	.10
.3977	Above 5400	56.36	17.3	11.3	.073	.11

The average quantum yield for the change from form B to form C of an ethanol solution of this spiran at 3130 Å. is 0.15 ± 0.07 and at 3660 Å. is 0.12 ± 0.06 mole/einstein. The uncertainty results from uncertainty in the extinction coefficient.

If a highly colored solution is formed and allowed to stand, the color fades. At 26.5° the first-order rate constant is $7.5 \pm 1.0 \times 10^{-4}$ sec.⁻¹. At 6° it was found to be 4.28×10^{-6} sec.⁻¹ which gives an activation energy of 23 kcal.

When the colored solution is irradiated with visible light, photofading occurs. The quantum yield for the visible light from the S-100 lamp through a 3-69 filter was 0.10 ± 0.05 .

Since visible light can effect the fading it seems possible that ultraviolet absorbed by the color form might also be effective. If it is, the photostationary state would have less colored form than otherwise. The equation for the photostationary rate can be written

$$\phi_B I_B = k[C] + \phi_C I_C \quad (2)$$

where

k is the thermal fading rate constant

I is light absorbed per liter per second

and subscripts refer to the non-colored (B) and colored (C) forms. Photostationary states were measured for 3660 and 3130 Å. light which gave quantum yields ϕ_C , of 0.4 and 0.7 mole/einstein. This increase in ϕ_C with energy per quanta seems reasonable. For 3130, 3660 and 5400 Å. the energy/einstein is 91.3, 78.1 and 59.2 kcal./einstein.

The thermal equilibrium shows only a small shift to the colored form between 26 and 50° so that ΔH must be small.

DETERMINATION OF THE IONIZATION CONSTANTS OF SOME PHENYLMERCURY COMPOUNDS¹

BY S. S. PARIKH AND THOMAS R. SWEET

Department of Chemistry, The Ohio State University, Columbus 10, Ohio

Received April 26, 1961

For many years the effects of various phenylmercury compounds on plants and animals have been studied. The purpose of this work is to determine the ionization constants for phenylmercuric acetate and phenylmercuric propionate.

These constants were obtained by potentiometric titrations of phenylmercuric hydroxide solutions with standard acetic acid and propionic acid solutions. In order to calculate these values, the ionization constant for phenylmercuric hydroxide was needed. This value has been reported by Waugh, Walton and Laswick² and also was redetermined in the present work.

Experimental

Reagents. Phenylmercuric Hydroxide.—This was obtained as a chemically pure sample from Metalsalts Corporation. Its purity was checked by the following analyses: %C, theor., 24.45; exptl., 24.61, 24.67; %H, theor., 2.05; exptl., 2.21, 2.23; %Hg, theor., 68.07; exptl., 67.80, 68.07, 68.25. An equivalent weight of 295.66 was determined by adding an excess of KBr and titrating with standard acid.² The theoretical equivalent weight is 294.72.

Phenylmercuric Hydroxide Solution.—A weighed quantity of phenylmercuric hydroxide was transferred to a volumetric flask. Carbon dioxide-free nitrogen gas was passed into the flask for one hour to flush out all carbon dioxide gas in the flask. Carbon dioxide-free water was added until the flask was about three quarters full and the liquid was brought to near boiling until all the phenylmercuric hydroxide went into solution. During this time and also while the solution was cooled to room temperature and diluted to the mark with distilled water, nitrogen was passed in at a slow rate. The solution was standardized by adding about 4 g. of potassium bromide to 50 ml. of the solution. Phenylmercuric bromide precipitated and the free hydroxide was titrated with a standard perchloric acid solution.

Preliminary Studies.—It was apparent that a saturated potassium chloride salt bridge should not be placed directly into the phenylmercuric hydroxide solution since this would result in the formation of insoluble phenylmercuric chloride and a consequent change in pH. For this reason a saturated sodium nitrate salt bridge was used. In order to prevent contact of carbon dioxide with the solution, nitrogen gas was continuously passed into the cell compartment. However, when a 0.01 M phenylmercuric hydroxide solution was titrated with 0.01 M HNO₃ under these conditions, a small amount of precipitate was observed in the solution and also on the tip of the salt bridge. This was attributed to the formation of phenylmercuric nitrate.

When a 0.01 M perchloric acid solution was used with a 0.01 M phenylmercuric hydroxide solution, no precipitate was observed in the solution. A thin film of precipitate could be seen on the tip of the sodium nitrate salt bridge if the salt bridge was left in contact with the phenylmercuric hydroxide solution for several minutes. The error resulting from this source was minimized by taking only one pH reading with each salt bridge-phenylmercuric hydroxide solution combination. When 0.01 M phenylmercuric hydroxide was titrated with 0.01 M acetic acid or 0.01 M propionic acid, the solution appeared the same as described above for the 0.01 M perchloric acid.

Procedure.—A 250-ml. beaker with a five hole rubber

(1) Taken in part from the master's thesis of S. S. Parikh presented to the Graduate School of The Ohio State University, December, 1960.

(2) T. D. Waugh, H. F. Walton and J. A. Laswick, *J. Phys. Chem.*, **59**, 395 (1955).

(8) Supplied by Dr. William McBride of these laboratories.

stopper and a 150-ml. beaker were placed in a water-bath maintained at $25 \pm 0.04^\circ$. The holes in the stopper of the larger beaker were used for a nitrogen gas inlet tube, a buret tip, a gas outlet tube, a Beckman blue bulb glass electrode (No. 40495), and one arm of a sodium nitrate salt bridge. The other arm of the salt bridge was placed in the 150-ml. beaker. This beaker contained a saturated solution of sodium nitrate and a Beckman saturated calomel electrode. Carbon dioxide-free nitrogen was passed into the dry 250-ml. beaker to displace all carbon dioxide. Nitrogen was passed into the beaker continuously until after the reading was obtained, thus keeping it carbon dioxide-free and stirring the solution.

Fifty ml. of phenylmercuric hydroxide solution was transferred to the 250-ml. beaker and a known volume of standard acid solution was added from the buret. After the solution was thoroughly mixed, a saturated sodium nitrate salt bridge was introduced and the pH was determined immediately. The entire procedure was repeated for the next volume of acid. Each time a pH reading was obtained, a new salt bridge and a new phenylmercuric hydroxide solution were used.

Results

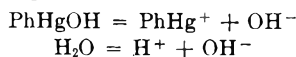
Table I shows the data and results for the ionization constant of phenylmercuric hydroxide. The average of the three values closest to the half equivalence point was 1.3×10^{-10} and this is taken as the best value for K_b . In the table, T_{HClO_4} and T_{PhHgOH} indicate, respectively, the total added perchloric acid concentration and the total added phenylmercuric hydroxide concentration after correction for dilution.

TABLE I

IONIZATION CONSTANT FOR PHENYLMERCURIC HYDROXIDE
Normality of perchloric acid = 0.01055; molarity of phenylmercuric hydroxide solution = 0.009503; initial vol. of phenylmercuric hydroxide sol. = 50.00 ml.

Vol. of HClO ₄ added	pH	$T_{\text{HClO}_4} \times 10^3$	$T_{\text{PhHgOH}} \times 10^3$	$K_b \times 10^{10}$
0.00	7.63			
5.02	5.04	0.998	8.610	1.42
10.00	4.66	1.755	7.920	1.02
18.38	4.29	2.824	6.949	1.29
25.09	4.04	3.512	6.328	1.33
28.24	3.94	3.793	6.073	1.31
34.00	3.71	4.254	5.656	1.30

In developing the equation used for calculating results, these equilibria were considered



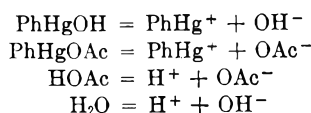
By combining equations for conservation of species, electrical neutrality and ionization constants, an equation was obtained

$$K_b = \frac{\frac{K_w^2}{[\text{H}^+]} + K_w T_{\text{HClO}_4} - K_w [\text{H}^+]}{[\text{H}^+] T_{\text{PhHgOH}} - K_w - [\text{H}^+] T_{\text{HClO}_4} + [\text{H}^+]^2}$$

A K_w value of 1.008×10^{-14} was used.³

Table II shows the data and results for the ionization constant for phenylmercuric acetate. The average of the three values closest to the half equivalence point is 1.5×10^{-5} and is taken as the best value.

In developing the equations for calculating the results, these equilibria were considered



The ionization constant K for phenylmercuric acetate was calculated from the equations

$$[\text{PhHg}^+] = \frac{T_{\text{PhHgOH}} - T_{\text{HOAc}} + \frac{[\text{H}^+]^2}{K_a} - \frac{K_w}{K_a} + [\text{H}^+] - \frac{K_w}{[\text{H}^+]}}{\frac{K_w}{[\text{H}^+] K_b} - \frac{[\text{H}^+]}{K_a}}$$

$$[\text{OAc}^-] = [\text{H}^+] + [\text{PhHg}^+] - \frac{K_w}{[\text{H}^+]}$$

$$[\text{PhHgOAc}] = T_{\text{HOAc}} - [\text{OAc}^-] \left\{ \frac{[\text{H}^+]}{K_a} + 1 \right\}$$

$$K = \frac{[\text{PhHg}^+][\text{OAc}^-]}{[\text{PhHgOAc}]}$$

A K_a value of 1.754×10^{-5} for acetic acid⁴ and a K_b value of 1.31×10^{-10} for phenylmercuric hydroxide were used in these calculations.

TABLE II

IONIZATION CONSTANT OF PHENYLMERCURIC ACETATE
Normality of acetic acid = 0.01008; molarity of phenylmercuric hydroxide soln. = 0.009503; initial vol. of phenylmercuric soln. = 50.00 ml.

Volume of acetic acid added	pH	$T_{\text{HOAc}} \times 10^3$	$T_{\text{PhHgOH}} \times 10^3$	$K \times 10^5$
0.00	7.63			
2.67	6.25	0.510	9.030	0.82
10.74	5.70	1.784	7.821	1.57
20.00	5.43	2.881	6.788	1.45
24.71	5.29	3.334	6.360	1.47
28.02	5.20	3.620	6.090	1.48
33.00	5.02	3.780	5.399	1.48

Table III shows the data and results obtained for the ionization constant of phenylmercuric propionate. The average of the three values closest to the half equivalence point is 3.1×10^{-5} and is taken as the best value.

TABLE III

IONIZATION CONSTANT FOR PHENYLMERCURIC PROPIONATE
Normality of propionic acid = 0.01321; molarity of phenylmercuric hydroxide soln. = 0.009299; initial vol. of phenylmercuric soln. = 50.00 ml.

Volume of propionic acid added	pH	$T_{\text{HOPr}} \times 10^3$	$T_{\text{PhHgOH}} \times 10^3$	$K \times 10^5$
0.00	7.56			
5.91	5.68	1.396	8.316	3.11
10.31	5.47	2.258	7.709	3.12
16.00	5.25	3.202	7.045	3.14
17.64	5.19	3.445	6.874	3.14
19.60	5.12	3.720	6.680	3.11
24.95	4.92	4.397	6.203	3.12
29.79	4.73	4.932	5.827	3.13
34.43	4.55	5.387	5.507	3.06

The equilibria considered and the equations used to calculate the ionization constant for phenylmercuric propionate correspond to those for phenylmercuric acetate. 1.336×10^{-5} was used as the ionization constant for propionic acid.⁴

The ionization constants were found to be 1.3

(3) H. S. Harned and B. B. Owen, "The Physical Chemistry of Electrolytic Solutions," Reinhold Publ. Corp., New York, N. Y., 1958, p. 638.

(4) Ref. 3, p. 755.

$\times 10^{-10}$ for phenylmercuric hydroxide, 1.5×10^{-5} for phenylmercuric acetate, and 3.1×10^{-5} for phenylmercuric propionate. Each of these values was found to be constant for experimental points taken over a wide range of ($T_{\text{acid}}/T_{\text{PhHgOH}}$) values. The constant for the hydroxide is further substantiated since it was used in calculating both of the other constants. The value for phenylmercuric hydroxide found in the present work agrees with the value of 1.0×10^{-10} that has been reported.² These constants may be used in estimations of equilibrium constants for the interaction of phenylmercury compounds with groups such as the sulfhydryl group in biological materials.

SORPTION OF SULFUR HEXAFLUORIDE BY ARTIFICIAL ZEOLITES

BY DANIEL BERG AND WILLIAM M. HICKAM

Westinghouse Central Laboratories, Pittsburgh 35, Pennsylvania

Received April 26 1961

The small and uniform size of the intracrystalline pores left by the removal of water from hydrated crystalline zeolites results in "molecular sieve" action. Molecules of large diameter are excluded from the pores; smaller diameter molecules may be sorbed in the intracrystalline pores. With mixtures of molecules of diameter smaller than the sieve pore sizes preferential sorption may take place.

Habgood¹ has studied the kinetics of Molecular Sieve action for nitrogen-methane mixtures. In this case nitrogen diffuses more rapidly into the small pores and is preferentially taken up in the early stages of sorption but methane has a higher affinity for the sieve and is preferentially sorbed at equilibrium.

In this work we are interested in studying the sorption of a molecule of roughly 5 Å. diameter, namely, SF₆, as a function of temperature and pressure and the selective sorption in mixtures of SF₆ and air.

Experimental Procedure

A gas circulatory system with mass spectrometer² was used in measuring sorption of SF₆ by the Molecular Sieve. This system offers several advantages over other equipment used for similar measurements. The calibrated volume and manometer permits accurate determination of the quantity of gas used. The system is attached to the mass spectrometer which provides analysis of the gas when desired. When mixtures of gases are being used the circulating pump ensures that the gas above the sieve is of uniform composition. This condition, combined with the mass spectrometric analysis, permits calculation of the quantity of each component adsorbed even though there are large temperature gradients in the system due to heating of the sieve.

A weighed amount of sieve was placed in the system. The sieve was evacuated and heated to about 200° to remove adsorbed gases. Sulfur hexafluoride was introduced at known pressure in the known volume of the gas circulatory system which was isolated from the sieve. When the SF₆ was exposed to the sieve the pressure dropped immediately and the sieve became heated. The procedure of filling the reservoir to a known pressure of SF₆ and then opening the sieve to the reservoir was repeated sev-

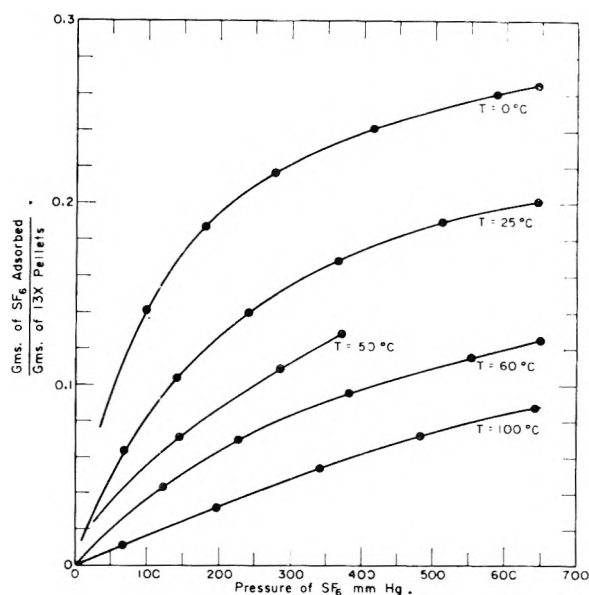


Fig. 1.—Adsorption of SF₆ on #13X Molecular Sieve pellets as a function of temperature and pressure.

eral times till the desired equilibrium pressure and temperature were reached. Knowledge of the system volume and pressure and the gas composition allowed the weight of SF₆ adsorbed on the sieve to be calculated for each final pressure above the sieve. The procedure was repeated with the sieve at equilibrium temperatures ranging from 0 to 100°. The reversibility of the adsorption also was established by evacuating measured quantities of SF₆ from the reservoir and then allowing the sieve to come to equilibrium temperature and pressure.

Sulfur hexafluoride from General Chemical Co., Pittsburgh, Pa., of greater than 99% purity was used. Mass spectrometrically identified tank impurities found were O₂, N₂, A, CF₄ and H₂O. With the exception of water and slight amounts of nitrogen the impurities are not sorbed by the Molecular Sieve at room temperature and higher.

There are four pore size sieves of Molecular Sieve available from the Linde Co., Tonawanda, N.Y. These include the 4A type of about 4 Å. pore width, 5A type to approximately 5.1 Å. pore width, 10X of about 10 Å. and 13X type of roughly 13 Å. pore width. They are synthetic alkali metal aluminosilicates. Both powder and 3.2 mm. pellets were used. The pellets are made by binding the powder with an inert clay-type binder amounting to 20% of the total weight of the pellet. Some of the properties of the 4A synthetic zeolites have been described by Breck, Eversole, Milton, Reed and Thomas³ and the crystal structure has been determined by Reed and Breck.⁴

Results and Discussion

The results of the sorption of pure SF₆ on type 13X Molecular Sieve are shown in Fig. 1 where the grams of SF₆ sorbed per gram of pellet is plotted as a function of the pressure of SF₆ for various Molecular Sieve temperatures. It should be remembered that the pellets contain 20% of inert clay binder. The true sorption fractions are 20% higher than graphed. This was confirmed by measuring pure 13X powder in a similar experiment. Type 10X gives similar curves. Both the 4A and 5A Molecular Sieve sorb less than 0.01 g. of SF₆ for each gram of pellet at 25° and 1 atmosphere.

From a plot of the pressure of SF₆ above the

(1) H. W. Habgood, *Can. J. Chem.*, **36**, 1384 (1958).

(2) L. C. Seala, W. M. Hickam and A. Langer, *Rev. Sci. Instr.*, **29**, 988 (1958).

(3) D. W. Breck, W. G. Eversole, R. M. Milton, T. B. Reed and T. L. Thomas, *J. Am. Chem. Soc.*, **78**, 5963 (1956).

(4) T. B. Reed and D. W. Breck, *ibid.*, **78**, 5972 (1956).

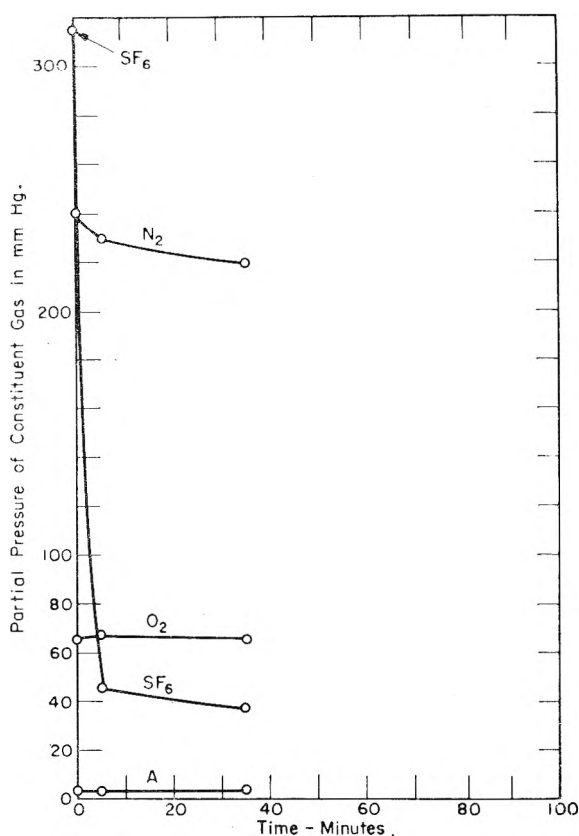


Fig. 2.— Adsorption of SF₆ from an air-SF₆ mixture by 13X sieve at 25°.

sieve against the reciprocal absolute temperature for various per cent. by weight adsorbed SF₆ one can determine the heat of adsorption by means of the equation

$$\log \frac{P_2}{P_1} = \frac{\Delta H}{2.3R} \left(\frac{1}{T_1} - \frac{1}{T_2} \right)$$

In this equation ΔH is the heat of adsorption (cal./mole), R is a constant equal to 2 cal./degree-mole, and P_1 , P_2 , T_1 , T_2 are the respective pressures and absolute temperatures. From such a plot ΔH was calculated to be about 5 kcal./mole. This means that heat is given off when the SF₆ is adsorbed and conversely heat is required to desorb the SF₆. The heat of sublimation of SF₆ is 5.64 kcal./mole at -64°. The value of 5 kcal./mole is typical for physical adsorption.

The diameter of SF₆ calculated from the S-F distance of 1.58 Å,⁶ the F tetrahedral covalent radius of 0.7 Å, and the less probable F⁻ ionic radius of 1.4 Å,⁷ leads to a value of 3.86 to 4.56 Å., both of which are smaller than the requisite 5 Å. size for the 5A Molecular Sieve. Using the relationship derived from kinetic theory,⁸ $\eta = 0.499\rho\bar{v}L$ where ρ is the density, \bar{v} the average velocity and L the mean free path, it is found that the cross-section calculated from the viscosity η is 6.4 Å. Apparently SF₆ is too large to penetrate the pores

of the Molecular Sieve with 5 Å. diameter or smaller pores. It is clear that the diameter computed from the ionic and/or covalent bond radii is not the correct one to use. It is more appropriate to use the cross-section computed from kinetic theory which considers the collision size and not the electron cloud size.

It should be noted that not only is the size of the molecule important from the standpoint of getting into the pores of the sieve, but it is necessary for the molecule to be adsorbed on the surface of the sieve. The adsorption on the surface depends on the magnitude of the interaction of the molecule with the surface. Since dipole-dipole interaction may be large, polar molecules interact with the polar surface of the sieve to a large extent, so that, if the polar molecule is small enough, a large quantity will be adsorbed. Non-polar molecules which may possess a quadrupole moment are adsorbed by the molecule being polarized by the surface of the sieve (a weak dipole is induced in the non-polar molecule by the polar surface of the sieve). If the non-polar molecule is small enough to enter the pores of the sieve and if the polarizability of the molecule in one direction is sufficient to have a large enough dipole induced in the non-polar molecule, the non-polar molecule will be adsorbed. In this qualitative discussion we are assuming that the temperature is constant because it is really the ratio of the energy of interaction of the molecule (polar or non-polar) and the surface to the thermal energy of the gaseous molecules (of the order of kT) which is important, as well as the size of the pores and molecules. SF₆ has a polarizability of 16.51⁹ which is almost 4 times that of oxygen or nitrogen and would be expected to physisorb more readily than O₂ or N₂. The larger interaction energy of the SF₆ molecule with the surface of the sieve as compared to that between SF₆ molecules makes it possible to obtain adsorption of the SF₆ above the critical temperature of SF₆ (46°). For example, at 60° and 1 atmosphere pressure, the sieve adsorbs about 15% by weight of SF₆. Assuming a surface area of 800 meters²/g.¹⁰ and using the thickness of the adsorbed monolayer of SF₆ as 6 Å. the calculated volume of SF₆ adsorbed on the surface of one gram of sieve is about 0.5 cm.³. Hence, the density of the adsorbed 0.15 g. of SF₆ in a volume of 0.5 cm.³ at 60° would be 0.3 g./cm.³. This compares to a liquid density of 0.73 g./cm.³ at the critical point.¹¹ A rough general rule is that the higher the value of the critical temperature of the gas the more the gas will be adsorbed at any temperature if the pores are larger than the molecules. The general rule is understandable if it is recalled that, above the critical temperature, a gas cannot be liquefied no matter what the pressure, and that the critical temperature gives a measure of the interaction of the molecules of the gas.

Additional experiments were performed with known mixtures of SF₆ and air. In Fig. 2 are

(5) W. C. Schumb and E. L. Gamble, *J. Am. Chem. Soc.*, **52**, 4302 (1930).

(6) T. G. Pearson and P. L. Robinson, *J. Chem. Soc.*, 1427 (1933).

(7) L. Pauling, "The Nature of the Chemical Bond," Third Edition, Cornell University Press, Ithaca, N. Y., 1960, pp. 247, 514.

(8) E. A. Kennard, "Kinetic Theory of Gases," McGraw-Hill Book Co., New York, N. Y., 1938, p. 147.

(9) H. E. Watson, G. Rao and K. L. Ramaswamy, *Proc. Roy. Soc. (London)*, **143**, 558 (1934).

(10) P. E. Eberly, *J. Phys. Chem.*, **65**, 68 (1961).

(11) K. E. MacCormack and W. S. Schneider, *Can. J. Chem.*, **29**, 699 (1951).

shown curves illustrating the selective adsorption of SF₆ from a 50% air and 50% SF₆ mixture. The SF₆ adsorption characteristics of the sieve are found to be independent of the air concentration. The SF₆ commercially available contains impurities of CF₄, O₂, N₂, A and H₂O. With the exception of water, and slight amounts of nitrogen, the other impurities are not adsorbed by the sieve and thus this provides a means for purifying SF₆. Mild heating removes the SF₆ and not the water. The SF₆ interacts through an induced dipole whereas water adsorbs by dipolar interaction.

THE HEAT OF FORMATION OF CF₂

BY LEO BREWER, JOHN L. MARGRAVE,¹ RICHARD F. PORTER AND KARL WIELAND

Department of Chemistry, University of California, Berkeley, California
Received April 27, 1961

Available data for the heat of formation of CF₂ are based on the general analogy of the C-F system with the C-H system² or on rates of reaction of Na with fluorinated methanes,³ and suggest $\Delta H_f^0 \leq -18$ kcal./mole. No lower limit on the heat has been suggested. Margrave⁴ has concluded recently from a mass spectrometric study of C₂F₄ and the appearance potential of CF₂⁺ that $\Delta H_f^0 \approx -30 \pm 10$ kcal./mole.

Further evidence regarding CF₂ has been deduced by determining the lowest temperature at which CF₂ bands may be detected in absorption in the system CF₄-graphite.⁵ The first faint, but clearly visible bands (2487 and 2457 Å.) appear at 1830°K. from the reaction CF₄(g) + C(s) = 2CF₂(g) with $P_{CF_4} = 0.18$ atm. From the very diffuse nature of the bands, it is likely that a minimum of 0.0015 mm. of CF₂ at 1800°K. is required for detection, while the maximum amount is probably 0.015 mm. at 1800°K., depending on the transition probability. These pressures, along with the known heat of formation of CF₄(g),⁶ and other standard thermodynamic functions, lead one to calculate $\Delta H_f^0(\text{CF}_2) \leq -30$ kcal./mole at 298°K.

A comparison also can be made with the Si-Cl system for which Schafer and Nickl⁷ have reported the heat of formation of the analogous molecule SiCl₂ as -30 kcal./mole. One can compare the heat of atomization of SiCl₂ (192 kcal./mole) with the heat of atomization of SiCl₄ (365 kcal./mole) and establish the ratio

$$\frac{\Delta H_a(\text{MX}_2)}{\Delta H_a(\text{MX}_4) - \Delta H_a(\text{MX}_2)} = 1.11$$

A similar value for this ratio appears to hold for the Si-F system.⁸ If exactly the same ratio holds

(1) University of Wisconsin, Madison, Wisconsin.

(2) R. Potocki and D. Mann, Natl. Bur. Standards Report 1439, February 15, 1952.

(3) J. Reed and B. Rabinovitch, *J. Phys. Chem.*, **61**, 598 (1957).

(4) J. L. Margrave, *J. Chem. Phys.*, **31**, 1432 (1959).

(5) J. L. Margrave and K. Wieland, *J. Chem. Phys.*, **21**, 1552 (1953); R. F. Porter and K. Wieland, unpublished work, 1953.

(6) C. A. Neugebauer and J. L. Margrave, *J. Phys. Chem.*, **60**, 1318 (1956).

(7) H. Schafer and J. Nickl, *Z. anorg. u. allgem. Chem.*, **274**, 250 (1953).

(8) A. Kansan and J. L. Margrave, unpublished work, University of Wisconsin, 1961.

for the C-F system, $\Delta H_a(\text{CF}_2) = 243$ kcal./mole and $\Delta H_f^0(\text{CF}_2) = -36$ kcal./mole.

Thus, it appears that the heat of formation of CF₂(g) is considerably more negative than previously thought with the correct value in the range -35 ± 10 kcal./mole.

REACTION OF ATOMIC HYDROGEN WITH SOLIDS AT -195°¹

BY VINCENT J. DECARLO AND F. O. RICE

Department of Chemistry, Georgetown University, Washington 7, D. C.
Received May 1, 1961

This work was started with the idea of synthesizing LiH₃. The fundamental notion is that negative ions tend to grow in order to give more room for the electronic cloud and consequently one might expect, given proper conditions, that the proton in lithium hydride could incorporate two hydrogen atoms to form the ion H₃⁻. The method used was that developed by Klein and Scheer² in which hydrogen atoms react with various substances frozen on a liquid nitrogen-cooled surface. Our results (largely negative) are shown in Table I.

TABLE I

ACTION OF ATOMIC HYDROGEN ON VARIOUS SUBSTANCES UNDER VARIOUS TEMPERATURES

Substance	Temp., °C.	Results
Li	-195	No reaction
Li	100	Fast reaction
Na, Hg, Cd, Mg		
Zn, Bi, Ge, Ga	-195	No reaction
Ca	-195	Very slow reaction
Ba	-195	H atoms go to H ₂ which is absorbed. No further reactions
	100	
Cu	-195	Apparently an unstable hydride first forms and then decomposes as concn. increases
HN ₂	-195	Very slow reaction
HN ₃	-150	Very slow reaction
COS	-195	Very slow reaction
Acetic anhydride	-195	No reaction
n-Butylamine	-195	No reaction
Isobutylamine	-195	No reaction
Ethyl alcohol	-195	No reaction
Amyl alcohol	-195	No reaction
Acetone	-195	Very slow reaction
n-Propyl alcohol	-195	Very slow reaction
Carbon tetrachloride	-195	Very slow reaction
Isobutyl alcohol	-195	Slow reaction
sec-Butyl alcohol	-195	Slow reaction
t-Butyl alcohol	-195	Slow reaction
n-Butyl alcohol	-195	Slow reaction (faster than the three previous)
Ethyl iodide	-195	Fast reaction

To our very great surprise, ethyl iodide reacts readily with hydrogen atoms at -195°; the white solid turns orange and gives a positive test for free iodine using starch indicator. We positively

(1) Presented at the Fifth International Symposium on Free Radicals, Uppsala, Sweden, July, 1961.

(2) R. Klein and M. D. Scheer, *J. Phys. Chem.*, **62**, 1011 (1958).

identified ethane, both by the mass spectrometer and gas chromatography, in the fraction removed at -80° , which seems to consist only of ethane. In addition a yellow non-volatile solid remained, which we did not identify.

Acknowledgment.—This work was supported in part by the National Science Foundation, Grant #G-9649, and the Atomic Energy Commission, Contract #1954-C.

STUDIES OF THE COPPER(II)-ALANINE AND PHENYLALANINE SYSTEMS IN AQUEOUS SOLUTION. DISSOCIATION AND FORMATION CONSTANTS AS A FUNCTION OF TEMPERATURE¹

BY R. M. IZATT,^{2a} J. W. WRATHALL,^{2b} AND K. P. ANDERSON

Department of Chemistry, Brigham Young Univ., Provo, Utah

Received May 12, 1961

Many formation constant data have been reported for metal ion-amino acid systems at a single temperature.^{3,4} The copper(I)-alanine,³⁻⁵ and the copper(II)-phenylalanine^{3,4,6} systems have been studied and formation constants reported at 25° and various ionic strength values. However, few studies of the temperature dependence of the formation constants of metal ion-amino acid systems, and, it appears, no data for the reaction of Cu^{++} with alanine or phenylalanine at temperatures other than 25° have been reported.

pK_D values are known at various ionic strengths for the stepwise dissociation of protons from protonated alanine at 0°, 20°, and 1.0, 12.5, 25, 37.5 and 50°⁸; and from protonated phenylalanine at 20°⁹ and 25°.⁹⁻¹² ΔH^0 values at 25° for the stepwise proton dissociation from protonated alanine have been determined by a calorimetric method¹³ and from the temperature dependence of the equilibrium constants.^{7,8}

This paper presents equilibrium constants calculated to infinite dilution for the stepwise reaction of copper(II) ion with alanate and phenylalanate ions, and for the stepwise dissociation of protons from protonated alanine and phenylalanine at 0, 10, 20, 30 and 40°. From the temperature

dependence of these constants, ΔH^0 values for the reactions are calculated. ΔS^0 values are calculated from ΔH^0 and ΔF^0 values.

Experimental

Procedure.—The pH titrations were made in solutions of low ionic strength in a manner similar to that described previously for the Cu^{++} -acetylacetonate system.¹⁴ Titrations were performed with a Beckman Model GS pH meter employing glass and saturated calomel electrodes.

Reagents.—A stock copper(II) perchlorate solution was prepared by dissolving C.P. CuO wire in a concd. HClO_4 - HNO_3 mixture, precipitating $\text{Cu}(\text{OH})_2$ with NaOH solution, washing with water, and dissolving in HClO_4 of known concentration. The solution was standardized with respect to Cu^{++} by conventional analytical procedures. Stock ligand solutions were prepared by dissolving weighed quantities of C.P. alanine and phenylalanine in water.

Buffers.—Bates¹⁵ has summarized and discussed the work of the National Bureau of Standards in determining pH values of standard reference solutions for use in pH titrations. Buffer solutions used in the present study were prepared by dissolving the C.P. salts, potassium hydrogen phthalate (pH 4)¹⁶ and a KH_2PO_4 - Na_2HPO_4 mixture (pH 7),¹⁷ in the required amounts of water and standardizing by conventional means to give solutions equivalent to those whose pH values have been determined from e.m.f. measurements by the National Bureau of Standards.

Calculations.—Molarity quotients for ligand-proton dissociation were determined by pH titration of two portions of each ligand solution with HClO_4 and NaOH , respectively. Molarity quotients for the stepwise reaction of each ligand with Cu^{++} were determined from \bar{n} and free ligand concentration by the method of Block and McIntyre.¹⁸ Thermodynamic equilibrium constants were calculated from the molarity quotients using a modified form of the Debye-Hückel equation.¹⁹ The calculations were made with an IBM 650 computer.

Results

Thermodynamic pK_{Dn} values for proton dissociation from the ligands and $\log K_n$ values for stepwise complex formation of each ligand anion, L^- , with Cu^{++} are given in Table I, together with ΔH^0_n and ΔS^0_n values calculated from the equilibrium constants. Comparison data from the literature are provided where these were determined under experimental conditions of temperature and ionic strength similar to those used here.

Plots of $1/T$ vs. pK_{D2} and $\log K_n$ are linear; however, the corresponding plot of $1/T$ vs. pK_{D1} in the case of each ligand shows curvature. The causes of this curvature which is observed in many carboxylic and related acids have been discussed by Gurney.²⁰

Discussion

$\log K_1$ is greater for the Cu(II)-alanine than for the Cu(II)-phenylalanine system, whereas the values of $\log K_2$ are close together and slightly greater for the copper(II)-phenylalanine. The first formation constant for the Cu(II)-alanine system might be expected to be greater than that for the phenylalanine system due to the greater basicity of the alanate ion (Table I); however, the relative

(1) Supported in part by NIH Grant A-2170 and Res. Corp. Grant 2370. Presented at the 139th ACS Meeting, St. Louis, Mo., March, 1961.

(2) (a) To whom inquiries concerning this article should be sent; (b) taken in part from the M.S. Thesis of Jay W. Wrathall.

(3) "Stability Constants," compiled by J. Bjerrum, G. Schwarzenbach, and L. G. Sillen, Special Publication No. 6, The Chemical Society (London), 1957.

(4) S. Chaberek and A. E. Martell, "Organic Sequestering Agents," John Wiley and Sons, Inc., New York, N.Y., 1959, Appendix 3.

(5) J. Curchod, *J. chim. phys.*, **53**, 182 (1956).

(6) J. Curchod, *ibid.*, **53**, 256 (1956).

(7) G. E. K. Branch and S. Miyamoto, *J. Am. Chem. Soc.*, **52**, 863 (1930).

(8) P. K. Smith, A. C. Taylor and E. R. B. Smith, *J. Biol. Chem.*, **122**, 109 (1937).

(9) H. R. Almond, R. J. Kerr and C. Niemann, *J. Am. Chem. Soc.*, **81**, 2856 (1959).

(10) J. C. Nevenzel, W. E. Shelberg and C. Niemann, *ibid.*, **71**, 3024 (1949).

(11) S. Miyamoto and C. L. A. Schmidt, *J. Biol. Chem.*, **90**, 165 (1930).

(12) P. Hirsch, *Biochem. Z.*, **147**, 433 (1924).

(13) J. M. Sturtevant, *J. Am. Chem. Soc.*, **64**, 726 (1942).

(14) R. M. Izatt, W. C. Fernelius and B. P. Block, *J. Phys. Chem.*, **59**, 80 (1955).

(15) R. G. Bates, *Chimica*, **14**, 111 (1960).

(16) W. J. Hamer, G. D. Pinching and S. F. Acree, *J. Research Natl. Bur. Standards*, **36**, 47 (1946).

(17) R. G. Bates and S. F. Acree, *ibid.*, **34**, 373 (1945).

(18) B. P. Block and G. H. McIntyre, *J. Am. Chem. Soc.*, **75**, 5667 (1953).

(19) R. M. Izatt, C. G. Haas, B. P. Block and W. C. Fernelius, *J. Phys. Chem.*, **68**, 1133 (1954).

(20) R. W. Gurney, "Ionic Processes in Solution," McGraw-Hill Book Co., New York, N. Y., 1953.

TABLE I

Temp., °C.	Proton dissociation			-NH ₃ ⁺			log K ₁	Cu ⁺⁺ -L ⁻ log K ₂	Interaction			
	pK _{D1}	ΔH ⁰ , kcal./mol.	ΔS ⁰ , e.u.	pK _{D2}	ΔH ⁰ , kcal./mol.	ΔS ⁰ , e.u.			ΔH ⁰ , kcal./mol.	ΔH ⁰ , e.u.	ΔS ⁰ , e.u.	S ₂ ⁰ , e.u.
	Ligand, alanine											
0	2.43			10.57			8.93	7.37				
10	2.39			10.30			8.96	7.29				
20	2.37			10.04			8.77	7.12				
	(2.22) ^a			(9.97) ^a			8.75	7.13				
25	(2.34) ^b			(9.87) ^b			8.68	7.00				
	(2.35) ^c	(0.6) ^c		(9.87) ^c	(10.8) ^c		8.63	7.04				
	(2.35) ^d	(0.8) ^d	(-3.0) ^d	(9.83) ^d	(11.0) ^d	(-8.0) ^d	(8.51) ^b	(6.85) ^b	(8.40) ^c	(7.36) ^c		
30	2.36			9.78			8.63	6.99				
40	2.36			9.48			8.58	6.86				
							8.53	6.93				
							8.39	6.68				
							8.29	6.69				
0-40		0.7	-3.6		10.6	-9.8	8.34	6.63				
	Ligand, phenylalanine											
0	2.28			9.95			8.65	7.45				
10	2.21			9.66			8.62	7.44				
20	2.20			9.38			8.45	7.26				
	(2.04) ^a			(9.31) ^a			8.38	7.21				
25	(2.16) ^f			(9.15) ^f			8.37	7.08				
30	2.23			9.15			8.24	7.08				
40	2.20			8.89			(7.70) ^g	(6.94) ^c				
							8.37	6.94				
							8.23	6.96				
							8.12	6.79				
							8.03	6.78				
							8.02	6.76				
0-40		0.6	8.3		10.3	-7.8						

^a Results of Albert,³ 0.005 *F* CuCl₂, 0.01 *F* HA, no activity correction. ^{b,c,d} Results of Monk,³ Keefer,³ and Smith, *et al.*,⁸ respectively; all values corrected to infinite dilution. ^e Calorimetric results of Sturtevant.¹³ ^f Results of Neverzel, *et al.*,¹⁰ obtained in 0.1 *F* NaCl. ^g Results of Curchod,⁶ μ not given.

magnitudes of the log *K*₂ values are surprising. The coordinated ligand in the 1:1 phenylalanine complex apparently affects the Cu in such a way as to cause it to have greater than expected affinity for the second phenylalanate ion. Cu⁺⁺ has completed d_{xy}, d_{xz}, d_{yz}, and d_{z²} orbitals, and has a single electron in the d_{x²-y²} orbital. Because of this electron distribution Cu-(II) complexes are commonly square planar.²¹

The above result, then, could arise because of the electron withdrawing character of the phenyl group in the 1:1 Cu⁺⁺-phenylalanine complex which would reduce the d-electron density along the *x-y* axes of the copper atom, thus lowering the repulsion between the single copper d electron and the donor atom electrons of the second entering phenylalanate ion making possible a bond of greater than expected stability in the 1:2 Cu⁺⁺-phenylalanine complex.

For a given ligand, the Δ*H*⁰ values are seen to be about the same for the formation of both complex species. The higher log *K*₁ value in each case is a result of the entropy contribution. This entropy effect can be attributed to (a) the purely statistical effect which prevents successive formation constants from being equal, and (b) differences in the hydra-

tion of the species in solution upon complex formation. The first step of the stepwise complex formation results in the removal of the highly hydrated Cu⁺⁺ ion from solution, and results in a greater increase in entropy than the second step, which does not involve such a highly charged ion.

The results of the ligand proton dissociation measurements are typical of those which have been found for simple α-amino acids.²⁰ The increased p*K*_D value for the -NH₃⁺ group relative to the -COOH group for both ligands is an enthalpy effect since 10 kcal./mole more heat is associated with proton ionization from the -NH₃⁺ than from the -COOH group, whereas the entropy changes are nearly the same.

The data presented here have been calculated on the assumption that stepwise formation of CuL₂ describes completely the reaction of L⁻ with Cu⁺⁺. The results obtained by using this assumption have been consistent. It is of interest, however, to note that other workers have presented evidence that alanine, under certain experimental conditions, forms these various species in addition to those assumed here: CuHL⁺⁺,^{5,22} Cu(HL)₂⁺⁺²² and CuL₃.²³ Curchod⁶ has found evidence for the formation of only CuL⁺ and CuL₂ in the case of phenylalanine.

(21) D. P. Graddon, "An Introduction to Co-ordination Chemistry," Pergamon Press, London, 1961.

(22) J. Curchod, *J. chim. phys.*, **53**, 125 (1956).

(23) R. M. Keefer, *J. Am. Chem. Soc.*, **68** 2320 (1946).

PROTON N.M.R. SPECTROSCOPY. XII.
TETRAMETHYLSILANE: SOME
OBSERVATIONS CONCERNING LINE
WIDTH AND LINE SHAPE

BY GEORGE VAN DYKE TIERS

Contribution No. 199 from the Central Research Department of the
Minnesota Mining and Manufacturing Co., St. Paul 19, Minnesota

Received May 16, 1961

It has become customary to consider that individual nuclear magnetic resonance (n.m.r.) lines, when not broadened by exchange may be described by the theoretical Lorentzian line shape.¹ It is recognized nevertheless that "in practice, line shapes are not always well represented by the Lorentz-type curve."¹ For mobile liquids such as tetramethylsilane at ordinary temperatures the "natural line width" (in cycles per second, c./sec., measured at half-maximal height) is given by the expression $1/\pi T_2$ where $T_2 \cong T_1$ as a rule.^{1,2} By direct measurement upon neat tetramethylsilane it has been found that $T_1 \geq 16.7$ sec.³ from which the natural line width would be estimated as 0.019 c./sec.; this is perhaps tenfold narrower than the best resolution attainable with present spectrometers. Even when air-saturated, a 5% solution of tetramethylsilane in carbon tetrachloride has $T_1 = 2.6$ sec., and thus 0.12 c./sec. line width. For this reason the assumption that the observed line shape can be treated as Lorentzian⁴ and that consequently all broadenings are additive,^{4b} may be incorrect and might result in substantial errors in kinetic measurements. It is therefore of interest to characterize line shape in terms of its approach to Lorentzian behavior, especially when spectrometer resolution has been optimized by careful attention to experimental details. The recently introduced Varian A-60 NMR Spectrophotometer has been found particularly suitable for such a study, since it combines inherently excellent resolution, convenience of operation and remarkable reproducibility of signal intensity and of sweep rate.

Experimental

The equipment used was the Varian A-60 NMR Spectrophotometer, kindly made available for trial and inspection.⁵ The air-saturated tetramethylsilane solution, 5% by volume in CCl_4 , was Varian Standard Sample No. 902337-05, and was contained in a 5 mm. o.d. thin-walled precision tube. All spectra were run at maximal expansion of sweep width, 1 c./sec. = 10 mm. on the chart. The minimal RF field setting (0.02 milligauss, nominal value) was chosen in order to minimize saturation.

For the optimization of "field shape" the slowness of decay of the ringing pattern at sweep rate 0.50 c./sec. per second was used as the criterion, it being required that exactly the same monotonic decay pattern be observed for

(1) J. A. Pople, W. G. Schneider and H. J. Bernstein, "High-Resolution Nuclear Magnetic Resonance," McGraw-Hill Book Co., Inc., New York, N. Y., 1959, p. 37.

(2) While T_2 is never longer than T_1 , it has in certain cases been found to be somewhat shorter; see J. G. Powles and D. Cutler, *Nature*, **180**, 1344 (1957) and **184**, 1123 (1959).

(3) F. A. Bovey, private communication. See also F. A. Bovey, *J. Chem. Phys.*, **32**, 1877 (1960).

(4) Ref. 1, (a) p. 45-46; (b) p. 220-224.

(5) During the Second Conference on Experimental Aspects of NMR Spectroscopy, Mellon Institute, Pittsburgh, 1961, the equipment was put on display by the manufacturer, Varian Associates.

both sweep directions. At the best setting of the field-homogeneity controls the decay was roughly exponential, being characterized by a half-life of 0.76 sec.; upon division by $\ln 2$ one obtains " T_2 " = 1.1 sec.,⁶ and from this the Lorentzian line width 0.29 c./sec. The spacings of wiggle maxima and minima were in exact agreement with the calculated values for the sweep rate used.⁶ The analysis of Jacobsohn and Wangness^{6,7} gives $\Delta\nu = 0.31$ c./sec. and $\Delta\nu' = 0.79$ c./sec., while the observed values (14 meas.) are 0.43 ± 0.01 c./sec. and 0.91 ± 0.01 c./sec., in fair agreement⁷; the true resonance position was taken as the mid-point between first maxima obtained from sweeps in both directions, as these were highly reproducible. The slowest sweep rate available, 0.10 c./sec. per second, was used for the line shape studies; since this was about three times the rate below which wiggles are not observed,⁷ considerable filtering was introduced (dial setting 0.2) in order to minimize the effects of wiggles. While this procedure is admittedly open to question, the observed $\Delta\nu$, 0.18 ± 0.01 c./sec. (20 meas.) shows no decrease in agreement with the calculated value, 0.13 c./sec.⁷ The response rate of the recorder did not appear to be limiting, since six of the measurements were made at double the amplitude, without any detectable change in $\Delta\nu$.

The results of twenty line width measurements are given in Table I.

Peak heights in fourteen of the runs, made at amplitude setting 0.63, averaged 50.6 mm. (± 1.7 mm. std. dev., per run) and those from the remaining six runs, at amplitude setting 1.25, averaged 96.9 mm. (± 1.7 , std. dev., per run). This good reproducibility of heights is certainly very reassuring when accurate width measurements at various percentage heights are desired.

An additional spectral feature readily observed is the spin-spin coupling between methyl protons and Si^{29} , present in 8.4% abundance. The coupling constant for tetramethylsilane, $J(\text{Si}^{29}\text{H}) = 6.57 \pm 0.02$ c./sec., was obtained from ten measurements; it may be compared with a previous value of 6.68 ± 0.04 c./sec. obtained with a Varian V-4300-240.00 Mc./sec. spectrometer.

Discussion

From the values cited in Table I it is seen that the somewhat broadened line, resulting from moderately rapid conformational isomerization (conformerization) of perfluorocyclohexane,⁸ does indeed show the virtually Lorentzian shape expected for a line narrow relative to the separation of the exchanging species. However, for the hundredfold narrower line from tetramethylsilane, a significant deviation from the Lorentzian shape is noted. Since the relative line widths, R_H , fall about halfway between those for the Lorentzian and Gaussian curves, one might plausibly suggest an approximately Gaussian distribution of Lorentzian lines, resulting perhaps from tiny random inhomogeneities in the magnetic field. Among other "experimental" causes of broadening might be (a) slow exchange, (b) unrecognized multiplicity, and (c) too fast rate of sweep. While in the present case the first two of these can be ruled out *a priori*, it will be instructive to examine their effects along with those of fast sweep.

(6) Ref. 1, p. 41; the envelope of wiggle maxima (or minima) is given by the exponential factor in equation 3-83, and from equation 3-84 the spacings (in c./sec.) of wiggle maxima or minima "far down the tail" is simply $1/\Delta t$, where Δt is the time elapsed after traversing the resonance position.

(7) B. A. Jacobsohn and R. K. Wangness, *Phys. Rev.*, **73**, 942 (1948); the displacement $\Delta\nu$ (c./s.) of the first maximum from the true resonance position is given by $\Delta\nu = x(d\nu/dt)^{1/2}/(2\pi)^{1/2}$ where x has the value 0.9 to 1.1 for the sweep rates used in the present article. The displacement $\Delta\nu'$ of the first minimum is found from the same equation by letting x be 2.8. Wiggles are not observed if the sweep rate, $d\nu/dt$ (in c./sec.²) $\leq 1/8\pi T_1$.

(8) G. V. D. Tiers, *Proc. Chem. Soc.*, 389 (1960); all experimental procedures are described there. The line width at half-height, $W_{1/2}$, was 23.93 ± 0.08 c./sec. at 25.5° .

TABLE I
RELATIVE LINE WIDTHS, R_H ,^a FOR OBSERVED N.M.R. LINES, AND FOR LORENTZIAN AND GAUSSIAN LINE SHAPES, AT VARIOUS PERCENTAGE HEIGHTS, H

	R_{10}	R_{20}	R_{30}	Relative line width, R_H^a		R_{70}	R_{80}	R_{90}
				R_{40}	R_{60}			
Lorentzian line shape	3.000	2.000	1.527	1.225	0.816	0.655	0.500	0.333
Obsd. n.m.r. of cyclo- C_6F_{12} ^b	3.13 ± 0.04	2.04 ± 0.02	1.54 ± 0.01	1.24 ± 0.01	0.82 ± 0.01	0.66 ± 0.01	0.52 ± 0.01	0.33 ± 0.03
Obsd. n.m.r. of $(CH_3)_4Si$ ^c	2.49 ± 0.06	1.72 ± 0.03	1.39 ± 0.01				0.53 ± 0.01	
Gaussian line shape ^d	1.823	1.523	1.319	1.150	0.859	0.718	0.567	0.390

^a The R_H values are expressed relative to the full line width at half-height, $W_{1/2}$ (occasionally referred to by the incorrect contraction "half-width"). ^b See ref. 8. ^c The line width, $W_{1/2}$, was 0.326 ± 0.007 c./sec. ^d The line width, $W_{1/2}$, is 2.345σ where σ is the "standard deviation"; see ref. 9.

TABLE II
LINE WIDTH RATIOS, L_H , AT VARIOUS PERCENTAGE HEIGHTS, H , FOR SEVERAL HYPOTHETICAL N.M.R. CASES, RELATIVE TO A LORENTZIAN LINE OF THE SAME HALF-HEIGHT WIDTH

	L_{10}	L_{20}	L_{30}	Line width ratios, L_H^a				
				L_{40}	L_{60}	L_{70}	L_{80}	L_{90}
Slow exchange ^b								
$W_{1/2} = 0.5$	0.853	0.878	0.910	0.947	1.075	1.187	1.386	1.857
$W_{1/2} = 1.0$.743	.790	.844	.911	1.116	1.287	1.580	2.232
Binomial multiplet ^c								
Comp. $W = 5J$.813	.872	.926	.969	1.035	1.060	1.086	1.100
Comp. $W = 2J$.684	.802	.885	.952	1.043	1.087	1.095	1.143
Gaussian line limits	.608	.762	.865	.939	1.051	1.096	1.134	1.170
Theor. fast sweep ^d								
$a^{1/2}T_2 = 1$.72	.83	.92	.96	1.04	1.1	1.2	1.3
$a^{1/2}T_2 = 2$.66	.79	.89	.95	1.04	1.07	1.1	1.1
$(CH_3)_4Si$, obsd.								
$d\nu/dt = 0.1$ c./sec. ^{2e}	$.83 \pm 0.02$	$.86 \pm 0.01$	0.91 ± 0.01				1.06 ± 0.02	
$d\nu/dt = 0.5$ c./sec. ^{2f}	.69	.80	.89	.95	1.04	1.1	1.1	1.2

^a The L_H ratios are as described in the text. ^b Exact calculation according to ref. 1, p. 223, eq. 10-29, where $\Delta = \nu_A - \nu_B$. ^c Fifteen individual Lorentzian component lines of half-height width W and spacing J , the intensities being given by the binomial coefficients. These curves approximate to Gaussian distribution of Lorentzian lines; see ref. 9. ^d Taken from ref. 7, Fig. 2; $a^{1/2}T_2 = (2\pi d\nu/dt)^{1/2}T_2$. See ref. 6. ^e Calcd. value of $a^{1/2}T_2 = 0.9$. ^f Experimental errors ca. ± 0.03 . Calcd. value of $a^{1/2}T_2 = 2.0$. $W_{1/2} = 0.58$ c./sec.

For this purpose it is convenient to take the theoretical Lorentzian curve as the standard, and to define a width ratio, L_H , as R_H (observed)/ R_H (Lorentzian), where R_H signifies the relative line widths based upon the half-height width. If an observed line is Lorentzian, then all L_H are unity; and if not Lorentzian the curve may be characterized by a table or plot of L_H vs. H . Such a comparison is made in Table II.

Slow exchange between two equal sites may be readily recognized experimentally, since it leads to abnormal breadth above the half-height. A single measurement of L_{30} or L_{90} in principle could permit a fairly accurate estimate of Δ , the shielding difference between the sites, if for some experimental reason this could not be observed directly.

The effects of multiplicity cannot be characterized as readily. The values listed in Table II are only typical of a many-component first-order multiplet which is not a common case. They were included because they provide a close approximation⁹ to the hypothetical Gaussian distribution of Lorentzian lines. The L_H values obtained from the theoretical curves for "fast" sweep⁷ (*i.e.*, producing "ringing") are also in-

cluded. It is interesting to note that one cannot distinguish between the patterns of L_H -values for these two cases. To be sure, the fast-sweep curves are not symmetrical, but the skewed Gaussian curve is well known.¹⁰

In order to decide on experimental grounds between these two causes of non-Lorentzian behavior it was necessary to examine the effect upon the L_H -values produced by changing the sweep rate. If a Gaussian distribution of magnetic field inhomogeneities were dominant, little or no change in the L_H values should be noted. If, on the other hand, one were to assume a fundamentally-Lorentzian line distorted by too-rapid sweep,⁷ then a predictable change in L_H -values would be observed. The experimental results of Table II correspond remarkably well with the numerical values of L_H calculated for "fast sweep." At sweep rate 0.5 c./sec. per second the *a priori* calculated value of $a^{1/2}T_2$ ⁷ is approximately 2.0, and the correspondence of the observed L_H -values with the theoretical is excellent. At sweep rate 0.1 c./sec. per second the *a priori* value of $a^{1/2}T_2$ is just below 0.9, and it is apparent that slight de-

(9) F. Mosteller, R. E. K. Rourke and G. B. Thomas, Jr., "Probability and Statistics," Addison-Wesley, Inc., Reading, Mass., 1961, pp. 275-287.

(10) J. C. Bartlett and D. M. Smith, *Can. J. Chem.*, **38**, 2057 (1960), have provided an interesting treatment of asymmetrical gas-chromatographic peaks based on the skewed Gaussian.

viations from the theoretical L_H values for $a^{1/2}T_2 = 1.0$ are in the right direction.

There is clearly no experimental basis for a claim of non-Lorentzian line shape, since all measurements are quantitatively in accord with theory for a Lorentzian line of half-height width 0.29 c./sec., slightly distorted and broadened by sweep rates just slightly too rapid. It is interesting that this is so, since the natural line width is only about 0.12 c./sec. Further and more careful studies of line shape on various n.m.r. spectrometers would perhaps enable a less tentative statement to be made. In this connection it may be noted that the Si^{29} satellites, for which $J(\text{Si}^{29}\text{H}) = 6.63$ c./sec., may be used as internal calibration of sweep when the older-type n.m.r. instrument is used; the short-term instabilities in sweep rate would, however, make necessary a much larger number of measurements than were required in the present work.

I am grateful to Varian Associates, Inc., for making available this remarkably fine new spectrometer, and to Mr. Robert Jones of that company for instruction in its use.

THE HEAT CONTENT AND HEAT CAPACITY OF BORON NITRIDE FROM 298 TO 1689°K.¹

By R. A. McDONALD AND D. R. STULL

Thermal Laboratory, The Dow Chemical Company, Midland, Michigan
Received May 4, 1961

This work was undertaken to fill in the gap between the low temperature data of Dworkin, Sasmor and Van Artsdalen² and the high temperature investigation of Magnus and Danz³ and to extend the measurements to higher temperatures.

Experimental

Material.—A cylindrical sample of boron nitride having a density of about 1.95 g. cc.⁻¹ was obtained through the courtesy of the Research and Development Division of the Carborundum Company, Niagara Falls, New York. After roasting, extracting with methanol to remove boron oxide, and vacuum drying, the sample was assayed: boron, 42.81% (43.58% theoretical); nitrogen, 56.85 ± 0.4% (56.42% theoretical). X-Ray diffraction revealed only well crystallized boron nitride of the graphite structure.

Enthalpy.—The heat content relative to 298.15°K. was measured in a "drop" calorimeter similar to the one described by Southard.⁴ A 5.154-g. portion of the boron nitride was sealed in a platinum-10% rhodium alloy capsule (14.011 g.) by arc welding under 8 cm. helium pressure. The temperature of the capsule in the furnace was measured with a platinum vs. platinum-10% rhodium thermocouple, the hot junction nearly touching the top of the capsule. The thermocouple had been calibrated at the gold point (1063.0°) and corrections were assumed to be linear.

Correction for the heat content of the container and heat loss during the drop was obtained by measuring the heat content of a similar empty capsule. Observations of the heat content of aluminum oxide (Calorimetry Conference Synthetic Sapphire) also were made to check the accuracy of the apparatus.

(1) This work was done for the Advanced Research Project Agency under U. S. Air Force Contract No. AF 33(616)-6149.

(2) A. S. Dworkin, D. J. Sasmor and E. R. Van Artsdalen, *J. Chem. Phys.*, **22**, 837 (1954).

(3) A. M. Magnus and H. Danz, *Ann. Physik*, [4] **81**, 407 (1926).

(4) J. C. Southard, *J. Am. Chem. Soc.*, **63**, 3142 (1941).

(5) G. T. Furukawa, T. B. Douglas, R. E. McCoskey and D. C. Ginnings, *J. Research Natl. Bur. Standards*, **57**, 67 (1956).

TABLE I

ENTHALPY OF $\alpha\text{-Al}_2\text{O}_3^a$

T , °K.	$H_T - H_{298.15}$, cal. mole ⁻¹ Obs.	cal. mole ⁻¹ NBS eq. ^b	Deviation obsd. - calcd.	% Dev. from NBS
278.8	-353.8	-355.8	+ 2.0	+0.56
329.6	615.8	619.9	- 4.1	-0.66
448.3	3246.4	3297.4	- 51.0	-1.55
539.4	5569.1	5591.5	- 22.4	-0.40
655.7	8803.2	8712.5	+ 90.7	+1.04
761.3	11736	11671	+ 65	+0.56
893.8	15455	15505	- 50	-0.32
1128.2	22436	22500	- 64	-0.28
1267.0	26758	(26726) ^c	+ 32	+0.12
1463.0	32902	(32765) ^c	+137	+0.42
1619.6	37849	(37630) ^c	+219	+0.58

^a Molecular weight, 101.96 g. mole⁻¹. ^b Furukawa, *et al.*, ref. 5. ^c Extrapolated.

TABLE II

OBSERVED ENTHALPY OF BN^a

T , °K.	$H_T - H_{298.15}$, cal. mole ⁻¹	T , °K.	$H_T - H_{298.15}$, cal. mole ⁻¹
279.5	-83.2	1120.7	7183.3
279.5	-83.4	1299.1	9193.3
408.3	648.1	1381.8	10160
455.6	910.3	1504.5	11572
656.3	2545.1	1603.0	12802
884.3	4728.6	1682.5	13651
902.9	4893.0		

^a Molecular weight, 24.83 g. mole⁻¹.

TABLE III

SMOOTHED ENTHALPY AND HEAT CAPACITY OF BN

T , °K.	$H_T - H_{298.15}$, cal. mole ⁻¹	C_p , cal. mole ⁻¹ deg. ⁻¹	T , °K.	$H_T - H_{298.15}$, cal. mole ⁻¹	C_p , cal. mole ⁻¹ deg. ⁻¹
300	7.45	4.69	1000	5898.4	10.6
350	263.2	5.54	1050	6432.2	10.8
400	559.2	6.28	1100	6975.2	10.9
450	890.2	6.93	1150	7526.2	11.1
500	1252.2	7.50	1200	8084.4	11.2
550	1640.5	8.00	1250	8648.8	11.3
600	2051.4	8.42	1300	9218.6	11.4
650	2482.2	8.76	1350	9793.0	11.5
700	2929.4	9.09	1400	10371	11.6
750	3391.8	9.39	1450	10953	11.7
800	3868.5	9.66	1500	11537	11.7
850	4358.2	9.93	1550	12122	11.7
900	4860.5	10.2	1600	12708	11.7
950	5374.2	10.4	1650	13294	11.7

Results

The observed enthalpies of α -aluminum oxide are compared with values calculated from the work of Furukawa,⁵ *et al.*, in Table I. We have taken the liberty of extrapolating their equation to compare the results above 1200°K.

The observed enthalpies of boron nitride are given in Table II and smoothed values of enthalpy and heat capacity are presented in Table III. The smoothed values were obtained by graphically smoothing the first differences.

The data of Magnus and Danz³ are in good agreement with our measurements of the heat content of boron nitride and the low temperature heat capacities of Dworkin, Sasmor and Van Artsdalen² join smoothly with our values.

COMMUNICATIONS TO THE EDITOR

ELECTRON SPIN RESONANCE OF AROMATIC HYDROCARBONS ON SILICA-ALUMINA CATALYSTS

Sir:

It has been reported that the adsorption of certain polynuclear aromatic hydrocarbons on silica-alumina cracking catalysts results in the formation of a positive radical-ion from the hydrocarbon, which exhibits typical electron spin resonance spectra.^{1,2} It was tacitly assumed that this was the result of an interaction involving only the hydrocarbon and an acid site on the surface of the catalyst. Experiments in this laboratory have indicated that this may not be true in many cases, and that the sometimes unsuspected presence of oxygen exerts a strong influence on the results. Oxygen is not eliminated easily from experimental materials, especially catalysts.

A sample of granulated silica-alumina cracking catalyst was contained in one lower arm of a 5-mm. h-shaped glass tube and a small amount of perylene was placed in the other lower arm. The tube was attached to a high-vacuum system and the catalyst (but not the perylene) was heated at 500° until the pressure did not rise above one micron when the pump valve was closed for a few seconds. The perylene was degassed by sublimation to the tube wall just above the lower end. The catalyst was cooled to about 100° and the perylene to -195° and the tube was exposed to vapor from degassed benzene in another tube attached to the vacuum system. The benzene had been degassed by three cycles of alternate pumping while frozen and melting under its own vapor pressure. When enough benzene had condensed in the perylene arm the h-tube was removed from the vacuum system by sealing off above the juncture of the lower arms. No resonance absorption could be detected in either the catalyst or the perylene-benzene arm at this stage.

The perylene then was transferred to the catalyst by means of the benzene as a solvent. The catalyst was instantly colored purple on contact with the solution. The benzene was returned to the other arm by cooling the arm in liquid nitrogen and the catalyst arm was sealed off just below the juncture. The colored catalyst then exhibited a 9-line electron spin resonance spectrum essentially identical with those already reported.^{1,2}

In a similar experiment the catalyst arm was provided with a vent to atmosphere at the lower end, and hydrogen was passed over the catalyst at 500° for two hours before the vent was sealed and evacuation was begun. In this case the catalyst became only slightly colored on contact with the perylene solution and the spin resonance absorption was reduced in amplitude to one-third of the amplitude obtained with the unhydrogenated catalyst.

- (1) J. J. Rooney and R. C. Pink, *Proc. Chem. Soc.*, 70 (1961).
- (2) D. M. Brouwer, *Chem. & Ind. (London)*, 177, No. 6 (1961).

In another experiment, anthracene was used with no solvent and was deposited on the catalyst under vacuum by heating at 170°. Very little spin resonance was found. When air was admitted to the tube, a large electron spin resonance absorption immediately appeared.

These observations and others along the same vein can perhaps be taken as evidence for the formation of positive radical-ions by electron-transfer to oxygen from a hydrocarbon-proton complex³ which might be expected from interaction of the hydrocarbon with a protonic acid site on the catalyst. On the other hand, while it is known that interactions of several aromatic hydrocarbons with certain strong Lewis acids yield positive radical-ions⁴ which may be expected to be paramagnetic, it may be that oxygen can accept an electron from a covalent complex of a hydrocarbon with a weaker Lewis acid site, again forming a paramagnetic radical-ion.

In either case it is obviously necessary in experiments designed to examine the interaction of acid-type catalysts and hydrocarbons to control the presence of oxygen (and presumably of other oxidizing agents) and to account for its effects if present.

UNION RESEARCH CENTER
UNION OIL COMPANY OF CALIFORNIA
BREA, CALIFORNIA

JAMES K. FOGO

RECEIVED JUNE 15, 1961

(3) W. Ij. Aalbersberg, J. Gaaf and E. L. Mackor, *J. Chem. Soc.*, 905 (1961).

(4) W. Ij. Aalbersberg, G. J. Hooijink, E. L. Mackor and W. P. Weijland, *ibid.*, 3055 (1959).

THE INFLUENCE OF X-RAYS ON CATALYTIC ACTIVITY AS RELATED TO INCORPORATED RADIOACTIVITY

Sir:

It has been reported in the literature¹⁻³ that the addition of millicurie amounts of radioactive S³⁵ to MgSO₄-Na₂SO₄ catalysts markedly increases their activity for the dehydration of cyclohexanol at 365 to 415°. The percentage increase in reaction rate was reported proportional to the logarithm of the specific activity, reaching 171% at an activity of 105.2 mc./g. On the other hand, irradiation of a MgSO₄ catalyst with externally produced 800-kev. electrons while the reaction was proceeding was reported to have had no effect. Since pure MgSO₄ was used in the latter tests while MgSO₄ containing 0.52 to 21.87% Na₂SO₄ was used in the former, and since the range of 800-kev. electrons in MgSO₄ is of the order of only 0.08 cm., the question of

(1) A. A. Balandin, V. I. Spitsyn, N. P. Dobroselskaya and I. E. Mikhailenko, *Doklady Akad. Nauk S.S.S.R.*, 121, 495 (1958).

(2) V. I. Spitsyn, *Izvest. Akad. Nauk S.S.S.R., Otdel. Khim. Nauk*, 1296 (1958).

(3) A. A. Balandin, V. I. Spitsyn, N. P. Dobroselskaya, D. Verehtschinski and P. Glozounov, Paper 68, 2nd International Congress on Catalysis, Paris, 1960.

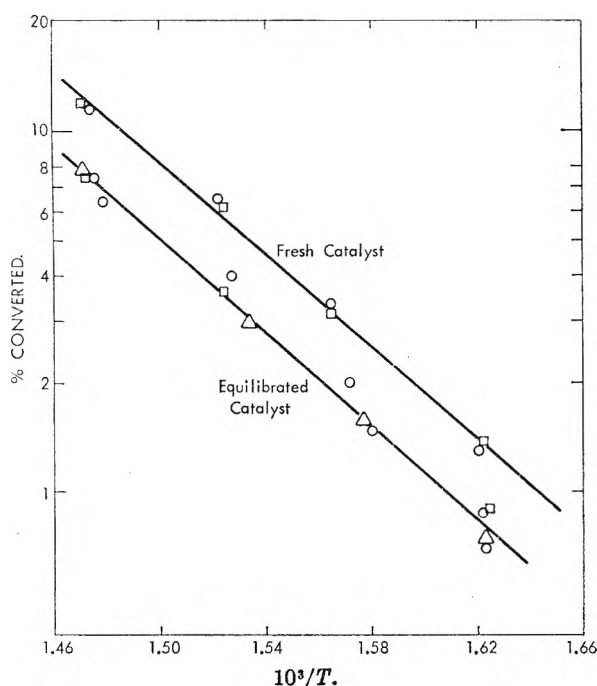


Fig. 1.—Arrhenius plot: catalyst, 0.0500 g. MgSO_4 ; \circ no radiation; \square irradiated, 180 kv., 15 ma., 123 rad./min.; \triangle irradiated, 300 kv., 5 ma., 113 rad./min.

whether externally supplied radiation could cause an effect similar to that resulting from the incorporation of radioactive sulfur remained in doubt.

In this work catalysts composed of MgSO_4 and $\text{MgSO}_4\text{-Na}_2\text{SO}_4$ have been irradiated while the dehydration reaction was taking place using a Norelco MG300 constant potential X-ray machine. Electrons were thus generated throughout the catalyst bed to simulate more closely the incorporation of S^{35} . The X-ray beam attenuation was less than 10%. Dose rates of 113 rad./min. (300 kv., 5 ma.) and 123 rad./min. (180 kv., 15 ma.), as measured by Fricke dosimeters and corrected for electron density, were used. On the basis of total energy absorbed, using 50 kev. as the average energy of the S^{35} beta particle, this corresponds to ~ 67 mc./g. of S^{35} . Compton and photoelectron energy-spectrum calculations, however, show that relatively few electrons of energies greater than 100 kev. are generated by the X-rays. If it is postulated that only these higher energy electrons are effective in producing changes in catalytic activity, the X-rays are equivalent to ~ 14 mc./g.

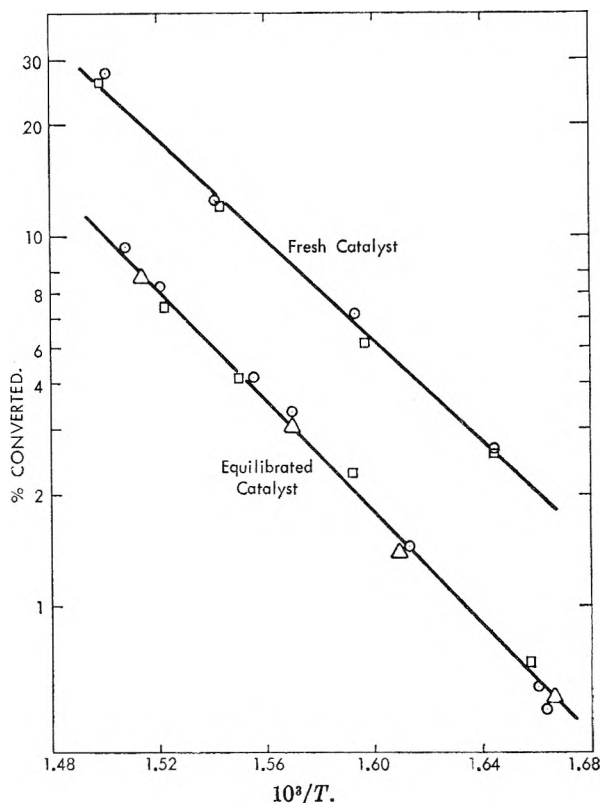


Fig. 2.—Arrhenius plot: catalyst, 0.1500 g. $\text{MgSO}_4\text{-4\% Na}_2\text{SO}_4$; \circ no radiation; \square irradiated, 180 kv., 15 ma., 123 rad./min.; \triangle irradiated, 300 kv., 5 ma., 113 rad./min.

of S^{35} . The reported data indicated that 67 mc./g. of S^{35} would produce a 154% increase in rate and 14 mc./g. a 97% increase in rate, so that in either case the effect should be easily observable. No such rate increases were found, however, on either fresh catalyst or catalyst brought to equilibrium activity by several hours' use (Fig. 1 and 2).

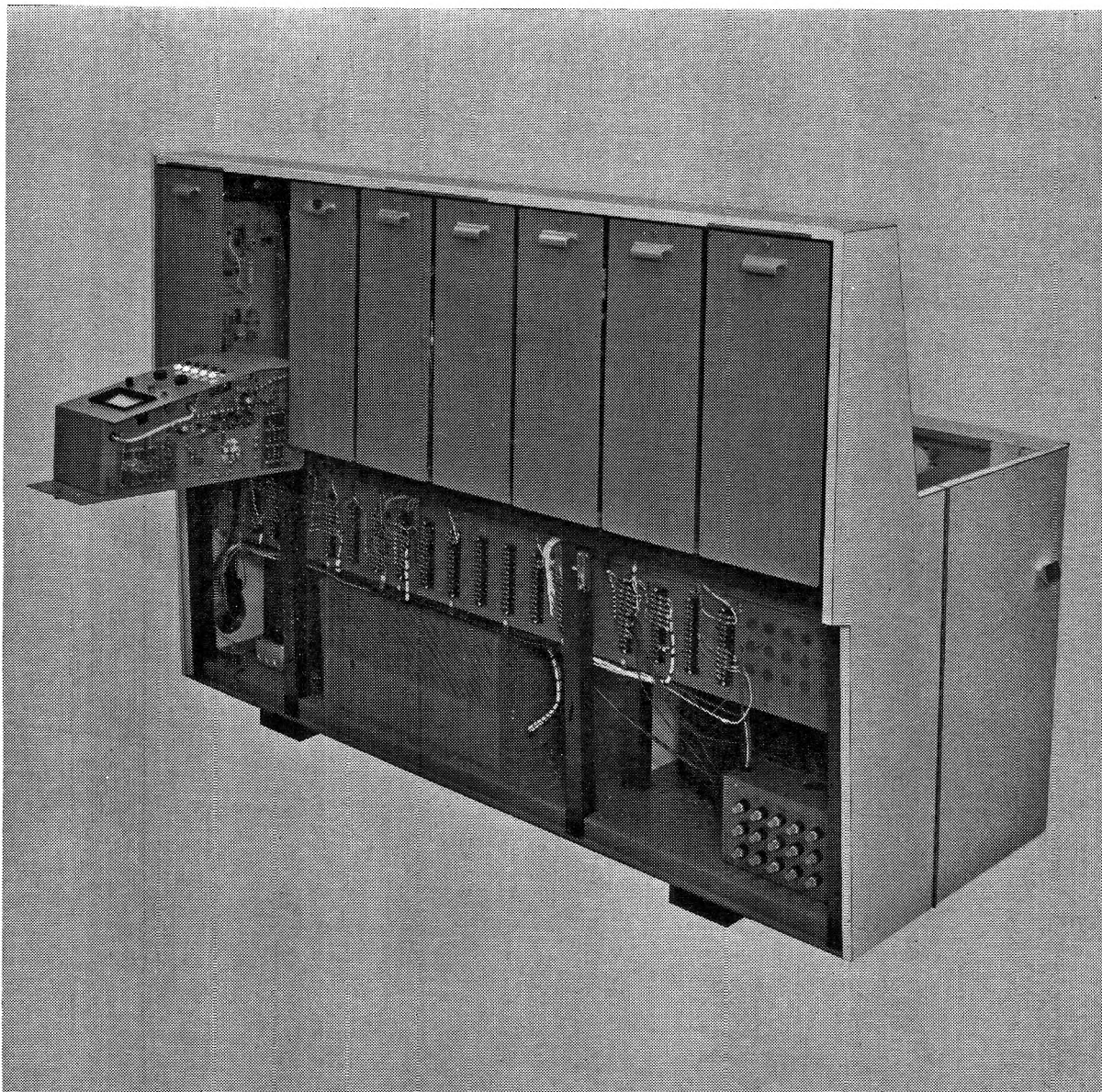
It thus appears that the effect of the addition of radioactive sulfur to these catalysts cannot be caused by any mechanism involving only the beta particles, but must be a result of physical or chemical changes related to the conversion of sulfur atoms to atoms of chlorine.

DEPARTMENT OF CHEMISTRY
UNIVERSITY OF TENNESSEE
KNOXVILLE, TENNESSEE, AND
OAK RIDGE NATIONAL LABORATORY
POST OFFICE BOX X
OAK RIDGE, TENNESSEE

NORMAN A. KROHN

HILTON A. SMITH

RECEIVED JULY 14, 1961



Behind this mass spectrometer: precision and accuracy for graduate chemistry studies

Here's the "instrument man's mass spectrometer" that goes hand in hand with graduate chemistry studies. CEC's new 21-130 Laboratory Mass Spectrometer, a medium-priced instrument, is used by many universities and colleges to perform analyses for research grants... and to attract contracts from industry.

The 21-130 permits graduate students to perform analyses with the same precision and high accuracy achieved by the largest mass spectrometers used in industry. This instrument helps support graduate training programs... complements other chemistry instruc-

tion with its capabilities in identifying and measuring unknown materials in gases and liquids.

Among its features: a mass range from m/e 2 to 230 continuous with unit resolution up to m/e 200... a built-in direct-writing oscillograph that records the full dynamic range without manual attenuation.

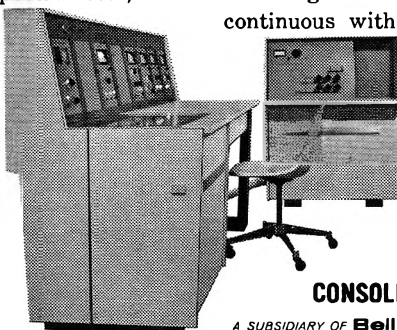
For complete information, call your nearest CEC sales and service office or write for Bulletin CEC 21130-X10.

Analytical & Control
Division

CEC

CONSOLIDATED ELECTRODYNAMICS/pasadena, calif.

A SUBSIDIARY OF **Bell & Howell** · FINER PRODUCTS THROUGH IMAGINATION



Just Published: Volume 12 (September 1961)

ANNUAL REVIEW OF

PHYSICAL CHEMISTRY

Editors: H. EYRING, C. J. CHRISTENSEN, H. S. JOHNSTON

Editorial Committee: J. BIGELEISEN, N. R. DAVIDSON, H. EYRING, D. F. HORNIG, J. E. MAYER,
W. H. STOCKMAYER

CONTENTS:

Physical Organic Chemistry	<i>A. N. Bourns and Erwin Buncel</i>
Marine Geochemistry	<i>Edward D. Goldberg</i>
Physical Properties of High Polymers	<i>K. H. Illers, H. G. Kilian, and R. Kosfeld</i>
The Statistical Mechanics of Chemical Processes	<i>Robert M. Mazo</i>
Kinetics of the Solid State	<i>Norman H. Nachtrieb</i>
Surface Catalysis	<i>Hugh Taylor</i>
Nuclear and Electron Spin Resonance	<i>S. I. Weissman</i>
Electrolyte Solutions	<i>Harold L. Friedman</i>
Solutions of Nonelectrolytes	<i>Berni J. Alder</i>
Electrode Processes	<i>Heinz Gerischer</i>
Molecular Electronic Spectroscopy	<i>D. A. Ramsay</i>
Vibration-Rotation Spectroscopy	<i>Bernard Kirtman, Margaret L. Benston, and Paul C. Cross</i>
Quantum Theory: Electronic Structure and Reactivity of Large Organic Molecules	<i>Takayuki Fueno</i>
Thermochemistry and Thermodynamic Properties of Substances	<i>Bruno J. Zwolinski and Alfred Danti</i>
High Temperature Chemistry	<i>Paul W. Gilles</i>
Ion Exchange	<i>Robert Kunin</i>
Radiation Chemistry	<i>John L. Magee</i>
Kinetics of Gas Phase Reactions	<i>W. D. Walters</i>
Proteins and Synthetic Polypeptides	<i>Ephraim Katchalski and Izchak Z. Steinberg</i>

514 pages

Author and Subject Indexes

Volumes 1 to 11 also available

\$7.00 postpaid (U.S.A.); \$7.50 postpaid (elsewhere)

ANNUAL REVIEWS, INC.

231 Grant Avenue, Palo Alto, California